

Kiyotake Ishikawa *Editor*

Experimental Models of Cardiovascular Diseases

Methods and Protocols

EXTRAS ONLINE



Humana Press

METHODS IN MOLECULAR BIOLOGY

Series Editor

John M. Walker

School of Life and Medical Sciences
University of Hertfordshire
Hatfield, Hertfordshire, AL10 9AB, UK

For further volumes:
<http://www.springer.com/series/7651>

Experimental Models of Cardiovascular Diseases

Methods and Protocols

Edited by

Kiyotake Ishikawa

Icahn School of Medicine at Mount Sinai, New York, NY, USA



Editor

Kiyotake Ishikawa
Icahn School of Medicine at Mount Sinai
New York, NY, USA

ISSN 1064-3745

ISSN 1940-6029 (electronic)

Methods in Molecular Biology

ISBN 978-1-4939-8596-8

ISBN 978-1-4939-8597-5 (eBook)

<https://doi.org/10.1007/978-1-4939-8597-5>

Library of Congress Control Number: 2018947193

© Springer Science+Business Media, LLC, part of Springer Nature 2018

This work is subject to copyright. All rights are reserved by the Publisher, whether the whole or part of the material is concerned, specifically the rights of translation, reprinting, reuse of illustrations, recitation, broadcasting, reproduction on microfilms or in any other physical way, and transmission or information storage and retrieval, electronic adaptation, computer software, or by similar or dissimilar methodology now known or hereafter developed.

The use of general descriptive names, registered names, trademarks, service marks, etc. in this publication does not imply, even in the absence of a specific statement, that such names are exempt from the relevant protective laws and regulations and therefore free for general use.

The publisher, the authors and the editors are safe to assume that the advice and information in this book are believed to be true and accurate at the date of publication. Neither the publisher nor the authors or the editors give a warranty, express or implied, with respect to the material contained herein or for any errors or omissions that may have been made. The publisher remains neutral with regard to jurisdictional claims in published maps and institutional affiliations.

Printed on acid-free paper

This Humana Press imprint is published by the registered company Springer Science+Business Media, LLC part of Springer Nature.

The registered company address is: 233 Spring Street, New York, NY 10013, U.S.A.

Preface

Cardiovascular disease continues to be the leading global cause of death. The number of patients suffering from these diseases is expected to further grow in the next decade due to the aging population worldwide as well as lifestyle changes in developing countries. Thorough research is ongoing to combat these diseases; however much remains to be elucidated before we fully understand the fundamental pathophysiological processes. Meanwhile, new therapeutic approaches are being actively explored in various areas including pharmacological, cell, gene, and device therapies. Common to both of these research areas is the importance of designing appropriate and reproducible experiments. Among the various factors, the disease model is the essential element that determines the quality and efficiency. Accordingly, employing appropriate experimental models is the key to obtaining successful and reproducible results.

The aim of this book is to provide methodological information on establishing reliable and reproducible experimental models of cardiovascular diseases. Practical and detailed protocols from expert laboratories will facilitate researchers in conducting experiments that focus on cardiovascular diseases, which will eventually lead to novel discoveries in cardiac biology and the development of effective therapeutic approaches.

I thank all expert authors for their dedication in describing detailed step-by-step methodologies that will help other researchers to reproduce their useful experimental cardiovascular disease models. We hope that the readers find *Experimental Models of Cardiovascular Diseases: Methods and Protocols* a useful reference for conducting and improving their projects.

New York, NY, USA

Kiyotake Ishikawa

Contents

Preface	v
Contributors	xi

PART I OVERVIEW

- 1 Experimental Models of Cardiovascular Diseases: Overview 3
Jae Gyun Oh and Kiyotake Ishikawa

PART II IN SILICO MODELS

- 2 An Introduction to Computational Modeling of Cardiac Electrophysiology and Arrhythmogenicity 17
Joshua Mayourian, Eric A. Sobie, and Kevin D. Costa

PART III IN VITRO MODELS

- 3 Isolation of Atrial and Ventricular Cardiomyocytes for In Vitro Studies 39
Jelena Plaćić and Jens Kockskämper
- 4 Cardiomyocyte Differentiation from Mouse Embryonic Stem Cells 55
Adam T. Lynch, Silvia Mazzotta, and Stefan Hoppler
- 5 Cardiomyocyte Differentiation from Human Embryonic Stem Cells 67
Silvia Mazzotta, Adam T. Lynch, and Stefan Hoppler
- 6 Induction of Human Induced Pluripotent Stem Cells to Cardiomyocytes Using Embryoid Bodies 79
Takeshi Hatani, Kenji Miki, and Yoshinori Yoshida
- 7 Measuring Cardiomyocyte Contractility and Calcium Handling In Vitro 93
Przemek A. Gorski, Changwon Kho, and Jae Gyun Oh

PART IV EX VIVO MODELS

- 8 Langendorff Perfusion Method as an Ex Vivo Model to Evaluate Heart Function in Rats 107
Makino Watanabe and Takao Okada
- 9 Methods for the Preparation of an Excised, Cross-Circulated Rat Heart 117
Koiji Obata and Miyako Takaki
- 10 Optical Action Potential Mapping in Acute Models of Ischemia–Reperfusion Injury: Probing the Arrhythmogenic Role of the Mitochondrial Translocator Protein 133
Zeki Ilkan, Benjamin Strauss, Chiara Campana, and Fadi G. Akar

- 11 Cardiac Tissue Engineering Models of Inherited and Acquired
Cardiomyopathies 145
*Irene C. Turnbull, Joshua Mayourian, Jack F. Murphy, Francesca Stillitano,
Delaine K. Ceholski, and Kevin D. Costa*
- 12 Badimon Perfusion Chamber: An Ex Vivo Model of Thrombosis 161
*M. Urooj Zafar, Carlos G. Santos-Gallego, Lina Badimon,
and Juan J. Badimon*

PART V SMALL ANIMAL MODELS

- 13 Ischemic Model of Heart Failure in Rats and Mice 175
*Jiqiu Chen, Delaine K. Ceholski, Irene C. Turnbull, Lifan Liang,
and Roger J. Hajjar*
- 14 Conventional Method of Transverse Aortic Constriction in Mice 183
Jimeen Yoo, Vadim Chepurko, Roger J. Hajjar, and Dongtak Jeong
- 15 Characterization of the Differential Progression of Left
Ventricular Remodeling in a Rat Model of Pressure Overload
Induced Heart Failure. Does Clip Size Matter? 195
Antoine H. Chaanine and Roger J. Hajjar
- 16 Isoproterenol-Induced Heart Failure Mouse Model Using
Osmotic Pump Implantation 207
Sunny C. Chang, Shuxun Ren, Christoph D. Rau, and Jessica J. Wang
- 17 Rat Model of Cardiotoxic Drug-Induced Cardiomyopathy 221
*Takehiro Nakahara, Takashi Tanimoto, Artiom D. Petrov, Kiyotake
Ishikawa, H. William Strauss, and Jagat Narula*
- 18 Pulmonary Artery Hypertension Model in Rats by Monocrotaline
Administration 233
Carlos Bueno-Beti, Yassine Sassi, Roger J. Hajjar, and Labouaria Hadri
- 19 The Sugen 5416/Hypoxia Mouse Model of Pulmonary
Arterial Hypertension 243
Carlos Bueno-Beti, Labouaria Hadri, Roger J. Hajjar, and Yassine Sassi
- 20 Mouse Model of Wire Injury-Induced Vascular Remodeling 253
Aya Nomura-Kitabayashi and Jason C. Kovacic
- 21 The Mouse Aortocaval Fistula Model with Intraluminal Drug Delivery 269
Toshihiko Isaji and Alan Dardik

PART VI LARGE ANIMAL MODELS

- 22 A Pig Model of Myocardial Infarction: Catheter-Based Approaches 281
Olympia Bikou, Shin Watanabe, Roger J. Hajjar, and Kiyotake Ishikawa
- 23 Ovine Model of Ischemic Mitral Regurgitation 295
*Dae-Hee Kim, Brittan Morris, J. Luis Guerrero, Suzanne M. Sullivan,
Judy Hung, and Robert A. Levine*
- 24 Canine Model of Pacing-Induced Heart Failure 309
Jeffery C. Powers and Fabio Recchia

25	Swine Model of Mitral Regurgitation Induced Heart Failure <i>Shin Watanabe, Olympia Bikou, Roger J. Hajjar, and Kiyotake Ishikawa</i>	327
26	Pig Model of Increased Cardiac Afterload Induced by Ascending Aortic Banding <i>Olympia Bikou, Satoshi Miyashita, and Kiyotake Ishikawa</i>	337
27	Large Porcine Model of Profound Acute Ischemic Cardiogenic Shock <i>Ole K. Møller-Helgestad, Hanne B. Ravn, and Jacob E. Møller</i>	343
28	Chronic Pulmonary Artery Embolization Models in Large Animals <i>Jaume Aguero, Nadjib Hammoudi, Olympia Bikou, Kenneth M. Fish, Iratxe Zaragoikoetxea, Roger J. Hajjar, and Kiyotake Ishikawa</i>	353
29	Modeling Pulmonary Hypertension: A Pig Model of Postcapillary Pulmonary Hypertension <i>Olympia Bikou, Kiyotake Ishikawa, Kenneth M. Fish, Iratxe Zaragoikoetxea, Roger J. Hajjar, and Jaume Aguero</i>	367
30	Development and Multiparametric Evaluation of Experimental Atherosclerosis in Rabbits <i>Max L. Senders, Mark E. Lobatto, Raphael Soler, Olivier Lairez, Carlos Pérez-Medina, Claudia Calcagno, Zahi A. Fayad, Willem J. M. Mulder, and Francois Fay</i>	385
	<i>Index</i>	401

Contributors

- JAUME AGUERO • *Centro Nacional de Investigaciones Cardiovasculares Carlos III (CNIC), Madrid, Spain; Hospital Universitari i Politècnic La Fe, Valencia, Spain; Cardiovascular Research Center, Icahn School of Medicine at Mount Sinai, New York, NY, USA*
- FADI G. AKAR • *Cardiac Bioelectricity Research Laboratory, Cardiovascular Institute, Icahn School of Medicine at Mount Sinai, New York, NY, USA*
- JUAN J. BADIMON • *AtheroThrombosis Research Unit, Cardiovascular Institute, Icahn School of Medicine at Mount Sinai, New York, NY, USA*
- LINA BADIMON • *Cardiovascular Research Center, Hospital Santa Cruz and San Pablo, School of Medicine of the Autonomous, University of Barcelona, Barcelona, Spain*
- OLYMPIA BIKOU • *Cardiovascular Research Center, Icahn School of Medicine at Mount Sinai, New York, NY, USA*
- CARLOS BUENO-BETI • *Cardiovascular Research Center, Icahn School of Medicine at Mount Sinai, New York, NY, USA*
- CLAUDIA CALCAGNO • *Translational and Molecular Imaging Institute, Icahn School of Medicine at Mount Sinai, New York, NY, USA*
- CHIARA CAMPANA • *Cardiac Bioelectricity Research Laboratory, Cardiovascular Institute, Icahn School of Medicine at Mount Sinai, New York, NY, USA*
- DELALINE K. CEHOLSKI • *Cardiovascular Research Center, Icahn School of Medicine at Mount Sinai, New York, NY, USA*
- ANTOINE H. CHAANINE • *Division of Cardiovascular Diseases, Mayo Clinic, Rochester, MN, USA*
- SUNNY C. CHANG • *Division of Cardiology, Department of Medicine, David Geffen School of Medicine at UCLA, Los Angeles, CA, USA*
- JIQIU CHEN • *Cardiovascular Research Center, Icahn School of Medicine at Mount Sinai, New York, NY, USA*
- VADIM CHEREPKO • *Department of Cardiology/Cardiovascular Research Center, Icahn School of Medicine at Mount Sinai, New York, NY, USA*
- KEVIN D. COSTA • *Cardiovascular Research Center, Icahn School of Medicine at Mount Sinai, New York, NY, USA*
- ALAN DARDIK • *Vascular Biology and Therapeutics Program, Yale School of Medicine, New Haven, CT, USA; Department of Surgery, Yale School of Medicine, New Haven, CT, USA; Department of Surgery, VA Connecticut Healthcare System, West Haven, CT, USA*
- ZABI A. FAYAD • *Translational and Molecular Imaging Institute, Icahn School of Medicine at Mount Sinai, New York, NY, USA*
- FRANCOIS FAY • *Translational and Molecular Imaging Institute, Icahn School of Medicine at Mount Sinai, New York, NY, USA; Department of Chemistry and Pharmaceutical Science, York College of the City University of New York, Jamaica, NY, USA*
- KENNETH M. FISH • *Cardiovascular Research Center, Icahn School of Medicine at Mount Sinai, New York, NY, USA*
- PRZEMEK A. GORSKI • *Cardiovascular Research Center, Icahn School of Medicine at Mount Sinai, New York, NY, USA*
- LAHOUARIA HADRI • *Cardiovascular Research Center, Icahn School of Medicine at Mount Sinai, New York, NY, USA*

- ROGER J. HAJJAR • *Department of Cardiology/Cardiovascular Research Center, Icahn School of Medicine at Mount Sinai, New York, NY, USA*
- NADJIB HAMMOUDI • *Cardiovascular Research Center, Icahn School of Medicine at Mount Sinai, New York, NY, USA*
- TAKESHI HATANI • *Department of Cardiovascular Medicine, Graduate School of Medicine, Kyoto University, Kyoto, Japan; Center for iPS Cell Research and Application, Kyoto University, Kyoto, Japan*
- STEFAN HOPPLER • *Institute of Medical Sciences, Foresterhill Health Campus, University of Aberdeen, Aberdeen, Scotland, UK*
- JUDY HUNG • *Cardiac Ultrasound Laboratory, Massachusetts General Hospital, Harvard Medical School, Boston, MA, USA*
- ZEKI ILKAN • *Cardiac Bioelectricity Research Laboratory, Cardiovascular Institute, Icahn School of Medicine at Mount Sinai, New York, NY, USA*
- TOSHIHIKO ISAJI • *Vascular Biology and Therapeutics Program, Yale School of Medicine, New Haven, CT, USA; Department of Surgery, Yale School of Medicine, New Haven, CT, USA; Department of Vascular Surgery, The University of Tokyo, Tokyo, Japan*
- KIYOTAKE ISHIKAWA • *Cardiovascular Research Center, Icahn School of Medicine at Mount Sinai, New York, NY, USA*
- DONGTAK JEONG • *Department of Cardiology/Cardiovascular Research Center, Icahn School of Medicine at Mount Sinai, New York, NY, USA*
- CHANGWON KHO • *Cardiovascular Research Center, Icahn School of Medicine at Mount Sinai, New York, NY, USA*
- DAE-HEE KIM • *Cardiac Imaging Center, Asan Medical Center, College of Medicine, University of Ulsan, Seoul, Korea; Division of Cardiology, Asan Medical Center, College of Medicine, University of Ulsan, Seoul, Korea; Cardiac Ultrasound Laboratory, Massachusetts General Hospital, Harvard Medical School, Boston, Massachusetts, USA*
- JENS KOCKSKÄMPER • *Faculty of Pharmacy, Institute of Pharmacology and Clinical Pharmacy, Biochemical and Pharmacological Center (BPC) Marburg, University of Marburg, Marburg, Germany*
- JASON C. KOVACIC • *Cardiovascular Research Center, Icahn School of Medicine at Mount Sinai, New York, NY, USA*
- OLIVIER LAIREZ • *Translational and Molecular Imaging Institute, Icahn School of Medicine at Mount Sinai, New York, NY, USA; Cardiac Imaging Center, University Hospital of Toulouse, Toulouse, France*
- ROBERT A. LEVINE • *Cardiac Ultrasound Laboratory, Massachusetts General Hospital, Harvard Medical School, Boston, Massachusetts, USA*
- LIFAN LIANG • *Cardiovascular Research Center, Icahn School of Medicine at Mount Sinai, New York, NY, USA*
- MARK E. LOBATTO • *Department of Radiology, Academic Medical Center, Amsterdam, The Netherlands*
- J. LUIS GUERRERO • *Surgical Cardiovascular Laboratory, Massachusetts General Hospital, Harvard Medical School, Boston, MA, USA*
- ADAM T. LYNCH • *Institute of Medical Sciences, Foresterhill Health Campus, University of Aberdeen, Aberdeen, Scotland, UK*
- JOSHUA MAYOURIAN • *Cardiovascular Research Center, Icahn School of Medicine at Mount Sinai, New York, NY, USA*
- SILVIA MAZZOTTA • *Institute of Medical Sciences, Foresterhill Health Campus, University of Aberdeen, Aberdeen, Scotland, UK*

- KENJI MIKI • *Center for iPS Cell Research and Application, Kyoto University, Kyoto, Japan*
- SATOSHI MIYASHITA • *Cardiovascular Research Center, Icahn School of Medicine at Mount Sinai, New York, NY, USA*
- OLE K. MØLLER-HELGESTAD • *Research Unit of Cardiology, Department of Cardiology, Odense University Hospital, Odense, Denmark*
- JACOB E. MØLLER • *Research Unit of Cardiology, Department of Cardiology, Odense University Hospital, Odense, Denmark*
- BRITTAN MORRIS • *Surgical Cardiovascular Laboratory, Massachusetts General Hospital, Harvard Medical School, Boston, MA, USA*
- WILLEM J. M. MULDER • *Translational and Molecular Imaging Institute, Icahn School of Medicine at Mount Sinai, New York, NY, USA; Department of Medical Biochemistry, Academic Medical Center, Amsterdam, The Netherlands*
- JACK F. MURPHY • *Cardiovascular Research Center, Icahn School of Medicine at Mount Sinai, New York, NY, USA*
- TAKEHIRO NAKAHARA • *Division of Cardiology, Icahn School of Medicine at Mount Sinai, New York, NY, USA; Molecular Imaging and Therapy Section, Memorial Sloan Kettering Cancer Center, New York, NY, USA; Department of Diagnostic Radiology, Keio University School of Medicine, Tokyo, Japan*
- JAGAT NARULA • *Division of Cardiology, Icahn School of Medicine at Mount Sinai, New York, NY, USA*
- AYA NOMURA-KITABAYASHI • *Cardiovascular Research Center, Icahn School of Medicine at Mount Sinai, New York, NY, USA*
- KOJI OBATA • *Department of Physiology, Gifu University Graduate School of Medicine, Gifu, Japan*
- JAЕ GYUN OH • *Cardiovascular Research Center, Icahn School of Medicine at Mount Sinai, New York, NY, USA*
- TAKAO OKADA • *Department of Physiology, Juntendo University Faculty of Medicine, Tokyo, Japan*
- CARLOS PÉREZ-MEDINA • *Translational and Molecular Imaging Institute, Icahn School of Medicine at Mount Sinai, New York, NY, USA*
- ARTIOM D. PETROV • *Division of Cardiology, Icahn School of Medicine at Mount Sinai, New York, NY, USA*
- JELENA PLAČKIĆ • *Faculty of Pharmacy, Institute of Pharmacology and Clinical Pharmacy, Biochemical and Pharmacological Center (BPC) Marburg, University of Marburg, Marburg, Germany*
- JEFFERY C. POWERS • *Department of Physiology, Cardiovascular Research Center, Lewis Katz School of Medicine at Temple University, Philadelphia, PA, USA*
- CHRISTOPH D. RAU • *Division of Cardiology, Department of Medicine, David Geffen School of Medicine at UCLA, Los Angeles, CA, USA*
- HANNE B. RAVN • *Department of Cardiothoracic Anesthesia, The Heart Center, Rigshospitalet, Copenhagen, Denmark*
- FABIO RECCHIA • *Department of Physiology, Cardiovascular Research Center, Lewis Katz School of Medicine at Temple University, Philadelphia, PA, USA*
- SHUXUN REN • *Division of Cardiology, Department of Medicine, David Geffen School of Medicine at UCLA, Los Angeles, CA, USA*
- CARLOS G. SANTOS-GALLEGÓ • *AtheroThrombosis Research Unit, Cardiovascular Institute, Icahn School of Medicine at Mount Sinai, New York, NY, USA*

- YASSINE SASSI • *Cardiovascular Research Center, Icahn School of Medicine at Mount Sinai, New York, NY, USA*
- MAX L. SENDERS • *Translational and Molecular Imaging Institute, Icahn School of Medicine at Mount Sinai, New York, NY, USA; Department of Medical Biochemistry, Academic Medical Center, Amsterdam, The Netherlands*
- ERIC A. SOBIE • *Department of Pharmacology and Systems Therapeutics, Icahn School of Medicine at Mount Sinai, New York, NY, USA*
- RAPHAEL SOLER • *Translational and Molecular Imaging Institute, Icahn School of Medicine at Mount Sinai, New York, NY, USA; Department of Vascular and Endovascular Surgery, Timone Hospital, Marseille, France*
- FRANCESCA STILLITANO • *Cardiovascular Research Center, Icahn School of Medicine at Mount Sinai, New York, NY, USA*
- BENJAMIN STRAUSS • *Cardiac Bioelectricity Research Laboratory, Cardiovascular Institute, Icahn School of Medicine at Mount Sinai, New York, NY, USA*
- H. WILLIAM STRAUSS • *Division of Cardiology, Icahn School of Medicine at Mount Sinai, New York, NY, USA; Molecular Imaging and Therapy Section, Memorial Sloan Kettering Cancer Center, New York, NY, USA*
- SUZANNE M. SULLIVAN • *Surgical Cardiovascular Laboratory, Massachusetts General Hospital, Harvard Medical School, Boston, MA, USA*
- MIYAKO TAKAKI • *Department of Physiology, Gifu University Graduate School of Medicine, Gifu, Japan; Department of Orthopaedic Surgery, Nara Medical University School of Medicine, Nara, Japan*
- TAKASHI TANIMOTO • *Division of Cardiology, Icahn School of Medicine at Mount Sinai, New York, NY, USA; Wakayama Medical University, Wakayama, Japan*
- IRENE C. TURNBULL • *Cardiovascular Research Center, Icahn School of Medicine at Mount Sinai, New York, NY, USA*
- JESSICA J. WANG • *Division of Cardiology, Department of Medicine, David Geffen School of Medicine at UCLA, Los Angeles, CA, USA*
- MAKINO WATANABE • *Department of Physiology, Juntendo University Faculty of Medicine, Tokyo, Japan*
- SHIN WATANABE • *Cardiovascular Research Center, Icahn School of Medicine at Mount Sinai, New York, NY, USA*
- JIMEEN YOO • *Department of Cardiology/Cardiovascular Research Center, Icahn School of Medicine at Mount Sinai, New York, NY, USA*
- YOSHINORI YOSHIDA • *Center for iPS Cell Research and Application, Kyoto University, Kyoto, Japan*
- M. UROOJ ZAFAR • *AtheroThrombosis Research Unit, Cardiovascular Institute, Icahn School of Medicine at Mount Sinai, New York, NY, USA*
- IRATXE ZARRAGOIKOETXEA • *Hospital Universitari i Politècnic La Fe, Valencia, Spain; Cardiovascular Research Center, Icahn School of Medicine at Mount Sinai, New York, NY, USA*

Part I

Overview



Chapter 1

Experimental Models of Cardiovascular Diseases: Overview

Jae Gyun Oh and Kiyotake Ishikawa

Abstract

Cardiovascular disease is one of the most common causes of deaths in clinics. Experimental models of cardiovascular diseases are essential to understand disease mechanism, to provide accurate diagnoses, and to develop new therapies. Large numbers of experimental models have been proposed and replicated by many laboratories in the past. Models with significant advantages are chosen and became more popular. Particularly, feasibility, reproducibility, and human disease resemblance are the common key factors for frequently used cardiovascular disease models. In this chapter, we provide a brief overview of these experimental models used for in vitro, in vivo, and in silico studies of cardiovascular diseases.

Key words Animal model, Myocardial infarction, Cardiomyocyte, Electrophysiology, Modeling, Pulmonary hypertension, Heart failure, Left ventricle, Rodents, Large animals

1 Introduction

Prevalence of cardiovascular disease (CVD) has been increasing worldwide, and the recent report from AHA (Heart Disease and Stroke Statistics—2017 Update) [1] indicates over 90 million US adults have at least one CVD, which is expected to increase more in a rapid pace. Extensive research focusing on prevention, diagnosis, and treatment of CVD has improved outcomes of patients with CVD; however, efforts continue to improve further. Importantly, bench science has been the driving force for this achievement and will continue to play major roles in future research.

Various models of CVD have contributed to new therapeutic discovery and identification of disease pathophysiology. In vitro models allow fast, efficient, and controllable experiments using cells or tissues. In contrast, in vivo models allow evaluation of mechanisms and therapeutic efficacy in more complex biology system. Recent advances in computation and software also enabled reliable in silico modeling of CVDs. To provide an overview of these models that aim at simulating human CVD, this chapter concisely reviews experimental models of CVD. Detailed protocols

to produce these models are provided in the following chapters of the book (*Experimental Models of Cardiovascular Diseases*), and the relevant chapter numbers are included as references.

2 In Silico Models

Recent advances in computing and technology now enable various approaches to model diseases in silico. By integrating data of key elements obtained from experiments, these models can help understand complex and dynamic biology as a system, offer high-throughput and efficient analysis, and provide novel insights into biological mechanisms. For example, cardiomyocyte action potential has been successfully modeled by integrating data from respective ion channel properties and contributed to understanding the impact of genetic disorders of each ion channels or effect of drugs [2]. These data can be further applied to more complex systems such as tissue or organ level electrophysiology (Chapter 2). The myocardial contraction was modeled using various methods such as finite-element analysis [3] and provided a spectrum of new mechanistic insights. Cardiac contractility as a part of systemic hemodynamics has been modeled using pressure–volume loop concept [4] and is a useful approach to estimate and understand how interventions affect these factors. Furthermore, similar to other areas of research, computational approaches are the main drivers of analyzing mass data and extracting important biological information. As the technologies advance, in silico approaches are expected to become more powerful and may replace many of in vitro and in vivo experiments in the future.

3 In Vitro Models

The key advantages of in vitro modeling systems are the availability of a large number of cells and precise control of experimental conditions that provide ability to efficiently conduct signaling pathway studies, cell-specific mechanistic studies and high-throughput drug screenings. Primary isolated cells and immortalized cell lines have contributed enormously in improving our understandings in the molecular and physiological regulation of cardiovascular system, and recently, human embryonic and induced pluripotent stem cell (ESC and iPSC, respectively) derived cells joined these repertoires, offering new in vitro approaches to study cardiovascular diseases.

3.1 Primary Isolated Cardiomyocytes

Neonatal cardiomyocytes, which are commonly isolated from 1- to 5-day-old rats, are one of the most popular in vitro model systems of cardiac function and disease. These cells are relatively easy to

isolate and culture, while offering feasible manipulation of gene expression profiles [5]. Various types of pathophysiological stimulations can be applied on neonatal cardiomyocytes, all mimicking *in vivo* cardiac pathology. Cardiac hypertrophy is induced by drugs such as norepinephrine [6], angiotensin II [7], and endothelin-1 [8]. Mechanical stretch can be applied directly on cells to simulate cardiac volume overload associated myocardial stretch [9]. In addition, ischemia–reperfusion is replicated by hypoxia–reoxygenation [10] or oxygen-scavenging compound (e.g., Na₂S₂O₄) treatments [11]. These stimulations often lead to cellular responses that closely represent cardiomyocyte changes *in vivo* setting, such as hypertrophy, apoptosis, autophagy, and fetal gene expression, rendering them a reliable model of cardiac diseases. Notwithstanding, immature morphology [12] and some dissociation in gene expression profiles compared to adult cardiomyocytes [13] are limitations of this cell type.

In contrast, adult cardiomyocytes (Chapter 3) more closely represent morphology as well as the behavior of cells in the intact human heart. Cells can be isolated from animal hearts of different age, sex, and species including human using enzymatic digestion protocols. Additionally, cardiomyocyte isolation from transgenic animals and diseased animals allow for a wide spectrum of experiments focusing on gene function as well as pathological stimuli. Most notably, thanks to the mature sarcomeric structure and ion channels, these cells also bear sophisticated experimental approaches such as patch-clamp [14], contractility measurements (Chapter 7) [15], and Ca²⁺ imaging studies [16, 17]. Technical difficulties in isolation procedures and culture are the limitation of this cell type. However, above invaluable advantages motivate researchers to continue working on these cells, and they remain one of the most frequently used models for *in vitro* cardiac research.

3.2 Immortalized Cell Lines

To overcome the limited culturing ability of primary cardiomyocytes [18], efforts have been made to establish immortalized cardiac cells. Representative cardiac immortalized cell lines include H9c2 [19], ANT-T-antigen [20], AT-1cells [21], MC29 [22], HL-1 [23], and AC16 [24]. These cells originate from cardiac cells and thus retain similar gene expression profiles and phenotypic characteristics of their origin. For example, H9c2 cells are derived from myoblast cell line, which was isolated from embryonic BDIX rat ventricular tissue, and AC16 cells from human ventricular tissues (by fusion with SV40 transformed human fibroblasts). Cell line-specific features and limitations need to be well recognized when using these cells, and validation in other cardiac models is likely necessary. Nevertheless, feasibility in culture and ability to use cells after freeze-thaw cycles render them a useful *in vitro* modeling system.

3.3 ESC and iPSC Derived Cardiomyocytes

Cardiomyocyte-like cells can be induced from pluripotent stem cells such as ESCs (Chapters 4 and 5) and iPSCs (Chapter 6). There is a recent surge on use of these cells as tools for modeling cardiac diseases in vitro. The key advantage is that these cells can be obtained from patients without excising the actual heart. This enables application of cardiac precision medicine by taking into account the individual variability of genomic profiles. Examples include mechanistic studies of gene disorders [25] and screening of potentially harmful drugs that can induce QT prolongation or cardiotoxicity [26]. Challenges remain, however, in cost and effort extensive methods to create these cells as well as physiologically and structurally immature cell status after induction. When these limitations are addressed by new approaches, stem cell-derived cardiomyocytes may become the primary choice of cell type for the majority of in vitro research.

3.4 In Vitro Models of Vascular Disease

Vascular endothelial cells (EC)s and smooth muscle cells (SMC)s are the two commonly studied cell types when modeling vascular diseases in vitro. Pathological modifications of these cells in vivo lead to atherosclerosis, restenosis, hypertension, and aneurysm that are all tightly connected to cardiovascular deaths. Key signaling pathways that contribute to these diseases are sought, and at the same time, methods to enhance angiogenesis are studied using ECs and SMCs. Primary cells can be obtained by enzymatic digestion of the vascular tissues from the variety of animals including human. Unlike cardiomyocytes, they easily proliferate on a culture dish and well tolerate freeze-thaw cycles, thus offer easier use of primary cells. Similar to cardiac cell models, ESC and iPSC derived ECs [27], as well as SMCs [28] have also been developed to model vascular diseases. Commonly performed mechanistic studies using these cells include proliferation, migration, contraction, secretion, and angiogenesis assays. To more closely reflect in vitro setting, cells are sometimes cultured in flow conditions or cultured together with other cell types to address cell interactions.

4 Ex Vivo Tissue Models

Although cell-based models offer efficient and fine-tuned experiments focusing on respective cell types, they usually lack in three-dimensional structure and interactions with other cell types. Ex vivo models of CVD can be used to overcome this limitation while maintaining fine-tuned experimental conditions. Majority of previously proposed ex vivo models use fresh organs explanted from animals or humans. Whole-heart perfusion using Langendorff system (Chapter 8) [29] or inter-animal cross-circulation (Chapter 9) [30] allows for precisely controlled physiological studies at the organ level. These approaches played pivotal roles in establishing the basis of our current understandings in cardiac physiology by

studying pressure–volume relationships, cardiac work, and myocardial oxygen consumption. Sophisticated studies on cardiac electrophysiology are also available using Langendorff system [31]. Optical mapping of Ca^{2+} sensitive fluorescence probes allows for detection of cardiac electric activities with high spatial and temporal resolution in the whole heart as well as in a piece of tissue that can be artificially perfused (Chapter 10). By changing the composition of perfusate, tailored experiments with different circulating concentrations of ions or drugs can be examined [32]. In addition, the impact of ischemia, as well as reperfusion injury may be studied in these ex vivo hearts by temporally or permanently ligating the coronary arteries. One limitation of these freshly explanted organ/tissues is difficulties in maintaining their integrities for long-term. Therefore, these models are mainly used for acute experiments. In contrast, bioengineering approaches allow for a chronic culture of tissues for long-term experiments using tissue engineering techniques from cultured cells [33]. Three-dimensional structure offers better replication of in vivo physiology compared to cell cultures. In addition, incorporation of human iPSC-induced cardiomyocytes allows for experiments on patient-specific disorders (Chapter 11). Continued efforts on improving the technique will likely lead to the development of the engineered whole heart in future.

Similar to the heart, protocols for ex vivo perfusion of vasculatures have also been developed [34]. Serial imaging with high spatial resolution is available using this approach, and may lead to new discoveries in atherosclerosis research. Atherosclerotic plaque rupture and thrombosis cause sudden onset disease and can be fatal, requiring efficient preventive approaches. For evaluating the risk of thrombosis events and to test the efficacies of antithrombotic drugs in specific patient, an ex vivo thrombosis model has been developed (Chapter 12).

5 In Vivo Models

Cardiac function and biology in vivo are meticulously regulated by interplays of various stimuli from outside the heart, such as hemodynamic, neurohormonal, and inflammatory signalings [35]. These signals are activated to maintain body homeostasis; however, sustained activation of these signals provokes cardiac pathophysiological responses. Importantly, cardiac dysfunction induces activation of pathological signaling, while these signals deteriorate cardiac function, thus forming a positive feedback loop in both acute and chronic settings. To understand the cardiac disease pathophysiology and effect of therapeutics in the complex biological system, in vivo models are essential. A variety of animal models have been proposed, and we will briefly review commonly used in vivo experimental models in the following sections.

5.1 Small Animal Models

Rodent models play pivotal roles in vivo cardiovascular research for several reasons [36]. These include anatomical similarity to human heart (four chambers) and vasculatures, easy housing and reasonable cost, fast gestation and short lifespan, and less ethical concerns compared to more advanced species. Owing to the established gene manipulation techniques and feasibility, mouse models offer in-depth analysis of gene function and disease mechanisms. High similarity in many genes between mice and human [37], together with established research tools for detecting gene and protein expressions in mice render them the most popular in vivo model system for cardiovascular research. Rat models, on the other hand, have larger heart and vessel sizes that offer easier surgical manipulation to induce diseases and provide a larger amount of tissues compared to mouse models. Rats are also physiologically closer to the human compared to mice.

Apart from transgenic CVD models, the model induction methods are mostly similar in mice and rats. Surgical manipulation is more challenging in mice due to its smaller size. However, once the researchers have become familiar with the necessary skills, higher throughput research is available in mice. Cardiac ischemia models include permanent coronary ligation and ischemic–reperfusion, both using similar techniques (Chapter 13). Location and the length of ligation determine the size of injury as well as survival after model induction. At the chronic stage, the heart remodels with systolic dysfunction similar to human after MI [38]. It also seems that the infarct healing processes are faster in mice than more advanced species [39]. Another popular method to induce heart failure is pressure overload using surgical banding of the aorta (Chapters 14 and 15). In mice, the heart initially becomes hypertrophic followed by cardiac dilation and systolic dysfunction at the later stage [40]. The speed of disease progression depends on the location of the banding (ascending or transverse) and the degree of the stenosis. In contrast, latter changes are not always observed in rats after aortic banding [41]. Drug-induced cardiac disease models are also commonly employed. Osmotic pumps are used to continuously infuse angiotensin or isoproterenol (Chapter 16) [42], while cardiotoxicity drugs such as doxorubicin are injected systemically (Chapter 17) [43]. Injection of monocrotaline can easily induce pulmonary hypertension in rats (Chapter 18) [44]. In contrast, the effect of monocrotaline in mice is not very reliable and hypoxia-induced pulmonary hypertension is more commonly used when using mice (Chapter 19).

For inducing vascular remodeling, wire injury method (Chapter 20) [45], as well as balloon inflation methods [46], are commonly employed. Disruption of endothelium and stretching of the vasculature with high cholesterol diets induce vascular lesions at the chronic stage. Artery to venous fistula model is also a useful tool to study venous remodeling (Chapter 21) [47].

5.2 Large Animal Models

Key advantages of large animal models are the similarities in size, anatomy, and physiology to the human heart. These features enable research using clinically applicable imaging devices as well as clinical sized therapeutic devices including the endovascular catheters. Similar physiology and more complex immune system compared to rodents make it easier to predict human responses to new therapeutic approaches. A large amount of tissue samples is available at necropsy and different assays can be conducted in the identical animal, which is sometimes difficult in small rodent hearts. Limitations of large animal experiments include difficulty in enrolling a large number of animals due to the cost and space limitations, higher ethical concerns, and limited research resources such as antibody and primers. Nevertheless, their important roles in bridging the bench science to clinical practice for drug development, testing clinical devices, and evaluating cardiac imaging modalities make them an essential step before clinical application of these approaches.

Variety of large animal models have been proposed using different species including pigs, dogs, sheep, rabbits, and nonhuman primates. To examine any therapeutic or diagnostic approaches in clinically relevant setting, large animal models should exhibit similar disease phenotype as the targeted clinical population. Among the cardiac diseases, ischemia-induced disease models are most commonly used. Myocardial infarction can be induced by both catheter-based (Chapter 22) [48] and surgical (Chapter 23) [49] approaches and provide a reproducible and controllable degree of systolic dysfunction. Acute studies focusing on reducing the initial myocardial injury associated with ischemia and subsequent reperfusion injury, as well as chronic studies focusing on preventing or reversing the progressive cardiac dysfunction and remodeling can be designed using these models. Other ischemic models include coronary embolization models that develop diffuse cardiac dysfunction (Chapter 27) [50], and chronic ischemia models with hibernating myocardium [51]. Presence of mitral regurgitation in post-MI heart is a risk factor for adverse events, and animal models of this condition have been developed in pigs [52] and sheep (Chapter 23) [53, 54].

Nonischemic cardiac disease models can be induced by continuous tachypacing (tachycardia-induced myopathy) (Chapter 24) [55], volume overload by valvular regurgitation (Chapter 25) [56] or artery to venous shunt [57], pressure overload by aortic banding (Chapter 26) [58] or renal wrapping [59], and cardiac toxic drug injection [60]. Pressure overload-induced models somewhat resemble clinically common heart failure phenotype; heart failure with preserved ejection fraction, but the lack of obesity and metabolic diseases, as well as difficulty in using aged animals, make it challenging to replicate clinical phenotype completely. Right heart failure without accompanying pulmonary hypertension can be induced by

pulmonary artery constriction [61]. Pulmonary embolism model mimics clinical pulmonary hypertension patients with chronic thromboembolic pulmonary hypertension (Chapter 28) [62]. Our group has recently established a post-capillary pulmonary hypertension model that accompanies right ventricular dysfunction (Chapter 29) [63]. Together, these models offer options for choosing appropriate pulmonary hypertension models for experiments in large animals.

A rabbit model of atherosclerosis is a popular vascular disease model for studying imaging and therapeutics for atherosclerosis (Chapter 30) [64]. Combination of high-fat diet and balloon injury to induce vascular lesions are also employed in other species. Aortic dissection and aortic aneurysm models have also been developed in large animals [65].

6 Conclusion

All models described above have their own advantages and limitations. It is important for the researchers to design the experiments based on their solid hypothesis and use appropriate models to answer their hypothesis. Detailed protocols described in each chapter for creating these models in this book should allow for successful and reproducible experiments.

Acknowledgments

This work is supported by NIH R01 HL139963 (K.I.), AHA-SDG 17SDG33410873 (K.I.), and AHA 17POST33410877 (J.G.O.).

References

1. Benjamin EJ, Blaha MJ, Chiuve SE, Cushman M, Das SR, Deo R, de Ferranti SD, Floyd J, Fornage M, Gillespie C, Isasi CR, Jimenez MC, Jordan LC, Judd SE, Lackland D, Lichtman JH, Lisabeth L, Liu SM, Longenecker CT, Mackey RH, Matsushita K, Mozaffarian D, Mussolini ME, Nasir K, Neumar RW, Palaniappan L, Pandey DK, Thiagarajan RR, Reeves MJ, Ritchey M, Rodriguez CJ, Roth GA, Rosamond WD, Sasson C, Towfighi A, Tsao CW, Turner MB, Virani SS, Voeks JH, Willey JZ, Wilkins JT, Wu JHY, Alger HM, Wong SS, Muntner P, Comm AHAS, Subcomm SS (2017) Heart disease and stroke statistics-2017 update: a report from the American Heart Association. Circulation 135 (10):E146–E603. <https://doi.org/10.1161/Cir.0000000000000485>
2. O'Hara T, Virag L, Varro A, Rudy Y (2011) Simulation of the undiseased human cardiac ventricular action potential: model formulation and experimental validation. PLoS Comput Biol 7(5):e1002061
3. Dorri F, Niederer PF, Lunkenheimer PP (2006) A finite element model of the human left ventricular systole. Comput Methods Biomed Engin 9(5):319–341
4. Santamore WP, Burkhoff D (1991) Hemodynamic consequences of ventricular interaction as assessed by model analysis. Am J Phys 260 (1 Pt 2):H146–H157
5. Louch WE, Sheehan KA, Wolska BM (2011) Methods in cardiomyocyte isolation, culture, and gene transfer. J Mol Cell Cardiol 51 (3):288–298. S0022-2828(11)00250-1 [pii].

- <https://doi.org/10.1016/j.yjmcc.2011.06.012>
6. Simpson P, McGrath A, Savion S (1982) Myocyte hypertrophy in neonatal rat heart cultures and its regulation by serum and by catecholamines. *Circ Res* 51(6):787–801
 7. Sadoshima J, Izumo S (1993) Molecular characterization of angiotensin II – induced hypertrophy of cardiac myocytes and hyperplasia of cardiac fibroblasts. Critical role of the AT1 receptor subtype. *Circ Res* 73(3):413–423
 8. Sakai S, Shimojo N, Kimura T, Tajiri K, Maruyama H, Homma S, Kuga K, Mizutani T, Aonuma K, Miyachi T (2014) Involvement of peptidyl-prolyl isomerase Pin1 in the inhibitory effect of fluvastatin on endothelin-1-induced cardiomyocyte hypertrophy. *Life Sci* 102(2):98–104. S0024-3205 (14)00343-9 [pii]. <https://doi.org/10.1016/j.lfs.2014.03.018>
 9. Komuro I, Kaida T, Shibasaki Y, Kurabayashi M, Katoh Y, Hoh E, Takaku F, Yazaki Y (1990) Stretching cardiac myocytes stimulates protooncogene expression. *J Biol Chem* 265(7):3595–3598
 10. Acosta D, Puckett M (1977) Ischemic myocardial injury in cultured heart cells: preliminary observations on morphology and beating activity. *In Vitro* 13(12):818–823
 11. Peng K, Qiu Y, Li J, Zhang ZC, Ji FH (2017) Dexmedetomidine attenuates hypoxia/reoxygenation injury in primary neonatal rat cardiomyocytes. *Exp Ther Med* 14(1):689–695. <https://doi.org/10.3892/etm.2017.4537>. ETM-0-04537 [pii]
 12. Brette F, Orchard C (2003) T-tubule function in mammalian cardiac myocytes. *Circ Res* 92 (11):1182–1192. <https://doi.org/10.1161/01.RES.0000074908.17214.FD>. 92/11/1182 [pii]
 13. Gilsbach R, Preissl S, Gruning BA, Schnick T, Burger L, Benes V, Wurch A, Bonisch U, Gunther S, Backofen R, Fleischmann BK, Schubeler D, Hein L (2014) Dynamic DNA methylation orchestrates cardiomyocyte development, maturation and disease. *Nat Commun* 5:5288. ncomms6288 [pii]. <https://doi.org/10.1038/ncomms6288>
 14. Bhargava A, Lin X, Novak P, Mehta K, Korchev Y, Delmar M, Gorelik J (2013) Super-resolution scanning patch clamp reveals clustering of functional ion channels in adult ventricular myocyte. *Circ Res* 112 (8):1112–1120. <https://doi.org/10.1161/CIRCRESAHA.111.300445>
 15. Gaitas A, Malhotra R, Li T, Herron T, Jalife J (2015) A device for rapid and quantitative measurement of cardiac myocyte contractility. *Rev Sci Instrum* 86(3):034302. <https://doi.org/10.1063/1.4915500>
 16. Moshal KS, Tippuraju SM, Vacek TP, Kumar M, Singh M, Frank IE, Patibandla PK, Tyagi N, Rai J, Metreveli N, Rodriguez WE, Tseng MT, Tyagi SC (2008) Mitochondrial matrix metalloproteinase activation decreases myocyte contractility in hyperhomocysteinaemia. *Am J Physiol Heart Circ Physiol* 295(2):H890–H897. 00099.2008 [pii]. <https://doi.org/10.1152/ajpheart.00099.2008>
 17. Cagalinec M, Waczulikova I, Ulicna O, Chorvat D Jr (2013) Morphology and contractility of cardiac myocytes in early stages of streptozotocin-induced diabetes mellitus in rats. *Physiol Res* 62(5):489–501. 932467 [pii]
 18. Marvin WJ Jr, Robinson RB, Hermsmeyer K (1979) Correlation of function and morphology of neonatal rat and embryonic chick cultured cardiac and vascular muscle cells. *Circ Res* 45(4):528–540
 19. Kimes BW, Brandt BL (1976) Properties of a clonal muscle cell line from rat heart. *Exp Cell Res* 98(2):367–381
 20. Steinhelper ME, Lanson NA Jr, Dresdner KP, Delcarpio JB, Wit AL, Claycomb WC, Field LJ (1990) Proliferation in vivo and in culture of differentiated adult atrial cardiomyocytes from transgenic mice. *Am J Phys* 259(6 Pt 2): H1826–H1834. <https://doi.org/10.1152/ajpheart.1990.259.6.H1826>
 21. Delcarpio JB, Lanson NA Jr, Field LJ, Claycomb WC (1991) Morphological characterization of cardiomyocytes isolated from a transplantable cardiac tumor derived from transgenic mouse atria (AT-1 cells). *Circ Res* 69(6):1591–1600
 22. Jaffredo T, Chestier A, Bachnou N, Dieterlen-Lievre F (1991) MC29-immortalized clonal avian heart cell lines can partially differentiate in vitro. *Exp Cell Res* 192(2):481–491
 23. Claycomb WC, Lanson NA Jr, Stallworth BS, Egeland DB, Delcarpio JB, Bahinski A, Izzo NJ Jr (1998) HL-1 cells: a cardiac muscle cell line that contracts and retains phenotypic characteristics of the adult cardiomyocyte. *Proc Natl Acad Sci U S A* 95(6):2979–2984
 24. Davidson MM, Nesti C, Palenzuela L, Walker WF, Hernandez E, Protas L, Hirano M, Isaac ND (2005) Novel cell lines derived from adult human ventricular cardiomyocytes. *J Mol Cell Cardiol* 39(1):133–147. S0022-2828(05)00076-3 [pii]. <https://doi.org/10.1016/j.yjmcc.2005.03.003>
 25. Moretti A, Bellin M, Welling A, Jung CB, Lam JT, Bott-Flugel L, Dorn T, Goedel A,

- Hohnke C, Hofmann F, Seyfarth M, Sinnecker D, Schomig A, Laugwitz KL (2010) Patient-specific induced pluripotent stem-cell models for long-QT syndrome. *N Engl J Med* 363(15):1397–1409. NEJMoa0908679 [pii]. <https://doi.org/10.1056/NEJMoa0908679>
26. Burridge PW, Li YF, Matsa E, Wu H, Ong SG, Sharma A, Holmstrom A, Chang AC, Coronado MJ, Ebert AD, Knowles JW, Telli ML, Witteles RM, Blau HM, Bernstein D, Altman RB, Wu JC (2016) Human induced pluripotent stem cell-derived cardiomyocytes recapitulate the predilection of breast cancer patients to doxorubicin-induced cardiotoxicity. *Nat Med* 22(5):547–556. nm.4087 [pii]. <https://doi.org/10.1038/nm.4087>
27. Zhang J, Chu LF, Hou Z, Schwartz MP, Hacker T, Vickerman V, Swanson S, Leng N, Nguyen BK, Elwell A, Bolin J, Brown ME, Stewart R, Burlingham WJ, Murphy WL, Thomson JA (2017) Functional characterization of human pluripotent stem cell-derived arterial endothelial cells. *Proc Natl Acad Sci U S A* 114(30):E6072–E6078. <https://doi.org/10.1073/pnas.1702295114>
28. Ji H, Kim HS, Kim HW, Leong KW (2017) Application of induced pluripotent stem cells to model smooth muscle cell function in vascular diseases. *Curr Opin Biomed Eng* 1:38–44. <https://doi.org/10.1016/j.cobme.2017.02.005>
29. Langendorff O (1895) Untersuchungen am überlebenden saugethierherzen (investigations on the surviving mammalian heart). *Arch Ges Physiol* 61:291–332
30. Suga H, Hisano R, Goto Y, Yamada O, Igarashi Y (1983) Effect of positive inotropic agents on the relation between oxygen consumption and systolic pressure volume area in canine left ventricle. *Circ Res* 53(3):306–318
31. Frommeyer G, Milberg P, Witte P, Stypmann J, Koopmann M, Lucke M, Osada N, Breithardt G, Fehr M, Eckardt L (2011) A new mechanism preventing proarrhythmia in chronic heart failure: rapid phase-III repolarization explains the low proarrhythmic potential of amiodarone in contrast to sotalol in a model of pacing-induced heart failure. *Eur J Heart Fail* 13(10):1060–1069
32. Motloch LJ, Ishikawa K, Xie C, Hu J, Aguero J, Fish KM, Hajjar RJ, Akar FG (2017) Increased afterload following myocardial infarction promotes conduction-dependent arrhythmias that are unmasked by hypokalemia. *JACC Basic Transl Sci* 2(3):258–269. <https://doi.org/10.1016/j.jabts.2017.02.002>
33. Kim DE, Lee EJ, Martens TP, Kara R, Chaudhry HW, Itescu S, Costa KD (2006) Engineered cardiac tissues for in vitro assessment of contractile function and repair mechanisms. *Conf Proc IEEE Eng Med Biol Soc* 1:849–852. <https://doi.org/10.1109/EMBS.2006.259753>
34. Van Epps JS, Chew DW, Vorp DA (2009) Effects of cyclic flexure on endothelial permeability and apoptosis in arterial segments perfused ex vivo. *J Biomech Eng* 131(10):101005. <https://doi.org/10.1115/1-3192143>
35. Sutton MG, Sharpe N (2000) Left ventricular remodeling after myocardial infarction: pathophysiology and therapy. *Circulation* 101(25):2981–2988
36. Camacho P, Fan H, Liu Z, He JQ (2016) Small mammalian animal models of heart disease. *Am J Cardiovasc Dis* 6(3):70–80
37. Guenet JL (2005) The mouse genome. *Genome Res* 15(12):1729–1740. <https://doi.org/10.1101/gr.3728305>
38. Patten RD, Hall-Porter MR (2009) Small animal models of heart failure: development of novel therapies, past and present. *Circ Heart Fail* 2(2):138–144. <https://doi.org/10.1161/CIRCHEARTFAILURE.108.839761>
39. Dewald O, Ren G, Duerr GD, Zoerlein M, Klemm C, Gersch C, Tincey S, Michael LH, Entman ML, Frangogiannis NG (2004) Of mice and dogs: species-specific differences in the inflammatory response following myocardial infarction. *Am J Pathol* 164(2):665–677. [https://doi.org/10.1016/S0002-9440\(10\)63154-9](https://doi.org/10.1016/S0002-9440(10)63154-9)
40. Furihata T, Kinugawa S, Takada S, Fukushima A, Takahashi M, Homma T, Masaki Y, Tsuda M, Matsumoto J, Mizushima W, Matsushima S, Yokota T, Tsutsui H (2016) The experimental model of transition from compensated cardiac hypertrophy to failure created by transverse aortic constriction in mice. *Int J Cardiol Heart Vasc* 11:24–28. <https://doi.org/10.1016/j.ijcha.2016.03.007>
41. Chaanine AH, Gordon RE, Kohlbrenner E, Benard L, Jeong D, Hajjar RJ (2013) Potential role of BNIP3 in cardiac remodeling, myocardial stiffness, and endoplasmic reticulum: mitochondrial calcium homeostasis in diastolic and systolic heart failure. *Circ Heart Fail* 6(3):572–583. <https://doi.org/10.1161/CIRCHEARTFAILURE.112.000200>
42. Wang JJ, Rau C, Avetisyan R, Ren S, Romay MC, Stolin G, Gong KW, Wang Y, Lusis AJ (2016) Genetic dissection of cardiac remodeling in an isoproterenol-induced heart failure

- mouse model. PLoS Genet 12(7):e1006038. <https://doi.org/10.1371/journal.pgen.1006038>
43. Robert J (2007) Preclinical assessment of anthracycline cardiotoxicity in laboratory animals: predictiveness and pitfalls. Cell Biol Toxicol 23(1):27–37. <https://doi.org/10.1007/s10565-006-0142-9>
 44. Stenmark KR, Meyrick B, Galie N, Mooi WJ, McMurtry IF (2009) Animal models of pulmonary arterial hypertension: the hope for etiological discovery and pharmacological cure. Am J Physiol Lung Cell Mol Physiol 297(6):L1013–L1032. <https://doi.org/10.1152/ajplung.00217.2009>
 45. Sata M, Maejima Y, Adachi F, Fukino K, Saiura A, Sugiura S, Aoyagi T, Imai Y, Kurihara H, Kimura K, Omata M, Makuchi M, Hirata Y, Nagai R (2000) A mouse model of vascular injury that induces rapid onset of medial cell apoptosis followed by reproducible neointimal hyperplasia. J Mol Cell Cardiol 32(11):2097–2104. <https://doi.org/10.1006/jmcc.2000.1238>
 46. Gabeler EE, van Hillegersberg R, Statius van Eps RG, Sluiter W, Gussenhoven EJ, Mulder P, van Urk H (2002) A comparison of balloon injury models of endovascular lesions in rat arteries. BMC Cardiovasc Disord 2:16
 47. Lu DY, Chen EY, Wong DJ, Yamamoto K, Protack CD, Williams WT, Assi R, Hall MR, Sadaghianloo N, Dardik A (2014) Vein graft adaptation and fistula maturation in the arterial environment. J Surg Res 188(1):162–173. <https://doi.org/10.1016/j.jss.2014.01.042>
 48. Ishikawa K, Aguero J, Tilemann L, Ladage D, Hammoudi N, Kawase Y, Santos-Gallego CG, Fish K, Levine RA, Hajjar RJ (2014) Characterizing preclinical models of ischemic heart failure: differences between LAD and LCx infarctions. Am J Physiol Heart Circ Physiol 307(10):H1478–H1486. <https://doi.org/10.1152/ajpheart.00797.2013>
 49. Galvez-Monton C, Prat-Vidal C, Diaz-Guemes I, Crisostomo V, Soler-Botija C, Roura S, Llucia-Valldperas A, Perea-Gil I, Sanchez-Margallo FM, Bayes-Genis A (2014) Comparison of two preclinical myocardial infarct models: coronary coil deployment versus surgical ligation. J Transl Med 12:137. <https://doi.org/10.1186/1479-5876-12-137>
 50. Lavine SJ, Prcevski P, Held AC, Johnson V (1991) Experimental model of chronic global left ventricular dysfunction secondary to left coronary microembolization. J Am Coll Cardiol 18(7):1794–1803
 51. Ishikawa K, Ladage D, Takewa Y, Yaniz E, Chen J, Tilemann L, Sakata S, Badimon JJ, Hajjar RJ, Kawase Y (2011) Development of a preclinical model of ischemic cardiomyopathy in swine. Am J Physiol Heart Circ Physiol 301(2):H530–H537. <https://doi.org/10.1152/ajpheart.01103.2010>
 52. Ishikawa K, Watanabe S, Hammoudi N, Aguero J, Bikou O, Fish K, Hajjar RJ (2018) Reduced longitudinal contraction is associated with ischemic mitral regurgitation after posterior MI. Am J Physiol Heart Circ Physiol 314(2):H322–H329. <https://doi.org/10.1152/ajpheart.00546.2017>
 53. Beeri R, Chaput M, Guerrero JL, Kawase Y, Yosefy C, Abedat S, Karakikes I, Morel C, Tisosky A, Sullivan S, Handschumacher MD, Gilon D, Vlahakes GJ, Hajjar RJ, Levine RA (2010) Gene delivery of sarcoplasmic reticulum calcium ATPase inhibits ventricular remodeling in ischemic mitral regurgitation. Circ Heart Fail 3(5):627–634. <https://doi.org/10.1161/CIRCHEARTFAILURE.109.891184>
 54. Hung J, Solis J, Guerrero JL, Braithwaite GJ, Muratoglu OK, Chaput M, Fernandez-Friera L, Handschumacher MD, Wedeen VJ, Houser S, Vlahakes GJ, Levine RA (2008) A novel approach for reducing ischemic mitral regurgitation by injection of a polymer to reverse remodel and reposition displaced papillary muscles. Circulation 118(14 Suppl):S263–S269. <https://doi.org/10.1161/CIRCULATIONAHA.107.756502>
 55. Ojaimi C, Qanud K, Hintze TH, Recchia FA (2007) Altered expression of a limited number of genes contributes to cardiac decompensation during chronic ventricular tachypacing in dogs. Physiol Genomics 29(1):76–83
 56. Watanabe S, Fish K, Bonnet G, Santos-Gallego CG, Leonardson L, Hajjar RJ, Ishikawa K (2018) Echocardiographic and hemodynamic assessment for predicting early clinical events in severe acute mitral regurgitation. Int J Cardiovasc Imaging 34(2):171–175
 57. Alyono D, Ring WS, Anderson MR, Anderson RW (1984) Left ventricular adaptation to volume overload from large aortocaval fistula. Surgery 96(2):360–367
 58. Ishikawa K, Aguero J, Oh JG, Hammoudi N, Fish LA, Leonardson L, Picatoste B, Santos-Gallego CG, Fish KM, Hajjar RJ (2015) Increased stiffness is the major early abnormality in a pig model of severe aortic stenosis and predisposes to congestive heart failure in the absence of systolic dysfunction. J Am Heart

- Assoc 4(5). <https://doi.org/10.1161/JAHA.115.001925>
- 59. Munagala VK, Hart CYT, Burnett JC Jr, Meyer DM, Redfield MM (2005) Ventricular structure and function in aged dogs with renal hypertension: a model of experimental diastolic heart failure. *Circulation* 111(9):1128–1135
 - 60. Van Vleet JF, Greenwood LA, Ferrans VJ (1979) Pathologic features of adriamycin toxicosis in young pigs: nonskeletal lesions. *Am J Vet Res* 40(11):1537–1552
 - 61. Schmitt JD, Doerge H, Post H, Coulibaly M, Sellin C, Popov AF, Sossalla S, Schoendube FA (2009) Progressive right ventricular failure is not explained by myocardial ischemia in a pig model of right ventricular pressure overload. *Eur J Cardiothorac Surg* 35(2):229–234. <https://doi.org/10.1016/j.ejcts.2008.09.010>
 - 62. Aguero J, Ishikawa K, Fish KM, Hammoudi N, Hadri L, Garcia-Alvarez A, Ibanez B, Fuster V, Hajjar RJ, Leopold JA (2015) Combination proximal pulmonary artery coiling and distal embolization induces chronic elevations in pulmonary artery pressure in Swine. *PLoS One* 10(4):e0124526. <https://doi.org/10.1371/journal.pone.0124526>
 - 63. Aguero J, Ishikawa K, Hadri L, Santos-Gallego C, Fish K, Hammoudi N, Chaanine A, Torquato S, Naim C, Ibanez B, Pereda D, Garcia-Alvarez A, Fuster V, Sen-gupta PP, Leopold JA, Hajjar RJ (2014) Characterization of right ventricular remodeling and failure in a chronic pulmonary hypertension model. *Am J Physiol Heart Circ Physiol* 307(8):H1204–H1215. <https://doi.org/10.1152/ajpheart.00246.2014>
 - 64. Fan J, Kitajima S, Watanabe T, Xu J, Zhang J, Liu E, Chen YE (2015) Rabbit models for the study of human atherosclerosis: from pathophysiological mechanisms to translational medicine. *Pharmacol Ther* 146:104–119
 - 65. Kloster BO, Lund L, Lindholt JS (2015) Induction of continuous expanding infrarenal aortic aneurysms in a large porcine animal model. *Ann Med Surg (Lond)* 4(1):30–35

Part II

In Silico Models



Chapter 2

An Introduction to Computational Modeling of Cardiac Electrophysiology and Arrhythmogenicity

Joshua Mayourian, Eric A. Sobie, and Kevin D. Costa

Abstract

Mathematical modeling is a powerful tool to study the complex and orchestrated biological process of cardiac electrical activity. By integrating experimental data from key components of cardiac electrophysiology, systems biology simulations can complement empirical findings, provide quantitative insight into physiological and pathophysiological mechanisms of action, and guide new hypotheses to better understand this complex biological system to develop novel cardiotherapeutic approaches. In this chapter, we briefly introduce *in silico* methods to describe the dynamics of physiological and pathophysiological single-cell and tissue-level cardiac electrophysiology. Using a “bottom-up” approach, we first describe the basis of ion channel mathematical models. Next, we discuss how the net flux of ions through such channels leads to changes in transmembrane voltage during cardiomyocyte action potentials. By applying these fundamentals, we describe how action potentials propagate in models of cardiac tissue. In addition, we provide case studies simulating single-cell and tissue-level arrhythmogenesis, as well as promising approaches to circumvent or overcome such adverse events. Overall, basic concepts and tools are discussed in this chapter as an accessible introduction to nonmathematicians to foster an understanding of electrophysiological modeling studies and help facilitate communication with dry lab colleagues and collaborators.

Key words Cardiac electrophysiology, Systems biology, Quantitative systems pharmacology, Models of disease, Ion channels, Torsades de pointes, Arrhythmias

1 Introduction

1.1 Why Do We Need Mathematical Models in Basic and Translational Research?

Biological processes exhibit different layers of complexity that obscure the interpretation of experimental findings. First, many biological phenomena are nonlinear, whereby small changes in one system component can lead to large changes in overall behavior. Second, biological processes are multiscale, which means that the translation of behavior from one spatial scale (e.g., the cell) to another (e.g., the organ) is not always straightforward. Such complexity forces experimentalists to utilize a simplified representation, or a model, of a given system in order to address a biological question. Independent of one’s biological interests, three fundamental questions are commonly asked [1]: (1) what mechanisms

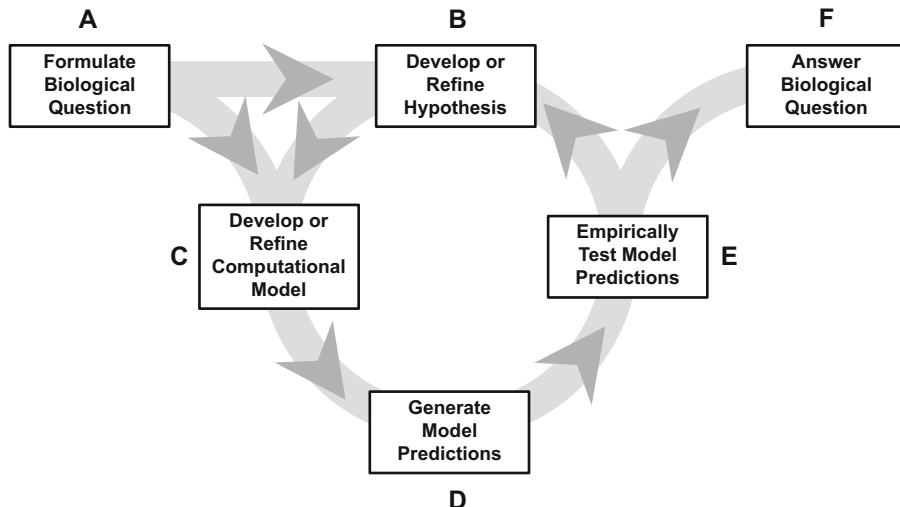


Fig. 1 Typical flowchart for incorporating mathematical modeling into an experimental study to answer biological questions. (a) Well-defined research questions lead to (b) the development of hypotheses and (c) appropriate modeling approaches. Iterating through (d) model development, fine-tuning, and (e) experimental validation can lead to refined hypotheses (b) or answers to biological questions (f). Figure redrawn from [1]

regulate my biological process? (2) how do my findings translate in a multiscale context? and (3) how can I extract meaningful biological information from my big data set? Each of these issues can be addressed with computational methods.

Experimentalists utilize conceptual models to develop causal relationships; computational models use mathematical equations to describe such relationships. Both types of models help build intuition, contextualize data, and generate hypotheses [1]. Together, these two approaches provide complementary information and can yield greater insights than either strategy used in isolation [2, 3].

A typical flowchart to incorporate mathematical modeling into an experimental study involves a well-defined research question, model development/refinement, and experimental validation, leading to refined hypotheses or answers to biological questions (Fig. 1). In this chapter, we discuss methods to incorporate mathematical modeling into experimental cardiac electrophysiology under healthy and diseased conditions.

1.2 Multiscale Characteristics of Cardiac Electrophysiology Models and Their Applications

Like other biological processes, cardiac electrophysiology has complex nonlinear and multiscale characteristics (Fig. 2). By integrating experimental data from key components of cardiac electrophysiology, systems biology simulations can complement empirical findings, provide quantitative insight into physiological and pathophysiological mechanisms of action, and guide new hypotheses to better understand this complex biological system and develop novel cardiotherapeutic approaches.

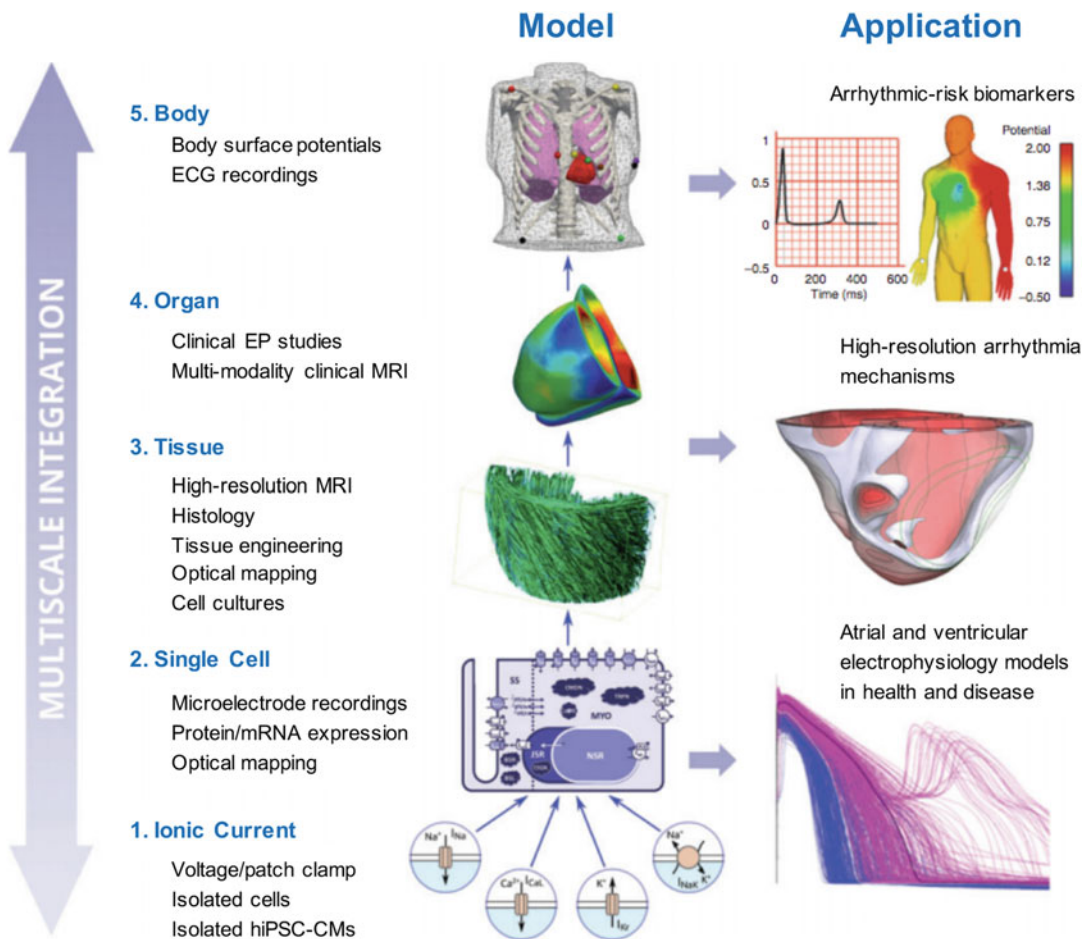


Fig. 2 Multiscale integration of experimental data into mathematical models to predict healthy and diseased cardiac electrophysiology. From bottom to top: (1) voltage/patch clamp data are used to develop models of cardiac ion channels; (2) the net effects of all cardiac ion channels/pumps/etc. are used for single-cell cardiomyocyte models; together, these models can be perturbed to simulate physiologic and pathophysiologic single-cell electrophysiology. (3–5) tissue-, organ-, and body-level simulations utilize image-based anatomical models; incorporating single-cell models with electrical excitation through tissue allows for higher-order predictions of arrhythmia. The right panel illustrates *in silico* applications for each respective scale. Figure adapted from [37] with permission

Fine-tuned movements of ions into and out of the cardiomyocyte are at the core of cardiac electrophysiology. Individual cardiomyocytes have distinct ion channels, each with their own kinetics and properties that regulate the magnitude and rate of ions fluxing into and out of the cell (Fig. 2, item 1). The activity of a given ion channel can be mathematically modeled with sufficient voltage clamp data obtained by measuring ion channel activity while holding a cell's transmembrane voltage for a set amount of time at a range of values (for more details, *see* Subheading 2.1). Tireless efforts and collaborations between experimentalists and dry lab

colleagues have led to models of each key ion moving through compartments of the cardiomyocyte. By accounting for the net effects of all key ion channels/pumps/exchangers in cardiomyocytes, mathematical modelers have been successful in simulating whole-cell electrophysiology (Fig. 2, item 2; for more details see Subheading 2.2). Experimentally, cellular electrophysiology can be assessed via single cell imaging and microelectrodes, whereas tissue-level measurements are commonly made with electrode arrays and optical mapping. Higher-order models can be subsequently developed by accounting for electrical excitation through image-based anatomical representations of tissue comprised of *in silico* single-cell models (Fig. 2, items 3–5).

Throughout this chapter, we sequentially demonstrate that each order of model—from ion currents to whole cell to tissue level—has its own utility and contributes to modeling and predicting specific types of physiology and pathophysiology (Fig. 2, right panel).

1.3 Chapter Overview

In the remainder of this chapter, we briefly introduce *in silico* methods to describe the dynamics of physiological and pathophysiological single-cell and tissue-level cardiac electrophysiology (Fig. 2, items 1–3), aiming to provide a primer that will enable nonmathematicians to better communicate with computational modeling colleagues and understand the related scientific literature. Following a brief review of the basics of human ventricular cardiomyocyte electrophysiology (Subheading 1.4), we adopt a “bottom-up” approach that starts by describing the basis of ion channel mathematical models (Subheading 2.1). Next, we discuss how the net flux of ions through key channels leads to changes in transmembrane voltage during cardiomyocyte action potentials (Subheading 2.2). By applying these fundamentals, we describe how action potentials propagate in models of cardiac tissue (Subheading 2.3). Finally, for each of these latter sections, we also provide case studies and applications of simulating single-cell and tissue-level electrophysiological pathology (Subheadings 3.1 and 3.2, respectively).

1.4 Brief Overview of Adult Human Cardiomyocyte Electrophysiological Properties

As a reference for the nonelectrophysiologist, we first provide a brief overview on cardiomyocyte electrophysiology. As illustrated in Fig. 3, the human adult ventricular cardiomyocyte (hCM) has five phases of the cardiac action potential: (0) upstroke; (1) early repolarization notch; (2) plateau; (3) late repolarization; and (4) diastole. Specific ion channels dominate each of these respective phases: (0) sodium current; (1) transient outward potassium current; (2) L-type calcium current; (3) rapid and slow delayed rectifier potassium currents; and (4) inward rectifier potassium current. Figure 3 illustrates how these channels contribute to the action potential, and when they are active during the ventricular action potential.

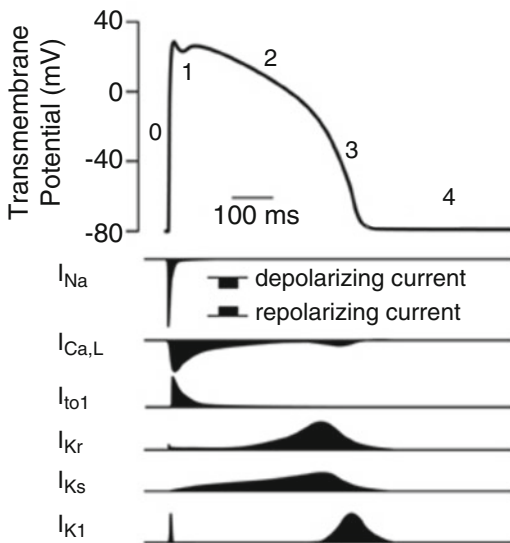


Fig. 3 Overview of cardiomyocyte action potential electrophysiology. Human adult ventricular cardiomyocytes have distinct action potential waveforms with unique underlying ion current contributions. Phases 0–4 of an excited adult ventricular cardiomyocyte action potential (looking at transmembrane potential over time) correspond to upstroke (mainly due to the sodium current, I_{Na}), early repolarization notch (mainly due to transient outward K^+ current type 1, I_{to1}), plateau (mainly due to L-type calcium current, $I_{Ca,L}$), late repolarization (mainly due rapid and slow delayed rectifier K^+ currents, I_{Kr} and I_{Ks} , as well as the inward rectifier K^+ current, I_{K1}), and diastole (mainly due to I_{K1} and others not shown), respectively. Adapted from [38] with permission

Myocytes from different regions of the heart (e.g., atria compared with ventricles) contain different ionic current constituents, and, as a result, exhibit different action potential shapes. Similarly, important differences in ion channels and action potential waveforms are observed between mature adult human cardiomyocytes and human stem cell-derived cardiomyocytes (hiPSC-CMs) that are often used in the experimental setting. More specifically, hiPSC-CMs have prominent funny currents, or pacemaker currents, which contribute to hiPSC-CM automaticity that is not evident in adult ventricular myocytes (Fig. 3) [4]. Mathematical models can describe these differences, and even help predict how findings from hiPSC-CMs may translate to healthy and diseased adult ventricular myocytes [3]. Below, we describe how to mathematically model individual families of ion currents; specifically, we use the hERG rapid delayed rectifier K^+ current (I_{Kr}) as a case example.

2 Methods

2.1 How to Model Ion Channel Activity

Cellular electrophysiology depends on the movement of sodium, potassium, calcium, and other ions across semipermeable cellular and intracellular membranes. However, the lipid bilayer has an extremely high resistance that acts as an electrical insulator; transmembrane ion channels control the flux of specific ions across cell membranes [5].

Ions flow through an ion channel down an electrochemical gradient—that is, ion flux is influenced by both diffusional and electric field forces. When ion x 's movement in one direction of a channel due to diffusion is equal and opposite to the rate of movement due to the electric field, equilibrium is achieved. This occurs when the transmembrane voltage (V_m), defined by present-day convention as intracellular minus extracellular voltage, is equal to the Nernst equilibrium potential (E_x) that can be calculated using an equation derived by the physical chemist and Nobel Laureate, Walther Nernst, in the late nineteenth century:

$$E_x = \frac{RT}{zF} \ln \left(\frac{[x_o]}{[x_i]} \right) \quad (1)$$

That is, for an ion with a known charge z at constant temperature T , E_x increases in magnitude when the disparity between intracellular and extracellular concentration ($[x_i]$ and $[x_o]$, respectively) of a given ion x increases. Note that R and F are the ideal gas constant and Faraday's constant, respectively. Mathematical modelers can therefore keep track of intracellular and extracellular concentrations of ions to calculate E_x over time. Using the present-day convention, the logarithmic term in E_x is positive if the extracellular concentration of an ion is greater, and negative if the intracellular concentration of an ion is greater.

When deviating from equilibrium, the net driving force of ion x outward (based on convention) can be defined as $(V_m - E_x)$. If $V_m > E_x$, the outward diffusion forces (e.g., K^+ is higher intracellularly than extracellularly) outweigh inward electric forces, leading to a net flux of a given ion out of the cell through its channel (this is common in several cardiomyocyte K^+ ion channels, as E_K is approximately -90 mV, and a cardiomyocyte's V_m ranges from approximately -90 mV to $+40$ mV). Conversely, if $V_m < E_x$, the inward diffusion forces (e.g., Na^+ is higher extracellularly than intracellularly) outweigh outward electric forces, leading to a net flux of a given ion into the cell through its channel (this is common in the cardiomyocyte Na^+ ion channel, which leads to Phase 0 depolarization as in Fig. 3).

Using this framework, the current I of ion x is proportional to the electrochemical driving force $(V_m - E_x)$, with the proportionality coefficient \mathcal{G}_x , defined as the conductance, or the ability of

electrical charge to flow through the ion channel. The conductance is generally not modeled as a constant, but rather simulated to account for the average number of channels within a cell membrane that are open at a particular time.

Macroscopically, the number of open voltage gated channels changes over time in response to V_m . Computational electrophysiologists describe these changes mathematically using macroscopic channel kinetic equations. In a simple case, a channel can be modeled as switching between active and inactive states using first-order rate processes. The average percent of open channels (x_1) over time can therefore be described by two variables: (1) its steady state value, $x_{1,\infty}$, defining the average percent of open channels over a sufficiently extended period of time; and (2) its time constant, τ_{x1} , defining how quickly x_1 approaches $x_{1,\infty}$. Based on these definitions, $x_{1,\infty}$ ranges between 0 and 1, where it increases at higher transmembrane voltages. Mathematically, x_1 obeys the differential equation:

$$\frac{dx_1}{dt} = \frac{x_{1,\infty} - x_1}{\tau_{x1}} \quad (2)$$

That is, the instantaneous change in x_1 is such that it approaches $x_{1,\infty}$ (i.e., if x_1 is less than $x_{1,\infty}$, there is a positive instantaneous change in x_1 to approach its steady-state value $x_{1,\infty}$; on the other hand, if x_1 is greater than $x_{1,\infty}$, there is a negative instantaneous change in x_1 to approach its steady-state value $x_{1,\infty}$) at a rate proportional to $1/\tau_{x1}$ (i.e., the smaller the τ_{x1} , the faster it will approach the steady-state value). Importantly, both $x_{1,\infty}$ and τ_{x1} are functions of transmembrane voltage, as demonstrated in Fig. 4. Numerical methods are used to update x_1 values over time, thereby simulating the temporal evolution of ion channel gating at a given voltage, by: (1) discretizing changes in time (e.g., time increments of 0.0025 ms); (2) calculating the right hand side of the differential equation—recall that $x_{1,\infty}$ and τ_{x1} are functions of transmembrane voltage, so this value must be known; (3) multiplying the values from the previous two steps; (4) adding step 3 to the previous value of x_1 ; and (5) repeating steps 1–4.

In more complex cases, a channel can again switch between open and closed states; however, in addition, it can also be inactivated—or blocked—by specialized subunits of a channel, adding another layer of complexity. The switch between the two states—inactivated or not inactivated—can be modeled using similar first-order rate processes. However, the steady-state values typically decrease, rather than increase, at higher transmembrane voltages. Nevertheless, the same differential equation typically applies to model inactivation.

This approach was utilized by Tong et al. to model the hERG delayed rectifier current (I_{Kr}) [6]. To formulate such a model, it is necessary to develop relationships between the transmembrane

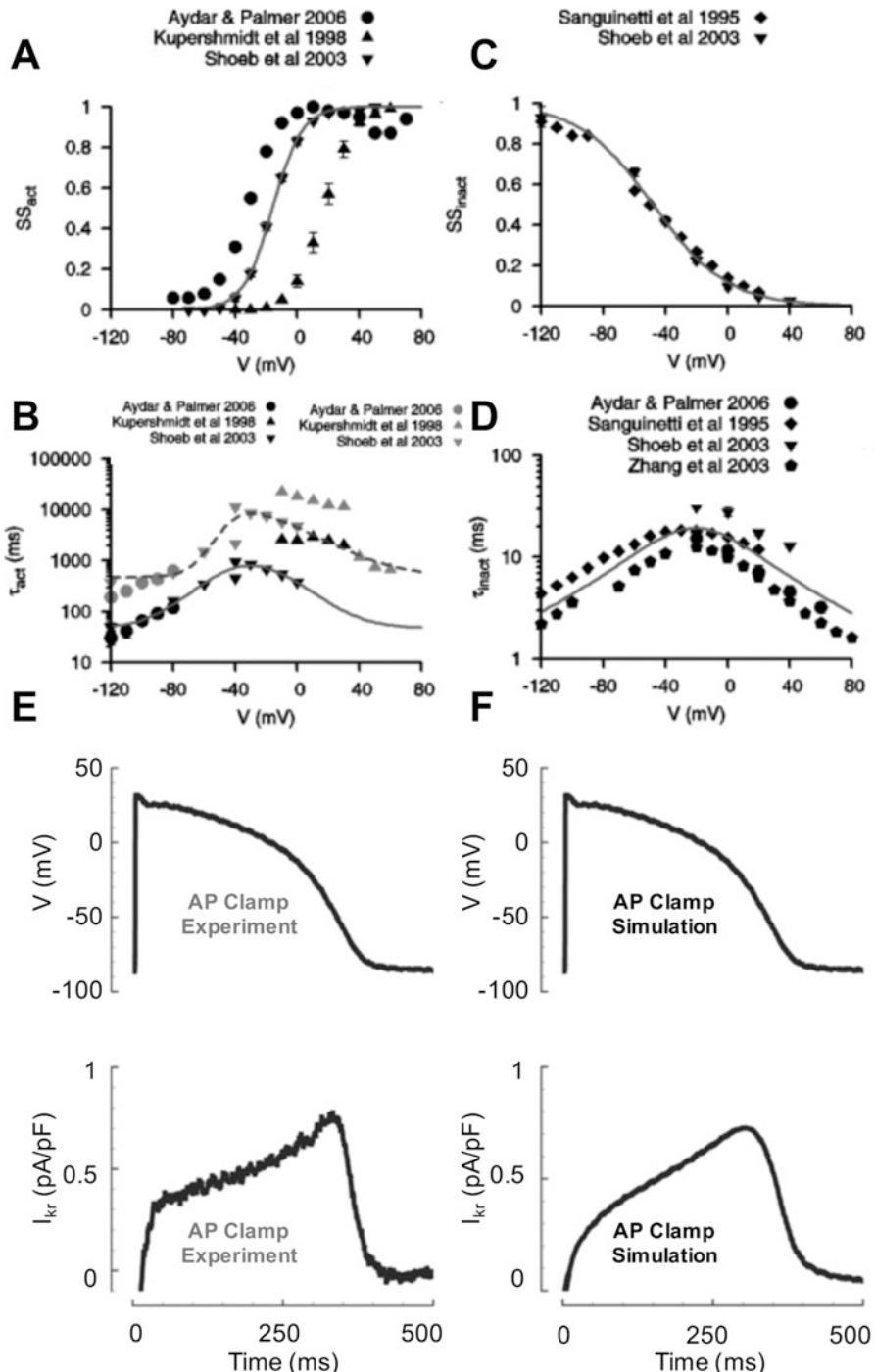


Fig. 4 Modeling the hERG rapid delayed rectifier ion channel. Tong et al. [6] developed a model of the hERG delayed rectifier channel by determining relationships between the transmembrane voltage (V) and (a) steady-state activation (ss_{act}), (b) activation time constant (τ_{act}), (c) steady-state inactivation (ss_{inact}), and (d) inactivation time constant (τ_{inact}) using data from full length hERG clones expressed in different expression systems [7–10]. Lines represent best fit equations to experimental data points. Note two different activation

voltage and steady-state activation, activation time constant, steady-state inactivation, and inactivation time constant. This was done by Tong et al. [6] by extracting data from full length hERG clones expressed in different expression systems [7–10], as shown in Fig. 4a–d, respectively.

The theory behind gating kinetics motivates the use of the sigmoidal-shaped function to relate voltage and steady-state variables, as shown in Fig. 4a, c. On the other hand, normal distribution-shaped functions (as in Fig. 4b, d) or exponential decay-shaped functions (not shown) are commonly used to relate voltage and time constants. The parameters within each equation are typically found through algorithms to minimize the error between the function outputs and experimental data points. Both activation and inactivation variables obey the differential Eq. (2) previously shown; in this case, the resulting conductance ($\mathcal{G}_{\text{hERG}}$) was defined as the product of the maximum conductance constant, activation variables (each a function of time and voltage, as previously described), and the inactivation variable (a function of time and voltage, as previously described), which can be inserted into the hERG ion current equation, $I_{\text{hERG}} = \mathcal{G}_{\text{hERG}}(V_m - E_K)$.

More sophisticated models have been developed to refine the hERG model specifically for its contributions to the cardiomyocyte action potential. For example, using a similar methodology to that described herein, O’Hara et al. [11] developed a more complex, but more cardiomyocyte-specific, representation of the delayed rectifier potassium current. As shown in Fig. 4e, f, it is highly representative of experimental hERG activity throughout the cardiac action potential.

In the next section, we demonstrate how O’Hara et al. [11] used their hERG model (and other key action potential ion channel/pump models) to simulate whole-cardiomyocyte action potentials. While other human ventricular models have been successfully developed [12–14], we focus on the O’Hara et al. model [11] for its current use as an *in silico* component of the Comprehensive *in vitro* Proarrhythmia Assay (CiPA) initiative, which we describe further in Subheading 3.1 [15].

2.2 How to Model Whole-Cardiomyocyte Electrophysiology

As outlined in Subheading 1.4, several key ion channels are active at different phases of the cardiac action potential. Each of these channels can be modeled using the framework described in Subheading 2.1, with slight modifications to account for unique properties of

Fig. 4 (continued) gates were incorporated into the Tong et al. [6] hERG model by using the same steady-state activation equations from Panel (a), each with different activation time constants τ_{hn1} and τ_{hn2} from Panel (c). (e, f) Other models (e.g., O’Hara et al. [11]) have been developed to better reflect the hERG delayed rectifier current (I_K) contribution during an adult human cardiomyocyte action potential. Panels (a) through (d) adapted from [6] with permission. Panels (e) and (f) adapted from [11] with permission

each channel. The net flux of ions (I_{total}) through key channels (for a schematic of all channels/pumps/etc. involved in the O’Hara et al. human adult cardiomyocyte model, *see* Fig. 5a) [11] leads to changes in transmembrane potential (V_m) over time, obeying the following differential equation:

$$\frac{dV_m}{dt} = -\frac{I_{\text{total}} + I_{\text{stim}}}{C_m} \quad (3)$$

where C_m is the constant capacitance of the cell (proportional to cell size) and I_{stim} is the artificial stimulus provided in the simulation (adult ventricular myocytes do not excite on their own, thus requiring artificial activation in the model). Note that the negative term in front of the right hand side of the equation is due to the present-day convention of current previously described. Similar to the differential Eq. (2), numerical methods can be used to update V_m values over time (allowing for simulations of the transmembrane voltage over time) by (1) discretizing changes in time (e.g., time increments of 0.0025 ms); (2) calculating the right hand side of the differential equation (recall each ion channel has its own gates, so for each gate, the numerical methods for solving respective gating differential equation (Subheading 2.1) must be used); (3) multiplying the values from the previous two steps; (4) adding step 3 to the previous value of V_m ; and (5) repeating steps 1–4.

By doing so, the O’Hara et al. model [11] was able to successfully simulate adult cardiomyocyte action potentials (Fig. 5b) that look remarkably similar to experimental action potentials from three select adult cardiomyocytes (Fig. 5c) and was within experimental variability for several characteristics of the action potential, including resting membrane potential, peak voltage, and maximum rate of voltage increase (Fig. 5d–f). Furthermore, by accounting for net fluxes of calcium into and out of four key cellular compartments—such as bulk myoplasm (myo), junctional sarcoplasmic reticulum (JSR), network sarcoplasmic reticulum (NSR), and subspace (SS)—the O’Hara et al. model [11] could also simulate intracellular calcium (in myo) over the duration of the action potential, which was also remarkably similar to experimental calcium transient characteristics (Fig. 5g–i).

2.3 How to Model Cardiac Tissue Strands

Myocardium is made up of individual cardiomyocytes connected by intercalated disks, embedded within the extracellular matrix; in the context of cardiac tissue electrophysiology, gap junctions play a key role by allowing for intercellular propagation of action potentials throughout the myocardial tissue. To simulate tissue-level electrophysiology, mathematical modelers extend the single-cell model (Subheading 2.2) by accounting for ion flow through gap junctions between neighboring cells. Figure 6 illustrates this method and the

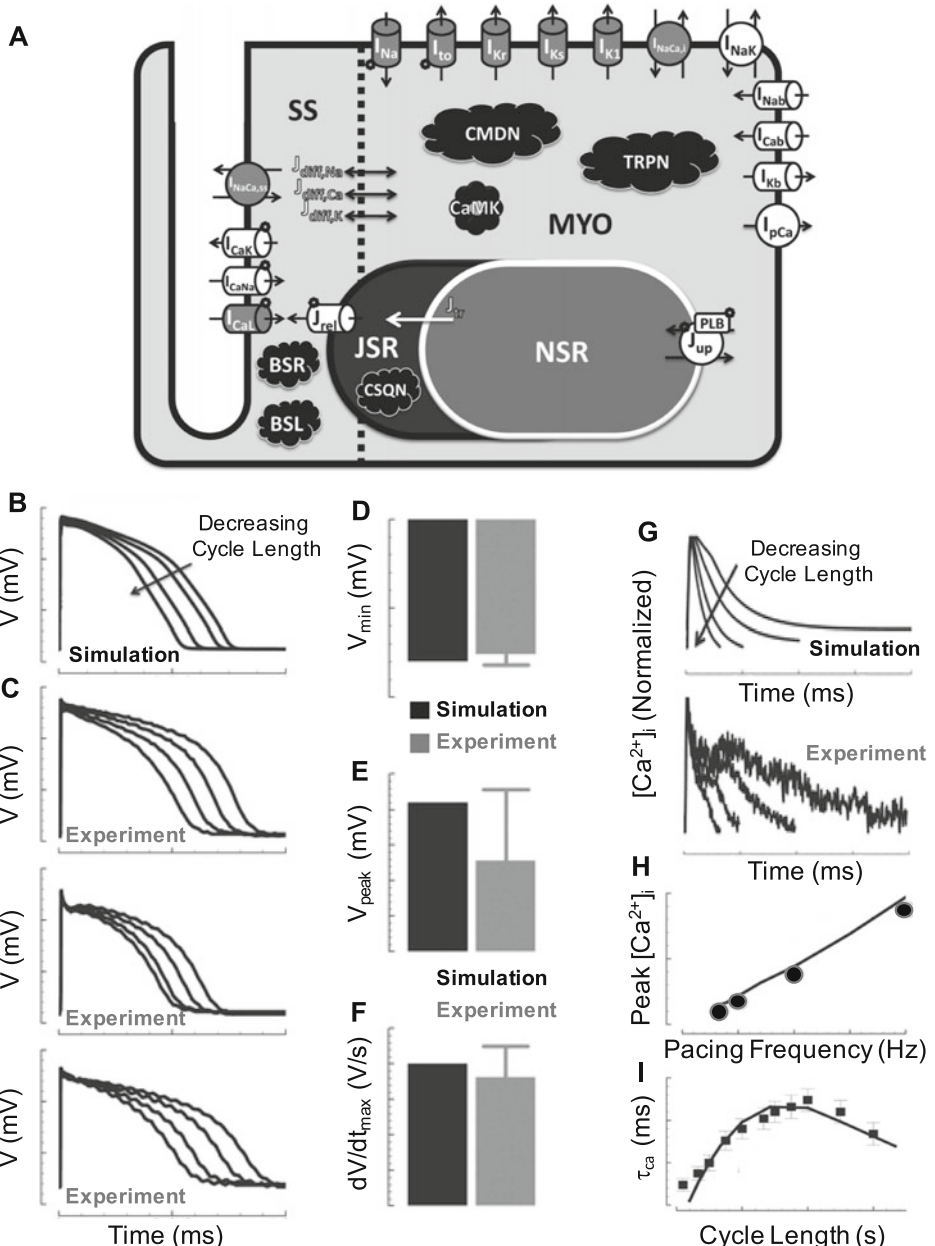


Fig. 5 Modeling the human adult cardiomyocyte action potential. (a) Schematic of the types of ion channels/pumps/exchangers modeled; the net effects of these channels/pumps/exchangers in their given compartment are used to model whole cell electrophysiology. Four main compartments are accounted for, including (1) bulk myoplasm (myo), (2) junctional sarcoplasmic reticulum (JSR), (3) network sarcoplasmic reticulum (NSR), and (4) subspace (SS); for details, see [11]. Comparison of the (b) simulated and (c) three select experimental adult cardiomyocyte action potentials during electrical pacing with varying cycle length (inverse of frequency). (d–f) Comparison of simulated and experimental characteristics of the action potential, including resting membrane potential (V_{min}), peak voltage (V_{peak}), and maximum rate of voltage increase (dV/dt_{max}), respectively. (g) By accounting for net fluxes of calcium into and out of each key cellular compartment, O'Hara et al. [11] could also simulate intracellular calcium ($[Ca^{2+}]_i$) over the duration of the action potential (top); comparison to experimental $[Ca^{2+}]_i$ transients (bottom). (h, i) Comparison of simulated and experimental characteristics of the calcium transient, including peak $[Ca^{2+}]_i$ and decay time constant (τ_{ca}), respectively. Adapted from [11] with permission.

resultant simulations in the simplest tissue case—a one-dimensional strand of myocytes, also referred to as a “cable model”.

In this example, cells are connected end-to-end through gap junctions. Gap junctions contain proteins called connexins, and these form channels that connect the intracellular spaces of two adjacent myocytes. As a result of the connexin proteins, gap junctions allow the flow of electrical charge (i.e., they are conductive). To this end, flow between two cells can be modeled analogously to an ion channel. Just as there was an electrochemical driving force ($V_m - E_x$) for a single-cell’s ion channel, there is a driving force through a gap junction between cells 1 and 2 of ($V_{m,1} - V_{m,2}$); if cell 1 has a higher voltage than neighboring cell 2 (i.e., $V_{m,1} > V_{m,2}$), then cation flux is driven from cell 1 to cell 2 (Fig. 6a). This gets scaled by the constant gap junctional conductance, \mathcal{G}_{gap} , to compute the gap junctional current. Keep in mind, each cell has its own electrophysiological properties that can be described by whole-cell models (Fig. 6b). Altogether, each cell within the tissue strand can be mathematically approximated as:

$$\frac{\Delta V_{m,cell\ n}}{\Delta t} = -\frac{I_{total,n} + I_{stim,n} + \mathcal{G}_{gap}(V_n - V_{n-1}) + \mathcal{G}_{gap}(V_n - V_{n+1})}{C_m} \quad (4)$$

where, for a given cell n with transmembrane voltage $V_{m,cell\ n}$, the change in voltage over time can be approximated as single-cell changes (from $I_{total,n}$ and $I_{stim,n}$), in addition to the fluxes through gap junctions to neighboring cells to the left ($\mathcal{G}_{gap}(V_{m,n} - V_{m,n-1})$) and right ($\mathcal{G}_{gap}(V_{m,n} - V_{m,n+1})$) of cell n . Yet again, as an extension to the whole-cell calculations (Subheading 2.2), numerical methods can be used to update voltage values of all cells in a tissue over time by: (1) discretizing changes in time; (2) calculating the right hand side of the differential equation (recall each cell has its own voltage and channels, so for each cell’s gates—which are dependent on voltage—the numerical methods used to solve each gating differential equation (Subheading 2.1) must be implemented); (3) multiplying the values from the previous two steps; (4) adding step 3 to the previous value of V_m for each cell; and (5) repeating steps 1–4. Note that I_{stim} does not necessarily need to excite all cells at once, as we discuss below.

Figure 6c illustrates simulation results of action potentials propagating from cell 1 (the only excited cell) to cell 100 connected in series. Note a delay in activation from cell-to-cell, which reflects the intrinsic resistance to ionic flux through the gap junctions. A typical metric used to characterize this delay is called the conduction

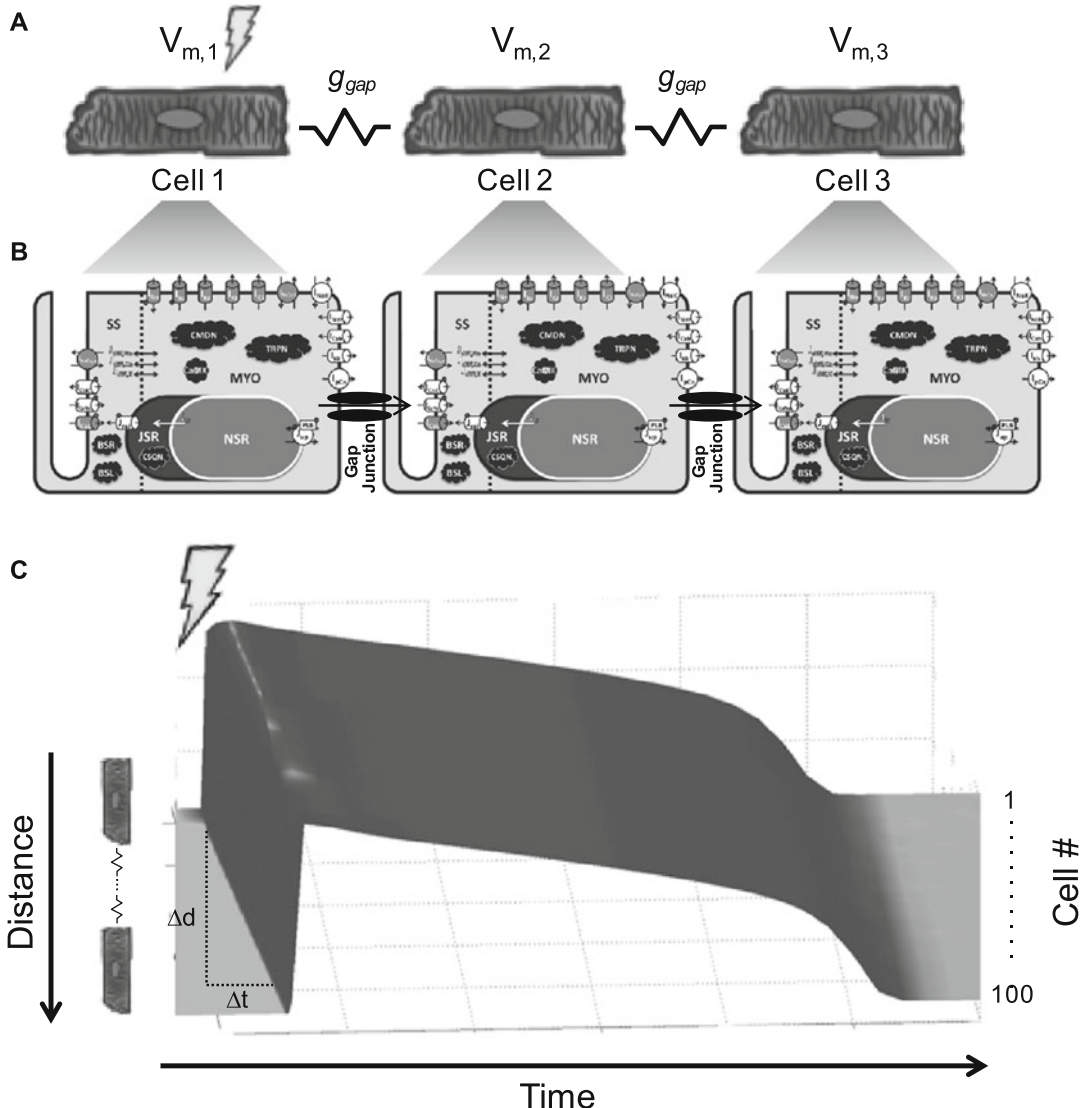


Fig. 6 Modeling action potential propagation in a one-dimensional tissue strand. **(a)** Schematic of action potential propagation when cells are coupled to each other—cell 1 is excited, leading to depolarization; $V_{m,1}$ therefore has a higher voltage than neighboring cell 2, driving cation flux from cell 1 to cell 2, and so forth. **(b)** This can be represented with electrophysiological models, where each cell has its own whole-cell model (e.g., O'Hara et al. cell model [11]), and ions flow down the electrochemical gradient through gap junctional channels with constant conductance, g_{gap} . **(c)** Simulation results of action potentials propagating from excited cell 1 to cell 100. The speed of propagation from one cell to the next can be calculated by the conduction velocity ($\Delta d/\Delta t$). Panel **(b)** adapted from [11] with permission. Panel **(c)** adapted from [39] with permission

velocity (CV); the greater the conduction velocity, the less the delay. Measuring the difference in time of activation between a cell near the beginning of the strand and the end of the strand (defined as Δt) and the spatial distance between these two cells (defined as Δd), conduction velocity is calculated as $CV = \Delta d/\Delta t$ (Fig. 6c). Physiologic CV

along the fiber direction in healthy adult human myocardium can decrease appreciably in the setting of fibrosis or other pathologies or interventions that diminish the integrity or expression level of gap junction proteins, leading to irregular heartbeats. Therefore, CV is recognized as a valuable metric when attempting to predict myocardial arrhythmic potential.

3 Applications of Cardiac Electrophysiology Models

3.1 Applications of Single-Cell Models: Predicting Torsadogenic Drugs

In this section, we provide an example of the utility and promise of computational approaches to model whole-cell electrophysiological pathology and emerging drug toxicity screening technologies.

Torsades de pointes (TdP) is a rare but lethal form of polymorphic ventricular tachycardia [16]. In addition to congenital long QT syndrome, antiarrhythmic and noncardiac drugs have been implicated in causing TdP [17]. Drug-induced TdP is a leading cause of drug relabeling or withdrawal from the market, second only to drug-induced hepatotoxicity [18, 19]; this has led to the establishment of regulatory cardiotoxicity testing [20–22]—including in vitro measurements on hERG current inhibition, animal model QT assays, and clinical examination of QT interval in healthy volunteers—that is both expensive and of limited predictive value for subsequent clinical trials [23, 24]. Given early drug development attrition rates of 80–90% and only 10% commercial success [25, 26] with development costs on the order of two to three billion dollars [27], it is of great interest for pharmaceutical companies to economically and effectively screen whether a drug under development is likely to be torsadogenic [28].

Recent work has demonstrated the promise of integrating systematic simulations with machine learning to successfully predict pharmacological toxicity [29]. Lancaster and Sobie [29] simulated the individual effects of a panel of 86 drugs on cardiomyocyte action potential and calcium transient metrics by incorporating each of their empirical inhibitory effects on hERG delayed rectifier K⁺ channel, L-type calcium channel, and sodium channel activity (Fig. 7a). This was accomplished by scaling the maximum conductance as a function of the half-maximal inhibitory concentration (IC_{50}) value, and the effective free therapeutic plasma concentration (EFTPC).

By inputting the simulated effects of each drug on 13 action potential (Fig. 7a) and calcium transient (Fig. 7b) metrics into a support vector machine (SVM) learning algorithm (SVM divides the input metrics into two regions—e.g., torsadogenic and nontorsadogenic—separated by a linear boundary), Lancaster and Sobie [29] were able to classify drugs as torsadogenic or nontorsadogenic with superior sensitivity and specificity (Fig. 7c) and lower misclassification rates (Fig. 7d) in comparison to conventional

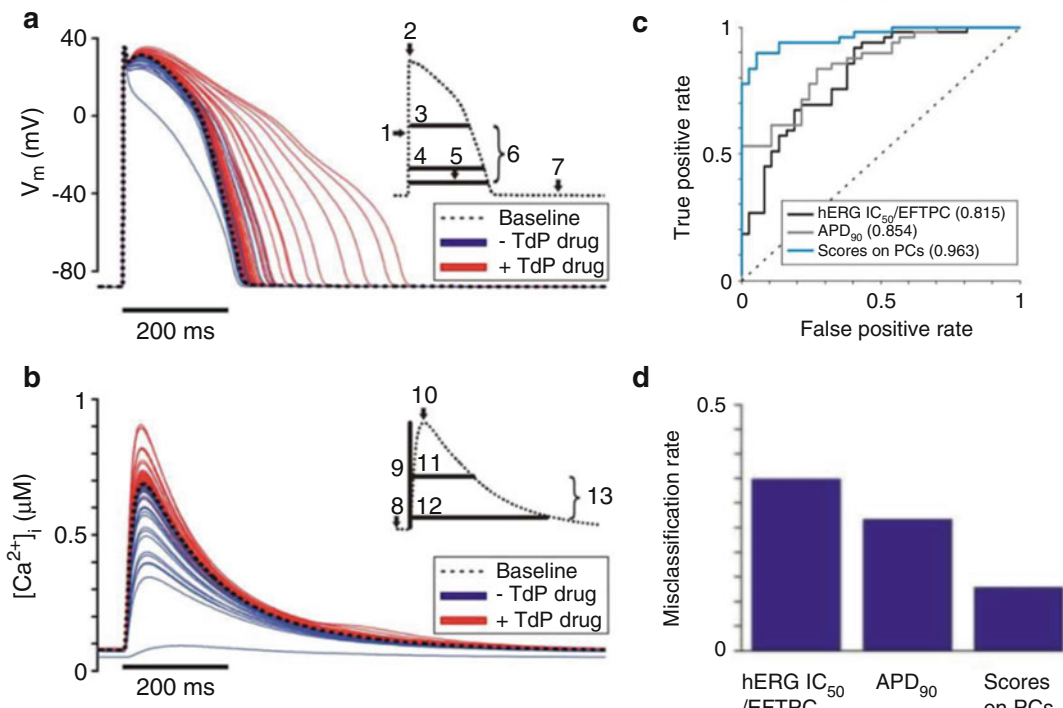


Fig. 7 Using single-cell models to predict drug-induced arrhythmias. By simulating effects of 86 drugs on 13 metrics (inset) from human adult ventricular myocyte (a) action potentials and (b) calcium transients, Lancaster and Sobie were able to classify drugs as torsadogenic or nontorsadogenic with superior (c) sensitivity and specificity and (d) misclassification rates compared to conventional methods [e.g., using IC_{50} values from hERG channel inhibition assays (hERG IC_{50} /EFTPC), or from simulations of action potential duration alone (APD₉₀)]. Figure adapted from [29] with permission

methods [e.g., using IC_{50} values from hERG channel inhibition assays (hERG IC_{50} /EFTPC), or from simulations of action potential duration alone (APD₉₀)].

These promising quantitative systems pharmacology approaches are gaining traction; currently, in silico modeling of human ventricular electrical activity is an integral part of the CiPA initiative to more effectively detect and avoid drug-induced TdP for new drugs seeking regulatory approval from the Food and Drug Administration (FDA) [15].

3.2 Applications of Tissue-Level Models: Predicting Stem Cell Effects on Electrical Properties of Fibrotic Heart Tissue

In this final section, we provide an example of using computational approaches to model tissue-level electrophysiology pathology and therapeutic interventions.

Human bone marrow-derived mesenchymal stem cells (hMSCs) offer a promising approach to treat heart failure [30]. To date, clinical benefits of hMSC therapy have achieved statistical significance, but typically remain modest in effect and not long lasting [31–34], representing an opportunity for improvement.

A better understanding of underlying cardioactive mechanisms could help optimize future hMSC-based therapies. These mechanisms involve antifibrotic and ion channel remodeling effects of hMSC paracrine signaling, as well as direct hMSC–myocyte heterocellular coupling [3].

In our recent study [3], in silico findings provided insights that help resolve disparate reports of potential proarrhythmic risks of hMSCs *in vitro* [35] that contradict *in vivo* reports of hMSCs having no effect [36] or even favorable cardioprotective effects [34] on arrhythmogenesis in preclinical animal studies and clinical trials. To do so, we extended one-dimensional tissue strands to two-dimensional tissue sheets (Fig. 8a), with cells coupled end-to-end in the x direction, as well as side-to-side in the y direction. Heterogeneous cell populations comprised of cardiac myocytes and fibroblasts were used to simulate cardiac tissue with either low levels or high levels of fibrosis. The former is more representative of *in vitro* cell culture with minimal fibrosis, whereas the latter represents *in vivo* models where hMSCs are used therapeutically post-myocardial

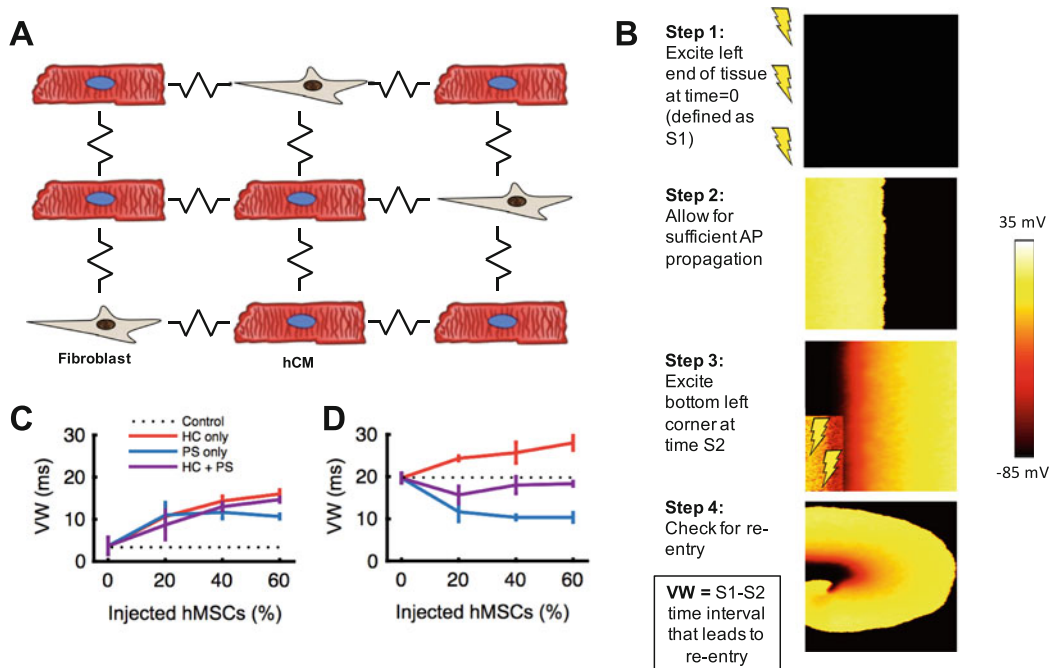


Fig. 8 Modeling hMSC electrophysiological effects on 2D fibrotic cardiac tissue. (a) Schematic of two-dimensional cell–cell coupling between human adult ventricular myocytes (hCMs) and fibroblasts. In this case, action potentials can propagate both in the x and y directions, rather than just along one dimension as in Fig. 6. (b) Steps for performing two-dimensional vulnerable window (VW) analysis by observing electrical wavefront propagation patterns in a 5×5 -cm square region of simulated cardiac tissue. VWs of (c) low fibrotic and (d) high fibrotic cardiac tissue with varying levels of human mesenchymal stem cell heterocellular coupling (HC) and/or paracrine signaling (PS) interventions. Panel (b) adapted from [40] with permission. Panels (c) and (d) adapted from [3] with permission

infarction. Note that myocyte–myocyte gap junctional conductances are higher than myocyte–fibroblast gap junctions (i.e., there is more resistance in myocyte–fibroblast coupling), leading to slower CV when adding fibrosis into cardiac tissue simulations.

Slowed conduction could lead to arrhythmogenesis, warranting a systematic method to test arrhythmic responses. In the context of cardiac tissue, a metric called the vulnerable window (VW) is often used [3]. A typical protocol for VW analysis is shown in Fig. 8b; a higher VW corresponds to a higher risk of arrhythmogenesis.

In simulations more closely representing healthy myocyte monolayers (Fig. 8c), both hMSC paracrine signaling (PS) and heterocellular coupling (HC) are predicted to increase arrhythmogenicity compared to hMSC-free control conditions. However, in VW simulations of highly fibrotic cardiac tissue (Fig. 8d), hMSC paracrine signaling-only conditions were predicted to be antiarrhythmic by decreasing VW compared to control, whereas HC between hMSCs and cardiomyocytes caused the VW to increase [3]. VW analyses further predicted that hMSC supplementation (involving both PS and HC mechanisms) did not adversely impact fibrotic cardiac tissue arrhythmogenesis, and may even be antiarrhythmic [3]. These simulations could help explain why hMSCs are often reported as safe [36] or even antiarrhythmic [34] in clinical trials where paracrine effects are present despite low cell engraftment.

Acknowledgments

This work was supported by NIH/NHLBI 1F30HL134283-01A1 (JM) and NIH/NHLBI R01HL132226 (KDC).

References

1. Yang JH, Saucerman JJ (2011) Computational models reduce complexity and accelerate insight into cardiac signaling networks. *Circ Res* 108(1):85–97. <https://doi.org/10.1161/CIRCRESAHA.110.223602>
2. Mayourian J, Ceholski DK, Gonzalez DM, Cashman TJ, Sahoo S, Hajjar RJ, Costa KD (2018) Physiologic, pathologic, and therapeutic paracrine modulation of cardiac excitation-contraction coupling. *Circ Res* 122(1):167–183
3. Mayourian J, Cashman TJ, Ceholski DK, Johnson BV, Sachs D, Kaji DA, Sahoo S, Hare JM, Hajjar RJ, Sobie EA, Costa KD (2017) Experimental and computational insight into human mesenchymal stem cell paracrine signaling and heterocellular coupling effects on cardiac contractility and arrhythmogenicity. *Circ Res* 121(4):411–423. <https://doi.org/10.1161/CIRCRESAHA.117.310796>
4. Karakikes I, Ameen M, Termglinchan V, Wu JC (2015) Human induced pluripotent stem cell-derived cardiomyocytes: insights into molecular, cellular, and functional phenotypes. *Circ Res* 117(1):80–88. <https://doi.org/10.1161/CIRCRESAHA.117.305365>
5. Plonsey R, Barr RC (2007) Bioelectricity: a quantitative approach, 3rd edn. Springer, New York
6. Tong WC, Tribe RM, Smith R, Taggart MJ (2014) Computational modeling reveals key contributions of KCNQ and hERG currents to the malleability of uterine action potentials underpinning labor. *PLoS One* 9(12):e114034. <https://doi.org/10.1371/journal.pone.0114034>
7. Sanguinetti MC, Jiang C, Curran ME, Keating MT (1995) A mechanistic link between an inherited and an acquired cardiac arrhythmia:

- HERG encodes the IKr potassium channel. *Cell* 81(2):299–307
8. Shoeb F, Malykhina AP, Akbarali HI (2003) Cloning and functional characterization of the smooth muscle ether-a-go-go-related gene K₊ channel. Potential role of a conserved amino acid substitution in the S4 region. *J Biol Chem* 278(4):2503–2514. <https://doi.org/10.1074/jbc.M208525200>
 9. Kupershmidt S, Snyders DJ, Raes A, Roden DM (1998) A K₊ channel splice variant common in human heart lacks a C-terminal domain required for expression of rapidly activating delayed rectifier current. *J Biol Chem* 273(42):27231–27235
 10. Zhang S, Kehl SJ, Fedida D (2003) Modulation of human ether-a-go-go-related K₊ (HERG) channel inactivation by Cs⁺ and K₊. *J Physiol* 548(Pt 3):691–702. <https://doi.org/10.1113/jphysiol.2003.039198>
 11. O’Hara T, Virag L, Varro A, Rudy Y (2011) Simulation of the undiseased human cardiac ventricular action potential: model formulation and experimental validation. *PLoS Comput Biol* 7(5):e1002061. <https://doi.org/10.1371/journal.pcbi.1002061>
 12. Grandi E, Pasqualini FS, Bers DM (2010) A novel computational model of the human ventricular action potential and Ca transient. *J Mol Cell Cardiol* 48(1):112–121. <https://doi.org/10.1016/j.jmcc.2009.09.019>
 13. ten Tusscher KH, Noble D, Noble PJ, Panfilov AV (2004) A model for human ventricular tissue. *Am J Physiol Heart Circ Physiol* 286(4): H1573–H1589. <https://doi.org/10.1152/ajpheart.00794.2003>
 14. ten Tusscher KH, Panfilov AV (2006) Alternans and spiral breakup in a human ventricular tissue model. *Am J Physiol Heart Circ Physiol* 291(3):H1088–H1100. <https://doi.org/10.1152/ajpheart.00109.2006>
 15. Colatsky T, Fermini B, Gintant G, Pierson JB, Sager P, Sekino Y, Strauss DG, Stockbridge N (2016) The comprehensive in vitro proarrhythmia assay (CiPA) initiative – update on progress. *J Pharmacol Toxicol Methods* 81:15–20. <https://doi.org/10.1016/j.jpharmthera.2016.06.002>
 16. Sauer AJ, Newton-Cheh C (2012) Clinical and genetic determinants of torsade de pointes risk. *Circulation* 125(13):1684–1694. <https://doi.org/10.1161/CIRCULATIONAHA.111.080887>
 17. Yap YG, Camm AJ (2003) Drug induced QT prolongation and Torsades de pointes. *Heart* 89(11):1363–1372
 18. Shah RR (2013) Drug-induced QT interval prolongation: does ethnicity of the thorough QT study population matter? *Br J Clin Pharmacol* 75(2):347–358. <https://doi.org/10.1111/j.1365-2125.2012.04415.x>
 19. Shah RR (2006) Can pharmacogenetics help rescue drugs withdrawn from the market? *Pharmacogenomics* 7(6):889–908. <https://doi.org/10.2217/14622416.7.6.889>
 20. Fermini B, Hancox JC, Abi-Gerges N, Bridgland-Taylor M, Chaudhary KW, Colatsky T, Correll K, Crumb W, Damiano B, Erdemli G, Gintant G, Imredy J, Koerner J, Kramer J, Levesque P, Li Z, Lindqvist A, Obejero-Paz CA, Rampe D, Sawada K, Strauss DG, Vandenberg JI (2016) A new perspective in the field of cardiac safety testing through the comprehensive in vitro proarrhythmia assay paradigm. *J Biomol Screen* 21(1):1–11. <https://doi.org/10.1177/1087057115594589>
 21. Cavero I, Crumb W (2005) ICH S7B draft guideline on the non-clinical strategy for testing delayed cardiac repolarisation risk of drugs: a critical analysis. *Expert Opin Drug Saf* 4(3):509–530. <https://doi.org/10.1517/14740338.4.3.509>
 22. Shah RR (2005) Drugs, QTc interval prolongation and final ICH E14 guideline: an important milestone with challenges ahead. *Drug Saf* 28(11):1009–1028
 23. Redfern WS, Carlsson L, Davis AS, Lynch WG, MacKenzie I, Paethorpe S, Siegl PK, Strang I, Sullivan AT, Wallis R, Camm AJ, Hammond TG (2003) Relationships between preclinical cardiac electrophysiology, clinical QT interval prolongation and torsade de pointes for a broad range of drugs: evidence for a provisional safety margin in drug development. *Cardiovasc Res* 58(1):32–45
 24. Gintant G (2011) An evaluation of hERG current assay performance: translating preclinical safety studies to clinical QT prolongation. *Pharmacol Ther* 129(2):109–119. <https://doi.org/10.1016/j.pharmthera.2010.08.008>
 25. Fermini B, Fossa AA (2003) The impact of drug-induced QT interval prolongation on drug discovery and development. *Nat Rev Drug Discov* 2(6):439–447. <https://doi.org/10.1038/nrd1108>
 26. Shah RR (2002) Drug-induced prolongation of the QT interval: regulatory dilemmas and implications for approval and labelling of a new chemical entity. *Fundam Clin Pharmacol* 16(2):147–156
 27. Avorn J (2015) The \$2.6 billion pill--methodologic and policy considerations. *N Engl J Med* 372(20):1877–1879. <https://doi.org/10.1056/NEJMmp1500848>

28. Gintant G, Fermini B, Stockbridge N, Strauss D (2017) The evolving roles of human iPSC-derived cardiomyocytes in drug safety and discovery. *Cell Stem Cell* 21(1):14–17. <https://doi.org/10.1016/j.stem.2017.06.005>
29. Lancaster MC, Sobie EA (2016) Improved prediction of drug-induced Torsades de pointes through simulations of dynamics and machine learning algorithms. *Clin Pharmacol Ther* 100(4):371–379. <https://doi.org/10.1002/cpt.367>
30. Karantalis V, Hare JM (2015) Use of mesenchymal stem cells for therapy of cardiac disease. *Circ Res* 116(8):1413–1430. <https://doi.org/10.1161/CIRCRESAHA.116.303614>
31. Karantalis V, DiFede DL, Gerstenblith G, Pham S, Symes J, Zambrano JP, Fishman J, Pattany P, McNiece I, Conte J, Schulman S, Wu K, Shah A, Breton E, Davis-Sproul J, Schwarz R, Feigenbaum G, Mushtaq M, Suncion VY, Lardo AC, Borrello I, Mendizabal A, Karas TZ, Byrnes J, Lowery M, Heldman AW, Hare JM (2014) Autologous mesenchymal stem cells produce concordant improvements in regional function, tissue perfusion, and fibrotic burden when administered to patients undergoing coronary artery bypass grafting: the prospective randomized study of mesenchymal stem cell therapy in patients undergoing cardiac surgery (PROMETHEUS) trial. *Circ Res* 114(8):1302–1310. <https://doi.org/10.1161/CIRCRESAHA.114.303180>
32. Heldman AW, DiFede DL, Fishman JE, Zambrano JP, Trachtenberg BH, Karantalis V, Mushtaq M, Williams AR, Suncion VY, McNiece IK, Ghersin E, Soto V, Lopera G, Miki R, Willens H, Hendel R, Mitrani R, Pattany P, Feigenbaum G, Oskouei B, Byrnes J, Lowery MH, Sierra J, Pujol MV, Delgado C, Gonzalez PJ, Rodriguez JE, Bagno LL, Rouy D, Altman P, Foo CW, da Silva J, Anderson E, Schwarz R, Mendizabal A, Hare JM (2014) Transendocardial mesenchymal stem cells and mononuclear bone marrow cells for ischemic cardiomyopathy: the TAC-HFT randomized trial. *JAMA* 311(1):62–73. <https://doi.org/10.1001/jama.2013.282909>
33. Meyer GP, Wollert KC, Lotz J, Pirr J, Rager U, Lippolt P, Hahn A, Fichtner S, Schaefer A, Arseniev L, Ganser A, Drexler H (2009) Intracoronary bone marrow cell transfer after myocardial infarction: 5-year follow-up from the randomized-controlled BOOST trial. *Eur Heart J* 30(24):2978–2984. <https://doi.org/10.1093/euroheartj/ehp374>
34. Hare JM, Fishman JE, Gerstenblith G, DiFede Velazquez DL, Zambrano JP, Suncion VY, Tracy M, Ghersin E, Johnston PV, Brinker JA, Breton E, Davis-Sproul J, Schulman IH, Byrnes J, Mendizabal AM, Lowery MH, Rouy D, Altman P, Wong Po Foo C, Ruiz P, Amador A, Da Silva J, McNiece IK, Heldman AW, George R, Lardo A (2012) Comparison of allogeneic autologous bone marrow-derived mesenchymal stem cells delivered by transendocardial injection in patients with ischemic cardiomyopathy: the POSEIDON randomized trial. *JAMA* 308(22):2369–2379. <https://doi.org/10.1001/jama.2012.25321>
35. Chang MG, Tung L, Sekar RB, Chang CY, Cysyk J, Dong P, Marban E, Abraham MR (2006) Proarrhythmic potential of mesenchymal stem cell transplantation revealed in an in vitro coculture model. *Circulation* 113 (15):1832–1841. <https://doi.org/10.1161/CIRCULATIONAHA.105.593038>
36. de Jong R, Houtgraaf JH, Samiei S, Boersma E, Duckers HJ (2014) Intracoronary stem cell infusion after acute myocardial infarction: a meta-analysis and update on clinical trials. *Circ Cardiovasc Interv* 7(2):156–167. <https://doi.org/10.1161/CIRCINTERVENTIONS.113.001009>
37. Rodriguez B, Carusi A, Abi-Gerges N, Ariga R, Britton O, Bub G, Bueno-Orovio A, Burton RA, Carapella V, Cardone-Noott L, Daniels MJ, Davies MR, Dutta S, Ghetti A, Grau V, Harmer S, Kopljar I, Lambiase P, Lu HR, Lyon A, Minchale A, Muszkiewicz A, Oster J, Paci M, Passini E, Severi S, Taggart P, Tinker A, Valentin JP, Varro A, Wallman M, Zhou X (2016) Human-based approaches to pharmacology and cardiology: an interdisciplinary and intersectorial workshop. *Europace* 18 (9):1287–1298. <https://doi.org/10.1093/europace/euv320>
38. Hoekstra M, Mummery CL, Wilde AA, Bezziina CR, Verkerk AO (2012) Induced pluripotent stem cell derived cardiomyocytes as models for cardiac arrhythmias. *Front Physiol* 3:346. <https://doi.org/10.3389/fphys.2012.00346>
39. Yang PC, Kurokawa J, Furukawa T, Clancy CE (2010) Acute effects of sex steroid hormones on susceptibility to cardiac arrhythmias: a simulation study. *PLoS Comput Biol* 6(1):e1000658. <https://doi.org/10.1371/journal.pcbi.1000658>
40. Mayourian J, Savizky RM, Sobie EA, Costa KD (2016) Modeling electrophysiological coupling and fusion between human Mesenchymal stem cells and Cardiomyocytes. *PLoS Comput Biol* 12(7):e1005014. <https://doi.org/10.1371/journal.pcbi.1005014>

Part III

In Vitro Models



Chapter 3

Isolation of Atrial and Ventricular Cardiomyocytes for In Vitro Studies

Jelena Plačkić and Jens Kockskämper

Abstract

High quality cardiomyocyte isolation is of critical importance for successful studies of myocardial function at the cellular and molecular level. Although previous work has established isolation procedures for various species, it still remains challenging to produce consistently a high yield of viable and healthy cardiomyocytes. The basis for the most successful and reproducible isolation of cardiomyocytes from intact hearts is the Langendorff retrograde perfusion technique. Here, we will illustrate in detail all practical aspects of the enzyme-based Langendorff isolation of rat atrial and ventricular cardiomyocytes. This includes a series of obligatory steps starting from quick aortic cannulation to rinse the heart from blood, short perfusion of the heart with Ca^{2+} -free solution to dissociate cells at the level of intercalated discs, followed by longer perfusion with low Ca^{2+} -containing enzyme solution in order to disrupt the extracellular matrix network, extraction of the released cardiomyocytes and gentle Ca^{2+} reintroduction to allow cells to return gradually to normal cytosolic Ca^{2+} levels. The average yield of intact viable ventricular myocytes that can be achieved with our protocol is $\approx 70\%$ (range $\approx 50\text{--}90\%$). For atrial myocytes, in general, it is slightly ($\approx 10\%$) lower than for ventricular myocytes. The yield depends on the age of the rat and the degree of cardiac remodeling such that digestion of older and more remodeled hearts (more fibrosis) usually results in lower yields. Isolated atrial and ventricular cardiomyocytes may be employed for studies of cardiomyocyte function (e.g., shortening/contraction, intracellular $[\text{Ca}^{2+}]$ transients) as well as for biochemical and molecular biological studies (e.g., immunoblotting, PCR).

Key words Langendorff retrograde heart perfusion, Cardiomyocyte isolation, Collagenase digestion, Atrial and ventricular cardiomyocytes

1 Introduction

Isolated adult cardiomyocytes represent an essential tool for the investigation and understanding of cardiac structure and function at the cellular and molecular level in health and disease. Studies on embryonic and neonatal cultured cardiomyocytes cannot be easily extrapolated to the adult myocardium, since these cells differ from adult cardiomyocytes in morphology and ultrastructure as well as the expression of important ion channels, Ca^{2+} -regulating and contractile proteins [1]. Similar arguments apply for the more

recently employed cardiomyocytes derived from induced pluripotent stem cells [2]. Isolated cardiomyocytes have the advantage to be free of neural and humoral influences, providing the ideal setting for a highly controllable experimental environment. Additionally, isolation of cardiomyocytes offers the possibility to select cells from distinct areas of the heart including, for example, the left or right atrium, the left or right ventricle, infarcted diseased regions or the cardiac conduction system. High quality cardiomyocyte isolation is of critical importance for successful studies with both freshly isolated and cultured cells, as adult cardiomyocytes can be transfected for gene transfer studies [1, 3].

Starting from the 1970s until today, various isolation approaches have been developed. Cardiomyocyte isolation may differ between mammalian species. Principally, however, each isolation procedure includes a series of obligatory steps, and many critical factors relevant for obtaining functionally intact, Ca^{2+} -tolerant cardiomyocytes have been identified [4]. Despite previous work, however, it still remains challenging to prepare consistently a large yield of high-quality cardiomyocytes.

From all species, rats and mice are perhaps those most frequently used for the isolation of cardiomyocytes. The basis for the most reproducible and highest quality enzymatic isolation of viable cardiomyocytes from intact hearts is the Langendorff retrograde perfusion technique. With this technique, the heart is perfused via cannulation of the aorta. The perfusion buffer fills the coronary vasculature by flowing opposite to normal physiologic flow (retrogradely) down the ascending aorta with the aortic valve closed under pressure [5]. The protocol that will be introduced here describes the isolation of atrial and ventricular cardiomyocytes from rat heart and represents a modification of previously published procedures, e.g., [1, 3, 4, 6–8]. It has been used for the last 7 years in our laboratory with a consistently large yield of healthy atrial [9] and ventricular [10] cardiomyocytes.

The major steps of this protocol for the isolation of cardiomyocytes are quick aortic cannulation using low Ca^{2+} -containing Tyrode's solution to rinse the heart from blood, short perfusion of the heart with Ca^{2+} -free solution to dissociate cells at the level of the intercalated discs, followed by longer perfusion with low Ca^{2+} -containing proteolytic enzyme solution in order to cleave the connections of the individual cells with the extracellular matrix network, extraction of the released cardiomyocytes and gentle Ca^{2+} reintroduction to allow cells to return gradually to normal cytosolic Ca^{2+} levels.

In the following, we will illustrate in detail all practical aspects of the isolation of rat atrial and ventricular cardiomyocytes, stressing the most critical steps necessary for successful cell preparation.

2 Materials

2.1 Equipment

1. Langendorff apparatus running in the constant flow mode.
2. A light microscope or magnifying glasses for dissection.
3. A stainless steel cannula of suitable size (diameter in the range of 2–3 mm, depending on the size of the rat) with graves.
4. Surgical silk (5-0 size).
5. Scissors.
6. Forceps.
7. 300 µm sieve cloths.

2.2 Solutions

Prepare all solutions using demineralized, ultrapure water (ddH₂O), processed with the Milli-Q Reference A+ system. 18.2 Ω molecular biology grade H₂O is highly recommended. All solutions for the isolation should be freshly prepared from the basic isolation Tyrode's solution (*see Table 1*).

1. Basic isolation Tyrode's solution (*see Note 1*): 130 mM NaCl, 5.4 mM KCl, 0.5 mM MgCl₂, 0.33 mM NaH₂PO₄, 25 mM HEPES, 22 mM glucose, 0.01 U/mL insulin (pH = 7.4).
2. Cannulation solution: isolation solution with 0.15 mM CaCl₂ and 2 U/mL heparin (*see Note 2*).
3. Cardioplegic solution (ice cold): cannulation solution with 25 mM KCl.
4. Ca²⁺-free solution: isolation solution containing 0.4 mM EGTA (*see Note 3*), 10 mM 2,3-butanedione monoxime (BDM) and 2 U/mL heparin.
5. Enzyme solution: isolation solution containing 0.2 mM CaCl₂, 10 mM BDM, 0.8 mg/mL type 2 collagenase (CLS-2, Worthington, USA), 0.05 mg/mL type XIV protease (Sigma-Aldrich) (*see Note 4*).
6. Stop solution for atrial myocytes: isolation solution containing 0.2 mM CaCl₂, 10 mM BDM.
7. Stop solution for ventricular myocytes: isolation solution containing 0.5 mM CaCl₂, 10 mM BDM (*see Note 5*), 2 mg/mL BSA.
8. Ca²⁺ solution 1: isolation solution containing 1 mM CaCl₂, 2 mg/mL BSA.
9. Ca²⁺ solution 2: isolation solution containing 1.5 mM CaCl₂.

Table 1
Solutions made from the basic isolation Tyrode's solution. Amount required for one cell preparation

Solution name	Basic isolation Tyrode's solution	Substance	Final concentration
1. Cannulation solution	250 ml	CaCl ₂	0.15 mM
		Heparin	2 U/ml
2. Ca ²⁺ -free solution	50 ml	EGTA	0.4 mM
		BDM	10 mM
		Heparin	2 U/ml
3. Enzyme solution	50 ml	Collagenase	0.8 mg/ml
		Protease	0.05 mg/ml
		CaCl ₂	0.2 mM
		BDM	10 mM
4. Stop solution for ventricular myocytes	15 ml	CaCl ₂	0.5 mM
		BDM	10 mM
		BSA	2 mg/ml
5. Ca ²⁺ solution 1	15 ml	CaCl ₂	1 mM
		BSA	2 mg/ml
6. Ca ²⁺ solution 2	100 ml	CaCl ₂	1.5 mM

200 ml of the cannulation solution use for preparing the cardioplegic solution

Before adding enzymes, take 1 ml of this solution, heat up to 37°C and use it as a stop solution for atrial myocytes

3 Methods

3.1 Setting up the Langendorff Apparatus

1. For the isolation procedure, the Langendorff apparatus is running in the constant flow mode, where perfusion of the heart is achieved by a peristaltic pump filling a compliance chamber to which the aortic cannula is attached. Check the flow rate of the peristaltic pump regularly and adjust to 3 mL/min, as this is of great importance for appropriate perfusion and successful isolation.
2. Clean and noncontaminated tubing and chambers of the Langendorff system are also very important factors. Make sure that the Langendorff system is thoroughly washed after every isolation procedure (*see Note 6*).
3. Switch on the water bath to warm up the water bath-jacketed tubes of the Langendorff system in order to keep the circulating perfusion solutions at 37 °C throughout the Langendorff heart perfusion. The temperature of the perfusate should also be checked regularly.
4. Oxygenate all solutions that are going to be used for perfusion to maintain sufficient O₂ supply and prevent hypoxic conditions of the heart (through bubbling with 100% O₂ through sintered glass oxygenators) (*see Note 7*).
5. Fill the Langendorff apparatus with oxygenated cannulation solution and draw any air bubbles out of the compliance chamber (the “bubble trap” space) to protect the heart from coronary occlusion.
6. For efficient fixing of the aorta to the cannula, make sure that a suitably sized (2 mm diameter for younger rats and 2.5–3 mm for older rats) stainless steel cannula with a couple of graves and appropriate 5-0 surgical silk is used.

3.2 Excision and Cannulation of the Heart

1. Prepare the settings for the cannulation (*see Fig. 1a*) and fill the syringe with the heparin-containing cannulation solution. Remove all air bubbles from the syringe to prevent air from entering the coronary arteries.
2. Anaesthetize and kill the rat according to the protocol approved by your local animal welfare authorities. In our case, the rat is anaesthetized by isoflurane and killed by decapitation.
3. Make a cut from the mid abdomen to the diaphragm, hold the sternum with curved serrated forceps and cut bilaterally. Reflect the thoracic cage to expose the heart. Inject the heparin solution (1000 U/mL) directly into the heart (*see Note 8*) to prevent blood clotting during the excision of the heart.
4. Carefully trim away any surrounding noncardiac tissue, e.g., lungs and connective tissue.

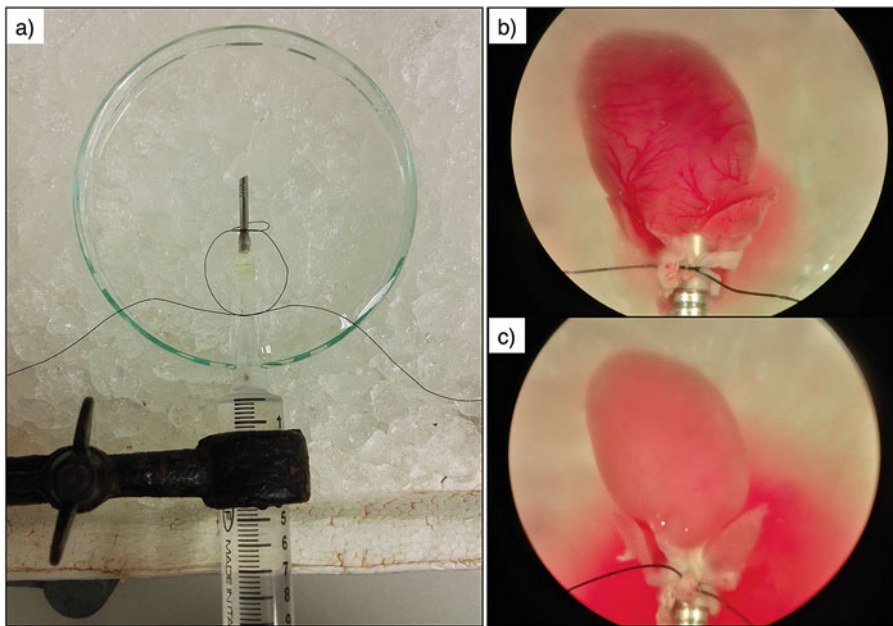


Fig. 1 Cannulation of the heart through the ascending aorta. (a) Cannula is initially detached from the Langendorff apparatus and fixed to the syringe filled with the cannulation solution. The syringe is mounted below the dissection microscope and above the 100 mm petri dish with the ice-cold oxygenated cardioplegic solution. (b) After the aorta is ligated to the cannula (c) putting pressure on the syringe fills the coronary arteries with cannulation solution and rinses blood from the heart leaving the coronary arteries whitish. Since cannulation solution contains low Ca^{2+} concentration, the heart should contract weakly, which helps in removing the blood

5. Lift the heart slightly using fine curved serrated forceps, excise the heart from the thoracic cavity and put it into a beaker with the oxygenated ice-cold cardioplegic solution. Then, gently press it (with the scissors or a small spatula) to remove some initial blood.
6. Transfer the heart to the 100 mm culture dish (*see Fig. 1a*) with oxygenated ice-cold cardioplegic solution (*see Note 9*).
7. After you identify the aorta and its cranial branches, which are usually hidden behind the thymus, cut the aorta below its first branch. Rapidly slip the heart on the aortic cannula. Then, make a double knot with the surgical silk to ensure tight ligature and inject the cannulation solution into the heart (*see Fig. 1b, c*).
8. Transfer the heart to the Langendorff system (*see Note 10*).

3.3 Perfusion and Digestion of the Heart

1. Perfuse the heart with oxygenated, heparin-containing cannulation solution at a rate of 3 mL/min to remove the residual blood. When you start the perfusion with the cannulation solution, the tubing of the Langendorff apparatus should be placed in the oxygenated Ca^{2+} -free solution. When the heart stops beating, Ca^{2+} -free solution has reached the heart.

2. When the Ca^{2+} -free solution has reached the heart, the tubing of the Langendorff apparatus should be placed in the oxygenated enzyme solution. After 4 min, the enzyme solution has to reach the heart (*see Note 11*).
3. Perfuse the heart with the enzyme solution at a rate of 3 mL/min until it becomes swollen, soft and pale (*see Note 12*, Fig. 2). When pressed gently with the forceps, the ventricles lose shape and the heart hangs like a bag (*see Fig. 2g*). In a drop of the solution taken from the surface of the heart, lots of isolated cells can be found. The atria might be digested (a few minutes) faster than the ventricles. They should be harvested when they have become flaccid, pale and easy to remove (*see Note 13*).

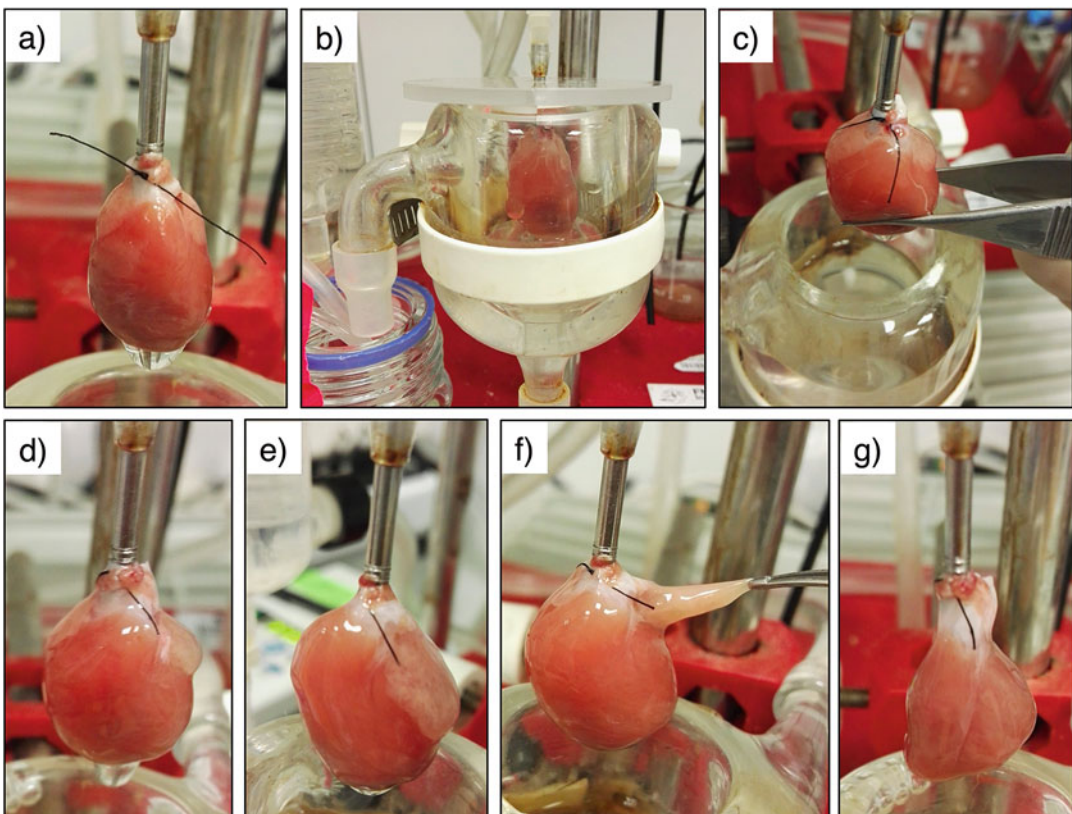


Fig. 2 Perfusion and digestion of the heart. (a) The heart is attached to the Langendorff system and initially perfused with the cannulation solution, followed by 4 min perfusion with Ca^{2+} -free solution at a rate of 3 mL/min. (b) Afterwards, the heart is perfused with the enzyme solution. During the perfusion with the enzyme solution, the perfused heart is immersed in a water bath-jacketed organ bath filled with enzyme solution to achieve efficient digestion of the heart from inside and outside. (c) Occasionally, the course of digestion should be observed by palpation of the heart with the forceps or fingers. (d) When digested, ventricles become swollen, soft, and pale and (e) the atria appear flaccid, pale, bigger and (f) easy to remove by pulling with the forceps without cutting. (g) When pressed with the forceps, the ventricles lose shape and the heart hangs like a bag

3.4 Preparing the Atrial Myocytes

- Take the left and right atrium and put each into a beaker with 0.5 mL of the stop solution for the atrial myocytes preheated to 37 °C.
- With two fine forceps, gently dissect the atrial tissue (*see Fig. 3a*). Afterwards, place the beakers with the atrial tissue on a rocking platform to facilitate cell dissociation.
- Start the slow Ca²⁺ adaptation steps (*see Note 14*) by adding solutions with increasing Ca²⁺ concentrations every 2 min according to the scheme in Table 2.

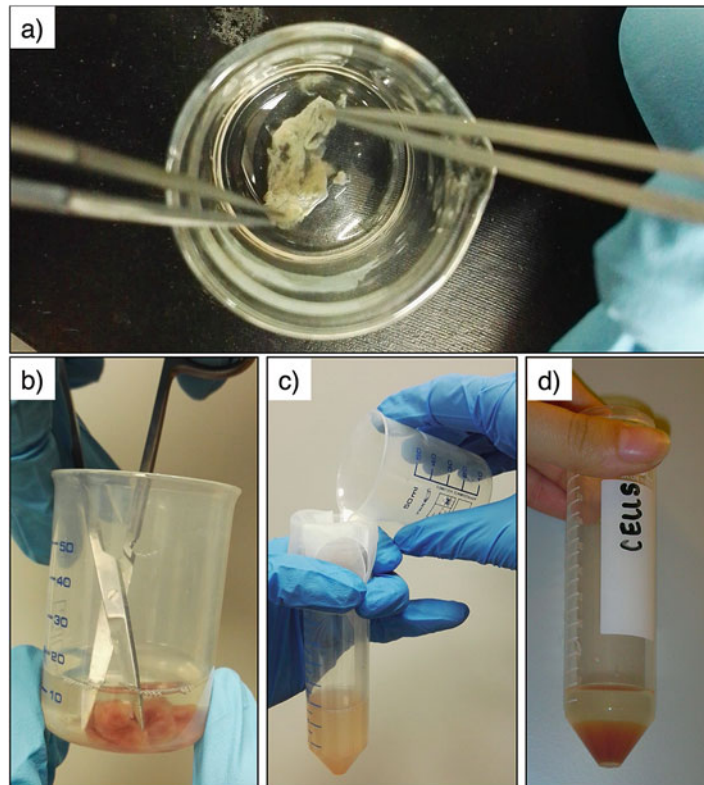


Fig. 3 Preparation of atrial and ventricular myocytes. (a) Following removal of an atrium, it is transferred to a beaker with the stop solution for atrial myocytes (preheated to 37 °C), and the atrial tissue is gently dissected by means of two fine forceps to facilitate cell dissociation. Afterwards, the beaker with the atrial tissue is placed on a rocking platform and Ca²⁺ is stepwise reintroduced to reach physiological Ca²⁺ concentration at RT. (b) The ventricle is removed and transferred to a beaker with the stop solution for ventricular myocytes (preheated to 37 °C) and gently chopped to release the cells. (c) The undigested tissue is removed by filtration through sieve cloths with 300 µm pores and (d) the cells are left to settle down by gravity. Afterward, the cells are gradually adapted to increasing Ca²⁺ concentrations at RT.

Table 2**Scheme of atrial myocyte adaptation to physiological Ca²⁺ concentration**

Solution	Volume	Final Ca ²⁺ concentration	
Stop solution for atrial myocytes (37°C)	500 µl	0.2 mM	The atria are taken and dissected in this solution
Ca ²⁺ adaptation on the rocking platform			
Stop solution for ventricular myocytes (37°C)	5 x 100 µl	0.35 mM	
Ca ²⁺ solution 1 (1 mM Ca ²⁺ , RT)	4 x 100 µl 3 x 200 µl	0.675 mM	
Ca ²⁺ solution 2 (1.5 mM Ca ²⁺ , RT)	4 x 250 µl 2 x 500 µl	1.1 mM	
	Stop rocking, wait 10 min, remove 2 mL, start rocking again		
	4 x 500 µl	1.3 mM	
	Stop rocking, remove the remaining tissue, wait 10 min, gently remove some solution if necessary to concentrate the cell suspension		

3.5 Preparing the Ventricular Myocytes

- Put the ventricles (*see Note 15*) into a beaker with ≈10 mL of the stop solution for ventricular myocytes preheated to 37 °C.
 - Gently chop the ventricles (*see Fig. 3b, Note 16*).
 - Remove the undigested tissue by filtration through sieve cloths with 300 µm pores (*see Fig. 3c*).
 - Let the cells settle down by gravity (*see Fig. 3d, Note 17*) for 10 min and gently aspirate the supernatant.
- After the Ca²⁺ adaptation procedure and adjustment of the density of the atrial myocyte suspension, seed the atrial myocytes (*see Fig. 4b*) on laminin-coated coverslips (or culture dishes) and leave the cells to attach to the bottom of the coverslips (or culture dishes) for about 20 min. They are now ready for experimentation.

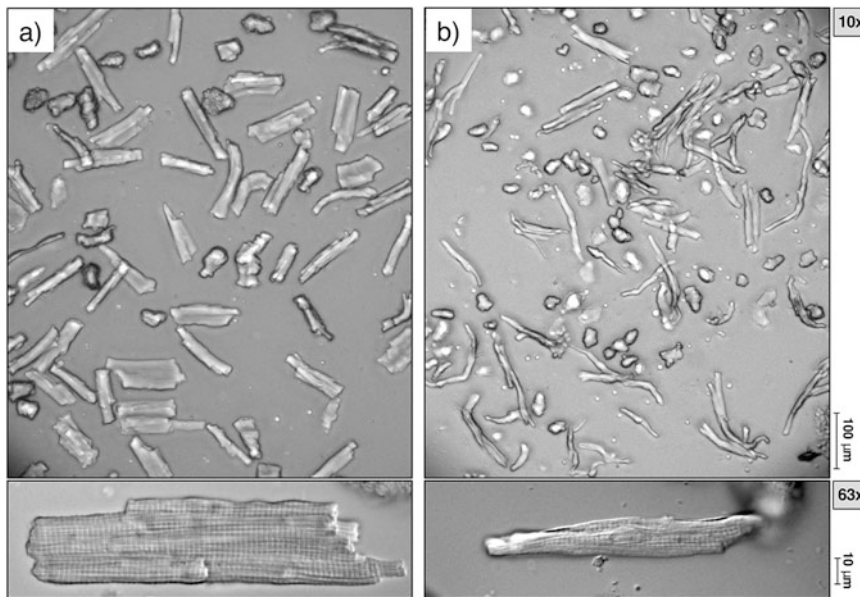


Fig. 4 Light microscopy images of atrial and ventricular myocytes after complete preparation. (a) Ventricular myocytes have a more rectangular shape, whereas (b) atrial myocytes are smaller and more spindle-shaped. Healthy cardiomyocytes exhibit clear cross-striations (bottom images) and do not show any spontaneous contractions at rest. Images were recorded on a Leica DMI3000B microscope using 10× (top) or 63× (bottom) objective lenses, respectively, and processed using ImageJ software

5. Add \approx 5–10 mL of Ca^{2+} solution 1 (RT) without mixing the cell suspension. Adapt the cells to the Ca^{2+} solution 1 for 10 min, then gently aspirate the supernatant.
6. Add \approx 5–10 mL of Ca^{2+} solution 2 (RT) and allow 10 min for the adaptation of the cells.
7. Isolated ventricular myocytes (*see Fig. 4b, Note 18*) can be stored at RT and used for experimentation within 12 h after isolation.
8. Before plating the ventricular myocytes, adjust the concentration of the cell suspension by dilution with Ca^{2+} solution 2. Ventricular myocytes can be plated on laminin-coated coverslips (or culture dishes) like the atrial myocytes (*see step 4* in Subheading 3.4, *see Note 19*).

4 Notes

1. Basic isolation Tyrode's solution without insulin can be kept in the refrigerator for 2–3 weeks. On the day of cell isolation add insulin and prepare all solutions freshly from the basic isolation Tyrode's solution. For one cell isolation use 500 mL of basic isolation Tyrode's solution (*see Table 1*). Besides insulin and

glucose used here, other additions to the isolation Tyrode's solution (e.g., amino acids, fatty acids, adenosine, pyruvate, taurine, vitamins) have been used by other investigators in an effort to improve the yield and viability of isolated cells, e.g., [11]. The potential effects of these additions are not entirely clear though. Since we obtain good results with our combination of insulin and glucose, we prefer to use this simple and effective isolation solution.

2. Prepare 5 kU/mL heparin stock solution in sterile phosphate-buffered saline (PBS), keep it in the refrigerator and use it for a couple of months.
3. Prepare 100 mM EGTA stock solution (pH 7.4) and use it for up to a year.
4. As an alternative, instead of using type 2 collagenase and type XIV protease, enzymatic digestion of the heart can be performed using liberase. In contrast to type 2 collagenase, which is a crude preparation of collagenases and other proteases (e.g., clostrypain, caseinase) with varying activities and relatively high lot-to-lot variability, liberase represents a defined mix of highly purified collagenases and other proteases with high activity and minimal lot-to-lot variability. It is more often used for isolation of cardiomyocytes from mouse hearts [8]. Some investigators report on improved results (better cell yield, more single cardiomyocytes) when using liberase for isolation of cardiomyocytes from rat hearts [12]. We have tested a combination of 0.1 mg/mL liberase (Liberase TM Research Grade, Roche) and 0.15 mg/mL trypsin (10× liquid 2.5% Trypsin, Sigma Aldrich) for isolation of atrial and ventricular cardiomyocytes from rat hearts. In our hands, results obtained with liberase digestion did not greatly differ from those obtained with collagenase. The higher lot-to-lot variability of protease activities from type 2 collagenase preparations requires, however, that concentrations and digestion times may have to be adjusted when using a new lot of type 2 collagenase for cardiomyocyte isolation.
5. BDM reversibly inhibits cardiac contractile activity and protects the myocardium from damage [3, 13, 14]. However, since BDM acts as a chemical, i.e., nonspecific, phosphatase, it may exert multiple effects on cardiomyocyte function, including impaired Ca^{2+} handling [3, 14, 15]. Hence, BDM should be washed out prior to the experiments, and final Ca^{2+} solution 1 and 2 do not contain any BDM.
6. To clean the tubing of the Langendorff apparatus, wash it right after every isolation first with plenty of distilled water at high speed, then with 50% ethanol at lower speed to allow enough time for disinfection of the system and finally again with plenty

of water. Do not forget to clean the compliance chamber (“bubble trap” space) and water-jacketed organ bath as well.

7. For the mouse cardiomyocyte isolation, some laboratories recommend that all solutions for perfusing the heart should be filtered through 0.2 µm sterile filters, e.g., [8, 11]. While this is certainly crucial when cardiomyocytes are used for cell culture, it is less clear whether this is also important when cardiomyocytes are used for experimentation within the next couple of hours after isolation. In the case of rat cardiomyocytes, we find that filtration through 0.2 µm sterile filters does not make a difference with regard to the quality of freshly isolated cells.
8. The injection of heparin is important to prevent blood clotting. The isolation procedure could also be done without injecting the heparin, but in this case excision of the heart and cannulation should be done even faster (<2 min). If the killing is performed by decapitation, the heparin should be injected directly into the heart, but if it is done by cervical dislocation (often done when mice are used), where the circulation remains intact, the heparin could be injected into the liver rather than the heart, to prevent possible injury of the heart. For injection, prepare 1 mL of 1000 U/mL heparin (from a 5 kU/mL heparin stock solution) and recalculate how much of 1000 U/mL heparin you need to inject, having in mind that 1000 U of heparin are required for 1 kg body weight of the rat. For example, for 300 g body weight of the rat, you would need to inject 0.3 mL of 1000 U/mL heparin.
9. The cardioplegic solution is used for cardiac arrest. The high potassium concentration in this solution depolarizes the cardiomyocytes and prevents contractions, thus reducing cellular ATP consumption.
10. Quick and efficient cannulation and transfer of the heart to the Langendorff system is crucial for the quality of the cardiomyocyte preparations. During the isolation procedure, the cannula should not be inserted too deeply into the aorta, as this can lead to mechanical damage of the aortic valve leaflets, causing inefficient perfusion and poor digestion of the heart. During the cannulation, most of the blood should be removed from the heart, as shown in Fig. 1b, c. To make the cannulation easier, use of a dissection microscope or magnifying glasses is recommended. While transferring the heart to the Langendorff apparatus, special care should be taken on preventing air entering the coronary vasculature, as this may lead to emboli and microvascular obstruction with detrimental effects on outcome, i.e., quality and yield of cardiomyocytes. The total time taken from the moment of opening the thorax until the heart is mounted and perfused on the Langendorff system should be as

short as possible to avoid cell damage caused by ischemia and hypoxia. We recommend a time of less than 6 min and usually perform these steps within 3–5 min.

11. The time taken from the moment when the heart stops beating until the enzyme solution reaches the heart (i.e., the time in Ca^{2+} -free solution) should not exceed 4 min, as a critical time, above which reintroduction of Ca^{2+} -containing solution causes massive damage of the heart with release of large amounts of lactate dehydrogenase, a phenomenon termed “calcium paradox” [16]. In Ca^{2+} -free solution, the surface glycocalyx of the cardiomyocytes gets disrupted and intercalated discs are separated. This results in an increased Ca^{2+} permeability of the sarcolemma, leading to contracture and cell death after restoration of extracellular Ca^{2+} concentration [17]. Furthermore, elevated intracellular Na^+ levels after exposure to Ca^{2+} -free solution accompany the development of the calcium paradox, favoring Ca^{2+} overload when extracellular Ca^{2+} is elevated back to normal levels (due to activation of reverse mode $\text{Na}^+/\text{Ca}^{2+}$ exchange) [17]. Thus, limiting the time of exposure of the heart to Ca^{2+} -free solution is crucial to attenuate the calcium paradox and to minimize membrane damage by EGTA (which by itself is able to separate the glycocalyx from the sarcolemmal lipid bilayer). Therefore, if necessary, you should readjust the speed of the peristaltic pump in this step to achieve this goal.
12. The duration of the digestion varies and could last any time between 20 and 80 min. It depends on several factors, including enzyme activities (*see Note 4*), age, sex and strain of rat or disease model (cardiac remodeling). When we use healthy male Wistar-Kyoto rats aged 12–16 weeks [9, 10], typical digestion times using type 2 collagenase and type XIV protease are in the range of 20–40 min. When using older rats or rat models exhibiting cardiac remodeling, in particular fibrosis, digestion times increase. For example, for old (15–20 months) spontaneously hypertensive rats with a high degree of cardiac hypertrophy and fibrosis, digestion times of 40–80 min are required. Maintenance of the heart temperature at 37 °C throughout the Langendorff perfusion is also critical for the successful digestion of the heart. This is accomplished by using water bath-jacketed tubes for keeping the circulating enzyme solution at 37 °C and by immersion of the perfused heart in a water bath-jacketed organ bath filled with enzyme solution. In this way, the heart is digested more efficiently from inside and outside (*see Fig. 2b*). For successful digestion of the heart and a high yield of viable isolated cardiomyocytes, however, the enzymes should be used at the lowest effective concentrations to minimize the risk of cell injury by hydrolysis of crucial surface residues. In addition, the extracellular Ca^{2+} concentration

during enzymatic digestion of the heart must be sufficiently high (0.2 mM) to preserve the structural integrity of the sarcolemma and glycocalyx, attenuating injury of cardiomyocytes from the calcium paradox and allowing for sufficient activity of collagenase, but—at the same time—low enough to ensure separation of the cells at their intercalated discs [3, 4, 17]. The enzyme solution can be recirculated during longer digestion in order to minimize the amount of the enzymes used.

13. The best sign that the atria are well digested is if you can easily pull them off the heart with the forceps without cutting them.
14. Aiming to restore physiological extracellular Ca^{2+} concentration, Ca^{2+} concentration should be increased gradually and slowly to allow the atrial myocytes to return to normal intracellular Ca^{2+} concentration without the risk of Ca^{2+} overload [3].
15. It is possible to separate the right and left ventricle for isolation of right and left ventricular myocytes. The easiest way is to cut off first the right ventricular wall for isolation of right ventricular myocytes and to use the remainder (left ventricular wall with septum) for the isolation of left ventricular myocytes.
16. To facilitate the release of ventricular myocytes, dissociate the ventricular tissue by gently pipetting the tissue pieces using plastic Pasteur pipettes with differently sized, manually cut openings (7, 5 and 3 mm diameter) until the large pieces of ventricular tissue are dispersed in the cell suspension. Avoid, however, vigorous agitation to prevent mechanical stress and cell injury.
17. Similarly, as in the case of atrial myocytes, in order to prevent cell damage, the extracellular Ca^{2+} concentration should be increased stepwise to allow the cells to reach normal intracellular Ca^{2+} concentration without becoming Ca^{2+} overloaded. Ventricular myocytes, however, are less sensitive to this Ca^{2+} adaptation than atrial myocytes. Therefore, less adaptation steps are required. After the filtration step, do not centrifuge the cell suspension to precipitate the cells. Let them settle down by gravity and take great care while aspirating and adding solutions during Ca^{2+} adaptation. Do not try to aspirate the entire supernatant and always add the solutions gently to the wall of the falcon tube without mixing the cell suspension.
18. Immediately after the isolation, healthy cardiomyocytes with distinct cross-striations may be quiescent or show a few irregular contractions. The low-frequency spontaneous activity, however, disappears with time. Moribund cells, on the other hand, show constant high-frequency spontaneous contractions, often in a wave-like manner, and finally develop contracture. Dead cells can be identified as round, granulated debris. The average

yield of intact viable ventricular myocytes that can be achieved with our protocol is $\approx 70\%$ (range $\approx 50\text{--}90\%$). This depends—again—on the age of the rat and the degree of cardiac remodeling such that digestion of older and more remodeled hearts (more fibrosis) usually results in lower yields. For atrial myocytes, in general, the yield is slightly ($\approx 10\%$) lower than for ventricular myocytes. Ventricular myocytes typically remain in good condition for up to 12 h after isolation, atrial myocytes for up to 8 h after isolation.

19. Laminin is used to foster attachment of the cells to the coverslips. Glass coverslips or glass-bottomed culture dishes should be coated with 50 $\mu\text{g}/\text{mL}$ laminin (diluted in Ca^{2+} solution 2 or PBS) for 1–2 h at room temperature. After the incubation period, remove the remaining laminin, plate the cells and allow them to attach for about 20 min before being loaded with fluorescent dyes.

References

1. Mitcheson JS, Hancox JC, Levi AJ (1998) Cultured adult cardiac myocytes: future applications, culture methods, morphological and electrophysiological properties. *Cardiovasc Res* 39(2):280–300
2. Streckfuss-Bomeke K, Wolf F, Azizian A, Stauske M, Tiburcy M, Wagner S, Hubser D, Dressel R, Chen S, Jende J, Wulf G, Lorenz V, Schon MP, Maier LS, Zimmermann WH, Hasenfuss G, Guan K (2013) Comparative study of human-induced pluripotent stem cells derived from bone marrow cells, hair keratinocytes, and skin fibroblasts. *Eur Heart J* 34(33):2618–2629. <https://doi.org/10.1093/euroheartj/ehs203>
3. Louch WE, Sheehan KA, Wolska BM (2011) Methods in cardiomyocyte isolation, culture, and gene transfer. *J Mol Cell Cardiol* 51 (3):288–298. <https://doi.org/10.1016/j.yjmcc.2011.06.012>
4. Dow JW, Harding NG, Powell T (1981) Isolated cardiac myocytes. I. Preparation of adult myocytes and their homology with the intact tissue. *Cardiovasc Res* 15(9):483–514
5. Bell RM, Mocanu MM, Yellon DM (2011) Retrograde heart perfusion: the Langendorff technique of isolated heart perfusion. *J Mol Cell Cardiol* 50(6):940–950. S0022-2828 (11)00095-2 [pii]. <https://doi.org/10.1016/j.yjmcc.2011.02.018>
6. Isenberg G, Klockner U (1982) Calcium tolerant ventricular myocytes prepared by preincubation in a “KB medium”. *Pflugers Arch* 395 (1):6–18
7. Mitra R, Morad M (1985) A uniform enzymatic method for dissociation of myocytes from hearts and stomachs of vertebrates. *Am J Phys* 249(5 Pt 2):H1056–H1060
8. O’Connell TD, Rodrigo MC, Simpson PC (2007) Isolation and culture of adult mouse cardiac myocytes. *Methods Mol Biol* 357:271–296. <https://doi.org/10.1385/1-59745-214-9:271>
9. Pluteanu F, Hess J, Plackic J, Nikanova Y, Preisemberger J, Bukowska A, Schotten U, Rinne A, Kienitz MC, Schafer MK, Weihe E, Goette A, Kockskamper J (2015) Early subcellular Ca^{2+} remodelling and increased propensity for Ca^{2+} alternans in left atrial myocytes from hypertensive rats. *Cardiovasc Res* 106 (1):87–97. <https://doi.org/10.1093/cvr/cvv045>
10. Plackic J, Preissl S, Nikanova Y, Pluteanu F, Hein L, Kockskamper J (2016) Enhanced nucleoplasmic Ca^{2+} signaling in ventricular myocytes from young hypertensive rats. *J Mol Cell Cardiol* 101:58–68. <https://doi.org/10.1016/j.yjmcc.2016.11.001>
11. Roth GM, Bader DM, Pfaltzgraff ER (2014) Isolation and physiological analysis of mouse cardiomyocytes. *J Vis Exp* 91:e51109. <https://doi.org/10.3791/51109>
12. van Deel ED, Najafi A, Fontoura D, Valent E, Goebel M, Kardux K, Falcao-Pires I, van der Velden J (2017) In vitro model to study the effects of matrix stiffening on Ca^{2+} handling and myofilament function in isolated adult rat cardiomyocytes. *J Physiol* 595

- (14):4597–4610. <https://doi.org/10.1113/JP274460>
- 13. Mulieri LA, Hasenfuss G, Ittleman F, Blanchard EM, Alpert NR (1989) Protection of human left ventricular myocardium from cutting injury with 2,3-butanedione monoxime. *Circ Res* 65(5):1441–1449
 - 14. Blanchard EM, Smith GL, Allen DG, Alpert NR (1990) The effects of 2,3-butanedione monoxime on initial heat, tension, and aequorin light output of ferret papillary muscles. *Pflugers Arch* 416(1–2):219–221
 - 15. Adams W, Trafford AW, Eisner DA (1998) 2,3-Butanedione monoxime (BDM) decreases sarcoplasmic reticulum Ca content by stimulating Ca release in isolated rat ventricular myocytes. *Pflugers Arch* 436(5):776–781
 - 16. Zimmerman AN, Hulsmann WC (1966) Paradoxical influence of calcium ions on the permeability of the cell membranes of the isolated rat heart. *Nature* 211(5049):646–647
 - 17. Piper HM (2000) The calcium paradox revisited: an artefact of great heuristic value. *Cardiovasc Res* 45(1):123–127



Chapter 4

Cardiomyocyte Differentiation from Mouse Embryonic Stem Cells

Adam T. Lynch, Silvia Mazzotta, and Stefan Hoppler

Abstract

In vitro generated mammalian cardiomyocytes provide experimental models for studying normal mammalian cardiomyocyte development, for disease modeling and for drug development. They also promise to inform future therapeutic strategies for repair of injured or diseased myocardium. Here we provide reliable protocols for differentiation of mouse embryonic stem cells into functional cardiomyocytes, together with Notes about trouble shooting and optimizing such protocols for specific cell lines.

Key words Mouse embryonic stem cell, Cardiomyocytes, Heart, In vitro differentiation

1 Introduction

Embryonic stem (ES) cells are pluripotent cells derived from the inner cell mass (ICM) of the early blastocyst [1, 2], which can be propagated ex vivo under appropriate conditions. When cultured in pro-pluripotency conditions, ES cells can self-renew indefinitely. In contrast, addition of pro-differentiation factors can induce ES cells to differentiate into any of the approximately 200 cell types comprising an adult organism [3]. This therefore makes them a powerful model to study developmental process with relative ease [4], and also offer potential in regenerative medicine therapies [3]. Various protocols have been developed to direct pluripotent stem cells into the cardiovascular lineage. In this chapter we focus on protocols using mouse ES cells (mESCs), while the following chapter (*see* Chapter 5) describes protocols for human ES cells (hESCs). When ES cells are cultured as three-dimensional spheroids, termed “embryoid bodies” (EBs), they are capable of differentiating into derivatives of all three germ layers (endoderm, mesoderm, and ectoderm), and can spontaneously generate beating cardiomyocytes [5, 6]. However, the proportion of cardiomyocytes within this population is often very low, usually less than 3%, and also relies

upon the use of animal-derived products in culture. More recent efforts to generate enriched cultures of cardiomyocytes have sought to recapitulate embryonic development more faithfully by manipulating those signaling pathways *in vitro* which normally control cardiac development *in vivo*. Such protocols have succeeded in recapitulating heart development step by step, differentiating pluripotent stem cells into functional cardiomyocytes by careful exposure to growth factors or bioactive small molecules at appropriate developmental stages. In contrast to the embryoid body approach, highly enriched populations of cardiomyocytes (98% in some cell lines) can be generated in feeder-free conditions [7]. To accomplish studying heart development and disease mechanisms accurately and reliably, efficient protocols to direct the differentiation of pluripotent stem cells into cardiomyocytes are therefore required. In this chapter, we outline protocols to differentiate mouse ES cells into cardiomyocytes, which can be used as a model to study embryonic heart development.

2 Materials

All solutions should be sterile and prepared endotoxin-free. Many vendors provide cell culture-grade reagents preprepared and sterilized for convenience. Reagents should be stored according to the manufacturer's instructions, and prepared media should be stored at 4 °C unless otherwise stated. All work should be carried out in class II laminar flow cabinets, and all materials entering the cabinets should be sprayed with 70% ethanol first. Cells should be maintained and differentiated in a dedicated, humidified cell culture incubator set to 37 °C and 5% CO₂. The morphology of pluripotent stem cells and differentiated cells should be observed with an inverted light microscope.

1. Feeder-dependent or feeder-independent mouse ES cells such as E14-Tg2A [8] or R1 [9]. Cell lines can be purchased commercially from several vendors, including the ATCC cell bank. Mouse ES cells used here are in the so-called naïve state of pluripotency [10].
2. ES LIF Media: Prepare by supplementing Glasgow's Minimal Essential Media (GMEM), 10% fetal bovine serum (FBS) (*see Note 1*), 2 mM L-glutamine, 1× nonessential amino acids, 1 mM sodium pyruvate, 0.1 mM β-mercaptoethanol, 1000 U/mL leukemia inhibitory factor (LIF) (for source, *see Note 2*).
3. EB Differentiation Media: Prepare by supplementing Dulbecco's Modified Eagle's Medium (DMEM), 15% FBS, 2 mM L-glutamine, 0.1 mM nonessential amino acids, 1 mM sodium

- pyruvate, 0.1 mM β -mercaptoethanol, 50 μ g/mL L-ascorbic acid.
4. Dulbecco's phosphate buffered saline (D-PBS) without Mg^{2+} or Ca^{2+} (2.67 mM KCl, 1.47 mM KH_2PO_4 , 136.9 mM NaCl, and 8.1 mM Na_2HPO_4 , pH 7.4).
 5. Trypsin (0.05%)-EDTA (0.5 mM) in D-PBS. Filter-sterilized (0.22 μ m filter).
 6. 70% ethanol (v/v).
 7. 100 mm cell culture-treated petri dishes (NuncTM).
 8. 6-well cell culture-treated plates.
 9. Flat bottomed, cell culture-treated 96-well plates (Greiner).
 10. 0.1% gelatin solution: 0.1% (w/v) gelatin from porcine skin (Sigma. *See Note 3*) dissolved in MilliQ water or D-PBS. Autoclave to sterilize.
 11. 0.4% Trypan Blue Solution.
 12. Cryopreservation media: 50% FBS, 40% ES LIF medium, 10% DMSO. Store at -20 °C for 1 year.
 13. DMEM/F-12 (already combined).
 14. N2B27 2i + LIF medium: N2B27 is a fully defined, serum-free basal medium which can be purchased ready-prepared or assembled in-house. This comprises DMEM/F-12 combined at a 1:1 ratio with 1× N-2 Supplement (Gibco): Neurobasal® Medium (Gibco) containing 1× B-27 minus vitamin A supplement (Gibco). When the medium is required for ES cell cultivation, aliquots of N2B27 medium are supplemented with 1 μ M PD0325901, 3 μ M CHIR99021, and 1000 U/mL LIF. Use 2i LIF medium within 1 week.
 15. Serum-free differentiation (SFD) medium: prepare by assembling 3 parts IMDM (Iscove's Modified Dulbecco's Medium) to 1 part Ham's F-12, supplemented with 2 mM L-glutamine, 50 μ g/mL L-ascorbic acid, 1× N-2 supplement, 1× B-27 supplement (Gibco), 0.05% BSA (bovine serum albumin), and 4.5×10^{-4} M MTG (α -monothioglycerol).
 16. Cardiomyocyte differentiation medium: prepare by supplementing 1× StemPro-34 medium with 2 mM L-glutamine, 0.45 mM ascorbic acid, 5 ng/mL human VEGF, 10 ng/mL bFGF, and 50 ng/mL FGF10.
 17. TryPLE Express (Gibco) or StemPro-34 Accutase[®] (Gibco).
 18. Activin A (R & D, prepare according to manufacturer's instructions).
 19. BMP-4 (R & D, prepare according to manufacturer's instructions).

20. Human-VEGF (R & D, prepare according to manufacturer's instructions).
21. b-FGF (R & D, prepare according to manufacturer's instructions).
22. FGF10 (R & D, prepare according to manufacturer's instructions).
23. StemProTM-34 medium (Gibco).

3 Methods

Some mouse ES cell lines require culturing on a feeder layer of mitotically inactivated mouse embryonic fibroblasts (MEFs), whereas other cell lines can be cultured feeder-free. For ease of manipulation, feeder-free cell lines are recommended. This protocol will deal with feeder-independent mouse ES cell lines. Should feeder-dependent cells be used, various well-established protocols exist which describe the feeder-dependent maintenance of ES cells [11].

3.1 Subculture of Mouse ES Cells in Serum-Containing Medium

1. Prepare a 100 mm cell culture-treated petri dish by flooding with 10 mL of 0.1% gelatin. Place in the 37 °C cell culture incubator for 30 min prior to use.
2. Thaw a vial of cryopreserved feeder-independent mouse ES cells (such as E14-Tg2A cells) in a 37 °C water bath until only a small ice crystal remains. Immediately transfer to the hood and dilute the thawed cells 1:10 into prewarmed DMEM, and centrifuge at $300 \times g$ for 5 min to pellet the cells. Aspirate off the media to remove the DMSO and resuspend the cells in 10 mL of ES LIF medium. Plate out approximately 1×10^6 cells per 100 mm plate in 10 mL ES LIF media per plate.
3. Grow the ES cells in a humidified 37 °C cell culture incubator in 5% CO₂. Feed the cells daily by aspirating off the old media and gently replacing with 10 mL of prewarmed ES LIF medium. After 2–3 days, the plate should be nearly confluent.
4. Upon reaching 70–90% confluence, aspirate off the media and wash with prewarmed D-PBS. Add 2.5 mL of trypsin–EDTA solution and place into the tissue culture incubator for 2–3 min. Cell detachment is complete if colonies are visibly moving when the plate is angled and tapped.
5. Neutralize the trypsin by adding 7.5 mL of prewarmed ES LIF medium. Transfer the cell suspension to a sterile 15 mL FalconTM tube and gently centrifuge at $300 \times g$ for 5 min at room temperature to pellet the cells.

6. Aspirate off the medium and thoroughly resuspend the cell pellet in 10 mL of ES LIF medium. *It is important to thoroughly disperse the clumps into single cells by gently pipetting up and down, to prevent undesired differentiation.*
7. Using a hemocytometer or automatic cell counter, count the number of cells and calculate the concentration of cells. For greater accuracy, use 0.4% trypan blue solution to determine the number of viable cells.
8. Plate out approximately 1×10^6 cells onto a 0.1% gelatin-coated 100 mm plate, taking note of the passage number (*see Note 4*). The remaining cells can be cryopreserved (*see below*).
9. To cryopreserve cells, use a hemocytometer or automatic cell counter to count the number of cells. Centrifuge the cells at $300 \times g$ for 5 min and resuspend the cell pellet at a concentration of $1\text{--}2 \times 10^6$ cells/mL in prechilled cryopreservation media. Dispense 1 mL aliquots of cell suspension into cryovials and transfer to Mr. Frosty™ Freezing Container. Immediately place the container in a -80°C freezer, and transfer to liquid N₂ the next day for long-term storage.

3.2 Differentiation of Mouse Embryonic Stem Cells

Mouse Embryonic stem cells differentiate into a variety of cell types, including cardiomyocytes, when cultured as Embryoid Bodies (EBs). Various protocols exist for the generation of EBs [6]. In general, there are two main approaches. One method employs the hanging drop protocol whereby droplets of ES cells are pipetted onto the lid of a petri dish, which is then inverted, causing the ES cells to coalesce under gravity to generate spheroids and undergo differentiation (Fig. 1). The second approach uses suspension culture in which ES cells are cultivated in noncoated petri dishes and allowed to spontaneously generate three-dimensional aggregates. The suspension culture technique is beneficial for the large-scale generation of EBs, but produces aggregates of significantly different sizes. The first protocol will describe the more reproducible hanging drop method (Subheading 3.2.1). The second protocol, described later in Subheading 3.2.2 uses EBs generated by suspension culture. EB-mediated differentiation of ES cells using conventional protocols (such as the one described in Subheading 3.2.1) generates fewer than 3% mature cardiomyocytes, as determined by intracellular flow cytometry for TNNT2 [12]. More recent protocols (e.g., Subheading 3.2.2) have succeeded in generating enriched cardiomyocyte populations containing approximately 70% TNNT⁺ cells, and therefore may be more appropriate to study cardiac development in greater detail [7, 13]. Whilst this second protocol (Subheading 3.2.2) represents the most efficient method for generating cardiomyocytes to date from mouse ES

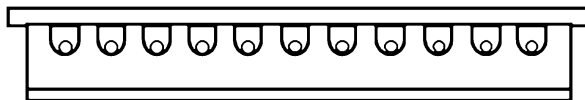


Fig. 1 Schematic representation of the differentiation of mouse ES cells into cardiomyocytes by embryoid bodies (EBs) via hanging drops. EBs are generated by using a multichannel pipette to dispense 25 μ L droplets containing 1000 cells per droplet onto the lid of a 150 mm bacterial-grade petri dish. The dish is inverted to allow the formation of spheroids by gravity, which undergo spontaneous differentiation when cultured in prodifferentiation media

cells, it is absolutely imperative to predetermine the optimal concentration of BMP4 and Activin A by titration (*see Note 5*). This protocol also employs EBs for day 0–4 of differentiation (Fig. 3) (*see Note 6*). This method also utilizes serum-free conditions to maintain the ES cells [14], in contrast to the conditions described in Subheading 3.1 (*see Note 7*).

3.2.1 Embryoid Body-Mediated Differentiation into Cardiomyocytes

1. Trypsinize cells as above (Subheading 3.1, steps 4 and 5). After centrifugation, thoroughly resuspend the cells in EB differentiation medium. It is essential to ensure a single-cell suspension. Count the number of cells accurately using a hemocytometer or automatic cell counter. For embryoid body (EB) generation, it is advisable to use 0.4% trypan blue exclusion during the cell count for increased accuracy.
2. Calculate the number of cells required so that a 25 μ L droplet will contain 1000 cells.
3. Using a multichannel pipette, dispense 25 μ L droplets onto the lid of a nontreated 150 mm bacterial-grade petri dishes (Fig. 1). Ensure droplets do not touch each other.
4. Flood the base of the petri dish with D-PBS and carefully invert the droplet-containing lid.
5. Place into the cell culture incubator for 4 days. If molecular analyses are to be undertaken, use a P1000 pipette tip to collect EBs from each day of differentiation and isolate RNA/protein (including day 0) (*see Note 8*).
6. After 4 days (96 h post-differentiation), carefully transfer each droplet, containing one embryoid body each, onto a 0.1% gelatin-coated 12-well plate. Place approximately 10 EBs into each well, containing 1 mL of EB differentiation media.
7. The next day (day 5), the EBs will have attached to the dish and will begin to undergo extensive morphological changes (Fig. 2).
8. Feed the cells every day with EB differentiation media. Sheets of spontaneously contracting cells will usually be observed by day 8, using an inverted light microscope.

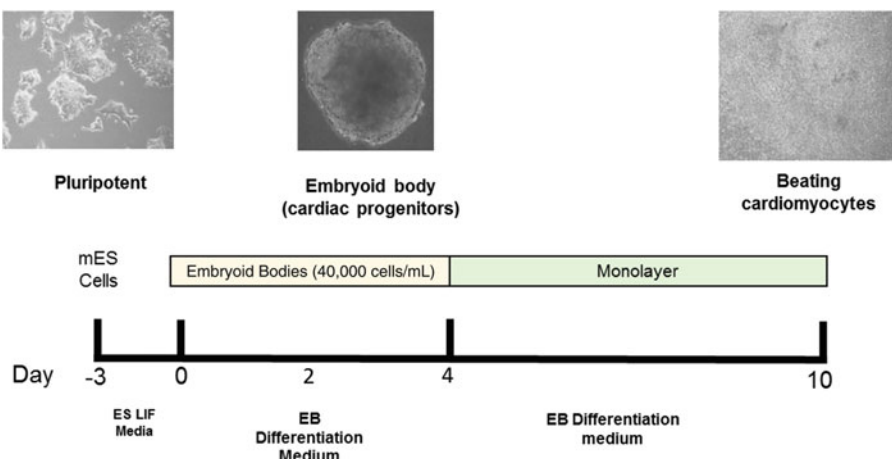


Fig. 2 Timeline of Embryoid body (EB)-mediated differentiation of mouse ES cells into cardiomyocytes. Mouse ES cells are cultured in serum-containing media until confluent. To generate EBs, ES cells are generated by hanging drops (Fig. 1) for 4 days. After 4 days, EBs are directly plated out onto 0.1% gelatin-coated wells to enhance cardiac differentiation. Spontaneous contraction is typically observed after day 10

3.2.2 High-Efficiency Differentiation of Mouse ES Cells into Cardiomyocytes

1. Prepare a tissue culture-treated 6-well plate by flooding each well with 2 mL of 0.1% gelatin. Place in the 37 °C incubator for 30 min.
2. Thaw a vial of cryopreserved, low passage number E14-Tg2A mouse ES cells (*see Note 4*) in a 37 °C water bath until only a small ice crystal remains. Immediately transfer to the hood and dilute 1:10 in prewarmed DMEM/F-12 and centrifuge gently at 300 × g for 5 min at room temperature to pellet the cells. Aspirate off the DMSO-containing medium and thoroughly resuspend the cells into single-cell suspensions in N2B27 2i + LIF medium. Plate approximately 0.4×10^6 cells per well of a 0.1% gelatin-coated 6-well plate.
3. Feed the cells daily for 2–3 days (with fresh N2B27 2i + LIF medium), until 70–90% confluence is reached. Mouse ES colonies cultured in 2i + LIF medium are prone to detachment (*see Note 9*), and therefore pour media gently when feeding.
4. Upon reaching 70–90% confluence, remove the medium and carefully wash with D-PBS. Add 500 μL of TryPLE Express or Accutase® and place into the 37 °C cell culture incubator for 3–5 min until the colonies have detached.
5. Dilute the detached cells with 2 mL of prewarmed DMEM/F-12 and pool the wells together into a 15 mL Falcon™ tube. Centrifuge at 300 × g for 5 min and remove the supernatant.
6. Thoroughly resuspend the cells into single-cell suspensions in SFD medium and count the number of cells with a hemocytometer or automatic cell counter, performing trypan blue exclusion.

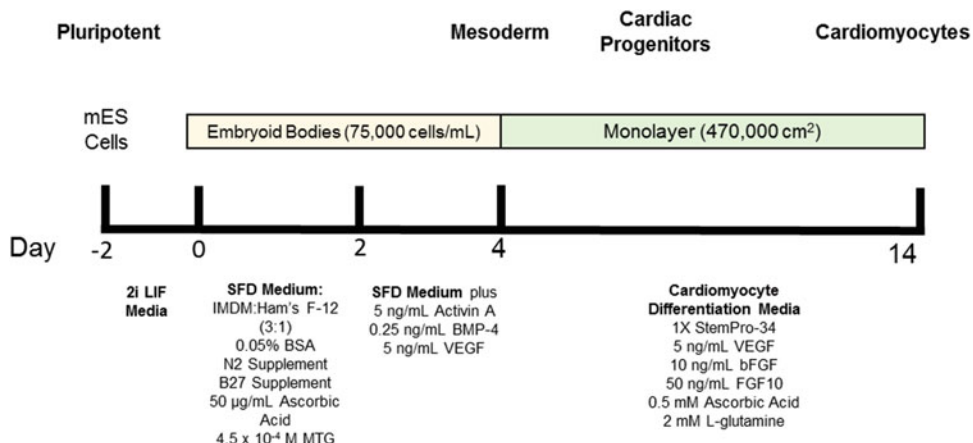


Fig. 3 Timeline of the growth factor-induced, high-efficiency differentiation of mouse ES cells into cardiomyocytes. Mouse ES cells are cultured in 2i LIF media (serum-free) until confluent. Embryoid bodies (EBs) are then generated as a suspension culture for 2 days in serum-free differentiation (SFD) medium. After 2 days, EBs are dissociated and then reaggregated in SFD medium supplemented with Activin A, BMP4, and VEGF (see Note 7). After a further 2 days, EBs are dissociated and plated out in a monolayer in SFD medium supplemented with VEGF, bFGF, and FGF10. Spontaneously contraction is typically observed after day 8 of differentiation

7. In nontreated bacterial-grade petri dishes, plate out 7.5×10^4 cells/mL in 10 mL of SFD medium to generate EBs as free-floating spheroids. Place into the cell culture incubator for 48 h (Fig. 3).
8. After 48 h, collect the EBs in a 15 mL Falcon™ tube and allow the aggregates by gravity to settle to the bottom of the tube, or centrifuge gently ($300 \times g$ for 5 min). Carefully aspirate off the medium and wash gently with D-PBS. Allow the EBs to resettle (or centrifuge gently) and aspirate off the D-PBS. Add 1 mL of Accutase® or TryPLE and place into the cell culture incubator for 3–5 min. Homogenize the cells to break up the EBs into single cells. Upon dissociation, add 9 mL of DMEM/F-12 and centrifuge at $300 \times g$ for 5 min.
9. Remove the supernatant and thoroughly resuspend the cell pellet in SFD medium supplemented with 5 ng/mL Activin A, 0.25 ng/mL BMP-4 (see Note 5), and 5 ng/mL VEGF. Plate out 7.5×10^4 cells/mL in SFD medium plus growth factors in 100 mm nontreated bacterial-grade petri dishes (as in step 7). Leave in the incubator for a further 48 h.
10. At day 4 of differentiation, prepare a flat-bottomed tissue culture-treated 96-well plate by flooding the wells with 100 µL of 0.1% gelatin, and place in the cell culture incubator for 30 min.
11. Dissociate the EBs as in step 8. Carefully count the number of cells using a hemocytometer or automatic cell counter

incorporating trypan blue exclusion. Plate out 470,000 cells/cm² (1.25×10^5 cells/well) in a 0.1% gelatin-coated, flat-bottomed tissue culture-grade 96-well plate in cardiomyocyte differentiation medium.

12. Feed the cells every day with cardiomyocyte differentiation medium. Spontaneous contraction will typically be observed by day 8.
13. If desired, quantify the differentiation efficiency by flow cytometry (*see Note 10*).

3.3 Protocol Variations and Applications

The EB-mediated differentiation of mouse ES cells into cardiomyocytes is a simple and widely used protocol to study cardiac development without the requirement for expensive reagents or time-consuming protocol optimization. However, the low efficiency of TNNT⁺ cells generated in this approach is problematic to study cardiac differentiation in isolation. The high-efficiency differentiation protocol described here is the most efficient method to direct the differentiation of mouse ES cells into cardiomyocytes to date [7], and has been utilized in multiple publications to study cardiac development [13, 15]. A variation on this protocol utilizes a monolayer-based approach, bypassing the necessity to generate and dissociate EBs [16], but is less efficient at generating cardiomyocytes. Other protocols have been described in the literature to differentiate mouse ES cells into cardiomyocytes by manipulation of Wnt/β-catenin signaling. Stimulation of Wnt/β-catenin signaling during early differentiation [17] or inhibition during later stages [18] enhances cardiac differentiation in EBs. However, no protocol for mouse ES cells manipulating Wnt/β-catenin signaling alone has yet generated enriched populations of cardiomyocytes comparable to the well-established protocol in human ES cells [19] (*see Chapter 5*). *See Note 10* for further characterization of in vitro differentiated cardiomyocytes.

4 Notes

1. Many different commercial suppliers provide FBS which differs significantly in price and suitability. For ease-of-use, stem-cell qualified FBS is available which has been preselected for cultivation of ES cells. However, non-ES cell-qualified FBS can also be used if it is tested in-house for its suitability to maintain ES cells in an undifferentiated state. For labs wishing to save money on FBS, it is common practice to acquire small samples (often provided free-of-charge) of different lots of FBS and cultivate ES cells in the different lots to determine which FBS batch is most suitable. Suitability is assayed in-house as previously described [20]. Higher concentrations of FBS (such as

15–20%) might also be required to maintain mouse ES cells in an undifferentiated state, and should be predetermined for each specific cell line.

2. Concentrated LIF can be purchased commercially (ESGRO, Millipore) or can be generated in-house by transfection of Cos7 cells with a LIF-bearing plasmid (such as pCAGGSLIF) and harvesting the conditioned medium [21].
3. For stem cell protocols it is often important to optimize the exact conditions for successful differentiation or maintenance of pluripotency. While we have not always tested several different suppliers, but where we found that switching suppliers might affect the success of the protocol, we have listed the supplier that we use successfully with the protocols presented here.
4. It is good practice to take note of the passage number (i.e., the number of times cells have been split). Although mouse ES cells have the capacity to self-renew indefinitely, continual subculturing can lead to karyotypic abnormalities including chromosomal translocations, trisomy, loss of Y-chromosome in male cell lines, and X-chromosomal instability in female cells [22]. Whilst it is possible to check the karyotype by chromosomal counting and molecular diagnostics, a general rule-of-thumb is to only utilize cells at low passage numbers, ideally below P30. It is preferable to use serum-containing medium for long-term propagation (*see Note 7*).
5. Titration of BMP4 and Activin A concentrations must be performed prior to initiating differentiation, regardless of the cell line used. Small variations in concentrations of these growth factors significantly affect the outcome of differentiation and must therefore be optimized. It is also recommended to titrate every time a new batch of BMP4 or Activin A is purchased, as subtle differences in concentration will affect cardiomyocyte yield.
6. A variation of this protocol utilizes a monolayer-based approach, bypassing the requirements for EBs during differentiation, but leads to reduced cardiomyocyte yields compared to EB-mediated method [16].
7. Recent evidence suggests that long-term cultivation of mouse ES cells in serum-free conditions causes chromosomal abnormalities and epigenetic erasure [23]. To maintain a normal karyotype, it is therefore recommended that cells are routinely cultivated in serum-containing media, and adapted to serum-free media prior to differentiation. Once cells have been adapted to serum-free, they can be immediately differentiated or stocks frozen, and used for differentiation at a later time

point. Cells should not be routinely subpassaged in serum-free conditions.

8. Due to the smaller size of the EBs during the early time course of differentiation, more EBs will be needed for molecular analyses earlier during differentiation (days 1–5), compared to later on, when EBs have grown to a larger size. Collect at least 20 EBs per experimental day for RNA and protein extraction during early differentiation and approximately 10–15 EBs for later stages.
9. It may be preferable to supplement N2B27 2i LIF medium with 2% FBS. This helps to maintain good attachment of the ES cell colonies when using trypsin-EDTA [24]. Alternatively, use Accutase instead of trypsin-EDTA to split the cells.
10. Whilst RT-qPCR and immunoblotting can be used to identify cardiomyocyte markers (such as *TNNT2* and *MYH6*), the most efficient and accurate method to quantify the proportion of mature cardiomyocytes in the differentiated population is to utilize flow cytometry for *TNNT2* [13].

Acknowledgments

We thank the Bruneau lab (Gladstone Institute) and the Martinez-Arias lab (University of Cambridge) for helpful advice regarding mouse ES cell culture. We thank Kate Watt and Yvonne Turnbull (University of Aberdeen), for lab management and technical support, the British Heart Foundation (PG/13/23/30080) for research funding, and the Institute of Medical Sciences (University of Aberdeen) for PhD studentship funding.

References

1. Evans MJ, Kaufman MH (1981) Establishment in culture of pluripotential cells from mouse embryos. *Nature* 292(5819):154–156
2. Thomson JA, Itskovitz-Eldor J, Shapiro SS, Waknitz MA, Swiergiel JJ, Marshall VS et al (1998) Embryonic stem cell lines derived from human blastocysts. *Science* 282 (5391):1145–1147
3. Murry CE, Keller G (2008) Differentiation of embryonic stem cells to clinically relevant populations: lessons from embryonic development. *Cell* 132(4):661–680
4. Zhu Z, Huangfu D (2013) Human pluripotent stem cells: an emerging model in developmental biology. *Development* 140(4):705–717
5. Itskovitz-Eldor J, Schuldiner M, Karsenti D, Eden A, Yanuka O, Amit M et al (2000) Differentiation of human embryonic stem cells into embryoid bodies compromising the three embryonic germ layers. *Mol Med* 6 (2):88–95
6. Kurosawa H (2007) Methods for inducing embryoid body formation: in vitro differentiation system of embryonic stem cells. *J Biosci Bioeng* 103(5):389–398
7. Kattman SJ, Witty AD, Gagliardi M, Dubois NC, Niapour M, Hotta A et al (2011) Stage-specific optimization of activin/nodal and BMP signaling promotes cardiac differentiation of mouse and human pluripotent stem cell lines. *Cell Stem Cell* 8(2):228–240
8. Magin TM, McWhir J, Melton DW (1992) A new mouse embryonic stem cell line with good

- germ line contribution and gene targeting frequency. *Nucleic Acids Res* 20(14):3795–3796
- 9. Nagy A, Rossant J, Nagy R, Abramowitz Newerly W, Roder JC (1993) Derivation of completely cell culture-derived mice from early-passage embryonic stem cells. *Proc Natl Acad Sci U S A* 90(18):8424–8428
 - 10. Nichols J, Smith A (2009) Naive and primed pluripotent states. *Cell Stem Cell* 4 (6):487–492
 - 11. Conner DA (2001) Mouse embryonic stem (ES) cell culture. In: Current protocols in molecular biology. Wiley, Hoboken
 - 12. Bondue A, Lapouge G, Paulissen C, Semeraro C, Iacovino M, Kyba M et al (2008) Mesp1 acts as a master regulator of multipotent cardiovascular progenitor specification. *Cell Stem Cell* 3(1):69–84
 - 13. Wamstad JA, Alexander JM, Truty RM, Shrikumar A, Li F, Eilertson KE et al (2012) Dynamic and coordinated epigenetic regulation of developmental transitions in the cardiac lineage. *Cell* 151(1):206–220
 - 14. Ying Q-L, Wray J, Nichols J, Batlle-Morera L, Doble B, Woodgett J et al (2008) The ground state of embryonic stem cell self-renewal. *Nature* 453(7194):519–523
 - 15. Ishida H, Saba R, Kokkinopoulos I, Hashimoto M, Yamaguchi O, Nowotschin S et al (2016) GFRA2 identifies cardiac progenitors and mediates cardiomyocyte differentiation in a RET-independent signaling pathway. *Cell Rep* 16(4):1026–1038
 - 16. Kokkinopoulos I, Ishida H, Saba R, Coppen S, Suzuki K, Yashiro K (2016) Cardiomyocyte differentiation from mouse embryonic stem cells using a simple and defined protocol. *Dev Dyn* 245(2):157–165
 - 17. Ueno S, Weidinger G, Osugi T, Kohn AD, Golob JL, Pabon L et al (2007) Biphasic role for Wnt/beta-catenin signaling in cardiac specification in zebrafish and embryonic stem cells. *Proc Natl Acad Sci* 104(23):9685–9690
 - 18. Wang H, Hao J, Hong CC (2011) Cardiac induction of embryonic stem cells by a small molecule inhibitor of Wnt/β-catenin signaling. *ACS Chem Biol* 6:192–197
 - 19. Lian X, Zhang J, Azarin SM, Zhu K, Hazeltine LB, Bao X et al (2012) Directed cardiomyocyte differentiation from human pluripotent stem cells by modulating Wnt/β-catenin signaling under fully defined conditions. *Nat Protoc* 8 (1):162–175
 - 20. Walker JM, Jackson M, Taylor AH, Jones EA, Forrester LM (2010) Mouse cell culture, Methods in molecular biology, vol 633. Springer, New York, pp 29–56
 - 21. Smith AG (1991) Culture and differentiation of Embryonic stem cells. *J Tissue Cult Methods* 13(330):89–94
 - 22. Gaztelumendi N, Nogués C (2014) Chromosome instability in mouse embryonic stem cells. *Sci Rep* 4:5324
 - 23. Yagi M, Kishigami S, Tanaka A, Semi K, Mizutani E, Wakayama S et al (2017) Derivation of ground-state female ES cells maintaining gamete-derived DNA methylation. *Nature* 548(7666):20–22
 - 24. Tamm C, Galitó SP, Annerén C (2013) A comparative study of protocols for mouse embryonic stem cell culturing. *PLoS One* 8(12):1–10



Chapter 5

Cardiomyocyte Differentiation from Human Embryonic Stem Cells

Silvia Mazzotta, Adam T. Lynch, and Stefan Hoppler

Abstract

In vitro generated human cardiomyocytes hold the ultimate promise for heart patients for repair of injured or diseased myocardium, but they also provide experimental models for studying normal cardiomyocyte development, for disease modeling and for drug development. Here we provide reliable protocols for differentiation of human embryonic stem cells into functional cardiomyocytes, together with Notes about troubleshooting and optimizing such protocols for specific cell lines. This chapter also briefly discusses other published protocols and those further adapted for differentiation of induced pluripotent stem cells into cardiomyocytes.

Key words Human embryonic stem cells, Human pluripotent stem cells, Human induced pluripotent stem cells, Human cardiomyocytes, Human heart development, In vitro differentiation, Wnt signaling

1 Introduction

Human embryonic stem cells were first isolated and described in 1998 [1]. The potential of human embryonic stem cells (hESCs) is particularly exciting as it offers great opportunities for future therapies in regenerative medicine [2]; additionally, hESCs represent experimentally accessible models for studying human developmental biology [3]. Originally, hESCs were efficiently maintained in vitro by culturing them on a feeder layer of mitotically inactivated mouse embryonic fibroblasts [1]; however, a number of feeder-free protocols were later developed [4]. Various protocols have also been developed to direct human pluripotent stem cells into the cardiovascular lineage [5]. Improvements to cardiomyocyte differentiation protocols came particularly from the observation that temporal modulation of Wnt/β-catenin signaling enhances cardiac differentiation in ES cells [6, 7]. More recent efforts to generate enriched cultures of cardiomyocytes have sought to recapitulate embryonic development more faithfully by manipulating those signaling pathways in vitro which normally control cardiac

development *in vivo*. Such protocols have succeeded in recapitulating heart development step by step, differentiating pluripotent stem cells into functional cardiomyocytes by careful exposure to growth factors or bioactive small molecules at appropriate developmental stages. Highly enriched populations of cardiomyocytes (up to 98% using some human pluripotent stem cell lines) can be generated in fully defined, animal-free culture conditions [8], and have been successfully transplanted into primate models of myocardial infarction [9]. In addition to generating enriched populations of cardiomyocytes for regenerative therapies, pluripotent stem cells can also be used to study the mechanistic basis of cardiovascular diseases. By using induced pluripotent stem (iPS) cells [10] derived from patients with genetic cardiac diseases, iPS cells can be differentiated into cardiomyocytes to study the mechanistic basis underpinning diseases affecting the development of the heart [11]. Additionally, these patient-derived cardiomyocytes can also be utilized in high-throughput drug screens to develop novel drugs to treat cardiomyocyte dysfunction [12]. To accomplish studying heart development and disease mechanisms accurately and reliably, efficient protocols to direct the differentiation of pluripotent stem cells into cardiomyocytes are therefore required. In this chapter, we outline protocols to differentiate human ES cells into cardiomyocytes, which can be used as a model to study human embryonic heart development.

2 Materials

All solutions should be sterile and prepared endotoxin-free. Many vendors provide cell culture-grade reagents preprepared and sterilized for convenience. Reagents should be stored according to the manufacturer's instructions, and prepared media should be stored at 4 °C, unless otherwise stated. All work should be carried out in class II laminar flow cabinets, and all materials entering the cabinets should be sprayed with 70% ethanol first. Cells should be maintained and differentiated in a dedicated, humidified cell culture incubator set to 37 °C and 5% CO₂. The morphology of pluripotent stem cells and differentiated cells should be observed with an inverted light microscope.

2.1 Feeder-Dependent Human ES Cell Culture

1. Human ES cells [such as WA07 (H7) or WA09 (H9), WiCell]. Human embryonic stem cells used here are in the so-called primed state of pluripotency [13].
2. CF-1 mouse embryonic fibroblasts (MEFs), mitotically inactivated via γ -irradiation or mitomycin-C treatment (*see Note 1*).
3. 6-well plates (Corning, Costar) (*see Note 2*).
4. 15 mL Falcon® Tubes.

5. 0.1% gelatin solution: 0.1% (w/v) gelatin from porcine skin dissolved in MilliQ water and autoclaved to sterilize.
6. MEF media: DMEM GlutaMAX, 1× nonessential amino acids, 15% fetal bovine serum (*see Note 3*), 0.0007% β-mercaptoethanol, 1× penicillin/streptomycin.
7. hESC media: DMEM/F-12 (Gibco), 15% KnockOut Serum Replacement (KSR; Gibco) (*see Note 3*), 2 mM L-glutamine, 140 μM β-mercaptoethanol, 4 ng/mL Basic FGF, 1× nonessential amino acids, 1× penicillin/streptomycin.
8. D-PBS without Mg²⁺ or Ca²⁺ (2.67 mM KCl, 1.47 mM KH₂PO₄, 136.9 mM NaCl, and 8.1 mM Na₂HPO₄, pH 7.4).
9. Cryopreservation Media: prepare by combining 90% KSR with 10% DMSO.
10. Cryovials.
11. Mr Frosty™ Freezing Container.

2.2 Feeder-Independent Human ES Cell Culture

1. Human ES cells [such as WA07 (H7) or WA09 (H9), WiCell]. Human Embryonic Stem cells used here are in the so-called primed state of pluripotency [[13](#)].
2. 6-well tissue culture-treated plates.
3. 15 mL Falcon® Tubes.
4. Corning® Matrigel® hESC-qualified Matrix (*see Note 2*).
5. mTeSR1 (STEMCELL Technologies).
6. Accutase®.
7. D-PBS without Mg²⁺ or Ca²⁺ (2.67 mM KCl, 1.47 mM KH₂PO₄, 136.9 mM NaCl, and 8.1 mM Na₂HPO₄, pH 7.4).
8. Y-27632 (ROCK inhibitor, make up a stock solution of 10 mM in D-PBS).
9. Cryopreservation Media: 90% KSR, 10% DMSO.
10. Cryovials.
11. Mr Frosty™ freezing container.

2.3 Human ES Cell Differentiation into Cardiomyocytes

1. Corning® Matrigel® hESC-qualified Matrix (*see Note 2*).
2. D-PBS without Mg²⁺ or Ca²⁺ (2.67 mM KCl, 1.47 mM KH₂PO₄, 136.9 mM NaCl, and 8.1 mM Na₂HPO₄, pH 7.4).
3. 12-well plates (Corning, Costar) (*see Note 2*).
4. IWP-2 (Wnt signal inhibitor, make up stock solution of 5 mM in DMSO).
5. Y-27632 (ROCK inhibitor, make up a stock solution of 10 mM in D-PBS).
6. RPMI.

7. B-27 supplement without insulin.
8. B-27 supplement with insulin.
9. CHIR99021 (GSK3 inhibitor, make up stock solution of 25 mM in DMSO).
10. Wnt signaling activating medium: RPMI medium containing 1× B-27 supplement without insulin, supplemented with 12 µM CHIR99021.
11. Wnt signaling inhibiting medium: RPMI medium containing 1× B-27 supplement without insulin, supplemented with 5 µM IWP2.

3 Methods

Traditionally, mitotically inactivated mouse embryonic fibroblast (MEF) feeder cells were considered crucial to support and maintain human ES cells in the undifferentiated state (Subheading 3.1). However, in recent years reliable strategies for the culture of human ES cells independently of feeder cells have been introduced (Subheading 3.2). These initially relied on the use of Matrigel-coated plates and mTeSRTM1 media, but more recently several alternatives have been introduced to the market, offering equal or improved strategies to expand human pluripotent ES cells.

As compared to feeder-dependent cultures, feeder-free cultures are often more reproducible and reliable, bypassing issues such as quality/quantity of feeder cells, and batch-to-batch variability of the serum used to supplement MEFs media or the KnockOut serum replacement used to supplement hESC media. Although both methods are described below, feeder-free culturing is strongly recommended for more robust and reproducible results.

Relatively recent advances in the field have also led to the development of efficient and reproducible protocols for in vitro differentiation of cardiomyocytes. Importantly, when cells are maintained on feeders, depletion of the feeder layer is required for human ES cell differentiation into cardiomyocytes.

The cardiomyocyte protocol described in Subheading 3.3 is adapted from Lian et al., and was chosen among others as it allows for differentiation of human ES cells cultured independently of feeders into up to 98% cardiomyocytes [8]. Before starting this protocol, human ES cells must be grown in feeder-free conditions for at least three passages. However, human ES cells can generally be adapted from feeder-dependent culture to feeder-independent culture, therefore both strategies for maintaining pluripotent hES cells are described here.

3.1 Feeder-Dependent Maintenance of Human ES Cells

The first steps (1–7) describe the preparation of the MEF feeder cell layer:

1. Coat a 6-well plate in gelatin (*see Note 4*), by adding 1.5 mL 0.1% gelatin solution per well and incubating at room temperature for at least 15 min.
2. While gelatin coating is completing, retrieve a frozen vial of mitotically inactivated MEFs containing 900,000 cells and thaw contents into 37 °C waterbath.
3. Transfer contents of the vial to a 15 mL Falcon® Tube and dilute 1:10 with MEF medium.
4. Gently centrifuge the tube for 5 min at 300 × *g* to pellet the cells.
5. Discard the supernatant and carefully resuspend the pellet in 12 mL MEF medium.
6. Discard gelatin from wells by aspiration and gently dispense 2 mL MEFs per well to plate out the cells.
7. Incubate overnight at 37 °C, and expect plated cells to have a 70–80% confluence after 24 h (*see Note 5*).

The following steps (8–13) describe the establishment of human ES cell culture:

8. Once MEFs have attached in culture, thaw a vial of cryopreserved human ES cells in a 37 °C water bath (*see Note 6*).
9. Dilute the thawed clusters of cells (colonies) 1:10 into prewarmed hESC media in a 15 mL Falcon® Tube and gently centrifuge at 300 × *g* for 5 min to pellet the cells.
10. Gently aspirate off the media to remove the DMSO and resuspend the cells in 12 mL prewarmed hESC media gently, to avoid dissociating the hESC colonies (*see Note 6*).
11. Aspirate media from gelatin-coated plate containing MEFs, and gently wash once in warm D-PBS.
12. Tap the Falcon® Tube containing the human ES cell to mobilize colonies. Dispense 2 mL of cell suspension per well gently, to avoid disrupting the feeder layer. Swirl the plate to ensure even distribution of colonies, and incubate at 37 °C for 48 h (*see Note 7*).
13. After this initial incubation of 48 h, feed cells daily in hESC media, until colonies reach 70–80% confluency. Upon reaching 70–80% confluency, split cells (*see Note 8*).

The following steps (14–23) describe the splitting of a confluent human ES cell culture:

14. Discard culture media and rinse once in 2 mL D-PBS.
15. Remove D-PBS and add further 2 mL D-PBS per well. Incubate at 37 °C for 5–15 min, then observe colonies under the

inverted light microscope. Incubation can be stopped when colony edges are lifting.

16. Scrape colonies in D-PBS with the tip of a 5 mL pipette, making sure to hold the pipette perpendicular to the well. *Make sure not to break colonies excessively.*
17. Carefully transfer colonies to a 15 mL Falcon® Tube and add hESC media to a final volume of 10 mL. Colonies will still be visible as small aggregates, so let them settle at the bottom of the tube by gravity for 5–10 min at room temperature. *Do not prolong this incubation to avoid carrying MEF contamination.*
18. Carefully discard supernatant and resuspend colonies in 100 µL hESC media per well. *Do not pipette up and down to avoid breaking colonies.*
19. Remove media from a new MEF-containing plate and rinse in 2 mL D-PBS; remove D-PBS and dispense 2 mL hESC media per well of a precoated MEF-containing plate, as described above (**steps 1–7**).
20. Tap the Falcon® Tube containing the human ES cell to mobilize colonies. Using a p200 tip, gently pipette 100 µL of resuspended colonies per well.
21. Rock the plate back-and-forth to evenly distribute cells and incubate at 37 °C for 48 h.
22. After this initial incubation of 48 h, feed cells daily in hESC media, until colonies reach 70–80% confluence (as in **step 13**, *see Note 7*).
23. Upon reaching required confluence, cells can be split again (**steps 14–23**) or frozen (**steps 24–26**) (*see Note 8*).
The following steps (24–26) describe the freezing down of a human ES cell culture:
24. To freeze cells, repeat **steps 14–17**; carefully discard supernatant and resuspend the pellet in cryopreservation media.
25. Aliquot 1 mL cells per cryovial and store in Mr Frosty at –80 °C overnight.
26. Transfer to liquid nitrogen the following day.

3.2 Feeder-Independent Maintenance of Human ES Cells

1. Prepare a 6-well plate by coating wells with Matrigel (*see Note 9*).
The following steps (2–6) describe the establishment of human ES cell culture:
2. Thaw a vial of cryopreserved human ES cells in a 37 °C water bath until only a small ice crystal remains. Transfer to the hood and immediately dilute the thawed cells 1:10 into prewarmed DMEM/F-12 and gently centrifuge at 300 × g for 5 min to pellet the cells. Aspirate off the media to remove the DMSO

and resuspend the cells in 12 mL prewarmed mTeSR1 medium containing 10 µM Y-27632.

3. Dispense 2 mL of the cell suspension per well into all 6 wells of a Matrigel-treated 6-well plate (*see Note 10*). Rock the plate back-and-forth to ensure equal distribution of cells.
4. Grow the ES cells in the cell culture incubator for 48 h, with no media change (*see Note 7*).
5. After day 2, feed the cells daily with mTeSR1 (without Y-27632) by aspirating the old medium and carefully replacing with fresh media. After 2–3 days, the plate should be 70–90% confluent.
6. Upon reaching 70–90% confluence, proceed to splitting (*see Note 8*).

The following steps (7–13) describe the splitting of a confluent human ES cell culture:

7. Discard culture media and rinse once in 2 mL D-PBS.
 8. Discard D-PBS and add 1 mL of prewarmed Accutase per well. Place plate in the incubator for 5–10 min until single cells can be observed under the microscope.
 9. Upon detachment, gently dilute the Accutase by adding 3 mL of PBS. Transfer the cell suspension to a sterile 15 mL Falcon™ tube and centrifuge at $300 \times g$ for 5 min to pellet the cells.
 10. Aspirate off the supernatant and gently resuspend the pellet in 3 mL mTeSR1 containing 10 µM Y-27632. Carefully count the number of cells using a haemocytometer or automatic cell counter incorporating trypan blue exclusion.
 11. In a Matrigel-coated plate (*see Note 9*), plate 1.6×10^4 cells/ cm^2 in the appropriate volume of mTeSR1 containing 10 µM Y-27632.
 12. Feed the cells daily with mTeSR1 medium (without Y-27632) until the wells are 70–90% confluent.
 13. Upon reaching required confluence, cells can be split again (**steps 7–13**) or frozen (**steps 14–16**) (*see Note 8*).
- The following steps (14–16) describe the freezing down of a human ES cell culture:
14. To freeze cells, repeat **steps 7–9** in this section; discard supernatant and resuspend the pellet in the appropriate volume of cryopreservation media.
 15. Aliquot 1 mL cells per cryovial and store in Mr Frosty at -80°C overnight.
 16. Transfer to liquid nitrogen the following day.

3.3 Differentiation of Human ES Cells into Cardiomyocytes

1. Prepare hESC culture (Subheading 3.1, steps 14–22, or Subheading 3.2, steps 7–12) (*see Note 11*).
2. Upon reaching 70–90% confluence, aspirate the medium from plate/flask and rinse with D-PBS.
3. Proceed to cell detachment as described above (Subheading 3.2, steps 6–8).
4. Dispense $1.25\text{--}5 \times 10^4 \text{ cells/cm}^2$ (1.9×10^5 cells per well) in a Matrigel-coated 12-well plate (*see Note 12*).
5. Feed the cells daily with mTeSR1 medium (without Y-27632) for an additional 2 days.
6. After these 2 days (*considered Experimental Day 0*, *see Fig. 1*), rinse cells with D-PBS and feed them in prewarmed Wnt signaling activating medium (*see Note 13*).
7. Exactly 48 h later (*Experimental Day 2*), rinse the cells with D-PBS and feed them in prewarmed Wnt signaling inhibiting medium.
8. Exactly 48 h later (*Experimental Day 4*), rinse the cells with D-PBS and feed them in prewarmed RPMI medium containing $1\times$ B-27 supplement without insulin.
9. Exactly 48 h later (*Experimental Day 6*), rinse the cells with D-PBS and feed them in prewarmed RPMI medium containing

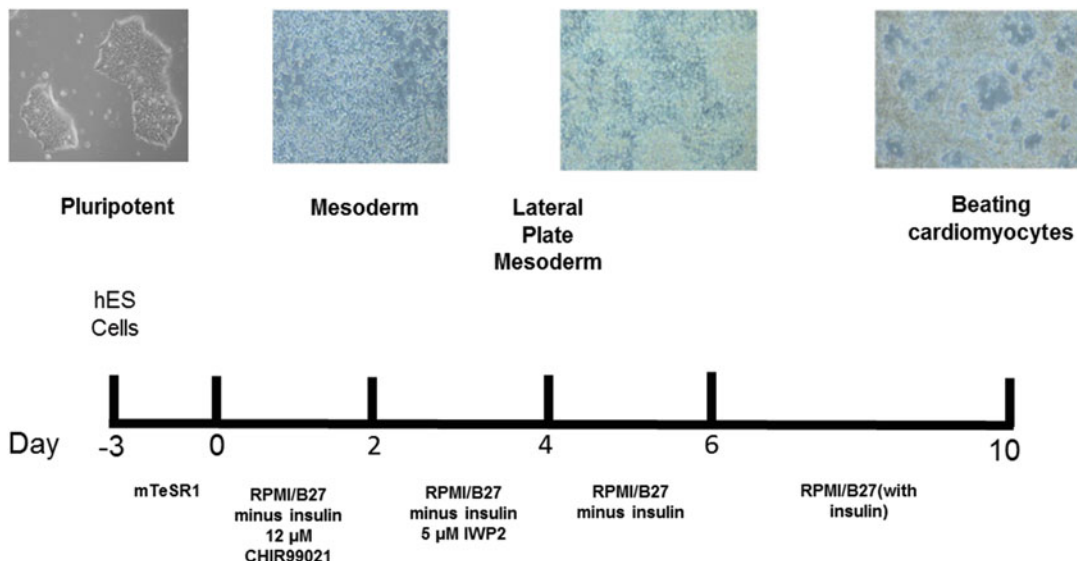


Fig. 1 Differentiation of human ES cells into cardiomyocytes by small-molecule inhibitors. Human ES cells are cultured in feeder-free conditions in mTeSR1 medium for 3 days. Monolayer differentiation is then performed by exposing the human ES cells to the Wnt/β-catenin agonist CHIR99021 for 2 days. After 2 days, the differentiating cells are exposed to the Wnt signaling inhibitor IWP2 for a further 2 days. At day 4 of differentiation, IWP2 is removed and spontaneously contracting cardiomyocytes are typically observed by day 9–10 of differentiation

$1 \times$ B-27 supplement (with insulin). Keep cells in this media for additional 4 days. Expect to observe spontaneous contraction between days 7 and 9 (*see Note 14*).

10. If desired, quantify the differentiation efficiency by intracellular flow cytometry (*see Note 15*).

3.4 Protocol Variations and Application to Human iPS Cells

The protocol discussed in this chapter is a variation of a previously published [14] efficient method to differentiate human ES cells into cardiomyocytes. This protocol is based on the temporal modulation of Wnt signaling [8]. A very similar protocol has recently been adapted for differentiation of cardiomyocytes from human iPS cells [15]. While this protocol is widely used, several other variations exists and have recently been reviewed [16] including differentiation in minimum, fully defined conditions [17] or coaddition of the Wnt/ β -catenin antagonist XAV939 to enhance cardiac differentiation [18]. Alternatively, cardiomyocytes can also be generated by exposure to Activin, BMP4, and LY294002, an inhibitor of phosphoinositide 3-kinases during early differentiation, followed by later inhibition of Wnt signaling [14]. The protocols described here generate mixed populations of cells containing atrial, ventricular, and pacemaker-like cells. Through differential retinoic acid signaling, highly enriched populations of atrial or ventricular cells can be generated *in vitro* [19], which offer great promise in differentiating specific subsets of cardiac cells for potential regenerative therapies. Various other methods have also been described (reviewed in [5, 16]) with varying differentiation efficiencies.

4 Notes

1. MEFs can be purchased ready-inactivated from various commercial suppliers. Alternatively, MEFs can be either isolated directly from mouse embryos, or purchased non-inactivated from commercial vendors. The MEFs are expanded for 3–4 passages and then mitotically inactivated by either mitomycin-C treatment or exposure to γ -irradiation. To perform this, the reader is directed to a previously described protocol [20]. We usually source our ready-inactivated MEFs from MTI-Globalstem, and the Materials and Methods described here have been optimized for these cells. If using other suppliers, adjust protocols according to supplier's instructions for culturing their inactivated MEFs.
2. For stem cell protocols it is often important to optimize the exact conditions for successful differentiation or maintenance of pluripotency. Although we have not always tested reagents from several different suppliers, we found that switching suppliers might affect the success of the protocol; therefore here

we list the supplier that we have used successfully to optimize the protocols presented here.

3. FBS and KnockOut Serum Replacement should be batch tested, for optimal and reproducible growth of cells.
4. Cell culture can be scaled up or down according to personal requirements. Other Costar plate formats or tissue culture flasks can be used as needed. The format chosen will depend on the number of colonies frozen per vial and will vary between cell lines. Additionally, variability in cell survival and attachment can be observed even between different frozen stocks of the same cell type.
5. The quality and quantity of MEFs are crucial for efficient support of hESC growth in the undifferentiated state. Therefore each batch of MEFs should be tested for effective inactivation and plating density prior to use. Effective inactivation can be confirmed by plating MEFs at a chosen density and counting them after 24 h of culture. Titration of MEF plating density is recommended for each batch of MEFs. In fact, cell viability and recovery after thawing are unpredictable, and therefore each batch of MEFs should be tested to ensure achievement of 70–80% confluence (following attachment of inactive cells, rather than growth) in the 24 h following thawing and plating. While MEFs can be kept in culture for up to 1 week prior use, with 1–2 media changes provided when required, the use of fresh MEFs is recommended when possible.
6. Human ES cells intended to be grown on feeder cells must be frozen as small clumps rather than single cells. Conversely, human ES cells intended to be grown independently of feeders can be frozen in either format. However, human ES cells frozen as single cells should always be thawed in the presence of 10 µM Y27632, for optimal cell recovery.
7. Cells should be monitored during these 48 h, as media change might be required in rare occasions. If 24 h after plating severe cell death is observed, together with spontaneous differentiation, media change should be considered at this stage.
8. Prior to splitting or freezing, observation of hESCs is necessary under the inverted light microscope, in order to identify possible differentiating colonies, which typically show irregular morphology and growth in multilayers. Identified differentiating colonies can be marked with a marker pen at the bottom of the plate, and removed by aspiration prior to splitting.
9. To culture human ES cells on Matrigel, using human ES cell-qualified Matrigel is recommended. Matrigel should be thawed overnight at 4 °C and aliquoted (on ice) out at the dilution factor recommended by the manufacturer. Aliquots should be frozen and always kept on ice when handling. To prepare tissue

cultureware with Matrigel, thaw an aliquot of Matrigel on ice and dilute into 24 mL of prechilled DMEM/F-12. Coat the bottom of a 6-well plate with 1 mL of diluted Matrigel and ensure the surface is fully coated. Incubate at room temperature for an hour. Alternatively, vessels can be coated and stored at 4 °C for 1 week (sealed) if not required immediately. Upon use, aspirate off the diluted Matrigel and immediately flood the well with an appropriate amount of mTeSR1 medium, making sure not to disturb the Matrigel layer.

10. Ideally cells should be plated at a density of 1.6×10^4 cells/cm², so adjust volumes according to the number of cells frozen per vial.
11. Human ES cells should be split or passaged in feeder-free conditions for at least three times before proceeding to cardiomyocyte differentiation.
12. Titrating the plating density is strongly encouraged for optimal results.
13. Titrating the CHIR99021 concentration may be necessary for efficient cardiac differentiation of specific cell lines. While some cell death at this stage is expected, if considerable apoptosis is observed following CHIR99021 treatment, titrate the CHIR99021 6–14 µM [8].
14. If regularly fed, cells can be maintained contracting in culture for several weeks. Temporary decreased contraction could be observed as a consequence of changes in temperature.
15. While RT-qPCR and immunoblotting can be used to identify cardiomyocyte markers (such as *TNNT2* and *MYH6*), the most efficient and accurate method to quantify the proportion of mature cardiomyocytes in the differentiated population is to utilize flow cytometry for *TNNT2* [8].

Acknowledgments

We are grateful to Po-Lin So and Bruce Conklin (Gladstone Institutes) for providing a modified version of the Lian et al. protocol for cardiomyocyte differentiation from human ES cells. We thank Kate Watt, and Yvonne Turnbull (University of Aberdeen), for lab management and technical support, Rory J Bonner (University of Aberdeen) for providing images, the British Heart Foundation (PG/12/75/29851) for research funding, and the Institute of Medical Sciences (University of Aberdeen) for PhD studentship funding.

References

1. Thomson JA, Itskovitz-Eldor J, Shapiro SS, Waknitz MA, Swiergiel JJ, Marshall VS et al (1998) Embryonic stem cell lines derived from human blastocysts. *Science* 282 (5391):1145–1147
2. Murry CE, Keller G (2008) Differentiation of embryonic stem cells to clinically relevant populations: lessons from embryonic development. *Cell* 132(4):661–680
3. Zhu Z, Huangfu D (2013) Human pluripotent stem cells: an emerging model in developmental biology. *Development* 140(4):705–717
4. Xu C, Inokuma MS, Denham J, Golds K, Kundu P, Gold JD et al (2001) Feeder-free growth of undifferentiated human embryonic stem cells. *Nat Biotechnol* 19(10):971–974
5. Mummery CL, Zhang J, Ng ES, Elliott DA, Elefanty AG, Kamp TJ (2012) Differentiation of human embryonic stem cells and induced pluripotent stem cells to cardiomyocytes: a methods overview. *Circ Res* 111(3):344–358
6. Wang H, Hao J, Hong CC (2011) Cardiac induction of embryonic stem cells by a small molecule inhibitor of Wnt/β-catenin signaling. *ACS Chem Biol* 6:192–197
7. Yang L, Soonpaa MH, Adler ED, Roepke TK, Kattman SJ, Kennedy M et al (2008) Human cardiovascular progenitor cells develop from a KDR+ embryonic-stem-cell-derived population. *Nature* 453(7194):524–528
8. Lian X, Zhang J, Azarin SM, Zhu K, Hazeltine LB, Bao X et al (2012) Directed cardiomyocyte differentiation from human pluripotent stem cells by modulating Wnt/β-catenin signaling under fully defined conditions. *Nat Protoc* 8 (1):162–175
9. Chong JJH, Yang X, Don CW, Minami E, Liu Y-W, Weyers JJ et al (2014) Human embryonic-stem-cell-derived cardiomyocytes regenerate non-human primate hearts. *Nature* 510 (7504):273–277
10. Takahashi K, Tanabe K, Ohnuki M, Narita M, Ichisaka T, Tomoda K et al (2007) Induction of pluripotent stem cells from adult human fibroblasts by defined factors. *Cell* 131 (5):861–872
11. Davis RP, Casini S, Van Den Berg CW, Hoekstra M, Remme CA, Dambrot C et al (2012) Cardiomyocytes derived from pluripotent stem cells recapitulate electrophysiological characteristics of an overlap syndrome of cardiac sodium channel disease. *Circulation* 125 (25):3079–3091
12. Mordwinkin NM, Burridge PW, Wu JC (2014) A review of human pluripotent stem cell-derived cardiomyocytes for high-throughput drug discovery, cardiotoxicity screening and publication standards. *J Cardiovasc Transl Res* 6(1):22–30
13. Nichols J, Smith A (2009) Naive and primed pluripotent states. *Cell Stem Cell* 4 (6):487–492
14. Mazzotta S, Neves C, Bonner RJ, Bernardo AS, Docherty K, Hoppler S (2016) Distinctive roles of canonical and noncanonical Wnt signaling in human embryonic cardiomyocyte development. *Stem Cell Reports* 7(4):764–776
15. Pei F, Jiang J, Bai S, Cao H, Tian L, Zhao Y et al (2017) Chemical-defined and albumin-free generation of human atrial and ventricular myocytes from human pluripotent stem cells. *Stem Cell Res* 19:94–103
16. Hausburg F, Jung JJ, Hoch M, Wolfien M, Rimbach C, David R (2017) (Re-) programming of subtype specific cardiomyocytes. *Adv Drug Deliv Rev* 120:147–167
17. Burridge PW, Matsa E, Shukla P, Lin ZC, Churko JM, Ebert AD et al (2014) Chemically defined generation of human cardiomyocytes. *Nat Methods* 11(8):855–860
18. Hwang GH, Park SM, Han HJ, Kim JS, Yun SP, Ryu JM et al (2017) Purification of small molecule-induced cardiomyocytes from human induced pluripotent stem cells using a reporter system. *J Cell Physiol* 232(12):3384–3395
19. Lee JH, Protze SI, Laksman Z, Backx PH, Keller GM (2017) Human pluripotent stem cell-derived atrial and ventricular cardiomyocytes develop from distinct mesoderm populations. *Cell Stem Cell* 21(2):179–194.e4
20. Conner DA (2001) Mouse embryo fibroblast (MEF) feeder cell preparation. In: *Current protocols in molecular biology*. Wiley, Hoboken



Chapter 6

Induction of Human Induced Pluripotent Stem Cells to Cardiomyocytes Using Embryoid Bodies

Takeshi Hatani, Kenji Miki, and Yoshinori Yoshida

Abstract

Specific cell lineages differentiated from human induced pluripotent stem cells (iPSCs) are promising sources for cell replacement therapy and are useful biomedical research tools for research on disease mechanisms and drug discovery. Among the different lineages, cardiac lineage has been one of the most efficiently differentiated through several established protocols. In this chapter, we describe our reproducible and highly efficient methodology for differentiating iPSCs into cardiomyocytes using embryoid bodies. We also describe methods to dissociate iPSC-derived cardiomyocytes and to evaluate iPSC-derived cardiomyocytes.

Key words Cardiac differentiation, Cardiomyocyte, Embryoid body, Human induced pluripotent stem cells, Reaggregation

1 Introduction

To differentiate pluripotent stem cells including human embryonic stem cells and human induced pluripotent stem cells (iPSCs) into specific lineages, it is advised to recapitulate important steps in early embryonic development by controlling the activation and inhibition of different signaling pathways in defined culture conditions [1]. In cardiac differentiation, pluripotent stem cells follow the fate of mesoderm. In this early stage, bone morphogenetic proteins (BMPs) and activin proteins, both of which are members of the transforming growth factor- β superfamily, wingless/INT proteins (WNTs), and fibroblast growth factors (FGFs) play key roles [2]. Managing these signal cascades properly promotes effective cardiac differentiation. In general, there are two major ways to induce cardiomyocytes, the embryoid bodies (EBs) approach and the monolayer approach [1, 2]. In EBs approach, the interaction of the cells in EBs mimics *in vivo* embryonic developmental processes to some extent. Recently, efficient generation of desired specific cardiac subtypes are reported using modified EB-based

methods [3, 4]. On the other hand, relatively uniform cardiomyocytes can be differentiated with the monolayer approach without the complex procedures. The monolayer protocols also do not require replating steps in some feeder-free iPSC culture systems. In this chapter, we describe our reproducible and highly efficient EB method, which was modified from previously reported protocols [5–7].

2 Materials

2.1 Human Induced Pluripotent Stem Cell (iPSC) Culture

1. Gelatin from porcine skin: make a 10× stock solution (1% w/v) dissolved in dH₂O and store at room temperature.
2. SNL medium: Dulbecco's Modified Eagle's Medium (DMEM) with high glucose, 7.5% fetal bovine serum (FBS), 2 mM L-glutamine, 50 U/mL penicillin–50 µg/mL streptomycin.
3. 0.25% trypsin–EDTA.
4. Dulbecco's phosphate-buffered saline without Ca or Mg (DPBS (-)).
5. Mitomycin-C: make a 0.4 mg/mL working solution dissolved in DPBS (-).
6. Recombinant human (rh) bFGF: 200 µL aliquots at 10 µg/mL in 1 mM DTT–0.1% BSA–DPBS (-) and stored at –30 °C.
7. iPSC medium: ES cell medium (ReproCELL), 4 ng/mL rhbFGF, 50 U/mL penicillin–50 µg/mL streptomycin.
8. Cell scraper.
9. 100 mm cell culture dish.
10. 60 mm cell culture dish.
11. Collagenase type IV: make a 1 mg/mL stock solution dissolved in dH₂O and store at –30 °C.
12. Calcium chloride: make a 0.1 M CaCl₂ stock solution dissolved in dH₂O and store at room temperature.
13. Collagenase, trypsin, and KSR (CTK) solution: 0.1 mg/mL Collagenase type IV, 0.25% trypsin, 20% (v/v) KnockOut Serum Replacement (KSR), 1 mM CaCl₂, all dissolved in dH₂O, and store at –30 °C.
14. 15 mL conical tube.
15. 50 mL conical tube.

2.2 Cardiomyocyte Differentiation

1. Accumax.
2. Iscove's Modified Dulbecco's Medium (IMDM).
3. StemPro-34 SFM (Thermo Fisher Scientific).

4. L-glutamine: make a 200 mM stock solution and store at -30 °C.
5. L-ascorbic acid: make a 5 mg/mL stock solution dissolved in dH₂O and store at -30 °C.
6. Transferrin: make a 30 mg/mL stock solution and store at 4 °C.
7. Monothioglycerol: make a 0.135 M working solution dissolved in StemPro-34 SFM and store at 4 °C.
8. Matrigel Matrix (Corning): make a 50% (v/v) stock solution dissolved in IMDM and store at -30 °C.
9. Y-27632: make a 10 mM stock solution dissolved in dH₂O and store at -30 °C.
10. rhBMP4: make a 100 µg/mL stock solution dissolved in 4 mM HCl-0.1% BSA-dH₂O and store at -80 °C, make a 10 µg/mL working solution dissolved in 4 mM HCl-0.1% BSA-dH₂O and store at 4 °C.
11. rhActivin A: make a 100 µg/mL stock solution dissolved in 0.1% BSA-DPBS (-) and store at -80 °C, make a 10 µg/mL working solution dissolved in 0.1% BSA-DPBS (-) and store at 4 °C.
12. rhbFGF: make a 100 µg/mL stock solution dissolved in 1 mM DTT-0.1% BSA-DPBS (-) and store at -80 °C, make a 10 µg/mL working solution dissolved in 1 mM DTT-0.1% BSA-DPBS (-) and store at 4 °C.
13. IWP-3: make a 10 mM stock solution dissolved in DMSO and store at -30 °C.
14. rhVEGF: make a 100 µg/mL stock solution dissolved in 0.1% BSA-DPBS (-) and store at -80 °C, make a 10 µg/mL working solution dissolved in 0.1% BSA-DPBS (-) and store at 4 °C.
15. SB431542: make a 10 mM stock solution dissolved in DMSO and store at -80 °C.
16. Dorsomorphin: make a 10 mM stock solution dissolved in DMSO and store at -80 °C.
17. Differentiation medium 1: StemPro-34 SFM, L-glutamine, L-ascorbic acid, transferrin, monothioglycerol, Matrigel matrix, Y-27632, and rhBMP4. Concentration and amount are shown in Table 1.
18. 2× Differentiation medium 2: StemPro-34 SFM, L-glutamine, L-ascorbic acid, transferrin, monothioglycerol, rhBMP4, rhActivin A, and rhbFGF. Concentration and amount are shown in Table 2.

Table 1
Differentiation medium 1

Products	Working solution	Final concentration
StemPro-34 SFM		
L-glutamine	200 mM	2 mM
L-ascorbic acid	5 mg/mL	50 µg/mL
Transferrin	30 mg/mL	150 µg/mL
Monothioglycerol	0.135 M	0.4 µM
Matrigel matrix	50% (v/v)	0.5% (v/v)
Y-27632	10 mM	10 µM
rhBMP4	10 µg/mL	2 ng/mL

Table 2
2× Differentiation medium 2

Products	Working solution	Final concentration
StemPro-34 SFM		
L-glutamine	200 mM	2 mM
L-ascorbic acid	5 mg/mL	50 µg/mL
Transferrin	30 mg/mL	150 µg/mL
Monothioglycerol	0.135 M	0.4 µM
rhBMP4	10 µg/mL	18 ng/mL
rhActivin A	10 µg/mL	12 ng/mL
rhbFGF	10 µg/mL	10 ng/mL

19. Differentiation medium 3: StemPro-34 SFM, L-glutamine, L-ascorbic acid, transferrin, monothioglycerol, Matrigel matrix, IWP-3, rhVEGF, SB431542, and dorsomorphin. Concentration and amount are shown in Table 3. SB431542 and dorsomorphin are added depending on the cell lines.
20. Differentiation medium 4: StemPro-34 SFM, L-glutamine, L-ascorbic acid, transferrin, monothioglycerol, and rhVEGF. Concentration and amount are shown in Table 4.
21. 96-well U-bottom ultralow attachment plate (Corning).
22. 6-well ultralow attachment plate (Corning).
23. Twenty-five milliliter reagent reservoir.

Table 3
Differentiation medium 3

Products	Working solution	Final concentration
StemPro-34 SFM		
L-glutamine	200 mM	2 mM
L-ascorbic acid	5 mg/mL	50 µg/mL
Transferrin	30 mg/mL	150 µg/mL
Monothioglycerol	0.135 M	0.4 µM
Matrigel matrix	50% (v/v)	0.5% (v/v)
IWP-3	10 mM	1 µM
rhVEGF	10 µg/mL	10 ng/mL
SB431542 ^a	10 mM	5.4 µM
Dorsomorphin ^b	2 mM	0.6 µM

^{a, b} These molecules are added depending on the cell lines

Table 4
Differentiation medium 4

Products	Working solution	Final concentration
StemPro-34 SFM		
L-glutamine	200 mM	2 mM
L-ascorbic acid	5 mg/mL	50 µg/mL
Transferrin	30 mg/mL	150 µg/mL
Monothioglycerol	0.135 M	0.4 µM
rhVEGF	10 µg/mL	5 ng/mL

2.3 Assessment of Differentiated Cells

1. 100× Dulbecco's phosphate-buffered saline (DPBS (+)) Preparation Reagent: make a 1× stock solution dissolved in DPBS (-) and store at 4 °C.
2. Collagenase type I: make a 2 mg/mL stock solution dissolved in 25% (v/v) FBS-1× DPBS (+) Preparation Regent and store at -30 °C.
3. DNase I: make a 1 mg/mL stock solution dissolved in dH₂O and store at -30 °C.
4. Five milliliter flow cytometry tube.
5. 24-well flat-bottom multiwell cell culture plate.
6. 96-well U-bottom tissue culture plate.

7. Fibronectin (Sigma-Aldrich): make a 1 mg/mL stock solution dissolved in dH₂O and store at -30 °C.
8. Flow cytometry buffer: 2% FBS (v/v) solution dissolved in DPBS (-) and store at 4 °C.
9. Saponin.
10. Permeabilization buffer: 0.5% (w/v) saponin solution dissolved in flow cytometry buffer.
11. Paraformaldehyde (PFA): make a 4% (g/w) stock solution dissolved in DPBS (-) solution and store at -30 °C.
12. Normal goat serum.
13. Troponin T (Thermo Fisher Scientific; 1:200).
14. APC goat anti-mouse IgG (BD Biosciences; 1:100).
15. Goat anti-mouse IgG-Alexa Fluor 546 (Life Technologies; 1:400).
16. Hoechst 33342 (Life Technologies; 1:10,000).
17. Bovine serum albumin (BSA).
18. Triton X-100.
19. Blocking buffer: 5% (v/v) normal goat serum, 0.1% (v/v) Triton X-100, and 0.1% BSA in DPBS (-).
20. PE mouse anti-human CD31 (BD Pharmingen; 2:50).
21. PE mouse anti-human CD49a (BD Pharmingen; 3:50).
22. PE mouse anti-human CD140b (BD Pharmingen; 5:50).
23. PE mouse anti-human CD90 (BD Pharmingen; 1:50).
24. PE/Cy7 mouse anti-human SIRPa (Biolegend; 3:50).

3 Methods

3.1 Maintenance of iPSCs

1. Add 310 µL of 0.4 mg/mL mitomycin-C solution directly to the medium in the 100 mm dish culturing SNL feeder cells and incubate at 37 °C for 2.25 h.
2. Aspirate the mitomycin-C containing medium and rinse twice with DPBS (-).
3. Add 0.5 mL of 0.25% trypsin-EDTA, swirl to cover the entire surface of the dish and incubate at room temperature for 2 min.
4. Add 3 mL of SNL medium to neutralize the trypsin and pipette the clumps to single cells using a 1000 µL pipette.
5. Count the cells with a TC20 automated cell counter (Bio-Rad) and dilute the dissociated cells with SNL medium at a concentration of 2.6×10^5 cells per 1 mL.

6. Seed the mitomycin-C treated SNL feeder cells to a 0.1% gelatin coated-60 mm dish at 7.8×10^5 cells/dish (e.g., 3 mL for a 60 mm dish).
7. Shake the dish briefly and place the dish into a 5% CO₂ incubator at 37 °C overnight (*see Note 1*).
8. Next day, aspirate the culture medium from the dish culturing iPSCs with approximately 90% confluence and rinse the dish once with DPBS (-).
9. Add CTK solution (e.g., 0.5 mL for a 60 mm dish) and incubate at room temperature for 2 min to detach the feeder cells.
10. Aspirate CTK solution and rinse the dish twice with DPBS (-). Add iPSC medium to the dish (e.g., 1 mL for a 60 mm dish).
11. Scrape the iPSC colonies using a cell scraper. Pipette them ~5 times to small clumps using a 1000 µL pipette.
12. Seed the iPSC clumps to a prepared SNL feeder dish. The split ratio is generally between 1:2 and 1:4, which depends on the cell line.

3.2 Cardiac Differentiation

We show the schematic procedure for the cardiac differentiation in Fig. 1. In our experience, the iPSC colonies which cover approximately 90% of the surface area of the culture dish are suitable for starting cardiac differentiation (Fig. 2) (*see Note 2*). We also show EBs of iPSC-derived cardiomyocytes at day 20 after differentiation (Fig. 2).

Day 0: Begin differentiation with Differentiation medium 1

1. Aspirate the medium from the dish and rinse once with DPBS (-). Add CTK solution and incubate at room temperature for 2 min to detach the feeders (*see Note 3*).
2. Aspirate CTK solution and rinse the dish twice with DPBS (-). Add Accumax (e.g., 1 mL for a 60 mm dish) and incubate at 37 °C for 5–8 min.
3. Pipette ~3 times with a 1000 µL pipette to dissociate into single cells and transfer the cells to a 15 mL conical tube (*see Note 4*).

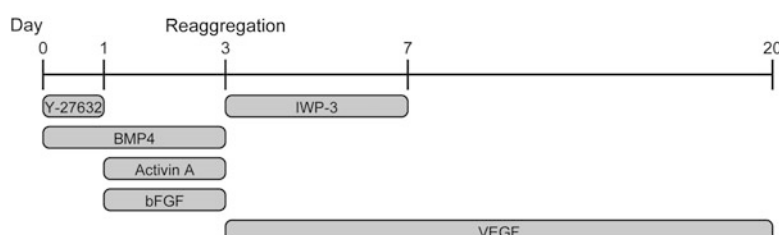


Fig. 1 The time course and small molecules used to generate cardiomyocytes by embryoid body formation

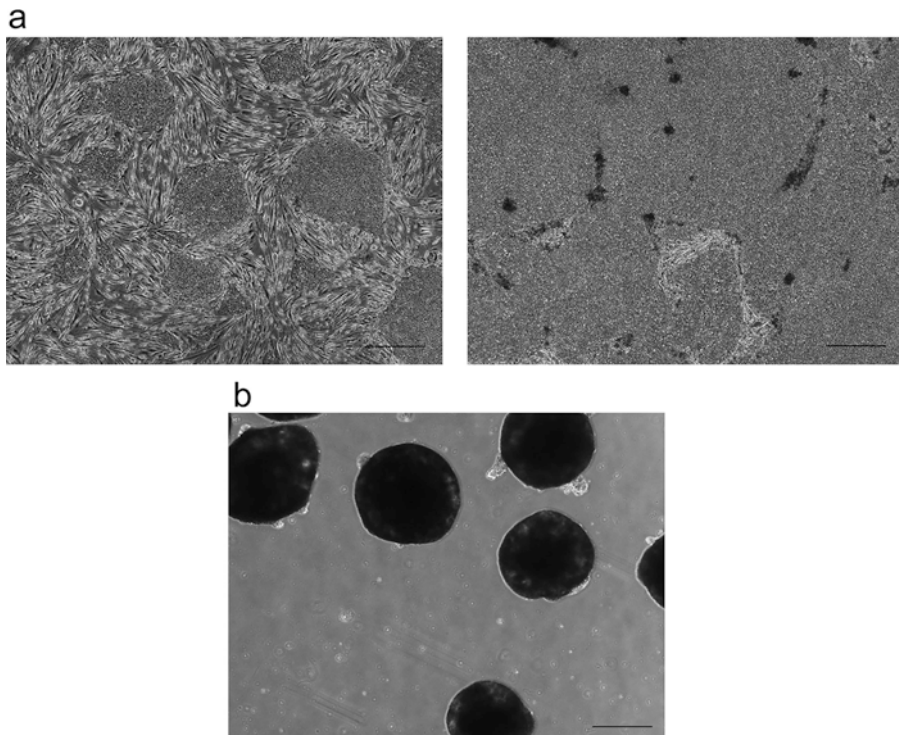


Fig. 2 Phase contrast images of iPSCs (a) and iPSC-derived cardiomyocytes (b). (a) iPSCs grow on mitomycin-C treated SNL feeders. After 2 days from passage, the confluence is low (left figure). After 6 days from passage, the confluence is about 90%, and iPSCs are ready for passage and induction into cardiomyocytes (right figure). Scale bars: 500 μ m. (b) iPSC-derived cardiomyocytes start beating at day 7. This image is pictured at day 20 after differentiation. Scale bar: 500 μ m

Add 6 mL of IMDM to the tube and centrifuge at $120 \times g$ for 5 min. During this time, prepare Differentiation medium 1 (Table 1) (*see Note 5*).

4. Aspirate the medium from the conical tube and suspend the pellet with 1–2 mL of Differentiation medium 1. Count the cells with a TC20 automated cell counter and dilute the dissociated cells with Differentiation medium 1 at a concentration of 5000–7000 cells per 70 μ L.
 5. Transfer the cell suspension to a reservoir and distribute the suspension to a 96-well U-bottom ultralow attachment plate at 70 μ L per well with a multichannel pipette.
 6. Place the plate into a 5% O₂ (hypoxic) incubator at 37 °C (*see Note 6*).
- Day 1: Add 2× Add xic) incubator at 32
7. Prepare 2× Differentiation medium 2 (Table 2).

8. Transfer 2× Differentiation medium 2 to a reservoir and add the media to the day 0 plate at 70 µL per well with a multichannel pipette (e.g., 140 µL per well totally).
 9. Place the plate into a 5% O₂ (hypoxic) incubator at 37 °C.
- Day 3: Change to Differentiation medium 3 (Reaggregation of EBs)
10. Transfer EBs from the 96-well U-bottom ultralow attachment plate to 15 mL conical tubes with a 1000 µL pipette. After EBs naturally fall, aspirate the supernatant.
 11. Add Accumax (e.g., 1 mL for a 15 mL conical tube) and incubate at 37 °C for 5–8 min. Pipette ~5 times with a 1000 µL pipette to dissociate into single cells (*see Note 4*). Add 6 mL of IMDM to the tube and centrifuge at 120 × g for 5 min. During this time, prepare Differentiation medium 3 (Table 3) (*see Notes 5 and 7*).
 12. Aspirate the media from the conical tube and suspend the pellet with 1–2 mL of Differentiation medium 3. Count the cells with a TC20 automated cell counter and dilute the dissociated cells with Differentiation medium 3 at a concentration of 20,000–30,000 cells per 100 µL (*see Note 8*).
 13. Transfer the cell suspension to a reservoir and distribute the suspension to a new 96-well U-bottom ultralow attachment plate at 100 µL per well with a multichannel pipette.
 14. Place the plate into a 5% O₂ (hypoxic) incubator at 37 °C (*see Note 6*).
- Day 7~: Change to Differentiation medium 4
15. Prepare Differentiation medium 4 (Table 4).
 16. Transfer EBs from the 96-well U-bottom ultralow attachment plate to a 6-well ultralow attachment plate (e.g., 25–35 EBs per well) with a 1000 µL pipette. After EBs naturally fall, aspirate the supernatant.
 17. Add 2 mL of Differentiation medium 4 to a well of a 6-well plate.
 18. Place the plate into a 5% O₂ (hypoxic) incubator at 37 °C (*see Note 6*).
 19. Perform media change every 2–3 days with Differentiation medium 4. After day 10, place the plate into a conventional O₂ incubator at 37 °C (*see Note 6*).

3.3 Evaluation of Differentiated Cardiomyocytes Using Flow Cytometry

Day 20 iPSC-derived cardiomyocytes are analyzed using flow cytometry (Fig. 3). Characterization of the efficiency of the cardiac differentiation can be done using cell surface makers without fixation or cardiac specific proteins with fixation.

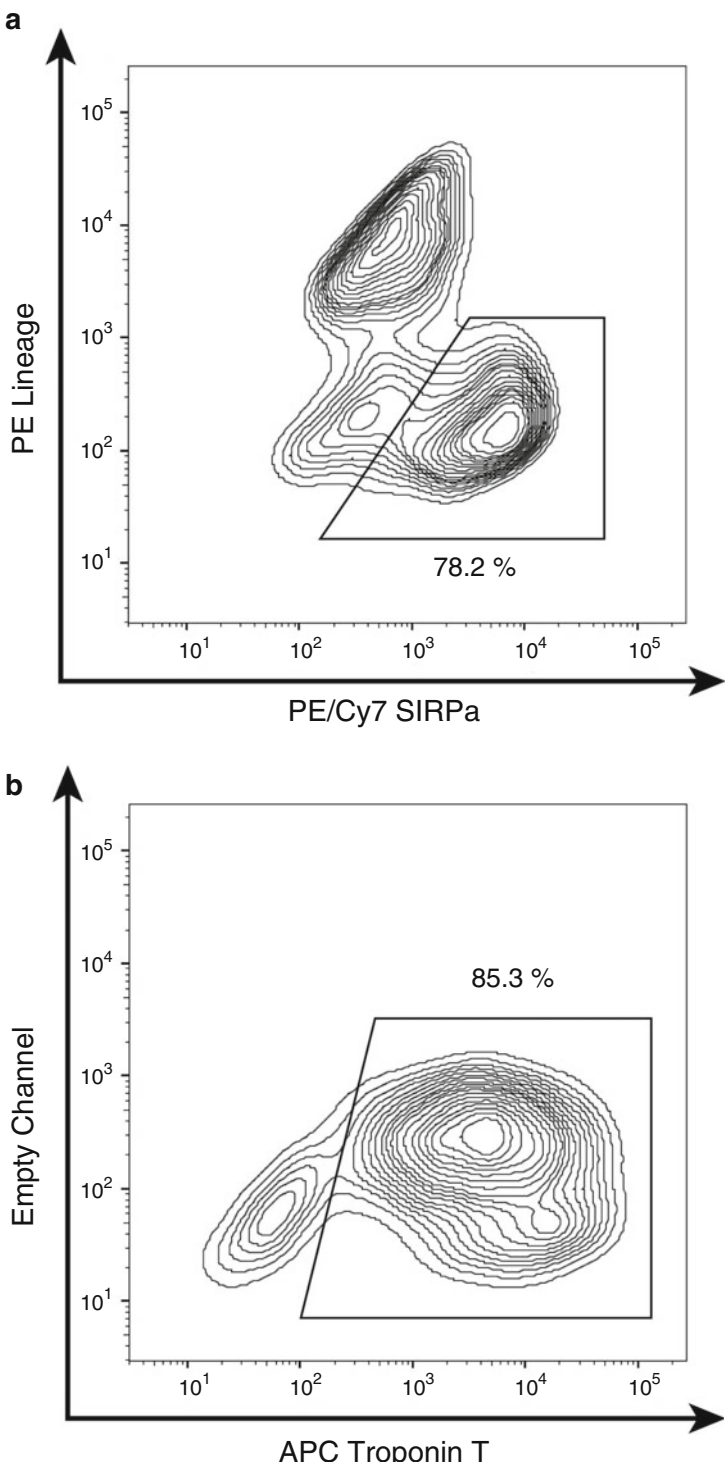


Fig. 3 Characterization of cardiomyocytes produced by EB formation using flow cytometry. **(a)** Flow cytometry analysis shows cardiomyocytes are distributed to the SIRPa (+) Lineage (-) fraction. The cells used in the analysis are day 20 after the start of differentiation. **(b)** Flow cytometry analysis shows cardiomyocytes are distributed to the Troponin T (+) fraction. The cells used in the analysis are day 20 after the start of differentiation

1. After EBs naturally fall, change the media from Differentiation medium 4–2 mg/mL collagenase type I solution containing 10 µg/mL DNase I (e.g., 2 mL to each well of a 6-well plate). Incubate at 37 °C for 3–4 h (*see Note 4*).
2. Transfer the media including the EBs to 15 mL conical tubes. After EBs naturally fall, aspirate the supernatant.
3. Add Accumax (e.g., 1 mL for a 15 mL conical tube) and incubate at 37 °C for 15–20 min. Pipette ~7 times with a 1000 µL pipette to dissociate into single cells (*see Note 4*). Add 6 mL of IMDM to the tube and centrifuge at 120 × g for 5 min.

3.3.1 Characterization of Differentiated Cells Using Cell Surface Markers Without Fixation

1. Aspirate the media from the conical tube and suspend the pellet with 50 µL of flow cytometry buffer containing PE mouse anti-human cardiac lineage antibodies (CD31, CD49a, CD90, and CD140b) and PE/Cy7 mouse anti-human SIRPa (*see Note 9*). The dilution ratio is shown above. Transfer the cell suspension to a 96-well U-bottom plate and incubate at 4 °C for 20–30 min.
2. Centrifuge at 760 × g for 2 min. Aspirate the supernatant and resuspend the pellet with 200 µL of flow cytometry buffer.
3. Centrifuge at 760 × g for 2 min. Aspirate the supernatant and resuspend the pellet with 200 µL of flow cytometry buffer.
4. Analyze with a flow cytometry.

3.3.2 Characterization of Differentiated Cells Using Cardiac Specific Proteins With Fixation

1. Aspirate the media from the conical tube and suspend the pellet with 200 µL of 4% PFA. Transfer the cell suspension to a 96-well U-bottom plate and incubate at room temperature for 30 min.
2. Centrifuge at 760 × g for 2 min. Aspirate the supernatant and resuspend the pellet with 200 µL of DPBS (−).
3. Centrifuge at 760 × g for 2 min. Aspirate the supernatant and resuspend the pellet with 200 µL of DPBS (−).
4. Make permeabilization buffer.
5. Centrifuge at 760 × g for 2 min. Aspirate the supernatant and resuspend the pellet with 200 µL of permeabilization buffer. Incubate at room temperature for 10 min.
6. Centrifuge at 760 × g for 2 min. Aspirate the supernatant and resuspend the pellet with 50 µL of permeabilization buffer and 1:200 dilution of a Troponin T mouse monoclonal primary antibody. Incubate at 4 °C for 30 min.
7. Centrifuge at 760 × g for 2 min. Aspirate the supernatant and resuspend the pellet with 200 µL of permeabilization buffer.

8. Centrifuge at $760 \times g$ for 2 min. Aspirate the supernatant and resuspend the pellet with 50 μ L of permeabilization buffer and 1:100 dilution of an APC goat anti-mouse secondary antibody. Incubate at room temperature for 30 min in dark.
9. Centrifuge at $760 \times g$ for 2 min. Aspirate the supernatant and resuspend the pellet with 200 μ L of flow cytometry buffer.
10. Centrifuge at $760 \times g$ for 2 min. Aspirate the supernatant and resuspend the pellet with 200 μ L of flow cytometry buffer.
11. Analyze with a flow cytometry.

3.4 Estimation of Differentiated Cardiomyocytes with Fluorescent Immunostaining

Day 20 iPSC-derived cardiomyocytes can be evaluated by fluorescent immunostaining using an antibody against Troponin T, as shown in Fig. 4.

1. To coat the wells of a 24-well plate with fibronectin, thaw a fibronectin stock solution and make 50 μ L/mL of fibronectin solution diluted with DPBS (−). Add 200 μ L of fibronectin solution to each well of a 24-well plate. Incubate at room temperature for 1 h.
2. Remove the solution, and add 400 μ L of Differentiation medium 4 containing 10,000–20,000 iPSC-derived cardiomyocytes sorted for SIRPa (+) Lineage (−) using flow cytometry. Incubate at 37 °C for 1 day.
3. Aspirate the medium and rinse the plate once with DPBS (−).
4. Remove the media and add 200 μ L of 4% PFA. Incubate at room temperature for 30 min.

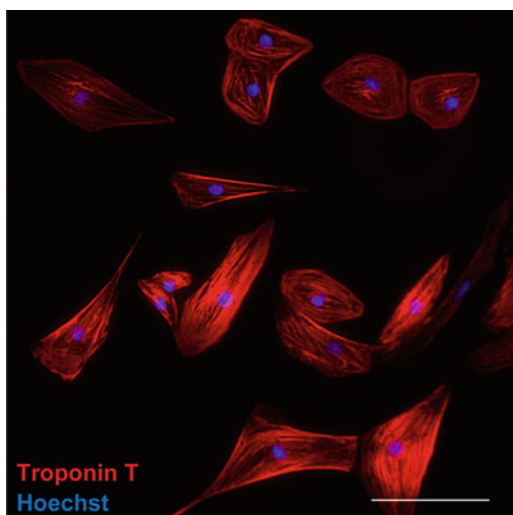


Fig. 4 Characterization of cardiomyocytes produced by EB formation using fluorescent immunostaining. The cells shown here are day 20 from the start of cardiac differentiation. Scale bar: 100 μ m

5. Make blocking buffer.
6. Wash three times with DPBS (-).
7. Add 200 µL of blocking buffer. Incubate at room temperature for 30 min.
8. Aspirate the media and add 200 µL of blocking buffer with 1:200 dilution of Troponin T mouse monoclonal primary antibody. Incubate overnight at 4 °C.
9. Remove the media and wash three times with DPBS (-).
10. Add 200 µL of 0.1% BSA–DPBS (-) with 1:400 dilution of Alexa Fluor 546 goat anti-mouse IgG. Incubate at room temperature for 2 h in dark.
11. Wash once with DPBS (-).
12. Add DPBS (-) with 1:10,000 dilution of Hoechst. Incubate for 20 s.
13. Wash once with DPBS (-).
14. Evaluate by fluorescence microscopy.

4 Notes

1. A SNL feeder dish should be used within 2 days.
2. Suitable growth of pluripotent cells is one of the most important variables for achieving efficient cardiac differentiation.
3. Long time treatment of CTK solution causes lower cardiac differentiation efficiency.
4. The number of pipetting times is one of the most important variables for achieving efficient cardiac differentiation. Adjust the Accumax treatment time and the collagenase treatment time to avoid too much pipetting.
5. Matrigel Matrix hardens at room temperature, and Matrigel Matrix should be added just before use.
6. Cardiomyocyte induction in 5% O₂ (hypoxic) incubator in the first 10 days promotes a higher efficiency in the cardiac differentiation.
7. Almost all iPSC lines can achieve efficient cardiac differentiation without using SB431542 or dorsomorphin. However, some iPSC lines achieve more efficient cardiac differentiation with addition of SB431542 and dorsomorphin to Differentiation medium 3 [6].
8. The number of cells making an EB is also one of the most important variables for achieving efficient cardiac differentiation. Reaggregation of EBs at day 3 contributes to uniformed size of EBs and efficient cardiac differentiation.

9. There is no specific antibody against cardiac cell surface. Instead, a combination of several cell surface makers, such as SIRPa and Lineage, is used to purify cardiomyocytes [8, 9]. As a result, contamination by noncardiomyocytes is a concern. We have succeeded in purifying iPSC-derived cardiomyocytes using cardiomyocyte-specific microRNA [10]. We also showed that iPSC-derived cardiomyocytes on day 20 after starting the differentiation have the highest engraftment rate in a myocardial infarction mouse model [11].

Acknowledgments

We greatly appreciate colleagues at our laboratories and the Department of Cardiovascular Medicine, Kyoto University. We thank Gordon Keller, Mark Gagliardi, Shunsuke Funakoshi, and Chikako Okubo for providing valuable advice and support for the differentiation method of cardiomyocytes, Ikue Takei, Misato Nishikawa, Azusa Inagaki, and Megumi Narita for technical support, and Peter Karagiannis for proofediting. We would like to express our heartfelt gratitude to Yoko Uematsu for her administrative support.

References

1. Burridge PW, Keller G, Gold JD et al (2012) Production of de novo cardiomyocytes: human pluripotent stem cell differentiation and direct reprogramming. *Cell Stem Cell* 10:16–28
2. Mummery CL, Zhang J, Ng ES et al (2012) Differentiation of human embryonic stem cells and induced pluripotent stem cells to cardiomyocytes: a methods overview. *Circ Res* 111:344–358
3. Protze SI, Liu J, Nussinovitch U et al (2017) Sinoatrial node cardiomyocytes derived from human pluripotent cells function as a biological pacemaker. *Nat Biotechnol* 35:56–68
4. Lee JH, Protze SI, Laksman Z et al (2017) Human pluripotent stem cell-derived atrial and ventricular cardiomyocytes develop from distinct mesoderm populations. *Cell Stem Cell* 21:179–194.e4
5. Yang L, Soonpaa MH, Adler ED et al (2008) Human cardiovascular progenitor cells develop from a KDR+ embryonic-stem-cell-derived population. *Nature* 453:524–528
6. Kattman SJ, Witty AD, Gagliardi M et al (2011) Stage-specific optimization of activin/nodal and BMP signaling promotes cardiac differentiation of mouse and human pluripotent stem cell lines. *Cell Stem Cell* 8:228–240
7. Willemse E, Spiering S, Davidovics H et al (2011) Small-molecule inhibitors of the Wnt pathway potently promote cardiomyocytes from human embryonic stem cell-derived mesoderm. *Circ Res* 109:360–364
8. Dubois NC, Craft AM, Sharma P et al (2011) SIRPA is a specific cell-surface marker for isolating cardiomyocytes derived from human pluripotent stem cells. *Nat Biotechnol* 29:1011–1018
9. Elliott DA, Braam SR, Koutsis K et al (2011) NKX2-5(eGFP/w) hESCs for isolation of human cardiac progenitors and cardiomyocytes. *Nat Methods* 8:1037–1040
10. Miki K, Endo K, Takahashi S et al (2015) Efficient detection and purification of cell populations using synthetic MicroRNA switches. *Cell Stem Cell* 16:699–711
11. Funakoshi S, Miki K, Takaki T et al (2016) Enhanced engraftment, proliferation, and therapeutic potential in heart using optimized human iPSC-derived cardiomyocytes. *Sci Rep* 6:19111



Chapter 7

Measuring Cardiomyocyte Contractility and Calcium Handling In Vitro

Przemek A. Gorski, Changwon Kho, and Jae Gyun Oh

Abstract

In vitro measurements of cardiomyocyte contractility and Ca^{2+} handling have been used as a platform for determining physiological consequence of various genetic manipulations and identifying potential therapeutic targets for the treatment of heart failure. The Myocyte Calcium and Contractility System (IonOptix) offers a simultaneous trace of sarcomere movements and changes of intracellular Ca^{2+} levels in a single cardiomyocyte. Herein, we describe a modified protocol for the isolation of adult cardiomyocytes from murine hearts and provide a step-by-step description on how to analyze cardiomyocyte Ca^{2+} transient and contractility data collected using the IonOptix system. In our modified protocol, we recommend a novel cannulation technique which simplifies this difficult method and leads to improved viability of isolated cardiomyocytes. In addition, a comprehensive analysis of intracellular Ca^{2+} handling, SR Ca^{2+} load, myofilament Ca^{2+} sensitivity, and cardiomyocyte contractility is described in order to provide important insights into myocardial mechanics.

Key words Intracellular calcium, Calcium handling, Cardiomyocyte, Contractility, Heart disease

1 Introduction

Intracellular calcium (Ca^{2+}) cycling plays a critical role in regulating systolic and diastolic function of cardiomyocytes [1, 2]. Numerous ion channels, transporters, and other intracellular Ca^{2+} handling proteins are involved in maintaining proper Ca^{2+} homeostasis and defects in these essential molecules often result in a severe malfunction of cardiomyocytes [3–6]. Therefore, analyses of Ca^{2+} handling in healthy and disease conditions can greatly advance our understanding of cardiac disease. Due to the lack of suitable immortalized cardiac cell lines and significant limitations of neonatal cardiomyocytes, isolated adult cardiomyocytes provide a powerful platform for studying cardiac dysfunction and complement murine models of heart disease [7–11].

In the present protocol, we describe a fast and reproducible method for isolating adult murine cardiomyocytes and provide

instructions on how to obtain a variety of measurements of cardiomyocyte contractility and Ca^{2+} handling using the Myocyte Calcium and Contractility System (IonOptix). Standard analysis of Ca^{2+} handling and cardiomyocyte contraction, evaluation of the sarcoplasmic reticulum (SR) Ca^{2+} reserve and the rate of diastolic Ca^{2+} removal, as well as the assessment of myofilament Ca^{2+} sensitivity are discussed in detail. Such measurements can be utilized in a variety of experimental settings to study the effects of small molecules, environmental stressors, infections, or genetic manipulations on cardiomyocyte function. Together, the use of these techniques may provide important mechanistic insights into Ca^{2+} -related signaling pathways and physiologically relevant characterization of cardiac disease.

2 Materials

2.1 Drugs

1. Heparin sodium: 1000 units/mL.
2. Ketamine–xylazine cocktail: ketamine and xylazine, at a ratio of 5:1, e.g., 65/13 mg/kg.

2.2 Equipment

1. Delicate suture tying forceps (2×): length: 9 cm, tip dimensions: 0.4 × 0.3 mm, curved.
2. Extra fine Graefe forceps (2×): length: 10 cm, tip dimensions: 0.5 × 0.5 mm, straight.
3. Spring scissors: length: 10 cm, tip diameter: 0.2 mm, cutting edge: 8 mm, straight.
4. Fine scissors: length: 10.5 cm, cutting Edge: 26 mm, straight.
5. Surgical suture: silk, 4-0.
6. Homemade perfusion cannula: *See Fig. 1c*.
7. Homemade cannula holder: *See Fig. 1c*.
8. Cell Strainer: Nylon, 100 μm pore size.

2.3 Apparatus

1. Dissecting microscope: Zoom range 1–8×.
2. Fluidic inline heater: internal dead volume is 35 $\mu\text{L}/\text{tubing}$.
3. Syringe pump: for caffeine injection.
4. Langendorff system: constant flow model (3 mL/min).
5. The Myocyte Calcium and Contractility System (IonOptix).

2.4 Solutions

1. Tyrode solution: 125 mM NaCl, 5 mM KCl, 2 mM NaH_2PO_4 , 1.2 mM MgSO_4 , 5 mM pyruvate, 11 mM glucose, 5 mM creatine, 5 mM L-carnitine, 5 mM taurine, 10 mM 2,3-butanedione-monoxime (BDM), 25 mM HEPES, pH 7.2.

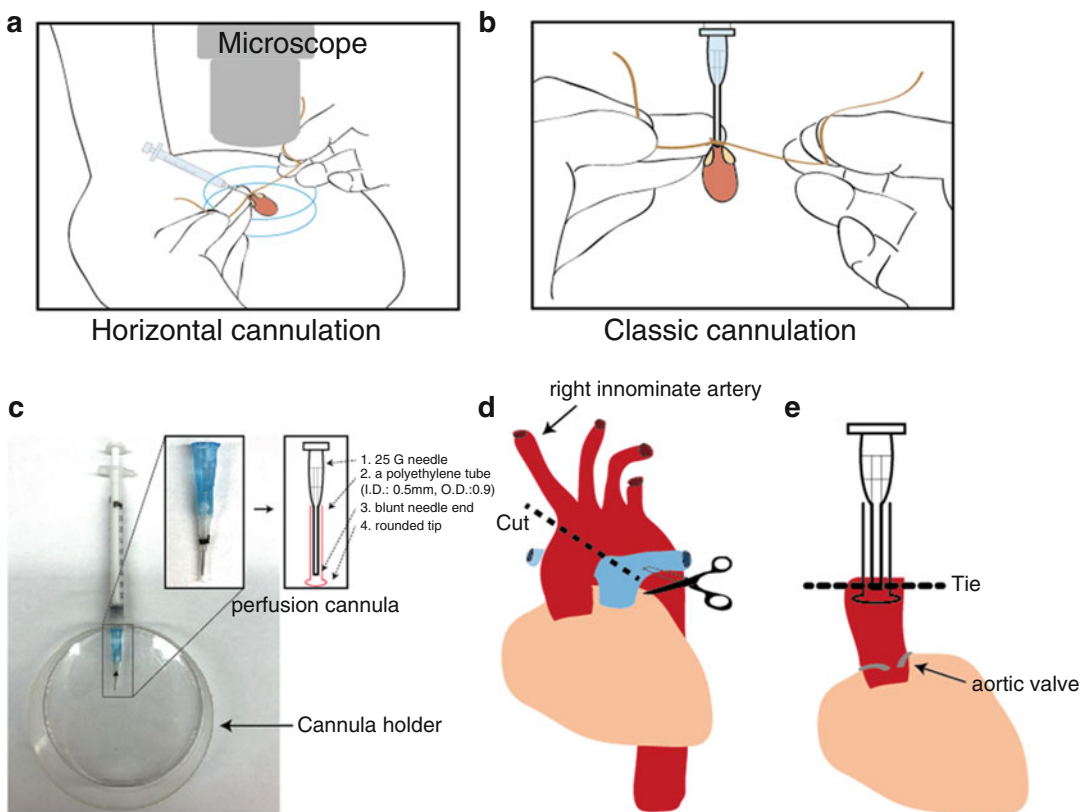


Fig. 1 General overview of the cannulation procedure. (a) Illustration of the horizontal cannulation setup described herein and (b) the commonly used (classic) cannulation setup. (c) A detailed schematic of the homemade horizontal cannulation apparatus. (d) Schematic diagram of a mouse heart illustrating the location of where the aortic arch should be cut off and (e) a proper ligation of the aorta to the Langendorff perfusion cannula

2. Enzyme solution: 250 units/mL Collagenase type B, 60 units/mL Hyaluronidase, Tyrode solution.
3. Ca^{2+} buffer: 1.2 mM CaCl_2 , Tyrode solution.
4. Blocking solution: 5% bovine serum albumin (BSA), Tyrode solution.
5. Caffeine solution: 10 mM caffeine, Tyrode solution.
6. Coating solution: 5 $\mu\text{g}/\text{mL}$ laminin, PBS.
7. Fura-2 AM (acetoxymethyl ester form): 1 μM Fura-2 AM, Ca^{2+} buffer.
8. PBS (regular phosphate-buffered saline): 137 mM NaCl, 2.7 mM KCl, 10 mM Na_2HPO_4 , 1.8 mM KH_2PO_4 , pH 7.4.
9. Culture medium: 0.1% bovine serum albumin (BSA), 1× insulin–transferrin–selenium (ITS), 10 mM BDM, 1× CD lipid (chemically defined lipid concentrate), 1× penicillin/streptomycin solution, M199 medium.

3 Methods

3.1 Isolation and Culture of Cardiomyocytes

1. Inject mouse with 150 units of heparin sodium into the peritoneal cavity.
2. Anesthetize mouse via intraperitoneal injection of ketamine–xylazine. After few minutes, confirm that the animal is fully anesthetized by the lack of toe pinch reflex.
3. Open the abdominal cavity under the xiphoid process with surgical scissors, lift the xiphoid process and open the chest. After cutting the inferior vena cava, inject Tyrode solution into the left ventricular apical region to remove blood from the chamber (*see Note 1*). Remove the pericardium, slightly lift the heart with curved forceps, identify the aortic arch, and excise the heart from the root of the aorta. Place the heart into a dish of ice-cold PBS.
4. Hold the aorta with two microdissecting forceps and mount it onto the Langendorff perfusion cannula (Fig. 1). Firmly ligate the aorta onto the cannula using surgical sutures (*see Notes 2 and 3*).
5. Transfer cannulated heart onto the Langendorff perfusion apparatus. Inspect the tubing and the cannulation needle to make sure there are no bubbles trapped in the perfusion system (*see Note 4*).
6. Perfusion the heart with Tyrode solution for 5 min at a rate of 3 mL/min. Switch the buffer to the enzyme solution and perfuse for 20 min (*see Note 5*).
7. Use forceps to grab the aorta and transfer the digested heart into a dish full of fresh blocking solution. Cut off the atria, the right ventricle and the atrioventricular junction area, leaving only the left ventricle (*see Note 6*).
8. Use fine scissors and forceps to cut the left ventricle into smaller pieces (~10 mm). Gently pipette the cell suspension up and down using a sterile 5 mL pipette to further dissociate the tissue.
9. Filter the cell suspension through a 100 µm nylon mesh filter into a 15 mL conical tube. Centrifuge at $50 \times g$ for 60 s and discard the supernatant (*see Note 7*).
10. Resuspend the cell pellet in a desired volume of culture media (10 mL) and plate the cell suspension on laminin-coated coverslips in an appropriate sized dish. Incubate at 37 °C and 2% CO₂ for 60 min to allow the cells to equilibrate and adhere to coverslips.
11. Remove plating media from the dish and replace with culture media. Depending on the experimental conditions, cardiomyocytes can be cultured for up to 72 h (Fig. 2).

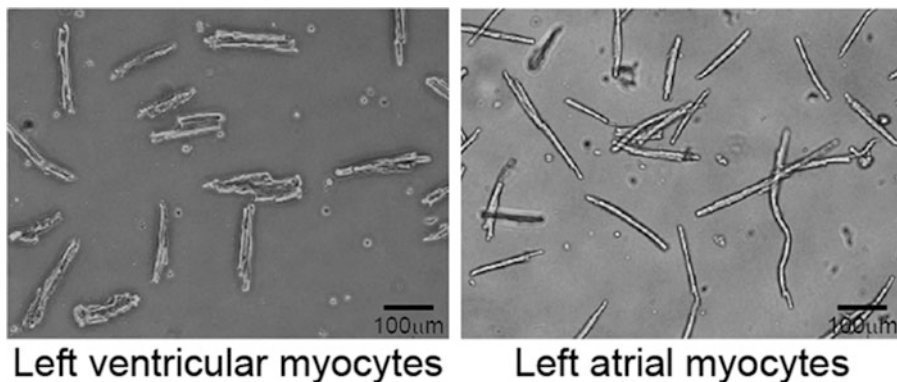


Fig. 2 Representative example of ventricular and atrial myocytes

3.2 Simultaneous Measurements of Intracellular Ca^{2+} Transients and Contractility

1. Power the IonOptix system ensuring that the arc lamp is initiated first.
2. Prime the buffer circulation system with Ca^{2+} buffer. Temperature should be held at 37 °C throughout the experiment using the fluidic inline heater.
3. Incubate cardiomyocytes with Fura-2 AM (1 μM) for 10 min (*see Note 8*).
4. Mount a glass coverslip with cardiomyocytes into the perfusion chamber and fasten.
5. Start perfusing the chamber (1.5 mL/min) with Ca^{2+} buffer and pace cardiomyocytes with 1 Hz field stimulation using MyoPacer field stimulator (10 V, 4 ms) for 5 min.
6. Use 40× objective lens to select a healthy cardiomyocyte (rod shape, sharp edge, clear cross striations, and no spontaneous contraction) for recording.
7. Center the selected cardiomyocyte in the field of view, line it up horizontally, and minimize the background area by adjusting the cell framing adapter. Adjust the focus of the microscope until sarcomere striations are clearly visible.
8. To measure cardiomyocyte shortening/relengthening, two recording tasks are available in the IonOptix system (*see Note 9*):
 - (a) Sarcomere length recording task: Align the sarcomere zone control (purple rectangular box) on an area of the cardiomyocyte containing well-defined sarcomeres and adjust the focus to optimize the peak of the power spectrum (red peak).
 - (b) Cell length recording task: Align the red and green selection lines on both edges which clearly show contrast between the cell edge and the background. Check whether the cursor indicates the edge during contraction.

9. Record the changes of sarcomere/cell length (15–20 stable contractions) under field stimulation. Since the IonOptix system provides simultaneous measurements of the change in the sarcomere/cell length of cardiomyocytes and Ca^{2+} recording of the Fura-2 AM fluorescence (excitation at 360/380 nm and emission at 510 nm), no additional set up is necessary to obtain Ca^{2+} transient data.

3.3 Analysis of Cardiomyocyte Contractility and Ca^{2+} Handling

Once the Ca^{2+} transients and contractility traces are acquired, data are analyzed with the IonWizard software according to the following instructions:

1. Create an ensemble average from 10 to 20 traces by selecting “Average Events” from the “Operations” pull-down menu (Fig. 3a).
2. Exclude any abnormal traces from the source data using inclusion indicators. Any bars drawn in red represent traces excluded from the current average (Fig. 3b).
3. Select the duration/end time to be analyzed in the ensemble average trace using transient mark editor.
4. Click the trace analysis button (M Tran) to analyze the ensemble average trace (Fig. 3c).
5. Contractility can be analyzed in a variety of ways:

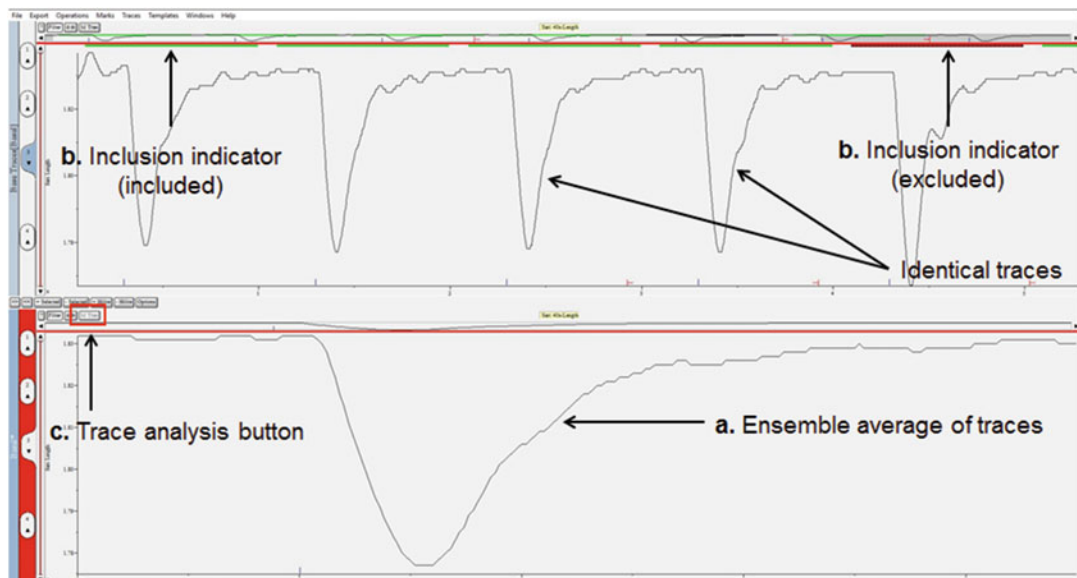


Fig. 3 Representative example of sarcomeric length measurement using the IonOptix system. (top panel) Sarcomere length tracing showing traces included and excluded (b) from the analysis. (bottom panel) Ensemble average of selected contractility traces (a) shown in the top panel. (c) Trace analysis button is indicated

For systolic function, one can assess the magnitude of contraction with fractional shortening or speed of contraction with time to peak shortening (bl% peak h, Fig. 4a), and maximal contraction velocity (dep v, Fig. 4b). Diastolic function can be analyzed by calculating time to 50% relaxation (t to bl 50%, Fig. 4c) and relaxation velocity (ret v, Fig. 4d).

6. For calcium transient analysis, baseline (bl, Fig. 4e), Ca^{2+} amplitude (peak h, Fig. 4f), tau (sin exp tau, Fig. 4g), and time to 50% baseline (t to bl 50%, Fig. 4h) parameters can be used to compare different data sets.

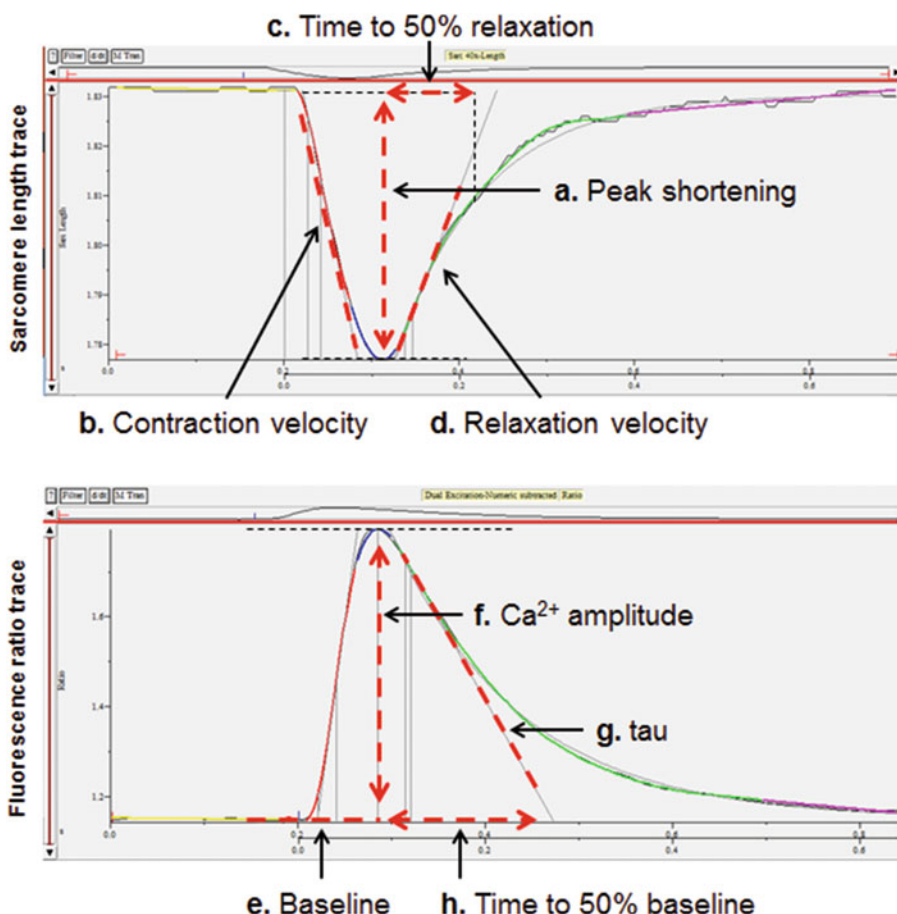


Fig. 4 (top panel) Ensemble average of contractility tracings after analysis. (a) Peak shortening, (b) contraction velocity, (c) time to 50% relaxation, and (d) relaxation velocity parameters are indicated. (bottom panel). Ensemble average of calcium transients after analysis. (e) Baseline, (f) Ca^{2+} amplitude, (g) tau, and (h) time to 50% baseline parameters are indicated

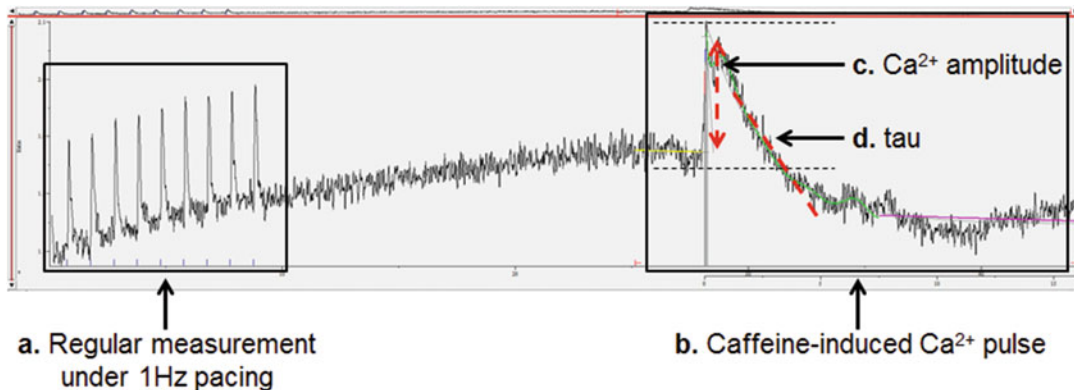


Fig. 5 Representative calcium transient trace from a SR Ca²⁺ reserve and diastolic Ca²⁺ removal measurement. (a) Initial phase of the experiment during which cardiomyocytes are paced at 1 Hz. (b) Ca²⁺ transient after the addition of caffeine into the system. (c) Ca²⁺ amplitude and (d) tau parameters are indicated

3.4 Assessment of SR Ca²⁺ Reserve and Diastolic Ca²⁺ Removal

Here, we describe how to record caffeine-induced Ca²⁺ pulses in isolated cardiomyocytes that can be used to extrapolate data which primarily reflect the contribution of SERCA2a and NCX to diastolic Ca²⁺ removal [12–14].

1. Prime a syringe pump with 60 µL of 80 mM caffeine solution (final caffeine concentration is 10 mM).
2. Start the recording and measure basal Ca²⁺ transient and contractility at 1 Hz pacing with Ca²⁺ buffer for 30 s (Fig. 5a).
3. Pause the recording and carefully adjust the position of the micropipette tip filled with caffeine solution nearby the target cardiomyocyte.
4. Resume the recording and inject caffeine solution rapidly.
5. To analyze caffeine-induced Ca²⁺ pulses (Fig. 5b), select only the pulse with a steep wave for analysis of the calcium removal function.
6. Measure the amplitude of the caffeine-induced Ca²⁺ pulse (peak h, Fig. 5c), indicating SR Ca²⁺ reserve.
7. Obtain the decay time constant of caffeine-induced Ca²⁺ pulse (sin exp tau, Fig. 5d), indicating NCX activity.

3.5 Assessment of Myofilament Ca²⁺ Sensitivity

Here, we describe a protocol used to assess the changes in myofilament Ca²⁺ sensitivity in isolated adult mouse cardiomyocytes.

1. Measure Ca²⁺ transients and contractility as described in Subheading 3.2.
2. Average the sarcomere length and Ca²⁺ transient data at steady-state (10–20 traces) and plot the phase-plane loop of the changes in sarcomere shortening vs. intracellular Ca²⁺ levels (Fig. 6).

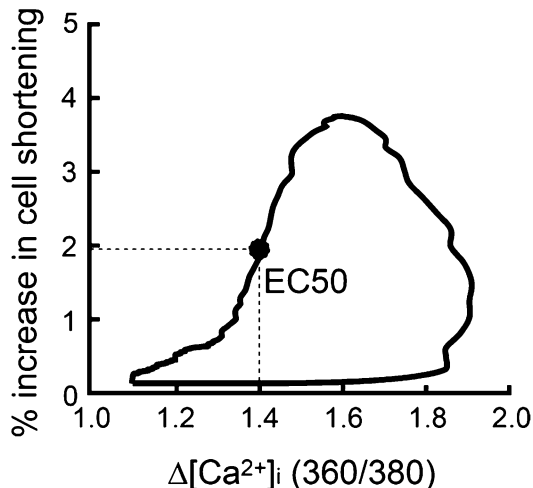


Fig. 6 Phase-plane plot of the delta changes in sarcomere shortening vs. intracellular Ca^{2+} level (Fura-2 ratio, 360/380) with the EC_{50} value (intracellular Ca^{2+} level at 50% sarcomere shortening) indicated

3. In each plot, define intracellular Ca^{2+} level at 50% sarcomere shortening (EC_{50}). Compare the loop plot and EC_{50} values for each condition to assess myofilament Ca^{2+} sensitivity between the tested groups (see Note 10).

4 Notes

1. Injection of Tyrode solution into the left ventricular apical region improves enzyme digestion of the heart by reducing the possibility of blood clotting inside the coronary artery.
2. In this protocol, horizontal cannulation is highly recommended as it presents several advantages over the classic (vertical needle insertion) cannulation method (Fig. 1a, b). First, the horizontal cannulation procedure can be performed under a dissecting microscope, which allows for easy visualization of the aorta leading to improved mounting onto the perfusion cannula. Second, cannulation time can be minimized down to 1 min increasing the yield of healthy cardiomyocytes. Moreover, the horizontal cannulation gives a chance to check the condition of cannulation and rectify it. The condition of cannulation can be tested by perfusing Tyrode solution through the cannula. If cannulation is successful, blood is removed from the coronary artery. If the blood vessel that was mounted on the needle is not the aorta, the cannulation procedure must be repeated. Finally, horizontal cannulation reduces strain on the heart during mounting, allowing for easier and more accurate tying of the surgical suture to the cannulation needle.

3. For cannulation of mouse hearts, blunt end needle (25 G) covered with a polyethylene tube (I.D.-0.50 mm, O.D.-0.90 mm) is used (Fig. 1c). The distal tip of the tube is rounded by high heat. Alternatively, a commercial animal-feeding needle (24G) can be used. The rounded polyethylene tube or the animal feeding needle will allow to secure the suture over the groove and prevent the heart from slipping off the cannula during perfusion.
4. Before cannulation make sure to trim the aorta as indicated in Fig. 1d (ideally below the aortic root distal to the right innominate artery). It is important to ensure that the end of the needle rests in the ascending aorta but that it does not extend through the aortic valve into the left ventricle (Fig. 1e).
5. The heart should appear scarlet over time indicative of proper enzyme digestion of the connective tissue. The perfusion should be stopped if the color of the heart turns pale as this means that cardiomyocytes have already started dying. At this point it is best to start the isolation again using another mouse heart.
6. It is important to note that the cell morphology and functional properties of cardiomyocytes differ significantly depending on the source. Therefore, before dissociating the heart tissue with forceps, it is possible to separate the heart into respective chambers in order to isolate chamber specific cardiomyocytes as desired (Fig. 2).
7. The supernatant contains nonmyocyte cells, including cardiac fibroblasts. To culture primary cardiac fibroblasts, centrifuge the supernatant at $500 \times g$ for 10 min and discard the supernatant (cell debris). Resuspend the cell pellet in 5% serum medium and plate the suspension onto cell culture dishes (uncoated). Incubate at 37°C in a cell culture incubator with 5% CO_2 for 2 h (preplating). At this time viable and healthy fibroblasts should have adhered to the dish. Check the cell confluence under the microscope (It should be around 50%). Fibroblasts should resemble small spherical bodies.
8. Fura-2 is light-sensitive. Perform all loading procedures and experiments in the dark.
9. The IonOptix system offers two methods to measure contractility: one based on measuring the changes of the total cardiomyocyte length and second based on the changes of sarcomere length. Total cardiomyocyte length measurements trace the movement of the two distal cell edges. Some studies report increases in the full length of cardiomyocytes at diastole as an index of cardiac hypertrophy [15, 16]. However, the length of cardiomyocytes from different compartments of the heart (e.g., atrium vs. ventricle) varies significantly. Usually, the

variability is higher than the changes in cell length due to hypertrophy. Therefore, using cardiomyocyte length as an index of cardiac hypertrophy is not recommended. If necessary, cardiomyocyte isolation from only one part of the heart (e.g., septum only) should be performed to minimize diversity in cell length. Another method to measure contractility is based on tracing the movement of sarcomere length. The average sarcomere length of healthy cardiomyocytes at diastole is 1.8 μm . If the cardiomyocyte isolation is not successful and the viability of cells is low, the intracellular Ca^{2+} is increased in diastole leading to shortening of the sarcomere length ($\sim 1.5 \mu\text{m}$). Therefore, routine monitoring of the sarcomere length should be helpful to maintain the consistency between Ca^{2+} transient and contractility measurements.

10. Higher EC_{50} value and a rightward shift of the loop trajectory are indicative of myofilament Ca^{2+} desensitization. This process is primarily caused by changes in the phosphorylation status of TnI and myobinding protein C which greatly affects myofilament's ability to bind Ca^{2+} [17–19].

Acknowledgments

PAG is supported by a fellowship from the Canadian Institutes of Health Research. JGO is supported by a fellowship from the American Heart Association (17POST33410877).

References

1. Fearnley CJ, Roderick HL, Bootman MD (2011) Calcium signaling in cardiac myocytes. *Cold Spring Harb Perspect Biol* 3:a004242
2. Kho C, Lee A, Hajjar RJ (2012) Altered sarco-plasmic reticulum calcium cycling: targets for heart failure therapy. *Nat Rev Cardiol* 12:717–733
3. Ather S, Respress JL, Li N, Wehrens XH (2013) Alterations in ryanodine receptors and related proteins in heart failure. *Biochim Biophys Acta* 1832:2425–2431
4. Despa S, Bers DM (2013) $\text{Na}(+)$ transport in the normal and failing heart: remember the balance. *J Mol Cell Cardiol* 61:2–10
5. Park WJ, Oh JG (2013) SERCA2a: a prime target for modulation of cardiac contractility during heart failure. *BMB Rep* 46:237–243
6. Shaw RM, Colecraft HM (2013) L-type calcium channel targeting and local signalling in cardiac myocytes. *Cardiovasc Res* 98:177–186
7. Chloupkova S, Psotova J, Miketova P (2001) Neonatal rat cardiomyocytes: a model for the study of morphological, biochemical and electrophysiological characteristics of the heart. *Biomed Pap Med Fac Univ Palacky Olo-mouc Czech Repub* 145:49–55
8. Haworth RA (1990) Use of isolated adult myocytes to evaluate cardiotoxicity. II. Preparation and properties. *Toxicol Pathol* 18:521–530
9. Haworth RA, Goknur AB, Cook MG, Decker RS (1990) Use of isolated adult myocytes to evaluate cardiotoxicity. I. Sugar uptake and protein synthesis. *Toxicol Pathol* 18:511–520
10. Lieu DK, Liu J, Siu CW, McNerney GP, Tse HF, Abu-Khalil A, Huser T, Li RA (2009) Absence of transverse tubules contributes to non-uniform $\text{Ca}(2+)$ wavefronts in mouse and human embryonic stem cell-derived cardiomyocytes. *Stem Cells Dev* 18:1493–1500

11. Simko F, Turcani M, Fizel A, Fizel'ova A (1986) The isolated cardiomyocyte: a prospective model for the experimental study of the heart muscle. *Cesk Fysiol* 35:414–428
12. Choi KM, Zhong Y, Hoit BD, Grupp IL, Hahn H, Dilly KW, Guatimosim S, Lederer WJ, Matlib MA (2002) Defective intracellular Ca(2+) signaling contributes to cardiomyopathy in type 1 diabetic rats. *Am J Physiol Heart Circ Physiol* 283:H1398–H1408
13. Yi T, Vick JS, Vecchio MJ, Begin KJ, Bell SP, Delay RJ, Palmer BM (2013) Identifying cellular mechanisms of zinc-induced relaxation in isolated cardiomyocytes. *Am J Physiol Heart Circ Physiol* 305:H706–H715
14. Oh JG, Kim J, Jang SP, Nguen M, Yang DK, Jeong D, Park ZY, Park SG, Hajjar RJ, Park WJ (2012) Decoy peptides targeted to protein phosphatase 1 inhibit dephosphorylation of phospholamban in cardiomyocytes. *J Mol Cell Cardiol* 56:63–71
15. Wei H, Jin JP (2014) A dominantly negative mutation in cardiac troponin I at the interface with troponin T causes early remodeling in ventricular cardiomyocytes. *Am J Physiol Cell Physiol* 307:C338–C348
16. Yu ZB, Wei H, Jin JP (2012) Chronic coexistence of two troponin T isoforms in adult transgenic mouse cardiomyocytes decreased contractile kinetics and caused dilatative remodeling. *Am J Physiol Cell Physiol* 303:C24–C32
17. Kunst G, Kress KR, Gruen M, Uttenweiler D, Gautel M, Fink RH (2000) Myosin binding protein C, a phosphorylation-dependent force regulator in muscle that controls the attachment of myosin heads by its interaction with myosin S2. *Circ Res* 86:51–58
18. Oh JG, Jeong D, Cha H, Kim JM, Lifirsu E, Kim J, Yang DK, Park CS, Kho C, Park S et al (2012) PICOT increases cardiac contractility by inhibiting PKCzeta activity. *J Mol Cell Cardiol* 53:53–63
19. Varian KD, Raman S, Janssen PM (2006) Measurement of myofilament calcium sensitivity at physiological temperature in intact cardiac trabeculae. *Am J Physiol Heart Circ Physiol* 290:H2092–H2097

Part IV

Ex Vivo Models



Chapter 8

Langendorff Perfusion Method as an Ex Vivo Model to Evaluate Heart Function in Rats

Makino Watanabe and Takao Okada

Abstract

The Langendorff Perfused Heart Model is an experimental procedure developed at the end of the nineteenth century by Oskar Langendorff. In this procedure, an excised heart has a cannula inserted into its aorta so that the heart can be retrogradely perfused via the coronary artery. The procedure has been improved in recent times, and these improvements are used to evaluate the direct effect of medication on the heart as well as the effect of ischemia–reperfusion injury on heart function. In this chapter, we describe protocols for evaluating heart function in Langendorff perfused rat heart.

Key words Langendorff perfusion, Rat heart, Heart function, Heart rate, Left ventricular pressure, Coronary perfusion pressure, Irreversible cardiac damage

1 Introduction

The Langendorff perfused heart model is an experimental procedure developed at the end of the nineteenth century by the German physiologist, Oskar Langendorff [1]. His experimental procedure was modified, and various types of animal species have been examined using the modified protocols, including rats, mice, guinea pigs, ferrets, dogs, cats, and other animals. Oxygenated physiological buffer is retrogradely perfused through the coronary artery via the aorta of an excised heart. During the experiment, heart functions such as heart rate (HR), left ventricular developed pressure (LVDP), and electrocardiographic data can be recorded. Although the Langendorff perfusion experiment is not a novel technique, it is well established, simple, and easy. This allows evaluation of heart function in isolated heart without the effects of neuroreflexes and humoral factors, which enables its use for the evaluation of the direct effects of medications on heart function, drug screening, as well as evaluation of the effects of ischemia–reperfusion (I/R) injury on heart function. The present chapter explicates our preparation method and general recording parameters using our

constant-flow isolated perfused rat heart model as an example. The same procedure can be performed on other animals as well. The experimental equipment and perfusion device will basically remain the same; however, changes in size may be necessary depending on the size of the animal (*see Note 1*).

There are reports on electrocardiogram and cardiac action potential recording in Langendorff perfused ex vivo hearts by other researchers [2, 3]. Differences in voltage potentials between the aortic root as the negative pole and the apex as the positive pole can be measured, and a waveform resembling that of a lead II electrocardiogram in human can be recorded. Furthermore, monophasic action potential can be recorded by mounting electrodes onto the surface of the heart. These techniques are very useful to evaluate the drug influences on cardiac excitation conduction.

2 Materials

Experimental buffers used in the experiment are prepared with deionized distilled water (DDW). The reagents to be used should be of high quality.

2.1 Buffers

Table 1 shows the composition of Modified Krebs–Henseleit buffer, and its recipe for 4× concentration stock buffer solution. When preparing the buffer solution, dilute the stock buffer solution (Table 1) four times. Add 2 mL/L CaCl₂ solution (1 mol/L) last (*see Note 2*). The amount of experimental buffer necessary for experiment depends on the number of animals, time of the experimental protocol and flow rate.

Table 1
Composition of Modified Krebs–Henseleit buffer, and its recipe for 5 L of 4× concentration stock buffer solution

	MW	Final conc. (mM)	g (for 5 L)
NaCl	58.44	110.0 (90.0)	128.57 (105.19)
NaHCO ₃	84.01	25.0	42.01
MgSO ₄ /7H ₂ O	246.48	1.2	5.916
KH ₂ PO ₄	136.09	1.2	3.266
KCl	74.56	4.7	7.009
Glucose	180.16	5.5	19.818
(Sucrose)	342.3	5.5	37.653

Numbers in NaCl bottom line indicate the concentration and amount for stock dissecting solution. For hypoxic perfusion, replace glucose with equimolar sucrose

1. Modified Krebs–Henseleit buffer (Table 1): NaCl 110.0 mM, NaHCO₃ 25.0 mM, MgSO₄ 1.2 mM, KH₂PO₄ 1.2 mM, KCl 4.7 mM, CaCl₂ 2.0 mM, glucose 5.5 mM. Adjust pH to 7.4 using hydrochloric acid (HCl). Saturate the solution by bubbling it with mixed gas (95% O₂–5% CO₂). For hypoxic perfusion, replace glucose with equimolar sucrose and bubble it with 95% N₂–5% CO₂.
2. Dissecting solution: NaCl 90.0 mM, NaHCO₃ 25.0 mM, MgSO₄ 1.2 mM, KH₂PO₄ 1.2 mM, KCl 24.7 mM, CaCl₂ 2.0 mM, glucose 5.5 mM (*see Note 3*). To prevent blood clot formation, add 1 mL/L of heparin and adjust pH to 7.4 using HCl. Saturate the solution by bubbling it with mixed gas (95% O₂–5% CO₂). Although it depends on the cannulation and trimming time, approximately 500 mL dissecting solution is required for three rat hearts.

2.2 Cannulation and Trimming Materials

1. An irrigator (*see Note 4*).
2. A chamber (*see Fig. 1*).
3. An auxiliary clip for fixing the cannula (*see Fig. 1*).
4. An arterial cannula (*see Note 5* and Fig. 2).
5. 3-0 silk suture.

2.3 Langendorff System (Fig. 3)

1. Two peristaltic pumps (*see Note 6*).
2. Two pressure transducers (for measuring LV pressure and coronary perfusion pressure).
3. Two pressure amplifiers (for measuring LV pressure and coronary perfusion pressure).
4. Data acquisition system or polygraph.
5. A bubble trap.
6. A heart chamber.

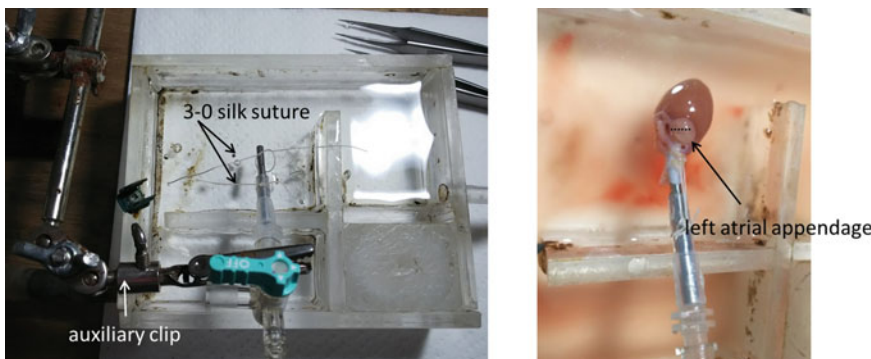


Fig. 1 Chamber used for cannulation (left panel), and cannulated heart (right panel). In the right panel, dotted line indicates the position of incision site on the left atrial appendage for LV balloon insertion

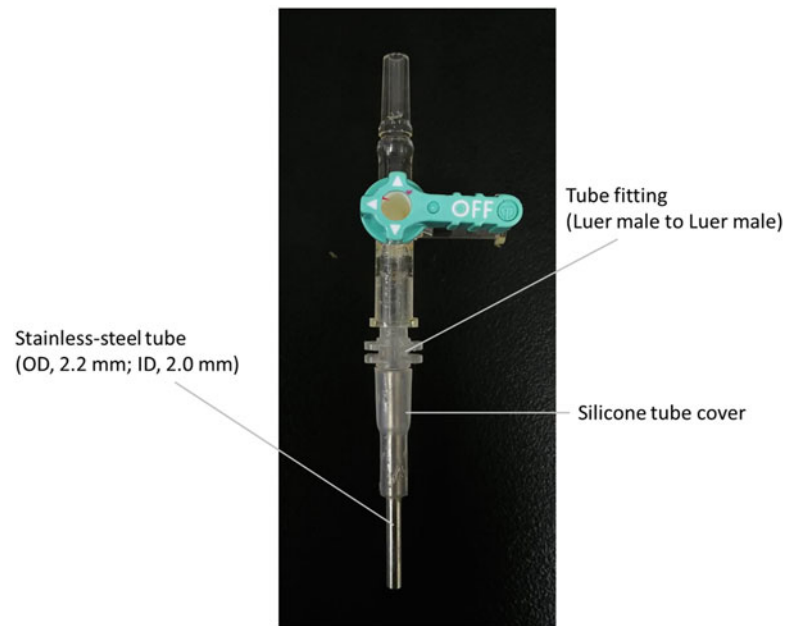


Fig. 2 A magnified view of the cannula structure

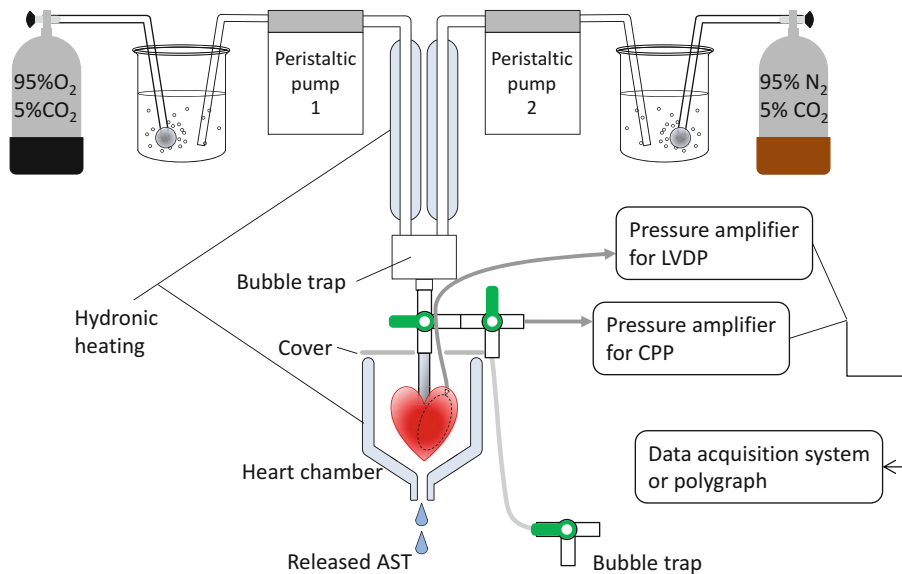


Fig. 3 Diagram of the Langendorff perfusion device for hypoxia–reoxygenation. Switching the pumps enables perfusion of solutions with different oxygen concentration

7. Constant-temperature bath and circulating pump.
8. Two glass hydronic heatings.
9. Two glass ball filters for fluid oxygenation.
10. 5% CO₂ mixture gas.

3 Methods

3.1 Preparation of Equipment

An illustration of the perfusion circuit device used in the experiment is shown in Fig. 3. Perform constant-flow perfusion using a peristaltic pump. Flow rate should be adjusted to coincide as closely as possible with the heart rate *in vivo* (*see Note 7*). Make the tubing from the hydronic heating circuit to the peristaltic pump as short as possible to reduce loss of the dissolved O₂ (*see Note 8*).

1. Prime the irrigator with the dissecting solution bubbled with mixed gas (*see Note 9*).
2. Completely remove air bubbles from the tube connections between the irrigator and the cannula (*see Note 10*).
3. Hang a 3-0 silk suture to ligate the aorta at the end of the cannula and fix the cannula using an auxiliary clip. Dip the cannula tip into the chamber filled with the dissecting solution (Fig. 1).
4. Warm the perfusate between the peristaltic pump and the heart using hydronic heating (*see Note 11*).
5. Any air present within the perfusate will appear as bubbles in the circuit after warming the solution. Install a bubble trap in the circuit to release these bubbles. A branching can be made in the cannula so that one side can be used as a vent line.
6. Once the cannula is branched, one end can be connected to a pressure amplifier so that coronary perfusion pressure (CPP) can be measured.

3.2 Dissection and Heart Isolation

To avoid ischemic preconditioning effects [4], the dissection, trimming, and experimental areas should be close to each other to minimize the time it takes to isolate the heart after decapitation, mounting the heart on the Langendorff perfusion device, and to begin the experiment.

1. Place the dissecting solution in a 20 mL beaker at room temperature.
2. Decapitate and exsanguinate a Sprague Dawley rat (weighing 300–350 g) (*see Note 12*).
3. Incise the skin and muscle layer following the costal margin starting at the bottom of the xiphoid process (*see Note 13*).
4. Lift the xiphoid process and cut out the diaphragm along the costal margin, continue the incisions on both left and right sides of the ribcage up to the first ribs.
5. Cut out the thymus.

6. Gently pinch the heart using the thumb and middle finger, and then insert scissors below it to cut the aorta and excise the heart (*see Note 14*).
7. Soak the excised heart in the beaker containing the dissecting solution.

3.3 Cannulation and Trimming

1. Insert the cannula into the aorta immediately, ligate the aorta with a 3-0 silk suture, and perfuse the aorta with dissecting solution (*see Note 15*).
2. While perfusing the dissecting solution, trim away any pieces of lung, trachea, or connective tissue that are attached around the heart and aorta.
3. Open a hole in the left atrial appendage for LV balloon insertion (Fig. 1, right panel: dotted line shows the position to open the hole).
4. Once trimming is completed, stop the perfusion, mount the heart on the perfusion device, and reperfuse immediately (<30 s) (*see Note 16*).
5. Insert the LV balloon connected to a catheter into the left ventricle via the hole in the left atrial appendage (*see Notes 17 and 18*). Anchor the catheter to the left atrial appendage with a 3-0 silk suture to prevent the LV balloon from being pushed out.
6. Fill the LV balloon with DDW until diastolic pressure reaches 2–5 mmHg (*see Note 19*).
7. The heartbeat will restart within several seconds after switching the perfusate from the dissecting solution to the modified Krebs–Henseleit buffer (without recirculation) (*see Note 20*).
8. Begin the experiment when the heart condition stabilizes after 15–20 min. Keep consistent flow during the experiment.

3.4 Experimental Protocol for Hypoxia–Reoxygenation Injury (*see Note 21*)

1. Let the heart stabilize with oxygenated modified Krebs–Henseleit buffer for 15–20 min.
2. Switch to hypoxic perfusion with sucrose Krebs–Henseleit buffer for 30 min (*see Note 22*).
3. Reoxygenate with modified Krebs–Henseleit buffer for 30 min (*see Note 23*).
4. Sequentially collect the coronary effluent during the experiment for measuring released aspartate aminotransferase (AST) levels (*see Notes 24 and 25*).

3.5 Data Evaluation

LV developed pressure (LVDP) is the difference between the LV pressure during contraction and relaxation. This is an indicator of myocardial contractile force; however, as LVDP changes according to the increases and decreases in HR, the pressure-rate product can be used as an indicator of heart function [5].

4 Notes

1. We previously performed Langendorff perfusion on the heart of an ICR mouse [6]; for a mouse weighing 30 g, we replaced a cannula with an 18-G blunt-ended needle and a 23-G intravenous cannula in place of a polyethylene tube for the LV balloon.
2. To prevent precipitation by the hydrogen calcium carbonate generation, add CaCl_2 last.
3. The basis of the dissecting solution is a Modified Krebs–Henseleit buffer. We use a potassium concentration >20 mM, higher than that of the modified Krebs–Henseleit buffer to arrest the heartbeat. To adjust the osmotic pressure, we reduce the concentration of NaCl by 20 mM. Using Ca-free buffer to arrest the heart can induce severe myocardial necrosis, i.e., Ca paradox [7]; hence, we do not use these Ca-free buffers.
4. We usually use the constant-flow perfusion system for washing out the blood in the coronary arteries.
5. For the 3-way stopcock, we use a stainless-steel tube (2.2 mm outer diameter, 2.0 mm inner diameter) connected via Luer fittings (Warner Instruments, CT, USA) (Fig. 2).
6. Experiments can be done using a single peristaltic pump, but using two peristaltic pumps as shown in Fig. 2 allows for better control of buffer exchange without time loss.
7. In vivo, heart rates of rats and mice are approximately 350 and 600 bpm, respectively. Appropriate flow rate for each heart should be determined based on the HR recorded during the preliminary experiments in same sized species. For example, the perfusion rate should be 13 mL/min for the heart of a standard rat weighing approximately 350 g and 2 mL/min for the heart of a standard mouse weighing approximately 30 g.
8. For the tubes connecting the peristaltic pump and the hydronic heating circuit, materials with low gas permeability (Tygon® tubing) are recommended.
9. When constant-pressure perfusion is not used, a peristaltic pump can be substituted. In such cases, the flow rate should be set at ≥ 15 mL/min to washout the blood in the coronary arteries as soon as possible.
10. If air is not completely removed from the circuit, it can enter the coronary artery when perfusion commences, which can result in an air embolism.
11. The hydronic heating circuit should be used to regulate the temperature so that the perfusion fluid entering the heart is maintained at 37 °C.

12. When the blood sample of an animal is required, administer pentobarbital into the peritoneal cavity as an anesthetic (135 mg/kg) instead of decapitation.
13. For collecting blood, make a longitudinal incision into the abdomen; then, use a heparinized syringe to collect blood from the abdominal vena cava, taking care not to injure the intestine.
14. It is not an issue if the lungs and trachea are excised together. However, take extra care to leave enough length of the aorta for cannula insertion.
15. If the cannula is properly inserted, it can be confirmed by visualization of blood wash out from the epicardial coronary arteries. If the cannula is inserted too deep, the tip of the cannula will block the coronary artery ostium, and perfusion cannot be performed.
16. To avoid air contamination during heart mounting, it is important to close the 3-way stopcock of the cannula at a position of 45°.
17. The LV balloon is made from latex. The size of the LV balloon will change depending on the size of the animal heart used. While the LV balloons are commercially available from ADInstruments (CO, USA) or Radnoti (CA, USA), LV balloon could be made using a condom (Fig. 4, lower panel). Connect the balloon to the end of a polyethylene tube with an outer diameter of 2 mm. Connect the tube to an 18-G blunt end needle (Warner Instrument, CT, USA), and then connect the needle to a pressure transducer (Fig. 4, upper panel).
18. The LV pressure can be measured by inserting a DDW-filled LV balloon attached to a catheter into the LV via the hole in the left atrial appendage.
19. For the heart of a standard rat weighing approximately 350 g, the amount of DDW injected into the LV balloon should be 0.2–0.4 mL.
20. HR can be recorded by entering the LV pressure signals into a data acquisition device, such as a PowerLab™ or polygraph.
21. Peristaltic pump can be stopped for 30 min to induce ischemia/reperfusion injury instead of hypoxic perfusion [8]. In this case, the heart should be immersed in warm modified Krebs–Henseleit buffer to maintain the temperature without perfusion.
22. HR and the LV pressure gradually decrease after starting the hypoxic perfusion. Prolonged hypoxia will cause cardiac arrest.
23. After reoxygenation (or reperfusion), HR and LV pressure gradually recover. At the end of reoxygenation, HR will

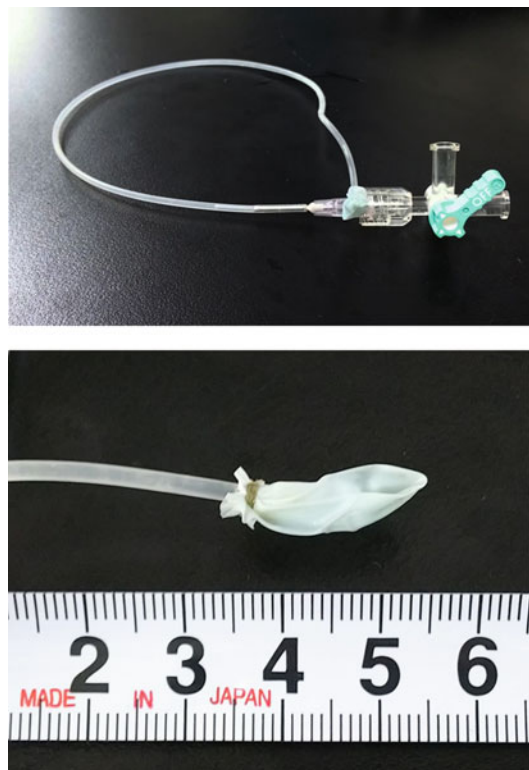


Fig. 4 View of the LV balloon as a whole (top), and a close-up view of the balloon section only (bottom)

completely recover but recovery of LV pressure is usually 50–60% of initial condition.

24. We usually collect the coronary effluent at immediately before hypoxic perfusion, 15 and 30 min after hypoxic perfusion, and 2, 5 and 15 min after reoxygenation. Measuring released AST levels in coronary effluent provides an indicator for irreversible myocardial damage. Creatine kinase is the most well-known cardiac enzyme; however, its instability makes it unsuitable for long-term sample storage. AST is comparatively stable; therefore, collected coronary effluent can be frozen and free AST levels can be measured later. For using effluent AST level as an indicator of irreversible myocardial damage, we normalize the amount of AST with heart weight and time [released AST level per heart weight per unit of time (IU/min/g)] [5]. During I/R (or hypoxia–reoxygenation) injury, released AST levels peaked around 2–5 min after reoxygenation.
25. Since there is no coronary effluent during ischemia in I/R injury protocol, AST measurement is not available.

References

1. Langendorff O (1895) Untersuchungen am überlebenden Säugetierherzen. *Pflügers Arch* 61:291–307
2. Frommeyer G, Milberg P, Witte P et al (2011) A new mechanism preventing proarrhythmia in chronic heart failure: rapid phase-III repolarization explains the low proarrhythmic potential of amiodarone in contrast to sotalol in a model of pacing-induced heart failure. *Eur J Heart Fail* 13:1060–1069
3. Kazusa K, Nakamura Y, Watanabe Y et al (2014) Effects of pH on nifekalant-induced electrophysiological change assessed in the Langendorff heart model of Guinea pigs. *J Pharmacol Sci* 124:153–159
4. Murry CE, Jennings RB, Reimer KA (1986) Preconditioning with ischemia: a delay of lethal cell injury in ischemic myocardium. *Circulation* 74:1124–1136
5. Watanabe M, Okada T (2003) Lysophosphatidylcholine-induced myocardial damage is inhibited by pretreatment of poloxamer 188 in isolated rat heart. *Mol Cell Biochem* 248:209–215
6. Watanabe M, Shinohara A, Matsukawa T et al (2011) Chronic magnesium deficiency decreases tolerance to hypoxia/reoxygenation injury in mouse heart. *Life Sci* 88:658–663
7. Frank JS, Rich TL, Beydler S, Kreman M (1982) Calcium depletion in rabbit myocardium. Ultrastructure of the sarcolemma and correlation with the calcium paradox. *Circ Res* 51:117–130
8. Kakigi R, Watanabe M, Iesaki T et al (2016) Acute exercise preserves cardiac function against ischemia-reperfusion injury. *J Physiol Sci* 66: S185



Chapter 9

Methods for the Preparation of an Excised, Cross-Circulated Rat Heart

Koji Obata and Miyako Takaki

Abstract

The Emax-Pressure-Volume Area (PVA)- VO_2 framework proposed by Dr. Suga for canine hearts has dramatically advanced the field of cardiac mechanical work and energetics, i.e., mechanoenergetics. He and his collaborators investigated mechanoenergetics in the left ventricle (LV) of excised, cross-circulated canine heart preparations. We instituted the excised cross-circulated rat whole heart preparations and found a curvilinear end-systolic pressure–volume relation (ESPVR) in the rat LV, in contrast to the linear ESPVR in canine, rabbit, and human LVs. Although Emax, the slope of the linear ESPVR, could be used as an index of LV contractility, it was not applicable for evaluating LV contractility in the rat LV. Thus, we proposed a new index of contractility, equivalent Emax (eEmax) in the rat LV. We also found a linear VO_2 -PVA relationship in the rat LV. Here, we introduce the methods for the preparation of excised, cross-circulated rat whole hearts and the eEmax-PVA- VO_2 framework in the rat LV. Using this method, we can obtain accurate LV volume and myocardial O_2 consumption in real time for estimating cardiac mechanoenergetics, which is very challenging in *in vivo* experiments.

Key words eEmax, Oxygen consumption, Mechanical work, Energetics, Pressure-volume area, Cross-circulation, Excitation–contraction coupling, Ca^{2+} handling, Langendorff apparatus

1 Introduction

Ex vivo mammalian heart preparations were first reported by Oscar Langendorff [1], who described an isolated model with retrograde perfusion using artificial crystalloid solution, i.e., the Langendorff heart (apparatus). Using this apparatus, the left ventricular (LV) mechanics with altering pressure, volume, and energetics could be estimated by measuring the O_2 consumption. Many cardiac physiologists and pharmacologists have performed experiments estimating the mechanisms of myocardial function, metabolism, as well as effects of myocardial inotropic drugs.

Dr. Suga proposed the Emax-Pressure-Volume Area (PVA)- VO_2 framework using the LV of excised, cross-circulated canine heart preparations [2, 3]. This blood-perfused heart preparation

was more physiological than the crystalloid-perfused heart preparation of the Langendorff apparatus. Subsequently, Dr. Takaki and her colleagues instituted ex vivo small animal heart preparations such as rats or guinea pigs under the cross-circulation method [4–6] based on previous methods [7]. Small animal heart preparations are less expensive and more compliant with animal welfare than canine heart preparations. Furthermore, rats are frequently used to create genetically engineered, and pathological models of human diseases such as transgenic and hypertensive rats, respectively. Although the slope of the linear ESPVR (end-systolic pressure–volume relation), i.e., Emax, could be used as an index of LV contractility in canine LV, Emax is not applicable for evaluating rat LV contractility because of a curvilinear ESPVR previously shown in vivo rat LV using the conductance catheter method [8]. Thus, we proposed a new index for LV contractility, an equivalent Emax (eEmax) [9, 10] and established the eEmax-PVA-VO₂ framework in LVs of rats.

Here, we introduce the method for ex vivo rat heart preparations with cross-circulation method. Using this method, we can obtain accurate LV volume (LVV) and myocardial O₂ consumption in real time and can change the LVV (preload) and heart rate according to designed protocols. Superior accuracy in volume measurements over in vivo evaluation approaches such as echocardiography and conductance catheter volumetry is a significant advantage. In addition, we can examine the direct effects of drugs on cardiac mechanoenergetics without neurohormonal factors, i.e. systemic effects. Although, several papers using this method and eEmax-PVA-VO₂ framework have been previously reported, this is the first report that describes detailed methodology of this preparation. This method has been used in pathological models such as those with LV hypertrophy and heart failure [11–13] to examine pharmacological effects [14–19] as well as the effects of foreign gene transfer on these models with mechanoenergetic analysis [20–27]. Furthermore, in transgenic rats, the mechanoenergetics of SERCA2a-overexpressed hearts were recently reported using this method [28, 29]. With the excised, cross-circulated rat heart preparations, technological advancements such as transgenic rat models can be employed and further promote our understanding in cardiac mechanoenergetics.

2 Materials

2.1 Experimental Animals and Surgical Instruments

1. Wistar rats (500–600 g and above) for metabolic supporter and blood supplier, as well as Wistar rats (350–500 g), or your experimental model rats (*see Note 1*) for heart donors.
2. Surgical instrument set: microscissors, surgical scissors, forceps, hemostats, retractors, bulldog clamps.

2.2 Perfusion Instruments

1. Polyethylene tube for carotid and jugular cannulae (Fr. No.7, 1.3 I.D. × 2.3 O.D. mm) (*see Note 2*).
2. Preparation of a thin latex balloon fitted into the LV for measuring the volume and pressure (Fr. No.4, 0.8 I.D. × 1.3 O.D. mm).
3. Pressure transducers.
4. Infusion drip with mesh filter.
5. Precision glass syringe.
6. Venous blood reservoir tube.
7. Oximeter blood oxygen content analyzer.
8. Syringe pumps.
9. Three-way stopcocks.
10. Silicon tube for peristaltic pump (1.6 I.D. × 4.9 O.D. mm).
11. Respirators.
12. Laboratory stand and Clip clamps.
13. Temperature control system (AutoMate Scientific).
14. Peristaltic tubing pump.
15. Disposable syringes (2.5-, 10-, 20-mL).
16. Disposable injection needles (21-gauge).
17. Silk 3-0 sutures.
18. Thermometer.
19. Water bath.
20. Sewing needle.

2.3 Measurement Instruments

1. Tubing flow measurements.
2. In-line oximeter probe.
3. Custom-made arteriovenous oxygen content difference analyzer (AVOX) (PWA-200S, SHOE TECHNICA Inc., Chiba, Japan).
4. AD converter.
5. Blood amplifier.
6. Bioelectric amplifier.
7. Trigger pulse generator.
8. Stimulator.
9. Isolator.
10. Blood lactate analyzer.

2.4 Others

1. Personal computer.
2. Software for recording and analyzing data.

2.5 Drugs

1. Pentobarbital sodium (50 mg/mL).
2. Heparin (1000 U/mL).
3. 0.5 mol/L KCl in distilled H₂O.
4. 1% CaCl₂ in distilled H₂O.
5. Ringer's lactate solution.
6. Saline solution.
7. 8.4% sodium bicarbonate.
8. 0.4 mg/mL atropine sulfate salt in saline.
9. 0.5 mg/mL L-phenylephrine in saline.

3 Methods

3.1 Experimental Preparation

3.1.1 Preparation of Anesthetized and Heparinized Rats

3.1.2 Preparation of the Balloon

In each experiment, three male rats are anesthetized with pentobarbital sodium (50 mg/kg) intraperitoneally, and used as blood supplier, metabolic supporter, and heart donor, respectively.

To measure the LVV and LV pressure (LVP), a thin balloon that can fit in the LV space is required. The balloon is made from the tip of a latex condom. The balloon is connected via polyethylene tube (Fr. No.4) onto the tip of the latex condom filled with water (to remove air), tied at 11–13 mm from the tip of the balloon with 3-0 surgical strings. A superfluous part of the latex balloon is removed, and the opposite side of the polyethylene tube is connected to a 21-gauge needle with the three-way stopcock, then connected to a pressure transducer and 0.005-mL precision glass syringe (*see Note 3*, Fig. 1).

3.1.3 Priming Heparinized Saline for all Tubes

All cannulae and tubes in the perfusion apparatus are thoroughly washed to remove detergents and primed with 5% heparinized saline (*see Note 4*).

1. Warm up custom-made arteriovenous oxygen content difference analyzer (AVOX) for 30 min and calibrate it with the water.
2. Prepare syringes (10-, 2.5-mL) filled with 1–2 mL heparin.
3. Calibrate the pressure transducers.
4. Heat up the water bath to 37 °C for heating the circuit.

3.1.4 Collecting Blood from Blood Supplier Rats

One Wistar rat is used as a blood supplier to extract its blood for priming the cross-circulation tubing and calibrating the AVOX. Approximately 15–20 mL of fresh oxygenated blood is obtained from each rat.

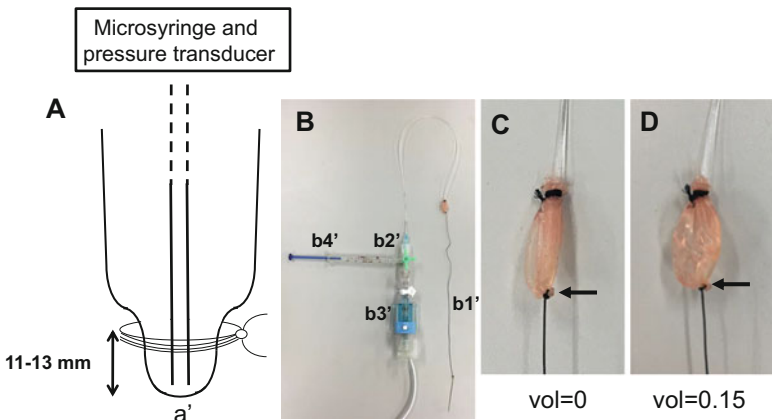


Fig. 1 Schematic illustration and of handmade balloon structure and the images of the balloon. (a) The handmade balloon for measuring LV volume and pressure uses the tip of a latex condom. The balloon is connected via polyethylene tube into the tip of a latex condom filled with water and tied at the 11 to 13 mm from the tip of the balloon (a') is tied with the 3-0 suture (the arrows in c and d) and connected to a sewing needle with this suture (about 15 cm) (b1'). B: A superfluous part is removed from the latex balloon. The opposite side of the polyethylene tube is connected to a 21-gauge needle with the three-way stopcock (b2') and connected to a pressure transducer (b3') and precision glass syringe (b4'). C: This image shows the intraballoon water volume of zero, indicating the balloon latex volume is 0.08 mL. D: This image shows the intraballoon water volume of 0.15 mL and thus a total of 0.23 mL LV volume, indicating the unstretched balloon volume (not to generate a pressure by itself) is below ~0.25 mL

1. Shave hair off the pectoral and cervical regions of the anesthetized rat using electric razor.
2. Fix the rat on the dissection station.
3. Lift the skin away from the abdominal cavity with forceps, and then use surgical scissors to cut the skin midsternally from the abdominal to the cervical site.
4. Identify the trachea in cervical area, partially incise it using the surgical scissors, and insert the intubation tube into the trachea. Tie the sutures to fix the tube to the trachea.
5. Connect the tube to the respirator and start ventilation ($0.11 \times$ body weight g/mL, 60 cycles/min) (see Note 5).
6. Open the chest midsternally under ventilation with supplemental O₂.
7. Remove the pericardial membrane.
8. Extract the oxygenated blood using a 21-gauge needle stabbed into the LV apex after injection of heparin (1000–1500 Units/1.0–1.5 mL) (see Note 6).
9. Load the collected blood onto the arterial and venous cuvettes, respectively, and calibrate the AVOX using the collected blood.

3.1.5 Preparation of Metabolic Supporter Rats

Another rat is used as the metabolic supporter for the excised heart. The bilateral common carotid arteries and right external jugular vein of this rat are cannulated and then connected to the arterial and venous cross-circulation tubing, respectively. The rat is continuously monitored: blood pressure should be maintained at about 100 mmHg (90–130 mmHg), and the body temperature at 37 °C under ventilation (see Note 7).

1. Repeat Subheading 3.1.4, steps 1–5. Place the heating plate under the station.
2. Identify the right (or left) external jugular vein, place two sutures under the vein and tie the distal end of the vein using one suture.
3. Incise the proximal site of the external jugular vein partially using the micro-scissors, insert the cannula for venous return and tie the other suture to fix the cannula to the vein.
4. Connect to the cross-circulation tubing using the three-way stopcock (Fig. 2, ②) after injection of heparin (1000–1500 Units/1.0–1.5 mL) into the metabolic supporter rat.

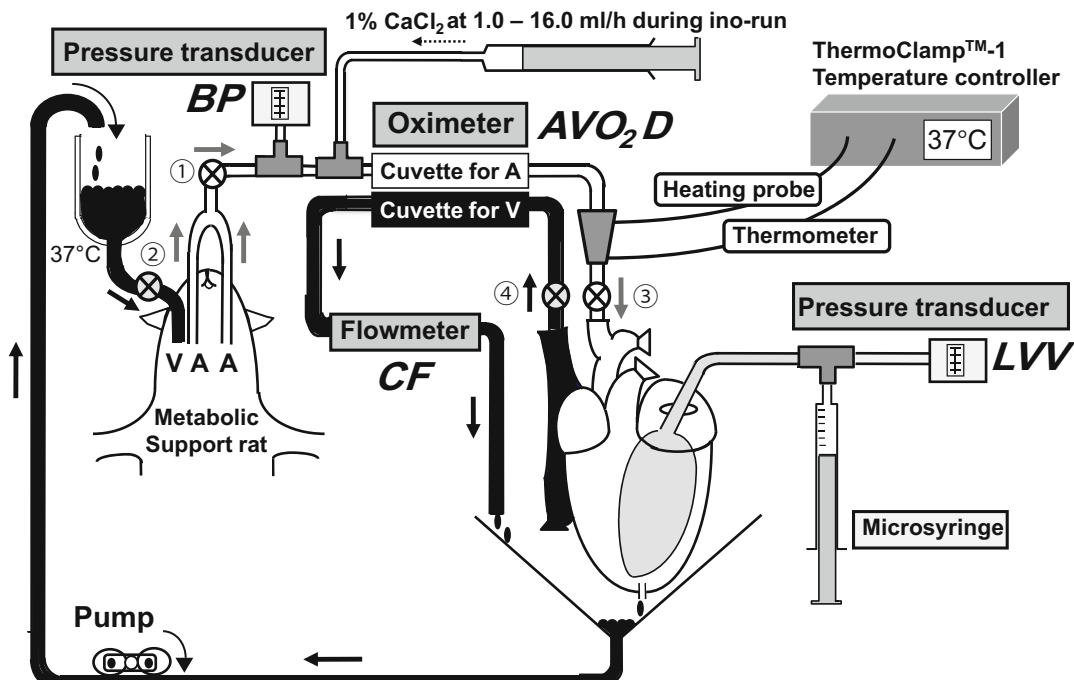


Fig. 2 Schematic illustration of experimental setting for the excised blood-perfused rat heart. A arterial blood, V venous blood, ΔVO_2 arteriovenous O_2 content difference, BP blood pressure of metabolic support rat that corresponds to perfusion pressure for the excised heart, CF coronary flow, LVP left ventricular pressure, LVV left ventricular volume. The all analog data of ΔVO_2 , BP, CF, LVP, and electrocardiogram (ECG) are converted to the digital format with PowerLab and read the data on PC

5. Identify the bilateral common carotid arteries, place two sutures under the arteries and tie the distal site of the arteries using one suture on both sides.
6. Incise the proximal end of the arteries partially using the microscissors, insert the cannulae for removing blood and tie the other suture to fix the cannulae to the arteries.
7. Connect the cross-circulation tubing and pressure transducer with the three-way stopcock (Fig. 2, ①). The pressure transducer is connected to the blood amplifier to monitor the systemic blood pressure. During this process, the three-way stopcock in the cross-circulation tubing should be closed.
8. Measure the rat rectal temperature and place a heating plate under the body to maintain the temperature at 37 °C (*see Note 7*).
9. Initiate additional continuous infusion of pentobarbital sodium at 7.5 mg/h with a syringe pump to maintain the anesthetic level in the metabolic supporter rat.

3.1.6 Preparation of Excised Hearts from Donor Rats

The cannulae are inserted into the aorta via the brachiocephalic artery (inflow cannula) and the right ventricle (outflow cannula) via the superior vena cava of the donor rat heart to connect the cross-circulation tubings from the metabolic supporter rat. The beating heart is excised from the body without interruption of the coronary perfusion and supported by cross-circulation to the metabolic supporter rat. The excised heart is maintained at 37 °C with a temperature control system (*see Note 8*).

1. Repeat Subheading 3.1.4, steps 1–6.
2. Maintain the operation field using retractors, remove any pericardial membrane and the thymus to improve exposure of the pulmonary artery, aorta, superior and inferior venae cavae (*see Note 9*).
3. Identify the brachiocephalic artery and place two sutures under it.
4. Tie the distal end of the brachiocephalic artery using a suture.
5. Clamp the proximal end of the brachiocephalic artery using the bulldog clamp, incise the artery partially using microscissors, insert the cannula for the blood infusion, remove the bulldog clamp and tie the other suture to fix the cannula to the artery following the injection of heparin (1000–1500 Units/1.0–1.5 mL) (*see Note 10*).
6. Place one suture under the distal ends of the ascending aorta, pulmonary artery, and inferior vena cava, respectively.
7. Place two sutures under the superior vena cava and tie the distal end using one suture.

8. Incise the superior vena cava partially using the micro-scissors, insert the cannula for removing blood into the right ventricle through the right atria, and tie the other suture to fix the cannula to the superior vena cava.
9. Connect the cannulae to the cross-circulation tubings for blood infusion and removal.
10. Open the three-way stopcock (Fig. 2, ③ and ④) and start cross-circulation between the excised heart and the metabolic supporter rat. Pay attention to the blood pressure in metabolic supporter rat (*see Note 11*).
11. Tie the ascending aorta, inferior vena cava, and the pulmonary artery with the sutures in this order.
12. Cut the brachiocephalic artery, descending aorta, inferior vena cava, pulmonary artery, and the connective tissues to remove the heart-lung section.
13. Fix the heart-lung section using laboratory stand with a clip clamp. Pay attention not to interrupt the coronary perfusion (*see Note 12*).
14. Remove the pericardial membrane, lung (cut the pulmonary veins), and other connective tissues.
15. Incise the left atrial appendage partially using the surgical scissors to insert the balloon connected to the sewing needle with thread in the excised beating heart.
16. Insert the needle from the left atrial appendage to the LV apex and pull down the needle with thread to bring the balloon into the LV chamber (*see Note 13*).
17. Connect the pressure transducer to the balloon tube. Check the developing LVP by infusion of water into the balloon and tie the balloon tube to the left atrial appendage.
18. Set the handmade pacing-electrodes on right atrial appendage for electrical pacing.
19. Set the handmade recording-electrodes in LV surface for electrocardiogram.

3.2 Oxygen Consumption Measurements

Myocardial O₂ consumption is the product of the coronary flow and arteriovenous O₂ content difference (AVO₂D) (Fig. 2).

1. Continuously measure total coronary blood flow with an ultrasonic flowmeter, in which the inline flow probe is placed in the middle of the coronary venous drainage tubing from the right ventricle.
2. The coronary AVO₂D is continuously measured by passing all the arterial and venous cross-circulation blood through the two cuvettes of the AVOX.

3.3 Electrocardiogram and Electrical Pacing

1. The LV epicardial electrocardiogram is recorded with a pair of handmade recording-electrodes.
2. Maintain the heart rate constant by the electrical pacing of the right atrium with a pair of handmade pacing-electrodes tipped with clips at 300 bpm using an electrical stimulator and its isolator.
3. Adjust the pacing rate to prevent incomplete relaxations or arrhythmia.

3.4 Myocardial Temperature Maintenance

Coronary perfusion of the excised heart is never interrupted during this preparation, and the excised heart is maintained at 37 °C with an in-line temperature control system, which is placed before (about 20 cm) the blood infusion cannula (Fig. 2).

3.5 Experimental Protocol

After the surgical preparation following the start of cross-circulation, allow the system to achieve hemodynamic stability for at least 30 min. At this time, the vol% value of AVOX must be calibrated with the oximeter blood oxygen content analyzer using arterial blood passing through the arterial cuvette and venous blood passing through the venous cuvette (see Note 14). Attention should be paid to maintain the various parameters i.e. blood pressure and body temperature of the metabolic supporter rat. The systemic arterial blood pressure of the metabolic supporter rat serves as the coronary perfusion pressure (90–130 mmHg) (see Notes 15 and 16). After the hemodynamic stability is established, control volume run (vol-run) is performed first, then an inotropic run (ino-run) with 1% CaCl₂ solution performed second, and a KCl-arrest for cardiac arrest with 0.5 mol/L KCl is performed last.

3.5.1 Control Volume Run (Vol-Run)

1. The volume-unloaded VO₂ is measured as close to zero as possible (see Note 17).
2. LVV is changed by adjusting the intraballoon water volume with the precision glass syringe in 0.025-mL steps from 0.08 mL to 0.23 mL, which is sum of intraballoon water volume (0, 0.025, 0.05, 0.075, 0.10, 0.125, 0.15 mL) and balloon latex volume (0.08 mL) (see Note 18).
3. LVP, VO₂, and PVA data during isovolumic contractions are simultaneously obtained at five to six different LVVs in each heart (Fig. 3).
4. To obtain the accurate data, the vol-run is performed at least two to three times (see Note 19).

3.5.2 Inotropic-Run (Ino-Run) During Ca²⁺ Infusion

After the vol-run, a Ca²⁺-induced inotropic run (Ca²⁺ ino-run) is performed during 1% CaCl₂ solution infusion with a syringe pump (see Note 20).

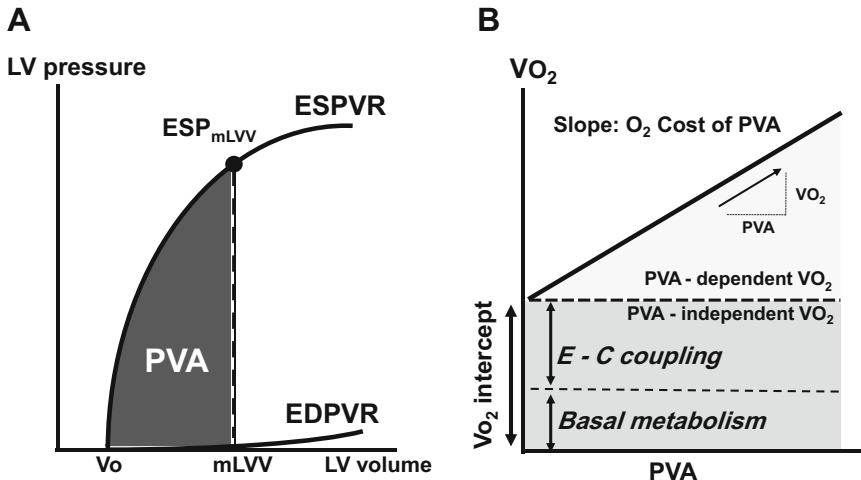


Fig. 3 Schematic illustration of framework of ESPVR-VO₂-PVA. **(a)** LV end systolic and diastolic pressure–LV volume relation, **(b)** VO₂–PVA relation. V_0 systolic unstressed LV volume, $mLVV$ midrange left ventricular volume, PVA pressure volume area, ESP end systolic pressure. PVA is defined as the area circumscribed by the curvilinear best-fit ESPVR, EDPVR, and the systolic portions of the ventricular P-V trajectories. PVA is normalized by LV mass (g). Mean ESP at $mLVV$ (ESP_{mLVV}) and PVA at $mLVV$ (PVA_{mLVV}) are calculated to assess LV mechanical work and energetics. The VO₂–PVA relationship is linear in the rat LV. Its slope represents the O₂ cost of PVA, and its VO₂ intercept represents the PVA-independent VO₂. The PVA-dependent VO₂ is consumed by myosin ATPase for cross-bridge cycling. The PVA independent VO₂ is composed of O₂ consumption for Ca²⁺ handling in excitation–contraction (E–C) coupling and basal metabolism

1. LVV is fixed at midrange LVV ($mLVV$) ($0.16\text{ mL} = 0.08\text{ mL}$ [V_0] plus 0.08 mL [a half value between the minimum and maximum water volume infused into the balloon]). At first, LVP, VO₂, and PVA data are obtained as zero Ca²⁺ before the Ca²⁺ infusion.
2. The intracoronary infusion of 1% CaCl₂ solution is started at 1.0 mL/h and the infusion rate of Ca²⁺ is gradually increased from 1.0 to 16.0 mL/h .
3. LVP, VO₂, and PVA data at each concentration are obtained until a decrease in end-systolic pressure (ESP) or arrhythmia due to Ca²⁺ overload is detected.
4. To obtain steady-state data, every data point is measured at 3 min- intervals after changing the infusion rate of Ca²⁺.

3.5.3 KCl-Arrest

Finally, to measure the basal metabolic O₂ consumption, cardiac arrest is induced by intracoronary infusion of KCl (0.5 mol/L) at $5\text{--}10\text{ mL/h}$ (calculated blood concentration: 0.03 mol/L) using a syringe pump (see Note 21).

1. The minimum volume loading is used to avoid volume-loading effects on the VO₂ data in KCl-arrest.

2. When cardiac arrest is identified on the electrocardiograms, VO₂ and PVA data are obtained in the steady-state after 3 min.
3. In each steady state, VO₂ and PVA data are repeatedly sampled (two to three times).
4. At the end of the experiment, the LV including the septum and right ventricular (RV) free wall are weighed separately (*see Note 22*).

4 Analysis

4.1 ESPVR and EDPVR (End Diastolic Pressure–Volume Relation) Are Needed for the Calculation of PVA, and the Estimated Systolic Unstressed Volume (V_0)

4.2 VO₂–PVA Relation and VO₂ for Excitation–Contraction (E-C) Coupling and Basal Metabolism

The best-fit ESPVR and EDPVR are obtained from five to six different pressure–volume data with the two different exponential functions by means of the least-squares method using the Delta-Graph software in Fig. 3a. The PVA is calculated as the area surrounded by ESPVR and EDPVR (Fig. 3a). Thus, V_0 is determined as the volume-axis intercept of the P-V relation by curve fitting with an equation (*see Note 23*).

Cardiac O₂ consumption is obtained as the product of coronary flow and AVO₂D. It is divided by heart rate (beats/min) to obtain O₂ consumption per beat (VO₂) in a steady state. The VO₂–PVA relationship is linear in the rat LV (*see Note 24*, Fig. 3b). Its slope represents the O₂ cost of PVA, while its VO₂ intercept represents the PVA-independent VO₂. The PVA-independent VO₂ is composed of VO₂ in E-C coupling and basal metabolism (Fig. 3b). Cardiac arrest is induced by intracoronary infusion of KCl (0.5 mol/L) at 5–10 mL/h to measure the basal metabolic O₂ consumption. In addition, PVA-independent VO₂ minus the basal metabolic VO₂ is VO₂ for Ca²⁺ handling in E-C coupling.

5 Notes

1. This protocol is performed under guidelines of your institution's animal care and use committee. Any rats can be used to fit the protocol regardless of the strain, age, and sex without any transfusion effects, but we recommend using larger animals to perform easier surgical operation, and use the same strain in each experiment.
2. The polyethylene tubes are stretched to appropriate diameters with alcohol ramp for the carotid artery, jugular vein, and brachiocephalic artery for blood-infusion, and the superior vena cava for blood-removal in the excised heart. In addition, some small holes should be made around the tip of the blood-removal cannula in the excised heart.

3. The balloon latex volume is 0.08 mL and the maximum unstretched balloon volume is below ~0.25 mL (Fig. 1).
4. The cannulae and tubes in this perfused apparatus should be as short as possible so that the dead space of the perfusion circuit is minimal. To avoid blood coagulation, heparin is administered in suitable quantity. The filters are placed under the excised heart (# 13 mm) and in the infusion drip (# 0.2 mm) to remove coagulated blood.
5. Supplemental O₂ for the metabolic supporter rat is recommended.
6. The syringe must be pulled as slowly as possible. Do not stop the heartbeat.
7. Systemic arterial blood pressure of the metabolic supporter rat is monitored in the arterial perfusion tubing with a pressure transducer. It serves as the coronary perfusion pressure (about 100 mmHg). The rectal temperature of the metabolic supporter rat is maintained at 36–38 °C throughout the experiment using the heating plate.
8. Temperature control system placed in the line system directly heats the perfused blood. Attention should be paid not to overheat the blood to prevent denaturation of serum proteins.
9. Cut the phrenic and vagus nerves running around the donor heart. The thymus is removed by holding and carefully tearing with the forceps, to prevent bleeding.
10. Be careful not to insert the cannula too close to the proximal end of the ascending aorta to prevent the aortic regurgitation. Failure of proper fixation of these cannulae may cause an unstable beating of heart preparation, and it may lead to non-preferred results.
11. Once the perfusion is started, the ventilation of the donor rat can be stopped, since it is unnecessary for the perfused heart and the ventilated lung also disturbs the excision of the heart from the body of the donor rat. If the blood pressure falls under 100 mmHg, the blood transfusion rate from venous return tank should be increased. The temperature control system should be started to maintain the cross-circulation system at 37 °C. At this time, the coronary blood flow of a donor heart is supplied by both the supporter rat and the donor rat itself.
12. The most appropriate position provides the highest coronary flow of the heart. Manually rotate the cannulae so that the posterior side of the heart faces the operator. At this time, the coronary blood flow of a donor heart is only supplied by the supporter rat. Thus, this operation is very important and should be performed as quickly and precisely as possible.

13. In the excised beating heart, the LV apex is punctured with a sewing needle to drain the thebesian and aortic regurgitant blood, if any. LV thebesian flow is negligible.
14. The arteriovenous O₂ content difference is calibrated to correct the vol% in the AVOX.
15. Arterial pH, PO₂, and PCO₂ of the metabolic supporter rat are maintained within their physiological ranges with supplemental O₂ and by addition of 3–4 mL of 8.4% sodium bicarbonate solution to the perfused blood throughout the experiment.
16. 0.5–1.0 mL atropine (0.4 mg/mL in saline) and 0.1–0.5 mL phenylephrine (0.5 mg/mL in saline) can be administered if necessary. We previously have confirmed that LV mechanoeenergetics data obtained by vol-run and Ca²⁺ ino-run were constant during 4–5 h after onset cross-circulation [16].
17. Systolic unstressed volume (V_0) is determined by filling the balloon to the level where peak isovolumic pressure, and hence pressure-volume area (PVA; see Sect. 4 Analysis), are zero. The sum of the intraballoon water and balloon material volumes are used as the initial estimate of V_0 .
18. The infusion of the intraballoon water volume could be performed in this order but not strictly in this order (0, 0.05, 0.10, 0.15, 0.125, 0.075, 0.025 mL). The vol-run must be repeated multiple times to obtain correct data. In fact, similar data can be obtained repeatedly if the perfused apparatus is prepared appropriately. The maximum intraballoon water volume as LVV must be infused not to exceed an end-diastolic pressure (EDP) of 20 mmHg.
19. All data are measured, sampled at 1 kHz for 5–10 s and averaged using the PowerLab unit and LabChart software in our laboratory.
20. The index for O₂ cost of LV contractility, indicates the VO₂ for Ca²⁺ handling in E-C coupling per unit LV contractility change in the rat heart. As described above, Emax cannot be used as an LV contractility index because of the curved ESPVR in the rat heart. Thus, eEmax is proposed, which is calculated as an ESP-V ratio of the specific virtual triangular PVA at a mLVV (PVA_{mLVV}) that is energetically equivalent to the real PVA_{mLVV} experimentally obtained (Fig. 4). The O₂ cost of LV contractility is obtained as the slope of this linear relation by plotting gradually increased PVA-independent VO₂, and eEmax values during stepwise increase in Ca²⁺ infusion. Ino-run can also be performed by other inotropic agents such as beta-agonist, dobutamine, which we previously reported [13].
21. The rate of intracoronary KCl-infusion is adjusted to abolish electrical excitation in monitoring ventricular electrocardiograms, and not to generate any KCl-induced constrictions of

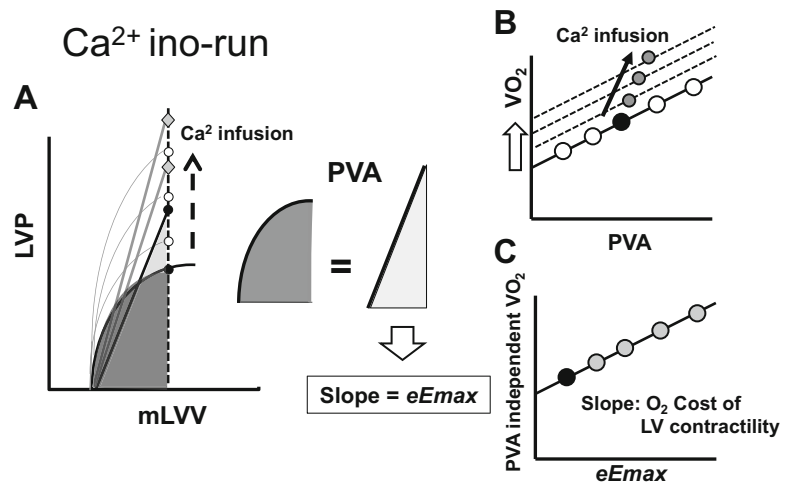


Fig. 4 Schematic illustration of framework of equivalent E_{max} (eE_{max})- VO_2 -PVA in Ca^{2+} induced inotropic run. **(a)** Control ESPVR (solid circle) and P-V data (open circle) during Ca^{2+} infusion at increased rates in steps at a midrange left ventricular volume (mLVV). **(b)** VO_2 -PVA data points and prospective VO_2 -PVA relationships, which show parallel shift at increased Ca^{2+} infusion rates in steps at mLVV. **(c)** The ratio of PVA independent VO_2 and eE_{max} , indicating the O_2 cost of LV contractility

the coronary vessels, by monitoring coronary flow (approximately 1.0 mL/min) and systemic blood pressure (corresponding to perfusion pressure) in the metabolic supporter rat to check the loss of perfusion pressure dependency.

22. The RV is kept collapsed by continuous hydrostatic drainage so that the RV PVA, and hence PVA-dependent VO_2 , are assumed to be negligible. The RV component of PVA-independent VO_2 is subtracted from the total VO_2 to yield LV VO_2 . The LV (including the septum), and the RV are weighed for normalization of LVV. Throughout each experiment, the mean concentration of hemoglobin and lactate in the perfused blood must be checked from time to time. The hemoglobin concentration should be more than 10 mg/dl. The lactate concentrations of arterial blood before passing through the excised heart and venous blood after passing through it are measured with Rapid Laboratory 860. The values of arteriovenous lactate difference throughout the experiment including the maximum LVV loading (i.e. the maximum O_2 demand) during vol-run should show a zero or minus difference, indicating no lactate production in the excised heart.
23. We obtain the best-fit ESPVR with the equation $ESP = A \{1 - \exp [-B(V - V_0)]\}$ by means of the least-squares method on a personal computer. We also obtain the best-fit end-diastolic pressure (EDP)-volume relation (EDPVR) with the

equation, $EDP = A' \{ \exp [B'(V - V'_0)] - 1 \}$. The correlation coefficients of the best-fit ESPVRs should be higher than 0.98. Systolic unstressed volume (V_0) should be determined as the volume at which peak isovolumic pressure, and hence, PVA is zero. Although, the residual PVA is small, LV peak pressure sometimes do not become zero because of the volume of the balloon membrane per se as well as high LV contractility.

24. The PVA-dependent VO_2 is consumed by myosin ATPase for cross-bridge cycling. The PVA independent VO_2 is composed of O_2 consumption for Ca^{2+} handling in E-C coupling and basal metabolism.

Acknowledgment

This work was supported in part by grants-in-aid NO. 25460283 for Scientific Research from the Ministry of Education, Culture, Sports, Science, and Technology of Japan.

Disclosures: None.

References

1. Langendorff O (1895) Untersuchungen am überlebenden saugethierherzen (investigations on the surviving mammalian heart). *Arch Ges Physiol* 61:291–332
2. Suga H, Hisano R, Goto Y et al (1983) Effect of positive inotropic agents on the relation between oxygen consumption and systolic pressure-volume area in canine left ventricle. *Circ Res* 53:306–318
3. Suga H (1990) Left ventricular (LV) mechanoenergetics has been well-investigated in canine hearts. Ventricular energetics. *Physiol Rev* 70:247–277
4. Matsushita T, Takaki M, Fujii W et al (1995) Left ventricular mechanoenergetics under altered coronary perfusion in Guinea pig hearts. *Jpn J Physiol* 45(6):991–1004
5. Hata Y, Sakamoto T, Hosogi S et al (1998) Linear O_2 use-pressure-volume area relation from curved end-systolic pressure-volume relation of the blood-perfused rat left ventricle. *Jpn J Physiol* 48(3):197–204
6. Hata Y, Sakamoto T, Hosogi S et al (1998) Effects of thapsigargin and KCl on the O_2 use of the excised blood-perfused rat heart. *J Mol Cell Cardiol* 30(10):2137–2143
7. Sakaki K (1980) Coronary vasoconstriction by locally administered acetylcholine, carbachol and bethanechol in isolated, donor-perfused, rat hearts. *Br J Pharmacol* 68:625–632
8. Tachibana H, Takaki M, Lee S et al (1997) New mechanoenergetic evaluation of left ventricular contractility in *in situ* rat hearts. *Am J Phys* 272:H2671–H2678
9. Tsuji T, Ohga Y, Yoshikawa Y et al (1999) New index for oxygen cost of contractility from curved end-systolic pressure-volume relations in cross-circulated rat hearts. *Jpn J Physiol* 49(6):513–520
10. Takaki M (2004) Left ventricular mechanoenergetics in small animals. *Jpn J Physiol* 54:175–207
11. Abe T, Ohga Y, Tabayashi N et al (2002) Left ventricular diastolic dysfunction in type II diabetes mellitus model rats. *Am J Physiol Heart Circ Physiol* 282(1):H138–H148
12. Ohga Y, Sakata S, Takenaka C et al (2002) Cardiac dysfunction in terms of left ventricular mechanical work and energetics in hypothyroid rats. *Am J Physiol Heart Circ Physiol* 283(2):H631–H641
13. Nakajima-Takenaka C, Sakata S, Kato S et al (2005) Detrimental effects after dobutamine infusion on rat left ventricular function: mechanical work and energetics. *Exp Physiol* 90(4):635–644
14. Kobayashi S, Yoshikawa Y, Sakata S et al (2004) Left ventricular mechanoenergetics after hyperpolarized cardioplegic arrest by nicorandil and after depolarized cardioplegic arrest by KCl.

- Am J Physiol Heart Circ Physiol 287(3): H1072–H1082
15. Yoshikawa Y, Hagihara H, Ohga Y et al (2005) Calpain inhibitor-1 protects the rat heart from ischemic-reperfusion injury: analysis by mechanical work and energetics. Am J Physiol Heart Circ Physiol 288(4):H1690–H1698
 16. Yoshikawa Y, Zhang GX, Obata K et al (2010) Cardioprotective effects of a novel calpain inhibitor, SNJ-1945 for reperfusion injury after cardioplegic cardiac arrest. Am J Physiol Heart Circ Physiol 298(2):H643–H651
 17. Yoshikawa Y, Zhang GX, Obata K et al (2010) A cardioprotective agent of a novel calpain inhibitor, SNJ-1945 exerts β_1 -actions on left ventricular mechanical work and energetics. Am J Physiol Heart Circ Physiol 299(2): H396–H401
 18. Hagihara H, Yoshikawa Y, Ohga Y et al (2005) $\text{Na}^+/\text{Ca}^{2+}$ exchange inhibition protects the rat heart from ischemic-reperfusion injury by blocking energy-wasting processes. Am J Physiol Heart Circ Physiol 288(4):H1699–H1707
 19. Nakajima-Takenaka C, Zhang GX, Obata K et al (2009) Left ventricular function of isoproterenol-induced hypertrophied rat hearts perfused with blood: mechanical work and energetics. Am J Physiol Heart Circ Physiol 297(5):H1736–H1743
 20. Sakata S, Lebeche D, Sakata Y et al (2006) Mechanical and metabolic rescue in a type II diabetes model of cardiomyopathy by targeted gene transfer. Mol Ther 13(5):987–996
 21. Sakata S, Lebeche D, Sakata Y et al (2007) Transcoronary gene transfer of SERCA2a increases coronary blood flow and decreases cardiomyocyte size in a type II diabetic rat model. Am J Physiol Heart Circ Physiol 292 (2):H1204–H1207
 22. Sakata S, Lebeche D, Sakata N et al (2007) Targeted gene transfer increases contractility and decreases oxygen cost of contractility in normal rat hearts. Am J Physiol Heart Circ Physiol 292:H2356–H2363
 23. Sakata S, Lebeche D, Sakata N et al (2007) Restoration of mechanical and energetic function in failing aortic-banded rat hearts by gene transfer of calcium cycling proteins. J Mol Cell Cardiol 42:852–861
 24. Sakata S, Liang L, Sakata N et al (2007) Preservation of mechanical and energetic function after adenoviral gene transfer in normal rat hearts. Clin Exp Pharmacol Physiol 34:1300–1306
 25. Kawase Y, Ly HQ, Prunier F et al (2008) Reversal of cardiac dysfunction following long term expression of SERCA2a by gene transfer in a pre-clinical model of heart failure. J Am Coll Cardiol 51(11):1112–1119
 26. Tsuji T, Del Monte F, Yoshikawa Y et al (2009) Rescue of Ca^{2+} overload-induced left ventricle dysfunction by targeted ablation of phospholamban. Am J Physiol Heart Circ Physiol 296 (2):H310–H317
 27. Takewa Y, Chemaly ER, Takaki M et al (2009) Mechanical work and energetic analysis of eccentric cardiac remodeling in a volume overload heart failure in rats. Am J Physiol Heart Circ Physiol 296(4):H1117–H1124
 28. Zhang GX, Obata K, Takeshita D et al (2012) Evaluation of left ventricular mechanical work and energetics of normal hearts in SERCA2a transgenic rats. J Physiol Sci 62:221–231
 29. Mitsuyama S, Takeshita D, Obata K et al (2013) Left ventricular mechanical and energetic changes in long-term isoproterenol-induced hypertrophied hearts of SERCA2a transgenic rats. J Mol Cell Physiol 59:95–106



Chapter 10

Optical Action Potential Mapping in Acute Models of Ischemia–Reperfusion Injury: Probing the Arrhythmogenic Role of the Mitochondrial Translocator Protein

Zeki Ilkan, Benjamin Strauss, Chiara Campana, and Fadi G. Akar

Abstract

Ischemia–reperfusion (I/R) injury causes dynamic changes in electrophysiological properties that promote the incidence of post-ischemic arrhythmias. High-resolution optical action potential mapping allows for a quantitative assessment of the electrophysiological substrate at a cellular resolution within the intact heart, which is critical for elucidation of arrhythmia mechanisms. We and others have found that pharmacological inhibition of the translocator protein (TSPO) is highly effective against postischemic arrhythmias. A major hurdle that has limited the translation of this approach to patients is the fact that available TSPO ligands have several confounding effects, including a potent negative ionotropic property. To circumvent such limitations we developed an *in vivo* cardiac specific TSPO gene silencing approach as an alternative. Here, we provide the methodological details of our optical action potential mapping studies that were designed to probe the effects of TSPO silencing in hearts from spontaneously hypertensive rats (SHR) that are prone to I/R injury.

Key words shRNA, Gene therapy, Adeno-associated virus, Arrhythmia, Mitochondria, Translocator protein, Optical mapping

1 Introduction

By predisposing to ischemic events, coronary artery disease is a leading cause of death and disability worldwide [1]. Prompt restoration of oxygenated blood flow to the ischemic myocardium is required for preventing irreversible cell damage and death. Unfortunately, restoration of blood flow, in itself, results in additional cardiac damage known as ischemia–reperfusion (I/R) injury [2]. On the one hand, mitochondrial dysfunction secondary to I/R injury causes further expansion of the infarcted zone leading

Zeki Ilkan and Benjamin Strauss contributed equally to this work.

to chronic heart failure, and on the other, it predisposes to ventricular tachyarrhythmias and sudden cardiac death. Effective strategies to limit postischemic arrhythmias have proven elusive owing to our incomplete understanding of the dynamically changing electrophysiological substrate during acute I/R injury. With the advent of optical imaging techniques using voltage sensitive dyes, spatiotemporal measurements of cardiac electrophysiological properties at a cellular level within the intact syncytium have become possible, paving the way for a more comprehensive understanding of post-ischemic arrhythmia mechanisms. Our work over the past 12 years has focused on the central role that the mitochondrial network plays in arrhythmogenesis [3–7]. We have found that stabilization of mitochondrial function through pharmacological inhibition of the translocator protein (TSPO) is highly effective against post-ischemic arrhythmias in structurally normal hearts [3]. The utility of this approach in chronic cardiovascular diseases such as hypertension, a major risk factor for I/R injury, remains unknown. Despite the impressive antiarrhythmic efficacy of pharmacological TSPO inhibition, available TSPO ligands have several confounding effects that limit their translatability to the clinic. This includes a potent negative ionotropic effect that arises from inhibition of the L-type calcium current by TSPO ligands such as 4'-chlorodiazepam [8]. To circumvent inherent limitations, including extracardiac toxicity, of pharmacological TSPO inhibitors, we developed an *in vivo* cardio-tropic TSPO gene silencing approach using adeno-associated virus serotype 9 (AAV9) as a gene delivery vector. In proof-of-concept studies, we applied our novel gene therapy approach to spontaneously hypertensive rats (SHR) which exhibit profound mitochondrial dysfunction and are particularly susceptible to I/R injury [9–15].

In this chapter, we provide an overview of these proof-of-concept studies. We describe in detail the optimized procedures that are needed to achieve chronic *in vivo* gene silencing of TSPO levels in SHR hearts (Figs. 1 and 2). We further document the *ex vivo* optical action potential mapping studies and acute I/R injury protocols that we performed to probe the electrophysiological consequences of chronic *in vivo* TSPO gene silencing (Figs. 3 and 4). We provide useful tips and key modifications to the standard I/R injury models and pacing protocols that we found useful for unmasking the antiarrhythmic efficacy of this gene therapy approach (Fig. 4).

2 Materials

2.1 shRNA Tail Vein Injection

1. Adult 10–13-week-old spontaneously hypertensive male rats (SHR).
2. Sterile physiological saline (0.9% sodium chloride injection).

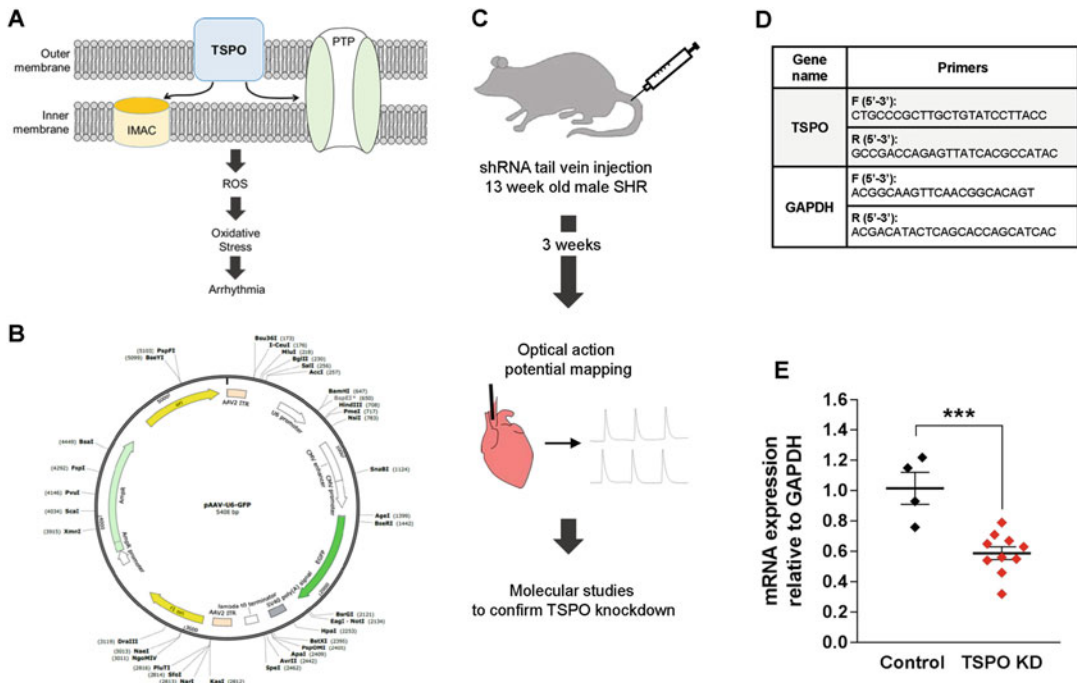


Fig. 1 Experimental design used to determine the electrophysiological effects of in vivo gene silencing of TSPO using AAV9-mediated gene transfer of shTSPO. **(a)** Schematic illustrating the regulation of the two key energy dissipating mitochondrial channels (the inner membrane anion channel, IMAC and the mitochondrial permeability transition pore, PTP) by TSPO. This complex of mitochondrial proteins mediates the regenerative process of reactive oxygen species (ROS)-induced ROS release, leading to oxidative stress and arrhythmias. **(b)** A schematic of the pAAV-U6-GFP plasmid map designed to induce in vivo TSPO silencing. **(c)** A summary of the procedures conducted in this study: 3 weeks after tail vein injection of 5×10^{11} gc/mL shTSPO, high-resolution optical action potential mapping was performed in ex vivo perfused rat hearts. The heart tissue was subsequently used in qPCR studies to confirm gene knockdown **(d)** The forward (F) and reverse (R) primer sequences for TSPO and GAPDH targets in the qPCR studies; **(e)** A consistent (~40%) reduction in TSPO RNA expression was observed in shRNA injected rat hearts, compared to controls where saline or no injections were performed. *** $P < 0.001$ by unpaired Student's *t*-test

3. Ketamine-HCl (100 mg/mL) and xylazine.
 4. AAV-CMV-GFP-U6-rm-TSPO-shRNA (shAAV-275192) stock solution [8×10^{13} genome copies per milliliter (gc/mL)].
 5. 1 mL syringes.
 6. 30G \times 1/2 in. (0.3 mm \times 13 mm) needles.
 7. 25G \times 5/8 in. (0.5 mm \times 16 mm) needles for intraperitoneal (IP) injections.
 8. 1.5 mL microcentrifuge tubes.
 9. Rat restrainer for tail vein injections.
 10. Electric heating pad or a table-mounted infrared heat lamp (with a 250 W lamp).

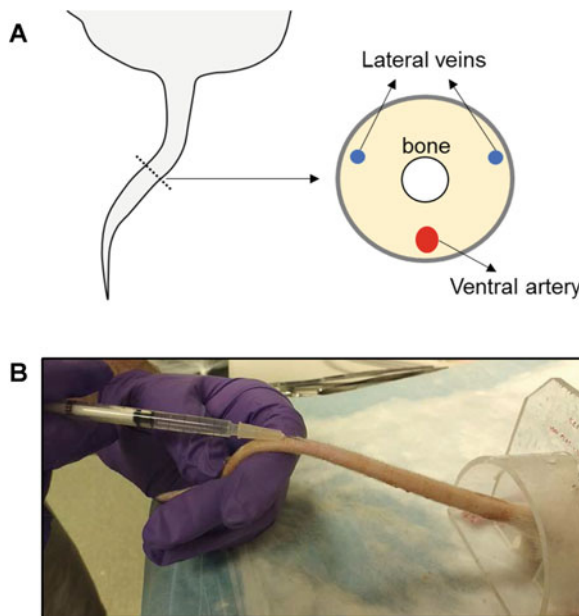


Fig. 2 An illustration of the rat tail veins and the injection procedure. (a) A simplified cartoon representation adapted from X-ray angiography images by Vanhoutte et al., 2002 [17]. (b) Injections were performed into either of the lateral veins as demonstrated

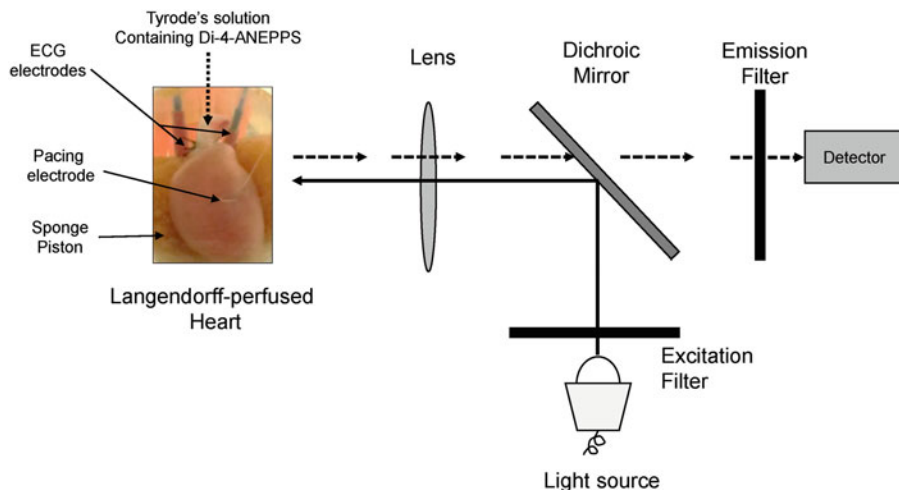


Fig. 3 The assembly of the Langendorff-perfused heart and a representation of the optical mapping system

2.2 Optical Mapping and Perfusion Systems

1. Charge coupled device (CCD) camera/detector.
2. Light source (Tungsten lamp).
3. Electrocardiogram (ECG) amplifier.
4. Pressure monitor.

5. Stimulator, Model S88.
6. PFA-coated silver wire: bare diameter 0.005", coated diameter 0.007", to be used as the pacing electrode (connected to the stimulator).
7. Thermistor thermometer.
8. Heating exchanger.
9. Bubble trap compliance chamber.
10. Plexiglass tissue bath with transparent (glass) imaging window.
11. Heat Circulating Pump 170051a with Digital One Controller. A heating coil should be immersed in the tissue bath to maintain temperature at 37 °C.
12. Peristaltic perfusion pump.
13. Pressure sensor.
14. Large water bath set at 37 °C.
15. Langendorff system.
16. Platinum-Cured Silicone Precision Tubing.
17. CardioPlex software (RedShirt Imaging, GA, USA).
18. AcqKnowledge Data Acquisition and Analysis Software (BIO-PAC Systems Inc., CA, USA).
19. Small alligator clips for cannulation.
20. Wax coated braided silk suture (4-0).

2.3 Langendorff Preparation and Optical Mapping Reagents

1. Tyrode's solution: 121.7 mM NaCl, 25.0 mM NaHCO₃, 4.81 mM KCl, 2.74 mM MgSO₄, 5.0 mM dextrose, 2.5 mM CaCl₂ (pH 7.40, perfused with 95% O₂-5% CO₂).
2. Blebbistatin (+/-).
3. Di-4-ANEPPS.
4. Heparin.
5. Sodium pentobarbital (390 mg/mL).

3 Methods

3.1 Anesthesia and Tail Vein Injection

1. After the arrival of animals into the local facility, allow for at least a 2-day acclimation period before subjecting them to experimental procedures.
2. For each rat to be injected with the shTSPO construct, prepare a microcentrifuge tube containing 5×10^{11} gc/mL AAV-CMV-GFP-U6-rm-TSPO-shRNA in 0.3 mL physiological saline, on ice. For example, if the stock solution is 8×10^{13} gc/mL, add 6.25 µL into 0.3 mL saline.

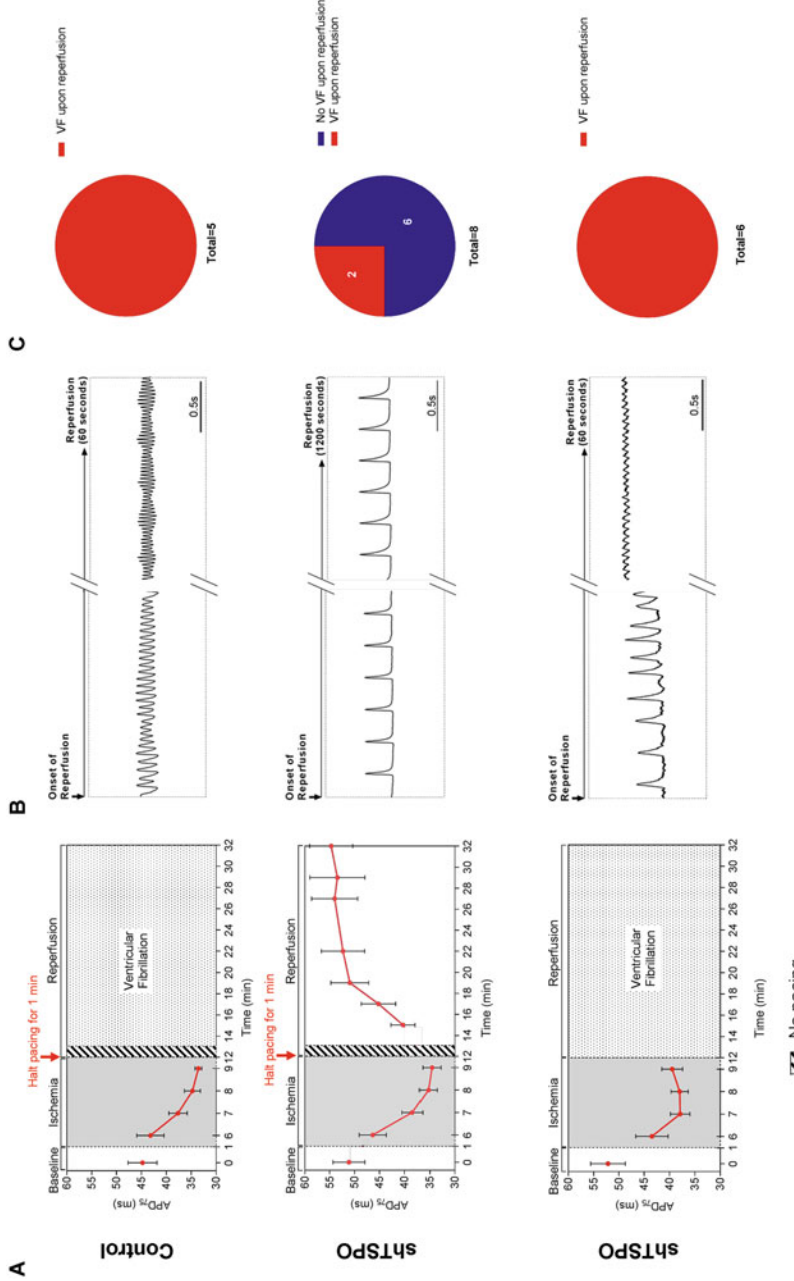


Fig. 4 The electrophysiological response of control and shTSPo hearts to ex vivo ischemia–reperfusion injury with and without pacing modification. (a) Quantification of APD₇₅ during the course of I/R protocols in control and shTSPo hearts. As expected, ischemia causes substantial action potential shortening, which is reversed upon reperfusion in some shTSPo but not control hearts. Successful recovery of the action potential and prevention of reperfusion-related VF in shTSPo hearts is dependent on a pacing modification (halt of pacing during the first 60 s of reperfusion). (b) Representative action potential traces recorded during the reperfusion phase highlighting the different electrophysiological outcomes. Reperfusion following 12 min of global no flow ischemia resulted in rapid onset of VF in control but not shTSPo hearts when pacing was halted during the first minute of reperfusion. When pacing is not halted during the initial phase of reperfusion, shTSPo hearts are also prone to the onset of arrhythmias. (c) Pie charts summarizing the incidence of reperfusion arrhythmias in control in shTSPo hearts subjected to standard and modified pacing protocols during I/R challenge

3. Into a 1 mL syringe, draw 0.4 mL saline followed by the 0.3 mL virus–saline mix. Leave aside.
4. Perform intraperitoneal (IP) injections of ketamine–xylazine into each animal to induce light sedation, in accordance with IACUC guidelines for rodent anesthesia.
5. Place lightly anesthetized rat into the restrainer and place the restrainer onto the preheated heating pad (*see Note 1*).
6. Locate the lateral tail veins on either side of the tail (Fig. 2a), and carefully inject the virus/saline mixture into the vein (Fig. 2b) (*see Note 2*).
7. Allow time for the effect of ketamine to wear off before placing the animals back into their cages.
8. Following the gene transfer procedure, maintain rats for at least 3–4 weeks to allow effective transfer of the introduced gene, before sacrifice.

3.2 Ex Vivo Optical Mapping

1. Turn on the light source, the heat circulating pump, and the 37 °C water bath 20–30 min prior to experimentation to allow for temperature equilibration.
2. Prepare fresh Tyrode's solution (~2 L per rat heart depending on the duration of the protocol). Place a petri dish containing Tyrode's solution in a –20 °C freezer for 30–40 min to allow the solution to become ice-cold without freezing.
3. Prime the perfusion system with oxygenated and pH equilibrated fresh Tyrode's solution for at least 20–30 min before the start of the experiment. The Tyrode's reservoir should be continuously oxygenated with 95% O₂–5% CO₂, and maintained in the 37 °C water bath throughout the experiment.
4. Aliquot 200 mL of Tyrode's solution in a beaker, and add required volumes of di-4-ANEPPS and blebbistatin to yield final concentrations of 1 μM and 10 μM, respectively. Mix well, and place the beaker in the 37 °C water bath to replace the Tyrode's reservoir from **step 3**.
5. Prior to surgery, perform IP injections of heparin, followed by pentobarbital to induce anesthesia in each animal.
6. After the successful induction of anesthesia, quickly excise the heart, and immerse in a petri dish containing ice-cold Tyrode's solution.
7. Locate the aorta and trim off excess tissue surrounding it. To confirm the identity of the vessel, apply light compression on the ventricles using tweezers, which will cause expulsion of the residual blood remaining in the ventricles through the aorta.
8. Perform cannulation with the aid of tweezers. Insert the cannula through the aorta until the base of aorta is reached.

Stabilize the heart on the cannula by placing a small alligator clip around the aorta. Ensure proper continuous perfusion.

9. Make two double knots around the aorta using two pieces of silk suture. Remove the alligator clip.
10. Consider removing the atria in order to prevent atrial stimulation of the ventricles, which would interfere with the applied pacing.
11. Monitor the perfusion pressure and maintain within a physiological range of 60–70 mmHg by varying the flow rate as necessary (*see Note 3*).
12. Insert the pacing electrode ~1 mm below the epicardial surface in the center of the anterior wall of the heart (Fig. 3) (*see Note 4*).
13. Immerse the cannulated and perfused heart in a tissue bath containing Tyrode's solution, and stabilize its position by gently pressing against a transparent imaging window with the help of a built-in sponge piston (Fig. 3).
14. Position the ECG electrodes on either side of the heart until a stable cardiac rhythm can be monitored.
15. Using the AcqKnowledge software, adjust the ECG sampling rate to 1000–2000 Hz.
16. Once it is ensured that a constant pressure, perfusion flow, and a stable cardiac rhythm are achieved, swiftly move the suction end of the perfusion system from the bucket containing Tyrode's solution to the beaker containing di-4-ANEPPS and blebbistatin in 200 mL of Tyrode's solution.
17. Allow constant perfusion for about 20 min. To confirm sufficient delivery of blebbistatin, visualize the heart through the live video camera: there will be minimal mechanical response to stimulation once a sufficient amount of blebbistatin has been delivered. To confirm adequate di-4-ANEPPS staining, record a test image of fluorescence to check for optical action potentials.
18. Determine the diastolic threshold for pacing (*see Note 5*). Set the pacing voltage to $1.2\times$ or $1.5\times$ the diastolic pacing threshold.
19. Maintain pacing at a steady state pacing cycle length (260–300 ms). Obtain 2 s optical action potential recordings every 30–60 s for at least 20 min. Use the last recording as the preischemia baseline measurement. Note the pressure and the perfusion rate during this recording.
20. Induce global no-flow ischemia by interrupting the perfusion flow for 12 min. This provides approximately 75% incidence of postischemic VF allowing one to determine efficacy of antiarrhythmic treatments. Shorter ischemia durations are associated

with lower incidence of postischemic VF which are optimal for evaluation of proarrhythmic factors [16]. During the ischemia phase, obtain 2-s recordings every 30–60 s (*see Note 6*).

21. At the end of the 12 min ischemia phase, restart perfusion by turning on the flow pump, and immediately halt pacing for the first minute of reperfusion (*see Note 7*). Ensure that the perfusion rate is adjusted to match the pressure levels that were recorded during the preischemia baseline recording. Adjust perfusion flow to match the preischemia perfusion pressure.
22. Obtain 2 s recordings every 30–60 s for the next 20 min of reperfusion (*see Note 8*).

4 Notes

1. As an alternative to the use of a heating pad, restrained rats can be placed under an infrared light source to prevent hypothermia under anesthesia. Care must be taken to prevent heat injuries or overheating, especially if a heating lamp is used. Placing the animal in the warm environment for a few minutes would also help dilate the tail veins and make them easier to locate.
2. Gently rub a gauze pad sprayed with 70% ethanol along the tail to clear the outer layers of the skin. This will enhance the visibility of the tail veins.
3. Before cannulation of the heart on the Langendorff apparatus, the perfusion rate is set at 15 mL/min. When there is no resistance at the end of the Langendorff apparatus, i.e., when the heart is not cannulated, the pressure sensor is calibrated to read 0 mmHg. After cannulation, the perfusion rate is varied as necessary to achieve a pressure range of 60–70 mmHg. It is important to continuously monitor the perfusion pressure to ensure its stability within the specified range. Pressure can be reinstated by varying the perfusion flow rate as necessary. As a metric of viability, we keep track of the perfusion flow-to-pressure ratio and volume conducted ECGs throughout the study.
4. It is useful to form a hook shape at the tip of the electrode to prevent detachment from the wall. To ease the insertion of the electrode, it may be threaded through a 26G × ½ in. needle. The needle is inserted into the anterior epicardium, midway between apex and base. After insertion, pull the needle out, leaving the electrode wire attached to the heart. Strip the insulating material from the tip of the wire that will be in contact with the heart prior to insertion.

5. To determine the diastolic threshold for pacing, slowly increase the voltage of the pulse (duration 1–2 ms) from 0 mV while monitoring the volume-conducted ECG. When a change in ECG morphology with clear evidence of 1:1 pacing is encountered, record the pulse duration and voltage as the diastolic threshold. Following this, increase the voltage value by 50% to reliably pace at $1.5 \times$ the diastolic threshold. In the event of loss of capture, slowly increase the voltage until capture is regained.
6. During ischemia, an abrupt drop in pressure will be observed due to termination of perfusion flow. It is important to avoid the overshoot in perfusion pressure at the onset of reperfusion by calibrating the flow to match the preischemia perfusion pressure.
7. Important: unless pacing is turned off during the first minute of reperfusion, the TSPO knockdown hearts will be prone to arrhythmias (Fig. 4a–c), and therefore it will not be possible to assess the recovery of the action potential duration (APD).
8. Monitor the ECG signals and action potentials during this period to detect any signs of arrhythmic activity, including ventricular tachycardia/fibrillation (VT/VF). For this study, we defined sustained VT/VF as episodes that did not spontaneously self-terminate within at least 5 min.

Acknowledgments

This work was supported by grants from the National Institutes of Health (R01 HL091923 and R21AG054211) and the American Heart Association (13GRNT17000046) to FGA.

References

1. Roth GA, Huffman MD, Moran AE et al (2015) Global and regional patterns in cardiovascular mortality from 1990 to 2013. *Circulation* 132(17):1667–1678. <https://doi.org/10.1161/CIRCULATIONAHA.114.008720>
2. Hausenloy DJ, Yellon DM (2013) Myocardial ischemia-reperfusion injury: a neglected therapeutic target. *J Clin Invest* 123(1):92–100. <https://doi.org/10.1172/JCI62874>
3. Akar FG, Aon MA, Tomaselli GF et al (2005) The mitochondrial origin of postischemic arrhythmias. *J Clin Invest* 115(12):3527–3535. <https://doi.org/10.1172/JCI25371>
4. Aon MA, Cortassa S, Akar FG et al (2006) Mitochondrial criticality: a new concept at the turning point of life or death. *Biochim Biophys Acta* 1762(2):232–240. S0925-4439(05)00105-5
5. Jin H, Nass RD, Joudrey PJ et al (2010) Altered spatiotemporal dynamics of the mitochondrial membrane potential in the hypertrophied heart. *Biophys J* 98(10):2063–2071. <https://doi.org/10.1016/j.bpj.2010.01.045>
6. Nederlof R, Xie C, Eerbeek O et al (2013) Pathophysiological consequences of TAT-HKII peptide administration are independent of impaired vascular function and ensuing ischemia. *Circ Res* 112(2):e8–e13. <https://doi.org/10.1161/CIRCRESAHA.112.274308>
7. Xie C, Hu J, Motloch LJ et al (2015) The classically cardioprotective agent diazoxide elicits arrhythmias in type 2 diabetes mellitus. *J*

- Am Coll Cardiol 66(10):1144–1156. <https://doi.org/10.1016/j.jacc.2015.06.1329>
- 8. Brown DA, Aon MA, Akar FG et al (2008) Effects of 4'-chlorodiazepam on cellular excitation-contraction coupling and ischaemia-reperfusion injury in rabbit heart. *Cardiovasc Res* 79(1):141–149. <https://doi.org/10.1093/cvr/cvn053>
 - 9. Seccia TM, Atlante A, Vulpis V et al (1998) Mitochondrial energy metabolism in the left ventricular tissue of spontaneously hypertensive rats: abnormalities in both adeninenucleotide and phosphate translocators and enzyme adenylate-kinase and creatine-phosphokinase activities. *Clin Exp Hypertens* 20(3):345–358
 - 10. Molgaard S, Faricelli B, Salomonsson M et al (2016) Increased myocardial vulnerability to ischemia-reperfusion injury in the presence of left ventricular hypertrophy. *J Hypertens* 34 (3):513–523.; discussion 523. <https://doi.org/10.1097/HJH.0000000000000826>
 - 11. Tang Y, Mi C, Liu J et al (2014) Compromised mitochondrial remodeling in compensatory hypertrophied myocardium of spontaneously hypertensive rat. *Cardiovasc Pathol* 23 (2):101–106. <https://doi.org/10.1016/j.carpath.2013.11.002>
 - 12. Jullig M, Hickey AJ, Chai CC et al (2008) Is the failing heart out of fuel or a worn engine running rich? A study of mitochondria in old spontaneously hypertensive rats. *Proteomics* 8 (12):2556–2572. <https://doi.org/10.1002/pmic.200700977>
 - 13. Meng C, Jin X, Xia L et al (2009) Alterations of mitochondrial enzymes contribute to cardiac hypertrophy before hypertension development in spontaneously hypertensive rats. *J Proteome Res* 8(5):2463–2475. <https://doi.org/10.1021/pr801059u>
 - 14. Ito H, Torii M, Suzuki T (1995) Decreased superoxide dismutase activity and increased superoxide anion production in cardiac hypertrophy of spontaneously hypertensive rats. *Clin Exp Hypertens* 17(5):803–816
 - 15. Power AS, Pham T, Loiselle DS et al (2016) Impaired ADP channeling to mitochondria and elevated reactive oxygen species in hypertensive hearts. *Am J Physiol Heart Circ Physiol* 310(11):H1649–H1657. <https://doi.org/10.1152/ajpheart.00050.2016>
 - 16. Lyon AR, Joudrey PJ, Jin D et al (2010) Optical imaging of mitochondrial function uncovers actively propagating waves of mitochondrial membrane potential collapse across intact heart. *J Mol Cell Cardiol* 49(4):565–575. <https://doi.org/10.1016/j.yjmcc.2010.07.002>
 - 17. Vanhoutte G, Verhoye M, Raman E et al (2002) In-vivo non-invasive study of the thermoregulatory function of the blood vessels in the rat tail using magnetic resonance angiography. *NMR Biomed* 15(4):263–269. <https://doi.org/10.1002/nbm.768>



Chapter 11

Cardiac Tissue Engineering Models of Inherited and Acquired Cardiomyopathies

Irene C. Turnbull, Joshua Mayourian, Jack F. Murphy,
Francesca Stillitano, Delaine K. Ceholski, and Kevin D. Costa

Abstract

The lack of biomimetic in vitro models of the human heart has posed a critical barrier to progress in the field of modeling cardiac disease. Human engineered cardiac tissues (hECTs)—autonomous, beating structures that recapitulate key aspects of native cardiac muscle physiology—offer an attractive alternative to traditional in vitro models. Here we describe the use of hECTs to advance our understanding and modeling of cardiac diseases in order to test therapeutic interventions, with a focus on contractile dysfunction in the setting of inherited and acquired forms of cardiomyopathies. Four major procedures are discussed in this chapter: (1) preparation of hECTs from human induced pluripotent stem cell-derived cardiomyocytes (hiPSC-CMs) on single-tissue and multitissue bioreactors; (2) data acquisition of hECT contractile function on both of these platforms; (3) hECT modeling of hereditary phospholamban-R14 deletion-dilated cardiomyopathy; and (4) cryo-injury and doxorubicin-induced hECT models of acquired cardiomyopathy.

Key words Tissue engineering, Genetic cardiomyopathy, Acquired cardiomyopathy, Contractility, Models of disease, Stem cells

1 Introduction

Nonischemic dilated cardiomyopathy (NIDCM), which is characterized by ventricular dilation and systolic dysfunction in the absence of coronary artery disease, is a major form of heart failure impacting 1 in 20,000 adults per year in the USA [1]. Inotropic support is a strategy of medical management for NIDCM, but it does not treat the underlying cause. This highlights a critical need to develop novel therapeutic strategies for restoring cardiac performance in NIDCM. Stem cell therapy has emerged as a promising approach to address this problem [2].

In our hands, human engineered cardiac tissues (hECTs)—capable of recapitulating key aspects of native cardiac muscle physiology [3]—provide a simple yet effective contractility assay to study

therapeutic strategies [4], such as stem cell-based cardiotherapies, in the context of healthy [5] and myocyte-depleted [6] conditions.

Nevertheless, to further progress the translational relevance of such findings (and other therapeutic interventions), it is necessary to continue improving hECT models of both ischemic and nonischemic cardiomyopathy. To this end, in this chapter, we highlight our recent efforts to advance hECT models of NIDCM and ischemic cardiomyopathy.

First, we provide step-by-step instructions on how to create hECTs with our single- and multi-hECT bioreactor platforms using human induced pluripotent stem cell-derived cardiomyocytes (hiPSC-CMs), and subsequently measure their contractile performance. Next, as one of the first cardiac tissue engineering groups to model familial dilated cardiomyopathy [7], we provide instructions on how to create an hECT model of inherited dilated cardiomyopathy (hereditary phospholamban-R14 deletion-dilated cardiomyopathy hECTs). Finally, motivated by *in vivo* animal models of acquired ischemic [8] and nonischemic [9] cardiomyopathy, we present instructions and original data on cryoinjury- and doxorubicin-induced hECT cardiomyopathy models, respectively.

Many *in vitro* disease models are evaluated exclusively using molecular and histology analysis. However, a strength of the hECT system is that it also provides a functional phenotype, which can be further analyzed for structural and molecular characteristics as desired. Altogether, this chapter complements our previous work to further support the use of hECTs as a system to help bridge a gap in traditional experimental models of the heart, in order to provide new opportunities for advancing our understanding of cardiac disease and therapeutics.

2 Materials

2.1 Cell Collection

1. hiPSCs (*see Notes 1 and 2*).
2. mTeSRTM 1.
3. 6-well tissue culture treated plates.
4. +I media: RPMI 1640, B-27 Supplement (50×), 1% penicillin–streptomycin.
5. –I media: RPMI 1640, B-27 Supplement Minus Insulin (50×), 1% penicillin–streptomycin.
6. 0.025% trypsin.
7. DMEM–F-12 Media, 1:1 nutrient mixture.
8. CHIR99021 (30 mM stock solution).
9. IWR-1 (10 mM stock solution).

10. 1× phosphate-buffered saline without calcium or magnesium (PBS, pH 7.4), sterile-filtered.
11. 15 mL conical tubes.
12. 1.5 mL Eppendorf tubes.

2.2 Tissue Formation

1. 5 mg/mL type-I collagen.
2. 1 M Sodium hydroxide NaOH.
3. 10× PBS (without calcium or magnesium).
4. Sterile ultrapure deionized water.
5. 10× Minimum Essential Medium (MEM).
6. 0.2 N HEPES pH 9.
7. Stem cell-qualified Matrigel.
8. Petri dishes 60 mm × 15 mm style and 100 mm × 20 mm style.

2.3 Bioreactor Construction

1. Sylgard 184 silicone elastomer kit (polydimethylsiloxane, or PDMS) custom molds.
2. Alcohol resistant black marker.
3. 2% bovine serum albumin (BSA).
4. Silicone vacuum grease.
5. Tweezers.

2.4 Data Acquisition

1. Laptop.
2. GRASS S88X stimulator (Astro-Med, West Warwick, RI).
3. High-speed monochrome camera, with the ability to capture images at up to 90 frames per second. Such as PixeLINK PL-B741 camera or similar.
4. Dissecting microscope. Olympus SZ61 or similar.
5. Carbon rods (for single-tissue data acquisition only).
6. Carbon plates (for multitissue data acquisition only).
7. Tungsten wire, gauge 0.010".
8. Plate heater (recommended for experiments where physiologic temperature condition is desired).
9. Boom microscope stand.
10. Gooseneck lamp.
11. Vibration isolation table. C-shape table that fits inside the laminar flow hood, this reduces transmission of vibration from the motor/blower to the bioreactor that is being tested.
12. Laminar flow hood.
13. Mirror (20 mm enhanced aluminum coated, right angle mirror, Edmund Optics).

14. Laboratory Jack 2× (for multitissue data acquisition only).
15. $\frac{3}{4}$ " spacers 4×.
16. LabVIEW (National Instruments, Austin, TX) and MATLAB (Natick, Massachusetts) software. Custom LabVIEW program used for data acquisition, and MATLAB script used for data analysis are available upon request from the authors.

3 Methods

3.1 Cardiomyocyte Differentiation of hiPSCs

1. To start the cardiomyocyte differentiation at 80–90% confluence (*see Note 3*) of hiPSCs in a 6-well plate, replace mTeSR™ 1 maintenance media (*see Note 4*) with 2 mL –I media containing CHIR99021 (10 μ M final concentration) per well.
2. After 24 h, wash with DMEM/F12 (*see Note 5*) and replace with 2 mL –I media per well.
3. After 48 h, wash with DMEM/F12 and replace with 2 mL –I media containing IWR-1 (5 μ M final concentration) per well.
4. After 24 h, wash with DMEM/F12 and replace with 2 mL –I media containing IWR-1 (5 μ M final concentration) per well.
5. After 24 h, wash with DMEM/F12 and replace with 2 mL –I media (without IWR-1) per well.
6. Repeat Subheading 3.1, step 5.
7. After 24 h, wash with DMEM/F12 and replace with 2 mL +I media per well.
8. Repeat Subheading 3.1, step 7 (*see Note 6*) up to days 20–30 of differentiation.

3.2 Preparing the Single-Tissue Bioreactor

1. Mark the tip of bioreactor posts with alcohol resistant black marker to facilitate later video tracking.
2. Assemble single-tissue bioreactor with inserts (Fig. 1a).
3. Sterilize (*see Note 7*).
4. In a laminar flow hood, using sterile tweezers, remove the PDMS mold from the autoclave bag; and while holding the mold with the tweezers, apply a spare amount of vacuum grease with the aid of a pipette tip to the bottom of the mold (*see Note 8*) and then place it on the 60 mm dish applying pressure so the mold adheres to the bottom of the dish.
5. Pipette approximately 150 μ L of 2% BSA into the well of the single-tissue bioreactor, and place in the incubator (37 °C and 5% CO₂) for 1 h.
6. Remove the BSA, then rinse by serial washes as follows, add approximately 150 μ L of 1× PBS, remove and repeat, then add

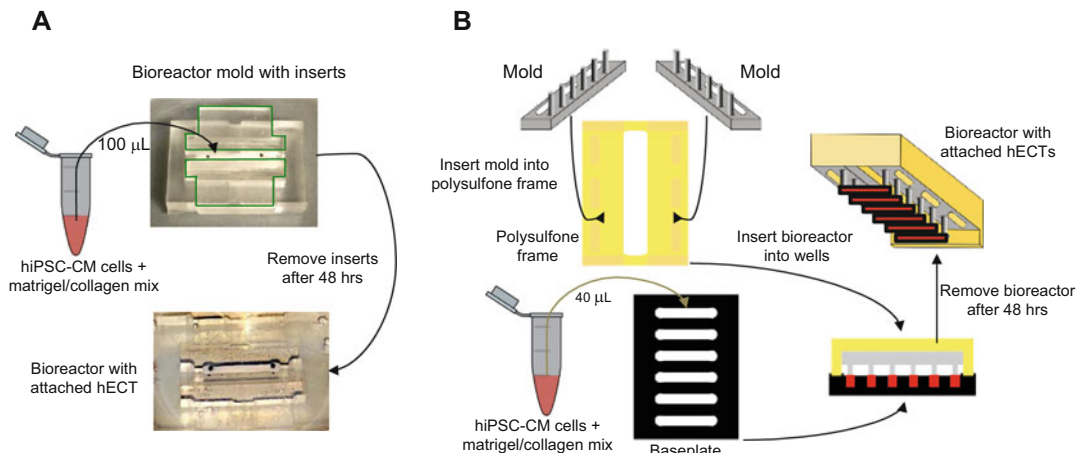


Fig. 1 Overview of hECT construction. hECTs are created either with (a) single-tissue or (b) multitissue bioreactors. For single-tissue bioreactors (a), a set volume of the cell–extracellular matrix mix is added to each well of the bioreactor. After 2 h of incubation the bioreactor is submerged in culture media for 48 h. Following hECT compaction, the inserts are slowly removed from the bioreactor. For multitissue bioreactors (b), a set volume of the cell–extracellular matrix mix is added to each well of the baseplate. Six pairs of bioreactor posts are then submerged into matching baseplate wells for 48 h. Following hECT compaction, the bioreactor is slowly lifted out of the baseplate with the tissues suspended between pairs of end-posts

approximately 150 μ L of distilled water, remove and repeat. After the second rinse of distilled water aspirate all the liquid from the well and leave the single-tissue bioreactor in the laminar flow hood to air dry.

3.3 Collecting hiPSC-CMs from the Monolayer

In our experience an effective time window to harvest the cells for hECT fabrication is between 20 and 30 days of differentiation, as convenient for experimental planning.

1. On the day of cell harvest, first wash cells once with 1 \times PBS.
2. Add 1 mL 0.025% trypsin per well (*see Notes 9 and 10*).
3. Incubate for 5 min at 37 °C and 5% CO₂.
4. Remove cells from each well mechanically using the 0.025% trypsin from each well.
5. Place trypsin–cell mix into 15 mL conical tube, and neutralize with equal amount of cold (4 °C) +I media.
6. Centrifuge at 300 \times *g* for 5 min.
7. Aspirate and resuspend with 10 mL +I media.
8. Count cells using hemocytometer.
9. Centrifuge at 300 \times *g* for 5 min (*see Note 11*).

3.4 Preparing the Collagen–Matrigel Mix

1. Keep all solutions on ice. Keep cells (hiPSC-CM) at room temperature. All volumes listed below are per hECT for the single-tissue bioreactor. For the multitissue bioreactor, multiply each volume by 0.4–0.6 (*see Note 12*).

2. Dilute 100.0 μ L of 5 mg/mL collagen stock to 3.125 mg/mL with 41.5 μ L of sterile ultrapure deionized water, 2.5 μ L of 1 M NaOH, and 16 μ L of 10 \times PBS, avoid bubbles when mixing.
3. Add 20.0 μ L of both 10 \times MEM and 0.2 N HEPES pH 9 to the dilute collagen mixture (previous step) to create the collagen mix.
4. Add stem cell-qualified Matrigel to the collagen mix (0.9 mg/mL final concentration).
5. Store the collagen–Matrigel mix on ice.

3.5 Forming hECTs on the Single-Tissue Bioreactor

For a schematic summarizing these steps, *see* Fig. 1a.

1. Aspirate supernatant from hiPSC-CM pellet.
2. Add 50 μ L of collagen–Matrigel mix per million cells (hiPSC-CM) to the cell pellet (*see Note 13*).
3. Add 100 μ L hiPSC-CMs + collagen–Matrigel mix into the well of the single-tissue bioreactor, avoid bubbles (*see Notes 14 and 15*).
4. Discard top lid of 60 mm dish; place 60 mm dish into 100 mm dish (*see Note 16*).
5. Add 1 mL of +I media into the edge of the 60 mm dish, being careful not to drop any media onto the bioreactor. This is to ensure the cell–collagen mixture does not get dehydrated during gel polymerization.
6. Place into incubator for 2 h at 37 °C and 5% CO₂, this is sufficient time for the collagen to polymerize.
7. Remove from incubator and place in sterile hood.
8. Slowly add approximately 14 mL +I media into 60 mm dish so that the entire bioreactor is covered with media (*see Note 17*).
9. Return assembly to incubator for 48 h at 37 °C and 5% CO₂.
10. Remove from incubator and bring to laminar flow hood; using sterile tweezers slowly remove the inserts and exchange media (half volume).
11. Continue half-media exchanges with +I media daily for tissue maintenance.

3.6 Preparing the Multitissue Bioreactor

For a schematic summary of these steps, *see* Fig. 1b. Carry out after steps described in Subheading 3.1.

1. Mark the tip of bioreactor posts with alcohol resistant black marker.
2. Sterilize (*see Note 7*).
3. Insert rack of bioreactor posts into polysulfone frame.

3.7 Forming hECTs Using the Multitissue Bioreactor

For a schematic summary of these steps, *see Fig. 1b*. Carry out after steps described in Subheadings 3.3 and 3.4.

1. Aspirate supernatant from hiPSC-CM pellet.
2. Add 40 μ L of collagen–Matrigel mix per million cells (hiPSC-CM) to the cell pellet (*see Note 18*).
3. Place baseplate in 60 mm dish.
4. Add 40 μ L hiPSC-CMs + collagen–Matrigel mix into each well of the baseplate (*see Note 14*).
5. Insert bioreactor into baseplate (*see Note 19*).
6. Discard top lid of 60 mm dish; place 60 mm dish into 100 mm dish (*see Note 16*).
7. Add 1 mL of +I media into edge of 60 mm dish to prevent dehydration of the gel.
8. Place into incubator for 2 h at 37 °C and 5% CO₂ for gel to polymerize.
9. Remove from incubator and bring to laminar flow hood.
10. Slowly add 14 mL +I media into 60 mm dish (*see Notes 17 and 20*).
11. Place into incubator for 48 h at 37 °C and 5% CO₂ (*see Note 21*).
12. Remove from incubator; slowly lift bioreactor out of baseplate (*see Note 22*), and place bioreactor into new 60 mm dish with 14 mL +I media.

3.8 Data Acquisition for Single-hECT and Multi-hECT Bioreactors

For a schematic summary of these steps, *see Fig. 2*.

1. Set up laminar hood with vibration isolation table, gooseneck lamp, boom stand, dissecting microscope and high-speed camera. For single-hECT bioreactors, place 60 mm dish with bioreactor on top of plate heater, and align microscope to view the hECT from the top (Fig. 2a). For multi-hECT bioreactor, include the laboratory jack, place spacers equally distant with mirror in the center, place the 100 mm dish containing the 60 mm dish with the multitissue bioreactor carefully on top of the spacers, and align the microscope to view the reflection of the multitissue bioreactor on the mirror (Fig. 2b, e) (*see Note 23*). Connect grass stimulator and camera to laptop.
2. Adjust microscope magnification and limit region of interest to have both posts of one hECT in view. Using an Olympus SZ61 microscope most of the acquisitions are done within the 1–1.5 \times magnification range (Fig. 2c). Our approach is to use a binary filter of the image to maximize contrast, which is why we use the black marker to mark the top of the posts.

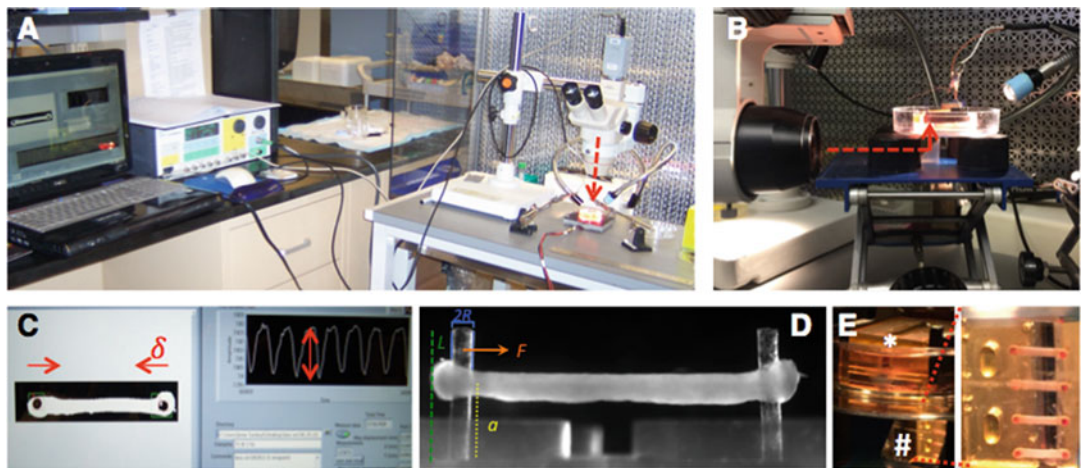


Fig. 2 Overview of hECT data acquisition. (a) Set up for data acquisition from hECT on single-tissue bioreactor. Camera viewing path (dotted red line) aligned with top view of hECT. (b) Set up for data acquisition from hECT multitissue bioreactor. Camera viewing path (dotted red line) aligned with mirror. (c) Screen view during data acquisition, live tracking of inward post-displacement during hECT contraction (δ), with corresponding measurement of the amplitude of each contraction (double headed arrow). (d) Side view of hECT on single-tissue bioreactor with embedded schematic of the measurements included in the calculation of force. (e) Multitissue bioreactor (*) with tissues submerged facing the bottom of the dish, and reflected image of hECT on mirror (#) to allow for imaging and data collection without manipulation of the hECT

3. Set the camera to capture at a high frame rate (90 frames per second) by increasing stepwise the speed and light level.
4. Using a custom LabVIEW program (available upon request), record the displacement of the posts without electrical stimulation to analyze the spontaneous contractile properties of the hECT.
5. Place carbon rods (or carbon plates) adjacent to the single-tissue (or the multitissue) bioreactor, respectively, and connect them to the grass stimulator electrodes (see Note 24).
6. Using a custom LabVIEW program, record the displacement of the posts with electrical stimulation (see Note 25).
7. Measure the post heights and tissue height on the posts by acquiring a side view image of the hECT as in Fig. 2d (see Note 26). For the single tissue bioreactor, place the mirror in the 60 mm dish along a long end of the bioreactor. For the multi-tissue bioreactor acquire side view images with the microscope looking directly through the 60 mm dish.
8. The data is then processed using a custom MATLAB script (available upon request) to produce the results for the different twitch parameters that are analyzed.

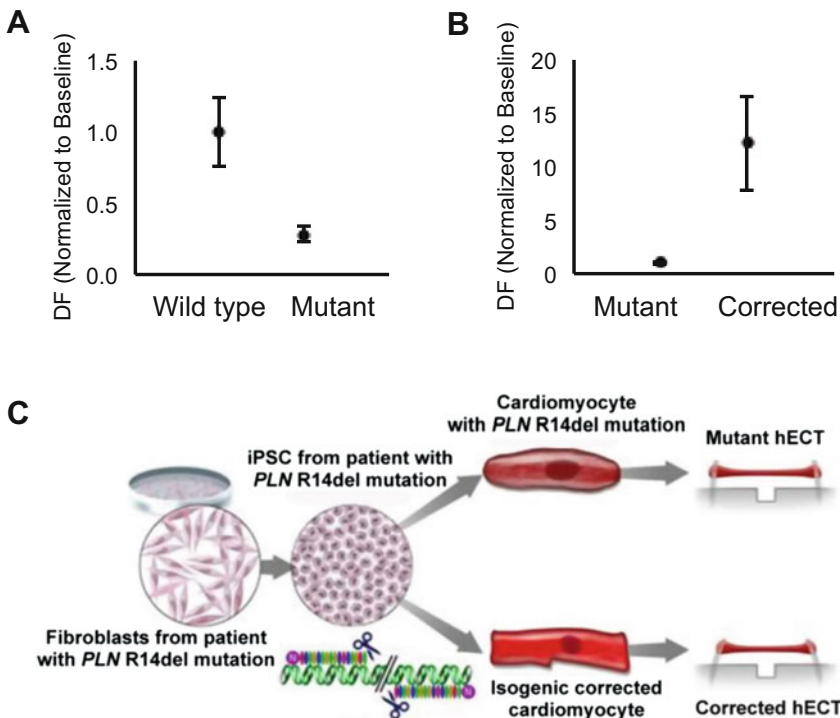


Fig. 3 hECT Inherited Models of Cardiac Disease. **(a)** Effects of model of inherited dilated cardiomyopathy on hECT developed force (DF) (mean \pm SEM, $n = 4\text{--}7$). **(b)** Effects of genetic correction of model of inherited dilated cardiomyopathy on hECT developed force (DF) (mean \pm SEM, $n = 4\text{--}7$). **(c)** Overview of method for inherited dilated cardiomyopathy model and genetic correction of the model; adapted from [7] with permission

3.9 hECT Model of Inherited Dilated Cardiomyopathy

Carry out steps in Subheadings 3.1 through 3.5 using hECT from distinct groups such as: wild type (hiPSC from healthy donor), mutant (hiPSC from patient carrier of the DCM- associated mutation) or isogenic corrected (using gene editing). Upon comparison of the contractile performance of the different groups, hECT fabricated with hiPSC-CM from the patient shows a phenotype of impaired contractile function when compared to wild type (Fig. 3a) that can be genetically corrected (Fig. 3b, c) (see Note 27).

- Follow steps described above in Subheading 3.5 to fabricate the hECTs.
- On day 5 of fabrication, switch to media with serum (composition of the media with serum are described in Note 17).
- Upon reaching day 7, pace hECTs using methods described above (see Subheading 3.8).
- Rinse with 1× PBS.
- Cover hECT in media with serum.
- Place in incubator if pacing at additional later time points is desired.

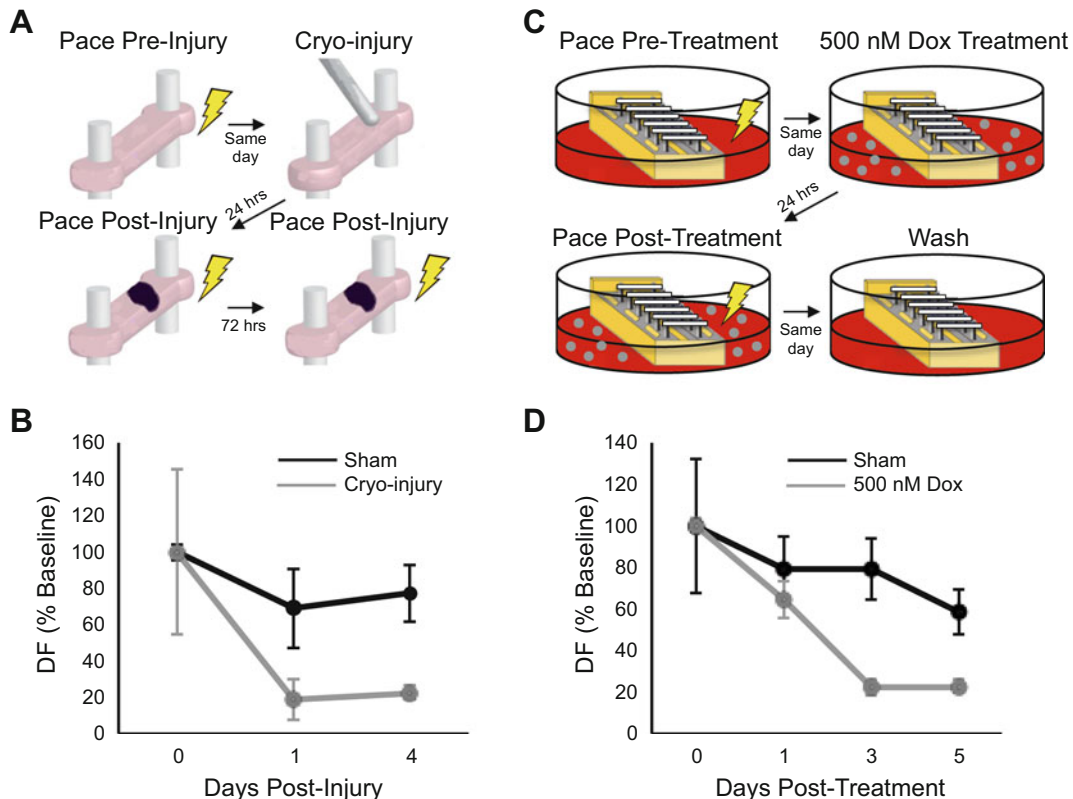


Fig. 4 hECT models of acquired cardiac disease. **(a)** Overview of cryo-injury method for acquired ischemic cardiomyopathy hECT model. **(b)** Effects of cryo-injury model (grey) on hECT developed force (DF) over time (mean \pm SEM, $n = 2\text{--}3$). **(c)** Overview of doxorubicin (Dox) method for acquired nonischemic cardiomyopathy hECT model. **(d)** Effects of 500 nM Dox (grey) on hECT DF over time (mean \pm SEM, $n = 4$)

3.10 Cryo-Injury hECT Cardiomyopathy Model

For a schematic summary of the steps, see Fig. 4a. The contractile performance of representative hECTs during this intervention is shown in Fig. 4b, where in acute injury you expect a decrease in function [8].

1. Follow steps described above in Subheadings 3.4 and 3.5 to fabricate the hECTs.
2. Six days post-tissue formation, pace hECTs using methods described above to measure preinjury baseline function (see Subheading 3.8).
3. Remove +I media to fully expose the hECT.
4. Lay a 1.6-mm diameter steel pin frozen in liquid nitrogen on the hECT for 5 s. For sham use a room temperature pin.
5. Add a few drops of +I media directly at the site where the steel pin is in contact with the hECT; this will thaw the region so the pin can be safely removed. Removing the frozen steel pin from

the hECT without previously warming it up with media will result in tearing off the portion of the hECT that is in contact with the frozen steel pin.

6. Cover hECT in +I media.
7. Place in incubator for 24 h at 37 °C and 5% CO₂.
8. Pace hECTs using methods described above (*see* Subheading 3.8) to measure short-term post-injury contractile function.
9. Rinse with 1× PBS.
10. Cover hECT in +I media.
11. Place in incubator for 72 h (or longer as desired) at 37 °C and 5% CO₂.
12. Pace hECTs using methods described above (*see* Subheading 3.8) to monitor long-term post-injury contractile function.

3.11 Doxorubicin-Induced hECT Cardiomyopathy Model

For a schematic summary of these steps, *see* Fig. 4c. The contractile performance of representative hECTs during this intervention is shown in Fig. 4d, where the doxorubicin treated hECT will show a sharp decrease in function [9] (*see* Note 28).

1. Five days post-tissue formation, pace hECTs using methods described above (*see* Subheading 3.8) to establish pre-doxorubicin baseline contractile function.
2. Rinse with 1× PBS.
3. Transfer bioreactor to new 60 mm dish with +I media containing 500 nM doxorubicin.
4. Place in incubator for 24 h at 37 °C and 5% CO₂.
5. Pace hECTs using methods described above (*see* Subheading 3.8) to measure short-term post-doxorubicin contractile function.
6. Rinse with 1× PBS.
7. Transfer bioreactor to new 60 mm dish with +I media.
8. Place in incubator for 48 h at 37 °C and 5% CO₂.
9. Pace hECTs using methods described above (*see* Subheading 3.8) to monitor long-term post-doxorubicin contractile function.
10. Repeat Subheading 3.11, steps 6 through step 9 as needed for longer term studies.

4 Notes

1. For Subheading 3.9, hiPSCs were generated from a patient with the PLN R14del mutation [7]. For Subheadings 3.10 and 3.11, the SKiPS-31.3 line was used. This line was

generated from dermal fibroblasts from a healthy 45-year-old male volunteer with no symptoms of cardiovascular disease [10].

2. Differentiations work best using hiPSCs between passages 30 and 70.
3. Confluency greatly affects differentiation efficiency.
4. E8 media can also be used for maintenance.
5. Washing away dead cells with DMEM/F12 helps improve differentiation efficiency.
6. At this stage of differentiation, changing media every 48 h (with 3 mL per well), rather than every 24 h (with 2 mL per well), is also a viable option. After day 10 of differentiation, it is not necessary to wash with DMEM:F12.
7. The PDMS molds can withstand sterilization cycles in a steam autoclave up to 121 °C.
8. The vacuum grease helps to adhere the mold to the bottom of the culture dish, so that in later steps, when the dish is filled with media, the single-tissue bioreactor will remain submerged. Avoid applying vacuum grease on the center of the mold because that will interfere with visualization of the tissue using an inverted microscope.
9. TrypLE Express can also be used for dissociation.
10. For poor differentiations, it is possible to improve hiPSC-CM purity by mechanically removing only the top layer of cells with the dissociation reagent and without incubation proceed to Subheading 3.3, step 5.
11. Working with 1.5-mL Eppendorf tubes is preferred when making hECTs; cells should be resuspended in 1 mL of +I media post-centrifugation/aspiration and transferred to an Eppendorf tube. Centrifugation is then repeated at $300 \times g$ for 5 min.
12. Using 0.4–0.6 scaling factors have proven successful in our hands. Scaling factor is dependent on desired amount of Matrigel–collagen mix to be used per tissue (*see Note 18*).
13. On average, one well from a six-well plate yields enough hiPSC-CM to fabricate one tissue using a single-tissue bioreactor.
14. To account for pipette error (and to help avoid bubbles), add 10% more of the cell–extracellular matrix mix into the pipette.
15. In the event of bubbles, aspirate the bubble using a 200 µL pipette tip. Let the bubble slowly rise to the top of the tip, and then return back into the well the cell–extracellular matrix that was aspirated with care to not return the bubble to the well.

16. Be sure that if you have relevant information on the lid, transcribe that information to the lid of the 100 mm dish. It also helps to label the bottom of the dish to keep record of the bioreactor inside the dish.
17. To improve compaction, add DMEM containing 10% neonatal bovine serum, 1% penicillin–streptomycin and 0.2% Amphotericin B instead of +I for the first 24–48 h.
18. Using 40–60 μL Matrigel–collagen mix per tissue has proven successful in our hands.
19. Confirm that bioreactor posts are submerged into the wells, but are not bent from touching the bottom or edges of the well.
20. May need to add more +I media to confirm that all hECTs are fully submerged into media.
21. Check on compaction; if compaction is progressing slower than expected it is okay to leave bioreactor in baseplate for an additional 24 h, on the other hand remove earlier if tissue compaction appears accelerated.
22. This method has been updated since [11]. While holding the baseplate at the bottom of the 60 mm dish, the bioreactor is slowly lifted vertically out of the baseplate into a new 60 mm dish with 14 mL +I media.
23. The multitissue bioreactor is maintained in culture and tested with the hECT facing the bottom of the dish; the reflected image on the mirror allows visualizing the tissue without requiring any direct manipulation.
24. To aid in connecting the carbon rods/plates to the grass stimulator electrodes, the electrodes can be fitted with alligator clips soldered to the end of the electrodes; tungsten wire can be looped tightly around the carbon rods/plates; lastly, clasp loose end of each tungsten wire with the alligator clips.
25. The protocol to follow for electrical stimulation should be determined per the experiment. We typically pace the hECT starting at low frequency (0.25 Hz), and then record hECT contractions (post displacement) at different frequencies using 0.25-Hz increments; bipolar field stimulation, 5 ms pulse duration, using a 12-V pulse wave (545 mV/mm and 480 mV/mm for single and multitissue bioreactor respectively).
26. The beam bending equation $F = \frac{3\pi ER^4}{2a^2(3L-a)}\delta$ is used to calculate the force (F) (Fig. 2c, d). Post length (L) and tissue height along the posts (a) are measured using a side view image of the hECT; the post displacement (δ) is measured during data acquisition using LabVIEW. The radius (R) and Young's modulus (E) are only required to be measured once upon

fabrication of a bioreactor, and thereafter the values remain constant. Developed Force (DF) is the difference between the maximum and minimum force during each twitch.

27. Furthermore, correction of the phenotype can be tested by using the isogenic control cell line. This has been previously described [7], demonstrating that by using genomic correction of the hiPSC-CM by a TALEN method of targeted gene editing, the corrected hECT showed enhanced contractile force compared to the isogenic mutant tissues (Fig. 3c).
28. In our experience, the adverse effect of doxorubicin on hECT contractile function is dependent on the initial developed force. For desired level of force reduction titrate doxorubicin between 0.25 and 2.0 μ M, administered for no longer than 48 h.

Acknowledgments

This work was supported by NIH/NHLBI K01HL133424 (ICT), NIH/NHLBI 1F30HL134283-01A1 (JM), American Heart Association 15POST25090116 (DKC), and NIH/NHLBI R01HL132226 (KDC).

References

1. Towbin JA, Lowe AM, Colan SD, Sleeper LA, Orav EJ, Clunie S, Messere J, Cox GF, Lurie PR, Hsu D, Canter C, Wilkinson JD, Lipshultz SE (2006) Incidence, causes, and outcomes of dilated cardiomyopathy in children. *JAMA* 296 (15):1867–1876. <https://doi.org/10.1001/jama.296.15.1867>
2. Mushtaq M, DiFede DL, Golpanian S, Khan A, Gomes SA, Mendizabal A, Heldman AW, Hare JM (2014) Rationale and design of the percutaneous stem cell injection delivery effects on neomyogenesis in dilated cardiomyopathy (the POSEIDON-DCM study): a phase I/II, randomized pilot study of the comparative safety and efficacy of transendocardial injection of autologous mesenchymal stem cell vs. allogeneic mesenchymal stem cells in patients with non-ischemic dilated cardiomyopathy. *J Cardiovasc Transl Res* 7 (9):769–780. <https://doi.org/10.1007/s12265-014-9594-0>
3. Turnbull IC, Karakikes I, Serrao GW, Backeris P, Lee JJ, Xie C, Senyei G, Gordon RE, Li RA, Akar FG, Hajjar RJ, Hulot JS, Costa KD (2014) Advancing functional engineered cardiac tissues toward a preclinical model of human myocardium. *FASEB J* 28 (2):644–654. <https://doi.org/10.1096/fj.13-228007>
4. Mayourian J, Ceholski DK, Gonzalez DM, Cashman TJ, Sahoo S, Hajjar RJ, Costa KD (2018) Physiologic, pathologic, and therapeutic paracrine modulation of cardiac excitation-contraction coupling. *Circ Res* 122 (1):167–183
5. Mayourian J, Cashman TJ, Ceholski DK, Johnson BV, Sachs D, Kaji DA, Sahoo S, Hare JM, Hajjar RJ, Sobie EA, Costa KD (2017) Experimental and computational insight into human mesenchymal stem cell paracrine signaling and heterocellular coupling effects on cardiac contractility and arrhythmogenicity. *Circ Res* 121 (4):411–423. <https://doi.org/10.1161/CIRCRESAHA.117.310796>
6. Serrao GW, Turnbull IC, Ancukiewicz D, Kim DE, Kao E, Cashman TJ, Hadri L, Hajjar RJ, Costa KD (2012) Myocyte-depleted engineered cardiac tissues support therapeutic potential of mesenchymal stem cells. *Tissue Eng Part A* 18(13–14):1322–1333. <https://doi.org/10.1089/ten.TEA.2011.0278>
7. Stillitano F, Turnbull IC, Karakikes I, Nonnenmacher M, Backeris P, Hulot JS, Kranias EG, Hajjar RJ, Costa KD (2016) Genomic

- correction of familial cardiomyopathy in human engineered cardiac tissues. *Eur Heart J* 37(43):3282–3284. <https://doi.org/10.1093/eurheartj/ehw307>
8. Strungs EG, Ongstad EL, O’Quinn MP, Palatinus JA, Jourdan LJ, Gourdie RG (2013) Cryoinjury models of the adult and neonatal mouse heart for studies of scarring and regeneration. *Methods Mol Biol* 1037:343–353. https://doi.org/10.1007/978-1-62703-505-7_20
9. Toyoda Y, Okada M, Kashem MA (1998) A canine model of dilated cardiomyopathy induced by repetitive intracoronary doxorubicin administration. *J Thorac Cardiovasc Surg* 115(6):1367–1373. [https://doi.org/10.1016/S0022-5223\(98\)70221-1](https://doi.org/10.1016/S0022-5223(98)70221-1)
10. Karakikes I, Senyei GD, Hansen J, Kong CW, Azeloglu EU, Stillitano F, Lieu DK, Wang J, Ren L, Hulot JS, Iyengar R, Li RA, Hajjar RJ (2014) Small molecule-mediated directed differentiation of human embryonic stem cells toward ventricular cardiomyocytes. *Stem Cells Transl Med* 3(1):18–31. <https://doi.org/10.5966/sctm.2013-0110>
11. Cashman TJ, Josowitz R, Gelb BD, Li RA, Dubois NC, Costa KD (2016) Construction of defined human engineered cardiac tissues to study mechanisms of cardiac cell therapy. *J Vis Exp* 109:e53447. <https://doi.org/10.3791/53447>



Chapter 12

Badimon Perfusion Chamber: An Ex Vivo Model of Thrombosis

M. Urooj Zafar, Carlos G. Santos-Gallego, Lina Badimon, and Juan J. Badimon

Abstract

The Badimon perfusion chamber is an ex vivo model of thrombosis that assesses the thrombogenicity of blood in humans and large animals. It works with native blood thereby excluding any interfering effects of anticoagulants unavoidable with the majority of platelet function testing methodologies. Each variable of the Virchow's triad (blood, blood flow, and endothelial wall) that modulates blood–vessel wall interaction and thrombus formation is incorporated in this perfusion model. These features make this device a valuable tool for the assessment of thrombogenic potential of various diseases and also gauging the efficacy of antithrombotic (anticoagulant and antiplatelet) treatments.

Key words Thrombus, Platelets, Perfusion, Arterial thrombosis, Venous thrombosis

1 Introduction

Acute thrombus formation over a disrupted atherosclerotic lesion or a site of endothelial denudation can lead to devastating consequences, including acute coronary syndrome and stroke [1]. Platelets play a central role in the pathophysiology of thrombus formation but additional factors such as severity of arterial injury and local rheology are also critical [2]. A wide variety of testing methodologies are available to assess the functional status of platelets (platelet aggregometry, multiple electrode aggregometry, VerifyNow®, PFA-100® System, ThromboElastoGraphy, Cone and Plate Analyzer, flow cytometry, etc.), however most of them focus only on the cellular component, frequently in a nonphysiological milieu (i.e., platelets in plasma or as washed platelets) or at best in whole blood with the interfering effect of an anticoagulant. As a result, most of these methodologies fail to account for the effect of shear forces arising from the flow of blood and the interactions of blood with the endothelium.

The Badimon perfusion chamber is an ex vivo model of thrombosis that allows the assessment of blood thrombogenicity in whole blood in the absence of any interfering anticoagulant. The model is unique in that it incorporates all three components of the Virchow's triad (blood, flow, and vessel wall). It has been utilized in the assessment of thrombogenic effects of various diseases (e.g., hyperlipidemia, diabetes, HIV, sickle cell disease, etc.) [3–7] and pathological states (arterial wall injury, atherosclerotic plaques, diesel exhaust inhalation, etc.) [8–12], in the investigation of pathophysiology of acute coronary syndromes [13–15], and in the testing of a wide array of pharmacological interventions (e.g., nitric oxide donors, anticoagulants, antiplatelet drugs, direct factor Xa inhibitors, direct thrombin inhibitors, statins, etc.) [16–22] in both preclinical and clinical studies.

1.1 Principle

The perfusion model works by exposing unaltered blood to thrombogenic tissue at controlled flow rates, thereby mimicking the real world *in vivo* conditions of blood flow as close as is currently achievable. The thrombogenic substrate most frequently used are segments of porcine aorta surgically stripped of the intimal layer to expose the deeper thrombogenic tunica media, but atherosclerotic specimens, isolated cell, as well as biomaterials can also be used. The interaction of flowing blood with the substrate activates platelets and the coagulation system, resulting in deposition of fibrin and platelets and subsequent formation of an acute thrombus over the surface of the substrate. The size of this thrombus can then be measured using digital planimetry.

1.2 Design

The Badimon Perfusion Chamber setup consists of three small Plexiglas® blocks connected in series using tightly fitting interconnecting tubes (Fig. 1). Each block consists of two interlocking pieces with a rectangular recess for the placement of thrombogenic substrate in between. A straight, cylindrical channel runs through the entire length of each block to allow passage of flowing blood. This channel exposes flowing blood to the thrombogenic substrate without interrupting its flow. Depending on the diameter of the channel in the perfusion chamber and the rate of perfusion (controlled by a peristaltic pump), the test can recreate shear rates for various conditions. In the most frequently utilized setup, the channel in the first block (chamber A) is of a larger diameter than the remaining two blocks (chambers B and C). The combination of the channel size and the calculated flow rate (10 mL/min) generates a shear rate of 212 s^{-1} in the first block and 1690 s^{-1} in the remaining two blocks, mimicking the rheological conditions of venous and moderately stenosed arterial flow respectively.

The three interconnected Plexiglas® blocks are attached on both ends with Tygon® tubing and placed inside a $37\text{ }^{\circ}\text{C}$ water bath (Fig. 2). The proximal Tygon® tubing connects to an IV

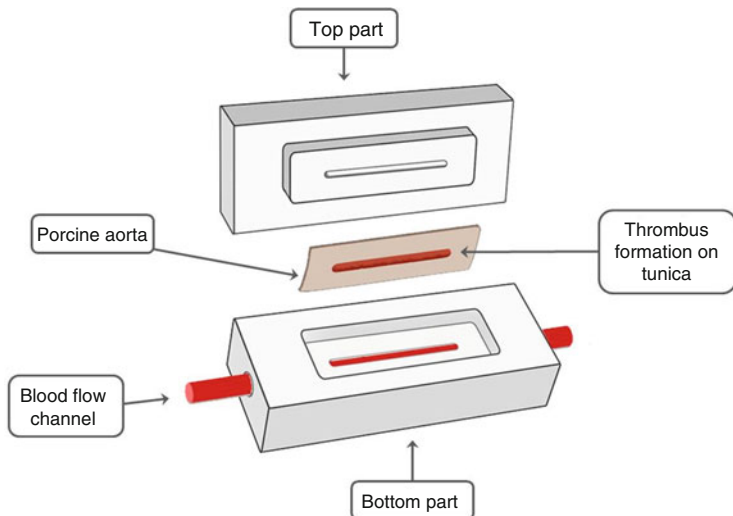


Fig. 1 Side view of an unassembled Plexiglas® block. The rectangular pieces of aorta are surgically stripped of the intimal layer in order to expose the thrombogenic tunica media but without creating any flaps. Those pieces of deendothelialized aorta are fit in the recessed area inside each of the three Plexiglas® blocks, with the medial surface facing the blood flow channel. The assembled block will be later submerged into the warm water bath

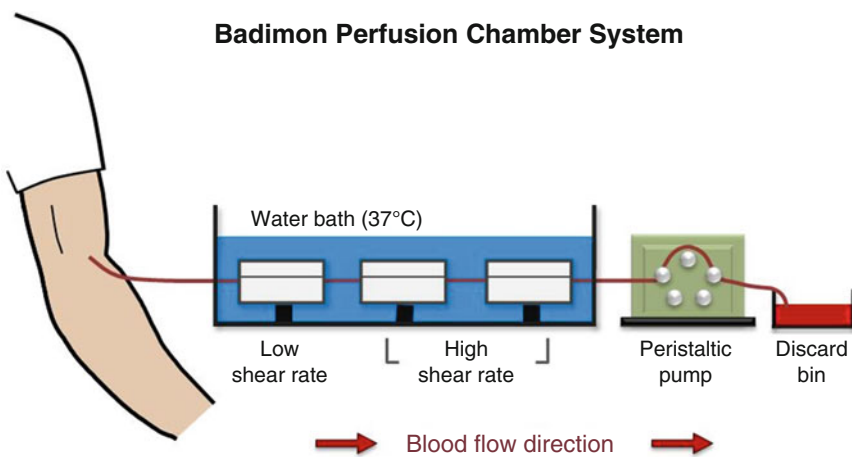


Fig. 2 Schematic depiction of the Badimon perfusion chamber system. Three Plexiglas® blocks are connected serially and submerged in a warm water bath. The blood flows from the patient's vein through the 19G IV catheter once the peristaltic pump is connected, and runs through the three Plexiglas® blocks (one for low shear rate and two blocks for the high shear rate) for 5 min. At the end of the experiment, each Plexiglas® block is opened, and the piece of aorta removed and fixed in 4% paraformaldehyde solution for ulterior histological staining

catheter in the patient's arm and serves to pass blood from the vein directly to the perfusion chamber, without any anticoagulation. The distal tubing passes through a peristaltic pump used to pull blood through the system at a constant flow rate, and ends in a discard bin for the collection of used blood. Placement of the pump distal to the perfusion setup avoids shearing and activation of the blood cells prior to their interaction with the substrates. When set up, the perfusion chamber forms a continuous channel starting from the IV catheter in patients arm, passing through each chamber in series and ending on the discard bin. This setup allows a constant, uninterrupted flow of nonanticoagulated blood through the system, exposing it to thrombogenic substrates at predetermined shear rates for the selected duration of time.

The tightly controlled setup minimizes the number of variables thereby allowing reproducible assessments of the pro/antithrombotic effects of various conditions and therapies. Comparisons of perfusion studies conducted in diseased patients versus healthy subjects can assess the thrombotic effects of various pathologies whereas conducting the tests before and after treatment administration can provide information about the efficacy of therapeutic interventions.

2 Materials

1. Plexiglas® blocks.
2. Connecting tubes.
3. Tygon® tubing.
4. Water bath with Thermomix-B water heater.
5. Phosphate-buffered saline (PBS), 0.1 M.
6. Paraformaldehyde, 4%.
7. Peristaltic pump.
8. Discard bin for collecting used blood.
9. Timer.
10. Thrombogenic substrate (Porcine surgically prepared aorta):
Pig aortas are purchased as whole.
11. Tissue cutting board.
12. Razor blades, single-edge industrial.
13. Tissue processing/embedding cassettes.
14. Stereo microscope with digital camera.
15. Image Pro Plus (IPP) software.

3 Methods

The day before the experiment, thrombogenic substrate (pieces of porcine aorta) should be removed from -70°C (*see* Subheading 3.1, step 1) and placed in 4°C fridge for overnight thawing. On the day of the experiment, the water bath should be filled up and started sufficiently ahead of time so that the water temperature is 37°C at the time of the experiment.

3.1 Prestudy Setup

1. Thaw the frozen aortas and clean to completely remove the adventitial layer. The cleaned aortas are cut open longitudinally and then into rectangular pieces small enough (approximately 1 in. \times 0.3 in.) to fit inside the Plexiglas® blocks. The individual pieces are then surgically stripped of the intimal layer in order to expose the underlying thrombogenic tunica media. This step is to be done carefully in order to ensure that the exposed surface is even and without flaps (*see* Note 1). The prepared substrates are stored in 0.1 M PBS at -70°C until the day of experiment.
2. The perfusion chamber system should be setup no earlier than 10 min prior to run. Setting up too early and letting the tissue sit in the system for prolonged duration can lead to swelling of thrombogenic tissue resulting in alterations in the shear rate.
3. Carefully select three pieces of surgically prepared porcine aortas, ensuring they are of similar thickness and free of any flaps (*see* Note 1). Place one piece of aorta in the recessed area inside each of the three Plexiglas® blocks, with the medial surface facing the blood flow channel.
4. Line up the three blocks in series (low shear-rate block at the proximal end), connect using the connecting tubes and place inside the holding container.
5. Attach a piece of Tygon® tubing (~18 in.) to the connecting tube at the distal end; pass the tubing through the peristaltic pump and place its unattached end into the discard bin.
6. To the connecting tube at the proximal end, attach two pieces of Tygon® tubing of unequal lengths (~10 and ~18 in.) using a three-way stopcock. The shorter tubing is immersed in 0.1 M PBS and used to flush the system, while the longer tubing will be attached to the intravenous catheter in the study subject's arm vein at the time of the experiment.
7. Flush the system with 0.1 M PBS to check for leaks (*see* Note 2).
8. Place the setup (holding container with three Plexiglas® blocks containing porcine aorta pieces) into the 37°C water bath.

3.2 Perfusion Chamber Run

An intravenous catheter (preferably at least 19 gauge or even larger inner diameter, to make sure the blood flow is steady) should be

placed in a mid-size vein in the subject's arm prior to experiment. A clean venipuncture is critical for avoiding platelet activation. The first 3 mL of blood should be discarded before starting the perfusion study. Collection of the discard should be used to check the quality of the venous access (*see Note 3*).

1. Set the peristaltic pump at 10 mL/min and timer for 5 min. Run the pump with proximal tubing placed in PBS for 1 min to prime the system.
2. After discarding the initial 3 mL of blood, attach the free end of the proximal Tygon® tubing to the intravenous catheter in the subject's arm vein.
3. Start the peristaltic pump.
4. When the blood flowing from the IV catheter toward the chamber reaches the 3-way stopcock, start the 5-min timer. Let the test run for exactly 5 min. Keep a watchful eye on the blood flow during this time to make sure there are no bubbles (*see Note 4*).
5. At the 5 min mark, switch the stopcock to change the inflow from the IV to the 0.1 M PBS solution and flush the system with PBS for 1 min (*see Note 5*).
6. Disconnect the proximal Tygon® tubing from the IV catheter and remove the distal tubing from the peristaltic pump. Remove the holding container from the water bath.
7. Slowly open each Plexiglas® block and remove the piece of aorta with great care to ensure that the thrombus formed on the surface is not dislodged. Place each piece of aorta in a separate, labeled tube containing 4% paraformaldehyde solution. Make sure the tissue is fully submerged in paraformaldehyde.
The tissues are left in paraformaldehyde for 24–72 h at room temperature for them to be fixed.

3.3 Poststudy Tissue Processing

1. Carefully remove each fixed piece of aorta from the test tube holding it from the corner using forceps. At all times, contact with the part of the aorta exposed to blood during the perfusion study must be avoided. Place the aorta (medial side up) on a clean tissue cutting board.
2. Cut off the edges of the tissue that did not come in contact with blood and discard them.
3. Cut the remaining tissue cross-sectionally into eight strips of approximately equal size.
4. Split the eight strips from each individual aorta piece equally into two prelabeled tissue embedding cassettes. Each chamber run would therefore yield six cassettes (two for each Plexiglas® block), each with four strips of aorta.

5. The cassettes are immersed in a container with 70% alcohol and sent to pathology services for tissue embedding, sectioning and staining.

3.4 Embedding, Sectioning, and Staining

The steps for tissue embedding, sectioning, and staining follow standard protocols utilized in most pathology departments.

1. Tissues are dehydrated in ethanol, cleared in xylene and embedded in paraffin.
2. Five micron sections are cut from each cassette and mounted on slides in duplicates. One slide is generated per cassette, each with approximately four sections (corresponding to the number of aorta strips in the cassette). Each run of the Perfusion Study therefore generates six slides; two for the low shear rate and four for the high shear rate. Each slide is labeled in accordance with the label on its corresponding cassette.
3. Slides are stained using Combined Masson's trichrome Elastin (CME) for the assessment of total thrombus area (Fig. 3 see Note 6).

3.5 Image Acquisition

Images of the slide sections are acquired using a digital camera attached to a stereo microscope. The acquisition is performed at 10× magnification using the available acquisition software (Leica Application Suite, Adobe Photoshop, Image J, etc.). Image of each high-shear section can be acquired in a single frame, however the low-shear sections are wider and will not fit in one frame. Each low-shear section is therefore acquired in two overlapping images. These two images are then merged (using Leica Application Suite, Fiji, etc.) before analysis.

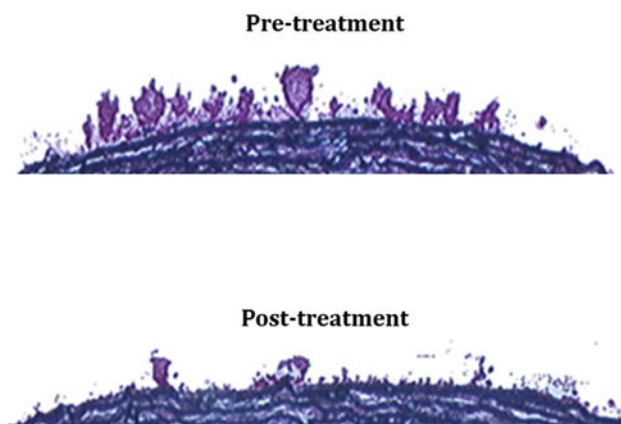


Fig. 3 Representative images of pretreatment and posttreatment (anti factor-Xa) thrombus size. Please note the tunica media in blue and the superimposed thrombus in light purple. Please note how the thrombus size is greatly reduced during Xa inhibitor treatment as compared with baseline (pretreatment situation)

3.6 Image Analysis

Images of chamber study sections are analyzed using Image Pro Plus (IPP) software. The software allows measurement of the area of total thrombus and/or its fibrin and platelet content, depending on the staining. Data for all images from a chamber study are averaged to generate one result for low shear and one for high shear rate.

1. Start the IPP program and open the images to be analyzed.
2. Select the proper Calibration settings for your microscope and magnification by clicking *Measure > Calibration > Select Spatial*. If the proper calibration has not been set, you will have to enter it manually (*see Note 7*).
3. Click the *Irregular AOI* button on the IPP toolbar (this allows you to trace objects on the image).
4. Trace an outline around the thrombi, making sure to exclude any non-thrombus tissue.
5. Click *Measure > Count/Size* from the toolbar (A new window will open up).
6. Check *Automatic Dark Objects* button in the new window and click the *Count* button. The dark object inside the tracing will now be highlighted in color. Check to make sure that the program is not over- or under-estimating the thrombus area (*see Note 8*).
7. Click *View > Statistics* in the new window and copy the results for *Sum* in an Excel sheet. Make sure the Excel file is properly formatted to keep track of the results for each subject, chamber, Plexiglas® block, and image.
8. Once all images are analyzed, calculate the average for all the low shear and the high shear image data for each chamber run to generate one low and one high shear rate result. These are your final results (*see Note 9*).

4 Notes

1. The presence of flaps leads to small pockets of elevated shear rates that can dramatically increase thrombus formation over the flaps. Stripped pieces of aorta that have macroscopically visible flaps should be discarded.
2. Leaks in the system will compromise the validity of the perfusion study. If the setup is not properly sealed, the peristaltic pump will start pulling in water from the temperature-controlled bath into the blood flow channel. This would lead to hemolysis, altered functionality of the platelets and reduced thrombus formation.

3. A good quality venous access is critical to the performance of the Badimon chamber study. If the blood flow is slow during the collection of the discard sample, it is likely to result in a suboptimal chamber study with falsely high thrombus formation due to stasis.
4. Bubbles (air or water) in the blood flow channel during a perfusion run indicate an inadequately placed IV catheter and/or a leak in the system. If the catheter is not placed properly in the subject's vein, the blood flow will get interrupted. As the peristaltic pump will continue its steady draw of 10 mL/min, the absence of blood will be filled up by air or water bubbles in the flow channel. Such scenarios will yield higher thrombus formation due to stasis. The study in such cases should be repeated after resolving the IV access problem.
5. Flushing removes the blood left standing in the chambers which would coagulate due to stagnation once the peristaltic pump is turned off. A perfusion study without a postrun flush would yield a falsely high thrombus formation.
6. Specialized staining options are utilized as needed per study protocol (e.g., anti-fibrin or CD42b antibody can be used to define the specific contribution to the formed thrombus of fibrin and platelets, respectively).
7. The calibration settings vary depending on the microscope and the camera being used. Consult an expert to properly configure these settings.
8. If the program is over/underestimating the thrombus area, select *Manual* in the *Count/Size* window instead of *Automatic Dark Objects* and click the *Select Ranges* button (a new window will open up). Click the dropper button and select the thrombus area until all the thrombi are highlighted. Now close the new window and click *Count* in the *Count/Size* window. Resume analysis as described earlier.
9. The results are reported as thrombus size (μm^2). This is usually reported as an absolute number (e.g., thrombus size $11845 \mu\text{m}^2$ baseline vs. $7100 \mu\text{m}^2$ 6 h after ticagrelor loading dose [20]), but a percentage may also be offered (e.g., reduction of 40% in thrombus size 6 h after ticagrelor loading dose [20]).

References

1. Santos-Gallego CG, Picatoste B, Badimon JJ (2014) Pathophysiology of acute coronary syndrome. *Curr Atheroscler Rep* 16(4):401. <https://doi.org/10.1007/s11883-014-0401-9>
2. Santos-Gallego CG, Bayon J, Badimon JJ (2010) Thrombi of different pathologies: implications for diagnosis and treatment. *Curr Treat Options Cardiovasc Med* 12(3):274–291. <https://doi.org/10.1007/s11936-010-0075-8>
3. Osende JI, Badimon JJ, Fuster V, Herson P, Rabito P, Vidhun R, Zaman A, Rodriguez OJ, Lev EI, Rauch U, Heftl G, Fallon JT, Crandall JP (2001) Blood thrombogenicity in type

- 2 diabetes mellitus patients is associated with glycemic control. *J Am Coll Cardiol* 38 (5):1307–1312
4. Badimon L, Badimon JJ, Galvez A, Turitto V, Fuster V (1989) Platelet interaction with vessel wall and collagen in pigs with homozygous von Willebrand's disease associated with abnormal collagen aggregation. *Thromb Haemost* 61 (1):57–64
 5. Glassberg J, Rahman AH, Zafar MU, Cromwell C, Punzalan A, Badimon JJ, Aledort L (2018) Application of phospho-CyTOF to characterize immune activation in patients with sickle cell disease in an ex vivo model of thrombosis. *J Immunol Methods* 453:11–19. <https://doi.org/10.1016/j.jim.2017.07.014>
 6. Badimon JJ, Badimon L, Turitto VT, Fuster V (1991) Platelet deposition at high shear rates is enhanced by high plasma cholesterol levels. In vivo study in the rabbit model. *Arterioscler Thromb* 11(2):395–402
 7. Shechter M, Merz CN, Paul-Labrador MJ, Kaul S (2000) Blood glucose and platelet-dependent thrombosis in patients with coronary artery disease. *J Am Coll Cardiol* 35 (2):300–307
 8. Badimon L, Badimon JJ, Galvez A, Chesebro JH, Fuster V (1986) Influence of arterial damage and wall shear rate on platelet deposition. Ex vivo study in a swine model. *Arteriosclerosis* 6(3):312–320
 9. Badimon L, Chesebro JH, Badimon JJ (1992) Thrombus formation on ruptured atherosclerotic plaques and rethrombosis on evolving thrombi. *Circulation* 86(6 Suppl):III74–III85
 10. Lucking AJ, Lundback M, Mills NL, Faratian D, Barath SL, Pourazar J, Cassee FR, Donaldson K, Boon NA, Badimon JJ, Sandstrom T, Blomberg A, Newby DE (2008) Diesel exhaust inhalation increases thrombus formation in man. *Eur Heart J* 29 (24):3043–3051. <https://doi.org/10.1093/eurheartj/chn464>
 11. Lucking AJ, Lundback M, Barath SL, Mills NL, Sidhu MK, Langrish JP, Boon NA, Pourazar J, Badimon JJ, Gerlofs-Nijland ME, Cassee FR, Boman C, Donaldson K, Sandstrom T, Newby DE, Blomberg A (2011) Particle traps prevent adverse vascular and prothrombotic effects of diesel engine exhaust inhalation in men. *Circulation* 123 (16):1721–1728. *CIRCULATIONAHA.110.987263* [pii]. <https://doi.org/10.1161/CIRCULATIONAHA.110.987263>
 12. Mailhac A, Badimon JJ, Fallon JT, Fernandez-Ortiz A, Meyer B, Chesebro JH, Fuster V, Badimon L (1994) Effect of an eccentric severe stenosis on fibrin(ogen) deposition on severely damaged vessel wall in arterial thrombosis. Relative contribution of fibrin(ogen) and platelets. *Circulation* 90(2):988–996
 13. Badimon L, Badimon JJ (1989) Mechanisms of arterial thrombosis in nonparallel streamlines: platelet thrombi grow on the apex of stenotic severely injured vessel wall. Experimental study in the pig model. *J Clin Invest* 84 (4):1134–1144. <https://doi.org/10.1172/JCI114277>
 14. Fernandez-Ortiz A, Badimon JJ, Falk E, Fuster V, Meyer B, Mailhac A, Weng D, Shah PK, Badimon L (1994) Characterization of the relative thrombogenicity of atherosclerotic plaque components: implications for consequences of plaque rupture. *J Am Coll Cardiol* 23(7):1562–1569. 0735-1097(94)90657-2 [pii]
 15. Badimon L, Badimon JJ, Turitto VT, Fuster V (1989) Role of von Willebrand factor in mediating platelet-vessel wall interaction at low shear rate; the importance of perfusion conditions. *Blood* 73(4):961–967
 16. Zafar MU, Farkouh ME, Osende J, Shimbo D, Palencia S, Crook J, Leadley R, Fuster V, Chesebro JH (2007) Potent arterial antithrombotic effect of direct factor-Xa inhibition with ZK-807834 administered to coronary artery disease patients. *Thromb Haemost* 97 (3):487–492
 17. Zafar MU, Ibanez B, Choi BG, Vorchheimer DA, Pinero A, Jin X, Sharma RK, Badimon JJ (2010) A new oral antiplatelet agent with potent antithrombotic properties: comparison of DZ-697b with clopidogrel a randomised phase I study. *Thromb Haemost* 103 (1):205–212. <https://doi.org/10.1160/TH09-06-0378>
 18. Zafar MU, Vilahur G, Choi BG, Ibanez B, Viles-Gonzalez JF, Salas E, Badimon JJ (2007) A novel anti-ischemic nitric oxide donor (LA419) reduces thrombogenesis in healthy human subjects. *J Thromb Haemost* 5 (6):1195–1200. <https://doi.org/10.1111/j.1538-7836.2007.02543.x>
 19. Zafar MU, Vorchheimer DA, Gaztanaga J, Velez M, Yadegar D, Moreno PR, Kunitada S, Pagan J, Fuster V, Badimon JJ (2007) Antithrombotic effects of factor Xa inhibition with DU-176b: phase-I study of an oral, direct factor Xa inhibitor using an ex-vivo flow chamber. *Thromb Haemost* 98(4):883–888
 20. Zafar MU, Zafar M, Baber U, Smith DA, Sartori S, Contreras J, Rey-Mendoza J, Linares-Koloffon CA, Escolar G, Mehran R, Fuster V, Badimon JJ (2017) Antithrombotic potency of ticagrelor versus clopidogrel in type-2 diabetic patients with cardiovascular

- disease. *Thromb Haemost* 117 (10):1981–1988. <https://doi.org/10.1160/TH17-04-0277>
21. Dangas G, Badimon JJ, Smith DA, Unger AH, Levine D, Shao JH, Meraj P, Fier C, Fallon JT, Ambrose JA (1999) Pravastatin therapy in hyperlipidemia: effects on thrombus formation and the systemic hemostatic profile. *J Am Coll Cardiol* 33(5):1294–1304
22. Hayes R, Chesebro JH, Fuster V, Dangas G, Fallon JT, Sharma SK, Collier BS, Badimon L, Marmur JD, Badimon JJ (2000) Antithrombotic effects of abciximab. *Am J Cardiol* 85 (10):1167–1172

Part V

Small Animal Models



Chapter 13

Ischemic Model of Heart Failure in Rats and Mice

Jiqiu Chen, Delaine K. Ceholski, Irene C. Turnbull, Lifan Liang,
and Roger J. Hajjar

Abstract

Temporary or permanent left coronary artery (LCA) ligation is the most widely used model of heart failure. In the present protocol, we describe the materials necessary for the procedure, key steps of the LCA ligation, triphenyl tetrazolium chloride (TTC) staining, and calculation of myocardial infarction (MI) size after ischemia–reperfusion (I/R) injury (30 min/24 h) in rats and mice. We discuss precautions and tips regarding the operation before and after surgery, both *in vivo* and *ex vivo*. The aim of this chapter is to describe the details of LCA surgery and provide recommendations for current and future surgical operators.

Key words Rodent, Ischemia, Ischemic heart failure, Surgical, Coronary artery ligation, Ischemia–reperfusion

1 Introduction

Animal models are one of the most important ways in which to study pathogenic mechanisms, treatment approaches, and drug development for cardiovascular diseases. Rodent models (mainly rats and mice) are wildly used in basic biomedical scientific research and have withstood the test of time [1]. Left coronary artery (LCA) ligation is the most common procedure to induce heart failure through myocardial infarction (MI) in rodents, canines, sheep, and several other animals [2]. The LCA in large animals can be visualized with angiography *in vivo* to determine the occluding location and control (relatively) the range of myocardial injury. On the other hand, the small size of rodent hearts results in their LCAs invisible to the surgical operator in almost 50% of cases *in vivo* [3]. Although it is well established that it is difficult to obtain a consistent degree of heart failure in rodents [4], the simplicity and low cost of the rodent model make it worthwhile to continue to strive to achieve better and more reliable results for modeling cardiovascular disease (*see Note 1*).

In the present protocol, we describe the critical steps of LCA ligation and provide tips to obtain an MI model as reliable and reproducible as possible.

2 Materials

1. Sprague-Dawley male rats, body weight = 250–280 g, or C57 wild-type (WT) male mice, body weight = 25–30 g (*see Note 2*).
2. KAX mix: ketamine (100 mg/mL), acepromazine (10 mg/mL), xylazine (20 mg/mL) (*see Notes 3 and 4*).
3. Ventilator: small animal ventilators. For rats: 6–8 cc/min, 90 breaths/min. For mice: 3 cc/min, 110 breaths/min (Fig. 1a) (*see Note 5*).
4. Intubation tube: 16–14 G catheter for rats, 20 G catheter for mice (Fig. 1b) (*see Note 6*).
5. Surgical microscope (Fig. 1c).
6. Silk sutures: 2-0, 4-0 for chest and skin closure; 6-0, 7-0 for LCA ligation.
7. Oxygen: 500 mL/min, tabletop Vaporizers. Isoflurane: 0.5–1.0% when necessary (when the animals are moving) (*see Note 7*).

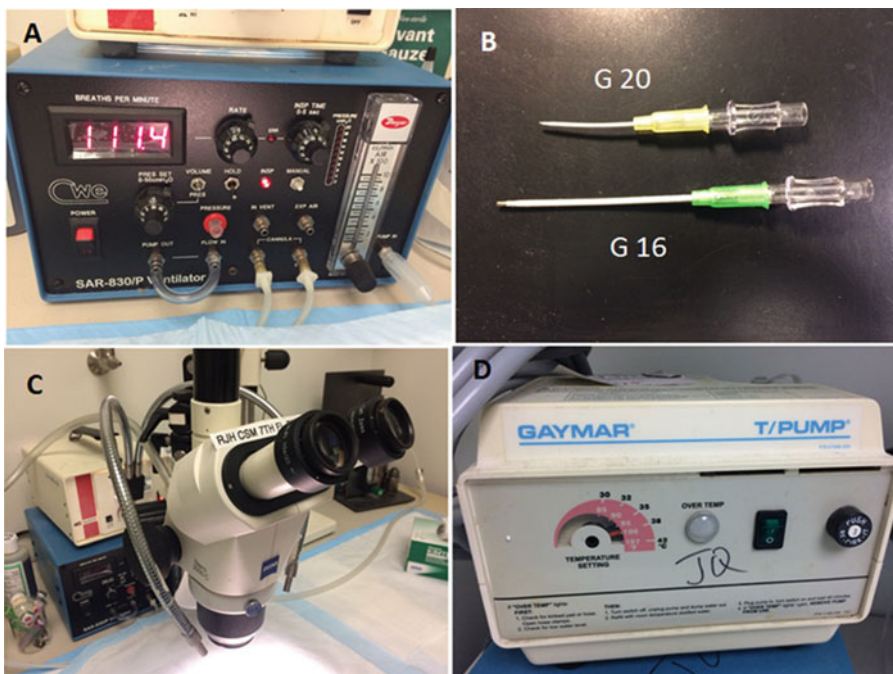


Fig. 1 Key instruments for cardiac surgery in rodents. (a) Ventilator. (b) Intubation. 20G catheter for mice and 16G for rats. (c) Surgical microscope. (d) Heating pad system

Table 1
K-H buffer formulation

Name	FW	mM	g/L
NaCl	58.5	118.5	7.0
KCl	74.5	4.8	0.35
MgCl ₂ ·6H ₂ O	203.3	1.2	0.24
KH ₂ PO ₄	136.09	1.2	0.16
CaCl ₂	110.9	2.5	2 mL/0.5 M
NaHCO ₃	84	2.1	2.1
HEPES	260	5	5
D-H ₂ O			1000 mL

FW = formula weight

8. Heating pads with pump, Temperature = 98 °F (Fig. 1d).
9. TTC solution: *triphenyl tetrazolium chloride*. 5 ~ 15 mL of 1.5% TTC in PBS.
10. 10% formaldehyde.
11. Phthalo Blue dye.
12. Langendorff system.
13. K-H buffer: NaCl, KCl, MgCl₂·6H₂O, KH₂PO₄, CaCl₂, NaHCO₃, HEPES, distilled water, pH = 7.35 (Table 1).

3 Methods

3.1 Rat LCA Permanent Ligation

1. Anesthetize the animals using KAX mix. For rats, mix 2 mL ketamine, 0.3 mL acepromazine, 0.3 mL xylazine and intraperitoneally inject 100 µL/g (animal weight) of this mixture (*see Notes 3 and 4*).
2. As soon as it is anesthetized, remove the mouse's hair on the left side of chest. Tape the mouse's right hind-paw to the table, and tape its left hind-paw on top of its right hind-paw in a manner that slightly torques the body so the left side of the chest is facing more skyward. Clear the skin with 10% povidone-iodine and 70% ethanol.
3. Open left chest at fourth intercostal space and open pericardium slightly.
4. Ligate the LCA using a 6-0 silk suture at the mid LCA level (*see Note 8*). A successful LCA ligation is verified by visual inspection of the change in apex color (*see Note 9*) (Fig. 2).

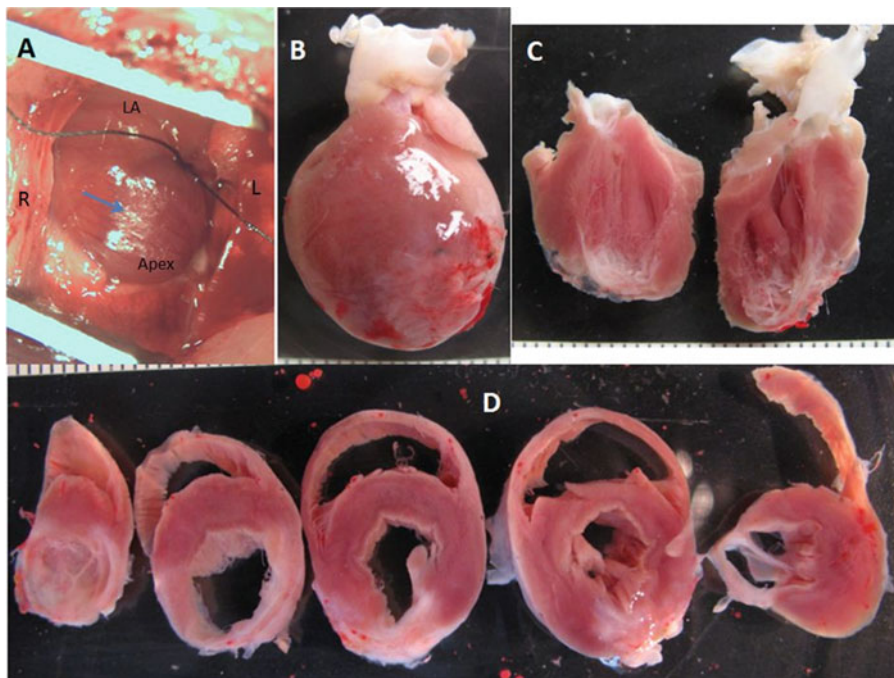


Fig. 2 Left coronary artery (LCA) ligation and myocardial infarction (MI) in rats. (a) LCA ligation in a rat *in vivo*. LA = left atrium, R = right, L = left. The color of the ischemic area is changed as indicated by arrow (b) Ex vivo view of MI. MI size could not be judged by white color of the scar. (c) Long axis view of MI in the left ventricle. (d) Cross-sectional view of MI in the left ventricle. MI size should be calculated using all slices according to methodology described (*see* “Evaluation of risk area and infarct size”)

5. Reexpand the lung by slightly occluding outlet tube of the ventilator. Close the chest with 2-0 silk suture on ribs and the skin [5].
6. Postsurgical monitoring is continued until the animal becomes conscious in a cage on heating pads (37 °C with O₂). Stop ventilation when animal has spontaneous breaths. Antibiotics will be given, if infection is a concern in surviving animals during the course of the study. All rodents are housed under identical conditions and will receive water and food ad libitum.

3.2 Mouse LCA Permanent Ligation

1. Anesthetize the animals using KAX mix. For mice, mix 1 mL ketamine, 0.1 mL acepromazine, 0.1 mL xylazine and dilute with 1 mL of 0.9% saline. Inject 0.06–0.08 mL of this diluted KAX mixture per mouse intraperitoneally.
2. Repeat Subheading 3.1, steps 2 and 3.
3. Ligate the LCA with a 7-0 silk suture. A successful LCA ligation is verified by visual inspection of the apex color (*see Note 9*).
4. Close the chest with 6-0 silk sutures and skin with 4-0 silk sutures [4].
5. Postsurgical monitoring is continued as in rats.

3.3 Ischemia–Reperfusion Injury

1. Repeat Subheading 3.1, steps 1–3.
2. After 30 min, the LCA ligature is released and reperfusion is visually confirmed (*see Note 10*).
3. Repeat Subheading 3.1, steps 4 and 5 [6].

3.4 Evaluation of Risk Area and Infarct Size

1. Reanesthetize rats/mice after 24 h of I/R injury.
2. Inject heparin (0.3 mL of 1000 U/mL, rat) intravenously through the tail vein before excising the heart.
3. Mount the heart on a Langendorff apparatus and perfuse for 3 min under constant pressure (100 cmH₂O) with K-H buffer at room temperature (*see Note 11*).
4. Reocclude the LCA with the suture that was left after reperfusion and perfuse the heart with 5% Phthalo Blue dye in 0.9% normal saline for 3 min (Fig. 3a).
5. Excise the right ventricle and freeze the left ventricle at –20 °C for 10 min, then section the left ventricle into 5–7 transverse slices (2 mm/rat, 1 mm/mouse).
6. Incubate the slices in 15 mL of 1.5% TTC solution for 20 min at 37 °C and then fix them in 10% formaldehyde. Twenty-four hours later, the slices are weighed and photographed.
7. Make digital imaging on each transverse slice (Fig. 3b). The blue regions represent nonischemic normal tissue, red regions represent risk area (ischemic but noninfarcted), and unstained pale white regions represent infarcted tissue (Fig. 3c). The blue, red, and white areas are outlined on each color image and measured using imaging software. On each side of each slice, the fraction of the LV area representing infarcted tissue is calculated, and the average of two images is multiplied by the weight of the section to determine the absolute weight of infarcted tissue in each slice.
8. Measure ischemic parameters as percentage [6], instead of absolute area, in order to buffer impact of ligature level on MI size (*see Note 12*).

$$\text{Ischemic area} = \text{Infarct area} + \text{Risk area}.$$

$$\text{Infarct size/LV mass (\%)} = \sum \text{Infarct weight in each section} / \text{Total LV weight} \times 100 (\%).$$

$$\text{Risk area/LV mass (\%)} = \sum \text{Red region weight in each section} / \text{Total LV weight} \times 100 (\%) \text{ (Fig. 3d, e).}$$

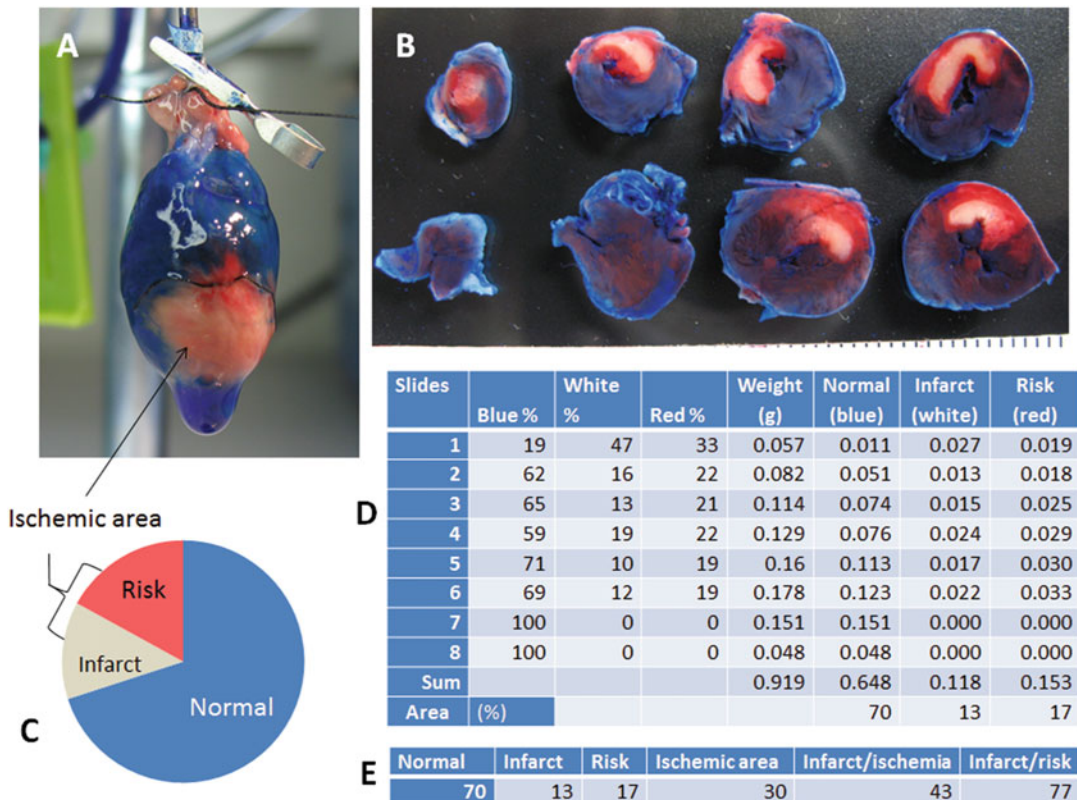


Fig. 3 TTC staining and measurement of ischemic and infarct size in rats. **(a)** Langendorff perfusion with Phthalo Blue dye. **(b)** After TTC staining. **(c)** Illustration of ischemic area. **(d)** Example calculation of risk, infarct, and ischemic size from eight slices of the heart shown in **(b)**. Columns 5, 6, and 7 equal columns 1, 2, and 3 multiplied by column 4. **(e)** Calculation of risk/infarct area and infarct/risk size

4 Notes

1. The surgery for MI roughly takes 30 min. Surgical mortality is around 30% both in rats, and a little bit higher in mice.
2. There are some variations in anatomy and pathophysiologic response to ischemic injury between animal strains and genders [3]. These factors should be considered during experimental design.
3. The ratio of KAX should be adjusted for rats and mice.
4. Proper anesthesia and dosage are critical. Ketamine plus xylazine is usually not enough. Inadequate anesthesia is a common cause of intubation failure, while excessive anesthesia can result in death.
5. After opening the chest, the inspiratory time should be increased from 0.3 to 0.45 s.
6. Blunt the tip of the catheter and curve it slightly (Fig. 1b).
7. It is important to provide oxygen and keep the animal warm.

8. The LCA is visible in nearly half of rats and slightly more than half of mice. When the LCA is invisible, the vessel path could be assumed from front third of left atrial edge to ventricular apex [3].
9. The change in apex color is not an absolute index of MI, meaning some MIs may be smaller or subtransmural even though the apex color turns white.
10. I/R injury is more difficult in mice than rats. Approximately 50% of I/R will result in transmural MI. A 45 min ischemia will not result in significantly more injury compared with a 30 min ischemia, but will likely increase mortality especially in mice.
11. TTC staining is more difficult in mice than in rats. Part of the reason for this is that the mouse aorta is smaller and Langendorff mounting is more difficult.
12. The level of ligation on the LCA has a key role in MI size and cardiac dysfunction. Slight deviation (<0.5 mm in mice) in ligature placement can result in significant variation in MI size and LV function. It is necessary to fully understand the characteristics of the LCA and the surrounding capillaries in order to reasonably interpret experimental results (Fig. 4).

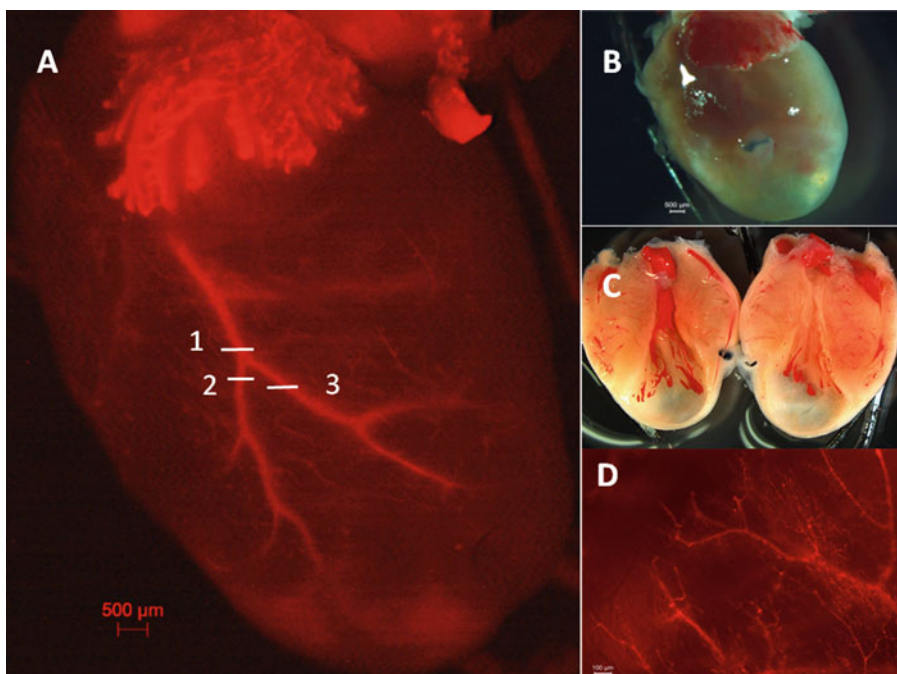


Fig. 4 Left coronary artery ligation and myocardial infarction in mice. (a) Fluorescent imaging of LCA ex vivo. The level of ligation on the LCA has a strong impact on MI size and cardiac dysfunction. Ligation of LCA at: position 1 could induce a large MI with high mortality; position 2 could lead to injury of ventricular septum and severe conduction block; and position 3 could result in a small MI. (b) Transmural MI results in a very thin LV wall in mice but the MI size still needs to be confirmed and measured in an opened heart (c). (d) Capillaries could be visualized in the ischemic border zone in situ

Acknowledgments

This work is supported by NIH R01 HL117505, HL 119046, HL129814, 128072, HL131404, R01HL135093, a P50 HL112324, and two Transatlantic Fondation Leducq grants. We would like to acknowledge the Gene Therapy Resource Program (GTRP) of the National Heart, Lung, and Blood Institute, National Institutes of Health. DKC is supported by a fellowship from the American Heart Association (15POST25090116). ICT is supported by NIH/NHLBI K01 HL 133424-01.

References

1. Houser SR, Margulies KB, Murphy AM, Spinale FG, Francis GS, Prabhu SD, Rockman HA, Kass DA, Molkentin JD, Sussman MA, Koch WJ, American Heart Association Council on Basic Cardiovascular Sciences, Council on Clinical Cardiology, Council on Functional Genomics and Translational Biology (2012) Animal models of heart failure: a scientific statement from the American Heart Association. *Circ Res* 111(1):131–150. <https://doi.org/10.1161/RES.0b013e3182582523>
2. Patten RD, Hall-Porter MR (2009) Small animal models of heart failure: development of novel therapies, past and present. *Circ Heart Fail* 2(2):138–144. <https://doi.org/10.1161/CIRCHEARTFAILURE.108.839761>
3. Chen J, Ceholski DK, Liang L, Fish K, Hajjar RJ (2017) Variability in coronary artery anatomy affects consistency of cardiac damage following myocardial infarction in mice. *Am J Physiol Heart Circ Physiol* 313(2):H275–H282. <https://doi.org/10.1152/ajpheart.00127.2017>
4. Chen J, Hammoudi N, Benard L, Ceholski DK, Zhang S, Lebeche D, Hajjar RJ (2016) The probability of inconstancy in assessment of cardiac function post-myocardial infarction in mice. *Cardiovasc Pharm Open Access* 5(5). <https://www.ncbi.nlm.nih.gov/pmc/articles/PMC5130155/>
5. Chen J, Chemaly ER, Liang LF, LaRocca TJ, Yaniz-Galende E, Hajjar RJ (2011) A new model of congestive heart failure in rats. *Am J Phys Heart Circ Phys* 301(3):H994–H1003. <https://doi.org/10.1152/ajpheart.00245.2011>
6. Chen J, Chemaly E, Liang L, Kho C, Lee A, Park J, Altman P, Schecter AD, Hajjar RJ, Tarzami ST (2010) Effects of CXCR4 gene transfer on cardiac function after ischemia-reperfusion injury. *Am J Pathol* 176(4):1705–1715. <https://doi.org/10.2353/ajpath.2010.090451>



Chapter 14

Conventional Method of Transverse Aortic Constriction in Mice

Jimeen Yoo, Vadim Chepurko, Roger J. Hajjar, and Dongtak Jeong

Abstract

Transverse aortic constriction is a widely used surgical model to reflect the progression from cardiac hypertrophy to heart failure states due to left ventricular pressure overload in mice. It produces afterload increase on the left ventricle in which compensated hypertrophy initially occurs in the first 2 weeks. This develops into maladaptive remodeling of the left ventricle and atrium, leading to heart failure. This model is useful for cardiac studies since transverse aortic constriction can be consistently replicated and has low surgical mortality. Additionally, the gradual progression to cardiac failure makes it a valuable method to evaluate the efficacy of potential therapeutic intervention. We introduce this chapter to offer practical approaches to facilitate a simple methodology for transverse aortic constriction.

Key words Transverse aortic constriction, TAC, Microsurgery, Heart failure, Hypertrophy

1 Introduction

Multiple models of heart disease using microsurgical methods have been created to recapitulate human heart disease conditions [1]. Usage of each model is dependent on the major cause of disease including aortic constriction, pulmonary artery constriction, and myocardial infarction. There are several methods for aortic constriction, with the most popular being ascending aortic constriction (AAC) [2, 3] and transverse aortic constriction (TAC) [4, 5]. AAC progresses quickly to heart failure within hours to days due to the close ligation placement around the origin of the aorta, which leads to rapid pressure overload in the left ventricle. In contrast, in TAC, the ligation occurs on the aortic arch between the innominate and left carotid arteries. Due to the innominate artery reducing some of the pressure in the left ventricle, hypertrophy and heart failure develop at a slower pace than AAC.

TAC was first conducted by Rockman et al. [5] in 1991, and has since been modified to be less invasive and time consuming [6]. Now it is an accepted and valuable model to understand

fundamental molecular processes and phenotypes critical in hypertrophy and heart failure. Additionally, its replicability, low surgical mortality, and its gradual progression to cardiac failure make TAC a widely used model. Up to 2 weeks post TAC surgery, contractility initially seems to improve due to compensated hypertrophy. During this time, cardiac structural remodeling occurs in which the left ventricle wall thickens. However, after 8 weeks, chronic pressure overload in the left ventricle causes decompensated cardiac hypertrophy and eventually heart failure occurs. Eventually, both left ventricle and atrial dilation (Fig. 1) can be observed in end stage of heart failure [7].

Thus, depending on the subjects of interest, both cardiac hypertrophy and heart failure can be generated by TAC. The progression of cardiac dysfunction over time can be evaluated by changes in cardiac parameters, body mass, and cardiac mass (Table 1). Increase in mortality can also be followed. We observe

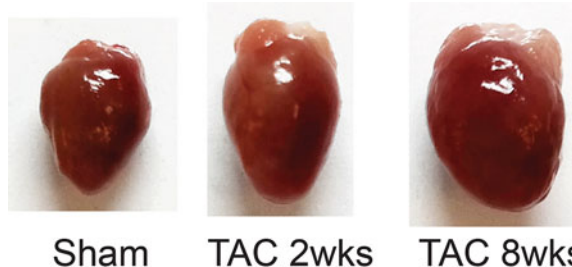


Fig. 1 Progression of structural changes of sham mice, 2 weeks post TAC, and 8 weeks post TAC are shown. The left ventricle becomes enlarged due to increased afterload. Changes in the left atrium are also visible. Initially, the left atrium is red and similarly sized with the right atrium, which progressively enlarges to a transparent pink with a spongy texture

Table 1

The progression of change in cardiac parameters, heart weight, and body weight for three groups of mice are shown: sham before surgery ($n = 5$), hypertrophy 2 weeks post TAC ($n = 10$), and heart failure 8 weeks post TAC ($n = 10$)

	Sham	Hypertrophy (2 weeks)	Heart Failure (8 weeks)
Body weight (g)	34.3 ± 0.5	31.7 ± 2.3	31.7 ± 0.5
Heart weight (mg)	127 ± 4.3	194.2 ± 6.6	297.8 ± 6.6
Fractional shortening % (FS)	63.5 ± 2.3	69.3 ± 1.9	34.2 ± 0.9
Left ventricular systolic dysfunction (LVSD)	1.12 ± 0.1	1.45 ± 0.4	1.2 ± 0.4
Heart rate (bpm)	599.6 ± 15.2	597 ± 19.8	605 ± 14.1

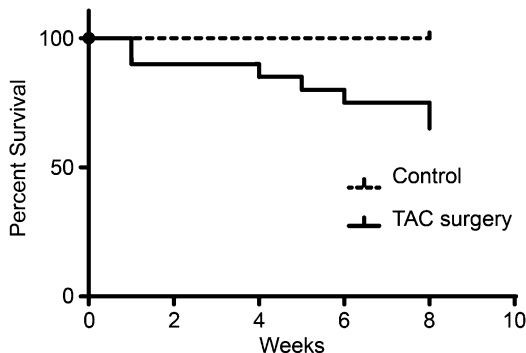


Fig. 2 Survival probability is plotted over 8 weeks since TAC surgery. Groups were sham-operated mice ($n = 12$) and TAC operated mice ($n = 20$)

survival percentages of 65% 8 weeks post TAC (Fig. 2). Here we describe our modified procedure for TAC with an operation time of 25–30 min to create a model with left ventricular pressure overload. We evaluate surgery success by echocardiogram 3 days post surgery.

2 Materials

2.1 Animal Care

All procedures were approved by and performed in accordance with the Institutional Animal Care and Use Committee (IACUC) of the Icahn School of Medicine at Mount Sinai. The investigation conforms with the Guide for the Care and Use of Laboratory Animals published by the US National Institutes of Health (NIH Publication No. 85-23, revised 1996). We usually use male *B6C3F1* mice aged 8–10 weeks (weight, 25–30 g).

2.1.1 Site Preparation

1. 70% isopropyl alcohol.
2. Warming blanket (15" \times 22").
3. Temperature-controlled water system.
4. Hot bead sterilizer for instruments.
5. Small animal ventilator.
6. Stereomicroscope for microsurgery.

2.1.2 Surgery

1. 27G1/2 needle.
2. Anesthesia: ketamine, xylazine.
3. Depilatory cream.
4. Cotton application.
5. Gauze.
6. Surgical paper tape.
7. Povidone-iodine solution.

8. Sterile drape.
9. Sterile gloves.
10. Suture: 5/0 vicryl, 6/0 silk sutures, 7/0 silk sutures.
11. PE 90 Tubing with a 22 G catheter needle for tracheal intubation.
12. Instruments: cautery pen, blunt scissors, blunt retractors, curved forceps, straight forceps, ligation aid, needle holder with suture cutter.
13. Surgery platform.
14. Heat lamp.

2.1.3 Echocardiography

1. Anesthesia: ketamine.
2. Surgical paper tape.
3. Depilatory cream.
4. Cotton applicator.
5. Gauze.
6. Ultrasound transmission gel.
7. Warming blanket (15" × 22").
8. Doppler echocardiogram.

3 Methods

3.1 Preparation of Operating Field and Procedure

Operating field and instrumentation are shown in Figs. 3 and 4, respectively.

1. Disinfect operating field with 70% isopropyl alcohol.
2. Disinfect surgical plastic platform with 70% isopropyl alcohol.
3. Disinfect surgical instruments in hot bead sterilizer.
4. To make a 90° curved needle holder for ligation, using a needle holder, remove the sharp end of a 27 gauge 1.5 in. needle to blunt the end. Curve it 90° with the needle holder and smooth the tip by rubbing the end on a sharpening stone. Cut the needle again to make a 0.5–1 cm spacer and rub the end on a sharpening stone to smooth the tip, as shown in Fig. 4. This will be used as the 0.4-mm spacer during ligation.

3.2 Preparation of Mice

1. Anesthetize mice by intraperitoneal injection using Ketamine (95 mg/kg) + Xylazine (5 mg/kg).
2. Confirm adequate level of anesthesia with a negative response to toe pinch reflex.
3. Remove hair from the neck to chest area using depilatory cream. Apply an even layer and remove the cream with gauze 2 min post application.

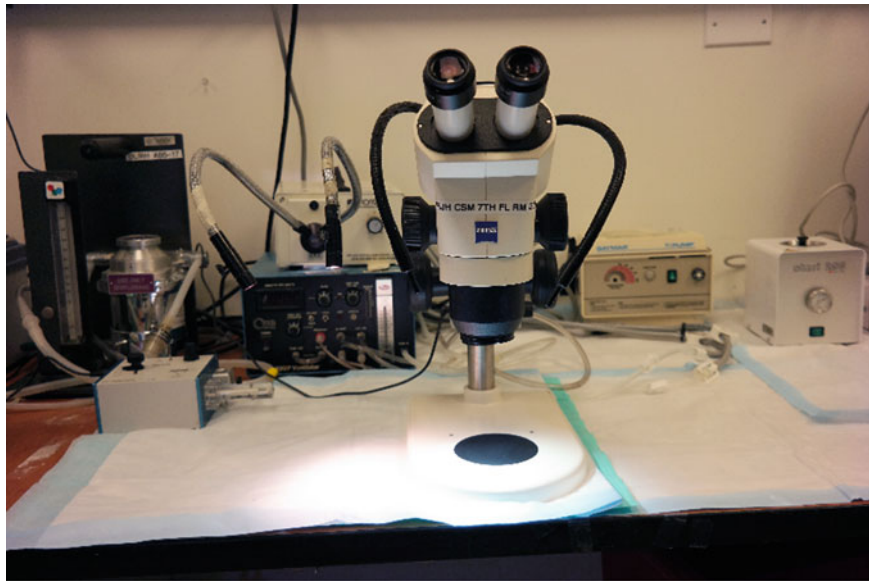


Fig. 3 Operating field arrangement is depicted. Note that the heating pad is connected to a circulating water pump

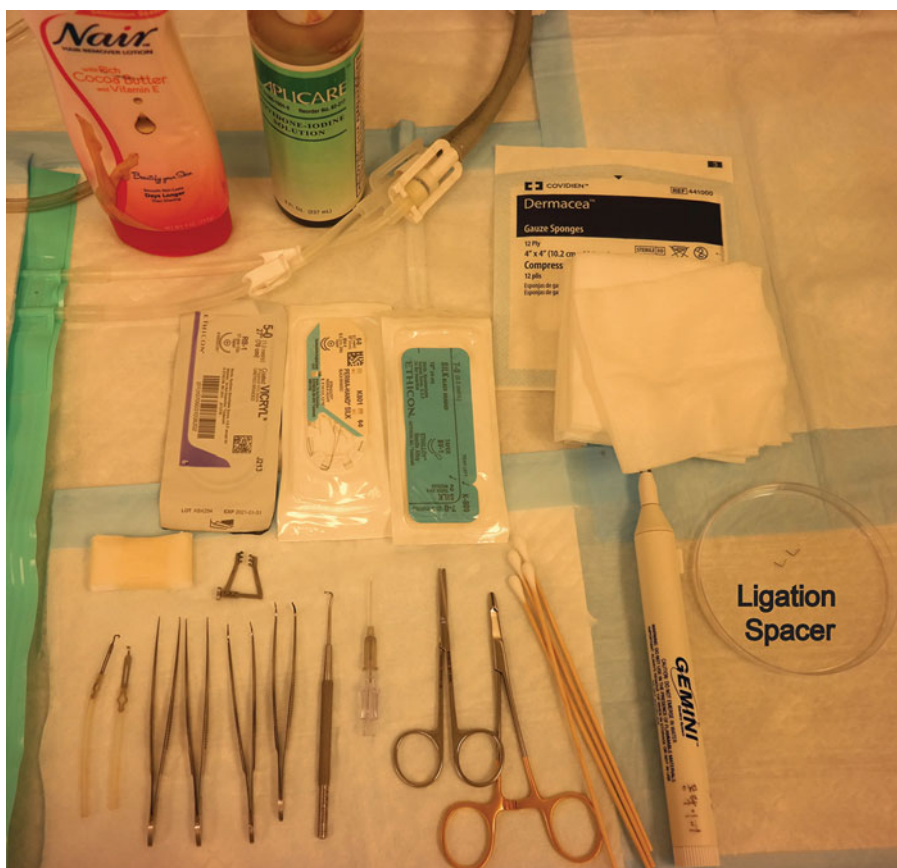


Fig. 4 Instrumentation and materials needed for surgery are shown

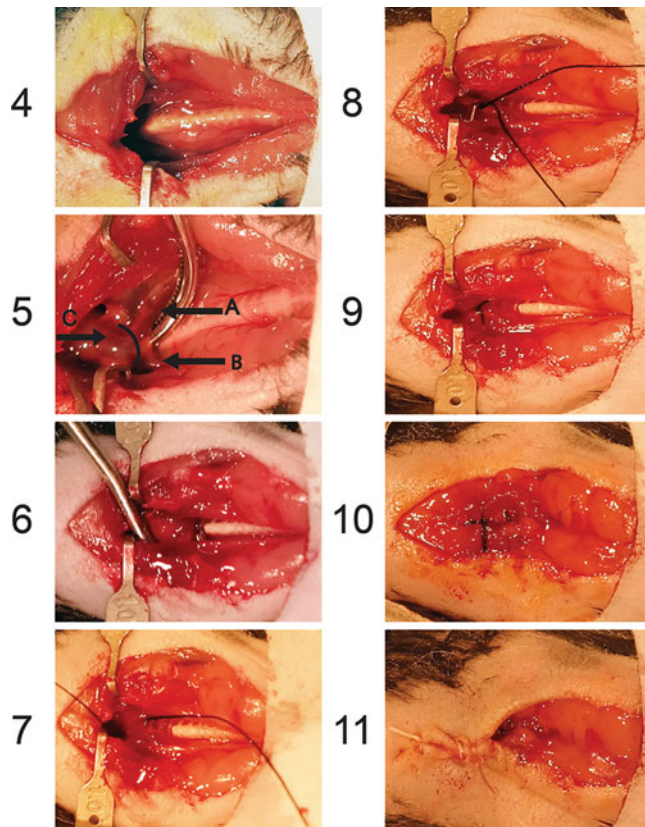


Fig. 5 Surgical procedure in Subheading 3.4 is shown in stepwise manner from procedures 4–11. In step 5, the innominate carotid, left common carotid, and aortic arch are labeled A, B, and C, respectively

4. In a supine position, put the upper front teeth of the mouse in the string on the platform to extend the neck. Tape limbs to plastic plate to immobilize their positions.
5. Pull tongue to the side with forceps and insert tracheal intubation tube (*see Note 1*). Connect ventilator and set to tidal volume of 0.1 mL and a respiratory rate of 120 breaths per minute.
6. Disinfect the depilated skin with povidone–iodine.
7. Place sterile drape on area of surgery.

3.3 Surgery

The surgical procedure from 4 to 11 can be followed in Fig. 5.

1. Begin with partial thoracotomy under a surgical microscope by creating a 2 cm incision in the skin to the second rib with blunt scissors.
2. Pull salivary glands toward head and separate muscle with cautery pen.

3. Separate the muscle on trachea at the midline toward both sides. If the tracheal tube was correctly inserted, it will be easily visible within the trachea.
4. Cut the sternum about 5 mm with scissors and open with a blunt retractor about 10 mm wide.
5. Separate the thymus lobes (which are white in color) to reveal the transverse aortic arch and two carotid arteries (*see Note 2*).
6. Place ligation aid below aortic arch from head side.
7. Put 7/0 silk suture into the hole of the ligation aid and pull the aid out to place the suture beneath the aortic arch between the innominate and left common carotid arteries.
8. Tie a double knot with the overlaid 27-gauge needle used as a spacer.
9. Immediately remove needle, leaving a discrete region of constriction, and cut the ends of the suture. Confirm successful ligation (*see Note 3*).
10. Close the chest wall using 6/0 silk suture with a simple interrupted suture pattern (*see Note 4*).
11. Close the skin with a 5/0 vicryl suture in a continuous suture pattern (*see Note 4*).
12. Disinfect suture site with povidone-iodine, remove intubation tube, and return mouse to the cage.
13. Inject 0.1 mg/kg buprenorphine intraperitoneally as postoperative analgesia (3 times a day for 4 days).
14. Leave cage under heat lamp and monitor for 2 h.
15. Provide mouse with soft food with proper hydration.

3.4 Doppler Echocardiography

Three days post surgery, confirm successful ligation of the aorta with echocardiography.

1. Anesthetize the mouse (3% isoflurane mixed with 0.5 L/min 100% O₂) in the induction chamber.
2. Perform a toe or tail pinch to confirm sedation. The level of anesthesia can be adjusted to obtain a target heart rate of 350 ± 50 beats per minute (bpm).
3. Remove hair from the neck to chest using depilatory cream. Apply an even layer and remove the cream with gauze 2 min post application.
4. Place the anesthetized mouse in a supine position on top of the heating pad to maintain body temperature. It is important to maintain the body temperature within a narrow range ($37.0^{\circ}\text{C} \pm 0.5^{\circ}\text{C}$) to get reliable and consistent results.
5. Apply ultrasound gel to the mouse's chest. A probe that is at least 20-MHz should be used to perform pulsed wave Doppler

to measure the jet velocity between the proximal and distal sites where TAC was conducted.

6. Place the Doppler probe on the right lateral position of the chest (the tip of the probe will be facing toward the left) and adjust the probe to the same plane of the aortic arch. Using B-Mode (two-dimensional (2D) imaging), obtain view along the parasternal short axis.
7. Measure the jet flow velocity between the proximal and distal sites where TAC was conducted. Calculate the pressure gradient using the simplified Bernoulli equation below. Mice should have pressure gradient of at least 30 mmHg.

$$\Delta P = 4V^2; P = \text{pressure (mmHg)}, \\ V = \text{peak jet velocity (m/s)} [8].$$

8. Allow the mouse to recover on warming blanket from anesthesia. See Notes 5 and 6 if animals are not reaching pressure overload or having high mortality. See Note 7 for an alternative method for measuring the pressure gradient before sacrificing mice.

3.5 Evaluating Systolic Function of the Heart

Conduct an echocardiogram 2 weeks post TAC for hypertrophy and 6–8 weeks post TAC for heart failure. Figure 6 and Table 1 show representative images and values for the progression of TAC-induced cardiac dysfunction.

1. Anesthetize with 100 mg/kg ketamine.
2. Remove hair from the neck to chest using depilatory cream. Apply an even layer and remove the cream with gauze 2 min post application.
3. Place mouse in supine position and tape to platform.
4. Apply ultrasound gel to mouse chest. Use a probe that is at least 14-MHz.

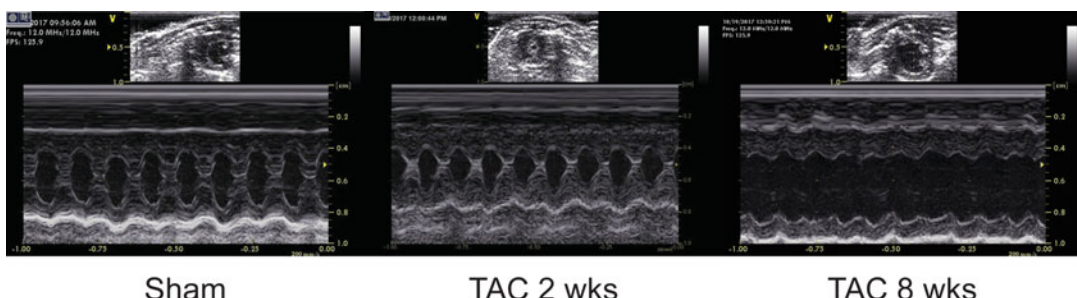


Fig. 6 Representative echocardiogram figures for SHAM, 2 weeks post TAC, and 8 weeks post TAC are shown. Two weeks post TAC mice shows a phenotype of cardiac hypertrophy, represented by a smaller cavity and thicker ventricular wall. On the other hand, 8 weeks post TAC mice show a significantly enlarged left ventricular cavity with dilatation of the left ventricular wall

5. Using B-Mode (2D imaging), hold the ultrasound probe with a 90° angle between the probe and the heart to obtain short-axis view. A proper image in this orientation will include the left ventricle and a slight portion of the right ventricular wall. All measurement of cardiac systolic function is evaluated at the papillary muscle level.
6. Switch to M-mode echocardiography to obtain fine measurements of cardiac dimensions and contractility. Store acquired images for evaluation of systolic left ventricular functional parameters.
7. Allow mice to recover on warming blanket from anesthesia. See **Note 8** for choosing mice for future heart failure studies.

4 Notes

1. In case of difficulty intubating, begin by placing the mouse in supine position and put the upper front teeth of the mouse in the string on the platform to extend the neck. Tape limbs to plastic plate to immobilize their positions. Place a 2 cm cervical incision on the skin above trachea. Separate both salivary glands and muscles to expose trachea. Locate the lamp above the neck to identify trachea. Then, pull tongue to the side with forceps and perform intratracheal intubation.
2. If there is difficulty locating the aortic arch due to obstruction, the thymus can be removed as its involution makes it mostly inactive for immunity in adulthood. The aortic arch can be found below and slightly anterior to the trachea.
3. The pulsation difference between the right and left carotid arteries can be compared to verify successful surgery. Gently separate the muscle on both sides of mouse neck to expose both right and left carotid arteries. Then, confirm that the right carotid artery has an augmented pulsation due to increased blood pressure than that of the left carotid artery after constriction.
4. For complete chest closure, at least two stitches are required. Remove potential air that settled in the chest cavity (optional). For closure of the skin, five to six stiches will be sufficient.
5. Potential causes of not achieving the pressure overload phenotype include: (1) Damage to the suture has occurred during operation, and (2) Suture may have loosened during the operation.
6. Potential causes of high mortality include: (1) Constriction site may be too tight if extra tissues are constricted together. (2) Internal bleeding may have occurred if sharp instruments are used instead of blunt instrumentation. This occurs most

frequently when there is damage to the left atrium during the ligation step or to the vessels during chest closure. (3) Old mice are used instead of the suggested young, 8–12 week old mice. Young mice will give higher consistency. Older animals are more difficult to conduct surgery due to visceral fat around the organs.

7. An alternative method for measuring the pressure gradient can be followed. At the time of sacrifice, both right and left carotid arteries are cannulated by two catheters to measure the pressure gradient. This method shows highly accurate values of pressure gradients for individual animals. However, it may alter blood flow, which eventually affects the pressure gradient value. Therefore, careful and quick assessment using a catheter is critical.
8. Additional echocardiography should be performed to evaluate cardiac function before using mice. Cardiac functional parameters will be measured in B and M mode. In B mode, change in left ventricular cavity size can be measured. In M mode, other detail cardiac parameters can be measured. Representative values are summarized in Table 1. If referencing our parameters, note that mice are anesthetized with ketamine only, which maintains heart rate over 550 rpm. Depending on the purpose of the study, different anesthesia can be used but values for cardiac function will vary [9].

Acknowledgments

This work is supported by NIH R01 HL117505, HL 119046, HL129814, 128072, HL131404, R01HL135093, a P50 HL112324, and two Transatlantic Fondation Leducq grants. We would like to acknowledge the Gene Therapy Resource Program (GTRP) of the National Heart, Lung, and Blood Institute, National Institutes of Health for providing the gene vectors used in this study.

References

1. Breckenridge R (2010) Heart failure and mouse models. *Dis Model Mech* 3(3–4):138–143. <https://doi.org/10.1242/dmm.005017>
2. Schunkert H, Dzau VJ, Tang SS, Hirsch AT, Apstein CS, Lorell BH (1990) Increased rat cardiac angiotensin converting enzyme activity and mRNA expression in pressure overload left ventricular hypertrophy. Effects on coronary resistance, contractility, and relaxation. *J Clin Invest* 86(6):1913–1920. <https://doi.org/10.1172/JCI114924>
3. Weinberg EO, Schoen FJ, George D, Kagaya Y, Douglas PS, Litwin SE, Schunkert H, Benedict CR, Lorell BH (1994) Angiotensin-converting enzyme inhibition prolongs survival and modifies the transition to heart failure in rats with pressure overload hypertrophy due to ascending aortic stenosis. *Circulation* 90(3):1410–1422
4. Furihata T, Kinugawa S, Takada S, Fukushima A, Takahashi M, Homma T, Masaki Y, Tsuda M, Matsumoto J, Mizushima W, Matsushima S, Yokota T, Tsutsui H (2016) The experimental

- model of transition from compensated cardiac hypertrophy to failure created by transverse aortic constriction in mice. *Int J Cardiol Heart Vasc* 11:24–28. <https://doi.org/10.1016/j.ijcha.2016.03.007>
5. Rockman HA, Ross RS, Harris AN, Knowlton KU, Steinhelper ME, Field LJ, Ross J Jr, Chien KR (1991) Segregation of atrial-specific and inducible expression of an atrial natriuretic factor transgene in an in vivo murine model of cardiac hypertrophy. *Proc Natl Acad Sci U S A* 88(18):8277–8281
6. Zaw AM, Williams CM, Law HK, Chow BK (2017) Minimally invasive transverse aortic constriction in mice. *J Vis Exp* (121). <https://doi.org/10.3791/55293>
7. De Jong AM, Van Gelder IC, Vreeswijk-Baudoin I, Cannon MV, Van Gilst WH, Maass AH (2013) Atrial remodeling is directly related to end-diastolic left ventricular pressure in a mouse model of ventricular pressure overload. *PLoS One* 8(9):e72651. <https://doi.org/10.1371/journal.pone.0072651>
8. Hartley CJ, Reddy AK, Madala S, Entman ML, Michael LH, Taffet GE (2011) Doppler velocity measurements from large and small arteries of mice. *Am J Physiol Heart Circ Physiol* 301(2):H269–H278. <https://doi.org/10.1152/ajpheart.00320.2011>
9. Stypmann J (2007) Doppler ultrasound in mice. *Echocardiography* 24(1):97–112. <https://doi.org/10.1111/j.1540-8175.2006.00358.x>



Chapter 15

Characterization of the Differential Progression of Left Ventricular Remodeling in a Rat Model of Pressure Overload Induced Heart Failure. Does Clip Size Matter?

Antoine H. Chaanine and Roger J. Hajjar

Abstract

Despite the use of inbred animals, phenotypic variability is usually encountered in rats subjected to pressure overload. This chapter describes techniques for creating a rat model of pressure overload by ascending aortic banding procedure and noninvasive characterization of the variable phenotypes by means of echocardiography. We address the variable phenotypes encountered in this model with moderate versus severe ascending aortic banding. We also describe some of the echocardiographic and hemodynamic parameters and the degree of interstitial fibrosis and extracellular matrix remodeling encountered in each of the different phenotypes.

Key words Ascending aortic banding, Pressure overload, Phenotypes, Hypertrophy, Heart failure, Myocardial remodeling, Fibrosis

1 Introduction

Heart failure (HF) is a prevalent disease affecting more than 23 million people worldwide [1]. Studies seeking to define the mechanisms leading to HF or to test novel HF therapeutics commonly use rodent models of pressure overload (PO) produced by ascending or transverse aortic banding as a time-telescoped model of human systemic hypertension or severe aortic stenosis. Following PO, there is a gradual increase in left ventricular (LV) wall thickness as a compensatory mechanism to adapt and to adequately reduce the increased LV wall stress; however, the development of concentric LV hypertrophy is maladaptive and is associated with the activation of a number of pathways that lead to myocardial remodeling and transition into a HF phenotype due to altered calcium handling, changes in metabolic patterns and gene expression as well as enhanced apoptosis and autophagy and extracellular matrix remodeling [2–6].

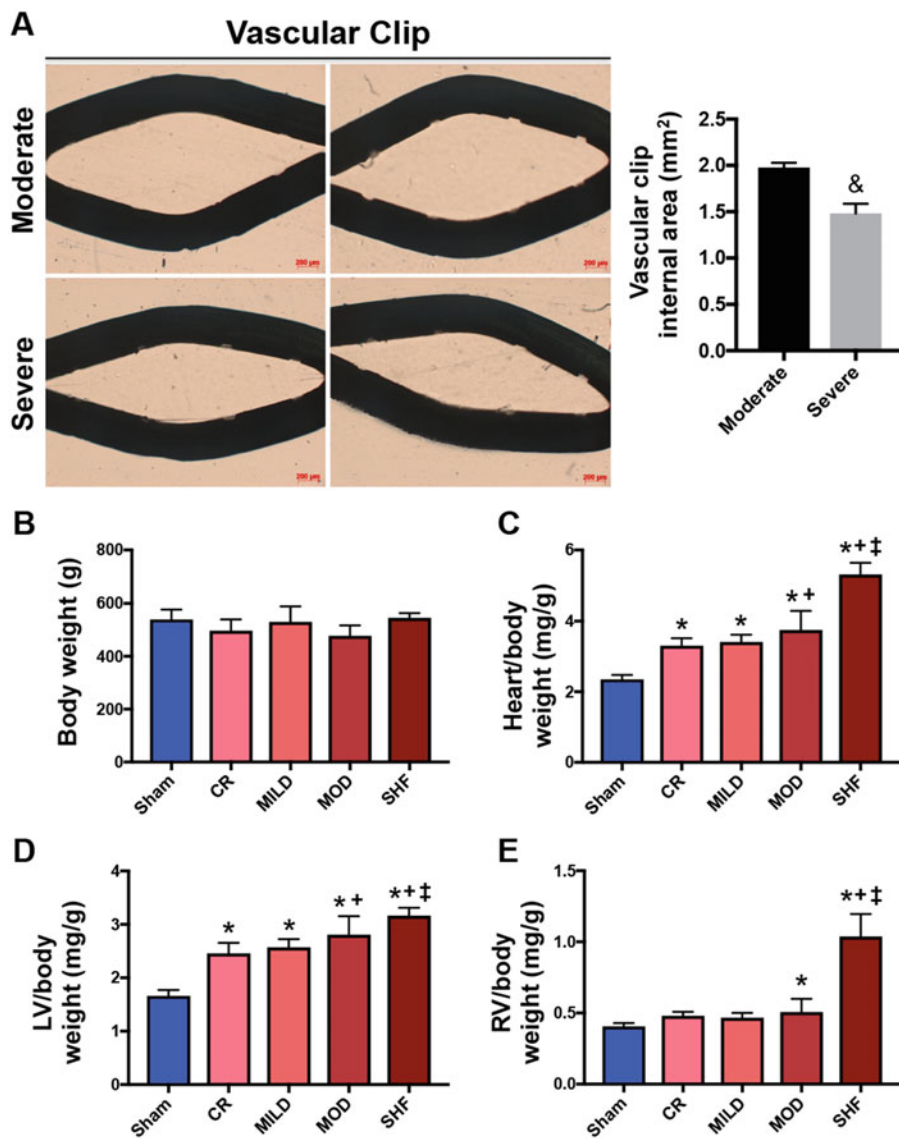


Fig. 1 (a) Vascular clip (hemoclip) internal area in moderate versus severe ascending aortic banding. $\& P < 0.05$ versus moderate. (b–e) Body weight and heart, left ventricle (LV) and right ventricle (RV) weight to body weight ratio in Sham, CR, MILD, MOD, and SHF phenotypes. * $P < 0.05$ vs. Sham, + $P < 0.05$ vs. CR and MILD, and $\ddagger P < 0.05$ vs. MOD. CR concentric remodeling, MILD mild eccentric remodeling, MOD moderate eccentric remodeling, SHF systolic heart failure

Despite the use of inbred rodent strains, there is tremendous phenotypic variability in LV chamber structure and function in aortic banding models [7–9]. Here we describe the different phenotypes encountered in Sprague Dawley rats subjected to ascending aortic banding (AAB) using a vascular clip with an internal area of 2 mm^2 (moderate AAB) and 1.5 mm^2 (severe AAB), Fig. 1a, respectively. The advantages of using a vascular clip compared to a stitch

for aortic banding is that the size of the vascular clip is standardized and is consistent between animals. Despite that, there remains phenotypic variability between animals that had developed severe PO and severe concentric hypertrophy with LV maximum pressure exceeding 200 mmHg and LV wall thickness of ≥ 3 mm, respectively. Also, failure rates exist due to unsuccessful banding or due to band internalization and periband aortic remodeling [9].

The phenotypes encountered with moderate AAB, vascular clip internal area of 2 mm^2 , 8 weeks post-AAB, and all having severe PO and severe concentric LV hypertrophy, are (1) compensated concentric remodeling (CR), (2) mild eccentric remodeling (MILD), and (3) moderate eccentric remodeling (MOD), none of them developing overt systolic dysfunction. The characterization of the aforementioned phenotypes is done by echocardiography and is described elsewhere in detail [10]. Of the total number of banded animals, these aforementioned phenotypes develop at a rate of 20% for each phenotype. Therefore, 60% of the banded animals develop the above phenotypes. The remaining 40% of the banded animals are distributed as follows: 20% death and 20% AAB failure and regression of hypertrophy due to above aforementioned reasons. The first two phenotypes, the CR and MILD, are more suitable to study diastolic dysfunction and therapies targeting diastolic dysfunction, while the MOD phenotype is more suitable to study pathways involved in, and therapies targeting, myocardial remodeling and prior to transition into a systolic HF phenotype. Differences between the three aforementioned phenotypes in regards to LV size and function, extracellular matrix remodeling, and alterations in myocardial signal transduction pathways involved in myocardial remodeling and oxidative capacity are published elsewhere [10].

The overt systolic HF (SHF) phenotype is encountered only with severe AAB, vascular clip internal area of 1.5 mm^2 , and at a rate of 13% of the totally banded animals. Of note, the CR, MILD and MOD phenotypes are encountered as well with severe AAB, at 8 weeks post-AAB; but at a slightly less percentage rate, of about 9% for each phenotype, when compared to moderate AAB. Moreover, severe AAB carries a higher post-operative mortality, within the first week post-AAB, compared to moderate AAB, 21% versus 5%, respectively. Thereafter, week 2 to week 8 post-AAB, the mortality rate is about the same between both, moderate and severe, groups, 15% vs. 19%, respectively. Failure rate between both groups is about the same, 20%. The phenotypic variability, mortality and failure rate percentages between moderate and severe AAB are summarized in Table 1.

Differences in body weight, heart weight, echocardiographic parameters, pressure-volume loop parameters, extracellular matrix remodeling and myocardial signal transduction between the different phenotypes are presented elsewhere [10, 11] and are summarized in Figs. 1b–e, 2, and 3. It is critical to properly characterize the different phenotypes in order to minimize variability in molecular

Table 1
Phenotypes, mortality, and failure rate percentages in moderate versus severe ascending aortic banding

Vascular Clip Internal Area		
Phenotypes, mortality and failure rates post-AAB	Moderate - 2 mm²(%)	Severe - 1.5 mm²(%)
Phenotypes: CR, MILD, MOD and SHF (week 8 post-AAB)		
CR	20	9
MILD	20	9
MOD	20	9
SHF	0	13
<i>Total</i>	<i>60</i>	<i>40</i>
Mortality		
Early (day 0 - day 7)	5	21
Late (week 2 - week 14) ^a	15	19
<i>Total</i>	<i>20</i>	<i>40</i>
Failure rate	20	20

Note: The different phenotypes develop 8 weeks post-AAB. It is not feasible to distinguish the different phenotypes at week 3 post-AAB, the time at which all phenotypes have severe concentric and compensated left ventricular hypertrophy
AAB ascending aortic banding, *CR* concentric remodeling, *MILD* mild eccentric remodeling, *MOD* moderate eccentric remodeling, *SHF* overt systolic HF

^aFor the late mortality majority of animals die between week 2 and week 8 post-AAB

expression between animals; and prior to implementing and studying effects of therapeutic strategies on myocardial function, structure, and signal transduction. The heart weight and LV weight to body weight ratio progressively increases from the CR and MILD phenotypes to the MOD phenotype and is the highest in the SHF phenotype, Fig. 1c, d. The difference in heart weight between the MOD and SHF phenotypes is mainly related to differences in RV weight rather than significant difference in LV weight. The RV to body weight ratio is increased in the MOD phenotype compared to Sham, and is much higher in the SHF phenotype compared to the other phenotypes, Fig. 1e. This correlates with the significantly higher LV end-diastolic pressure, Fig. 3b, and LV interstitial fibrosis, Fig. 3e, encountered in the SHF phenotype compared to the other phenotypes. Representative long and short parasternal axis two dimensional (2D) images and M-mode images at the level of the papillary muscle and aortic valve of the different phenotypes are presented in Fig. 2a. LV posterior wall thickness, LV end-diastolic and end-systolic volumes as well as LV ejection fraction are presented in Fig. 2b–e. Note that significant LV and left atrial remodeling is present in the MOD and SHF phenotypes only. Thus,

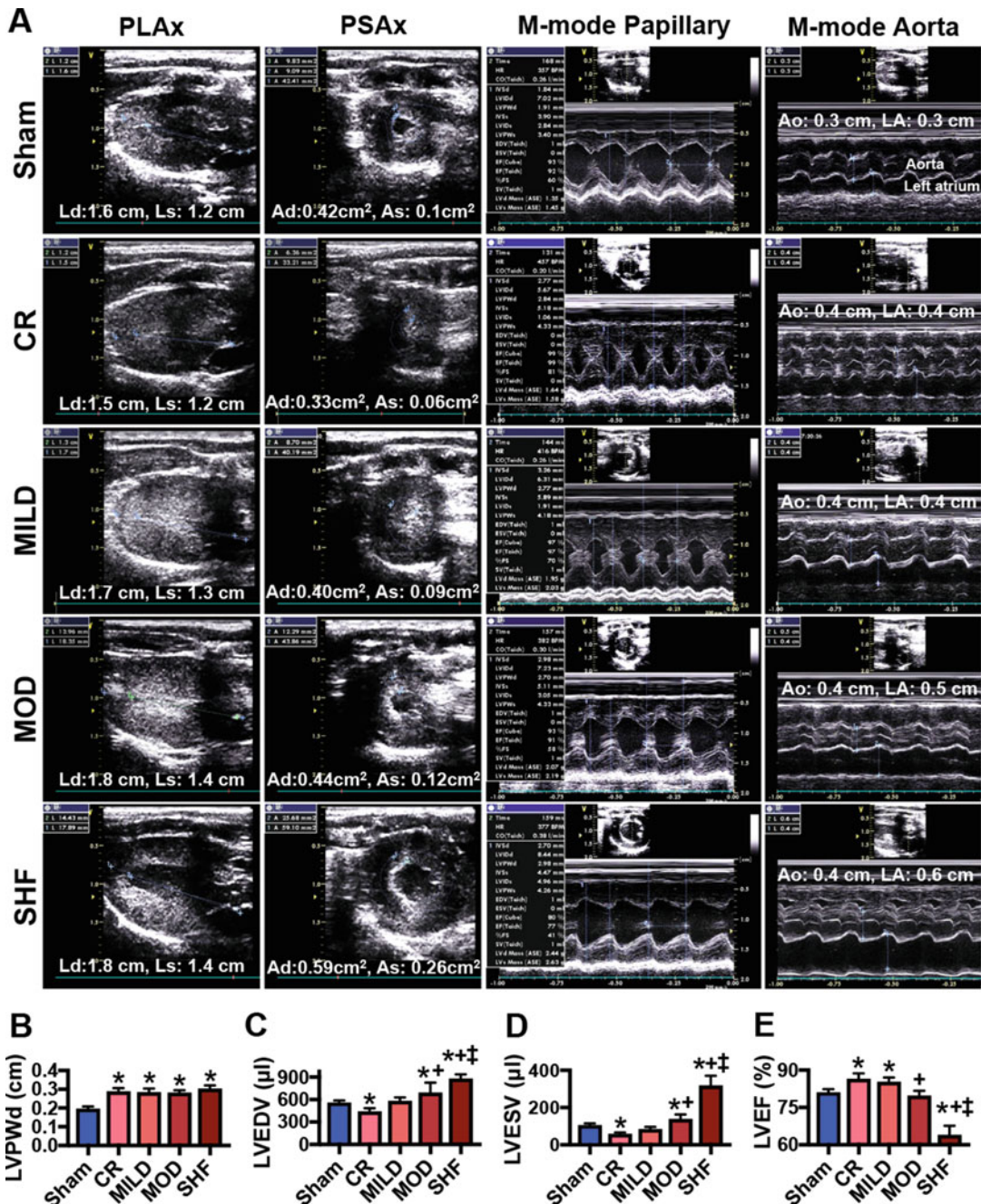


Fig. 2 (a) Representative echocardiography parasternal long (PLAx) and short (PSAx—at the level of papillary muscle) axis 2D images, traced in end-diastole and end-systole, as well as M-mode images at the level of papillary muscle and aortic valve of the different phenotypes. *Ld* length in diastole, *Ls* length in systole, *Ad* area in diastole and *As* area in systole. *Ao* aorta and *LA* left atrium. **(b–e)** LV posterior wall thickness in diastole (LVPWd), LV end-diastolic volume (LVEDV), LV end-systolic volume (LVESV) and LV ejection fraction (LVEF) in the different phenotypes. **P* < 0.05 vs. Sham, +*P* < 0.05 vs. CR and MILD, and ‡*P* < 0.05 vs. MOD

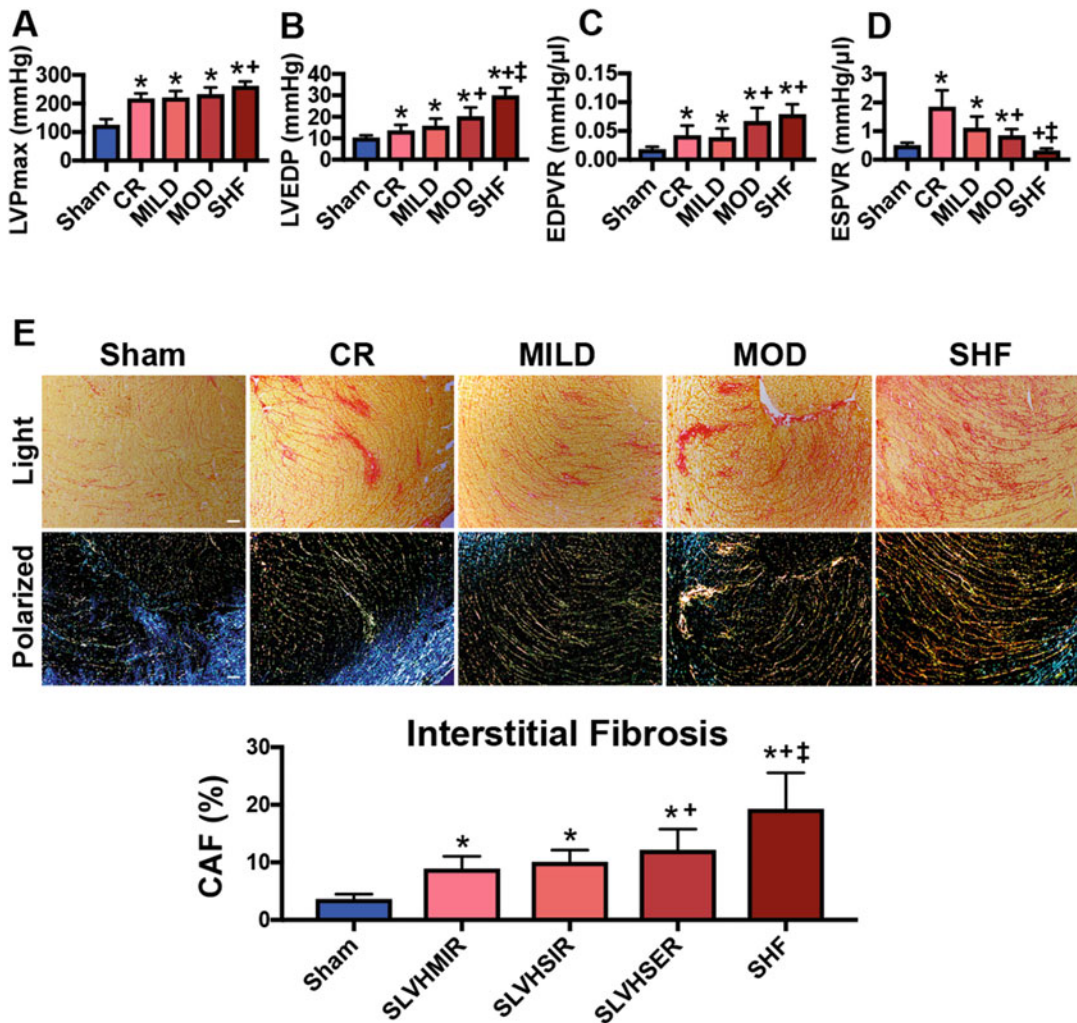


Fig. 3 (a-d) LV maximum pressure (LVPmax), LV end-diastolic pressure (LVEDP), end-diastolic pressure–volume relationship (EDPVR) and end-systolic pressure–volume relationship (ESPVR) in the different phenotypes. **(e)** LV interstitial fibrosis by light and polarized microscopy. Collagen I (yellow) and collagen III (green). * $P < 0.05$ vs. Sham, $^+P < 0.05$ vs. CR and MILD, and $^{\ddagger}P < 0.05$ vs. MOD. CAF collagen area of fibrosis

meticulous echocardiographic characterization of the different phenotypes is critically important. Pressure–volume loop parameters and interstitial fibrosis data are presented in Fig. 3. Note that the highest LV end-diastolic pressure is present in the SHF phenotype followed by the MOD phenotype. Both phenotypes have similar degree of myocardial stiffness, but myocardial contractility and efficiency gradually decreases with progressive LV remodeling and shift of LV volumes to the right. Also, there is progressive extracellular matrix remodeling associated with the degree of LV remodeling. More importantly, the increase in collagen I (yellow) and

collagen III (green), under polarized microscopy, becomes more significant in the MOD, but more so, in the SHF phenotypes, Fig. 3e. Thus, it is important to characterize and quantify not only the degree of interstitial fibrosis, but also collagen type.

2 Materials

2.1 Model Creation

1. A heating pad and warm blankets.
2. A mechanical ventilator for small animals, such as SAR-830/AP model.
3. Disinfectants: 70% isopropyl alcohol and povidone-iodine.
4. Anesthetics and analgesics: ketamine, xylazine, and buprenorphine.
5. 20 × 25 cm plastic board. Thickness should be about 3–5 mm.
6. Z-LITE fiber optic illuminator.
7. 100% cotton twine.
8. 2-0 and 3-0 vicryl taper sutures.
9. 14 and 16-Gauge angiocath for intubation and 25-Gauge needle for apical puncture.
10. Surgical tools: Hardened fine iris scissors, Tungsten Carbide Scissors (straight sharp/blunt), Adson forceps, one Graefe forceps straight and two Graefe forceps curved, Halsted-Mosquito Hemostats-straight, Kelly hemostats straight, Mayo-Hegar needle holder, chest retractors, Weck stainless steel Hemoclip ligation (cat# 533140) and stainless steel ligating clips (cat# 523435).
11. Sterile gauze and sterile cotton tipped applicators-6 in.
12. Surgical tape.

2.2 Evaluation of the Model

1. Echocardiography apparatus with a >14 MHz probe.
2. A 1.9F rat P-V catheter and a system (converter, recording and analysis software).
3. Hood, jars for staining, alcohol, xylene, and PicroSirius Red Stain kit.
4. Polarized light microscope.

3 Methods

3.1 Ascending Aortic Banding

The procedure is performed on 180–220 g male Sprague-Dawley rats.

1. The animal is anesthetized with Ketamine 65–75 mg/kg + Xylazine 2–5 mg/kg, intraperitoneally.

2. The hair is shaved on the surgical site (right thoracic area, lateral) under the right armpit.
3. After endotracheal intubation with 16-Gauge angiocath, mechanical ventilation is initiated with tidal volumes of 2 mL at 50 cycles/min and FiO_2 of 21%.
4. The animal is slowly turned to lie on its left side. The shaved area will be disinfected with topical application of povidone-iodine.
5. Right lateral thoracotomy, parallel to the ribs and 1 cm long, is performed 1 cm below the axilla, between the second and the third ribs, to access the ascending aorta (*see Notes 1–3*).
6. The thymus gland is gently dissected and then the aorta is identified, exposed and isolated from the superior vena cava by blunt dissection (*see Notes 4 and 5*).
7. Afterwards, a vascular clip (hemoclip), size described above, is placed around the ascending aorta, just above the aortic valve plane and prior to the takeoff of the brachiocephalic artery. The ascending aorta is gently lifted via a curved Graefe forceps with the left hand and the hemoclip, loaded into the hemoclip ligation tool, is placed in a horizontal plane over the ascending aorta using the right hand (*see Notes 6–8*).
8. The thorax will be then evacuated and closed using a 2-0 monofilament sutures. The muscle layer is sutured using 3.0 vicryl taper, then the skin incision is sutured using 3.0 cutting sutures.
9. Buprenorphine SR, 0.6–1 mg/kg, is then administered subcutaneously.
10. Finally, the animal is left to recover on heating pad with O_2 supply under regular monitoring. Once the animal shows signs of recovery from anesthesia (able to breath spontaneously—without evidence of gasping or use of accessory muscles for more than 2 min—and has good reflexes, red and warm extremities), it will be extubated and allowed to recover from anesthesia.

3.2 Echocardiography

Transthoracic echocardiography is performed to evaluate successful banding and disease progression.

1. Animal is sedated with ketamine 80–100 mg/kg injected intra-peritoneally (*see Notes 9 and 10*).
2. The chest hair is shaved on the procedure site.
3. Parasternal long and short axis—at the level of papillary muscle—2D views are obtained to calculate the LV end-diastolic (LVEDV) and end-systolic (LVESV) volumes as well as the ejection fraction of the LV (LVEF) using the area length

method: $V = 5/6 \times A \times L$; where V : is the volume in ml, A : is the cross sectional area of the LV cavity in cm^2 , obtained from the short axis 2D image in diastole and in systole, and L : is the diastolic length of the LV cavity in cm, measured from the long axis 2D image as the distance from the endocardial LV apex to the mitral-aortic junction (*see Notes 11–13*).

4. M-mode images are obtained from the short axis view at the level of the papillary muscle to measure the thickness of the septum (IVSd, cm) and the posterior wall at end-diastole (LVPWd, cm) as well as the LV end-diastolic (LVIDd, cm) and LV end-systolic internal dimensions (LVIDs, cm) and to calculate LV fractional shortening (LVFS, %) using the formula: $([\text{LVIDd} - \text{LVIDs}] \times 100/\text{LVIDd})$ (*see Notes 11 and 13*).
5. M-mode images at the level of the aortic valve are obtained to assess left atrial diameter, measured in diastole.

3.3 Invasive Pressure–Volume Loop Measurements

1. The animal is anesthetized with inhaled 5% (volume/volume) isoflurane for induction, and subsequently intubated using 14-Gauge angiocath and mechanically ventilated as noted above Subheading **3.1, step 3**.
2. Isoflurane is then lowered to 2–3% (volume/volume) for surgical incision. The chest is opened through a median sternotomy (*see Note 14*).
3. A rat P-V catheter is inserted into the LV apex through an apical stab performed with a 25G needle (*see Notes 15–17*).
4. Isoflurane is then adjusted (0.5–1%) to maintain anesthesia and a stable heart rate of approximately 350–400 bpm.
5. Hemodynamic recordings are performed 5 min after stable heart rate.
6. The intrathoracic inferior vena cava is transiently occluded to decrease venous return during the recording to obtain P-V end-systolic (ESPVR) and end-diastolic (EDPVR) relationships.
7. Linear fits of the ESPVR are used to calculate the end-systolic elastance (Ees) slope and volume intercept (V_0) and exponential of the EDPVR are used to derive the LV stiffness constant (β).
8. To adjust for the degree of LV hypertrophy, the dimensionless chamber stiffness index (DCSI) can be calculated by multiplying the EDPVR by the LV mass.
9. Blood resistivity is measured using a vendor supplied probe for rho value calibration.
10. Calibrate the pressure sensors and acquire pressure–volume data (*see Note 18*).

3.4 PicroSirius Red Staining in Fresh Frozen Tissue Sections

1. Slides, with LV sections about 7 μm thick, are fixed in 100% ETOH for 2 min then 50% ETOH for 2 min.
2. After three washes in deionized water, 3 min each, slides are stained with PicroSirius red stain for 1 h.
3. Then slides are washed in 0.5% acetic acid solution twice for 2 min.
4. Subsequently, slides are dehydrated by ethanol 95% and 100% bath, 2 min each.
5. After two baths of xylene, slides are mounted with Cyotseal 60 (Thermo Scientific, Waltham, MA, USA).
6. 4 \times and 10 \times magnification micrographs are taken by light microscopy and LV interstitial fibrosis is quantified from the 10 \times -magnified images using Image J software (NIH). At least ten fields per animal are quantified.
7. Polarized microscopy micrographs are taken under 4 \times magnification to assess for the collagen type, yellow: collagen I, and green: collagen III.

4 Notes

1. The dissection of the chest area, underneath the right armpit, should be performed with care in order to avoid injury/dissection of the right axillary artery.
2. Thoracotomy should be performed right underneath the armpit at the level of the second and third ribs. Thoracotomy performed between the first and second ribs or third and fourth ribs makes it harder to visualize the ascending aorta for placement of vascular clip.
3. When performing thoracotomy, care should be taken in order not to traumatize the right internal mammary artery, which usually runs medially and close to the sternum.
4. Gently dissect the two lobes of the thymus gland, as significant manipulation of the thymus gland will render it swollen, which impairs the visualization of the ascending aorta for the placement of the vascular clip.
5. Dissection of the aorta from the superior vena cava (SVC), via a curved Graefe forceps, should be done with care, as it is easy to injure/rupture the SVC, which is often fatal.
6. The hemoclip ligation tool should be adjusted, using a plastic precut twist tie—7", to obtain a vascular clip of the specified internal diameter of 1.5 mm^2 or 2 mm^2 .
7. After dissecting the aorta from the SVC, carefully lift the ascending aorta, using a curved Graefe forceps, and place the vascular band right before the takeoff of the brachiocephalic artery.

8. Be cautious not to band the brachiocephalic artery instead of the ascending aorta, which could happen if the aorta is not well visualized.
9. The animal must be completely sedated.
10. Animals that develop SHF are very sensitive to sedation and should be given half the dose of sedative that is administered to sham animals. Ketamine is a preferred agent over Isoflurane as the latter is associated with significant cardiodepressive effect.
11. Images should be acquired at heart rates between 370 and 420 beats/min.
12. Foreshortened long parasternal axis 2D images lead to false measurements. For quality control, the apex of the heart and the aortomitral angle should be well visualized. The length is measured from the apex (endocardium) to the aortomitral angle at end-diastole and end-systole.
13. Short parasternal axis 2D images are taken at the level of the papillary muscle. The area in diastole and in systole is measured by tracing the endocardium at end-diastole and end-systole.
14. Cardiac hemodynamics in this model of AAB can only be performed via an open chest, as the vascular clip is so tight, which makes it impossible to pass the P-V loop catheter retrogradely from the right carotid artery through the ascending aorta and into the LV.
15. Apical puncture in the diseased, PO, animals is associated with gushing of blood from the apex. It is very important to wear protective eyeglasses and work as fast as possible to insert the catheter through the apical puncture, without damaging the P-V loop catheter.
16. To lessen the amount of blood loss, it is best if the apical puncture is performed when the animal is under sedation with 3% inhaled isoflurane as the LV maximum pressure is significantly lower, compared to 0.5–1% inhaled isoflurane, due to the isoflurane-associated cardiodepressive effect.
17. If animal develops ventricular fibrillation, especially after apical puncture, gentle massage of the heart may revert it into normal rhythm. Also, it is important to ascertain that the animal is warm and to avoid air blowing into the chest from the surrounding to prevent ventricular arrhythmias and unstable rhythm.
18. The position of the catheter needs to be adjusted meticulously within the LV in order to obtain the highest volume and the best P-V loop shape. Also, care should be taken to ascertain that there is no biting of the catheter at end-systole which gives a falsely higher LV end-systolic pressure. In that case minute adjustment of the catheter position within the LV cavity can help resolve the problem.

Acknowledgments

This work is supported by NIH R01 HL117505, HL 119046, HL129814, 128072, HL131404, R01HL135093, a P50 HL112324, and two Transatlantic Fondation Leducq grants. We would like to acknowledge the Gene Therapy Resource Program (GTRP) of the National Heart, Lung, and Blood Institute, National Institutes of Health.

References

1. McMurray JJ, Petrie MC, Murdoch DR, Davie AP (1998) Clinical epidemiology of heart failure: public and private health burden. *Eur Heart J* 19(Suppl P):P9–P16
2. Berk BC, Fujiwara K, Lehoux S (2007) ECM remodeling in hypertensive heart disease. *J Clin Invest* 117(3):568–575. <https://doi.org/10.1172/jci31044>
3. Frey N, Olson EN (2003) Cardiac hypertrophy: the good, the bad, and the ugly. *Annu Rev Physiol* 65:45–79. <https://doi.org/10.1146/annurev.physiol.65.092101.142243>
4. Hill JA, Olson EN (2008) Cardiac plasticity. *N Engl J Med* 358(13):1370–1380. <https://doi.org/10.1056/NEJMra072139>
5. Kehat I, Molkentin JD (2010) Molecular pathways underlying cardiac remodeling during pathophysiological stimulation. *Circulation* 122(25):2727–2735. <https://doi.org/10.1161/circulationaha.110.942268>
6. Rothermel BA, Hill JA (2008) Autophagy in load-induced heart disease. *Circ Res* 103(12):1363–1369. <https://doi.org/10.1161/circresaha.108.186551>
7. Barrick CJ, Dong A, Waikel R, Corn D, Yang F, Threadgill DW, Smyth SS (2009) Parent-of-origin effects on cardiac response to pressure overload in mice. *Am J Physiol Heart Circ Physiol* 297(3):H1003–H1009. <https://doi.org/10.1152/ajpheart.00896.2008>
8. Barrick CJ, Rojas M, Schoonhoven R, Smyth SS, Threadgill DW (2007) Cardiac response to pressure overload in 129S1/SvImJ and C57BL/6J mice: temporal- and background-dependent development of concentric left ventricular hypertrophy. *Am J Physiol Heart Circ Physiol* 292(5):H2119–H2130. <https://doi.org/10.1152/ajpheart.00816.2006>
9. Lygate CA, Schneider JE, Hulbert K, ten Hove M, Sebag-Montefiore LM, Cassidy PJ, Clarke K, Neubauer S (2006) Serial high resolution 3D-MRI after aortic banding in mice: band internalization is a source of variability in the hypertrophic response. *Basic Res Cardiol* 101(1):8–16. <https://doi.org/10.1007/s00395-005-0546-3>
10. Chaanine AH, Sreekumaran Nair K, Bergen RH 3rd, Klaus K, Guenzel AJ, Hajjar RJ, Redfield MM (2017) Mitochondrial integrity and function in the progression of early pressure overload-induced left ventricular remodeling. *J Am Heart Assoc* 6(6). <https://doi.org/10.1161/jaha.117.005869>
11. Chaanine AH, Gordon RE, Kohlbrenner E, Benard L, Jeong D, Hajjar RJ (2013) Potential role of BNIP3 in cardiac remodeling, myocardial stiffness, and endoplasmic reticulum: mitochondrial calcium homeostasis in diastolic and systolic heart failure. *Circ Heart Fail* 6(3):572–583. <https://doi.org/10.1161/circheartfailure.112.000200>



Chapter 16

Isoproterenol-Induced Heart Failure Mouse Model Using Osmotic Pump Implantation

Sunny C. Chang, Shuxun Ren, Christoph D. Rau, and Jessica J. Wang

Abstract

Isoproterenol is used widely for inducing heart failure in mice. Isoproterenol is a nonselective beta-adrenergic agonist. The acute model mimics stress-induced cardiomyopathy. The chronic model mimics advanced heart failure in humans. In this chapter, we describe a protocol that we used to induce heart failure in 100+ strains of inbred mice. Techniques on surgical pump implantation and echocardiography are described in detail. We also discuss the impact of drug dosage, duration, mortality, age, gender, and strain on cardiac remodeling responses. The success of model creation may be assessed by echocardiogram or molecular markers. This chapter may be relevant to those who are interested in using this heart failure model.

Key words Heart failure, Isoproterenol, Mouse model, Cardiac remodeling, Mouse strains, Echocardiography

1 Introduction

Heart failure is a condition caused by inadequate pumping function of the heart. Several mouse models are available for basic investigations and preclinical testing. Left anterior descending artery ligation, transaortic constriction, and isoproterenol (ISO) aim at different cardiac pathologies [1]. Investigators should choose a model that best recapitulates their pathology of interest.

Both acute and chronic models of ISO have been used to study cardiac injury (Fig. 1). The acute model mimics stress-induced cardiomyopathy (SIC). SIC is characterized by apical segment ventricular dysfunction with basal segment sparing. It occurs in the setting of stressful life events. Adrenergic overstimulation has been postulated to play important roles in its pathogenesis [2, 3]. Protocols using one or few bolus injections have been described to mimic SIC. In contrast, the chronic model uses an implanted minipump to

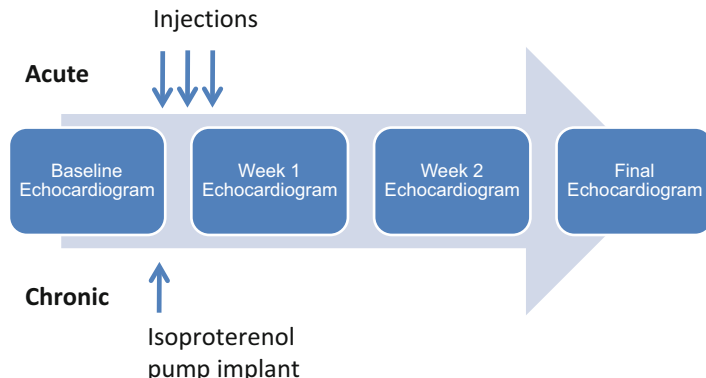


Fig. 1 Acute and chronic isoproterenol models

Table 1

Representative dosages, route of administration, and duration for chronic isoproterenol models of heart failure in mice

Strain	Age	Gender (see Note 6)	Dosage (mg/kg/d)	Route	Duration
C57BL/6 [12]	6–8 weeks	Male	3	s.c. daily	2 weeks
23 inbred mouse strains [13]	10–12 weeks	Male	10	s.c. osmotic pump	2 weeks
p110 γ (unknown genetic background) [14]	10–12 weeks	Male	15	Osmotic pump	7 days
100+ Hybrid Mouse Diversity Panel strains [8, 9]	10–12 weeks	Female	30	i.p. osmotic pump	3 weeks
C57BL/6 [15]	8 weeks	Male	40	s.c. osmotic pump	10 days
C57BL/6 [16]	6–8 weeks	Female	50	s.c. daily	7 days
BALB/c [17]	8–10 weeks	Male	60	s.c. daily	7 days
A/J C57BL/6J [18]	12–15 weeks	Male	100	s.c. daily	5 days
C57BL/6 [19]	8 weeks	Male	150	s.c. daily	7 days
AS-Ren mice [20]	3–5 months	NA	600	s.c. BID	Two consecutive days

release ISO continuously. This model mimics advanced heart failure where there is chronic adrenergic stimulation. A few representative protocols in literature are listed under Table 1.

Success for ISO model creation can be assessed *in vivo* by serial echocardiography demonstrating hypertrophy, dilation, and ventricular dysfunction. Histological findings include intramyocardial lipid accumulation and mild fibrosis [4]. Molecular signature from the collected heart tissue samples can be performed *ex vivo*. ISO causes cardiomyocyte ER stress, apoptosis, and a downregulation of beta-adrenergic receptors and adenyl cyclase activities [5–7].

In our previously published study performed across 105 Hybrid Mouse Diversity Panel (HMDP) strains, we used a dosage of 30 mg/kg/d over 21 days via the osmotic pump implanted intra-peritoneally [8, 9]. We observed striking interstrain variation in terms of response to interventricular wall and left ventricular mass hypertrophy, dilation, and ejection fraction (*see Note 1*). After 3 weeks of treatment, cardiac gene expression demonstrated significant changes between treatment and control groups across the HMDP [9]. The differentially expressed genes spanned cellular processes from extracellular matrix to inflammatory responses. These processes gave a glimpse of heart failure mechanisms due to beta-adrenergic stimulation. Here we describe the protocol we used for the preparation and surgical implantation of osmotic pumps and echocardiography.

2 Materials

1. Osmotic Pumps. Osmotic pumps of different sizes and drug duration are available for purchase from Alzet. We chose the ALZET Model 1004 minipumps with a 100 µL reservoir to administer isoproterenol over 3 weeks.
2. Isoproterenol (Concentration varies depending on the body weight of the animal due to constant flow rate.)
3. Depilatory cream.
4. Buprenorphine.
5. Ketamine.
6. Xylazine.
7. Ophthalmic ointment.
8. Surgical tools for mouse: scissors, forceps.
9. 5.0 absorbable suture.
10. 6.0 nonabsorbable suture.
11. Carprofen.
12. Amoxicillin.
13. Small animal anesthesia system: A tabletop anesthesia system that includes an isoflurane vaporizer/regulator, tubing,

induction chamber, face mask/nose cone, and passive scavenging system is required for echocardiography.

14. Echocardiography imaging system. An ultrahigh frequency ultrasound imaging system with cardiovascular analysis software, such as Visulsonics Vevo systems, is required for assessment of cardiac structure and function. We used a 30 MHz transducer for all image studies.

3 Methods

House animals in a vivarium with easy access to a surgical suite and an echocardiogram imaging system.

3.1 Anesthesia for Echocardiography

The use of inhaled isoflurane enables lesser trained operators to achieve physiologic images (*see Note 2*). Minimize measurement errors by using a uniform dosage of isoflurane throughout the experiment. Different mouse strains have varying susceptibility to isoflurane. Isoflurane dosage must be tailored to each mouse strain. Physiological heart rate for mice is around 600 bpm. Heart rate <475 bpm may be due to deep or prolonged sedation and should be avoided.

1. Fill the isoflurane regulator reservoir with isoflurane.
2. Turn on the oxygen to 2 L.
3. Turn on the isoflurane regulator to 1.25% or 1.5% to anesthetize each mouse in the induction chamber.
4. Once the mouse is appropriately sedated and secured on to the warmed echocardiography platform with tape, decrease isoflurane to a maintenance dosage of around 1%.
5. Take frequent notes of respiratory rate and heart rate.
6. Fine adjust isoflurane dosage as needed to maintain sedation without affecting heart rate and respiratory rate throughout the study.

3.2 Echocardiography

Echocardiography enables *in vivo* assessment of cardiac structures and function. Relevant measurements include left ventricular wall thickness, internal dimension, mass, and ejection fraction. Baseline assessment is helpful in controlling for biological variation. After isoproterenol treatment, reevaluation by echocardiogram can be performed as frequently as desired. In our study we monitored the mice weekly. The following steps are recommended to ensure accurate comparisons between serial studies.

1. Image the left ventricle in B-mode in the parasternal long-axis view.

2. Carefully adjust the mouse handling table to position the long-axis of the left ventricle in the same plane as the ultrasound beam. In practice, we place the aortic valve and the apex of the left ventricle in the same plane as the ultrasound beam. The aortic valve and the apex serve as fix points that remain invariant between serial studies on the same animal.
3. Adjust the tilt of the mouse handling table so that the long axis of the left ventricle is at 90° to the ultrasound beam.
4. Turn the ultrasound probe 90° to reveal the LV in short axis. Fine adjustments are made so that the maximum diameter of the LV is seen.
5. Perform M-mode through the middle of the left ventricle to image the walls and internal dimensions (*see Note 3*).

3.3 Preparation of Isoproterenol Osmotic Pump

Prepare osmotic pumps in a sterile environment such as a biosafety laboratory cabinet. The dosage of isoproterenol should be adjusted based on mortality and susceptibility to cardiac remodeling for each strain [8]. We chose 30 mg/kg/d to induce cardiac remodeling in most of the mouse strains. The osmotic pumps have a fixed delivery rate. The #1004 pump we chose has a pumping rate of 0.11 µL/h, duration of 28 days and reservoir volume of 100 µL. Prepare enough isoproterenol solution (~120 µL) as some volume will be lost in the filling tubing.

1. Weigh and record body weight for each mouse to calculate appropriate amounts of isoproterenol drug needed. *See Table 2*.
2. Use an analytical balance to weigh out the appropriate amount of isoproterenol for each mouse.
3. Dissolve isoproterenol in sterile 0.9% NaCl solution. Appropriate negative control for the experimental treatment is a solution identical to that used for solubilizing the isoproterenol drug, for example the 0.9% saline solution.

Table 2
Required dose of isoproterenol for commonly used animal weights

Isoproterenol 30 µg/g/d				
Body weight (g)	Daily dose (µg/d)	Flow rate (µL/d)	Concentration (µg/µL)	Isoproterenol (mg/120 µL)
20	600	2.64	227.3	27.3
21	630	2.64	238.6	28.6
22	660	2.64	250.0	30.0
23	690	2.64	261.4	31.4

4. Weigh the empty pump together with its flow modulator.
5. Draw the isoproterenol solution into a 1.0 mL small syringe. Attach the provided blunt-tipped, 27 gauge filling tube. Make sure that the syringe and filling tube are free of air bubbles.
6. Remove the flow moderator. Hold the pump in the upright position. Insert the filling tube through the opening at the top until it can go no further. This places the tip of the tube near the bottom of the pump reservoir.
7. Push the plunger of the syringe slowly to load the osmotic pump. When the solution appears at the outlet, stop filling and carefully remove the tube.
8. Wipe off excess solution and insert the flow moderator until the white flange is flushed with the top of the pump. Wipe off any overflow.
9. Weigh the filled pump to ensure that the fill volume is over 90% of the reservoir volume of 100 μ L.

3.4 Isoproterenol Osmotic Pump Surgical Implantation

Potential complications from isoproterenol pump surgery include infection and death. Therefore, survival surgery should be performed using sterile instruments, sutures, and septic procedures to minimize microbial infection. Surgeons should put on a surgical mask, bonnet and clean lab coat, and then wash and dry their hands before aseptically donning sterile gloves. Please *see Notes 3–5* regarding special considerations for age, gender, body size, and mortality rate with regards to surgical morbidity and mortality.

1. Prepare the animal by removing hair using a depilatory, such as Nair, at planned site of incision to minimize infections or other complications from incident hair. Perform this procedure in an area separate from where the surgery is to be conducted.
2. Administer buprenorphine 0.1 mg/kg s.c. to the back of the neck between the shoulder blades. Wait 10 min for the medication to work.
3. Anesthetize with 100 μ g/kg ketamine i.p. and 10 μ g/kg xylazine i.p.
4. Put ophthalmic ointment in the eyes to prevent the corneas from drying out.
5. Prepare the surgical site with an appropriate skin disinfectant, such as diluted Betadine or chlorhexidine. Alcohol is not an adequate disinfectant and its evaporation may lead to hypothermia in small animals.
6. Make a 1 cm long midline skin incision in the lower abdomen with surgical scissors. Carefully separate the skin from underlying connective tissues using blunt-ended scissors.

7. Use forceps to pick up the peritoneal wall. Cut a small (0.8 cm) hole in the musculoperitoneal layer and the peritoneal wall using fine surgical scissors while avoiding damage to the underlying bowel.
8. Insert the osmotic pump, flow moderator side first, into the peritoneal cavity.
9. Close the musculoperitoneal layer and the peritoneal wall with 5.0 absorbable sutures in an interrupted fashion.
10. Close the skin incision with 6.0 nonabsorbable sutures.
11. Move the animal to a warm, dry area, such as a dedicated incubator, and monitor it during recovery or overnight. Return the animal to its routine housing only after it has fully recovered from anesthesia.
12. To minimize pain and discomfort in the postoperative period, we recommend carprofen 5 mg/kg s.c., which may be repeated every 48 h as needed.
13. Administer antibiotic solution orally to prevent surgical site infections. For example, amoxicillin (0.25 mg/mL) in drinking water for 5 days.
14. Monitor every few days to check for complications (*see Notes 4 and 5*).
15. Remove nonabsorbable sutures after 7–10 days.

3.5 Tissue Collection

At the end of the protocol, endpoint assessment of cardiac structure and function using echocardiography may be performed. In our study, the minipump was capable of delivering constant isoproterenol dosage for 28 days. We made our end measurements at 21 days. After sublethal dosage of inhaled isoflurane followed by cervical dislocation, heart weight can be confirmed and heart and other tissues can be collected.

4 Notes

1. In our study, we included females from >100 inbred mouse strains. Isoproterenol caused a wide spectrum of cardiac remodeling phenotypes (Fig. 2 reproduced from PLoS Genet 2016 with permission from the Public Library of Science (PLOS) [9]). Expected time for the model development and weekly changes in echocardiography parameters for each strain are shown in Fig. 3 (reproduced from PLoS Genet 2016 with permission from PLOS) [9]. Overall, LVIDd and LVM increased over a period of 3 weeks. IVSd and FS increased in the first week but decreased by later time points. Of note, during the final assessment, most strains showed normal

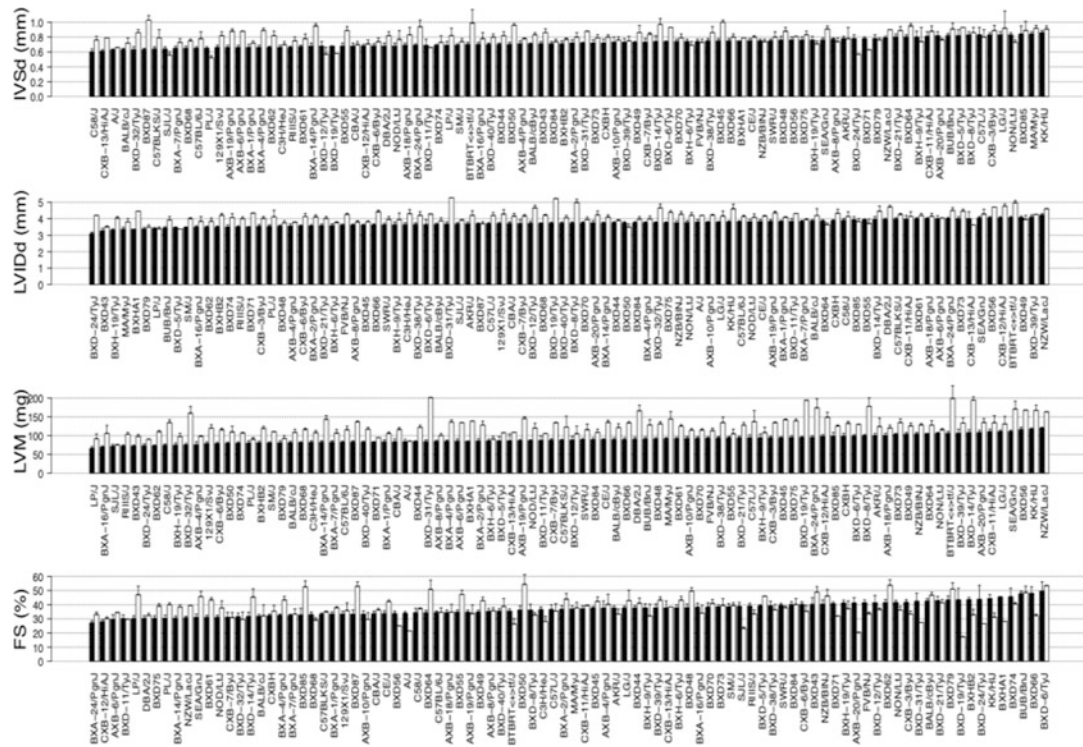


Fig. 2 Variation in echocardiographic measures of cardiac structure and function among HMDP mouse strains. Black bars represent measurements under the baseline condition in ranked order. White bars represent measurements after 3 weeks of continuous ISO infusion. *IVSd* Interventricular septal wall thickness, *LVIDd* Left ventricular diastolic diameter, *LVM* Left ventricular mass, *FS* Fractional shortening. Error bars represent the standard errors of the means

systolic heart function. With ongoing isoproterenol infusion, normal systolic function represents impaired contractile reserve.

2. Isoflurane can have a negative effect on cardiac chronotropy and inotropy. Echocardiogram may be performed without sedation by experienced operators.
 3. The sternum may cast a bony shadow over the image. The probe should be repositioned to image from a different rib interspace. The right ventricular wall may make it difficult to measure the interventricular wall borders. Measure cardiac dimensions in real time so that poorly delineated borders can be immediately reinterrogated by taking additional modified views. Accurate measurements are critical to the downstream comparisons.
 4. Age and body size. Mice weighing <20 g have a higher early surgical mortality associated with surgical procedures (death within 48 h). Allowing female mice to mature to at least 9–10 weeks of age will lower early surgical mortality.

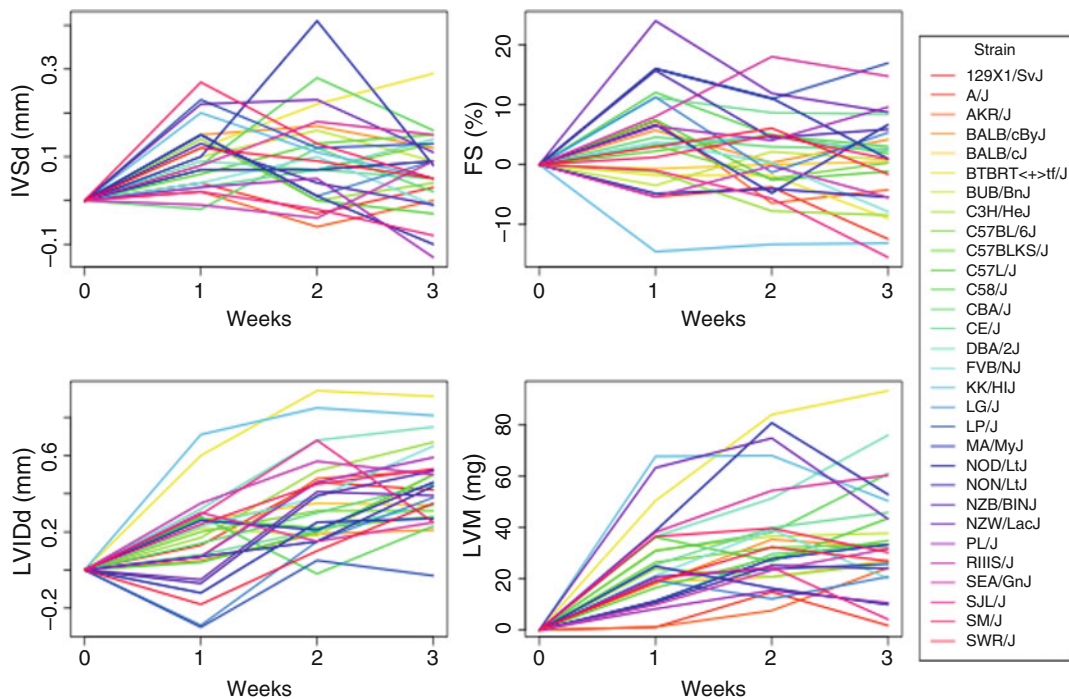


Fig. 3 The changes in echocardiographic measures compared to baseline at each ISO time point for individual classical inbred strains

5. Mortality rate and cardiac fibrosis. It is important to consider strain-specific rates of operative mortality and susceptibility to isoproterenol when planning an experiment (Table 3) [8]. In the HMDP study, 139 (29.6%) mice out of 470 mice in the isoproterenol treatment group died before the end of the protocol. Most (127) died within the first 48 h of treatment. Once mice survived the initial surgery, few died during the course of the study from heart failure complications. Specifically, 100% mortality occurred in BXA-12/PgnJ and BXD-34/TyJ; 86% in BTBRT<+>tf/J; 83% in NZW/LacJ; 64% in BXD40/TyJ; and 58% in BALB/cJ. Finally, ISO caused more cardiac fibrosis in some strains than in others. For example, the strain KK/Hij had markedly increased fibrosis after ISO stimulation (Fig. 4 reproduced from Circ Cardiovasc Genet 2015 with permission from Lippincott Williams & Wilkins) [8].
6. Gender. Sex differences in cardiovascular disease are well-known in the literature. Considerations regarding gender must be made when planning an experiment. In an ischemia reperfusion injury model, female mouse demonstrated higher postischemic contractile function and lesser ATP-depletion [10]. In a chronic isoproterenol model, Klingman et al. found

Table 3
Mouse strains and deaths in the isoproterenol group

Strain	Control	Isoproterenol	Deaths (<48 h)
129X1/SvJ	3	8	1
A/J	3	8	3
AKR/J	2	6	0
AXB-10/PgnJ	2	3	0
AXB-12/PgnJ	1	2	2
AXB-13/PgnJ	0	1	1
AXB-18/PgnJ	4	4	1
AXB-19/PgnJ	5	5	2
AXB-20/PgnJ	1	4	2
AXB-4/PgnJ	1	2	0
AXB-6/PgnJ	1	2	1
AXB-8/PgnJ	3	5	0
BALB/cByJ	2	4	1
BALB/cJ	6	12	7
BTBRT<+>tf/J	5	14	12
BUB/BnJ	3	8	3
BXA-1/PgnJ	2	3	1
BXA-11/PgnJ	1	1	0
BXA-12/PgnJ	1	3	3
BXA-14/PgnJ	4	5	0
BXA-16/PgnJ	2	4	0
BXA-2/PgnJ	3	4	1
BXA-24/PgnJ	5	8	4
BXA-4/PgnJ	4	4	0
BXA-7/PgnJ	5	5	0
BXA-8/PgnJ	1	2	1
BXD-1/TyJ	1	0	0
BXD-11/TyJ	2	2	1
BXD-12/TyJ	2	2	0
BXD-14/TyJ	1	3	0
BXD-15/TyJ	1	2	2

(continued)

Table 3
(continued)

Strain	Control	Isoproterenol	Deaths (<48 h)
BXD-19/TyJ	0	2	1
BXD-20/TyJ	0	1	1
BXD-21/TyJ	6	9	2
BXD-22/TyJ	0	1	1
BXD-24/TyJ	2	1	0
BXD-27/TyJ	1	3	3
BXD-31/TyJ	1	1	0
BXD-32/TyJ	4	5	2
BXD-33/TyJ	1	1	1
BXD-34/TyJ	2	5	5
BXD-38/TyJ	4	6	4
BXD-39/TyJ	2	3	0
BXD-40/TyJ	7	14	9
BXD43	2	5	0
BXD44	2	2	0
BXD45	3	4	2
BXD48	2	4	0
BXD49	3	3	0
BXD-5/TyJ	1	1	0
BXD50	4	5	1
BXD55	2	5	1
BXD56	3	4	3
BXD-6/TyJ	1	1	0
BXD61	4	7	2
BXD62	3	4	1
BXD64	3	3	0
BXD66	3	3	0
BXD68	3	5	0
BXD69	1	0	0
BXD70	3	4	1
BXD71	1	1	0

(continued)

Table 3
(continued)

Strain	Control	Isoproterenol	Deaths (<48 h)
BXD73	3	5	1
BXD74	2	2	0
BXD75	3	6	1
BXD79	3	4	0
BXD-8/TyJ	1	2	0
BXD84	3	6	1
BXD85	1	2	0
BXD86	2	2	2
BXD87	3	3	0
BXH-19/TyJ	1	3	0
BXH-6/TyJ	4	5	0
BXH-9/TyJ	1	2	0
BXHA1	0	1	0
BXHB2	4	5	0
C3H/HeJ	4	8	1
C57BL/6J	6	11	4
C57BLKS/J	3	5	3
C57L/J	2	3	0
C58/J	2	4	1
CBA/J	3	7	0
CE/J	2	3	0
CXB-11/HiAJ	2	3	1
CXB-12/HiAJ	4	6	2
CXB-13/HiAJ	2	5	1
CXB-3/ByJ	4	3	0
CXB-6/ByJ	3	7	4
CXB-7/ByJ	2	3	1
CXBH	2	5	1
DBA/2J	6	11	3
FVB/NJ	6	10	1
KK/Hij	2	4	0

(continued)

Table 3
(continued)

Strain	Control	Isoproterenol	Deaths (<48 h)
LG/J	4	4	1
LP/J	3	3	0
MA/MyJ	3	4	0
NOD/LtJ	3	7	0
NON/LtJ	4	6	1
NZB/BINJ	2	4	1
NZW/LacJ	3	6	5
PL/J	2	7	2
RIIIS/J	4	9	3
SEA/GnJ	3	9	5
SJL/J	2	7	2
SM/J	3	3	0
SWR/J	4	9	5

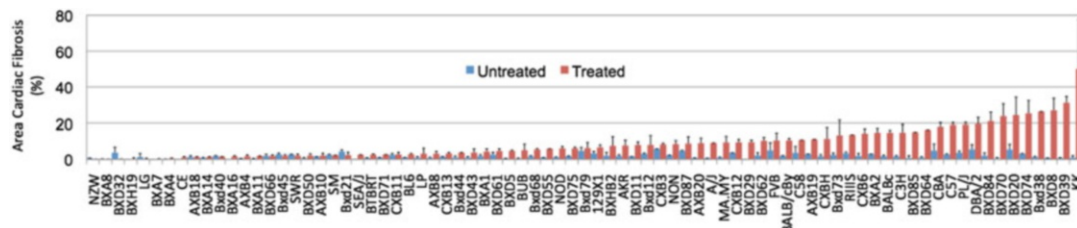


Fig. 4 Distribution of cardiac fibrosis before and after isoproterenol treatment in the HMDP. Data is organized based on the amount of fibrosis observed after isoproterenol treatment and displays mean +/- standard deviation

elevated heart to body weight ratio in males but not in females [11]. Finally, total norepinephrine levels in parotid and submaxillary glands were reduced in males but not in females.

Acknowledgments

The discussed protocol has been developed in the laboratory of Dr. Yibin Wang.

References

1. Balakumar P, Singh AP, Singh M (2007) Rodent models of heart failure. *J Pharmacol Toxicol Methods* 56(1):1–10
2. Yoshikawa T (2015) Takotsubo cardiomyopathy, a new concept of cardiomyopathy: clinical features and pathophysiology. *Int J Cardiol* 182:297–303
3. Kono T, Sabbah HN (2014) Takotsubo cardiomyopathy. *Heart Fail Rev* 19(5):585–593
4. Shao Y, Redfors B, Stahlman M, Tang MS, Miljanovic A, Mollmann H, Troidl C, Szardien S, Hamm C, Nef H, Boren J, Omerovic E (2013) A mouse model reveals an important role for catecholamine-induced lipotoxicity in the pathogenesis of stress-induced cardiomyopathy. *Eur J Heart Fail* 15 (1):9–22
5. Kudej RK, Iwase M, Uechi M, Vatner DE, Oka N, Ishikawa Y, Shannon RP, Bishop SP, Vatner SF (1997) Effects of chronic beta-adrenergic receptor stimulation in mice. *J Mol Cell Cardiol* 29(10):2735–2746
6. Zhuo XZ, Wu Y, Ni YJ, Liu JH, Gong M, Wang XH, Wei F, Wang TZ, Yuan Z, Ma AQ, Song P (2013) Isoproterenol instigates cardiomyocyte apoptosis and heart failure via AMPK inactivation-mediated endoplasmic reticulum stress. *Apoptosis* 18(7):800–810
7. El-Demerdash E, Awad AS, Taha RM, El-Hady AM, Sayed-Ahmed MM (2005) Probucol attenuates oxidative stress and energy decline in isoproterenol-induced heart failure in rat. *Pharmacol Res* 51(4):311–318
8. Rau CD, Wang J, Avetisyan R, Romay MC, Martin L, Ren S, Wang Y, Lusis AJ (2015) Mapping genetic contributions to cardiac pathology induced by beta-adrenergic stimulation in mice. *Circ Cardiovasc Genet* 8 (1):40–49
9. Wang JJ, Rau C, Avetisyan R, Ren S, Romay MC, Stolin G, Gong KW, Wang Y, Lusis AJ (2016) Genetic dissection of cardiac remodelling in an isoproterenol-induced heart failure mouse model. *PLoS Genet* 12(7):e1006038
10. Cross HR, Murphy E, Koch WJ, Steenbergen C (2002) Male and female mice overexpressing the beta(2)-adrenergic receptor exhibit differences in ischemia/reperfusion injury: role of nitric oxide. *Cardiovasc Res* 53(3):662–671
11. Klingman GI, McKay G, Ward A, Morse L (1973) Chronic isoproterenol treatment of mice: effects on catecholamines and rectal temperature. *J Pharm Sci* 62(5):798–801
12. Ma S, Yang D, Wang K, Tang B, Li D, Yang Y (2012) Cryptotanshinone attenuates isoprenaline-induced cardiac fibrosis in mice associated with upregulation and activation of matrix metalloproteinase-2. *Mol Med Rep* 6 (1):145–150
13. Berthonneche C, Peter B, Schupfer F, Hayoz P, Katalik Z, Abriel H, Pedrazzini T, Beckmann JS, Bergmann S, Maurer F (2009) Cardiovascular response to beta-adrenergic blockade or activation in 23 inbred mouse strains. *PLoS One* 4(8):e6610
14. Oudit GY, Crackower MA, Eriksson U, Sarao R, Kozieradzki I, Sasaki T, Irie-Sasaki J, Gidewicz D, Rybin VO, Wada T, Steinberg SF, Backx PH, Penninger JM (2003) Phosphoinositide 3-kinase gamma-deficient mice are protected from isoproterenol-induced heart failure. *Circulation* 108(17):2147–2152
15. Galindo CL, Skinner MA, Errami M, Olson LD, Watson DA, Li J, McCormick JF, McIver LJ, Kumar NM, Pham TQ, Garner HR (2009) Transcriptional profile of isoproterenol-induced cardiomyopathy and comparison to exercise-induced cardiac hypertrophy and human cardiac failure. *BMC Physiol* 9:23
16. Ren J, Yang L, Tian W, Zhu M, Liu J, Lu P, Li J, Yang L, Qi Z (2015) Nitric oxide synthase inhibition abolishes exercise-mediated protection against isoproterenol-induced cardiac hypertrophy in female mice. *Cardiology* 130 (3):175–184
17. Yang YH, Fang HL, Zhao M, Wei XL, Zhang N, Wang S, Lu Y, Yu XJ, Sun L, He X, Li DL, Liu JJ, Zang WJ (2017) Specific alpha7 nicotinic acetylcholine receptor agonist ameliorates isoproterenol-induced cardiac remodelling in mice through tgf-beta1/smads pathway. *Clin Exp Pharmacol Physiol* 44:1192–1200
18. Faulk MD, Ernsberger P, Vatner D, Hoffman RD, Lewis W, Strachan R, Hoit BD (2005) Strain-dependent beta-adrenergic receptor function influences myocardial responses to isoproterenol stimulation in mice. *Am J Physiol Heart Circ Physiol* 289(1):H30–H36
19. Li X, Zhang ZL, Wang HF (2017) Fusaric acid (fa) protects heart failure induced by isoproterenol (isp) in mice through fibrosis prevention via tgf-beta1/smads and pi3k/akt signaling pathways. *Biomed Pharmacother* 93:130–145
20. Vergaro G, Prud'homme M, Fazal L, Merval R, Passino C, Emdin M, Samuel JL, Cohen Solal A, Delcayre C (2016) Inhibition of galectin-3 pathway prevents isoproterenol-induced left ventricular dysfunction and fibrosis in mice. *Hypertension* 67(3):606–612



Chapter 17

Rat Model of Cardiotoxic Drug-Induced Cardiomyopathy

Takehiro Nakahara, Takashi Tanimoto, Artiom D. Petrov,
Kiyotake Ishikawa, H. William Strauss, and Jagat Narula

Abstract

Cardiotoxicity from cancer drugs remains a clinical problem. To find reliable markers of cardiotoxicity, animal models were proposed and potential new diagnostic markers have been actively investigated using these models. Here we describe our protocols, using male Sprague-Dawley rats, for inducing cardiomyopathy by single injection of high-dose doxorubicin (5–10 mg/kg) or multiple injections (2–4 times) of low-dose doxorubicin (2.5 mg/kg) with combined single injection of trastuzumab (10 mg/kg). The cardiotoxicity is evaluated by imaging modalities (echocardiography and nuclear imaging), serum troponin levels, and histopathological analyses.

Key words Doxorubicin, Traszmab, Cardiotoxicity, Echocardiography, Left ventricular ejection fraction, Troponin

1 Introduction

Although the remission rate of cancer therapy improved [1], cardiotoxicity from cancer drugs still remains the problem [2–4]. The myocardial damage from cancer drug leads to decreases in left ventricular ejection fraction (LVEF) and worsens the prognosis. To detect early signs of cardiotoxicity from cancer drugs, in particular doxorubicin (Dox) and recently trastuzumab (Trz), several animal models of cardiotoxicity (mouse, rat, and rabbit) were proposed and used for identifying diagnostic markers. These animal models are easy to create with high reproducibility; however, challenges remain in converting the dose and intervals from clinical regimen to animal protocols.

These models can be classified, depending on the injection protocols, into short-term models (~2 weeks) and long-term models (2–12 weeks). In rat short-term models, animals receive single dose (10–30 mg/kg) of Dox once I.V. or I.P. Other short-term models use 2–3.4 mg/kg of Dox every other day for six times, (cumulative dose of 12–20 mg/kg) [5–14]. For rat long-term

models, animals usually receive 1–5 mg/kg of Dox I.P. or I.V. every week for 2–12 weeks, with the cumulative dose of 3–25 mg/kg [15–27]. Trz (10 mg/kg) is commonly injected with or without Dox, based on clinical chemotherapy regimens that use both Trz and Dox [5, 21, 28]. In mouse short-term models, animals receive 6–20 mg/kg of Dox I.P. or I.V. for one time with or without Trz 10 mg/kg [29–40]. In mouse long-term models, animals receive 3–9 mg/kg of Dox I.P. or I.V. once every week or twice per week for 4–12 weeks (cumulative dose of 12–40 mg/kg) [37, 41–49]. Alternatively, Trz is combined to Dox in some of the chronic protocols. In rabbit models, animals receive 2 mg/kg of Dox every week for 1–8 weeks [50–54]. Although various study lengths have been used and animals seem to complete study protocols in each study, protocols are generally shorter in those using high-dose drugs, likely due to the short survival. For example, one study reported that 10 mg/kg Dox single injection resulted in 80% mortality at 28 days, whereas five weekly injections of 2 mg/kg Dox models survived approximately for 100 days [12]. Thus, short-term model with high-dose injection will be suitable to evaluate acute cardiotoxicity whereas low-dose long term model will be suitable to evaluate chronic cardiotoxicity. In this chapter, we describe our short-term protocols and the methods to detect cardiotoxicity in rats [5].

2 Material

For some materials, approvals may be required from appropriate institutional committees.

1. Animals: Sprague-Dawley 8-week-old male rats (*see Note 1*).
2. Rat normal diet.
3. Syringes (1 mL); measure dead space within the syringe for injecting exact dose.
4. IV catheters and needles (22G/23G).
5. Restrainer.
6. Isoflurane.
7. Oxygen.
8. Instruments for anesthesia including boxes and masks.
9. Gauze.
10. Phosphate buffered saline (PBS).
11. Saline.
12. Echocardiography with ECG leads and high frequency transducers (*see Note 2*).
13. Micro SPECT/CT (collimator for experimental animals) with nuclear tracers.

14. Heating pad.
15. ELISA kit.
16. Plate reader.
17. 4% paraformaldehyde (PFA).
18. Dimethyl sulfoxide (DMSO).
19. Doxorubicin (Dox).
20. Trastuzumab (Trz).

3 Methods

In our protocol, animals are imaged using echocardiography for every injection. Animals are anesthetized for echocardiography; however, they will be fixed in the restrainer without anesthesia for drug injections.

3.1 Injection

An overview of our injection protocol is described in **Note 3**.

1. Prepare Dox or Trz as calculated. Although ready-to-use Dox and Trz solutions are available, Dox powder can be solved with 4% dimethyl sulfoxide (DMSO). One milliliter of Saline is also prepared in a syringe for flush.
2. Evaluate baseline cardiac function (or during follow-up) as described later (Subheadings [3.2](#) and [3.3](#).).
3. After finishing echocardiography, the animals are inserted into a restrainer and the tail is pulled out from the bottom hole.
4. Immobilize the animal with a restrainer, fix the tail, and insert an IV catheter into the tail vein. Veins can be found on the lateral sides of the tail (Fig. 1). When inserting the IV catheter, check the back flow. When the back flow is observed, lean down the catheter and slightly push forward for only 1 mm in order to insert the catheter. Insert the catheter into the vein while pulling back the needle. After inserting the catheter, attach a syringe filled with saline and check whether blood can be drawn smoothly. Then inject saline (*see Note 4*).
5. Inject prepared Dox or Trz. Upon injection, immediately change the syringe and flush the drugs with saline.
6. After injection, remove the IV catheter from the vein and compress the wound firmly with gauze to treat bleeding (usually stops within 4–5 min).
7. After Isoflurane discontinuation, only oxygen is provided until the animal is awake.
8. Animal is put back to the cage and monitored until they are fully recovered from anesthesia.

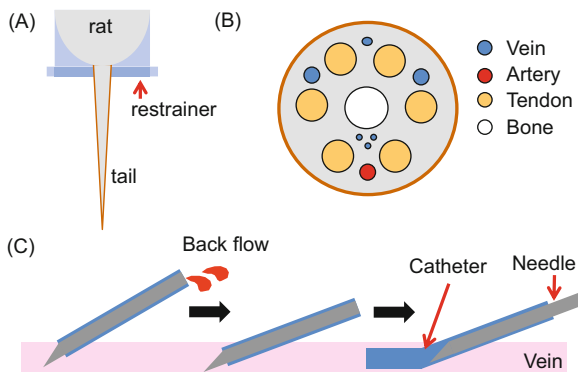


Fig. 1 Tips for injection. (A) Fix the animal with restrainer and pick up the tail and insert an IV catheter in the tail vein. (B) Target veins can be found on the lateral side of the tail. (C) When inserting the IV catheter, check the back flow. When back flow is observed, lean down the catheter and push forward for only 1 mm in order to insert the catheter. Insert the outer sheath into the vein, while pulling back the needle

3.2 Echocardiography

1. Anesthetize the animal with 2% isoflurane–98% oxygen (*see Note 5*).
2. Shave the body hair, especially on the chest, and fix the animal on a board. It is recommended to place a heating pad to maintain the body temperature during the imaging.
3. Attach ECG leads to limbs. Wrap with PBS-soaked gauze and clip the gauze with the metal. Attach ECG leads to the metal clips (Fig. 2).
4. Apply the probe on the chest and use 2D mode to obtain parasternal view (long-axis/short-axis), subxiphoid view and apical view (*see Note 6*).

3.3 Micro-SPECT/CT

1. Inject nuclear tracer into the tail vein (See Subheadings 3.1), and wait until the optimized timing for imaging.
2. Anesthetize the animal with 2% isoflurane–98% oxygen (*see Note 5*).
3. Fix the animal on SPECT/CT bed.
4. A micro-CT scan image is acquired using an X-ray tube operating at recommended setting.
5. Immediately after micro-CT scan, acquire micro-SPECT images in an optimized photopeak of nuclear tracers using multi pinhole collimator. Micro-SPECT images are reconstructed and transferred to image display and analysis.
6. The micro-SPECT images and micro-CT images can be fused using manufacturers' software.

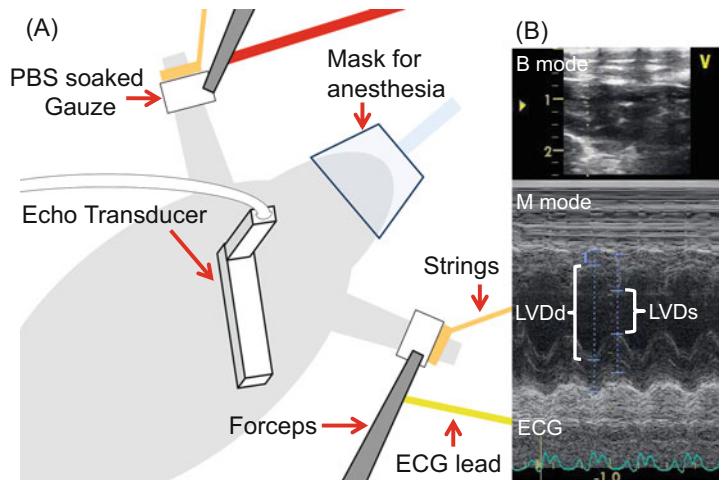


Fig. 2 Overview of echocardiography. **(A)** Acquire the echo images. Set the anesthetized animal in supine position and fix on a board. Limbs are pulled with strings to obtain good echo view. Then, the limbs are wrapped with PBS-Soaked gauze and the metal clips (forceps) are attached to the gauze. Attach ECG lead to the metal clips (forceps). To obtain echo images, apply the probe on the chest and use B mode to obtain parasternal view (long-axis/short-axis), subxiphoid view and apical view. **(B)** Parasternal view (long-axis). On the parasternal view (long-axis), obtain two dimensional images (B Mode) (upper image). Then set the cursor below of the mitral valve level. Following the cursor, M mode images are obtained (lower image). On the M mode, left ventricular parameters are measured to evaluate LV function. Set the cursor on the edge of LV walls and measure left ventricular diastolic diameter (LVDd) and left ventricular systolic diameter (LVDs). And left ventricular end diastolic volume (LVEDV), left ventricular end systolic volume (LVESV), stroke volume (SV), and LVEF are measured as below, following Teicholz method [55]. $LVEDV = 7 \times LVDd^3 / (2.4 + LVDd)$. $LVEDV = 7 \times LVDs^3 / (2.4 + LVDs)$. $SV = LVEDV - LVESV$. $EF = SV/LVEDV \times 100 (\%)$

3.4 Blood Sample Analysis

For evaluating cardiotoxicity using blood, cardiac troponin I can be used. Blood samples should be obtained before killing the animal. We obtain the blood from the portal vein or inferior vena cava.

1. Prepare syringes with 22 (23) G needle and tubes for centrifuge and serum storage. To obtain plasma, heparin should be placed in the centrifuge tube.
2. After the imaging is finished, keep the animals anesthetized.
3. Cut the abdominal skin and open abdomen.
4. Dislocate abdominal organs including intestines and lower liver to reveal the portal vein.
5. Insert a needle into the portal vein or inferior vena cava and withdraw 1–2 mL of blood (Fig. 3).

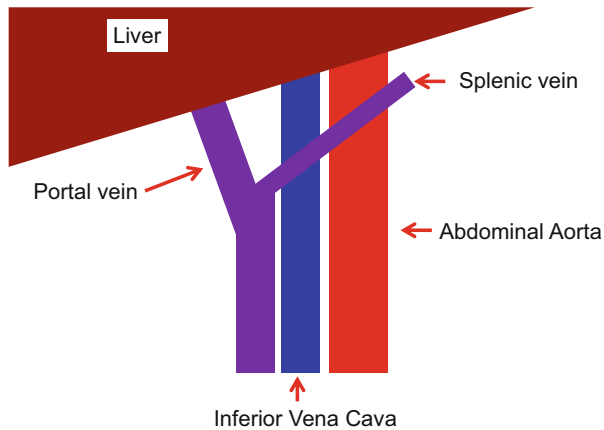


Fig. 3 A scheme of veins and arteries. To obtain blood, portal vein or inferior vena cava is easy to access on an anesthetized animal. This scheme shows frequent variation of portal vein and inferior vena cava

6. Transfer the blood to the tubes. For plasma, invert the tubes several times to mix the blood and heparin.
7. Approximately 30 min later in room temperature, centrifuge the tubes $1000\text{--}2000 \times g$ at 4°C for 10 min.
8. Retrieve serum and plasma using pipet and place them in new tubes for storage.
9. Unless serum/plasma is not used immediately, store in -80°C .
10. Using the ELISA kits and a plate reader, measure high-sensitive troponin I in the collected samples (*see Note 7*).

3.5 Histopathological Analysis

Histopathology is a sensitive method to detect cardiotoxicity from cancer drugs.

1. Cut organs and put them in each tube, separately (*see Note 8*).
2. Soak each sample in 4% PFA (1–2 mL) overnight.
3. Wash samples with PBS and store at 4°C up to 6 months.
4. Embed samples in Paraffin for staining. For immunofluorescence staining, samples are embedded in optimal cutting temperature (O.C.T.) compound and soaked into liquid nitrogen to freeze. After Paraffin (room temperature) or O.C.T. (frozen) embedding, sample are sectioned into $5\text{ }\mu\text{m}$ slices. Stain the slides for evaluation (*see Note 9*).

4 Notes

1. In this protocol, male rats are used. Female animals are also used in other protocols [6, 21, 22, 43].

2. The frequency of transducer should be set high (7.5–30 MHz) to assess the wall motion.
3. In our protocol, animals either receive single (5–10 mg/kg DOX) or multiple (2.5 mg/kg Dox every other day for 2, 3 or 4 injections) injections. Two groups also receive single dose of 10 mg/kg trastuzumab (Trz) in Dox multiple injection model. Single injection model and Dox with Trz model showed significant decrease in LVEF and myocardial damage in histology. Multiple Dox injection model showed no significant changes in LVEF, although it showed mitochondrial structural changes in histology. Serum troponin level did not change [5].
4. In IV catheters, there usually is a gap between the needle and the catheter (Fig. 1c). Confirmation of blood back flow helps to insert the catheter correctly. Drug leak into the interstitial space associated with inappropriate catheter placement will result in insufficient dose reaching to the heart. In addition, it can cause focal damage.
5. During the anesthesia for cardiac imaging, ECG changes (especially heart rate) should be monitored to avoid excessive anesthesia (approximate normal heart rate, mouse: 480–740/min, rat: 260–450/min, rabbit: 150–200/min). The respiratory rate will also help determining the depth of anesthesia (approximate normal respiratory rate, mouse: 180/min, rat: 90/min, rabbit: 30–60/min).
6. Echocardiography is performed before each injection and at the endpoint. Bidimensional (2D) and M-mode are used for assessing wall motion (damage). To evaluate function, LVEF is measured using Teichholz method in parasternal view (long-axis/short-axis). Because myocardial damage from cancer drugs cause diffuse hypokinesis, Teichholz method [55] is frequently used over other calculation methods, such as modified Simpson method, which measures focal impairments more accurately. Although it depends on size of the animals and spec of the echocardiography, Doppler and strain (Speckle tracking) can also be analyzed using high spec echocardiography and dedicated software.
7. Although cutoff points for Troponin I measurements in animal models are not clearly defined in literature; circulating troponin I level over 0.08 ng/mL [56, 57] (another study used over 0.03 ng/mL [58]) is commonly used as a cutoff limit for normal in clinical studies. Presence of cardiotoxicity is evaluated using this troponin I cutoff value. The protocols for ELISA assay should be followed the manufacturers' protocols.

8. We divide heart into four pieces, followed by short axis sectioning. To fix in 4% PFA, tissue size should be small, such as <1 cm.
9. To evaluate histopathology, grading method are used in HE staining [59, 60] (from inflammation, cardiomyocyte degeneration, apoptosis and necrosis, etc.), or electron microscopic (EM) analysis (inflammation, mitochondria changes, vacuoles, etc.) [60–62]. Picro-Sirius staining is used to detect fibrosis. To detect myocardial hypertrophy, wheat germ agglutinin (WGA) staining is used.

Acknowledgments

TN was supported by Uehara Memorial Foundation and SNMMI Wagner-Torizuka Fellowship. TT was supported by Japan Heart Foundation/Bayer Yakuhin Research Grant Abroad.

References

1. Zeng C, Wen W, Morgans AK, Pao W, Shu XO, Zheng W (2015) Disparities by race, age, and sex in the improvement of survival for major cancers: results from the National Cancer Institute Surveillance, Epidemiology, and End Results (SEER) program in the United States, 1990 to 2010. *JAMA Oncol* 1(1):88–96. <https://doi.org/10.1001/jamaoncol.2014.161>
2. Lenneman CG, Sawyer DB (2016) Cardio-oncology: an update on cardiotoxicity of cancer-related treatment. *Circ Res* 118 (6):1008–1020. <https://doi.org/10.1161/circresaha.115.303633>
3. Bloom MW, Hamo CE, Cardinale D, Ky B, Nohria A, Baer L, Skopicki H, Lenihan DJ, Gheorghiade M, Lyon AR, Butler J (2016) Cancer therapy-related cardiac dysfunction and heart failure: part 1: definitions, pathophysiology, risk factors, and imaging. *Circ Heart Fail* 9(1):e002661. <https://doi.org/10.1161/circheartfailure.115.002661>
4. Hamo CE, Bloom MW, Cardinale D, Ky B, Nohria A, Baer L, Skopicki H, Lenihan DJ, Gheorghiade M, Lyon AR, Butler J (2016) Cancer therapy-related cardiac dysfunction and heart failure: part 2: prevention, treatment, guidelines, and future directions. *Circ Heart Fail* 9(2):e002843. <https://doi.org/10.1161/circheartfailure.115.002843>
5. Nakahara T, Petrov A, Tanimoto T, Chaudhry F, Narula N, Seshan SV, Mattis JA, Pak KY, Sahni G, Bhardwaj A, Sengupta PP, Tiersten A, Strauss HW, Narula J (2018) Molecular imaging of apoptosis in cancer therapy related cardiac dysfunction before LVEF reduction. *JACC Cardiovasc Imaging* 2018 Feb 14. pii: S1936-878X(18)30005-6. <https://doi.org/10.1016/j.jcmg.2017.12.012>
6. Razmaraii N, Babaei H, Mohajjal Nayebi A, Asadnasab G, Ashrafi Helan J, Azarmi Y (2016) Cardioprotective effect of phenytoin on doxorubicin-induced cardiac toxicity in a rat model. *J Cardiovasc Pharmacol* 67 (3):237–245. <https://doi.org/10.1097/fjc.0000000000000339>
7. Zhang S, Meng T, Liu J, Zhang X, Zhang J (2015) Cardiac protective effects of dextrazoxane on animal cardiotoxicity model induced by anthracycline combined with trastuzumab is associated with upregulation of calpain-2. *Medicine* 94(4):e445. <https://doi.org/10.1097/md.0000000000000445>
8. Fernandez-Fernandez A, Carvajal DA, Lei T, McGoron AJ (2014) Chemotherapy-induced changes in cardiac capillary permeability measured by fluorescent multiple indicator dilution. *Ann Biomed Eng* 42 (12):2405–2415. <https://doi.org/10.1007/s10439-014-1110-9>
9. Salouge I, Ben Ali R, Ben Said D, Elkadri N, Kourda N, Lakhal M, Klouz A (2014) Means of evaluation and protection from doxorubicin-induced cardiotoxicity and hepatotoxicity in rats. *J Cancer Res Ther* 10 (2):274–278. <https://doi.org/10.4103/0973-1482.136557>

10. Hydock DS, Lien CY, Hayward R (2009) Anandamide preserves cardiac function and geometry in an acute doxorubicin cardiotoxicity rat model. *J Cardiovasc Pharmacol Ther* 14(1):59–67. <https://doi.org/10.1177/1074248408329449>
11. Hydock DS, Lien CY, Schneider CM, Hayward R (2008) Exercise preconditioning protects against doxorubicin-induced cardiac dysfunction. *Med Sci Sports Exerc* 40(5):808–817. <https://doi.org/10.1249/MSS.0b013e318163744a>
12. Hayward R, Hydock DS (2007) Doxorubicin cardiotoxicity in the rat: an in vivo characterization. *J Am Assoc Lab Anim Sci* 46(4):20–32
13. Panjrat GS, Patel V, Valdiviezo CI, Narula N, Narula J, Jain D (2007) Potentiation of Doxorubicin cardiotoxicity by iron loading in a rodent model. *J Am Coll Cardiol* 49(25):2457–2464. <https://doi.org/10.1016/j.jacc.2007.02.060>
14. Yurekli Y, Unak P, Ertay T, Biber Z, Medine I, Teksoz S (2005) Radiopharmaceutical model using ^{99m}Tc-MIBI to evaluate amifostine protection against doxorubicin cardiotoxicity in rats. *Ann Nucl Med* 19(3):197–200
15. Lim SC (2013) Interrelation between expression of ADAM 10 and MMP 9 and synthesis of peroxynitrite in doxorubicin induced cardiomyopathy. *Biomol Ther* 21(5):371–380. <https://doi.org/10.4062/biomolther.2013.034>
16. Oliveira MS, Melo MB, Carvalho JL, Melo IM, Lavor MS, Gomes DA, de Goes AM, Melo MM (2013) Doxorubicin cardiotoxicity and cardiac function improvement after stem cell therapy diagnosed by strain echocardiography. *J Cancer Sci Ther* 5(2):52–57. <https://doi.org/10.4172/1948-5956.1000184>
17. Hiona A, Lee AS, Nagendran J, Xie X, Connolly AJ, Robbins RC, Wu JC (2011) Pretreatment with angiotensin-converting enzyme inhibitor improves doxorubicin-induced cardiomyopathy via preservation of mitochondrial function. *J Thorac Cardiovasc Surg* 142(2):396–403. e393. <https://doi.org/10.1016/j.jtcvs.2010.07.097>
18. Lightfoot JC, D'Agostino RB Jr, Hamilton CA, Jordan J, Torti FM, Kock ND, Jordan J, Workman S, Hundley WG (2010) Novel approach to early detection of doxorubicin cardiotoxicity by gadolinium-enhanced cardiovascular magnetic resonance imaging in an experimental model. *Circ Cardiovasc Imaging* 3(5):550–558. <https://doi.org/10.1161/circimaging.109.918540>
19. Kenk M, Thackeray JT, Thorn SL, Dhami K, Chow BJ, Ascah KJ, DaSilva JN, Beanlands RS (2010) Alterations of pre- and postsynaptic noradrenergic signaling in a rat model of adriamycin-induced cardiotoxicity. *J Nucl Cardiol* 17(2):254–263. <https://doi.org/10.1007/s12350-009-9190-x>
20. Emanuelov AK, Shainberg A, Chepurko Y, Kaplan D, Sagie A, Porat E, Arad M, Hochhauser E (2010) Adenosine A3 receptor-mediated cardioprotection against doxorubicin-induced mitochondrial damage. *Biochem Pharmacol* 79(2):180–187. <https://doi.org/10.1016/j.bcp.2009.08.010>
21. Tatlidede E, Sehirli O, Velioglu-Ogunc A, Cetinel S, Yegen BC, Yarat A, Suleymanoglu S, Sener G (2009) Resveratrol treatment protects against doxorubicin-induced cardiotoxicity by alleviating oxidative damage. *Free Radic Res* 43(3):195–205. <https://doi.org/10.1080/10715760802673008>
22. Karagoz B, Suleymanoglu S, Uzun G, Bilgi O, Aydin S, Haholu A, Turken O, Onem Y, Kandemir EG (2008) Hyperbaric oxygen therapy does not potentiate doxorubicin-induced cardiotoxicity in rats. *Basic Clin Pharmacol Toxicol* 102(3):287–292. <https://doi.org/10.1111/j.1742-7843.2007.00196.x>
23. Anjos Ferreira AL, Russell RM, Rocha N, Plácido Ladeira MS, Favero Salvadori DM, Oliveira Nascimento MC, Matsui M, Carvalho FA, Tang G, Matsubara LS, Matsubara BB (2007) Effect of lycopene on doxorubicin-induced cardiotoxicity: an echocardiographic, histological and morphometrical assessment. *Basic Clin Pharmacol Toxicol* 101(1):16–24. <https://doi.org/10.1111/j.1742-7843.2007.00070.x>
24. Bennink RJ, van den Hoff MJ, van Hemert FJ, de Bruin KM, Spijkerboer AL, Vanderheyden JL, Steinmetz N, van Eck-Smit BL (2004) Annexin V imaging of acute doxorubicin cardiotoxicity (apoptosis) in rats. *J Nucl Med* 45(5):842–848
25. Koh E, Nakamura T, Takahashi H (2004) Troponin-T and brain natriuretic peptide as predictors for adriamycin-induced cardiomyopathy in rats. *Circ J* 68(2):163–167
26. Bertinchant JP, Polge A, Juan JM, Oliva-Lauraire MC, Giuliani I, Marty-Double C, Burdy JY, Fabbro-Peray P, Laprade M, Bali JP, Granier C, de la Coussaye JE, Dauzat M (2003) Evaluation of cardiac troponin I and T levels as markers of myocardial damage in doxorubicin-induced cardiomyopathy rats, and their relationship with echocardiographic and histological findings. *Clin Chim Acta* 329(1-2):39–51
27. Koh E, Ueda Y, Nakamura T, Kobayashi A, Katsuta S, Takahashi H (2002) Apoptosis in

- young rats with adriamycin-induced cardiomyopathy—comparison with pirarubicin, a new anthracycline derivative. *Pediatr Res* 51(2):256–259. <https://doi.org/10.1203/00006450-200202000-00021>
28. Kim YH, Park SM, Kim M, Kim SH, Lim SY, Ahn JC, Song WH, Shim WJ (2012) Cardio-protective effects of rosuvastatin and carvedilol on delayed cardiotoxicity of doxorubicin in rats. *Toxicol Mech Methods* 22(6):488–498. <https://doi.org/10.3109/15376516.2012.678406>
 29. Guenancia C, Li N, Hatchet O, Rigal E, Cottin Y, Dutartre P, Rochette L, Vergely C (2015) Paradoxically, iron overload does not potentiate doxorubicin-induced cardiotoxicity in vitro in cardiomyocytes and in vivo in mice. *Toxicol Appl Pharmacol* 284(2):152–162. <https://doi.org/10.1016/j.taap.2015.02.015>
 30. Sturgeon K, Schadler K, Muthukumaran G, Ding D, Bajulaie A, Thomas NJ, Ferrari V, Ryeom S, Libonati JR (2014) Concomitant low-dose doxorubicin treatment and exercise. *Am J Physiol Regul Integr Comp Physiol* 307(6):R685–R692. <https://doi.org/10.1152/ajpregu.00082.2014>
 31. Milano G, Raucci A, Scopuce A, Daniele R, Guerrini U, Sironi L, Cardinale D, Capogrossi MC, Pompilio G (2014) Doxorubicin and trastuzumab regimen induces biventricular failure in mice. *J Am Soc Echocardiogr* 27(5):568–579. <https://doi.org/10.1016/j.echo.2014.01.014>
 32. Walker JR, Sharma A, Lytwyn M, Bohonis S, Thliveris J, Singal PK, Jassal DS (2011) The cardioprotective role of probucol against anthracycline and trastuzumab-mediated cardiotoxicity. *J Am Soc Echocardiogr* 24(6):699–705. <https://doi.org/10.1016/j.echo.2011.01.018>
 33. Miyata S, Takemura G, Kosai K, Takahashi T, Esaki M, Li L, Kanamori H, Maruyama R, Goto K, Tsujimoto A, Takeyama T, Kawaguchi T, Ohno T, Nishigaki K, Fujiwara T, Fujiwara H, Minatoguchi S (2010) Anti-Fas gene therapy prevents doxorubicin-induced acute cardiotoxicity through mechanisms independent of apoptosis. *Am J Pathol* 176(2):687–698. <https://doi.org/10.2353/ajpath.2010.090222>
 34. Jassal DS, Han SY, Hans C, Sharma A, Fang T, Ahmadie R, Lytwyn M, Walker JR, Bhalla RS, Czarnecki A, Moussa T, Singal PK (2009) Utility of tissue Doppler and strain rate imaging in the early detection of trastuzumab and anthracycline mediated cardiomyopathy. *J Am Soc Echocardiogr* 22(4):418–424. <https://doi.org/10.1016/j.echo.2009.01.016>
 35. Daosukho C, Chen Y, Noel T, Sompot P, Nithipongvanitch R, Velez JM, Oberley TD, St Clair DK (2007) Phenylbutyrate, a histone deacetylase inhibitor, protects against Adriamycin-induced cardiac injury. *Free Radic Biol Med* 42(12):1818–1825. <https://doi.org/10.1016/j.freeradbiomed.2007.03.007>
 36. Li K, Sung RY, Huang WZ, Yang M, Pong NH, Lee SM, Chan WY, Zhao H, To MY, Fok TF, Li CK, Wong YO, Ng PC (2006) Thrombopoietin protects against in vitro and in vivo cardiotoxicity induced by doxorubicin. *Circulation* 113(18):2211–2220. <https://doi.org/10.1161/circulationaha.105.560250>
 37. Yi X, Bekererdjian R, DeFilippis NJ, Siddiquee Z, Fernandez E, Shohet RV (2006) Transcriptional analysis of doxorubicin-induced cardiotoxicity. *Am J Physiol Heart Circ Physiol* 290(3):H1098–H1102. <https://doi.org/10.1152/ajpheart.00832.2005>
 38. Shizukuda Y, Matoba S, Mian OY, Nguyen T, Hwang PM (2005) Targeted disruption of p53 attenuates doxorubicin-induced cardiac toxicity in mice. *Mol Cell Biochem* 273(1-2):25–32
 39. Liu FF, Stone JR, Schuldt AJ, Okoshi K, Okoshi MP, Nakayama M, Ho KK, Manning WJ, Marchionni MA, Lorell BH, Morgan JP, Yan X (2005) Heterozygous knockout of neuregulin-1 gene in mice exacerbates doxorubicin-induced heart failure. *Am J Physiol Heart Circ Physiol* 289(2):H660–H666. <https://doi.org/10.1152/ajpheart.00268.2005>
 40. Weinstein DM, Mihm MJ, Bauer JA (2000) Cardiac peroxynitrite formation and left ventricular dysfunction following doxorubicin treatment in mice. *J Pharmacol Exp Ther* 294(1):396–401
 41. Akolkar G, Bhullar N, Bews H, Shaikh B, Premecz S, Bordun KA, Cheung DY, Goyal V, Sharma AK, Garber P, Singal PK, Jassal DS (2015) The role of renin angiotensin system antagonists in the prevention of doxorubicin and trastuzumab induced cardiotoxicity. *Cardiovasc Ultrasound* 13:18. <https://doi.org/10.1186/s12947-015-0011-x>
 42. Su H, Gorodny N, Gomez LF, Gangadharmath U, Mu F, Chen G, Walsh JC, Szardenings K, Kolb HC, Tamarappoo B (2015) Noninvasive molecular imaging of apoptosis in a mouse model of anthracycline-induced cardiotoxicity. *Circ Cardiovasc Imaging* 8(2):e001952. <https://doi.org/10.1161/circimaging.114.001952>
 43. Dolinsky VW, Rogan KJ, Sung MM, Zordoky BN, Haykowsky MJ, Young ME, Jones LW, Dyck JR (2013) Both aerobic exercise and resveratrol supplementation attenuate

- doxorubicin-induced cardiac injury in mice. *Am J Physiol Endocrinol Metab* 305(2): E243–E253. <https://doi.org/10.1152/ajpendo.00044.2013>
44. Pramanik D, Campbell NR, Das S, Gupta S, Chenna V, Bisht S, Sysa-Shah P, Bedja D, Karikari C, Steenbergen C, Gabrielson KL, Maitra A, Maitra A (2012) A composite polymer nanoparticle overcomes multidrug resistance and ameliorates doxorubicin-associated cardiomyopathy. *Oncotarget* 3(6):640–650. <https://doi.org/10.18632/oncotarget.543>
45. Krishnamurthy K, Kanagasabai R, Druhan LJ, Ilangoan G (2012) Heat shock protein 25-enriched plasma transfusion preconditions the heart against doxorubicin-induced dilated cardiomyopathy in mice. *J Pharmacol Exp Ther* 341(3):829–839. <https://doi.org/10.1124/jpet.112.192245>
46. Maslov MY, Chacko VP, Hirsch GA, Akki A, Leppo MK, Steenbergen C, Weiss RG (2010) Reduced in vivo high-energy phosphates precede adriamycin-induced cardiac dysfunction. *Am J Physiol Heart Circ Physiol* 299(2): H332–H337. <https://doi.org/10.1152/ajpheart.00727.2009>
47. Deng S, Kruger A, Schmidt A, Metzger A, Yan T, Godtel-Armbrust U, Hasenfuss G, Brunner F, Wojnowski L (2009) Differential roles of nitric oxide synthase isozymes in cardiotoxicity and mortality following chronic doxorubicin treatment in mice. *Naunyn Schmiedebergs Arch Pharmacol* 380(1):25–34. <https://doi.org/10.1007/s00210-009-0407-y>
48. Niu J, Azfer A, Wang K, Wang X, Kolattukudy PE (2009) Cardiac-targeted expression of soluble fas attenuates doxorubicin-induced cardiotoxicity in mice. *J Pharmacol Exp Ther* 328(3):740–748. <https://doi.org/10.1124/jpet.108.146423>
49. Zhu W, Shou W, Payne RM, Caldwell R, Field LJ (2008) A mouse model for juvenile doxorubicin-induced cardiac dysfunction. *Pediatr Res* 64(5):488–494. <https://doi.org/10.1203/PDR.0b013e318184d732>
50. Lopez-Olmos V, Carreon-Torres E, Luna-Luna M, Flores-Castillo C, Martinez-Ramirez M, Bautista-Perez R, Franco M, Sandoval-Zarate J, Roldan FJ, Aranda-Frausto A, Soria-Castro E, Munoz-Vega M, Fragoso JM, Vargas-Alarcon G, Perez-Mendez O (2016) Increased HDL size and enhanced Apo A-I catabolic rates are associated with doxorubicin-induced proteinuria in New Zealand white rabbits. *Lipids* 51(3):311–320. <https://doi.org/10.1007/s11745-016-4120-6>
51. Lai R, Long Y, Li Q, Zhang X, Rong T (2011) Oxidative stress markers may not be early markers of doxorubicin-induced cardiotoxicity in rabbits. *Exp Ther Med* 2(5):947–950. <https://doi.org/10.3892/etm.2011.306>
52. Lai RC, Wang XD, Zhang X, Lin WQ, Rong TH (2012) Heart fatty acid-binding protein may not be an early biomarker for anthracycline-induced cardiotoxicity in rabbits. *Med Oncol* 29(3):2303–2308. <https://doi.org/10.1007/s12032-011-9843-x>
53. Barcin C, Kursaklioglu H, Safali M, Iyisoy A, Kose SB, Barindik N, Isik E (2005) Effect of octreotide in the prevention of doxorubicin cardiotoxicity. *Anadolu Kardiyol Derg* 5(1):18–23
54. Gambliel HA, Burke BE, Cusack BJ, Walsh GM, Zhang YL, Mushlin PS, Olson RD (2002) Doxorubicin and C-13 deoxydoxorubicin effects on ryanodine receptor gene expression. *Biochem Biophys Res Commun* 291(3):433–438. <https://doi.org/10.1006/bbrc.2002.6380>
55. Teichholz LE, Kreulen T, Herman MV, Gorlin R (1976) Problems in echocardiographic volume determinations: echocardiographic-angiographic correlations in the presence of absence of asynergy. *Am J Cardiol* 37(1):7–11
56. Cardinale D, Colombo A, Torrisi R, Sandri MT, Civelli M, Salvatici M, Lamantia G, Colombo N, Cortinovis S, Dessanai MA, Nole F, Veglia F, Cipolla CM (2010) Trastuzumab-induced cardiotoxicity: clinical and prognostic implications of troponin I evaluation. *J Clin Oncol Off J Am Soc Clin Oncol* 28(25):3910–3916. <https://doi.org/10.1200/jco.2009.27.3615>
57. Cardinale D, Sandri MT, Colombo A, Colombo N, Boeri M, Lamantia G, Civelli M, Peccatori F, Martinelli G, Fiorentini C, Cipolla CM (2004) Prognostic value of troponin I in cardiac risk stratification of cancer patients undergoing high-dose chemotherapy. *Circulation* 109(22):2749–2754. <https://doi.org/10.1161/01.cir.0000130926.51766.cc>
58. Sawaya H, Sebag IA, Plana JC, Januzzi JL, Ky B, Tan TC, Cohen V, Banchs J, Carver JR, Wiegers SE, Martin RP, Picard MH, Gerszten RE, Halpern EF, Passeri J, Kuter I, Scherrer-Crosbie M (2012) Assessment of echocardiography and biomarkers for the extended prediction of cardiotoxicity in patients treated with anthracyclines, taxanes, and trastuzumab. *Circ Cardiovasc Imaging* 5(5):596–603. <https://doi.org/10.1161/circimaging.112.973321>
59. Billingham ME, Mason JW, Bristow MR, Daniels JR (1978) Anthracycline

- cardiomyopathy monitored by morphologic changes. *Cancer Treat Rep* 62(6):865–872
60. Cove-Smith L, Woodhouse N, Hargreaves A, Kirk J, Smith S, Price SA, Galvin M, Betts CJ, Brocklehurst S, Backen A, Radford J, Linton K, Roberts RA, Schmitt M, Dive C, Tugwood JD, Hockings PD, Mellor HR (2014) An integrated characterization of serological, pathological, and functional events in doxorubicin-induced cardiotoxicity. *Toxicol Sci* 140(1):3–15. <https://doi.org/10.1093/toxsci/kfu057>
61. Friedman MA, Bozdech MJ, Billingham ME, Rider AK (1978) Doxorubicin cardiotoxicity. Serial endomyocardial biopsies and systolic time intervals. *JAMA* 240(15):1603–1606
62. Mackay B, Ewer MS, Carrasco CH, Benjamin RS (1994) Assessment of anthracycline cardiomyopathy by endomyocardial biopsy. *Ultrastruct Pathol* 18(1-2):203–211



Chapter 18

Pulmonary Artery Hypertension Model in Rats by Monocrotaline Administration

Carlos Bueno-Beti, Yassine Sassi, Roger J. Hajjar, and Lahouaria Hadri

Abstract

Pulmonary arterial hypertension (PAH) is a syndrome characterized by pulmonary vascular remodeling and vasoconstriction, leading to increased pulmonary vascular resistance, right ventricular pressure overload and, eventually, to right ventricular failure and premature death. Animal models have been an essential tool for understanding pulmonary hypertension pathophysiology and for the discovery and development of novel therapies.

MCT-induced PAH in rats leads to a significant increase in RV pressure and pulmonary vascular remodeling, as well as greater RV hypertrophy. In this chapter, we describe protocols for inducing and assessing the monocrotaline (MCT) rat model, the most classical and widely used *in vivo* model of PAH. Using this protocol, rats reproducibly develop pulmonary hypertension with a mean pulmonary pressure of ~40 mmHg approximately 4 weeks after single MCT administration.

Key words Pulmonary artery hypertension, Monocrotaline, Experimental model, Right ventricle hypertrophy, Right ventricle failure, Pulmonary vascular remodeling

1 Introduction

Pulmonary arterial hypertension (PAH) is characterized by various degrees of pulmonary arterial vessel remodeling leading to increased mean pulmonary artery pressure and pulmonary vascular resistance, right ventricular (RV) afterload and hypertrophy, and eventually to RV failure. Elucidating the pathobiology of PAH continues to be critical to design new effective therapeutic strategies, and appropriate animal models of PAH are necessary to achieve the task.

Monocrotaline (MCT)-induced PAH rat model has helped the scientific community to gain insight into the vascular remodeling process and its pathophysiology [1]. The advantages of MCT model are its technical simplicity, reproducibility, and relatively low cost.

MCT is a pyrrolizidine alkaloid derived from the plant *Crotalaria spectabilis* used to induce PAH in rats with a single subcutaneous injection. The MCT alkaloid is activated to the reactive pyrrole metabolite dehydromonocrotaline (MCTP) in the liver, a reaction that is highly dependent on cytochrome P-450 [2, 3]. When administered to rats, MCT recapitulates many features of human PAH, including induction of endothelial cell apoptosis within 4-days post-injection [4]. MCT causes endothelial cell damage by mechanisms that include disruption of intracellular membrane trafficking [5], disruption of endothelial nitric synthase and deregulation of nitric oxide signaling, leading to lung vascular changes [6], dysregulation of bone morphogenetic protein receptor II (BMPR II) and downstream Smad signaling [7], as well as oxidative stress response and apoptosis [8]. MCT also leads to pulmonary arterial medial hypertrophy and obstructive pulmonary vascular remodeling characterized by narrowing/obliteration of the vascular lumen due to the proliferation of pulmonary arterial smooth muscle cells (PASMCs), and resistance of PASMCs to apoptosis [9, 10]. It is also notable that the development of pulmonary hypertension occurs with delayed kinetics following a single exposure to MCT: PAH typically occurs 3–4 weeks after MCT challenge, yet MCT and MCTP are metabolized rapidly and cleared from the circulation [11]. The phenotype may result from delayed effects of endothelial injury versus persistent effects of MCT that has accumulated in erythrocytes, where it conserves its capability to interact with lung tissue.

Here we present detailed protocols for inducing PAH in rats by a single injection of MCT and functional and histological characterization of established PAH in this model.

2 Materials

2.1 Animals

1. 200–250 g male Sprague-Dawley Rats.
2. Rodent chow.
3. Rodent cages.
4. Rodent bedding.

2.2 PH Induction

1. Sterile 1-mL syringes.
2. 25G x 5/8" needles.
3. Monocrotaline (MCT) (Sigma-Aldrich).
4. 1N HCl solution.
5. pH meter.
6. 10N NaOH solution.

7. Dulbecco's phosphate buffered saline (DPBS, pH 7.4), sterile-filtered.
8. Analytical balance.

2.3 Functional PH

Characterization

1. Plexiglass induction chamber with lid.
2. Ventilator system and O₂ tank.
3. Isoflurane.
4. Heating pad.
5. Adhesive tape.
6. Dual goose-neck fiber-optic illuminator.
7. 16 G catheter.
8. Surgical silk.
9. Cotton swabs.
10. 25 G × 5/8" needles.
11. Gauze pads (2" × 2").
12. Surgical tools: small vessel cauterizer, Mayo scissors, blunt-nosed thumb forceps, Jansen retractor.
13. Pressure-volume control unit.
14. PV data acquisition and analysis software.
15. Rat 1.9F pressure-volume catheter.

2.4 Histological PH

Characterization

1. 50% O.C.T.: O.C.T. compound, PBS (1:1).
2. Disposable embedding molds.
3. Dry ice.
4. Cryostat.
5. Glass microscope slides.
6. Hematoxylin.
7. Eosin.
8. Ethanol.
9. Xylene.
10. Goat serum.
11. Primary antibodies.
12. Secondary antibody-fluorochrome conjugates.
13. 4,6-diamidino-2-phenylindole, dihydrochloride (DAPI).
14. Mounting medium.
15. Coverslips.
16. Bright light and confocal microscope.

3 Methods

3.1 Animals

- Let the animals to acclimate to the new environmental conditions of 12-h light–dark cycle at 18–20 °C and 40–50% humidity for a minimum of 24 h after reception from the commercial supplier (*see Note 1*).
- Randomly assign the animals to the control group (Control) or monocrotaline-treated group (MCT) and keep a record of their weights weekly from the beginning of the treatment.

3.2 PAH Induction

- Calculate the amount of MCT for injecting the animals at 60 mg/Kg. Completely dissolve MCT salt in 1–3 mL 1N HCl. Adjust pH to 7.4 with NaOH 10N. Add filtered-sterile PBS to prepare 20 mg/mL MCT solution (*see Note 2*).
- Inject the rats subcutaneously with MCT (60 mg/kg) in the ventral thorax (Fig. 1; *see Note 3*).
- Maintain the animals at 12-h light–dark cycle at 18–20 °C and 40–50% for 4 weeks and weigh them once a week to assess disease development (*see Note 4*).

3.3 Functional PH Characterization

- Place the tip of the 1.9F PV catheter in saline solution for 30 min. Turn on the pressure–volume control unit and run the data acquisition software.
- Preanesthetize the animals with 3–4% isoflurane mix with oxygen (0.5 L/min) in a Plexiglass induction chamber with a lid.
- Prepare the animal for the surgical procedure by shaving the chest and neck with a hair clipper. Keep the animal on a heating pad all the time.
- Place the animal on a platform with the neck next to one of the edges. Place the animal's head and neck straight by attaching a suture thread to its upper incisors and fix it to the platform with a tape. Secure the animal to the platform with tapes in the supine position. Then clean the surgical sites with alcohol.

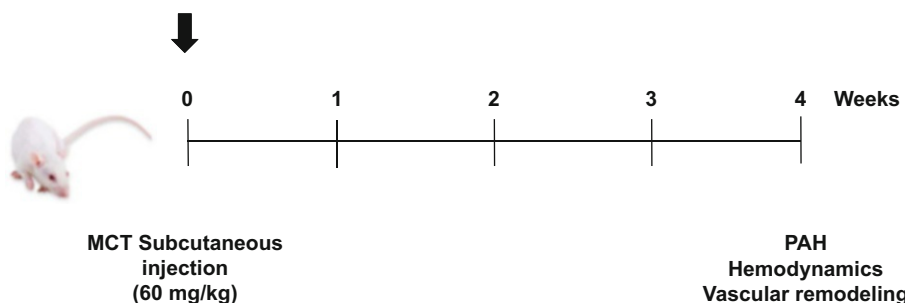
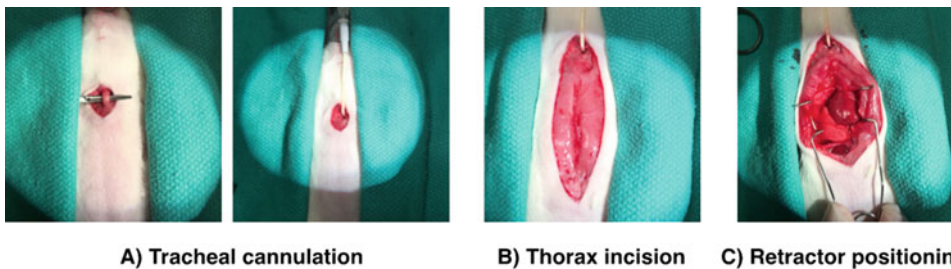


Fig. 1 Pulmonary arterial hypertension development. Experimental design for PAH development and characterization



A) Tracheal cannulation B) Thorax incision C) Retractor positioning

Fig. 2 Surgical procedure. Open chest procedure images. (a) Tracheal cannulation. Rats are intubated with 16G cannula and connected to a mechanical ventilator. (b) Thorax incision. A longitudinal incision is performed to expose the rib cage. (c) Sternotomy and retractor positioning. Open chest approach is achieved by medial sternotomy. A retractor is used to keep the chest open

5. Make a 2 cm incision in the midline neck region and visualize the trachea by blunt dissection. Place a surgical silk underneath the trachea and make a small incision cranial to the suture (Fig. 2a).
6. Insert the 16G catheter into the trachea and use the surgical silk to secure the cannula during the procedure (*see Note 5*).
7. Set the ventilator system to a respiration rate of 73 cycles per minute and a tidal volume of 1.84 mL and connect the ventilator system to the cannula through a modified Y-shape connector. Maintain the rat on a mixture of 100% oxygen with 2% isoflurane throughout the procedure.
8. Calibrate the PV catheter with saline solution at body temperature (*see Note 6*).
9. For the open-chest approach, make an incision above the xiphoid process throughout the sternum and separate the skin from the underlying tissue (Fig. 2b).
10. Cut across the sternum (sternotomy) and completely expose the chest cavity. Place the Jansen retractor to keep the chest open (Fig. 2c; *see Note 7*).
11. With a 25G × 5/8", stab the RV in the apex area and insert the 1.9F PV catheter through the hole until the most proximal electrode in the PV catheter is completely surrounded by cardiac tissue (*see Note 8*).
12. For mean pulmonary arterial pressure (mPAP) measurement move the inserted PV catheter in the RV upward to the Pulmonary Artery (PA) until the pressure waveform changes. Let the catheter to stabilize in the new position for 3 min, stop the ventilator system and start recording pulmonary artery diastolic and systolic pressures (PADP and PASP respectively) (*see Note 9*).
13. Record 3–6 values for each of the parameters (RVSP, PADP, and PASP) per rat using data acquisition software (Fig. 3b, c).

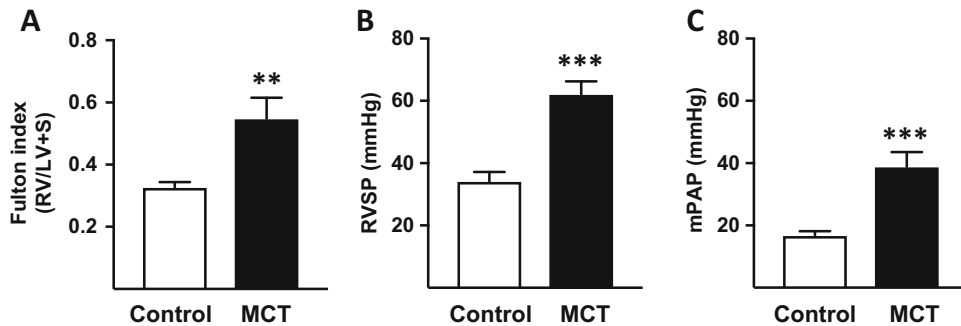


Fig. 3 Functional PAH characterization. Fulton Index (a), right ventricle systolic pressure (RVSP) (b) and mean pulmonary artery pressure (mPAP) (c) were measured in saline injected (Control) and MCT-treated animals after 4 weeks of MCT administration. ** $P < 0.01$ and *** $P < 0.001$ versus Control by Student's *t*-Test; $n = 5$ per group. MCT = Monocrotaline

3.4 Histological PH Characterization

1. Remove the right atria and perfuse the animal with 10 mL of PBS from the left ventricle to remove blood for the systemic circulation; then, remove the left atria and perfuse 10 mL of PBS from the RV to remove remaining blood out from the lungs.
2. Remove the lungs and the heart from the animal's body and dissect the RV from the LV and the septum. Record both weights and calculate the Fulton Index, a measure of heart hypertrophy, as $RV/LV + Septum$ (Fig. 3a).
3. Insufflate the lungs with 50% O.C.T. (*see Note 10*).
4. Prefill disposable embedding molds with O.C.T. and snap-freeze it on dry ice. Keep the samples at -80°C .
5. Prepare 8–10 μm sections with a cryostat and mount them on poly-L-lysine-treated slides (*see Note 11*).
6. Fix the slides with 4% PFA for 10 min.
7. Stain lung sections with Hematoxylin and Eosin for morphometric analysis and assessment of medial thickness (Fig. 4a)
8. For Immunohistochemistry, after fixing the sections, block them in 10% goat serum in DAKO antibody diluent solution for 1 h.
9. Wash the sections twice with PBS for 5 min.
10. Prepare the desired primary antibody mix in 1.5% goat serum in DAKO antibody diluent solution and incubate the sections overnight at 4°C .
11. Wash the sections twice with PBS for 5 min.
12. Add secondary antibody-fluorochrome conjugates in 1.5% goat serum in DAKO antibody diluent solution and incubate for 1 h at 37°C .

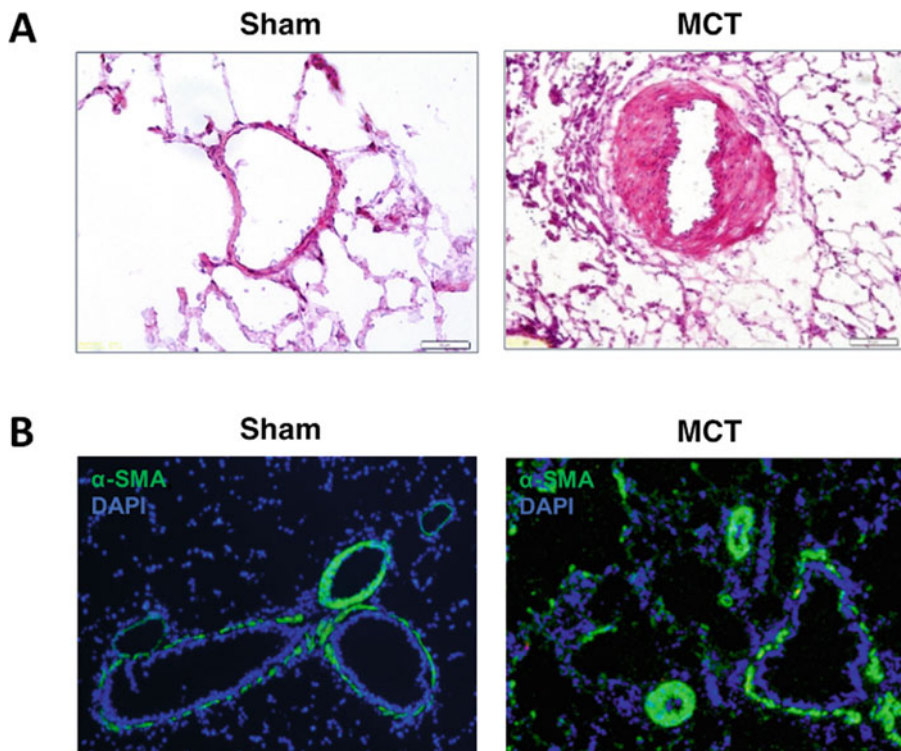


Fig. 4 Histological characterization of the PAH. **(a)** Hematoxylin and eosin staining. Hematoxylin and Eosin staining was performed in lung sections to determine blood vessel medial thickness. An increase in the medial thickness is observed in small arteries of monocrotaline-treated rats (MCT group) when compared to non-treated animals (Sham group). **(b)** Immunohistochemistry. Lung sections were incubated with α-smooth muscle actin (α-SMA; green) antibody and counterstained with 4',6-diamidino-2-phenylindole, dihydrochloride (DAPI; blue). Immunostaining revealed that blood vessel thickening in the MCT group is due to neointima formation, mainly composed of smooth muscle cells

13. Wash the sections twice with PBS for 5 min.
14. Counterstain the sections with DAPI solution
15. Rinse the sections once with PBS.
16. Mount the slides with mounting media and coverslips.
17. Take images of the mounted slides with a confocal microscope (Fig. 4b).

4 Notes

1. Animal treatments and surgical procedures were approved by the Icahn School of Medicine at Mount Sinai Institutional Animal Care and Use Committee and performed in accordance with the National Institutes of Health Guide for the Care and Use of Laboratory Animals.

2. Complete dissolution of MCT salt is critical for proper PAH induction and cytotoxicity reduction. Make sure that MCT is fully dissolved in HCl 1N and that no precipitate is formed during pH adjustment or PBS dilution.
3. For rats weighing 250–300 g, 1 mL of 20 mg/mL MCT solution per animal is injected. To avoid lesions due to MCT injection site cytotoxicity we strongly recommend administering MCT solution in at least three different areas.
4. During disease induction, check on animals daily for signals of distress like piloerection and difficulty in breathing. Body weight loss is a disease development indicator, as animals treated with MCT usually start losing weight 3 weeks after MCT administration.
5. To provide the correct amount of anesthetic and maintain the animal's normal breathing a proper intubation is required. Insufflate air to the lungs and check for an increase in the chest volume. If the cannula is not well positioned, and no increase in chest volume is observed, repeat the intubation procedure again. Instead, rats can be intubated without tracheal incision by orally inserting the 16G catheter.
6. Hold the tip of the PV catheter just under the surface of the saline solution for zero value. For higher pressure values immerse the catheter in the saline solution, the pressure should increase 0.75 mmHg per depth centimeter.
7. A sternotomy is an invasive procedure that can cause a significant amount of bleeding. Sternotomy must be performed throughout medial sternum preventing the disruption of blood vessels. If any vessel is damaged during the sternotomy, bleeding can be stopped by cauterizing the area. Note that any important blood loss may interfere with the hemodynamic parameters intended to be measured in this protocol for PH characterization.
8. Proper PV catheter positioning and stabilization is critical for acquiring good quality pressure data. After inserting the PV catheter, let it stabilize for 5 min. If the signal is distorted, replace the PV catheter to a more central position in the RV until the signal is stable. Stop the ventilator system for a few seconds during data recording.
9. Alternatively, if PA catheterization cannot be achieved through the apical stab wound, another stab can be performed in the central area of the RV, closer to the PA. mPAP is calculated from the following equation: $2/3 \text{ PADP} + 1/3 \text{ PASP}$. Values of mPAP higher than 25 mmHg at rest are the clinical definition of PH.

10. Perfusion with 50% O.C.T. in PBS is required to preserve the morphology and structure of the lungs for histological studies. Distribute 50% O.C.T. in PBS solution through all tissue evenly by using 1-mL syringes and 27G needles. You should observe an increase in the volume of the lungs.
11. After cutting the sections, let them dry for 30 min at room temperature. Then, cut sections can be stored at -80 °C for several months.

Acknowledgments

This work was supported by grants from the National Institutes of Health R01HL133554 to L.H., from the American Heart Association (AHA-17SDG33370112) to Y.S., and from the R01 HL117505, HL 119046, HL129814, 128072, HL131404, R01HL135093, a P50 HL112324, and two Transatlantic Foundation Leducq grants (R.J.H.). We would like to acknowledge the Gene Therapy Resource Program (GTRP) of the National Heart, Lung, and Blood Institute, National Institutes of Health.

References

1. Stenmark KR, Meyrick B, Galiè N et al (2009) Animal models of pulmonary arterial hypertension: the hope for etiological discovery and pharmacological cure. *Am J Physiol Lung Cell Mol Physiol* 297:L1013–L1032
2. Reid MJ, Lamé MW, Morin D et al (1998) Involvement of cytochrome P450 3A in the metabolism and covalent binding of ¹⁴C-monocrotaline in rat liver microsomes. *J Biochem Mol Toxicol* 12:157–166
3. Wilson DW, Segall HJ, Pan LC et al (1992) Mechanisms and pathology of monocrotaline pulmonary toxicity. *Crit Rev Toxicol* 22:307–325
4. Thomas HC, Lamé MW, Dunston SK et al (1998) Monocrotaline pyrrole induces apoptosis in pulmonary artery endothelial cells. *Toxicol Appl Pharmacol* 151:236–244
5. Sehgal PB, Mukhopadhyay S (2007) Dysfunctional intracellular trafficking in the pathobiology of pulmonary arterial hypertension. *Am J Respir Cell Mol Biol* 37:31–37
6. Huang J, Wolk JH, Gewitz MH et al (2010) Progressive endothelial cell damage in an inflammatory model of pulmonary hypertension. *Exp Lung Res* 36:57–66
7. Ramos M, Lamé MW, Segall HJ et al (2007) Monocrotaline pyrrole induces Smad nuclear accumulation and altered signaling expression in human pulmonary arterial endothelial cells. *Vasc Pharmacol* 46:439–448
8. Nakayama Wong LS, Lamé MW, Jones AD et al (2010) Differential cellular responses to protein adducts of naphthoquinone and monocrotaline pyrrole. *Chem Res Toxicol* 23:1504–1513
9. Kolettis T, Vlahos AP, Louka M et al (2007) Characterisation of a rat model of pulmonary arterial hypertension. *Hellenic J Cardiol* 48:206–210
10. Chesney CF, Allen JR (1973) Animal model: pulmonary hypertension, cor pulmonale and endocardial fibroelastosis in monocrotaline-intoxicated nonhuman primates. *Am J Pathol* 70:489–492
11. Estep JE, Lamé MW, Morin D et al (1991) [¹⁴C]monocrotaline kinetics and metabolism in the rat. *Drug Metab Dispos* 19:135–139



Chapter 19

The Sugen 5416/Hypoxia Mouse Model of Pulmonary Arterial Hypertension

Carlos Bueno-Beti, Lahouaria Hadri, Roger J. Hajjar, and Yassine Sassi

Abstract

Pulmonary hypertension is a rapidly progressive, life-threatening, and often fatal disease. Despite many new developments in pulmonary arterial hypertension (PAH) therapy, there is currently no cure for PAH, and new therapies are desperately needed. PAH pathobiology involves a remodeling process in pulmonary arteries that plays a critical role in elevating pulmonary arterial and right ventricle pressures. The discovery and development of new therapies requires animal models of PAH that mimic the human disease, including vascular remodeling.

Here we review and describe a detailed protocol for creating an *in vivo* model of Sugen/Hypoxia-induced PAH in mice that is commonly used to assess the efficiency of new therapies in PAH. Severe pulmonary hypertension can be established in 1 month using this protocol. Additional protocols to evaluate the model by invasive pressure measurements and histology are provided.

Key words Sugen 5416, Hypoxia, Pulmonary arterial hypertension model, Pulmonary vascular remodeling, Right ventricular hypertrophy

1 Introduction

Pulmonary arterial hypertension (PAH) is defined by the hemodynamic criteria of resting mean pulmonary artery pressure greater than 25 mmHg as assessed by right heart catheterization [1]. PAH is a cardiopulmonary disorder characterized by progressive vascular remodeling of the distal pulmonary arteries which results in elevated pulmonary arterial pressure, leading to right ventricle (RV) overload and ultimately death due to RV failure [2–4]. Vascular remodeling in PAH is the result of endothelial dysfunction, pathological proliferation and migration of smooth muscle cells, inflammation, and thrombosis [5–8].

Current therapies that target pathways involved in PAH disease pathogenesis improved quality of life and clinical outcomes in patients with PAH [7]; however, currently there is no cure for PAH. New therapeutic approaches that reverse pulmonary vascular

remodeling during pulmonary hypertension (PH) are being actively explored.

To investigate the efficiency of new treatments in PAH, pre-clinical models that recapitulate key pathophysiological features of the human disease are required. Characteristic features of the remodeled vasculature in patients with pulmonary hypertension include neointima hyperplasia, small pulmonary arterial medial and adventitial thickening, complex plexiform lesion formation, and capillary occlusion [9–11].

In contrast to the human disease, rodent models of PAH, such as monocrotaline (MCT) treatment in rats, lack remodeling processes and plexiform lesions relevant to the pathogenesis of human PAH [12–14]. A new murine model of PAH described in this protocol, although it does not completely replicate severe human PAH, displays many of the hallmarks of the human disease [15–17]. Combination of Sugen 5416 (SU5416, a vascular endothelial growth factor inhibitor) and exposure to chronic hypoxia has been proven to cause severe PAH with angio-obliterative lesions that are comparable to the plexiform lesions of PAH patients [18, 19].

Here we describe the method for inducing PAH in mice by combining chronic hypoxia and weekly Sugen 5416 injection, followed by measurement of hemodynamic parameters and histological PAH characterization. Severe pulmonary hypertension can be established in 1 month using this protocol.

2 Materials

2.1 Animals

1. Male C57BL/6 mice.
2. Rodent chow.
3. Water bottles.
4. Rodent cages.
5. Rodent bedding.

2.2 PH Induction

1. Semisealable hypoxia chamber (BioSpherix).
2. N₂ tank.
3. Oxygen controller ProOx 360 (BioSpherix).
4. Analytical balance.
5. Sugen 5416 (Cayman Chemical).
6. Dimethyl sulfoxide (DMSO).
7. Phosphate Buffered Saline (PBS).
8. Sterile 1-mL syringes.
9. 25G × 5/8" needles.

2.3 Functional PH Characterization

1. Anesthesia jar with lid.
2. Isoflurane.
3. Heating pad.
4. Adhesive tape.
5. Sterile suture packs.
6. 22G polyethylene catheter.
7. Mechanical ventilator/respirator system and O₂ tank.
8. Cotton swabs.
9. 25G × 5/8" needles.
10. Surgical tools: small vessel cauterizer, blunt scissors, blunted nosed thumb forceps, elastic hook retractors.
11. Pressure–volume (PV) control unit.
12. PV data acquisition and analysis software.
13. Mouse 1.2F PV catheter.

2.4 Histological PAH Characterization

1. 50% O.C.T./PBS: O.C.T. compound, PBS.
2. Disposable embedding molds.
3. Dry ice.
4. Cryostat.
5. Glass microscope slides, poly-L-lysine treated.
6. 4% paraformaldehyde (PFA) solution.
7. Hematoxylin.
8. Eosin.
9. Goat serum.
10. Primary antibodies.
11. Secondary antibody–fluorochrome conjugates.
12. 4,6-diamidino-2-phenylindole, dihydrochloride (DAPI).
13. Mounting medium.
14. Coverslips.
15. Bright light and confocal microscope.

3 Methods

3.1 Animals

1. Upon reception, house the animals socially (groups of five animals per cage) in ventilated rodent cages provided with appropriate bedding, rodent chow and water (*see Note 1*). Let them acclimate to the new environment (12-h light/dark cycle at 18–20 °C and 40–50% humidity) for at least 3 days.

2. Weigh the animals and, randomly assign them to each treatment group: Normoxia (Nox), hypoxia (Hy) or hypoxia + Sugen 5416 (SU) (HySU). Monitor the body weight, food and water consumption every other day.

3.2 PH Induction

1. Weigh the animals and prepare the SU for injection. Dissolve crystalline SU in DMSO to a concentration of 20 mg/mL. Then, dilute SU solution with PBS 1:3 (DMSO:PBS). Adjust pH to 7.2 (*see Note 2*).
2. Using 1-mL syringe with a 25G × 5/8" needles, inject HySU animals with SU at 20 mg/Kg subcutaneously in the abdominal area once a week during three consecutive weeks. Inject Nox and Hy animals with vehicle alone (Fig. 1).
3. Set the semisealable hypoxia chamber, the oxygen controller ProOx 360 and the N₂ tank as indicated in Fig. 2a and b. Establish a set-point of 10% O₂ in the ProOx 360 and let the system to reach the steady state (*see Note 3*).
4. Keep animals from Hy and HySU groups in normobaric hypoxia (10% O₂) for 3 weeks. After 3 weeks in hypoxia, place Hy and HySU animals under normoxic (21% O₂) conditions for one more week (*see Note 4*). The chambers can be opened every 3 days for 30 min to clean the cages and replenish food and water supplies.
5. Maintain normoxia animals in a semisealable chamber in 21% O₂ for 4 weeks.
6. During the hypoxia exposure time, inspect the animals daily looking for distress signals such as piloerection, loss of weight, and difficulty in breathing (*see Note 5*). Euthanasia should be performed if the animal is unable to eat or ambulate without significant and prompt improvement and without ability to correct the distress.

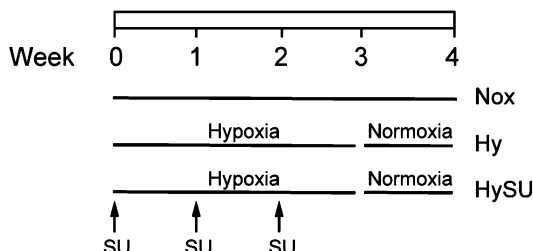


Fig. 1 Experimental design. Schematic representation of the treatment and oxygen level exposure for all animal groups during PH induction. *Nox* Normoxia, *Hy* Hypoxia, *HySU* Hypoxia + Sugen 5416, *SU* Sugen 5416

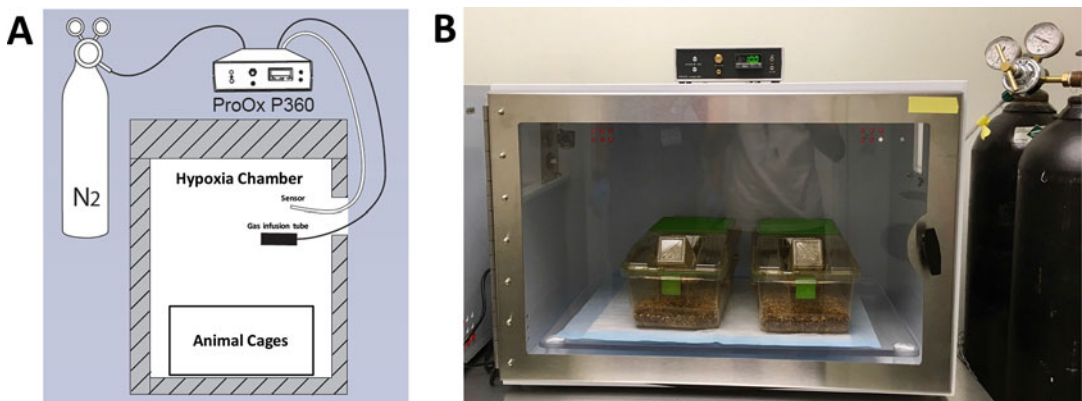


Fig. 2 Experimental setting for PH induction. (a) Schematic representation of the hypoxia system. Device display as indicated by BioSpherix Research Tools company. ProOx P360 detects variations in O₂ concentration and corrects them by infusing control gas through the gas infusion tube. (b) Picture of the BioSpherix system. The system installed in our laboratory is able to accommodate up to six cages per hypoxia chamber at once

3.3 Functional PH Characterization

1. Record weight and health status of each mouse prior to preanesthesia.
2. Preanesthetize mouse with 3–4% isoflurane in an anesthesia jar (0.20 mL of Isoflurane in 1 L jar). Verify appropriate anesthesia by applying noxious stimulus (i.e., tail pinch). Shave the animal's chest and neck with a hair clipper.
3. Situate mouse's neck up straight by attaching suture thread to the mouse's upper incisors and fix it to the heating pad. Secure the animal in supine position with the upper and lower extremities attached to the heating pad with tapes.
4. Clean surgical sites (neck and thorax) with alcohol.
5. With the mouse head pointing the operator, make an incision of 1 cm in the medial cervical skin. Separate the thyroid gland lobes and expose the trachea.
6. Carefully, pull out the tongue with atraumatic forceps and move it upwards. Transorally, intubate the animal with a 22-gauge polyethylene catheter. Through the neck incision, check that the catheter is properly placed inside the trachea (*see Note 6*).
7. Connect the catheter to a mechanical ventilator through a modified Y-shape connector and maintain the mouse on 2% isoflurane through all the surgical procedure. Ventilate with tidal volume of 0.12 mL, with 148 ventilation cycles per minute.
8. Before starting the surgery place the tip of the 1.2F PV catheter in PBS for 30 min. Turn on the pressure-volume control unit and initiate data acquisition software.

9. Calibrate the catheter with PBS at body temperature (*see Note 7*).
10. Make skin incision in the lower thorax area. Separate the skin from the chest wall and open the abdominal wall next to the sternal manubrium (*see Note 8*). Use elastic hook retractors to hold the rib cage in place.
11. Cut the diaphragm and expose the heart. Clean the area with cotton swabs and open the pericardium.
12. Stab apically the right ventricle (RV) with a 25G × 5/8" needle attached to a cotton swab. Remove the needle from the RV and insert the 1.2F PV catheter with the help of blunt-nosed thumb forceps through the stab hole towards the pulmonary artery direction. Make sure that the distal electrode of the catheter is fully surrounded by RV muscle (*see Note 9*).
13. Record all the data and take at least five values for the right ventricle systolic pressure (RVSP) per mouse and average (Fig. 3a). Carefully, remove the PV catheter from the RV and place it in PBS solution (*see Note 10*).
14. Once the pressure is recorded, perfuse the animal with 5 mL of PBS from the left ventricle (LV) to remove blood from the systemic circulation (*see Note 11*).
15. Isolate the heart and remove both atria. Carefully, dissect out the RV from the LV and the septum and weigh them. Right ventricular hypertrophy is assessed using the Fulton Index (calculated as RV weight/LV+Septum weight; Fig. 3b). As shown in Fig. 3, VEGFR inhibition exacerbates chronic hypoxia-induced RV pressure and hypertrophy.

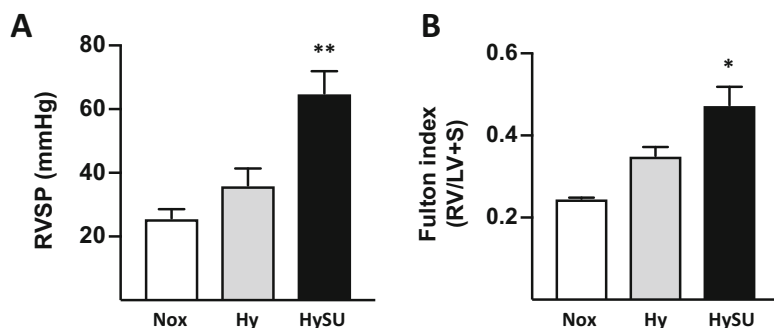


Fig. 3 Functional PH characterization. After 3 weeks of exposure to chronic hypoxia or chronic hypoxia + Sugen 5416 followed by 1 week in normoxia, right ventricular systolic pressure (a) and Fulton index (b) were determined and compared to control animals exposed to normoxia for 4 weeks. * $P < 0.05$ and ** $P < 0.01$ versus Hy using one-way ANOVA and Bonferroni's post hoc test; $n = 5$ per group. Nox Normoxia control group, Hy Hypoxia group, HySU Hypoxia + Sugen 5416 group

3.4 Histological PAH Characterization

1. Isolate the lung from the rest of the organs and tissues.
2. Prepare a solution of 50% O.C.T./PBS and insufflate the lungs (*see Note 12*).
3. Place the lung on disposable embedding molds pre-filled with O.C.T. and snap-freeze it on dry ice. Keep the samples at -80 °C after they are frozen.
4. Cut the lungs in 8 µm sections with a cryostat (*see Note 13*) and mount on poly-L-lysine-treated slides. Air-dry the sections at room temperature for 30 min.
5. Fix the slides with 4% PFA for 10 min.
6. For morphometric analysis and assessment of medial thickness of the lungs, perform hematoxylin and eosin staining (Fig. 4).
7. For Immunohistochemistry, after fixing the sections block them in 10% goat serum in Dako solution for 1 h. The alpha-smooth muscle actin (α -SMA) antibody can be for example used for confirming the medial hypertrophy.
8. Rinse the sections three times in PBS for 5 min each.
9. Dilute the primary antibody in 1.5% goat serum in Dako solution and incubate the sections in a humid chamber overnight at 4 °C.
10. Rinse the sections three times in PBS for 5 min each.
11. Add the secondary antibody-fluorochrome conjugates in 1% goat serum in Dako solution and incubate for 45–60 min in a humid chamber at 37 °C.
12. Rinse the sections three times in PBS for 5 min each.
13. Incubate the sections with DAPI solution for 5 min.
14. Rinse the sections once in PBS.

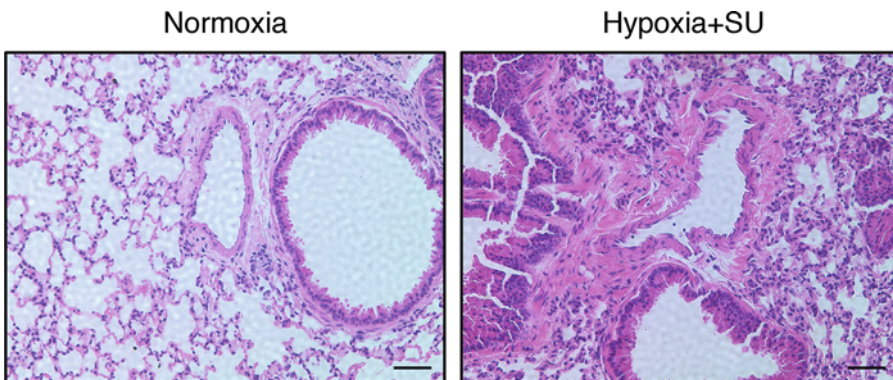


Fig. 4 Histological PH characterization. Representative lung sections stained with Hematoxylin/eosin of the indicated treatment group. Lung sections were stained for morphometric analysis and assessment of medial thickness. Scale bar: 50 µm

15. Mount the slides with a drop of mounting media. Seal coverslip with nail polish.
16. Observe the mounted slides with a confocal microscope.
17. For long-term storage, store slides in dark at 4 °C.

4 Notes

1. Male C57BL/6 mice (8–10 weeks old) were purchased from Charles River Laboratories, a commercial supplier licensed by the US Department of Agriculture. All the protocols using animals were performed in accordance with the National Institutes of Health Guide for the Care and Use of Laboratory Animals and approved by the Icahn School of Medicine at Mount Sinai Institutional Animal Care and Use Committee.
2. SU is provided as crystalline solid which does not dissolve in aqueous solutions. However, organic solvents like 100 % DMSO allow a complete dissolution of SU in small-volume compared to carboxymethylcellulose.
3. Oxygen controller ProOx P360 detects variations in O₂ concentration inside the semisealable hypoxia chamber and corrects it by infusing oxygen-rich or oxygen-poor control gas (N₂) through the gas infusion tube. Chamber ventilation is controlled passively by a fan that keeps the air flowing and by open holes in the sides of the chamber that allow stale air to be replaced. Pressures inside and outside the chamber stay the same (normobaric conditions). N₂ consumption will depend on the O₂ set-point and the hypoxia chamber size.
4. To induce moderate to severe PH (HySU group), mice are injected with SU (20 mg/kg) subcutaneously once-weekly and exposed to chronic normobaric hypoxia (10% O₂) for 3 weeks followed by one week in normoxia condition (21% O₂). Mild-to-moderate PH (Hy group) is induced by keeping the animals in chronic normobaric hypoxia for 3 weeks followed by 1 week in normoxia.
5. Decrease in body weight will be observed from the first week for the animals subjected to hypoxia. A 10% weight reduction in these animals is a reliable indication of disease development.
6. Manually insufflate air to the lungs through the catheter and double check that the intubation procedure has been performed properly. You should observe an increase in chest volume.
7. Use a 15-mL tube filled with PBS at 37 °C. For zero, hold the catheter a few millimeters under the surface of the PBS. Then,

submerge the catheter to a given depth and check the pressure; the output should be 0.75 mmHg for each centimeter of water depth it is submerged.

8. It is extremely important to avoid bleeding during the surgical procedure as significant blood loss could affect the hemodynamic parameter measurements. If blood vessels are damaged during the surgical procedure, use a small vessel cauterizer to stop bleeding.
9. This step is critical and all electrodes of the 1.2F PV catheter have to be immersed in the RV's cavity. Allow PV catheter to stabilize within the RV for 5 min before starting recording pressure data. If the PV catheter is not properly positioned the signal may be distorted. Adjust PV catheter position to a more central position within the RV and check that the signal is now stable. Best data recording is achieved when the ventilator is turned off a few seconds prior to and during the data recording.
10. For proper care of the PV catheter, place it in a 15-mL tube containing PBS. Clean and disinfect it at the end of experiments.
11. For a better exposure of the heart, make two lateral cuts through the rib cage up to the collarbone and lift the sternum away. Make an incision in the right atrium to allow the blood to leave the circulation.
12. For proper preservation of lung physiological structures it is required to insufflate them with 50% O.C.T. in PBS previous to snap-freezing. If all the lungs are intended for histological studies, lung insufflation can be performed through the trachea. Otherwise, lungs can be insufflated with 50% O.C.T. by using 1-mL syringes and 27G needles.
13. Set the cryostat temperature at -20 °C. Before starting the sectioning, let the O.C.T. block with the lung samples to temper. If the block is too cold, the specimen will curl, if it is too warm, it will stick to the knife. Unfixed slides can be stored at -80 °C for several months.

Acknowledgments

This work was supported by grants from the American Heart Association (AHA-17SDG33370112) to Y.S., from the National Institutes of Health R01HL133554 to L.H., and from the R01 HL117505, HL 119046, HL129814, 128072, HL131404, R01HL135093, a P50 HL112324, and two Transatlantic Foundation Leducq grants to R.J.H.

References

1. Galie N, Humbert M, Vachiery J-L et al (2016) 2015 ESC/ERS Guidelines for the diagnosis and treatment of pulmonary hypertension: The Joint Task Force for the Diagnosis and Treatment of Pulmonary Hypertension of the European Society of Cardiology (ESC) and the European Respiratory Society (ERS): Endorsed by: Association for European Paediatric and Congenital Cardiology (AEPC), International Society for Heart and Lung Transplantation (ISHLT). *Eur Heart J* 37:67–119
2. Humbert M, Sitbon O, Simonneau G (2004) Treatment of pulmonary arterial hypertension. *N Engl J Med* 351:1425–1436
3. Wilcox SR, Kabrhel C, Channick RN (2015) Pulmonary hypertension and right ventricular failure in emergency medicine. *Ann Emerg Med* 66:619–628
4. Simon MA, Pinsky MR (2011) Right ventricular dysfunction and failure in chronic pressure overload. *Cardiol Res Pract* 2011:568095
5. Dorfmüller P (2013) Pulmonary hypertension: pathology. *Handb Exp Pharmacol* 218:59–75
6. Guignabert C, Dorfmüller P (2017) Pathology and pathobiology of pulmonary hypertension. *Semin Respir Crit Care Med* 38:571–584
7. Huertas A, Perros F, Tu L et al (2014) Immune dysregulation and endothelial dysfunction in pulmonary arterial hypertension: a complex interplay. *Circulation* 129:1332–1340
8. Herve P, Humbert M, Sitbon O et al (2001) Pathobiology of pulmonary hypertension: the role of platelets and thrombosis. *Clin Chest Med* 22:451–458
9. Jonigk D, Golpon H, Bockmeyer CL et al (2011) Plexiform lesions in pulmonary arterial hypertension composition, architecture, and microenvironment. *Am J Pathol* 179:167–179
10. Pietra GG, Edwards WD, Kay JM et al (1989) Histopathology of primary pulmonary hypertension. A qualitative and quantitative study of pulmonary blood vessels from 58 patients in the National Heart, Lung, and Blood Institute, Primary Pulmonary Hypertension Registry. *Circulation* 80:1198–1206
11. Rubin LJ (1997) Primary pulmonary hypertension. *N Engl J Med* 336:111–117
12. Voelkel NF, Tuder RM (2000) Hypoxia-induced pulmonary vascular remodeling: a model for what human disease? *J Clin Investig* 106:733–738
13. Stenmark KR, Meyrick B, Galie N et al (2009) Animal models of pulmonary arterial hypertension: the hope for etiological discovery and pharmacological cure. *Am J Phys Lung Cell Mol Phys* 297:L1013–L1032
14. Bauer NR, Moore TM, McMurtry IF (2007) Rodent models of PAH: are we there yet? *Am J Phys Lung Cell Mol Phys* 293:L580–L582
15. Taraseviciene-Stewart L, Kasahara Y, Alger L et al (2001) Inhibition of the VEGF receptor 2 combined with chronic hypoxia causes cell death-dependent pulmonary endothelial cell proliferation and severe pulmonary hypertension. *FASEB J* 15:427–438
16. Abe K, Toba M, Alzoubi A et al (2010) Formation of plexiform lesions in experimental severe pulmonary arterial hypertension. *Circulation* 121:2747–2754
17. Ciucan L, Bonneau O, Hussey M et al (2011) A novel murine model of severe pulmonary arterial hypertension. *Am J Respir Crit Care Med* 184:1171–1182
18. Vitali SH, Hansmann G, Rose C et al (2014) The Sugen 5416/hypoxia mouse model of pulmonary hypertension revisited: long-term follow-up. *Pulm Circ* 4:619–629
19. Sakao S, Tatsumi K (2011) The effects of anti-angiogenic compound SU5416 in a rat model of pulmonary arterial hypertension. *Respiration* 81:253–261



Chapter 20

Mouse Model of Wire Injury-Induced Vascular Remodeling

Aya Nomura-Kitabayashi and Jason C. Kovacic

Abstract

We introduced the vascular remodeling mouse system induced by the wire injury to investigate the molecular and cellular mechanisms of cardiovascular diseases. Using these models, we focus on the adventitial cell population in the outermost layer of the adult vasculature as a vascular progenitor niche. Firstly we used the standard wire injury approach, leaving the wire for 1 min in the artery and retracting the wire by twisting out to expand the artery and denude the inner layer endothelial cells in the both peripheral artery and femoral artery. This method leads to adventitial lineage cell accumulation on the medial–adventitial border, but no contribution into the hyperplastic neointima. Since advanced atherosclerotic plaques in the mouse models and human clinical specimens show the elastic lamina in the media broken, we hypothesized that adventitial lineage cells contribute to acute neointima formation induced by the mechanical damage in both endothelial and medial layers. To make this intensive damage, next, we used the bigger diameter wire with no hydrophilic coating and repeated the ten-times insertion and retraction of the wire after leaving for 1 min in the femoral artery. The additional ten-times intensive movements of the wire lead to breakdown and rupture of the elastic lamina together with a contribution of adventitial lineage cells to the hyperplastic neointima. Here we describe these two different wire injury methods to induce different types of vascular remodeling at the point of adventitial lineage cell contribution to the hyperplastic neointima by targeting two separate locations of hind limb artery, the peripheral artery and femoral artery, and using two different diameter wires.

Key words Mouse, Angioplasty, Femoral artery, Peripheral artery, Wire injury, Endothelial cell denudation, Neointima hyperplasia, Adventitial lineage cells

1 Introduction

Neointima hyperplasia is known to form in the damaged vasculature caused by vascular grafting (vein to arterial) [1, 2] and interventional catheter treatment of coronary and peripheral artery atherosclerotic occlusions [3, 4]. To prevent postangioplasty restenosis, neointima formation has been intensively investigated in animal models including the mouse (Part 1, Re-Stenosis Models After Angioplasty in the book [5]). More than a decade ago, Sata's group established the femoral artery wire injury mouse model to produce neointima hyperplasia [6]. Many important advances have

been made using this surgical technique combined with mouse genetics in vascular remodeling research, including the role of stem cells, inflammation, medial smooth muscle cell phenotypic switching and extracellular matrix deposition [7–13]. Here we present two arterial wire injury methods, which could be considered “gentle” and “intensive,” with the latter model notable for allowing adventitial lineage cells to contribute to neointimal hyperplasia. Representative neointima hyperplasia with and without adventitial lineage cell contribution induced by these methods is demonstrated in Fig. 4. The protocols here are more detailed and the modified version of original wire injury methods [6, 14–16]. The modified parts are underlined in Notes. Wire injury procedures take less than 30 min when all steps work smoothly, and the survival rate of this surgery is high, more than 99% in our case. Neointima formation reaches the maximum at 3–4 weeks after artery wire injury and can be evaluated by the standard histological staining [6, 14–16].

2 Materials

2.1 Anesthesia Cocktail

Three hundred microliters of ketamine (100 mg/mL), 200 μ L xylazine (20 mg/mL), and 4 mL PBS.

2.2 Surgical Tools

Dumont #5 Forceps $\times 2$ (Fig. 1a), Dumont #5/45 Forceps $\times 2$ (Fig. 1b), Extra fine Graefe Forceps $\times 1$ (Fig. 1c), Extra Fine Micro Dissecting Scissors $\times 1$ (Fig. 1d), Moria Spring Scissors $\times 1$ (Fig. 1e), Halsey Micro Needle Holder $\times 2$ (Fig. 1f), Micro Serre-fine: Finescience #18055-02 $\times 1$ (Fig. 1g).

2.3 Suture

Ethicon 6-0 (Fig. 1h) and 5-0 (Fig. 1i) silk black suture.

2.4 Wires

1. Abbot Confianza Pro Asahi Guide Wire, # 20629-01, tip diameter 0.23 mm/0.009 in. (Fig. 1j), or similar.
2. Cook Fixed Core Wire Guide, #C-SF-15-15, tip diameter 0.38 mm/0.015 in. (Fig. 1k).

2.5 Others

1. Surgical microscope.
2. Gooseneck fiber-optic illuminator (*see Note 1*).
3. Heating mats (25 \times 15 cm for surgery and 50 \times 30 cm for the recovery cage) (*see Note 2*).
4. Plastic disk/plate with approx. 12 cm diameter (*see Note 3*).
5. Surgical tape (*see Note 4*).
6. Xylocaine (lidocaine-HCl, 10 mg/mL) (infiltration and nerve block), place in a 1 mL syringe.
7. PBS, place in 1 mL syringe and dishes.

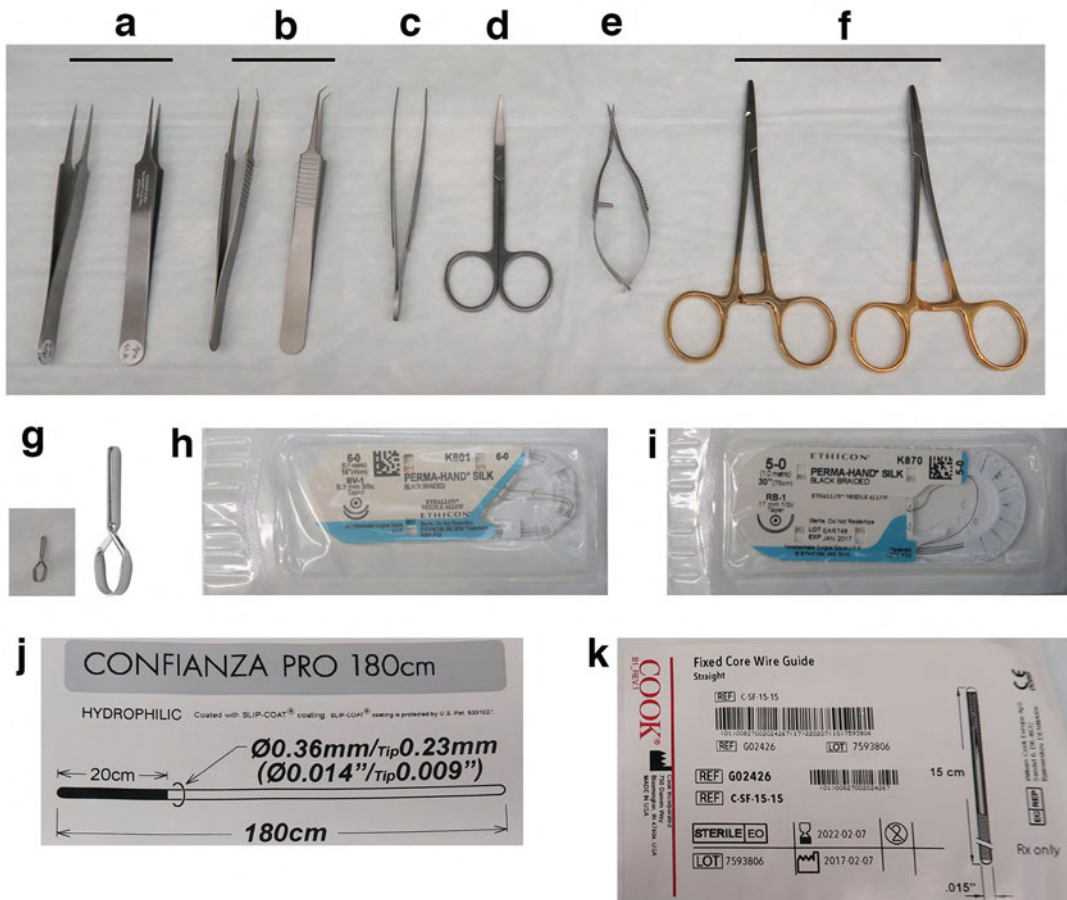


Fig. 1 Surgical tools and wires for mouse artery wire injury. Surgical tools to set up the wire injury are shown. (a) Dumont #5 Forceps, (b) Dumont #5/45 Forceps, (c) Extra fine Graefe Forceps, (d) Extra Fine Micro Dissecting Scissors, (e) Moria Spring Scissors, (f) Halsey Micro Needle Holder, (g) Micro Serrefine, (h) Ethicon 6-0, Perma-Hand SILK, BLACK BRAIDED, (i) Ethicon 5-0, Perma-Hand SILK, BLACK BRAIDED, (j) Abbot Confianza Pro Asahi Guide Wire, hydrophilic coated, # 20629-01, tip diameter 0.23 mm/0.009 in., (k) Cook Fixed Core Wire Guide, #C-SF-15-15, tip diameter 0.38 mm/0.015 in

8. Surgical disinfectant and 70% ethanol.
9. Hair remover lotion.
10. Sterile cotton-tipped swabs.
11. Sterile gauze 2" x 2".

2.6 Harvesting and Immunostaining of Wire Injured Artery

1. Fixation solutions: 20 mL/mouse, 1.5% PFA, 0.1% glutaraldehyde in PBS.
2. 15% sucrose in PBS.
3. OCT compound.
4. Cryo-mold (15 × 15 × 5 mm).

5. Anti-SMA antibody (SIGMA, #113200, 100-dilution).
6. Anti-PECAM antibody (BD, #550274, 10-dilution).
7. DAPI mounting media.
8. Alexa Fluor 649 anti-mouse IgG2a (500-dilution).
9. Alexa Fluor 488 anti-rat IgG (500-dilution).
10. Confocal microscope.

3 Methods

All procedures of experiments and surgery undertaken here are according to the regulation of Institutional Animal Care and Use Committee (IACUC) and the Center for Comparative Medicine and Surgery (CCMS) of the Icahn School of Medicine at Mount Sinai and are approved by them. In all steps, make sure that open tissue areas are intermittently moisturized with Xylocaine.

3.1 Peripheral Artery Wire Injury

3.1.1 Preparation of Surgical Tools

1. Cut the Abbot Confianza Pro Asahi Guide Wire, or a similar one, into an 8 cm length from the tip by the wire cutter, and soak the tip end into PBS in the 10 cm dish.
2. Soak sterilized surgical tools (*see Note 5*) and cut 6-0 silk sutures (~1.5 cm, two strings per mouse) and a 5-0 silk suture (~0.4 cm, one per mouse) into PBS in 10 or 6 cm plastic dishes.

3.1.2 Preparation of Mouse for Surgery

1. Measure the mouse body weight on the scale.
2. Anesthetize a mouse by intraperitoneal (IP) injection of the anesthesia cocktail in a 10 mL/body weight (kg) ratio, for example, 250 µL per 25 g mouse. The pedal reflex of the hind limb is checked to ensure an appropriate depth of anesthesia. All procedures will be completed within 30 min, before the mouse begins to awaken. In the event that the mouse begins to show any signs of waking prior to the end of the procedure, a small bolus of the anesthetic cocktail should be administered.
3. Remove the hair of the left leg from distal to proximal (heel to thigh) with the hair remover and wipe with PBS wet paper towel followed by 70% ethanol.
4. Place the mouse onto the plastic disk/plate in the supine position and extend the left hind limb straight and slightly abduct with surgical tapes (Fig. 2a) (*see Notes 3, 4, and 6*). Put this onto a heating mat draped with an absorbent pad during the surgery (*see Note 2*).
5. Place a folded Kimwipes under the leg to make the working field. Wet the leg and the paper bed with PBS, and wipe the left leg with the disinfectant and 70% ethanol.

3.1.3 Isolation of the Peripheral Artery

- Under the microscope, the bifurcation of the medial and lateral saphenous artery (SA) is clearly visible through the skin (blue arrow, Fig. 2a, h) [17]. Make a skin incision ~7 mm long longitudinally at approx. 5 mm distal position of the bifurcation of the medial and lateral SA, and detach the skin from the muscle around the exposed area for the last skin suturing. Moisturize opened area with a few drops of Xylocaine.
- Carefully separate the medial SA from the vein using #5/45 forceps.
- Tie the separated medial SA at approx. 4 mm distal position of the bifurcation with the edge of a presoaked 1.5 cm 6-0 silk suture (yellow arrowhead, Fig. 2b, e), and pull the other edge to keep gentle tension and tape it down over the leg (*see Note 7*).
- Place another presoaked 1.5 cm 6-0 suture under the proximal artery (Fig. 2e), and put a 0.4 cm presoaked 5-0 suture on the artery (Fig. 2f). Make a single bow tie with 6-0 string over the 5-0 string and artery together (Fig. 2g) for a temporary hemostat (*see Note 8*).
- Pinch the artery with the forceps between proximal and distal sutures several times to make the artery swollen. This action helps to introduce a wire into the artery.
- Place a few drops of Xylocaine over the surgical field to keep the artery moist through the procedure.

3.1.4 Creating Peripheral Artery Wire Injury

- Make a 45-degree angle cut on the medial SA (arteriotomy) closer to the posterior tie (light blue arrowhead, Fig. 2g) using the spring microscissors (Fig. 1e) (*see Note 9*).
- Lift the artery's cut flap with the #5/45 forceps, and put a prewetted Abbot (or similar) wire into the hole (*see Note 10*) by holding the wire gently from the top with another #5/45 forceps.
- Once the wire is advanced into the artery 2–3 mm, release the proximal single bow tie by pulling one string. Keep the wire steady to avoid slipping out from the artery during these steps. Remove the 5-0 short string and loosen the 6-0 suture over the artery to let the wire advance further into the proximal artery (*see Note 11*).
- Place a few drops of Xylocaine solution to keep wire and the artery moist. Use the Graefe forceps to guide the wire over the skin by gently pushing the muscle to adjust the curved SA/FA direction to help the wire insertion proximally about 1.4–2.0 cm (*see Note 12*).
- Leave the wire in the artery for 1 min to expand and damage the endothelial layer of the artery, and place a few drops of

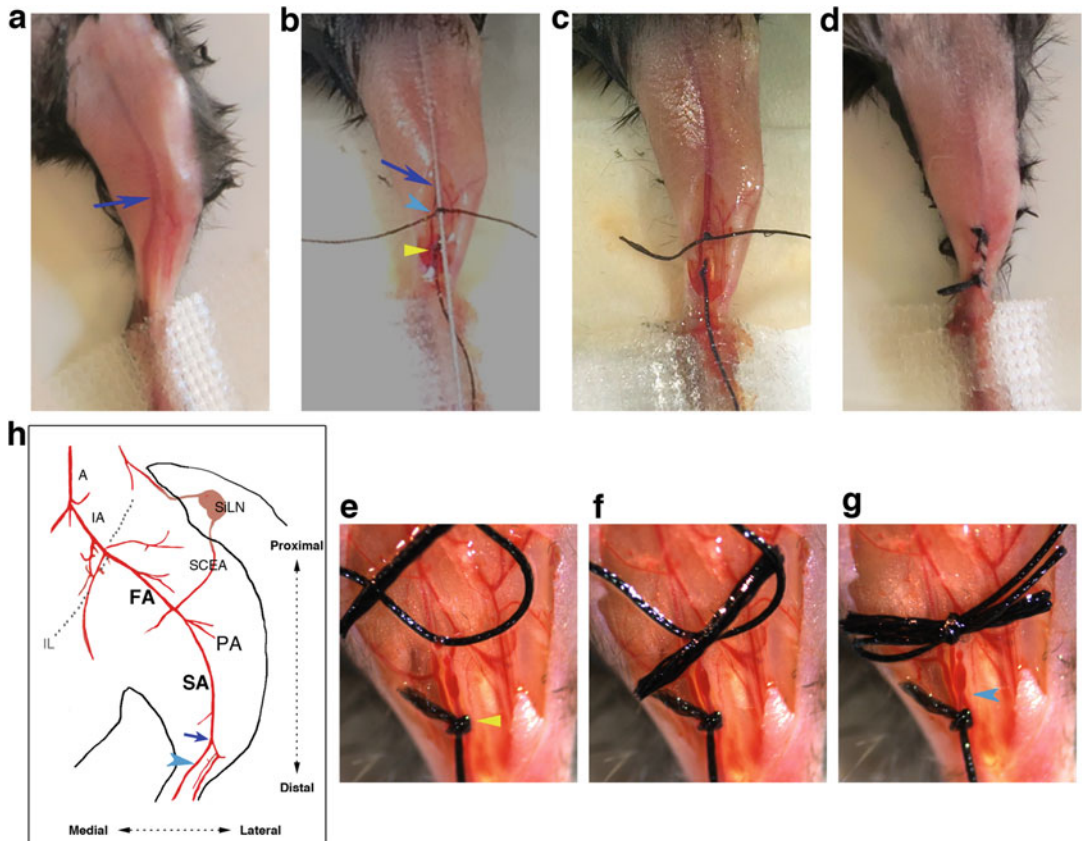


Fig. 2 Peripheral artery wire injury. (a) The bifurcation of the medial and lateral saphenous artery (SA) is clearly visible through the skin, indicated by the blue arrow. (b) The wire insertion is made through the medial SA to the proximal femoral artery (FA). Slight tension is applied by pulling the tied artery distally (yellow arrowhead), which aids in inserting the wire deeply into the proximal artery beyond the bifurcation of the SA (blue arrow). Temporally tie the preplaced 6-0 suture over the inserted wire proximal to the arteriotomy (light blue arrowhead). Panel (c) shows the swollen FA and SA after the wire is removed and no bleeding from the injured artery tied 1~2 mm proximal to the arteriotomy. (d) Skin closure is achieved by continuous suturing with the 5-0 silk. Panels (e–g) show how to make the single soft bow tie proximal to the wire insertion point (light blue arrowhead in the panel g) before making the arteriotomy. Panel (e) indicates a 6-0 suture placed under the proximal medial SA. Next (f) shows an ~0.4 cm presoaked 5-0 suture placed over the artery above the 6-0 suture, and making a single bow tie with the preplaced 6-0 suture over the 5-0 string and artery without taking out the loop edge out (g). (h) The diagram illustrates mouse hind limb arteries [17]. A Aorta, IA Iliac artery, IL Inguinal ligament, FA Femoral artery, SCEA Superficial caudal epigastric artery, SiLN Subiliac lymph node, PA Popliteal artery, SA Saphenous artery. Blue arrows in (a, b, h) show the bifurcation landmark of medial and lateral SA. Light blue arrowheads in (b, g, h) show the arteriotomy point in the medial SA. Yellow arrowheads (b, e) show the distal tie to pull the artery distally

Xylocaine. If keeping a record of the wire insertion length, measure it from the skin while waiting. Tie the preplaced 6-0 suture over the inserted wire proximal to the arteriotomy (light blue arrowhead, Fig. 2b).

6. Hold the tied suture's edge with the forceps, and slowly retract the wire twisting back using fingers in repeating rotations (*see Note 13*).
7. Before pulling out the wire completely, readjust the position of the pretied suture over the artery to 1–2 mm proximal to the arteriotomy.
8. Immediately after the wire is removed, tie the prepositioned suture firmly. Wash away the blood with PBS, and then make sure that there is no blood leakage from the tied area, and make another secure tie (Fig. 2c). Cut and clean out extra strings.
9. Place the wire into PBS immediately after taking out from the vessel, and wipe with gauze gently to prevent the tissue debris sticking on it, and keep in PBS for the next injury (*see Note 5*).

3.1.5 Skin Closure and Recovery

1. Close the skin with presoaked 5-0 silk suture (Fig. 2d).
2. Place the mouse back on the clean, prewarmed cage on the heating mat.
3. After the mouse has recovered, put some food on the bed and return the cage to the mouse room.
4. Next day, check the injured leg and mouse condition.

3.2 Femoral Artery (FA) Wire Injury

3.2.1 Preparation of Surgical Tools and Mouse

1. Cut a Cook Fixed Core Guide Wire with the wire-cutter into 1.5 cm (*see Note 14*), and soak in PBS in 6 cm dish. Presoak three of ~15.0 cm and two of 1.5 cm long 6-0 sutures and sterilized surgical tools in PBS.

3.2.2 Isolation of the Femoral Artery and Branches

2. After anesthetizing the mouse, remove the hair of the left leg around the thigh (Fig. 3a), and repeat steps in Subheading 3.1.2.
1. Make an ~0.5 cm skin incision longitudinally from the knee toward the medial thigh. The neurovascular bundle with the subcutaneous white fat (shown * in Fig. 3a) is a landmark, which covers the bifurcation of FA and popliteal artery (PA), distally located to the superficial caudal epigastric artery (SCEA, Fig. 3k) [17] (*see Note 15*).
2. Remove the membranous femoral sheath and subcutaneous fat tissue around the neurovascular bundle (Fig. 3b).
3. After pushing the separated nerve to the side to avoid its irritation, isolate the vascular bundle (no need to separate the vein and artery) using #5/45 forceps from the surrounding muscle and tissue. Loop two pre-wet 15 cm long 6-0 sutures

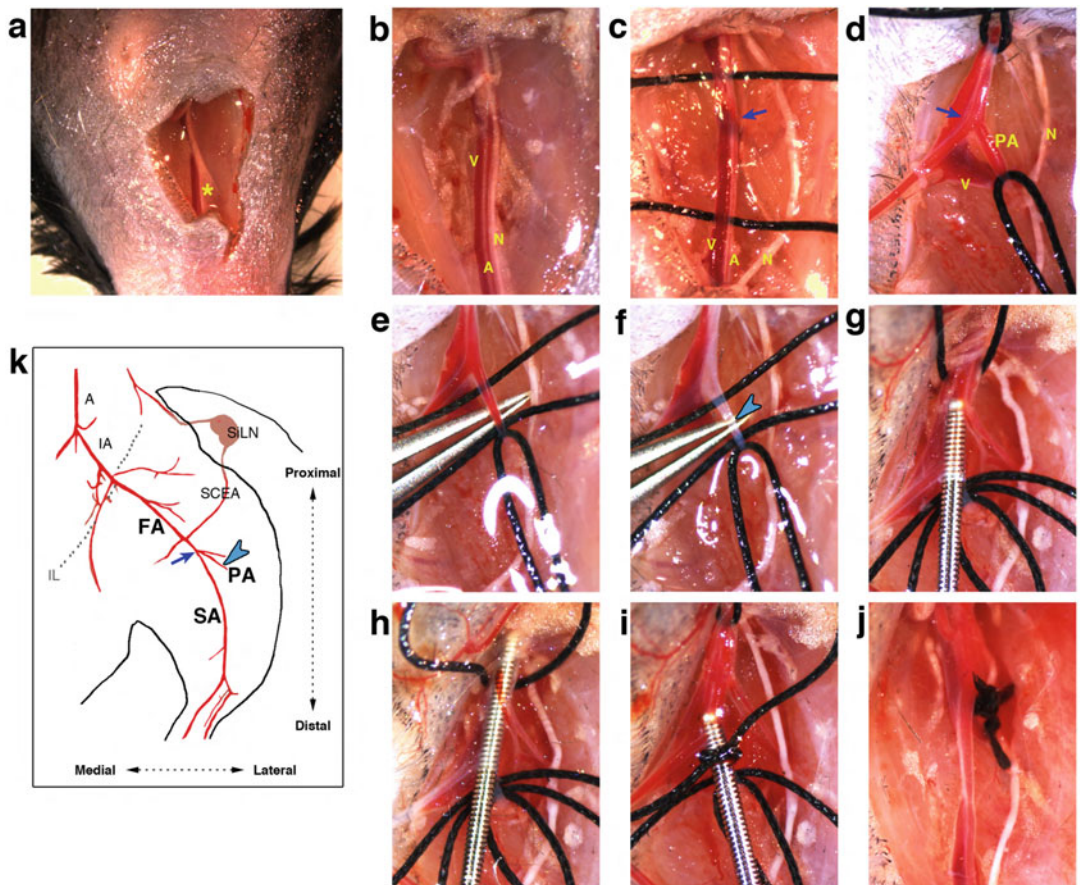


Fig. 3 Femoral artery (FA) wire injury. (a) The skin incision on the left hind limb made from the knee toward the medial thigh. Yellow asterisk shows a landmark subcutaneous white fat stream. (b) After removing the fat, the neurovascular bundle is clearly visible, but the bifurcation of the femoral artery (FA) and popliteal artery (PA) is still under the fat and muscle. Panel (c) shows the isolated nerve (N) placed away from the vessel, and two 6-0 sutures placed under the vascular bundle, both vein (V) and artery (A) together, at the proximal and distal position. The blue arrow points the bifurcation of the femoral and popliteal veins. Panel (d) shows the temporarily secured hemostat made between the proximal and distal vascular bundle by pulling the looped sutures proximomedially and distomedially (out of frame) respectively. The isolated PA is also stabilized with another 6-0 loop with gentle tension distolaterally. The bifurcation of FA and PA is indicated by the blue arrow. (e) Two additional 1.5 cm 6-0 sutures are placed under the PA. Putting the closed forceps tip under the PA near the distal suture help to visualize the PA clearly and guide the arteriotomy. (f) The arteriotomy indicated by the light blue arrowhead, allowing blood out from the hemostat artery. (g) The Cook wire is inserted from the PA branch into the FA about 2–3 mm. (h) Further wire insertion over the relaxed proximal suture into the proximal FA about 1 cm. (i) After creating the intensive wire injury, the pulled wire is tied over the artery with the preplaced 6-0 suture temporarily under the resecured hemostat before removing the wire from the PA. Panel (j) shows the firmly tied SA proximal to the arteriotomy and at the distal edge, without any blood leakage and with fully recovered blood flow through the FA to SA after removing all extra sutures. (k) The diagram illustrates mouse hind limb arteries [17]. Abbreviation: refer to Fig. 2h. Blue arrows in (c, d, k) show the bifurcation of FA and PA. Light blue arrowheads in (f, k) show the arteriotomy/wire insertion point in the PA

under the vascular bundle at the proximal and distal sites (Fig. 3c). The bifurcation of the FA and PA is still not visible, but the popliteal vein branched from the femoral vein is usually recognizable, indicated by the blue arrow (Fig. 3c). Moisten the open area with a drop of Xylocaine.

4. Secure the looped 6-0 sutures with the needle holders (Fig. 1f), and pull the proximal bundle proximomedially, and the distal bundle distomedially (*see Note 16*).
 5. These tensions help to expose and isolate the PA branch deeply running under the right side muscle.
 6. Carefully isolate the PA from the vein underneath the FA and PA (*see Note 17*) and loop a presoaked 15 cm 6-0 suture under the PA and hold it with the micro serrefine clamp and tape it with a gentle tension to distolaterally (Fig. 3d). Moisten the tissues as needed.
- 3.2.3 Creating Femoral Artery Wire Injury**
1. Place two more 1.5 cm 6-0 sutures under the PA (Fig. 3e). After securing hemostasis, make a 45-degree angle arteriotomy (light blue arrowhead, Fig. 3f) using the spring microscissors in the PA, far distally from the bifurcation of the FA (*see Note 18*). Moisten with a drop of Xylocaine.
 2. Lift the cut flap of the PA gently with the #5/45 forceps. Insert the pre-wet Cook wire toward the FA (Fig. 3g) (*see Note 19*).
 3. After inserting the wire securely about 3 mm in the FA, release the tension of the proximal suture for further wire insertion upward to the FA (Fig. 3h). Hold the wire using the Graefe (Fig. 1c) or #5/45 forceps and push the wire about 1 cm (wire length is 1.5 cm), which is enough to cover the proximal FA. Leave the wire for 1 min to expand the artery to damage the endothelial intima layer. To injure the medial layer, insert and retract the wire ten additional times (*see Note 20*).
 4. After making the intensive injury, gently retract (but do not remove) the wire and secure the hemostat again by pulling the proximal suture proximally.
 5. Re-position the preplaced 1.5 cm 6-0 suture at the proximal aspect of the incision point of the PA and pre-tie over the wire (Fig. 3i). Fully remove the wire from the PA, immediately tie the pre-tied suture firmly and make another secure knot (*see Note 21*). Soak the wire in PBS after removing from the artery to prevent the tissue debris sticking on it.
 6. Wash the blood away from the surgery area with PBS, and relax the proximal loop suture to restart the blood supply to the distal artery, and make sure that there is no blood leakage from the tied arteriotomy area of the PA.

7. Relax the distal loop suture to recover the full blood flow through the FA to SA. Recheck no blood leakage (*see Note 22*). After tying the distal edge of PA, remove all temporary hemostat sutures (Fig. 3j).
8. Repeat Subheading 3.1.5 for skin closure and recovery.

3.3 Cleaning and Maintaining the Wire

3.4 Harvesting and Immunostaining of Wire Injured Artery

Clean the PBS soaked wire with new gauze gently but thoroughly (*see Note 23*). Keep the wire in the original wire holder or the dish.

Key steps in harvesting, cryo-sectioning, and immunostaining are described below.

1. Perfusion the fixative solution after the PBS flushing into the blood circulation, and keep the dissected wire injured arteries in 15% sucrose in PBS at 4 °C overnight.
2. Embed arteries in the cryo-mold with OCT compound and cut into 6-μm cross sections.
3. The cryosections are stained with standard protocol and images acquired using a confocal microscope. Refer to Subheading 2.6 about common antibodies used for immunostaining.
4. Representative neointima hyperplasia with and without adventitial lineage cell contribution is demonstrating in Fig. 4 (*see Notes 24 and 25*).

4 Notes

1. For the femoral artery wire injury, the surgery area is deep, which allows liquids to pool in the surgical field. The upper light attached to the microscope makes a reflection on these liquids. If it prevents clear vision for the surgery, turn off the upper light and use a side light from the gooseneck fiber optic (*see Note 17*).
2. Using the heating mat during surgery to maintain body temperature facilitates mouse recovery, together with the additional heating mat under the recovering cage.
3. Using a plastic disk/plate to position the mouse on during the surgery gives the flexibility to adjust a suitable angle and position for the wire and tool access (*see Note 10*).
4. Transpore surgical tape is easy to cut into small pieces and not sticky unnecessarily, and it can stick on slightly wet surfaces by pushing out the moisture beneath.
5. Keep the surgical tools in PBS when not in use to release any debris and blood from them.

6. For peripheral artery wire injury, aligning the artery line of the medial saphenous to the proximal femoral makes the wire insertion much easier. Pull the leg to extend the knee straight, and abduct the lower leg below the knee slightly laterally.
7. Maintaining artery tension helps the wire insertion into the incision hole. Tape down the other side of the suture tied at the proximal artery on the foot with a 3 × 6 mm Transpore tape, and pull the sticking out suture under the tape to adjust the tension. Do not pull too much.
8. A temporary soft single bow tie can be released easily by pulling one of the suture ends. Making it proximal to the arteriotomy to prevent unnecessary blood loss and mess, makes wire insertion much easier. Make sure to have enough distance between the proximal and distal ties on the SA, and create the arteriotomy close to the distal tie (light blue arrowhead, Fig. 2g) to prevent the inserted wire from slipping out during the subsequent handling. Figure 2e–g shows step-by-step processes for how to make the soft single bow tie to create the temporary hemostat. The short 5-0 suture is a cushion to press the artery gently (Fig. 2f). Instead of taking out an edge of the looping suture during tying, keep pulling the middle of the loop and the other edge of the suture in the opposite direction to make a single bow tie (Fig. 2g). To release this bow tie, simply pull one end of the 6-0 suture.
9. Making a clean and adequate incision in the artery (arteriotomy) is one of the important points to achieve good wire insertion. Placing the forceps under the target artery gives a good contrast to see the depth of the cut (refer Fig. 3e). The arteriotomy should be in ~40% depth in the artery: if it's too deep, the artery will tear while inserting the wire.
10. Before inserting the wire, adjust the mouse/disk by 45-degrees to the left to make the wire insertion easier. Put the pre-wet wire beside the artery ready to use, and lift the cut flap of the artery with #5/45 forceps gently. Never flip or pull up the flap too much, it will cause tearing. Just hold the flap to keep the hole open. Hold the wire from the top with the #5/45 forceps and keep the wire angle parallel to the artery, and gently insert into the incision hole.
11. When releasing the proximal bow tie, keep the wire steady to avoid slipping out from the artery. Changing the forceps grab angle of the wire to the side helps the subsequent wire handling. Once the wire is in the artery, blood is held by the wire, but keep the 6-0 suture under the artery after loosening the tie for further steps.
12. Keep the wire and artery moist without making them sticky with Xylazine as well as with PBS for the shaved leg skin.

Gently push the muscle over the skin by the Graefe forceps to adjust the curved SA/FA artery alignment to guide wire insertion smoothly toward the proximal artery.

13. To retract the wire, hold the tied string at the wire insertion site with the left-hand forceps and hold the wire with your fingers. Make sure that the area is moist. Twisting/rotating the wire during retraction by your thumb and index/middle fingers, and repeat the right/left rotation gently and slowly until the wire tip comes closer to the exit. This motion will ensure thorough endothelial denudation in the peripheral artery using the Abbot wire.
14. The Cook wire has two round edges suitable for the wire injury—both can be used.
15. Locating the target arterial branch for femoral artery wire injury is easy once knowing the hind limb anatomical landmarks [17]. The middle and proximal thigh areas have more arterial branches compared with the distal limb. Refer to the diagram in Fig. 3k. Begin by locating the superficial caudal epigastric artery (SCEA) connecting to the subiliac lymph node (SiLN). This elongated free SCEA is quite easy to find. The target bifurcation of the femoral artery (FA) and popliteal artery (PA) is located distal to this SCEA branching out from the FA. Another landmark is a typical subcutaneous fat stream (yellow asterisk, Fig. 3a) along with a neurovascular bundle, and the target FA/PA bifurcation is under this fat and muscle. Once one is familiar with these landmarks, there is no need to dissect out the SCEA. Just make a small skin incision over the target area.
16. Holding the two looped sutures with the needle holders creates tension on the proximal and distal vascular bundles and secures the hemostat as well. Use enough length of suture (15 cm~) to allow the flexibility to adjust the tension and angle of vascular bundles (artery and vein together). Do not pull them too firmly or they can break. The needle holders add flexibility and increase working space.
17. The femoral and popliteal veins are bigger than the saphenous vein and easy to break. If the vein is damaged, press the area with a cotton swab to stop bleeding. Clean the blood pool with the dried and PBS absorbed cotton swabs. Isolation of the PA from the vein and placing a suture under PA are the most difficult steps of the FA wire injury procedure. Be patient to make an access path of the 6-0 suture by placing the closed #5/45 forceps tip under the PA without damaging the vein. If light reflection on the wet tissue makes it difficult to see the PA, turn off the upper light and use the side light source (*see Note 1*).

18. Make the arteriotomy in the distal PA to keep a secure distance to tie the PA after the injury and wire removal. The Cook wire diameter is ~2 times larger than the PA, and repeating insertion and retraction of the wire 10 times widen the incision hole and shortens the PA length from the arteriotomy to the bifurcation point.
19. When putting the Cook wire into the incision hole, do not just push the wire in, but try to gently overlay the edge of the cut flap of the PA onto the Cook wire.
20. After trying many different ways to induce an adventitial lineage cell contribution to neointima hyperplasia, only additional intensive wire injury with the ten-times repeated insertion and retraction of the Cook wire in the femoral artery worked to damage the medial layer and induced cell contribution. Without the intensive repeated movements, there was no adventitial cell contribution. Using the Abbot wire with this ten-times repeated insertion and retraction along with 1 min leaving in the FA did not make the cell contribution, and using the Cook wire for peripheral artery wire injury was unable to achieve wire insertion beyond 2–3 mm. Selecting a suitable wire injury method depends on the experimental aim and design. Here are the choices: (1) peripheral artery wire injury using the Abbot wire needs less handling than the Cook wire femoral artery injury, but the neointima has no adventitial lineage cell contribution. (2) Femoral artery wire injury using the Cook wire with an additional ten-times insertion and retraction gives adventitial lineage cell contribution to the hyperplastic neointima (Fig. 4).
21. Due to vessel foreshortening, the incision point of the PA becomes closer to the bifurcation of PA and FA after intensive wire injury. Therefore, carefully reposition the 6-0 suture before removing the wire and pre-tie it over the inserted wire as far distal as possible from the incision point. Ensure that the incision edge of the PA is protruding out distally from the tying position. When making another secure tie, do not break the first knot.
22. If there is blood leakage after fully releasing the hemostat, use the second preplaced 1.5 cm suture to stop the leak, and reassess.
23. The wires are reusable many times for mouse wire injury. The Abbot wire has the hydrophilic coating on the tip, so some membranous debris might be visible under the microscope after using a couple of times, but do not peel it off. When the Abbot wire insertion makes an unusual sticking stress during the insertion, it is a time to replace it. Clean the wires after soaking in the PBS by gently wiping with clean gauze. Keep

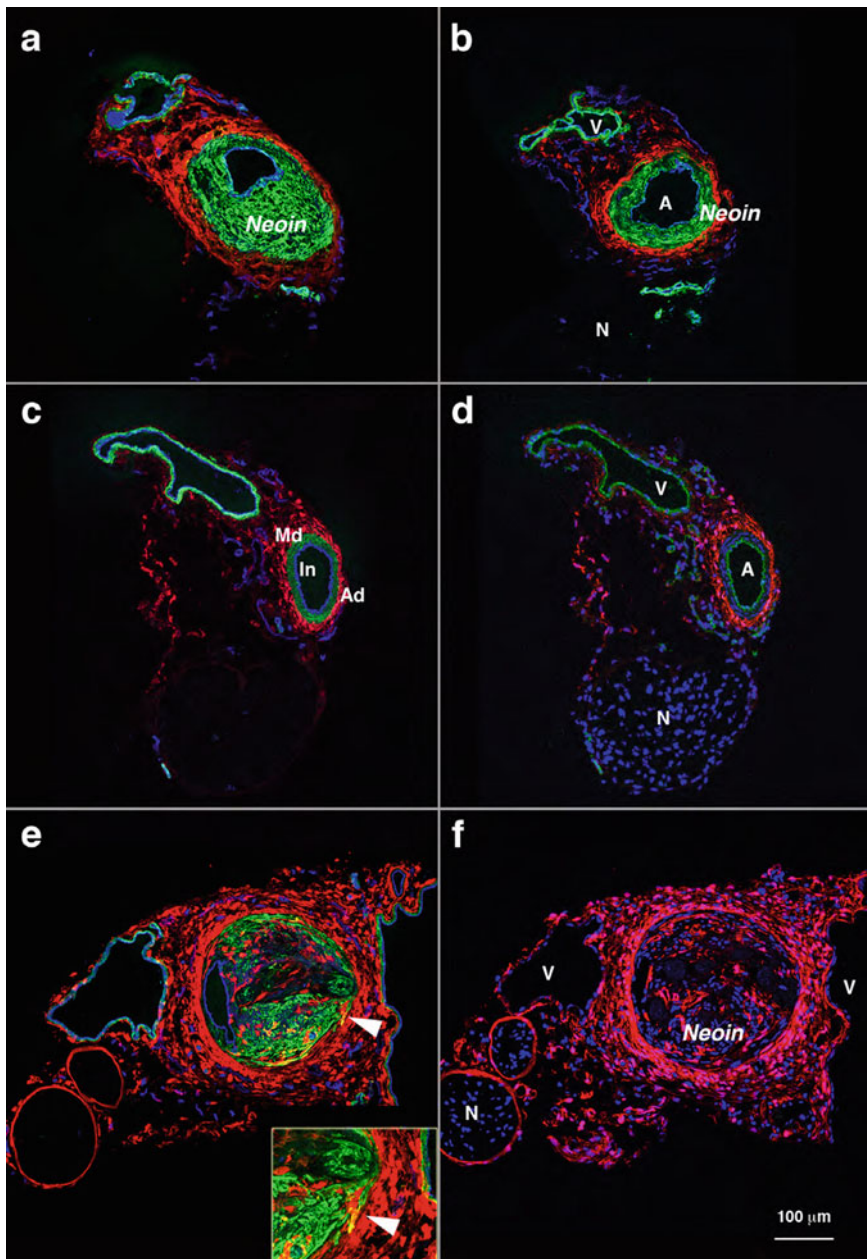


Fig. 4 Neointima hyperplasia with and without adventitial lineage cell contribution at 3-weeks after wire injury (see Notes 24 and 25). The cross-cut cryosections of the wire injured peripheral arteries (**a, b**), uninjured femoral artery (**c, d**), and wire injured femoral artery (**e, f**) are immunostained with anti-SMA, anti-PECAM antibodies and DAPI, and detected intrinsic tdTomato of the floxed out Rosa26-tdTomato. The tdTomato red signal represents the adventitial (Ad) lineage cells in all panels (**a-f**). Green and blue stained signals in the panels (**a, b, c, e**) indicate SMA positive cells in the neointima (Neoin) and medial layer (Md), and PECAM positive cells in the intima layer (In) and newly formed epithelial lining layer respectively. In panels (**d, f**), blue signals are DAPI positive nuclei, and PECAM positive intima layer shown in green (**d**). Panel (**f**) represents corresponding normal mouse IgG2a and rat IgG control staining using the sister section of (**e**). The femoral

them in the clean dish or wire tube, in which they originally came.

24. Representative neointima hyperplasia samples with and without adventitial lineage cell contribution are showing in Fig. 4. It summarizes the immunostaining results of both peripheral and femoral arteries 3-weeks after wire injury. The top row shows two examples of hyperplastic neointima from the injured peripheral arteries (Fig. 4a, b): adventitial lineage cells (tdTomato positive, red) (*See Note 25*) are not detected in the hyperplastic neointima (Neoin) (SMA positive, green). Uninjured normal femoral artery (Fig. 4c, d) has an intact PECAM positive intima layer (In) (blue in 4c or green in 4d). It lines the inside of well-organized intact medial layer (Md), which has elongated DAPI signal (blue, 4d) or SMA positive cells (green, 4c). And the red adventitial layer (Ad) surrounds them. However, in the femoral artery wire injured samples (bottom row, Fig. 4e, f), many adventitial lineage cells (red) are detected in the hyperplastic neointima (green, Fig. 4e): some of the adventitial lineage cells express SMA (double positive cells shown in yellow). The adventitial lineage cells accumulate around the neointima border, and a few red/yellow cells are crossing into the neointima from the adventitia (the insert shown at the higher magnification) as well. These data suggest that Cook wire's intensive injury of the femoral artery (1 min leaving in the artery plus 10-times repeats of the wire insertion and retraction) damages the medial layer additionally and allows the adventitial lineage cell migration and contribution to the hyperplastic neointima. On the other hand, the Abbot wire injury in the peripheral artery denudes the luminal endothelial cells but makes no damage to the medial layer, leading the adventitial lineage cells to remain outside the neointima without any contribution (*see Note 23*).
25. Mice used in Fig. 4 to track the adventitial lineage cells are tdTomato positive after the floxed-stop cassette out from the double transgenic mouse line harboring the inducible Cre and Rosa 26-tdTomato (JAX 007914).

Fig. 4 (continued) artery wire injured sample (e) shows adventitia lineage cells (red) contribute to the hyperplastic neointima (green). Many red or yellow colored cells are detected among the green cells, and the white arrowhead indicates red and yellow colored cells are crossing into the neointima from the adventitial layer: the insert shown at the higher magnification. However, adventitial lineage cells are not detected in the hyperplastic neointima in peripheral artery wire injured samples (a, b). V Vein, A Artery, N Nerve, Ad Adventitia, Md Media, In Intima, *Neoin* Neointima. Scale bar in (f) applies to all (a–f) except for the insert

Acknowledgments

We thank Microscope Core for the confocal microscope support and CCMS for the mouse husbandry care (Icahn School of Med at MSSM). We thank D. Yang (Icahn School of Med at MSSM) for the initial technical introduction and S. Hong (NHGRI) for the initial technical training of peripheral artery wire injury. We are grateful to Professor M. Sata (Tokushima Univ.) who established femoral artery wire injury technique originally for sharing information, and H. Kato (Tokyo Univ.) for the technical advice.

References

1. Collins MJ, Li X, Lv W et al (2012) Therapeutic strategies to combat neointimal hyperplasia in vascular grafts. *Expert Rev Cardiovasc Ther* 10:635–647
2. de Vries MR, Simons KH, Jukema JW et al (2016) Vein graft failure: from pathophysiology to clinical outcomes. *Nat Rev Cardiol* 13:451–470
3. Komiyama H, Takano M, Hata N et al (2015) Neoatherosclerosis: Coronary stents seal atherosclerotic lesions but result in making a new problem of atherosclerosis. *World J Cardiol* 7:776–783
4. Yahagi K, Kolodgie FD, Otsuka F et al (2016) Pathophysiology of native coronary, vein graft, and in-stent atherosclerosis. *Nat Rev Cardiol* 13:79–98
5. Sata M (2016) Mouse models of vascular diseases. Springer, Tokyo
6. Sata M, Maejima Y, Adachi F et al (2000) A mouse model of vascular injury that induces rapid onset of medial cell apoptosis followed by reproducible neointimal hyperplasia. *J Mol Cell Cardiol* 32:2097–2104
7. Sata M, Saiura A, Kunisato A et al (2002) Hematopoietic stem cells differentiate into vascular cells that participate in the pathogenesis of atherosclerosis. *Nat Med* 8:403–409
8. Passman JN, Dong XR, Wu SP et al (2008) A sonic hedgehog signaling domain in the arterial adventitia supports resident Scal+ smooth muscle progenitor cells. *Proc Natl Acad Sci U S A* 105:9349–9354
9. Kramann R, Schneider RK, DiRocco DP et al (2015) Perivascular Gli1+ progenitors are key contributors to injury-induced organ fibrosis. *Cell Stem Cell* 16:51–66
10. Kramann R, Goettsch C, Wongboonsin J et al (2016) Adventitial MSC-like cells are progenitors of vascular smooth muscle cells and drive vascular calcification in chronic kidney disease. *Cell Stem Cell* 19:628–642
11. Li C, Zhen G, Chai Y et al (2016) RhoA determines lineage fate of mesenchymal stem cells by modulating CTGF-VEGF complex in extracellular matrix. *Nat Commun* 7:11455
12. Yu B, Wong MM, Potter CM et al (2016) Vascular stem/progenitor cell migration induced by smooth muscle cell-derived chemokine (C-C Motif) ligand 2 and chemokine (C-X-C motif) ligand 1 contributes to neointima formation. *Stem Cells* 34:2368–2380
13. Zhu Y, Takayama T, Wang B et al (2017) Restenosis inhibition and re-differentiation of TGFbeta/Smad3-activated smooth muscle cells by resveratrol. *Sci Rep* 7:41916
14. Le V, Johnson CG, Lee JD et al (2015) Murine model of femoral artery wire injury with implantation of a perivascular drug delivery patch. *J Vis Exp* e52403:1–7
15. Takayama T, Shi X, Wang B et al (2015) A murine model of arterial restenosis: technical aspects of femoral wire injury. *J Vis Exp* e52561:1–6
16. Duckers HJ, Boehm M, True AL et al (2001) Heme oxygenase-1 protects against vascular constriction and proliferation. *Nat Med* 7:693–698
17. Kochi T, Imai Y, Takeda A et al (2013) Characterization of the arterial anatomy of the murine hindlimb: functional role in the design and understanding of ischemia models. *PLoS One* 8:e84047



Chapter 21

The Mouse Aortocaval Fistula Model with Intraluminal Drug Delivery

Toshihiko Isaji and Alan Dardik

Abstract

The arteriovenous fistula (AVF) is the most common type of vascular access currently used for hemodialysis, but long-term outcomes remain poor in many patients; understanding the basic mechanisms of venous remodeling within the fistula environment is critical to improve our understanding of AVF maturation. In this chapter, we describe a method to create a murine aortocaval fistula that allows intraluminal drug delivery. This model reliably recapitulates human AVF maturation and therefore is a good consideration to study venous remodeling.

Key words Arteriovenous fistula, Aortocaval fistula, Hemodialysis access, Animal model, Fistula maturation, Intraluminal drug delivery

1 Introduction

The number of patients with end-stage renal disease dependent on hemodialysis as renal replacement therapy continues to increase [1]. Arterial-venous fistulae (AVF) continue to be the most common access created for hemodialysis due to the lower rate of infection and thrombosis compared to prosthetic grafts and catheters. However, the one-year primary patency rates of AVF are only about 60% [2]; understanding the basic mechanisms of venous remodeling within the fistula environment is critical to improve our understanding of AVF maturation [3]. Veins adapting to the fistula environment may adapt in different ways than vein grafts adapting to the arterial environment, as the fistula has higher magnitudes and disturbed patterns of flow, lower pressure and lower resistance of the run-off vascular bed, as well as exposure to lower oxygen content in the mixed arterial and venous blood [4, 5].

To study venous remodeling in the context of an AVF, we have established a mouse aortocaval fistula model; this model has several advantages: First, unlike several models of AVF reported in larger animals, this mouse model capitalizes on the ability to use genetic

strains of mice to study human diseases. Second, this model uses manual pressure to achieve hemostasis without using sutures, which may cause the fistula occlusion, vessel stenosis and interference with subsequent molecular analysis. Third, this model can be adapted to easily deliver drugs intraluminally to the fistula endothelium at the same time as fistula creation [6]. Lastly, this simple model is easy to perform and master compared to the murine carotid to jugular AVF model using a perianastomotic cuff, a more technically demanding model [7].

A potential limitation of this model is that the AVF is made between the aorta and inferior vena cava (IVC); these are large central vessels, unlike the smaller peripheral vessels, such as the radial artery and cephalic vein, that are typically used for human vascular access. However, this model recapitulates the clinical course of human AVF maturation, including the development of early neointimal hyperplasia in approximately one-third of the cases [8]. Here we describe a method to create this model including its modification to use intraluminal drug delivery.

2 Materials

2.1 Anesthesia

Apparatus

1. Animal anesthesia machine including isoflurane vaporizer.
2. Induction chamber.
3. Inhalation mask and tube.

2.2 Surgical Tools

1. Dissecting microscope.
2. Micro forceps with teeth.
3. Surgical scissors.
4. Retractor.
5. Fine pointed forceps.
6. Micro clips.
7. Curved fine needle holder with lock.
8. 25 gauge needle (*see Note 1*).
9. 1 mL syringe.
10. Sterile cotton swabs.
11. Gauze.
12. 6-0 nonabsorbable sutures.
13. Saline.

3 Methods

3.1 Creating an Aortocaval Fistula in the Mouse

1. Anesthetize a C57BL/6 mouse, aged 8–10 weeks, with vaporized 2.5% isoflurane and 0.8 L/min oxygen administered into an acrylic induction chamber.
2. Remove the unresponsive mouse from the chamber. Confirm adequate anesthetization by lack of reaction to toe pinch. Place the mouse supine on the operation table and deliver vaporized 2.5% isoflurane by continuous inhalation with a silicone mask.
3. Ventral hair is removed from the neck to lower abdomen using a hair remover (*see Note 2*).
4. Make a midline abdominal incision from the level of the lower liver edge to just above the pubis.
5. Insert a retractor (Fig. 1a). Pull all of the bowels out of the abdominal cavity to the right side and wrap them with saline-soaked gauze. Pull the bladder and the seminal vesicles (in male mice) out to the caudal side (Fig. 1b) (*see Note 3*). Dissect the mesentery between rectum and retroperitoneum to obtain a full view of the aorta and IVC (Fig. 1c).

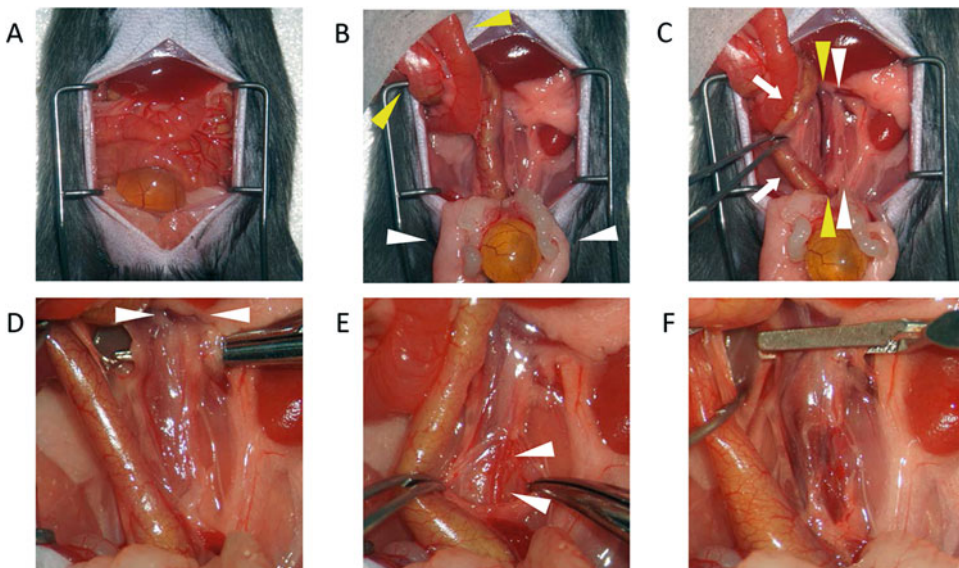


Fig. 1 Operative photos of creating an AVF in the mouse. (a) Insert a retractor after laparotomy. (b) Pull the bowel out to the right side (yellow arrowheads) and wrap them with a saline-soaked gauze. Pull the bladder and the seminal vesicles out to the caudal side (white arrowheads). (c) Dissect the mesentery of the rectum (white arrows) to obtain a full view of the aorta (white arrowheads) and IVC (yellow arrowheads). (d) Dissect the infrarenal aorta and IVC en bloc just below the left renal vein (white arrowheads). (e) Expose the puncture site of the aorta (white arrowheads) by dissecting surrounding tissues. (f) Clamp the infrarenal aorta and IVC en bloc

6. Dissect the infrarenal aorta and IVC en bloc from the surrounding retroperitoneal tissues to clamp them together (Fig. 1d) (*see Notes 4 and 5*).
7. Expose the puncture site of the aorta by dissecting surrounding tissues at approximately three-quarters of the distance from the left renal vein to the aortic bifurcation (Fig. 1e) (*see Notes 6–8*).
8. Bend a 25G needle to create a 45–60° angle approximately 4 mm from the needle tip (Fig. 2a). Grasp the needle with a curved needle holder (Fig. 2b) (*see Note 9*).
9. Clamp the infrarenal aorta and IVC en bloc with a single microsurgical clip (Fig. 1f) (*see Note 10*).
10. Grasp the connective tissue adjacent to the bifurcation and rotate the aorta medially and caudally so that the surface of the aorta is exposed and stretched slightly to the ventral side for the arterial puncture (*see Note 7*).
11. Keep the aorta in a rotated position and puncture through the aorta into the IVC using the 25G needle (Fig. 3a) (*see Note 11*).
12. Release the rotation and pull up the surrounding tissue from the left side of the aorta to cover the puncture site. Remove the needle and press the puncture site softly with a cotton-tipped swab for hemostasis (Fig. 3b) (*see Notes 12 and 13*).
13. Unclamp the aorta and IVC after confirmation of primary hemostasis. Upon declamping, light-colored arterial blood flowing into the IVC instead of dark-colored venous blood

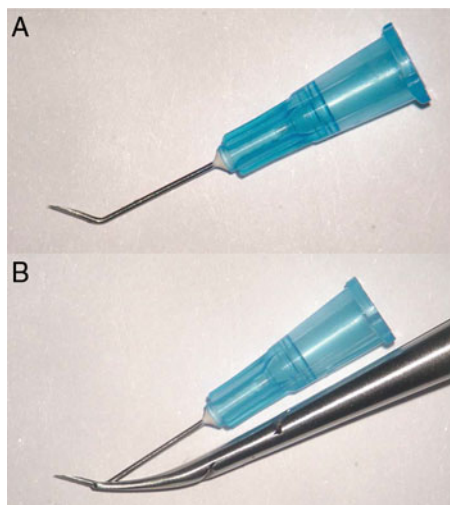


Fig. 2 (a) Bend a 25G needle to between a 45° and 60° angle approximately 4 mm from the needle tip. (b) Grasp the needle with a curved needle holder

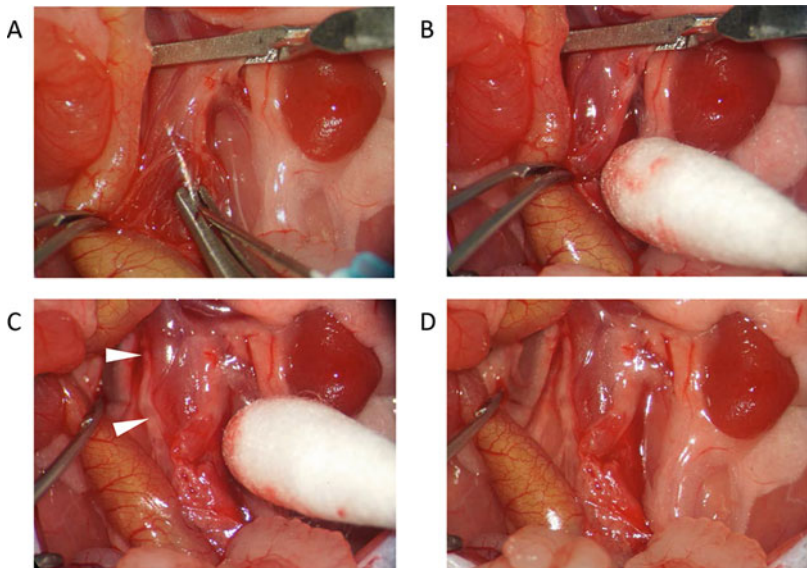


Fig. 3 Operative photos of creating an AVF in the mouse. **(a)** Puncture the aorta through into the IVC using the 25G needle. **(b)** Pull up the surrounding tissue from the left side of the aorta to cover the puncture site and press it softly with a cotton swab for hemostasis. **(c)** Unclamp the aorta and IVC. The change in color of IVC blood flow as well as dilated IVC can be observed (white arrowheads). **(d)** Confirm hemostasis

flow as well as a dilated IVC can be observed as proof of successful fistula creation (Fig. 3c) (*see Note 14*). Keep the puncture site covered for 1 additional minute to ensure hemostasis (Fig. 3d).

14. Return the organs to their natural position and close the abdomen with 6-0 sutures (*see Notes 15–18*).

3.2 Intraluminal Drug Delivery to the Mouse AVF

1. Repeat steps 1–7 in Subheading 3.1.
2. Dissect the aorta and IVC just below the aortic bifurcation from the surrounding tissues to prepare for distal clamping.
3. Repeat step 8 in Subheading 3.1
4. Attach a 1 mL syringe loaded with the drug to the 25G needle.
5. Place a single microsurgery clip across both the proximal aorta and the proximal IVC at the level just below the left renal vein (*see Note 19*). Place a second microsurgery clip across both the distal aorta and the distal IVC (*see Note 20*).
6. Repeat steps 10 and 11 in Subheading 3.1.
7. Keep holding the needle holder using the right hand and infuse the drug solution (100–200 μ L) using the left hand. Remain still and keep the position for up to 15 min.
8. Unclamp only the distal aorta and IVC.
9. Repeat steps 12–14 in Subheading 3.1.

4 Notes

1. 25 gauge needles are ideal for creating the fistula. We previously reported that using a 22 gauge needle increases postoperative mortality due to bleeding or acute cardiac failure and using a 28 gauge needle reduces postoperative patency [9].
2. Hair remover is preferred because hair that is left using a shaver may interfere with the postoperative ultrasound.
3. Cotton tipped swabs can be used to prevent injuries to the abdominal organs and to avoid bleeding.
4. Proximal clamping is enough to reduce the blood pressure. Distal clamping, which can interfere with the needle puncture, is not necessary.
5. Pay attention not to injure the small venous branches such as the lumbar veins during dissection of the proximal aorta and IVC. A caudal branch of the left renal vein can be included within the clamp if it is close to the left side of the aorta.
6. Do not puncture the aorta very proximally, or the fistula will not be completely established; the proximal portion of the infrarenal aorta is not closely attached to the IVC, with abundant connective tissue located between the two vessels.
7. The aorta needs to be rotated to obtain a front view of the puncture site, as puncturing the aorta straight into the IVC enables the fistula to mature quickly and to keep it patent. The aorta is positioned about 45° behind the IVC; hence the left side of the aorta must be adequately dissected posteriorly to allow rotation and exposure of the dorsal side of the IVC.
8. The crucial point of this model is not to dissect between the aorta and IVC.
9. Grasp the 25 gauge with a curved needle holder to maintain an optimal direction of the needle during puncture.
10. Clamp the proximal aorta and IVC en bloc without dissecting the connective tissue between them to avoid bleeding and prolonging the procedure. In addition, the dilated IVC, due to the proximal clamp, facilitates puncture into the IVC accurately.
11. Pay attention not to penetrate through the back wall of the IVC, which can be easily collapsed during puncture. The needle can be seen through the thin IVC wall in the case of successful puncture.
12. No suture is used to repair the arteriotomy; gentle pressure is applied for hemostasis in this model, which makes it more reproducible. Press the puncture site only to keep the surrounding tissues closely attached, but do not compress the

aorta against the IVC as it may lead to occlusion of the fistula. The appropriate degree of pressure to apply is part of the procedure learning curve.

13. Removal of the needle while compressing the puncture site can reduce bleeding.
14. Persistent light-colored arterial flow or pulsatile flow with alternate arterial and venous flows can be seen when the fistula is created successfully.
15. The average total procedure time is approximately 20 min.
16. After anesthesia terminates, the mouse is typically able to ambulate within about 15 min. Postoperatively, analgesia is given, and general status monitoring includes daily observation of wound healing, activity, and mobility.
17. Doppler ultrasound is performed post operatively to assess AVF patency and morphology, and blood flow in the aorta and IVC. The waveform of blood flow within the abdominal aorta proximal to the AVF is a clear indicator of AVF patency; a patent AVF shows sustained high diastolic flow (Fig. 4a), whereas an occluded AVF shows normal triphasic arterial waveforms (Fig. 4b).

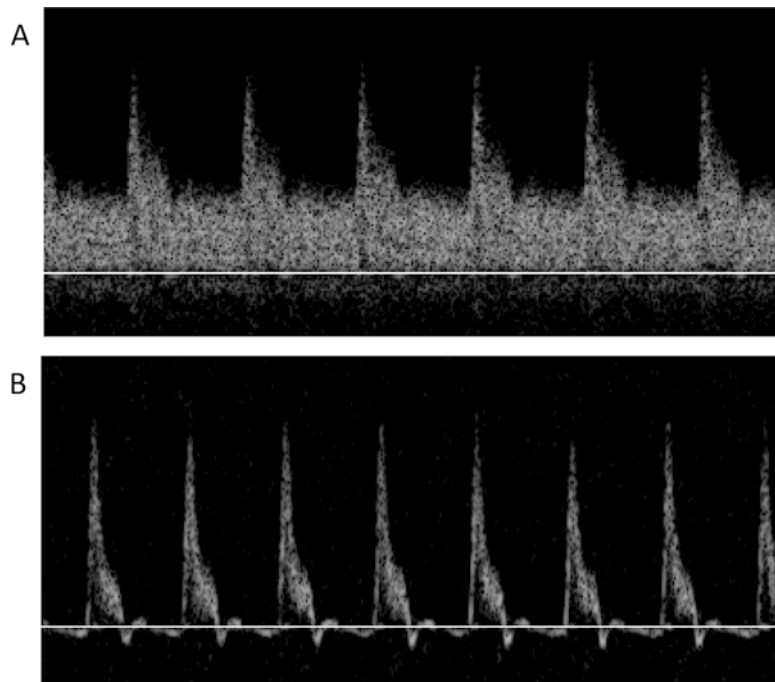


Fig. 4 Doppler analysis of the proximal abdominal aorta with a patent AVF shows sustained high diastolic flow (a), whereas that with an occluded AVF shows a normal triphasic arterial waveform (b)

18. Postoperative hemorrhage or acute heart failure may lead to early death within 24 h after surgery, whereas pulmonary embolism or limb ischemia with thrombosis potentially cause death after postoperative day 1; the survival rate on postoperative day 7 is approximately 90%. AVF technical success is confirmed on postoperative day 3, as a patent AVF on day 3 predicts persistence of the AVF at least until about day 21; the rate of AVF technical success on day 3 is approximately 70% [4].
19. The location of proximal clamping of the aorta and IVC can be modified to be just distal to the large lumbar veins that typically arise from the upper portion of the infrarenal IVC; excluding these lumbar veins will minimize drug dilution due to retrograde blood inflow as well as prevent drug loss from outflow, and thus promote efficient administration of the drug.
20. The micro clip that is used for clamping the distal aorta and IVC is inserted from the right side just below the aortic bifurcation so that it does not interfere with the needle puncture.

Acknowledgments

This work was supported in part by the National Institutes of Health Grant R01-HL128406 and the Merit Review Award I01-BX002336 from the United States Department of Veterans Affairs Biomedical Laboratory Research and Development Program, as well as through the resources and the use of facilities at the Veterans Affairs Connecticut Healthcare System (West Haven, CT).

References

1. Pisoni RL, Zepel L, Port FK, Robinson BM (2015) Trends in US vascular access use, patient preferences, and related practices: an update from the US DOPPS practice monitor with international comparisons. *Am J Kidney Dis* 65 (6):905–915. <https://doi.org/10.1053/j.ajkd.2014.12.014>
2. Gibson KD, Gillen DL, Caps MT, Kohler TR, Sherrard DJ, Stehman-Breen CO (2001) Vascular access survival and incidence of revisions: a comparison of prosthetic grafts, simple autogenous fistulas, and venous transposition fistulas from the United States Renal Data System Dialysis Morbidity and Mortality Study. *J Vasc Surg* 34(4):694–700. <https://doi.org/10.1067/mva.2001.117890>
3. Hu H, Patel S, Hanisch J, Santana J, Hashimoto T, Bai H, Kudze T, Foster T, Guo J, Yatsula B, Tsui J, Dardik A (2016) Future research directions to improve fistula maturation and reduce access failure. *Semin Vasc Surg* 29 (4):153–171. <https://doi.org/10.1053/j.semvascsurg.2016.08.005>
4. Yamamoto K, Li X, Shu C, Miyata T, Dardik A (2013) Technical aspects of the mouse aortocalval fistula. *J Vis Exp* 77:e50449. <https://doi.org/10.3791/50449>
5. Lu DY, Chen EY, Wong DJ, Yamamoto K, Prostak CD, Williams WT, Assi R, Hall MR, Sadaghianloo N, Dardik A (2014) Vein graft adaptation and fistula maturation in the arterial environment. *J Surg Res* 188:162–173. <https://doi.org/10.1016/j.jss.2014.01.042>
6. Hashimoto T, Yamamoto K, Foster T, Bai H, Shigematsu K, Dardik A (2016) Intraluminal drug delivery to the mouse arteriovenous fistula

- endothelium. *J Vis Exp* 109:e53905. <https://doi.org/10.3791/53905>
7. Castier Y, Lehoux S, Hu Y, Foteinos G, Tedgui A, Xu Q (2006) Characterization of neointima lesions associated with arteriovenous fistulas in a mouse model. *Kidney Int* 70(2):315–320. <https://doi.org/10.1038/sj.ki.5001569>
8. Yamamoto K, Protack CD, Tsuneki M, Hall MR, Wong DJ, Lu DY, Assi R, Williams WT, Sadaghianloo N, Bai H, Miyata T, Madri JA, Dardik A (2013) The mouse aortocaval fistula recapitulates human arteriovenous fistula maturation. *Am J Physiol Heart Circ Physiol* 305 (12):H1718–H1725. <https://doi.org/10.1152/ajpheart.00590.2013>
9. Yamamoto K, Protack CD, Kuwahara G, Tsuneki M, Hashimoto T, Hall MR, Assi R, Brownson KE, Foster TR, Bai H, Wang M, Madri JA, Dardik A (2015) Disturbed shear stress reduces Klf2 expression in arterial-venous fistulae in vivo. *Phys Rep* 3. <https://doi.org/10.14814/phy2.12348>

Part VI

Large Animal Models



Chapter 22

A Pig Model of Myocardial Infarction: Catheter-Based Approaches

Olympia Bikou, Shin Watanabe, Roger J. Hajjar, and Kiyotake Ishikawa

Abstract

Despite enormous efforts in treating myocardial infarction (MI) and subsequent heart failure, the recent statistics from the American Heart Association evidently show that there still remains room for improvements. To develop and translate new therapeutics toward clinics, large animal models that allow us to test new therapies in human-like conditions are of extraordinary importance. In this chapter, we describe detailed protocols for the creation of a closed-chest MI model in pigs. The advantages of this model include high survival rate (>90% after ischemia–reperfusion), adjustable MI size depending on coronary occlusion site, reproducible cardiac dysfunction, and relatively low invasive method. The temporary coronary occlusion method for ischemia–reperfusion injury as well as the permanent occlusion method, using clot injection or embolic coil implantation, are described. Furthermore, we describe the key steps needed for understanding, performing, and analyzing cardiac angiography and echocardiography in pigs.

Key words Myocardial infarction in pigs, Heart failure model, Ischemia–reperfusion, Embolic coil, Permanent coronary occlusion, Thrombus, Cardiac angiography in pigs, Echocardiography in pigs, Large animal

1 Introduction

Heart failure (HF) is a clinical syndrome, caused by a variety of causes [1]. According to the recent Statistics Update of the American Heart Association, the American adults affected by HF increased from 5.7 million in 2009–2012 to 6.5 million in 2011–2014 and the number of patients diagnosed with HF is expected to rise further by 2030 [2]. The increasing HF prevalence can be explained by the aging of the population on the one hand and by the better outcome of acute ischemic heart disease on the other hand. Therapeutics targeting patients suffering from an acute myocardial infarction (MI) have been progressively improving. This resulted in a higher survival rate after MI and increased risk of HF at the chronic stage [3].

Hence, ischemic heart disease continues to be one of the most common causes of clinical HF. Current clinically available treatments slow the progression of HF, but new therapies are desperately needed to protect or repair the heart from progressive detrimental processes associated with cardiac ischemia [4]. Animal models are essential in achieving this goal: animal models of HF allow us to identify novel mechanisms and new potential therapeutic targets. Once promising therapeutics have been identified, experiments using large animal models of HF will be necessary before translating them into humans. In addition, large animal models of HF allow for testing of clinical imaging modalities and clinical size devices.

In this chapter, we describe detailed protocols for creating a pig model of MI using catheter-based approaches. Advantages of this closed-chest MI model include high survival rate (>90% after ischemia–reperfusion), adjustable MI size depending on coronary occlusion site, reproducible cardiac dysfunction, and relatively low invasive method. Avoiding open chest surgery allows for easier and less traumatic access to the heart, and prevents surgery-associated adhesions and inflammations [5]. We describe the key steps needed for understanding, performing, and analyzing cardiac angiography and interventions as well as echocardiography in pigs. As for any clinical intervention, the investigator should be well familiar with the equipment used, anatomy of the heart and related structures as well as the potential perioperative complications and their managements.

2 Materials

2.1 Equipment

1. Swine (*see Note 1*).
2. Veterinary anesthesia ventilator suitable for large animals.
3. Syringe pumps for continuous infusion of fluids and anesthetics.
4. Vital monitors: electrocardiogram (ECG), ECG electrodes, conductive gel, pulse oximeter, capnography, pressure sensors.
5. Cardiac defibrillator.
6. Standard catheterization pack: syringes, needles, gauzes, bowls.
7. 6 Fr or larger sheaths.
8. 6 Fr or larger guiding catheters (*see Note 2*).
9. 0.035 inch wire.
10. 0.014 inch wire.
11. Coronary occlusion balloon (*see Note 3*).
12. Angiographic contrast.

13. Injection manifold.
14. Y-connector.
15. Embolic coil.
16. Disinfectants.
17. Heating mat.
18. Thermo blanket.
19. C-arm.
20. Echocardiography.

2.2 Drugs

1. Telazol (tiletamine/zolazepam).
2. Buprenorphine.
3. Propofol.
4. Antibiotics: cefazoline.
5. Atropine.
6. Amiodarone.
7. Furosemide.
8. Nitroglycerine.
9. Heparin.
10. Protamine.
11. Lidocaine.
12. Magnesium.
13. Pre-MI infusion solution: 0.9% sodium chloride solution 1,000 mL, amiodarone 3 mg/kg, potassium acetate 20 mEq, atropine 0.1 mg/kg (*see Note 4*).
14. Post-MI infusion solution: 0.9% sodium chloride solution 500 mL, amiodarone 3 mg/kg, potassium acetate 20 mEq.

3 Methods

3.1 Preparation and Anesthesia

1. Fast the animal overnight. Provide free access to water.
2. Induce anesthesia by intramuscular administration of 6.0 mg/kg Telazol (tiletamine/zolazepam). Administer pain medication (e.g., buprenorphine 0.03 mg/kg). Buprenorphine at higher dosages is effective for 8–12 h.
3. Transfer the animal to the preparation area and apply oxygen.
4. Monitor peripheral oxygen saturation and heart rate (pulse) continuously.
5. Intubate the pig and obtain a peripheral venous access.
6. Connect the tracheal tube to the ventilator. Shave the proximal part of the legs, in order to place the ECG electrodes. Apply gel

on the electrodes and tape them on the legs. This enables artefact-free monitoring, which is important for arrhythmia detection during coronary balloon occlusion.

7. Administer intramuscular prophylactic antibiotics (e.g., cefazoline, 25 mg/kg).
8. Transfer the animal to the surgical suite and connect to the ventilator. Intra-tracheal pressure should not exceed >20 mmHg continuously to prevent lung injury. End-respiratory CO₂ measurement is recommended to adjust the tidal volume and ventilation rate.
9. Maintain anesthesia using propofol (*see Note 5*). Heating pad should be placed under the animal to maintain body temperature during the procedure.
10. Pulse oximetry, ECG, heart rate and blood pressure monitoring should take place throughout the procedure.
11. Start intravenous saline infusion (body weight [kg] × 5–10 mL) to correct dehydration from overnight fasting (*see Note 6*).

3.2 Baseline Cardiac Assessment with Echocardiography

It is a good practice to conduct pre-MI echocardiography to screen for cardiac abnormalities and to evaluate the impact of MI. In order to acquire optimal images with echocardiography, it is essential to understand the anatomy of the pig heart. Compared to the human, the thoracic cavity of the pig is more “oval” in the anterior-posterior direction, basically because of the different standing posture. Also, the apex is placed more medial compared to the human. Fasting the animal as well as avoiding the excessive tidal volume is important to obtain good images of the heart.

1. Place the animal in the right lateral decubitus position (left side up). Apply sufficient amount of ultrasound gel on the chest (*see Notes 7 and 8*).
2. For the apical view, place the transducer substernal. An apical four-chamber view can be displayed (Fig. 1). For the apical three-chamber view, turn the transducer approximately 90° and side tilt slightly. Acquire and save the images for further offline analysis. Use the colour Doppler over the mitral and aortic valve to check regurgitation.
3. For evaluating the diastolic performance, use pulsed wave (PW) Doppler placed at the tips of the mitral valve in the left ventricle. The following flow velocities can be seen during LV diastole (sinus rhythm): the E-wave, representing the early passive filling of the ventricle, and the A-wave, which happens late in diastole, representing the atrial contraction.
4. Slow wall velocities can be assessed with Tissue Doppler Imaging (TDI). Place the PW-TDI sample volume at the level of the lateral mitral annulus. Note that septal wall will be infarcted at

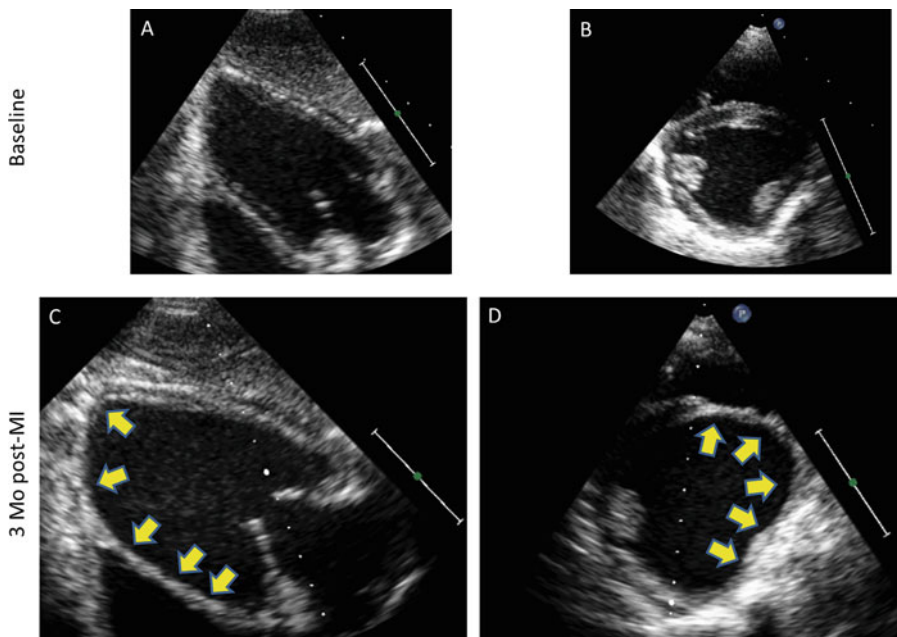


Fig. 1 Representative echocardiographic images before and 3 months after MI creation. **(A, B)** Before MI and **(C, D)** 3 months after MI creation. Note the remodeling of the left ventricle (ventricular dilation and thinning of the ventricular walls [arrows]), as well as enlargement of the left atrium. These are associated with decreased systolic function. **(A and C)** Apical longitudinal view. **(B and D)** Parasternal short axis view. Bars represent 5 cm

the time of follow-up. A systolic and two diastolic waves (E' : passive ventricle filling and A' : atrial contraction) will be displayed. The end-diastolic pressure can be estimated using these parameters.

5. Valve flow and function can be studied using colour Doppler over the aortic and the mitral valve, PW and continuous wave (CV) Doppler over the aortic and the mitral valve. For assessing trans-valvular flow, calculate the velocity time integral (VTI) by delineating the PW Doppler profiles.
6. For parasternal view, turn the pig to the left lateral decubitus position, right side up. Place the transducer at the third to fourth intercostal space. Following measurements can be obtained with parasternal view: LV outflow tract diameter, left atrial diameter, standard M-mode LV measurements, and short axis images.
7. For obtaining parasternal short axis view, turn the transducer 90° clockwise from the longitudinal view and tilt upward. If the image is suboptimal, try another intercostal space. Acquire LV images at the apical, papillary muscle, and basal levels (Fig. 1).

3.3 Induction of Myocardial Infarction

1. After completing the echocardiographic examination, start pre-MI infusion solution (300 mL/h) and intravenously administer following drugs before MI induction: amiodarone 1–3 mg/kg, atropine 0.1 mg/kg.
2. Place the swine in the dorsal position. Tie the legs loosely to the table, so that the animal is secured. Before the puncture, hind legs are tightly pulled caudolateral to stretch the vessels for preventing the vessel escape from the needle.
3. Clean and disinfect the groin area and apply some ultrasound gel. Place the vascular ultrasound probe on the skin proximal to the planned puncture site (*see Notes 9 and 10*).
4. Under ultrasound guidance, advance the needle. Correct the needle position based on the ultrasound image. Puncture the artery using a modified Seldinger's technique. Enter the skin at a 45° angle and make it lean during the pull back. Ensure good pulsatile blood flow before entering the wire.
5. Enter a J-Tip guide wire (*see Note 11*).
6. Exchange the puncture needle to arterial vascular sheath. Before inserting the sheath, make a skin incision large enough for the sheath to easily go through the skin layer (*see Note 12*).
7. Draw some blood for further analysis or thrombus injection (*see below Subheading 3.3, step 20a*) if necessary and administer heparin (200–300 IU/kg) intravenously. The activated coagulation time should be >250 s.
8. Make a small suture to secure the sheath in place. This prevents sheath dislodge during defibrillation in case of arrhythmias during coronary balloon occlusion.
9. Loosen the ropes that are tightly holding the hind legs.
10. For the right coronary artery angiogram: advance a 4 or 5 Fr coronary catheter to the ascending aorta with 0.035 inch wire guidance (*see Note 13*). Pull back the guide wire inside the catheter for 5–10 cm and rotate the catheter counterclockwise for engaging it to the right coronary artery (*see Note 14*).
11. Once the catheter is engaged to the coronary artery, remove the wire and connect to the injection manifold. Remove air inside the catheter and check the pressure (*see Notes 15 and 16*). Inject the contrast slowly while imaging the coronary with X-ray for test shot. Take an angiographic cine to obtain clear images of the right coronary artery in different views (*see Note 17*).
12. For the left coronary artery angiogram: pull back the catheter and exchange to the catheter for left coronary artery angiogram. Hockey stick catheter and sometimes JR (long tip) catheters can be used both for right and left coronary

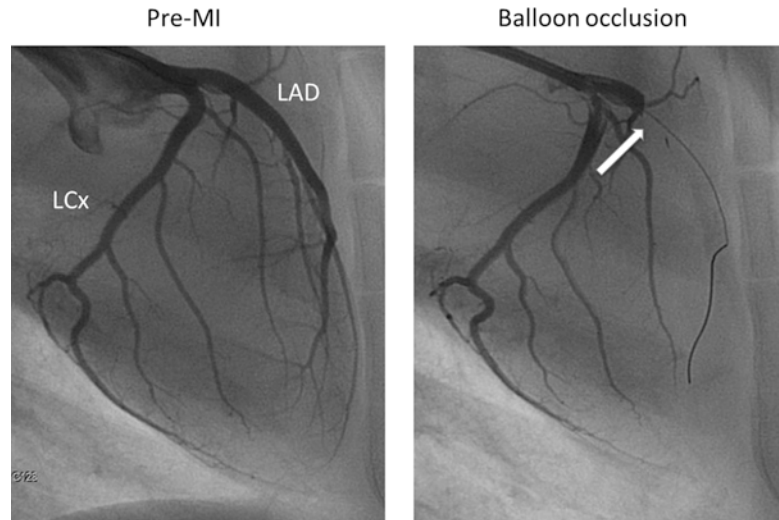


Fig. 2 Representative angiographic images before and during MI creation with balloon occlusion. (Left) Left coronary angiogram showing the LAD and LCx before balloon occlusion and (Right) during balloon occlusion. The arrow indicates the balloon position. *LAD* Left anterior descending artery, *LCx* Left circumflex artery

angiograms. Advance the catheter with 0.035 inch wire guidance to the ascending aorta and remove the wire. Connect the catheter to the manifold and flush. Check the pressure wave and adjust the position if the pressure wave is not normal (*see Note 15*). Rotate clockwise and engage the catheter to the left coronary artery ostium. Take an angiographic cine to obtain clear images of the left coronary artery in different views (*see Note 18* and Fig. 2).

13. Once the reference angiogram images are taken, evaluate the size of the target coronary artery and prepare a coronary balloon for occlusion. A balloon size that is $\times 1.2\text{--}1.5$ of the target coronary artery segment may be appropriate (*see Note 19* and Fig. 2).
14. Switch the catheter system to 6 or 7 Fr for inducing MI. Proceed the catheter with 0.035 inch wire guidance. Repeat Subheading 3.3, step 12.
15. Once the catheter is engaged to the left coronary artery, insert the balloon with 0.014 inch wire inside. Advance the balloon to the tip of the catheter and advance the 0.014 inch wire first, followed by the balloon while holding the wire (*see Note 20*).
16. Take cine images to confirm the location of the balloon. The balloon can occlude the side branch just next to the proximal marker as it also expands longitudinally. Place it at least

1 marker distal to the branch that should not be occluded (*see Note 21*).

17. Inflate the balloon (3–6 atm) at the desired location. Take a cine angiogram to confirm total occlusion. Pull back the guide catheter to disengage it from the left coronary ostium during MI, while pushing the balloon catheter to prevent it from pulling (*see Note 22*). Flush the catheter for pressure monitoring.
18. Monitor ECG and pressure continuously. Consider reducing propofol (*see Note 23*). Always be ready to use the external defibrillator after inflating the balloon and use appropriately as soon as the pig develops fatal arrhythmias (*see Notes 24 and 25*).
19. For ischemia–reperfusion injury: deflate the balloon and reperfuse after desired time (*see Note 26*).
20. For permanent occlusion: either clot injection through the balloon lumen or embolic coil implantation after reperfusion can be used.
 - (a) For clot injection, blood sample should be drawn before heparin injection and kept in glass tube. Take 1 cm³ cube thrombus and mix with 3 mL of contrast. Use a three way connector and crush the thrombus into small particles by rigorously pushing the mixture back and forth between the syringes. Inject 1 mL of this mixture into the coronary wire lumen before reperfusion (*see Note 27*). Slowly deflate the balloon after 3 min and check the coronary flow.
 - (b) For embolic coil implantation, deflate the balloon and withdraw the system. Use a 4 Fr coronary catheter and engage the left coronary artery as described in Subheading 3.3, step 12. Insert a 0.014 inch wire into the catheter and advance it to the artery that has been occluded. After the wire is deeply inserted into the target artery, advance the 4 Fr coronary catheter by gentle rotation and push while holding the wire. Advance the catheter to the distal of balloon-occluded site. Remove the wire and insert embolic coil into the catheter. Push the coil with 0.035 inch wire into the coronary artery. Remove the catheter once the coil is implanted, and perform angiogram if necessary (*see Note 28*).
21. Remove the sheath after stable hemodynamic status is established (*see Note 29*).
22. Recover the animal under continuous monitoring. Use a thermo blanket to maintain temperature. Apply furosemide 2.5 mg/kg and nitroglycerine 0.2 mg/kg for preventing

acute congestive heart failure. Apply postprocedural analgesics (e.g., buprenorphine, 0.03 mg/kg). Keep the animal well oxygenated (*see Note 30*).

23. After extubation of the pig, administer post-MI infusion solution 20 mL/h over 8 h.
24. Check animal health status daily. The majority of deaths occur within 24 h after MI. Mortality 48 h after MI is very low for this ischemia–reperfusion model. In our hands, survival rate for ischemia–reperfusion models is over 90%. In permanent occlusion models, pigs have higher mortality associated with arrhythmia. They can develop ventricular tachycardias after MI. Therefore ECG should be examined if the pigs develop any symptoms (*see Note 31*).

4 Notes

1. We have been able to catheterize animals over 9 kg by inserting 6 Fr sheath and using 5 or 6 Fr systems. However, the survival after the MI induction may be low in too young pigs. Regarding the pig breed, Hare group has reported that mini pigs are less tolerant to MI compared to the Yorkshire pigs. Therefore they induce a smaller infarct in mini pigs [6]. While we do not have experience in other species, same techniques can be applied for sheep. Dogs are known to have inherent collaterals between the coronary arteries, thus inducing reproducible MI with percutaneous approaches may be challenging.
2. Coronary balloons can be inserted through 4–5 Fr catheters, but continuous monitoring of the pressure through the catheter becomes difficult when the balloon catheter tightly fits in the guiding catheter. Optimal guiding catheter shape depends on size of the animal, access site, pig anatomy, and operator's preference. We use Hockey stick catheters in 20–30 kg pigs from femoral access. Different catheter types should be available in the lab for pigs with unique coronary anatomy.
3. The size of the coronary balloon depends both on the size and the occlusion site of the coronary artery and should be chosen accordingly. We use 3.5–4.0 mm short balloons (8 mm) for proximal LAD and LCx occlusions and 3.0–3.5 mm short balloons for mid LAD occlusions. Since the balloon pressure remains low (3–6 atm) during the occlusion, we use noncompliant balloons to prevent balloon slippage during defibrillation.
4. Preventing low potassium during and post-MI is important for reducing arrhythmias.

5. In our experience, propofol 10 mg/kg/h is necessary and sufficient for sedating naive Yorkshire pigs. Sick animals should receive reduced dose.
6. Hypovolumic condition during MI will result in low blood pressure. It is important to administer sufficient amount of fluid intravenously before inducing MI.
7. After initial setup, wait until the vital signs become stable. In order to have valid and reproducible results, pigs should not have tachycardia.
8. The thorax of the pig is more oval compared to the human, which sometimes makes the acquisition of clear images a challenge. Pig positioning is critical for acquiring good images: make the spine of the pig more “round,” by placing all four legs and the head close to each other. Image acquisition is optimized using brief periods of breath hold (<5 s).
9. The femoral artery runs in the femoral canal. The femoral canal is located between the *muscle sartorius* and the *muscle gracilis*. The femoral canal houses the nerve, the vein and the artery. The artery is located at the lateral part of the canal. The relationship between artery, nerve, and vein can be easily memorized by remembering VAN (vein, artery, nerve) from medial to lateral [7]. Because the palpation of the femoral pulse is very difficult to sense in swine, the anatomical landmarks are important for the orientation. The optimal location for the femoral artery puncture is best assessed with ultrasound. Over the years we observed less complications compared to the “blind” puncture technique.
10. Depending on the location, the vein can be found medial to the artery or beneath (more proximal). The artery has thicker wall compared to the veins. When applying pressure with the vascular ultrasound probe, veins can be easily flattened. Applying colour Doppler also helps distinguishing the vessels.
11. Never push the wire or the sheath against resistance. In case there is resistance while pushing the wire, pull out both the needle and the wire to prevent large vessel dissection and apply manual pressure to stop bleeding. The wire can easily dissect the artery and lead to occlusion of the vessel (*see below*).
12. Relevant complications in swine from the femoral artery punctures include:
 - (a) Dissection of the femoral artery: If the sheath is already placed, leave it until the end of procedure to prevent bleeding during balloon occlusion. Heparin can aggregate bleeding even if it stops once after the sheath removal. While most of the pigs stay asymptomatic in a case of femoral dissection, some do develop symptoms.

Examine the pig daily post procedure and adjust the medication accordingly.

- (b) Complete occlusion from thrombosis: Multiple failures of arterial puncture can result in complete thrombus occlusion. This may resolve as the time passes, but punctures to the other side should be performed by a well-experienced operator or with cut-down to secure an arterial access.
- 13. Wire should be always preceded first instead of the catheter to prevent vascular complications. This diagnostic angiogram can be skipped, but obtaining reference coronary angiogram for both right and left coronary arteries will improve estimation of infarct size.
- 14. From the femoral access, JR or Hockey stick catheters provide easy targeting of the right coronary artery: turn the catheter counterclockwise. Keeping the 0.035 wire inside the catheter facilitates catheter manipulation as it will serve as a core of the catheter. In pigs, the right coronary artery takeoff is slightly higher (more distal to the heart) than humans.
- 15. From wire removal to test injection is a set of manipulation that should always be performed after changing the catheter. Make sure by visual inspection that the air is removed from the system before injection. Do not inject anything if the pressure wave is not normal. In this case first, identify the problem. In most of the cases, the reason is one of the following: (1) catheter is wedging a small branch; (2) catheter is kinked; (3) air or thrombus is inside the catheter or tubes; (4) tube/catheter/manifold connection is loose.
- 16. For the right coronary artery, catheter can be engaged too deep in the coronary, and wedge the sinuatrial nodal branch. In this case, slowly clockwise and slightly pull back the catheter. Air injection can result in embolic infarction. In case the air was injected, administer multiple rapid saline injections into the coronary artery. This will dissolve air in many occasions.
- 17. In pigs, the right coronary artery is usually small and cranial views provide little information. RAO 90° and LAO 30° (or AP view) would provide sufficient information.
- 18. Depending on the planned occlusion location, optimal views are different. With RAO 90°, proximal part of the left coronary artery and circumflex artery can be separated well, i.e., left main bifurcation (proximal LAD and LCx). In contrast, LAO 30° is useful for seeing the mid to distal part of the LAD. Different angles should be examined until the operator understands the coronary circulation, especially for the targeting vessel. We use Hockey stick catheters for 20–40 kg pigs, but other catheters can be used as well. We have experienced more incidence of coronary dissection with the Amplatz type catheters, so very

soft tip catheters should be chosen for Amplatz type catheters in pigs.

19. Balloons that are too large can result in coronary dissection and chronic total occlusion. In contrast, small balloons may not completely occlude the artery and can minimize infarct size.
20. For targeting the LAD, rotate the catheter clockwise and for the LCx, slightly counterclockwise. Rotating the catheters too much will disengage the catheter. Always monitor the pressure. The wire should be inserted deeply so that balloon insertion can be facilitated and also the system position is stable during MI.
21. Precise placement of the balloon before inflation is critical to have reproducible infarct size. Repeated inflation–deflation can result in preconditioning of the heart and reduce infarct size significantly.
22. This will prevent blocking of the flow to nonoccluded coronary arteries.
23. Drug metabolism significantly reduces when the cardiac function decreases. Therefore, continuous 10 mg/kg/h propofol may sometimes lead to delayed recovery.
24. Severe hypotension can lead to more arrhythmic events. Try to maintain systolic aortic pressure of >60 mmHg. Low-dose phenylephrine infusion is recommended. Epinephrine usually leads to increased arrhythmias.
25. Immediate rhythm conversion is the key for successful model induction. Repeat defibrillation until the conversion is successful. During the recharging, chest compression should be performed to maintain systemic (including the heart) perfusion. Pressure monitoring is useful for evaluating the efficacy of chest compression. In pigs, compression should be done by pumping both lateral sides of the chest. Amiodarone, lidocaine, and magnesium may be considered if the arrhythmia is uncontrollable. Balloon location should be checked in these cases to determine if there was a dislocation of the balloon.
There are two peaks of arrhythmia events in Yorkshire pigs: 5–10 min and 25–35 min. Even if very frequent arrhythmias occur, pigs become rhythm-stable after 35 min in the majority of cases. Since early balloon deflation will lead to significantly less scar size, resuscitation should be continued until this arrhythmia surge has passed. Beta-blockers may be given to reduce the number of arrhythmias, but in this case the final infarct size may be reduced as well.
26. In our experience, at least 90 min occlusion is necessary for reproducible infarct induction. With shorter duration of occlusion, we found that some pigs have very small (less transmural)

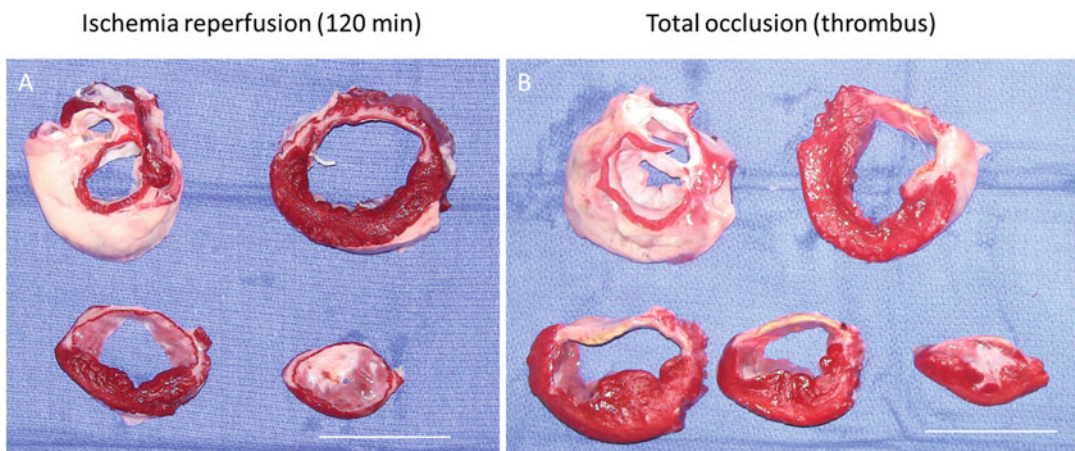


Fig. 3 Cross sections of the left ventricle after MI creation. The hearts are stained with triphenyl tetrazolium chloride to delineate the scar. **(A)** Left ventricular sections of a heart after MI creation by ischemia–reperfusion (temporary occlusion for 120 min). The heart is from the same pig shown in Fig. 1. **(B)** Left ventricular sections 2 months after permanent occlusion. Note the more transmural scar. Bars represent 5 cm

infarct, whereas others have almost semitransmural large infarct. Extending the occlusion time leads to increased transmurality of the infarct. Nevertheless, after reperfusion, we usually find a thin layer of viable myocardium in both endocardium and epicardium even with 120 min occlusion (Fig. 3).

27. This approach allows for transmural infarct induction with open coronary artery at the chronic stage (Fig. 3). Injection needs to be performed through the balloon lumen to prevent thrombus backflow to the nontarget branch or to the systemic circulation.
28. Remaining flow will diminish by thrombus formation as long as the coil is placed correctly inside the coronary artery. Make sure that the coil is placed distal to the occlusion site. Placing the coil proximal to the balloon occlusion site induces additional infarction and can lead to arrhythmia events during and after the recovery. For the same reason, implanting an embolic coil without preceding balloon occlusion is not recommended, since arrhythmias can occur without adequate monitoring.
29. Protamine can be used to facilitate hemostasis. Do not remove sheath while the pig is developing frequent arrhythmias.
30. Hypoxia increases incidence of arrhythmias.
31. Active infarct healing takes place for 4–6 weeks. When the embolic coil is placed, the healing takes longer.

Acknowledgments

This work is supported by NIH R01 HL139963 (K.I.), HL117505, HL 119046, HL129814, 128072, HL131404, HL135093, a P50 HL112324 (R.J.H.), AHA-SDG 17SDG33410873 (K.I.), and two Transatlantic Fondation Leducq grants. We would like to acknowledge the Gene Therapy Resource Program (GTRP) of the National Heart, Lung, and Blood Institute, National Institutes of Health. O.B. was supported by the Deutsche Herzstiftung.

References

1. Jessup M, Brozena S (2003) Heart failure. *N Engl J Med* 348(20):2007–2018. <https://doi.org/10.1056/NEJMra021498>
2. Benjamin EJ, Blaha MJ, Chiue SE, Cushman M, Das SR, Deo R, de Ferranti SD, Floyd J, Fornage M, Gillespie C, Isasi CR, Jimenez MC, Jordan LC, Judd SE, Lackland D, Lichtman JH, Lisabeth L, Liu S, Longenecker CT, Mackey RH, Matsushita K, Mozaffarian D, Mussolini ME, Nasir K, Neumar RW, Palaniappan L, Pandey DK, Thiagarajan RR, Reeves MJ, Ritchey M, Rodriguez CJ, Roth GA, Rosamond WD, Sasson C, Towfighi A, Tsao CW, Turner MB, Virani SS, Voeks JH, Willey JZ, Wilkins JT, Wu JH, Alger HM, Wong SS, Muntner P, American Heart Association Statistics Committee and Stroke Statistics Subcommittee (2017) Heart disease and stroke statistics-2017 update: a report from the American Heart Association. *Circulation* 135(10): e146–e603. <https://doi.org/10.1161/CIR.000000000000485>
3. Houser SR, Margulies KB, Murphy AM, Spinale FG, Francis GS, Prabhu SD, Rockman HA, Kass DA, Molkentin JD, Sussman MA, Koch WJ, American Heart Association Council on Basic Cardiovascular Sciences, Council on Clinical Cardiology, Council on Functional Genomics and Translational Biology (2012) Animal models of heart failure: a scientific statement from the American Heart Association. *Circ Res* 111 (1):131–150. <https://doi.org/10.1161/RES.0b013e3182582523>
4. Lecour S, Botker HE, Condorelli G, Davidson SM, Garcia-Dorado D, Engel FB, Ferdinand P, Heusch G, Madonna R, Ovize M, Ruiz-Meana M, Schulz R, Sluijter JP, Van Laake LW, Yellon DM, Hausenloy DJ (2014) ESC working group cellular biology of the heart: position paper: improving the preclinical assessment of novel cardioprotective therapies. *Cardiovasc Res* 104 (3):399–411. <https://doi.org/10.1093/cvr/cvu225>
5. Galvez-Monton C, Prat-Vidal C, Diaz-Guemes I, Crisostomo V, Soler-Botija C, Roura S, Llucia-Vallduperas A, Perea-Gil I, Sanchez-Margallo FM, Bayes-Genis A (2014) Comparison of two preclinical myocardial infarct models: coronary coil deployment versus surgical ligation. *J Transl Med* 12:137. <https://doi.org/10.1186/1479-5876-12-137>
6. McCall FC, Telukuntla KS, Karantalis V, Suncion VY, Heldman AW, Mushtaq M, Williams AR, Hare JM (2012) Myocardial infarction and intramyocardial injection models in swine. *Nat Protoc* 7(8):1479–1496. <https://doi.org/10.1038/nprot.2012.075>
7. Bangalore S, Bhatt DL (2011) Femoral arterial access and closure. *Circulation* 124(5): e147–e156. <https://doi.org/10.1161/CIRCULATIONAHA.111.032235>



Chapter 23

Ovine Model of Ischemic Mitral Regurgitation

Dae-Hee Kim, Brittan Morris, J. Luis Guerrero, Suzanne M. Sullivan, Judy Hung, and Robert A. Levine

Abstract

Ischemic mitral regurgitation (IMR) is a common complication of ischemic heart disease that doubles mortality after myocardial infarction and is a major driving factor increasing heart failure. IMR is caused by left ventricular (LV) remodeling which displaces the papillary muscles that tether the mitral valve leaflets and restrict their closure. IMR frequently recurs even after surgical treatment. Failed repair associates with lack of reduction or increase in LV remodeling, and increased heart failure and related readmissions. Understanding mechanistic and molecular mechanisms of IMR has largely attributed to the development of large animal models. Newly developed therapeutic interventions targeted to the primary causes can also be tested in these models. The sheep is one of the most suitable models for the development of IMR. In this chapter, we describe the protocols for inducing IMR in sheep using surgical ligation of obtuse marginal branches. After successful posterior myocardial infarction involving posterior papillary muscle, animals develop significant mitral regurgitation around 2 months after the surgery.

Key words Mitral regurgitation, Myocardial infarction, Sheep, Echocardiography, Tethering, Papillary muscle

1 Introduction

Ischemic mitral regurgitation (IMR) is a common complication of ischemic heart disease that doubles mortality after myocardial infarction (MI) and is a major driving factor increasing heart failure [1, 2]. Moderate or greater IMR occurs in ~500,000 patients/year in the USA—20% of those with new MI and 50% with systolic left ventricle (LV) failure [3–5]. Experimental and human studies have revealed a wide range of attributable factors, including mitral annular dilatation [6, 7], leaflet tethering [8, 9], altered LV geometry [10], and insufficient leaflet adaptations [11, 12]. IMR is caused by ischemic LV distortion: inferior wall bulging displaces the papillary

Electronic supplementary material: The online version of this chapter (https://doi.org/10.1007/978-1-4939-8597-5_23) contains supplementary material, which is available to authorized users.

muscle (PM) to which the leaflets are anchored [8–10, 13–24]. This tethers the leaflets into the LV cavity and restricts their closure [25, 26]. IMR reflects a deficiency in mitral valve (MV) leaflet tissue relative to the dilating ventricle [12]. Surgery for ischemic MR remains challenging; standard surgical therapy includes annular ring reduction (improving leaflet apposition by correction of posterior annular dilatation). Operative mortality is higher than in organic MR and the long-term prognosis is worse. The NHLBI-sponsored CTSN (Cardiothoracic Surgical Trials Network) has shown that annular ring reduction for IMR often fails: persistent MV tethering causes recurrent MR [27–32] in 33% of patients at 1 year and 59% at 2 years [33–36]. Failed repair associates with lack of reduction or increase in LV remodeling, with increased heart failure and related readmissions [34, 37].

Understanding mechanistic and molecular mechanisms of IMR has attributed to the development of large animal models close to the human. Newly developed therapies targeted to the primary causes can also be tested in these models. Sheep and swine resemble the coronary anatomy of humans closely, whereas dogs have an extensive coronary collateral supply and much faster heart rates [38]. The relatively comparable body size of sheep and swine and similar coronary anatomy and vasomotor responsiveness to human make them relevant for utilization of multiple diagnostic and therapeutic strategies. The most popular and classic ovine or swine model of chronic IMR can be made by ligating the obtuse marginal branches to induce a posterolateral infarct with PM involvement, which results in significant (moderate or greater) IMR. These highly reproducible models require a thoracotomy to occlude the target vessels [21]. Although the percutaneous techniques were developed, open chest models are usually preferred because they can allow for more comprehensive echo views and better resolution.

1.1 Advantage of Sheep Animal Model

The sheep is one of the most suitable models for cardiovascular research because it can be handled easily. The ovine model is currently accepted as the gold standard for mitral and aortic valve replacement. The size of the heart and chest cavity and vascular anatomy resemble those of the human. At cellular and molecular levels, the predominant (~100%) myosin heavy chain isoform in the sheep heart is similar to humans (~95%). The resting heart rate (60–120 bpm), systolic (~90–115 mmHg) and diastolic (~100 mmHg) pressure in sheep are akin to humans and so are the hemodynamic responses. However, sheep contractile and relaxation kinetics are slightly faster than humans [39]. Sheep do not have an abundant network of coronary collaterals like dogs and have a left-dominant coronary system, and the left and right

coronary arteries communicate with only minor overlap [40]; occlusion of a coronary artery can make distinct ischemic injuries with sharp border zone regions accordingly.

1.2 Mitral Valve Anatomy

Sheep heart has four cardiac valves with principally similar structures and locations to human. The gross morphology of the chordae attaching at the valve leaflet and the PM is very similar; on average, there are 12 chordae tendinea in each of the MV leaflet [41]. The anterior-posterior diameter of the mitral annulus is significantly smaller than that of human (25.8 ± 6.3 vs. 32.5 ± 5.6 mm), while the intercommissural diameters are similar. Notably, the fibrous continuity between the two fibrous trigones, termed the membranous septum, is completely absent in sheep [42].

1.3 Echocardiography

Echocardiography in the non open-chest model is challenging. Keel-shaped chest with narrow intercostal spaces makes difficult to locate the ultrasound transducer and limits the acoustic window. In addition, the presence of gas in the reticulorumen hampers the acquisition of subcostal and apical views [43]. Transducers with frequencies up to 5.0 MHz are generally preferred. During general anesthesia, sheep usually lie on its right decubitus position for left lateral thoracotomy. In this position, it is difficult to acquire apical images of the heart including apical four-, three-, and two-chamber views. Only parasternal short and long axis views are available so the parameters to be acquired are limited. Placing the probe on the left fourth intercostal space, craniodorsally oriented with 0° – 20° rotation, the left parasternal long axis view showing the LV outflow tract can be obtained. To acquire the short axis images of the above areas, the probe needs to be rotated perpendicular to the long axis plane, scanning from apex to base. Placing the transducer on the fourth or fifth intercostal space, just dorsal to the sternum and aiming dorsally and to the right, left parasternal four-chamber or five-chamber views can be obtained [44]. Even after left thoracotomy, although the resolution and image qualities are improved indeed (Fig. 1), making a pericardial cradle to suspend the heart [11, 45, 46] is essential to get apical images (*see Note 1*).

All parameters can be indexed to the body surface area (BSA) using the following equation.

$$\text{BSA } (\text{m}^2) = 0.84 \times \text{body weight } (\text{kg})^{0.66}$$

Several studies have proposed reference values for echocardiographic parameters in healthy sheep [44, 47–49]. However, care should be taken for interpretation of the results because the parameters will be affected by using sedatives or anesthetic agents.

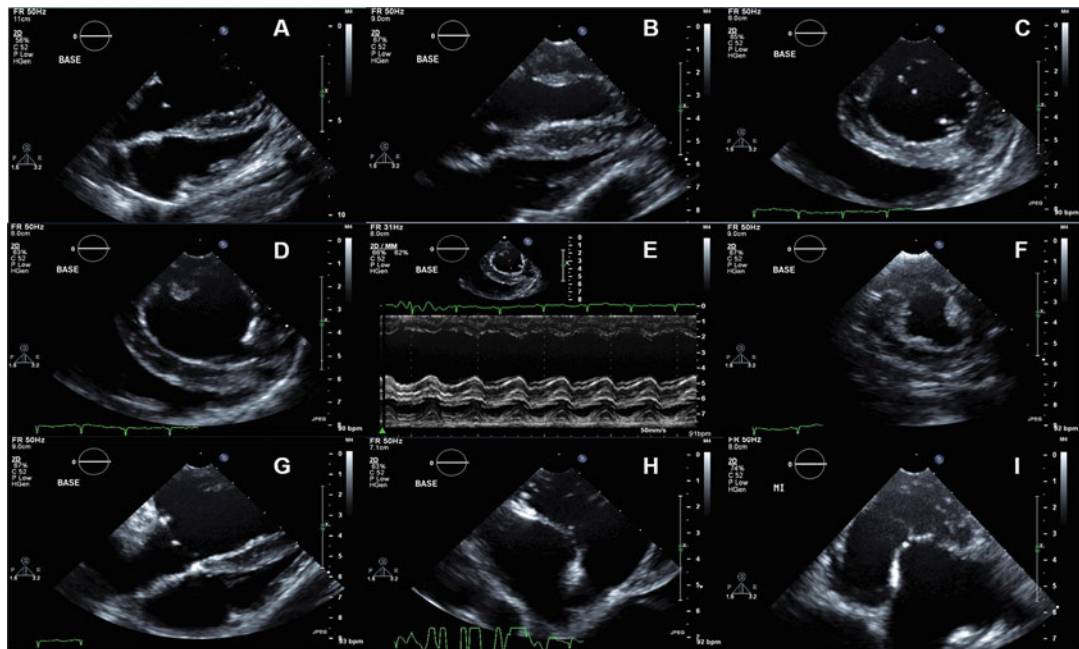


Fig. 1 Representative echocardiographic images available without pericardial cradle creation [(a–g) routine parasternal views, (h and i) lower parasternal views]. (a) RV focused view. (b) LV focused view. (c) Parasternal short axis view of the LV at MV level. (d) Parasternal short axis view of the LV at PM level. (e) M-mode tracing of the LV at the mid-ventricular short axis. (f) Short axis image of the LV at PM base (more apically displaced). (g) Lower parasternal MV focused view. (h) Lower parasternal three-chamber view. (i) Lower parasternal five-chamber view

1.4 Optimal Occlusion Site for Inducing IMR

Posterior myocardial infarction produces MR more often than anterior infarction [50]. The roles of papillary muscle infarction and annular dilatation in the pathogenesis of IMR are crucial. In previous studies, large acute posterior infarctions (32–35% of total LV, occlusion of OM1,2,3), involving the posterior PM, produce a moderate degree of acute MR [16, 51] and severe MR at several weeks later. After larger infarction with posterior PM infarction by occlusion of OM2, 3 and PDA (around 40% of total LV), severe MR developed in all sheep immediately after infarction [21]. However, two branch occlusion (usually OM2,3) model is usually preferred, because long-term survival is threatened in large infarction models. In one study, ligation of OM2 and OM3 infarcted $21.4 \pm 4.0\%$ (moderate infarct) of the LV with complete infarcts of the posterior PM and 11 out of 11 sheep developed a moderate degree of MR by six weeks after MI creation. Keep in mind that only 1+ MR develops immediately after MI creation when you ligate OM2 and OM3 [21] (Fig. 2). In our lab, after successful induction of moderate posterior infarctions (OM 2 and 3 occlusion), 2-month survival rate was 92% and 6-month survival rate was 83%.

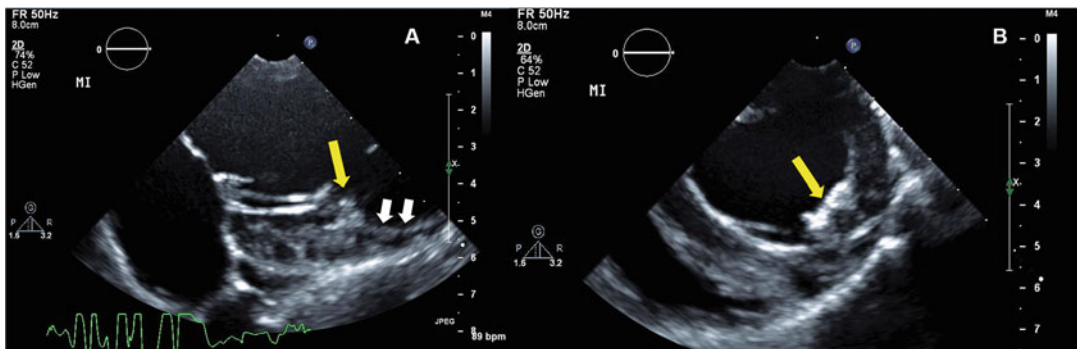


Fig. 2 Development of MR after MI creation. **(a)** No MR at baseline. **(b and c)** Trivial MR developed after MI creation. Even after OM2 and OM3 occlusion, only trivial MR develops immediately after MI creation. **(d)** Significant MR developed 2 months after MI creation

2 Materials

1. Adult Dorsett hybrid sheep (42–46 kg) (*see Note 2*).
2. Heated surgical table to maintain body temperature, table pad.
3. Mechanical ventilator and respiration hose for large animals.
4. Anesthesia machine with isoflurane vaporizer.
5. Vital monitors including pulse oximeter, blood pressure monitor, capnograph, rectal temperature monitor, ECG monitor.
6. Portable warming lamp.
7. Defibrillator with internal paddles.
8. Centrifuge.
9. –80 °C freezer.
10. Liquid nitrogen.
11. Vacutainers for blood sampling and cryogenic vials.
12. Induction: Intravenous propofol.
13. Alcohol swabs.
14. Endotracheal tube (7.5–8.0 mm).
15. Laryngoscope.
16. Anesthesia: isoflurane gas inhalant.
17. Artificial tears to prevent drying of eyes.
18. Tube gauze.
19. Suction canister, suction tubing and suction tip.
20. Sterile syringes, needles, etc.
21. 70% isopropyl alcohol.
22. Povidone–iodine.
23. Hydrogen peroxide.

24. Hair clippers (Oster size 40).
25. 18G angiocatheter for intravenous access.
26. Fabric tape to secure IV lines.
27. IV fluids (sodium chloride and lactated ringer's solution).
28. Amiodarone (50 mg/mL).
29. Analgesic: buprenorphine (0.3 mg/mL).
30. Antibiotic: cefazolin (1 g/vial).
31. Glycopyrrolate (0.2–0.4 mg).
32. Standard emergency drugs.
33. Ground plate.
34. Cautery.
35. #15 scalpel blade.
36. Basic surgical pack containing sterile drapes.
37. Sterile towels.
38. Sterile surgical instruments and chest retractor.
39. 0.7% Iodine povacrylex.
40. Echocardiography machine.
41. Sterile echo transducer covers.
42. 5Fr high-fidelity conductance catheter for the acquisition of pressure–volume loops.
43. Control unit and connected laptop for the pressure–volume loops acquisition.
44. Sutures: Silk and Prolene and Vicryl.
45. 11 blade.
46. 18Fr chest tube.
47. Bupivacaine 0.5% (5 mg/mL).
48. Lidocaine (20 mg/mL).
49. Heparin sodium (1000 USP units/mL).
50. Furosemide (10 mg/mL).
51. Flunixin meglumine (50 mg/mL).
52. Triple antibiotic ointment.

3 Methods

3.1 IMR Induction

1. Administer amiodarone 200 mg PO once daily for 2–3 days prior to surgery to prevent arrhythmia during surgery.
2. NPO the animal overnight prior to surgery.

3. After induction with propofol 0.5–1.5 mg/kg IV, shave the left jugular vein site with clippers and clean area with povidone–iodine and 70% isopropyl alcohol.
4. Cannulate the left jugular vein using an 18G angiocatheter.
5. Intubate the animal with a 7.5–8.0 mm endotracheal tube (depending on size of animal) with the aid of a laryngoscope.
6. Secure endotracheal tube with tube gauze.
7. Place animal on its right side down on heated surgical table and secure legs.
8. Ventilate animal at 15 mL/kg with 2–4% isoflurane and oxygen 3–4 L/min.
9. Place the vital monitors and begin monitoring and documenting isoflurane level and vital signs including respiration rate, heart rate, SpO₂, ETCO₂, blood pressure, muscle tone, and body temperature.
10. Apply artificial tears to both eyes to prevent drying.
11. Shave and clean left saphenous intravenous access site with 70% isopropyl alcohol and povidone iodine.
12. Obtain intravenous access in the left saphenous vein using an 18G angiocatheter.
13. Begin administration of IV fluids: lactated Ringer's solution and sodium chloride solution containing amiodarone 50 mg to prevent arrhythmia.
14. Administer analgesic buprenorphine 0.008–0.01 mg/kg, glycopyrrolate 0.4 mg to limit perioperative secretions of tracheal and bronchial secretions, and antibiotic cefazolin 1 g intravenously at least 15 min prior to chest wall incision.
15. Prepare surgical site using aseptic technique by shaving skin and cleaning site with 70% isopropyl alcohol, povidone–iodine.
16. Cover the animal with sterile drapes.
17. Clean surgical site with 0.7% Iodine povacrylex solution applicator to ensure asepsis of the skin.
18. Using a sterile #15 blade scalpel, make an approximately 13 cm long skin incision between and parallel to the fourth and fifth ribs (Fig. 3a).
19. Divide intercostal muscles and cauterize small bleedings.
20. Administer intercostal nerve block with 0.5% bupivacaine 0.5–1.0 mg/kg IM.
21. Place chest retractors and gently separate ribs being careful to avoid rib damage.

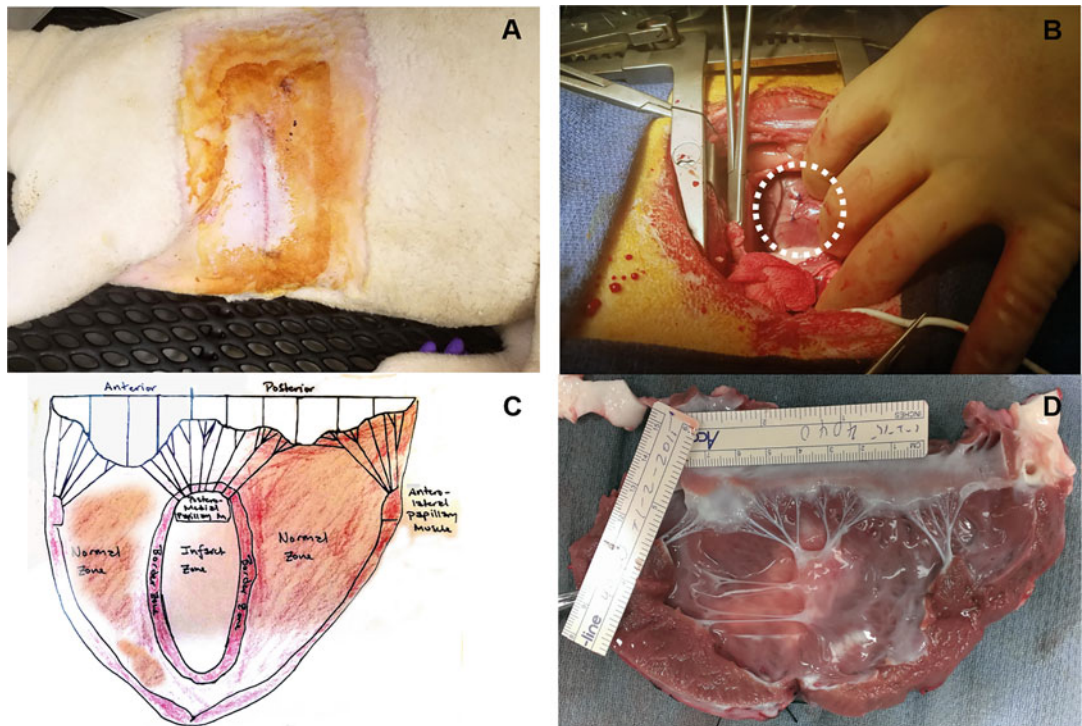


Fig. 3 (a) Incision site of lateral thoracotomy. (b) Occlusion of OM2 and OM3. (c) Illustration of the LV and MV dissections. (d) Real photo of dissected LV. The left atrium was opened and cut, and the LV wall was dissected from the anterolateral commissure thorough anterior PM

22. Open the pericardium to allow for coronary interventions and imaging. Following opening the pericardium from the apex to the base, a cradle is created (pericardial cradle creation, *see Note 1*).
23. Before myocardial infarction creation, acquire baseline two and three-dimensional echocardiography images using sterile echo transducer covers (*see Note 3*) and record baseline hemodynamic parameters (pressure–volume loop acquisition) using a 5F high fidelity conductance catheter placed in the left ventricle via the apex of the heart. Close the insertion site using purse string suture with Prolene (4-0).
24. Using Prolene (4-0) suture, permanently ligate the second and third obtuse marginal branches of the left circumflex coronary artery at their origins for myocardial infarction creation (Fig. 3b, *see Note 4*).
25. Repeat echocardiography and hemodynamic data acquisition as described in Subheading 3.1 (*see Note 5*).
26. Following completion of data collection and confirmation of stable vital sign and no recurrent ventricular arrhythmias, remove chest retractors.

27. Using an 11 blade, make a small (6–7 mm) incision between the fifth and sixth intercostal spaces and insert a 18Fr chest tube.
28. Begin closing the chest by approximating the ribs using Vicryl sutures.
29. Close the muscle in three layers using Vicryl antibacterial sutures and close the skin using Vicryl (3-0) sutures.
30. Administer 0.5% bupivacaine (0.5–1.0 mg/kg) intrapleurally via the chest tube for additional analgesia.
31. Evacuate the chest and remove the chest tube under negative pressure.
32. Administer furosemide 20–40 mg and cefazolin 1 g intravenously.
33. Wean animal off isoflurane general anesthesia in decrements of 0.5% until 0% is reached.
34. Remove left saphenous IV access and apply manual pressure to site for approximately 10–15 min until hemostasis is achieved.
35. Clean surgical sites and IV access sites with hydrogen peroxide and apply triple antibiotic ointment.
36. Move animal to transport pen for recovery from anesthesia before returning to animal facility.
37. Monitor all vital signs during recovery period including heart rate, SpO₂, blood pressure, and respiratory rate.
38. Once the animal begins to breathe on its own, decrease mechanical ventilator support until off and allow the animal to breathe room air while continuously monitoring SpO₂.
39. Extubate the animal when alert, swallowing, moving its head, and able to breathe normally on its own.
40. Continuously observe and monitor animal to ensure smooth and comfortable recovery while minimizing stress and discomfort.
41. Give additional buprenorphine 0.008–0.01 mg/kg IM or flunixin meglumine 1–2 mg/kg IM if pain is evident (fast heart rate, fast respiration rate, shaking, high blood pressure, teeth grinding).
42. Once conscious of environment, responding to external stimuli, and recovered from anesthesia, transport the animal back to the animal facility and continue to monitor postoperatively.
43. Provide postoperative analgesia with buprenorphine 0.008–0.01 mg/kg IM every 8–12 h for 72–96 h plus as needed and flunixin meglumine 1–2 mg/kg IM once every 24 h for 72–96 h postoperatively.

44. Observe and monitor animals 3–4 times daily for 3 days following surgery to ensure smooth and successful recovery.
45. Observe, interact with, and encourage socialization and activity during the postoperative period and daily thereafter to provide environmental enrichment and comfort.
46. For postmortem assessment of infarct size and MV apparatus, *see Note 6*.

4 Notes

1. Forming a pericardial cradle allows suitable fields for operation, an exposure of apex, which facilitates apical window of echocardiography and the insertion of high-fidelity catheter used for pressure–volume loop. It can be created by suturing multiple single stitches longitudinally along the open edges and attaching them to the chest retractor to keep the heart suspended throughout the procedure.
2. There is no data regarding gender difference in sheep after IMR model development. However, it is well recognized that there are distinct gender differences in epidemiology, pathophysiology, clinical manifestations, and outcomes of human MV and AV disease [52]. Life expectancy of a sheep is about 10–12 years. The use of sheep around 12 months of age, 40–45 kg allows for the testing of valve replacement, ring annuloplasty, because their valve size is comparable to that of humans [53]. The use of animals of similar age, weight and same gender is recommended for a good achievement.
3. For epicardial echocardiography, a sterile surgical probe cover (commercially available) can be used. A sterile latex glove soaked with ultrasound gel is a good alternative for the probe cover. Enough ultrasonic gel has to be applied for reducing near field artifact.
4. Using Prolene 4-0 (BB needle) suture, permanently ligate the second and third obtuse marginal branches of the left circumflex coronary artery at their origin for myocardial infarction creation. The Prolene suture should be placed around the OM2 and OM3 branches approximately 3–4 mm deep and 4 mm wide.
5. In our lab, considering the coronary artery anatomic variation, we ligate OM2 first. After carefully reviewing the extent of myocardial discoloration under direct visualization and echo images (regional wall motion abnormalities (RMWs) and papillary muscle involvement) (Fig. 4), we decide whether we ligate OM3 additionally. *See movie clips of echocardiographic images of normal and PM dysfunction after infarction (Movies 1a–1e)*.

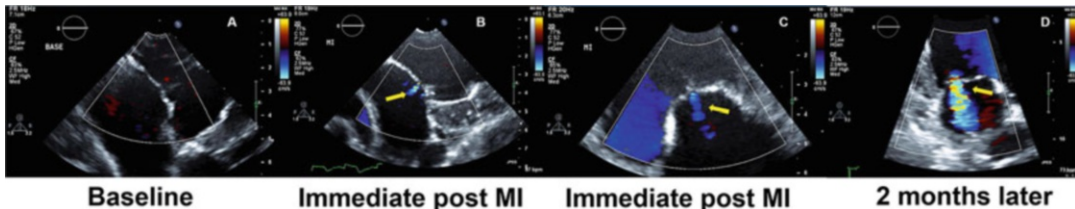


Fig. 4 Identification of PM dysfunction and regional wall motion abnormalities. **(a)** Modified parasternal long axis image showing PM and attached chordae. **(b)** Short axis image. You can see the dysfunctional PM (yellow arrow) by infarction and noncontracting myocardium (white arrows). See also Movies 1a–1e

6. After eviscerating the heart, we usually open the left atrium first, and dissect the LV wall from the anterolateral commissure thorough anterior-lateral PM (Fig. 3c, d). The photos with a ruler can be used for the further image analyses including infract area and mitral leaflet area. To establish a standard dissection method (Fig. 3c), communication with other researchers is encouraged (especially for histological analyses).

Acknowledgments

This study was supported in part by NIH grants R01 HL128099 and HL141917, and by support from the Ellison Foundation, Boston, MA.

References

1. Grigioni F, Detaint D, Avierinos JF, Scott C, Tajik J, Enriquez-Sarano M (2005) Contribution of ischemic mitral regurgitation to congestive heart failure after myocardial infarction. *J Am Coll Cardiol* 45(2):260–267
2. Grigioni F, Enriquez-Sarano M, Zehr KJ, Bailey KR, Tajik AJ (2001) Ischemic mitral regurgitation: long-term outcome and prognostic implications with quantitative Doppler assessment. *Circulation* 103(13):1759–1764
3. Lamas GA, Mitchell GF, Flaker GC, Smith SC Jr, Gersh BJ, Basta L, Moye L, Braunwald E, Pfeffer MA (1997) Clinical significance of mitral regurgitation after acute myocardial infarction. Survival and ventricular enlargement investigators. *Circulation* 96(3):827–833
4. Birnbaum Y, Chamoun AJ, Conti VR, Uretsky BF (2002) Mitral regurgitation following acute myocardial infarction. *Coron Artery Dis* 13(6):337–344
5. Trichon BH, Felker GM, Shaw LK, Cabell CH, O'Connor CM (2003) Relation of frequency and severity of mitral regurgitation to survival among patients with left ventricular systolic dysfunction and heart failure. *Am J Cardiol* 91(5):538–543
6. Popovic ZB, Martin M, Fukamachi K, Inoue M, Kwan J, Doi K, Qin JX, Shiota T, Garcia MJ, McCarthy PM, Thomas JD (2005) Mitral annulus size links ventricular dilatation to functional mitral regurgitation. *J Am Soc Echocardiogr* 18(9):959–963
7. Tibayan FA, Rodriguez F, Langer F, Zasio MK, Bailey L, Liang D, Daughters GT, Ingels NB Jr, Miller DC (2003) Annular remodeling in chronic ischemic mitral regurgitation: ring selection implications. *Ann Thorac Surg* 76(5):1549–1554, discussion 1554–1555
8. Yiu SF, Enriquez-Sarano M, Tribouilloy C, Seward JB, Tajik AJ (2000) Determinants of the degree of functional mitral regurgitation in

- patients with systolic left ventricular dysfunction: a quantitative clinical study. *Circulation* 102(12):1400–1406
9. Otsuji Y, Handschumacher MD, Schwammenthal E, Jiang L, Song JK, Guerrero JL, Vlahakes GJ, Levine RA (1997) Insights from three-dimensional echocardiography into the mechanism of functional mitral regurgitation: direct *in vivo* demonstration of altered leaflet tethering geometry. *Circulation* 96(6):1999–2008
 10. Kono T, Sabbah HN, Rosman H, Alam M, Jafri S, Goldstein S (1992) Left ventricular shape is the primary determinant of functional mitral regurgitation in heart failure. *J Am Coll Cardiol* 20(7):1594–1598
 11. Dal-Bianco JP, Aikawa E, Bischoff J, Guerrero JL, Hjortnaes J, Beaudoin J, Szymanski C, Bartko PE, Seybolt MM, Handschumacher MD, Sullivan S, Garcia ML, Mauskapf A, Titus JS, Wylie-Sears J, Irvin WS, Chaput M, Messas E, Hagege AA, Carpenter A, Levine RA, Leducq Transatlantic Mitral N (2016) Myocardial infarction alters adaptation of the tethered mitral valve. *J Am Coll Cardiol* 67(3):275–287
 12. Chaput M, Handschumacher MD, Tournoux F, Hua L, Guerrero JL, Vlahakes GJ, Levine RA (2008) Mitral leaflet adaptation to ventricular remodeling: occurrence and adequacy in patients with functional mitral regurgitation. *Circulation* 118(8):845–852
 13. Boltwood CM, Tei C, Wong M, Shah PM (1983) Quantitative echocardiography of the mitral complex in dilated cardiomyopathy: the mechanism of functional mitral regurgitation. *Circulation* 68(3):498–508
 14. Burch GE, De Pasquale NP, Phillips JH (1963) Clinical manifestations of papillary muscle dysfunction. *Arch Intern Med* 112:112–117
 15. Cochran RP, Kunzelman KS (1998) Effect of papillary muscle position on mitral valve function: relationship to homografts. *Ann Thorac Surg* 66(6 Suppl):S155–S161
 16. Gorman RC, McCaughan JS, Ratcliffe MB, Gupta KB, Streicher JT, Ferrari VA, St John-Sutton MG, Bogen DK, Edmunds LH Jr (1995) Pathogenesis of acute ischemic mitral regurgitation in three dimensions. *J Thorac Cardiovasc Surg* 109(4):684–693
 17. He S, Fontaine AA, Schwammenthal E, Yoganathan AP, Levine RA (1997) Integrated mechanism for functional mitral regurgitation: leaflet restriction versus coaptation force: *in vitro* studies. *Circulation* 96(6):1826–1834
 18. Kaul S, Spotnitz WD, Glasheen WP, Touchstone DA (1991) Mechanism of ischemic mitral regurgitation. An experimental evaluation. *Circulation* 84(5):2167–2180
 19. Komeda M, Glasson JR, Bolger AF, Daughters GT 2nd, MacIsaac A, Oesterle SN, Ingels NB Jr, Miller DC (1997) Geometric determinants of ischemic mitral regurgitation. *Circulation* 96(9 Suppl):II-128–II-133
 20. Kono T, Sabbah HN, Stein PD, Brymer JF, Khaja F (1991) Left ventricular shape as a determinant of functional mitral regurgitation in patients with severe heart failure secondary to either coronary artery disease or idiopathic dilated cardiomyopathy. *Am J Cardiol* 68(4):355–359
 21. Llaneras MR, Nance ML, Streicher JT, Lima JA, Savino JS, Bogen DK, Deac RF, Ratcliffe MB, Edmunds LH Jr (1994) Large animal model of ischemic mitral regurgitation. *Ann Thorac Surg* 57(2):432–439
 22. Llaneras MR, Nance ML, Streicher JT, Linden PL, Downing SW, Lima JA, Deac R, Edmunds LH Jr (1993) Pathogenesis of ischemic mitral insufficiency. *J Thorac Cardiovasc Surg* 105(3):439–442; discussion 442–433.
 23. Mittal AK, Langston M Jr, Cohn KE, Selzer A, Kerth WJ (1971) Combined papillary muscle and left ventricular wall dysfunction as a cause of mitral regurgitation. An experimental study. *Circulation* 44(2):174–180
 24. Otsuji Y, Handschumacher MD, Liel-Cohen N, Tanabe H, Jiang L, Schwammenthal E, Guerrero JL, Nicholls LA, Vlahakes GJ, Levine RA (2001) Mechanism of ischemic mitral regurgitation with segmental left ventricular dysfunction: three-dimensional echocardiographic studies in models of acute and chronic progressive regurgitation. *J Am Coll Cardiol* 37(2):641–648
 25. Godley RW, Wann LS, Rogers EW, Feigenbaum H, Weyman AE (1981) Incomplete mitral leaflet closure in patients with papillary muscle dysfunction. *Circulation* 63(3):565–571
 26. Levine RA, Schwammenthal E (2005) Ischemic mitral regurgitation on the threshold of a solution: from paradoxes to unifying concepts. *Circulation* 112(5):745–758
 27. Calafiore AM, Gallina S, Di Mauro M, Gaeta F, Iaco AL, D'Alessandro S, Mazzei V, Di Giambamarcò G (2001) Mitral valve procedure in dilated cardiomyopathy: repair or replacement? *Ann Thorac Surg* 71(4):1146–1152. discussion 1152–1143
 28. Grossi EA, Goldberg JD, LaPietra A, Ye X, Zakow P, Sussman M, Delianides J, Culliford AT, Esposito RA, Ribakove GH, Galloway AC, Colvin SB (2001) Ischemic mitral valve

- reconstruction and replacement: comparison of long-term survival and complications. *J Thorac Cardiovasc Surg* 122(6):1107–1124
29. Hung J, Papakostas L, Tahta SA, Hardy BG, Bollen BA, Duran CM, Levine RA (2004) Mechanism of recurrent ischemic mitral regurgitation after annuloplasty: continued LV remodeling as a moving target. *Circulation* 110(11 Suppl 1):II85–II90
 30. Kuwahara E, Otsuji Y, Iguro Y, Ueno T, Zhu F, Mizukami N, Kubota K, Nakashiki K, Yuasa T, Yu B, Uemura T, Takasaki K, Miyata M, Hamasaki S, Kisanuki A, Levine RA, Sakata R, Tei C (2006) Mechanism of recurrent/persistent ischemic/functional mitral regurgitation in the chronic phase after surgical annuloplasty: importance of augmented posterior leaflet tethering. *Circulation* 114(1 Suppl): I529–I534
 31. McGee EC, Gillinov AM, Blackstone EH, Rajeswaran J, Cohen G, Najam F, Shiota T, Sabik JF, Lytle BW, McCarthy PM, Cosgrove DM (2004) Recurrent mitral regurgitation after annuloplasty for functional ischemic mitral regurgitation. *J Thorac Cardiovasc Surg* 128(6):916–924
 32. Tahta SA, Oury JH, Maxwell JM, Hiro SP, Duran CM (2002) Outcome after mitral valve repair for functional ischemic mitral regurgitation. *J Heart Valve Dis* 11(1):11–18. discussion 18–19
 33. Acker MA, Parides MK, Perrault LP, Moskowitz AJ, Gelijns AC, Voisine P, Smith PK, Hung JW, Blackstone EH, Puskas JD, Argenziano M, Gammie JS, Mack M, Ascheim DD, Bagiella E, Moquete EG, Ferguson TB, Horvath KA, Geller NL, Miller MA, Woo YJ, D'Alessandro DA, Ailawadi G, Dagenais F, Gardner TJ, O'Gara PT, Michler RE, Kron IL (2013) Mitral-valve repair versus replacement for severe ischemic mitral regurgitation. *N Engl J Med* 370:23–32
 34. Goldstein D, Moskowitz AJ, Gelijns AC, Ailawadi G, Parides MK, Perrault LP, Hung JW, Voisine P, Dagenais F, Gillinov AM, Thourani V, Argenziano M, Gammie JS, Mack M, Demers P, Atluri P, Rose EA, O'Sullivan K, Williams DL, Bagiella E, Michler RE, Weisel RD, Miller MA, Geller NL, Taddei-Peters WC, Smith PK, Moquete E, Overbey JR, Kron IL, O'Gara PT, Acker MA, CTSN (2015) Two-year outcomes of surgical treatment of severe ischemic mitral regurgitation. *N Engl J Med* 374:344–353
 35. Kron IL, Hung J, Overbey JR, Bouchard D, Gelijns AC, Moskowitz AJ, Voisine P, O'Gara PT, Argenziano M, Michler RE, Gillinov M, Puskas JD, Gammie JS, Mack MJ, Smith PK, Sai-Sudhakar C, Gardner TJ, Ailawadi G, Zeng X, O'Sullivan K, Parides MK, Swayze R, Thourani V, Rose EA, Perrault LP, Acker MA (2015) Predicting recurrent mitral regurgitation after mitral valve repair for severe ischemic mitral regurgitation. *J Thorac Cardiovasc Surg* 149(3):752–761.e751
 36. Kron IL, Perrault LP, Acker MA (2015) We need a better way to repair ischemic mitral regurgitation. *J Thorac Cardiovasc Surg* 150 (2):428
 37. Vassileva CM, Boley T, Markwell S, Hazelrigg S (2011) Meta-analysis of short-term and long-term survival following repair versus replacement for ischemic mitral regurgitation. *Eur J Cardiothorac Surg* 39(3):295–303
 38. Scheuer J (1982) Effects of physical training on myocardial vascularity and perfusion. *Circulation* 66(3):491–495
 39. Milani-Nejad N, Janssen PM (2014) Small and large animal models in cardiac contraction research: advantages and disadvantages. *Pharmacol Ther* 141(3):235–249
 40. Gorman JH 3rd, Gorman RC, Plappert T, Jackson BM, Hiramatsu Y, St John-Sutton MG, Edmunds LH Jr (1998) Infarct size and location determine development of mitral regurgitation in the sheep model. *J Thorac Cardiovasc Surg* 115(3):615–622
 41. Hutchison J, Rea P (2015) A comparative study of the morphology of mammalian chordae tendinae of the mitral and tricuspid valves. *Vet Rec Open* 2(2):e000150
 42. Hill AJ, Iaizzo PA (2009) Comparative cardiac anatomy. In: Iaizzo PA (ed) *Handbook of cardiac anatomy, physiology, and devices*. Humana Press, Totowa, NJ, pp 87–108. https://doi.org/10.1007/978-1-60327-372-5_6
 43. Olsson K, Hansson K, Hydbring E, von Walter LW, Häggström J (2001) A serial study of heart function during pregnancy, lactation and the dry period in dairy goats using echocardiography. *Exp Physiol* 86(1):93–99
 44. Vloumudi EI, Fthenakis GC (2017) Ultrasonographic examination of the heart in sheep. *Small Rumin Res* 152(Supplement C):119–127
 45. Bartko PE, Dal-Bianco JP, Guerrero JL, Beaudoin J, Szymanski C, Kim DH, Seybolt MM, Handschumacher MD, Sullivan S, Garcia ML, Titus JS, Wylie-Sears J, Irvin WS, Messas E, Hagege AA, Carpentier A, Aikawa E, Bischoff J, Levine RA, Leducq Transatlantic Mitral N (2017) Effect of losartan on mitral valve changes after myocardial infarction. *J Am Coll Cardiol* 70 (10):1232–1244

46. Dal-Bianco JP, Aikawa E, Bischoff J, Guerrero JL, Handschumacher MD, Sullivan S, Johnson B, Titus JS, Iwamoto Y, Wylie-Sears J, Levine RA, Carpenter A (2009) Active adaptation of the tethered mitral valve: insights into a compensatory mechanism for functional mitral regurgitation. *Circulation* 120(4):334–342
47. Poser H, Semplicini L, De Benedictis GM, Gerardi G, Contiero B, Maschietto N, Valerio E, Milanesi O, Semplicini A, Bernardini D (2013) Two-dimensional, M-mode and Doppler-derived echocardiographic parameters in sedated healthy growing female sheep. *Lab Anim* 47(3):194–202
48. Locatelli P, Olea FD, De Lorenzi A, Salmo F, Vera Janavel GL, Hnatiuk AP, Guevara E, Crotogolini AJ (2011) Reference values for echocardiographic parameters and indexes of left ventricular function in healthy, young adult sheep used in translational research: comparison with standardized values in humans. *Int J Clin Exp Med* 4(4):258–264
49. Moses BL, Ross JN Jr (1987) M-mode echocardiographic values in sheep. *Am J Vet Res* 48(9):1313–1318
50. Becker AE (1991) Anatomy of the coronary arteries with respect to chronic ischemic mitral regurgitation. In: Vetter HO, Hetzer R, Schmutzler H (eds) Ischemic mitral incompetence. Steinkopff, Heidelberg, pp 17–24. https://doi.org/10.1007/978-3-662-08027-6_2
51. Gorman JH 3rd, Jackson BM, Gorman RC, Kelley ST, Gikakis N, Edmunds LH Jr (1997) Papillary muscle coordination rather than increased annular area facilitates mitral regurgitation after acute posterior myocardial infarction. *Circulation* 96(9 Suppl):II-124–II-127
52. Group EUCCS, Regitz-Zagrosek V, Oertelt-Prigione S, Prescott E, Franconi F, Gerdts E, Foryst-Ludwig A, Maas AH, Kautzky-Willer A, Knappe-Wegner D, Kintscher U, Ladwig KH, Schenck-Gustafsson K, Stangl V (2016) Gender in cardiovascular diseases: impact on clinical manifestations, management, and outcomes. *Eur Heart J* 37(1):24–34
53. Ahlberg SE, Bateman MG, Eggen MD, Quill JL, Richardson ES, Iaizzo PA (2013) Animal models for cardiac valve research. In: Iaizzo PA, Bianco RW, Hill AJ, St. Louis JD (eds) Heart valves: from design to clinical implantation. Springer US, Boston, MA, pp 343–357. https://doi.org/10.1007/978-1-4614-6144-9_14



Chapter 24

Canine Model of Pacing-Induced Heart Failure

Jeffery C. Powers and Fabio Recchia

Abstract

Tachypacing-induced heart failure is a well-established large animal model that recapitulates numerous pathophysiological, structural and molecular features of dilated cardiomyopathy and, more in general, of end-stage congestive heart failure. The left or the right ventricle is instrumented with pacing electrodes to impose supernormal heart rates, usually three times higher than baseline values, for a length of time that typically ranges between 3 and 5 weeks. The animal of choice is the dog, although this protocol has been successfully implemented also in pigs, sheep, and rabbits. This chapter provides detailed methodology and description of the dog model utilized in our laboratory, which is one of the variants described in literature. Chronic instrumentation is completed by adding probes and catheters necessary to obtain measures of cardiac function and hemodynamics and to withdraw blood samples from various vascular districts. The progression from compensated to decompensated heart failure is highly reproducible, therefore, due also to the phylogenetic proximity of dogs to humans, tachypacing-induced heart failure is considered a highly clinically relevant model for testing the efficacy of novel pharmacological and nonpharmacological therapeutic agents. This model typically produces heart failure as defined by an LV dP/dt max <1500 mmHg/s, end-diastolic pressure >25 mmHg, mean arterial pressure <85 mmHg, and an ejection fraction <35%. One can expect a mortality rate of 5–10% due to fatal arrhythmias.

Key words Pacing-induced heart failure, Dilated cardiomyopathy, Preclinical heart failure model, Congestive heart failure, Tachycardia-induced heart failure, Canine heart failure model

1 Introduction

More than 50 years ago, Whipple and colleagues tested whether high-frequency cardiac pacing in dogs could reproduce at experimental level a well-known form of human dilated cardiomyopathy caused by incessant tachyarrhythmia [1]. Perhaps those authors could not imagine at that time that they were providing the scientific community with one of the most valuable preclinical models of heart failure [2, 3] still utilized to date. Although the pacing protocol may vary among laboratories, dilated cardiomyopathy is always obtained by imposing a supernormal heart rate, at least three times higher than baseline values. This model is very reproducible and evolves over a predictable time course, and numerous studies

have shown that it recapitulates many of the fundamental characteristics of human heart failure, including progressive left ventricular chamber dilation, wall thinning, decreased contractility, neurohormonal activation, beta-adrenergic desensitization, and an array of cellular and molecular alterations [4–13]. Although initially tested in dogs, it was then successfully developed in pigs, sheep, rabbits, and even primates [14–20]. Cardiac tachypacing causes nonischemic cardiomyopathy. Despite its lower prevalence compared to ischemic cardiomyopathy as a cause of heart failure, dilated cardiomyopathy is particularly malignant and refractory to many pharmacological treatments, accounting for more than 50% cases of heart transplantation in the USA [21]. Therefore, cardiac tachypacing is valuable not only for *in vivo* and *ex vivo* studies on the pathophysiological and molecular mechanisms leading to progressive cardiac derangement, but also to test new curative interventions for nonischemic cardiomyopathy [22, 23].

This chapter provides a detailed description of the dog model utilized in our laboratory, which is one of the variants described in literature. First, dogs are chronically instrumented under sterile conditions, then, once the postsurgical recovery is complete, the cardiac pacing protocol is started, and the evolving functional deterioration can be monitored over time in the conscious state, devoid of confounding effects of anesthesia or surgical trauma. End-stage congestive heart failure is indicated by the life-threatening increase in left ventricular end-diastolic pressure up to 25 mmHg or higher.

2 Materials

2.1 Open-Chest Surgery/Pacing-Induced Heart Failure

1. Male mongrel hounds (22–25 kg, approximately 1 year old; male animals are typically used to avoid possible confounding effects of the menstrual or other sex-linked genetic variations [24, 25]).
2. Operating room with ability to maintain a sterile field.
3. Ventilator capable of tidal volumes of at least 1 L.
4. Sterile saline.
5. Acepromazine (to be administered via intramuscular injection).
6. Isoflurane.
7. Propofol (to be administered intravenously).
8. Jackets with pocket to allow external pacemaker to be stored.
9. Foam collar (Size 5) that can be trimmed to fit neck of animal.
10. Pacing electrodes that can be screwed into left ventricle and/or stitched to epicardial surface.
11. Sterile surgical kit.

12. Cefazolin (at least six doses of 1 g each to be reconstituted and administered via intramuscular injection).
13. Meloxicam (at least one injectable dose and five doses to be administered orally).
14. Azithromycin (at least five doses of up to 250 mg to be administered orally).
15. Fentanyl (transdermal patch, 75 µg/h).
16. Buprenorphine (0.3 mg/mL).
17. Euthasol (if not euthanizing via cardiectionomy under general anesthesia).
18. Echocardiograph capable of measuring, at a minimum, ejection fraction and LV free wall thickness.
19. Solid state pressure transducer to measure LV pressure (can be indwelling or guided invasively through the femoral artery; *see Note 1*).
20. Software capable of measuring, at a minimum, the following parameters: dP/dt max, systolic pressure, end-diastolic pressure, mean pressure.
21. Electrocautery.
22. Scalpel (10-blade).
23. Scalpel (11-blade).
24. Clippers.
25. Heated cage.

2.2 Chronic Instrumentation

1. Solid-state pressure transducer.
2. Doppler flow probe (3.0–4.0 mm diameter, Iowa Doppler Products).
3. Piezoelectric crystals (5 mm in diameter, two per animal).
4. Tygon tubing (0.09 inches in diameter).
5. Flowmeter/Sonomicrometer (Triton, Inc.).

3 Methods

3.1 Surgical Instrumentation and Postsurgical Recovery

1. Upon arrival at the facility, the animals should undergo a minimum of 1 week of acclimation and quarantine (*see Note 2*).
2. Fasting for a minimum of 18 h before the operation.
3. Anesthetize and place the animal in right lateral recumbent position. Fur is clipped on the left lateral and dorsal aspects of the thorax. Prepare the surgical sites with a series of three

betadine or chlorhexidine scrubs, each followed by an alcohol rinse.

4. Drape off the surgical field by the surgeon (*see Note 3* for action plan for adverse events).
5. A 10–15 mm skin incision is made between the ribs at the level of the fourth or fifth intercostal space. A disposable cautery instrument may be used for hemostasis during initial skin incision. The incision is deepened through the underlying intercostal muscles to the level of the thoracic cavity.
6. The pleura is incised, a rib retractor is placed, and the lungs are gently manipulated to expose heart and aorta. A segment of the descending thoracic aorta is suitably exposed for placement of the aortic catheter.
7. A purse string suture of 3-0 nonabsorbable suture material is placed in the aortic wall. A vascular clamp is used to partially clamp the aorta proximal to the catheter placement location.
8. A stab incision is made through the wall of the aorta in the center of the preplaced purse string suture.
9. The tip of a Tygon catheter (0.09 inch in diameter) is introduced into the lumen of the aorta and advanced approximately 5 mm.
10. The purse string suture is tightened to secure the catheter segment inserted in the aorta. The vascular clamp is released to reestablish normal blood flow within the aorta.
11. A single pexy suture (4-0 nonabsorbable) is used to secure the catheter to the aortic wall in order to provide additional stability.
12. The pericardium is then incised and held by forceps to the chest wall to create a pericardial cradle that lifts the heart and maintains it in surgical view.
13. A purse string suture of 4-0 nonabsorbable suture material is placed in the apical aspect of the left ventricle.
14. A stab incision is made through the wall of the left ventricle in the center of the preplaced purse string suture, and is widened with small forceps. If the transducer is inserted immediately (**step 15**), minimal bleeding should occur. If there is a delay in inserting the transducer, the suture can be pulled tight temporarily and then loosened just prior to insertion of the transducer.
15. A solid-state pressure transducer (5–6 mm in diameter) is inserted through the apex of left ventricle , and the purse string suture is tightened to hold it in place.
16. If a right ventricular catheter is needed, a stab incision is made through the wall of the right ventricle in the center of a

preplaced purse string suture. The tip of a Tygon catheter (0.09 inch in diameter) is inserted into the right ventricle and the purse string suture is tightened to hold it in place.

17. The left atrial appendage is lifted, a segment of the left circumflex coronary artery is dissected from the surrounding epicardium and connective tissue, and a cuff-type Doppler flow probe (0.5 mm length) is placed around it to measure blood flow. The wire is secured to the epicardial surface with a 2-0 nonabsorbable suture.
18. Disk-shaped piezoelectric crystals are placed on the left ventricular anterior and posterior free walls. First, a purse string suture of 2-0 nonabsorbable suture is placed on the posterior wall of the left ventricle. A stab incision is made through the wall in the center of the preplaced purse string suture, and the first dimension crystal is inserted in the ventricular cavity then pulled back to remain attached to the endocardial surface, and the purse string suture is tightened to hold it in place. This crystal is connected with a somomicrometer. The second crystal, also connected with a somomicrometer, is gently pushed against the epicardial surface of the left ventricular anterior wall and moved in various directions to find the best alignment with the first crystal. Then it is fixed to the internal surface of the ventricular wall as described for the first crystal.
19. A pair of pacing loop leads is attached to the epicardial surface of the left ventricular free wall with 4-0 nonabsorbable suture and one electrode is screwed into the epicardial surface with 2-0 nonabsorbable suture on the same surface, a few centimeters apart, avoiding coronary vessels.
20. A purse string suture of 4-0 nonabsorbable suture material is placed in the left atrial appendage. A stab incision is made through the wall of the left atrium in the center of the preplaced purse string suture. The tip of a Tygon catheter (0.09 inch in diameter) is inserted into the left atrium, and the purse string suture is tightened to hold it in place.
21. Each catheter is attached to a three-way stopcock, connected to a syringe and filled with sterile saline before surgical procedures.
22. After completing the placement of probes and catheters, a steel trocar (12-inch-long) is used to lead wires and catheters from the thoracic cavity subcutaneously to their exteriorization sites through the skin of the interscapular region. The trocar is passed through the thoracic wall musculature 1–2 intercostal spaces cranial or caudal to the surgical incision, and then passed subcutaneously.

23. A single 0.5–1.0 cm skin incision is made at each exteriorization site (a different site for each catheter or wire) and the trocar is passed through the skin incision.
24. The catheters are flushed and then closed by a knot (Since the catheters are identical in appearance, it is useful to tie a different number of knots in each catheter to distinguish them.).
25. The left ventricular pressure gauge wire and the pacing loop wires are passed together and exit through one skin incision. The flow probe wire and the two-dimension crystal wires pass together and exit through another skin incision.
26. When the surgery is complete, all catheters and wires are buried under the skin in correspondence of the exit points. They are all tied to thick silk sutures that come out of the skin incision sites. The sutures will be used to pull out catheters and wires when the postsurgical recovery is complete.
27. Each dorsal thoracic skin incision is closed with 1–2 sutures (2-0 nonabsorbable).
28. A chest tube (Pleura-Cath Chest Tube, 18 or 24 Fr) is placed to reduce postoperative pneumothorax. It is tied with a purse string of size 0 absorbable suture.
29. The thoracotomy is closed in layers: four ties of size 2 absorbable suture are placed around the ribs adjacent to the incision and tightened. The two muscle layers are closed with 2-0 absorbable suture in a simple interrupted pattern.
30. The subcutaneous tissues are closed with size 0 absorbable suture in a simple continuous pattern. The skin incision is closed with a continuous intradermic suture of sterile catgut.
31. A transdermal fentanyl patch (75 µg/h) is attached to the left dorsolateral lumbar region of the dog following closure of the thoracic incision and kept for 48 h after surgery. The position of the patch remains behind the following dressing so that it can be visually monitored for proper adherence to the skin.
32. After all surgical procedures are completed, the pneumothorax is reduced by repeatedly aspirating, via the chest tube, with a 50 mL syringe or suction tube until no air can be aspirated. The draining tube is then removed by pulling it out and the small exit wound sutured with no more than 2 silk stitches.
33. An additional dose of cefazolin (20 mg/kg I.M.) and of buprenorphine (0.01 mg/kg SQ), as well as meloxicam (0.2 mg/kg SQ) are given at the end of surgery.
34. Betadine should be applied to all surgical incisions. Surgical dressings are then placed over the surgical incision and the exit sites of the implanted instrumentation devices, and a wrap is placed around the thorax. Representative images of instrumented heart under X-ray fluoroscopy and surgery are shown in Fig. 1.

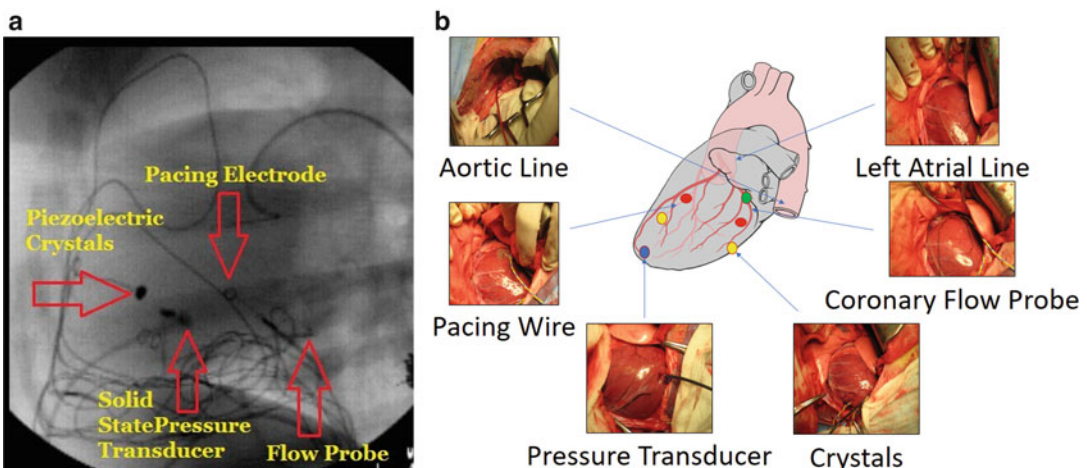


Fig. 1 Images of instrumented heart under X-ray fluoroscopy (a) and during open-chest surgery (b)

3.2 Anesthetic Recovery and Postoperative Care

1. During the postsurgical recovery, the dog is placed in a heated cage (*see Note 4*). Recovery from anesthesia is monitored by the staff.
2. The endotracheal tube is removed when the dog regains the swallowing reflex and/or coughs.
3. The following parameters are recorded every 15 min: temperature, heart rate, respiratory rate, and capillary refill time. This monitoring is continued until and the dog is awake and able to maintain sternal recumbency and rectal temperature is ~98 F.
4. Meloxicam is given at the dose of 0.1 mg/kg PO once daily for 5 days following surgery. Moreover, cefazolin is given at the dose of 40 mg/kg IM once daily for 5 days, followed by azithromycin at the dose of 5 mg/kg, orally, twice daily, for another 5 days. The dose of azithromycin is increased to 10 mg/kg if the dog temperature is >103.0 F (*see Note 5*).
5. Dogs are observed a minimum of twice daily by research personnel for 2 days following surgery, and at least once daily for the remaining 8 days of postsurgical recovery. The fentanyl patch is maintained for 48 h postoperatively (*see Note 6*).
6. Any suture that is nonabsorbable (silk or staples) is removed 10 days after surgery. During the entire postsurgical phase of the protocol, until final euthanasia, the dogs constantly wear custom-made vests to protect the exteriorized wires and to hold, when necessary, the pacemaker box. The vests are changed whenever they are damaged and/or dirty. The points of wires and catheter exteriorization are checked at least every 7 days for possible local skin infections.
7. Eating and defecating functions and rectal temperature are checked daily. If, during the time of the experimental protocol,

temperature is >103.0 F, antibiotic therapy is started again with 10 mg/kg azithromycin PO twice daily (*see Note 5*). A possible alternative to azithromycin is enrofloxacin (Baytril) at 5–20 mg/kg, once daily PO.

3.3 Experimental Protocols

3.3.1 Jackets

1. Once the 10-day postsurgical recovery is complete, wires and catheters can be exteriorized by gently pulling the silk threads that were left tied to their distal ends (buried under the skin) and sticking out of the skin. If the surgical wounds of the wires and catheters sites are well-healed, wires and catheters may be exteriorized earlier, but no sooner than day 7 after surgery. Performing this maneuver at 7 days rather than 10 days post-op renders it less traumatic, since the wound reparative tissue is still very soft. This procedure is preceded by local infiltration with 4 mL of 1% lidocaine.
2. Wires and catheters remain exteriorized for the rest of the protocol, until final euthanasia. They are protected by special jackets worn by the dog. Jackets are checked daily to ensure a proper and comfortable fit and, if torn, damaged or soiled they are replaced. They are changed at least once every 14 days or more frequently if needed. Soft tubular collars are also placed around the dogs' necks to prevent them from reaching the exteriorized wires and catheters.

3.3.2 Table Training

1. Dogs undergo training on the laboratory table starting no sooner than day 8 of the postsurgical recovery (which lasts 10 days) and is continued until the dog is deemed ready for an experiment in the conscious state (usually 2–3 sessions).
2. Training is performed for a maximum of once daily and consists of having the dogs rest on their right side on the study table for gradually increasing periods of time (starting at 15–30 min and increasing to 2 h) (*see Note 7*).
3. Dogs are never left unattended while on the study table. The maximum time a dog is on the table for training or assessment/testing procedures does not exceed three continuous hours and not exceed a total of 3 h per day.

3.3.3 Experiments in the Conscious State

1. Experiments can be started on day 10 after surgery. The dogs lie quietly on the laboratory table with the same modalities described in the “Table training” Subheading 3.3.2 and for the entire duration of the experiment.
2. Catheters are connected to pressure gauges and/or syringes and wires to the electronic equipment for hemodynamic measurements. Echocardiography is a regularly performed noninvasive procedure.

3.4 Coronary Vessels and Ventricular Catheterization

3.4.1 Catheterizations for Pressure Measurement and Blood Sampling

Coronary artery, coronary sinus, and ventricular catheterizations serve three purposes: blood pressure measurement, blood sampling and delivery of therapeutic agents.

1. A percutaneous cephalic catheter is placed in all animals for ready venous access in case emergency general sedation/anesthesia is required due to unforeseen procedural complications. Propofol is made available on site to rapidly induce rapid anesthesia during the procedure if some unforeseen procedural complications render it necessary.
2. Procedures for femoral artery or vein and peripheral vein cannulation (saphenous or cephalic vein) are similar. The skin is shaved with an electrical razor, disinfected with a disinfectant scrub followed by a rinse and then Betadine. The skin is infiltrated locally with 3–4 mL of 1% lidocaine and a 6–8 French sheath (depending on the size of the catheter) is inserted percutaneously in the vessel according to standard procedures, consisting in the introduction of a needle first, followed by a guidewire and finally the catheter is pushed in the vessel along the guidewire. No cutdown is necessary. One to two additional milliliters of lidocaine are injected in case the dog shows signs of sufferance.

The femoral artery is localized by palpation and the femoral vein is medial to it. In some cases, we might find useful an external Doppler echo probe to more precisely localize these two vessels. Catheterizations are then performed under sterile conditions unless the dog is undergoing a terminal experiment, immediately followed by euthanasia.

3. If the procedure is not terminal, a manual compression is applied with a sterile surgical sponge on the vessel, after catheter and sheath removal, in order to favor local blood coagulation. If the access is venous, the compression is held for 10 min and, if it is arterial, the compression is held for 20 min.
4. A tight multilayered sterile bandage is applied prior to final wrap, in order to provide the required pressure wrap. The bandage will be left in place for the following 12 h and the dog monitored while in the cage every 30 min for at least 3 h after the procedure. If proper hemostasis is achieved, adverse events are rare. Only the femoral artery catheterization, due to higher blood pressure in that vessel, can sometimes be followed by blood extravasation and swelling of the inguinal area. In that case a tighter bandage will be applied and, in cases the animal exhibits signs of limb swelling and/or pain and distress, veterinary input will be immediately sought to determine the optimal course of action. In some cases, especially in heart failure dogs, it may be very difficult to localize peripheral and femoral

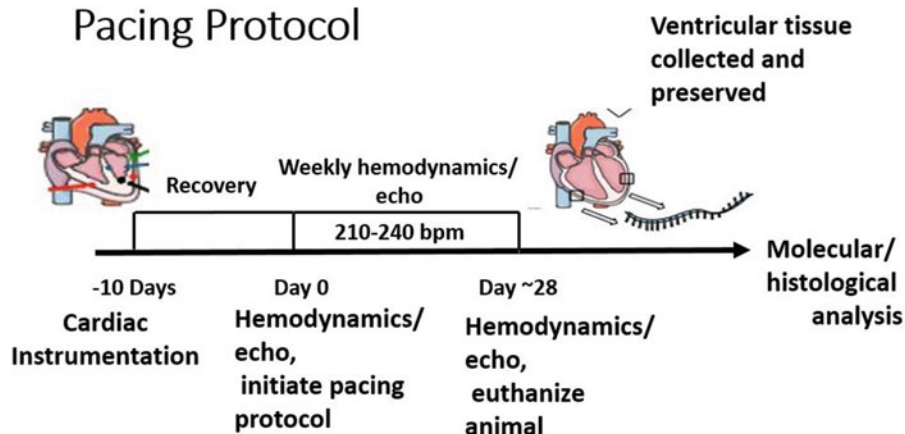


Fig. 2 Overview of pacing protocol

vessels. If the experiment is terminal, should coronary sinus catheterization be essential, one of the external jugular veins is utilized as an alternative. Given its very superficial position, this is easily identifiable and can be cannulated in conscious dogs using the same procedure described above. (Jugular vein cannulations are often performed in nonanesthetized human patients.)

3.5 Pacing-Induced Heart Failure

1. Heart failure is induced by high frequency cardiac pacing with an external pacemaker connected to the leads via external wires and carried on the shoulder, in the vest pocket. The pacing protocol is started no sooner than 10 days after surgery. It is summarized in Fig. 2.
2. Baseline hemodynamic and echocardiographic measurements are obtained (*see Notes 1 and 8*).
3. The left ventricle is then continuously paced at 210 beats/min for 3 weeks and, after the third week, the pacing rate is increased to 240 beats/min. The voltage generated by the pacemaker should be adjusted to the minimum sufficient to stimulate contraction at the desired rate (*see Notes 9 and 10*).
4. To assess the animals' progression into compensated/decompensated heart failure, cardiac function should be assessed every 7 days at a minimum (*see Note 9*).

3.6 Methods of Euthanasia

At the end of each experiment design in a specific protocol, the scientifically preferred means of euthanasia is cardiectomy under general anesthesia.

1. Anesthesia is induced with propofol (5 mg/kg I.V.) and the dog is intubated and ventilated with 100% oxygen and 5% isoflurane.

2. The chest is rapidly opened, and, while the heart is still beating, cardiac tissue samples are collected and immediately frozen for subsequent biochemical and molecular analysis. Other samples are fixed for histological analysis. Alternatively, the dogs can be rapidly euthanized with Euthasol (1 mL/10 lbs. I.V.) or sodium pentobarbital (100 mg/kg I.V.) followed by 20 mL of saturated KCl solution I.V.

4 Notes

1. Our standard battery of hemodynamic measurements consists of the following parameters: LV pressure (and thus LV dP/dt , LV systolic pressure, and LV end-diastolic pressure), aortic pressure (systolic, diastolic, mean), LV diameter (from piezoelectric crystals), coronary blood flow (from Doppler probe), and left atrial pressure (systolic, diastolic, mean). If there is an indwelling right ventricular catheter, systolic, end-diastolic, and dP/dt max can be measured in the right ventricle as well. If an indwelling catheter is not placed in the LV or if the catheter is rendered unusable (i.e., it stops working or the animal chews the externalized connector), a transducer can be inserted invasively through the femoral artery. This ideally requires three people: one to cannulate the artery, one to hold the opposite rear leg to expose the groin, and one to stay at the animal's head to distract it. To cannulate the right femoral artery, the animal should be lying on its right side. One person should be standing behind the animal holding its left rear leg up in the air with their right hand and holding its right leg parallel to the table with their left hand. The groin of the animal should be shaved. The person cannulating the artery should be able to locate the femoral artery easily by palpating the pulse. Once the artery is located, the area should be infiltrated with approximately 4 mL of 1% lidocaine. Approximately 0.5 cm caudal to the artery (so as to not immediately puncture the artery upon puncturing the skin), a 1 cm incision should be made, but only through the top layer of skin. A puncture needle should be inserted through the incision, through the next layer of skin, and then into the artery. Once the artery is punctured (as indicated by bright red, spurting blood; if the blood is dark red and/or oozing, you have punctured the femoral vein. Applying pressure for approximately 1 min should be sufficient to stop the bleeding), insert a guide wire through the needle, remove the needle, and then place a 6 or 7 Fr. sheath into the artery. At this point, a pressure catheter can be inserted through the sheath and ultimately into the LV. If this is a terminal procedure, no pressure bandage is necessary. If this is not a terminal procedure, direct pressure must be

applied to the wound immediately upon removal of the sheath until hemostasis occurs (typically 20 min). A pressure bandage must then be applied and left on the animal overnight. If multiple catheterizations need to be performed on the same animal over the course of the protocol, cannulation of the artery should be performed as distal as possible, so that the same leg can be used multiple times.

2. During the acclimation period, laboratory staff should interact with the animals at a minimum of once per day if possible. Since hemodynamic and echocardiographic measurements will be performed in the conscious state, familiarity with lab personnel minimizes the chance that the animals will be nervous, and thus in state of sympathetic overstimulation, when these measurements are taken.
3. Ventricular arrhythmia: dogs are monitored continuously during the surgical period with ECG. Dogs that develop ventricular arrhythmia are treated with lidocaine (2 mg/kg, I.V.). In case of ventricular fibrillation, dogs are defibrillated with a surgical manual defibrillator. Dogs that do not respond to these treatments are euthanized.

Infections: Clinical signs of infection may include discharge from catheter/wire sites, swelling and redness of skin surrounding exteriorization sites increased body temperature, decreased food consumption and activity, and weight loss. Should dogs show signs and symptoms of infection, staff veterinarians are consulted to determine the necessary treatments. Animals are euthanized if infections do not respond to treatment.

4. The body temperature of the animal can get as low as 95 degrees F if the chest is open for an extended period (>1.5 h). Hypothermia can be alleviated by placing a heating pad on the operating table, under the dog, throughout the duration of the surgery. Additionally, it is useful to preheat the recovery cage, for instance with a heater blowing hot air into it.
5. The body temperature of the animals is sensitive to their level of physical activity and excitement. This means that elevated temperature due to the animal jumping around in the cage or pressure washing of the kennel can give a false indication of fever. If an animal has a temperature of 103.0–103.5 F in the morning, and there is reason to think that it may be nonmicrobial in origin; temperature should be rechecked 2–3 h after the possible stimulus has taken place. At this point, if the temperature is still elevated, medical intervention should be undertaken aggressively to minimize the possibility of endocarditis. Additionally, if the temperature is higher than 103.5 F, it is safe to assume that it is not due to excitement or physical activity.
6. Any dogs exhibiting signs of pain, such as guarding of surgical site, lethargy and decreased appetite, is evaluated by the

veterinary staff and treated as deemed appropriated following examination. During the 10 days of postsurgical recovery, surgical incision care involves inspection (once a day) of the thoracotomy incision as well as the instrument exteriorization sites. The chest wraps and bandages are changed and the exteriorization sites are cleaned with dilute betadine in case of delayed healing. Possible sores are treated with antibiotic-based ointments. If cases of delayed healing are discovered, a veterinary consult is obtained for additional evaluation and treatment.

7. Leg restraints are used while the dog is lying on the table as a secondary measure to prevent the dog from jumping off the table. Experiments rely on surgically implanted cardiac monitoring devices that are connected to a data acquisition system through exteriorized catheters and wires. A dog that jumps from the table could not only hurt himself (e.g., pulling catheters and probes connected to heart and vessels), but could damage the wires, catheters, and monitoring equipment that are crucial for collecting data. The leg restraints are made of soft cotton rope material (commercially available from veterinarian supply companies) that are loosely placed around the dog's anterior legs at the level of the carpal joints. Restraints are not going to be used on the rear legs because the animal will innately try to use its front legs to lift its body up. With simple restraints to the front legs the dog's behavior will be impeded from using them. Dogs are acclimated to the leg restraints as part of the table training process.
8. Due to the anatomy of the dog, echocardiographic analysis can best be performed on a v-shaped table (Fig. 3). The four-chambered apical view can best be obtained parasternally on



Fig. 3 V-table to facilitate echocardiographic analysis

the left side of the dog's thorax at approximately the fifth rib space (this can vary between animals). This will involve the animal lying in its right side. Be sure that the staples have been removed from the thoracic incision, as these can obstruct the view. Two-chamber long and short axis views can best be obtained parasternally on the right side of the thorax at approximately the fifth rib space (this can vary between animals). This requires the animal to be on its left side. When switching from right to left laterally recumbency, many animals do not like being upside down, so the animal should be flipped on such a way that this does not occur.

9. The pacing rate is checked daily by auscultation with a stethoscope and/or palpation of the femoral pulse. If the animal is found not in pacing (either in sinus rhythm or pacing intermittently), the following steps should be followed: (1) ensure the pacing leads are connected to the terminals of the pacer, ideally with the screw lead connected to the negative terminal and the loop lead(s) connected to the positive terminal; (2) ensure the pacer batteries are properly charged, and change them out if they are not; (3) if these two conditions are met, increase the voltage of the pacer until the desired heart rate is resumed. If the heart still does not respond to pacing at maximum voltage, try applying different combinations of leads connections to the pacer. In rare cases, the formation of cardiac scar tissue around the pacing electrodes progresses with such rapidity that pacing cannot be resumed. If this occurs early enough in the pacing protocol (i.e., when no ventricular remodeling has been observed), the animal can be allowed a minimum of 1 week to recover and, if hemodynamics and echocardiography demonstrate that cardiac function and dimensions have returned to baseline values, the animal can be used as a normal control. If not, the animal may need to be euthanized. In this model, the first 3 weeks of pacing lead to compensated heart failure [22], in which the systolic function deteriorates, but pulmonary gas exchange is preserved, and the general condition of the animal remain stable, with no sign of sufferance. During the last week, when the pacing rate is set at 240 bpm, it is advisable to check cardiac function every other day since rapid decompensation can occur. We define end stage failure as the time when left ventricular end-diastolic pressure reaches 25 mmHg. From prior studies [22, 26], we know that this value of pressure is typically found during the fourth week of pacing (at the end of the study), concomitant with a drop in arterial PO₂, various signs of cardiac decompensation, including varying degrees and combinations of anorexia, lethargy, weight loss, exercise intolerance, tachypnea (increased respiratory rate), dyspnea (difficulty breathing), cyanosis (bluish mouth mucus membranes

from decreased blood oxygen levels), moist cough, peripheral edema (swelling of the extremities), pulmonary edema (fluid in the lungs), ascites (fluid in the abdomen), and rarely sudden death. By monitoring this combination of cardiac parameters and clinical signs, we know precisely how heart failure is progressing and are able to define as each animal approaches and enters decompensated heart failure. Every effort should be made to initiate the terminal studies as soon as animals show signs of decompensated failure and therefore minimize the time of this condition, which in general does not last for more than 24 h. Dyspnea is the most critical sign that prompts the performance of final experiment and euthanasia within the 24 h or simple euthanasia in case of impossibility to rapidly perform an experiment.

10. Dogs are euthanized before the end of the pacing protocol when they lose 20% or more of the baseline weight recorded on the day of arrival. Additionally, initiation of the pacing protocol can sometimes induce nausea during the first 1–2 days of pacing. This can sometimes be alleviated by administering Sucralfate 40 mg/kg PO in a slurry.

5 Acknowledgments

This work was supported by NIH grant R01HL129120-01A1.

References

1. Whipple GHS LT, Woodman EG, Theophilis C, Friedman S (1962) Reversible congestive heart failure due to chronic rapid stimulation of the normal heart. *Proc N Engl Cardiovasc Soc* 20:39–40
2. Recchia FA, Lionetti V (2007) Animal models of dilated cardiomyopathy for translational research. *Vet Res Commun* 31(Suppl 1):35–41. <https://doi.org/10.1007/s11259-007-0005-8>
3. Dixon JA, Spinale FG (2009) Large animal models of heart failure: a critical link in the translation of basic science to clinical practice. *Circ Heart Fail* 2(3):262–271. <https://doi.org/10.1161/CIRCHEARTFAILURE.108.814459>
4. Riegger AJ, Liebau G (1982) The renin-angiotensin-aldosterone system, antidiuretic hormone and sympathetic nerve activity in an experimental model of congestive heart failure in the dog. *Clin Sci (Lond)* 62(5):465–469
5. Wang W, Chen JS, Zucker IH (1991) Carotid sinus baroreceptor reflex in dogs with experimental heart failure. *Circ Res* 68 (5):1294–1301
6. Shannon RP, Komamura K, Stambler BS, Bigaud M, Manders WT, Vatner SF (1991) Alterations in myocardial contractility in conscious dogs with dilated cardiomyopathy. *Am J Physiol* 260(6 Pt 2):H1903–H1911. <https://doi.org/10.1152/ajpheart.1991.260.6.H1903>
7. Komamura K, Shannon RP, Pasipoularides A, Ihara T, Lader AS, Patrick TA, Bishop SP, Vatner SF (1992) Alterations in left ventricular diastolic function in conscious dogs with pacing-induced heart failure. *J Clin Invest* 89 (6):1825–1838. <https://doi.org/10.1172/JCII15787>
8. O'Rourke B, Kass DA, Tomaselli GF, Kaab S, Tunin R, Marban E (1999) Mechanisms of altered excitation-contraction coupling in canine tachycardia-induced heart failure, I: experimental studies. *Circ Res* 84(5):562–570
9. Smith CJ, Huang R, Sun D, Ricketts S, Hoegler C, Ding JZ, Moggio RA, Hintze TH

- (1997) Development of decompensated dilated cardiomyopathy is associated with decreased gene expression and activity of the milrinone-sensitive cAMP phosphodiesterase PDE3A. *Circulation* 96(9):3116–3123
10. Kiuchi K, Shannon RP, Komamura K, Cohen DJ, Bianchi C, Homcy CJ, Vatner SF, Vatner DE (1993) Myocardial beta-adrenergic receptor function during the development of pacing-induced heart failure. *J Clin Invest* 91(3):907–914. <https://doi.org/10.1172/JCI116312>
 11. Kirk JA, Chakir K, Lee KH, Karst E, Holewinski RJ, Pironti G, Tunin RS, Pozios I, Abraham TP, de Tombe P, Rockman HA, Van Eyk JE, Craig R, Farazi TG, Kass DA (2015) Pacemaker-induced transient asynchrony suppresses heart failure progression. *Sci Transl Med* 7(319):319ra207. <https://doi.org/10.1126/scitranslmed.aad2899>
 12. Traverse JH, Chen Y, Hou M, Li Y, Bache RJ (2007) Effect of K_{ATP} channel and adenosine receptor blockade during rest and exercise in congestive heart failure. *Circ Res* 100(11):1643–1649. <https://doi.org/10.1161/CIRCRESAHA.107.150219>
 13. Morimoto A, Hasegawa H, Cheng HJ, Little WC, Cheng CP (2004) Endogenous beta3-adrenoreceptor activation contributes to left ventricular and cardiomyocyte dysfunction in heart failure. *Am J Physiol Heart Circ Physiol* 286(6):H2425–H2433. <https://doi.org/10.1152/ajpheart.01045.2003>
 14. Martelli D, Silvani A, McAllen RM, May CN, Ramchandra R (2014) The low frequency power of heart rate variability is neither a measure of cardiac sympathetic tone nor of baroreflex sensitivity. *Am J Physiol Heart Circ Physiol* 307(7):H1005–H1012. <https://doi.org/10.1152/ajpheart.00361.2014>
 15. Lionetti V, Guiducci L, Simionici A, Aquaro GD, Simi C, De Marchi D, Burchielli S, Pratali L, Piacenti M, Lombardi M, Salvadori P, Pingitore A, Neglia D, Recchia FA (2007) Mismatch between uniform increase in cardiac glucose uptake and regional contractile dysfunction in pacing-induced heart failure. *Am J Physiol Heart Circ Physiol* 293(5):H2747–H2756. <https://doi.org/10.1152/ajpheart.00592.2007>
 16. Spinale FG, Coker ML, Thomas CV, Walker JD, Mukherjee R, Hebbar L (1998) Time-dependent changes in matrix metalloproteinase activity and expression during the progression of congestive heart failure: relation to ventricular and myocyte function. *Circ Res* 82(4):482–495
 17. Marcus NJ, Del Rio R, Schultz HD (2014) Reply from Noah J. Marcus, Rodrigo Del Rio and Harold D. Schultz. *J Physiol* 592(8):1905–1906. <https://doi.org/10.1113/jphysiol.2014.273565>
 18. Harada M, Tsuji Y, Ishiguro YS, Takanari H, Okuno Y, Inden Y, Honjo H, Lee JK, Murohara T, Sakuma I, Kamiya K, Kodama I (2011) Rate-dependent shortening of action potential duration increases ventricular vulnerability in failing rabbit heart. *Am J Physiol Heart Circ Physiol* 300(2):H565–H573. <https://doi.org/10.1152/ajpheart.00209.2010>
 19. Park M, Shen YT, Gaussin V, Heyndrickx GR, Bartunek J, Resuello RR, Natividad FF, Kitsis RN, Vatner DE, Vatner SF (2009) Apoptosis predominates in nonmyocytes in heart failure. *Am J Physiol Heart Circ Physiol* 297(2):H785–H791. <https://doi.org/10.1152/ajpheart.00310.2009>
 20. Rademaker MT, Cameron VA, Charles CJ, Richards AM (2005) Integrated hemodynamic, hormonal, and renal actions of urocortin 2 in normal and paced sheep: beneficial effects in heart failure. *Circulation* 112(23):3624–3632. <https://doi.org/10.1161/CIRCULATIONAHA.105.561308>
 21. Khatiwala JR, Everly MJ (2015) An update on cardiac transplantation in the United States based on an analysis of the UNOS registry. *Clin Transpl* 31:27–34
 22. Woitek F, Zentilin L, Hoffman NE, Powers JC, Ottiger I, Parikh S, Kulczycki AM, Hurst M, Ring N, Wang T, Shaikh F, Gross P, Singh H, Kolpakov MA, Linke A, Houser SR, Rizzo V, Sabri A, Madesh M, Giacca M, Recchia FA (2015) Intracoronary Cytoprotective gene therapy: a study of VEGF-B167 in a pre-clinical animal model of dilated cardiomyopathy. *J Am Coll Cardiol* 66(2):139–153. <https://doi.org/10.1016/j.jacc.2015.04.071>
 23. Pepe M, Mamdani M, Zentilin L, Csiszar A, Qanud K, Zacchigna S, Ungvari Z, Puligadda U, Moimas S, Xu X, Edwards JG, Hintze TH, Giacca M, Recchia FA (2010) Intramyocardial VEGF-B167 gene delivery delays the progression towards congestive failure in dogs with pacing-induced dilated cardiomyopathy. *Circ Res* 106(12):1893–1903. <https://doi.org/10.1161/CIRCRESAHA.110.220855>
 24. Simpson S, Edwards J, Emes RD, Cobb MA, Mongan NP, Rutland CS (2015) A predictive model for canine dilated cardiomyopathy-a meta-analysis of Doberman pinscher data. *PeerJ* 3:e842. <https://doi.org/10.7717/peerj.842>

25. Kiczak L, Tomaszek A, Paslawska U, Bania J, Noszczyk-Nowak A, Skrzypczak P, Paslawski R, Zacharski M, Janiszewski A, Kuropka P, Ponikowski P, Jankowska EA (2015) Sex differences in porcine left ventricular myocardial remodeling due to right ventricular pacing. *Biol Sex Differ* 6:32. <https://doi.org/10.1186/s13293-015-0048-4>
26. Mitacchione G, Powers JC, Grifoni G, Woitek F, Lam A, Ly L, Settanni F, Makarewicz CA, McCormick R, Trovato L, Houser SR, Granata R, Recchia FA (2014) The gut hormone ghrelin partially reverses energy substrate metabolic alterations in the failing heart. *Circ Heart Fail* 7(4):643–651. <https://doi.org/10.1161/CIRCHEARTFAILURE.114.001167>



Chapter 25

Swine Model of Mitral Regurgitation Induced Heart Failure

Shin Watanabe, Olympia Bikou, Roger J. Hajjar, and Kiyotake Ishikawa

Abstract

Mitral regurgitation (MR) is among the most common valvular heart diseases in clinics. MR induces volume overload of the heart and leads to heart failure (HF). Because physiological and molecular mechanisms in nonischemic HF are distinct from that of ischemic HF, a clinically relevant animal model of nonischemic HF is important for understanding the pathophysiology and developing new therapeutics targeting this HF phenotype. Additionally, the large animal model of MR provides opportunities to test new surgical and percutaneous approaches for correcting mitral valve insufficiency.

In this chapter, we describe protocols for inducing MR in pigs using percutaneous approaches. Specifically, mitral valve chords are cut by a cardiac biopsy catheter inserted either antegrade (transseptal through venous access) or retrograde (arterial access) into the left ventricle. Both acute and chronic HF can be induced using this technique, and left atrial enlargement can be found at the chronic stage.

Key words Heart failure, Mitral regurgitation, Nonischemic, Volume overload, Biopsy catheter, Echocardiography, Mitral insufficiency, Transseptal, Left atrial enlargement

1 Introduction

Mitral regurgitation (MR) is among the most common valvular heart diseases [1]. MR is classified as either primary or secondary. Primary causes are structural or degenerative abnormalities at any level of the mitral valve (MV) apparatus (leaflets, chordae tendineae, papillary muscles, mitral annulus). Secondary causes are those associated with left ventricular (LV) geometrical alterations that impair proper function of the MV apparatus, usually from LV dysfunction without organic MV diseases.

MR causes left atrial and LV volume overload and is one of the most prevalent causes of chronic nonischemic HF in clinics. The pathology and molecular mechanisms of heart failure (HF) due to MR is different from ischemic cause such as myocardial infarction [2, 3]. Considering that >30% of HF with reduced systolic function is reported to be of non-ischemic origin in clinic [4], large animal models of non-ischemic HF are essential for developing new

therapies, improving diagnostics, and deepening our understandings in pathophysiology.

Recent advances in percutaneous interventions provide options to treat mitral insufficiency without opening the chest. New devices are developed in a rapid pace, and efficacy as well as safety of these devices needs to be tested in animals before clinical application. A reproducible MR model is thus also useful for these applications. Importantly, enlarged left atrium (LA) in chronic MR model can be particularly useful to more closely replicate clinical MR condition.

In this chapter, we describe protocols for inducing MR by severing the mitral valve chordae tendinae in pigs, using two different percutaneous approaches. The antegrade approach method uses transseptal puncture to access the mitral valve chords through the LA. Using steerable sheath, this approach allows stable control of the catheter through a femoral venous access. Good understanding of 3D composition of the LV and LA is essential to avoid cardiac perforation as well as injury of the aortic root and surrounding tissues. In contrast, retrograde approach accesses the mitral valve cords from the aorta side via carotid arterial access. While this approach avoids risks of complications associated with transseptal puncture, catheter stability is somewhat hampered and access to the basal part of the LV (mitral valve itself) is challenging.

We previously reported that acute mortality of this procedure was 5.1% (2 out of 39 pigs) associated with massive MR. After successful induction of at least moderate MR, 30-days survival was 85.7% in pigs with moderate MR, whereas it was 47.6% in those with severe MR [5]. LA size increases significantly after 1 month (33.3 ± 2.5 mm vs. 39.8 ± 4.4 mm, before MR vs. 1 month post-MR). The procedure usually takes 30 min to 1 h, once the operator understands the anatomy and becomes familiar with the required skills. Because the procedure causes injuries to the mitral valve apparatus and sometimes to the endocardium, infective endocarditis may develop. Therefore, perioperative anti-infection medication is important to avoid this complication.

2 Materials

1. Pig (20–30 kg) (*see Note 1*).
2. Heating mat for maintaining the body temperature.
3. Mechanical ventilator for large animals.
4. Standard catheterization pack: sterile drape, syringes, puncture needle, etc.
5. Vital monitors including pressure sensors.
6. Contrast agent for angiogram.
7. 8 Fr introducer standard sheath for vascular access.

8. 70% isopropyl alcohol.
9. Povidone–iodine.
10. Analgesic: buprenorphine.
11. Anesthetics: Telazol (tiletamine/zolazepam) and propofol.
12. Heparin sodium.
13. Saline or phosphate buffered saline (PBS).
14. 8.5-Fr (inner lumen) Steerable introducer.
15. 8 Fr Long sheath.
16. Brockenbrough needle or 0.025 inch wire.
17. 5 or 6 Fr pig-tail catheter.
18. 7 Fr biopsy catheter.
19. Furosemide.
20. Nitroglycerin.
21. Cefazolin.
22. Gentamycin.

3 Methods

3.1 Antegrade Approach

1. Premedicate the animal using Telazol (tiletamine/zolazepam) (8.0 mg/kg) and buprenorphine (0.6 mg) (*see Note 2*).
2. Intubate the animal and then ventilate. Obtain a venous access on the ear vein. General anesthesia is maintained with Propofol (8–10 mg/kg/h) throughout the procedure (*see Note 2*).
3. Intravenously inject gentamycin (80 mg) before any additional intervention.
4. Place the animal in dorsal position on a heating mat. Tie its legs loosely to the table. Connect the monitors on the animal. The femoral puncture site is prepared with 70% isopropyl alcohol followed by povidone–iodine. Percutaneous punctures provide access to the vein and artery for sheath placements (*see Note 3*).
5. Puncture the femoral vein and the artery using the Seldinger technique with an echocardiographic guidance.
6. Insert 8.5-Fr steerable sheath into the femoral vein and 8 Fr standard sheath into the femoral artery.
7. Administer heparin sodium at the dose of 200–300 U/kg IV to achieve an activated coagulation time of >250 s.
8. Advance the pigtail catheter to the ascending aorta through the arterial sheath for monitoring the aortic pressure and prompt assessments of mitral regurgitation.
9. Advance the tip of the 8.5-Fr steerable sheath to the right atrium under fluoroscopy.

10. Bend the steerable sheath tip to 60°–80° and insert the tip into the right ventricle. Under 90° Right Anterior Oblique (RAO) imaging, the catheter should be facing toward the right side. Pressure change can be realized if the sheath is connected to the pressure sensor.
11. Rotate the steerable sheath clockwise for about 90°. The catheter will rotate toward the atrial septum. Move and adjust the catheter position to find a location where the catheter becomes fixed at the foramen ovale. This is the thinnest part of the atrial septum. Under X-ray, the catheter tip should be facing almost perpendicular to the image with RAO 90° (Fig. 1a). Slightly move the catheter counterclockwise and confirm that it moves

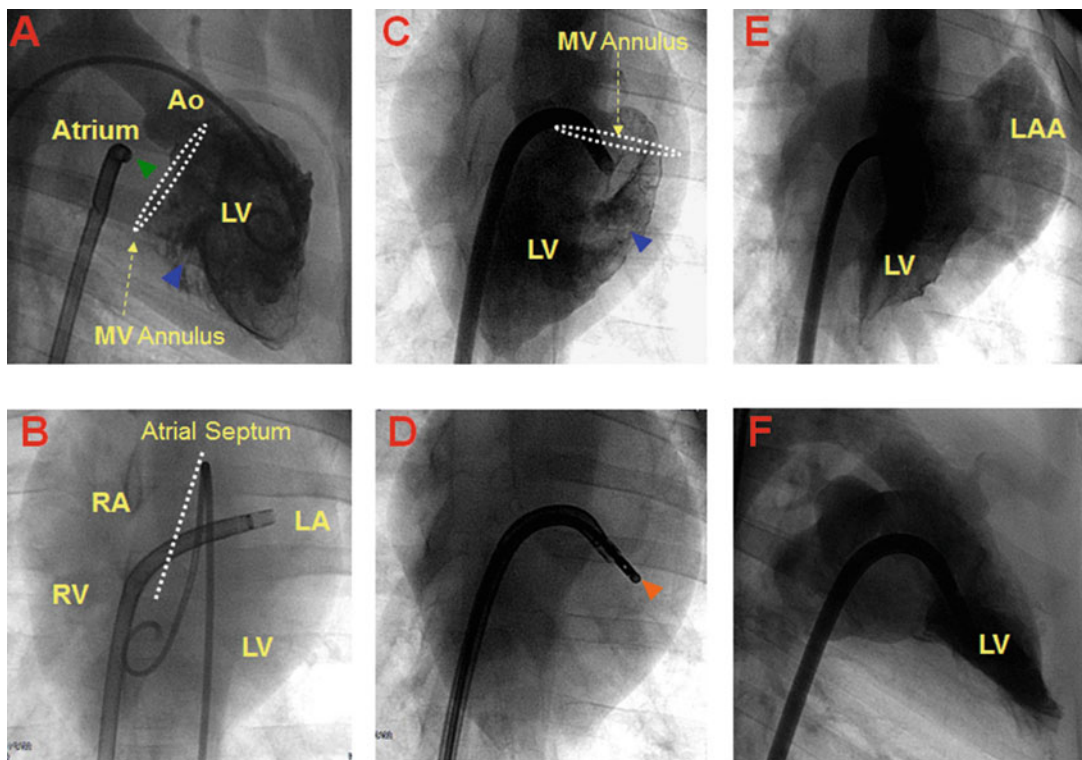


Fig. 1 Angiographic images during the procedure. (A) Left ventriculography with pigtail catheter in lateral view (RAO 90°). Green arrowhead indicates the tip of the steerable introducer at the fossa ovalis. Blue arrowhead indicates the papillary muscle. (B) AP view after advancing the introducer into the LA. (C) Left ventriculography from the sheath to check the position of the mitral valve and the papillary muscles in AP view. Blue arrowhead indicates the lateral papillary muscle. (D) AP view. Orange arrowhead shows the tip of the biopsy catheter positioned at the posterolateral part of the basal left ventricle for severing the chordae tendineae. (E, F) Representative left ventriculography in LV systolic phase after this procedure (AP and RAO 90°). Severe MR flow reaching the LA roof, LAA, and the pulmonary veins. (Ao Aorta, LA Left atrium, LAA LA appendage, LV Left ventricular, RA Right atrial, RV Right ventricular, MV Mitral valve, AP Anteroposterior, RAO Right anterior oblique)

toward right side. Moving toward left side with counterclockwise rotation indicates that the catheter is facing the right atrial free wall (180° reverse direction). In this case, place the catheter tip back into the right ventricle and repeat this step.

12. Change the fluoroscopic view to the anteroposterior (AP) direction. The catheter should be facing the septum.
13. Under fluoroscopic guidance, puncture the atrial septum at the foramen ovale using a Brockenbrough needle (*see Notes 4 and 5*) (Fig. 1). Inject small amount of contrast through the needle and confirm that the tip is inside the LA.
14. Once the Brockenbrough needle is inside the LA, proceed a dilator or a 5 Fr catheter. When advancing the dilator, pay attention to the tip of the needle as advancing the whole system may insert the needle too deep and can cause LA free wall perforation (*see Note 6*).
15. After insertion of the dilator into the LA, advance the steerable sheath. When there is a resistance at the septum, rotate the sheath slightly both clockwise and counterclockwise. This will facilitate catheter pass through the septal wall. Once the sheath is inside the LA, remove the dilator and the needle and connect the sheath to the pressure sensor. Flush the sheath with saline while paying careful attention not to inject air.
16. Advance a biopsy catheter to the tip of the steerable sheath.
17. Rotate the steerable sheath counterclockwise (*see Note 7*). Bend the sheath so that the tip faces posteroinferior wall of the LV (toward the bottom of the fluoro image in RAO 90°). Now, the sheath tip is positioned at the posterolateral part of the LV base. Rotate the sheath clockwise while monitoring the pressure and determine the location of the mitral valve (where the systolic pressure decreases from that of the LV to the LA).
18. Rotate the sheath back to counterclockwise direction. After the pressure wave has changed to the LV pressure, advance only the biopsy catheter while opening the tip widely. This will facilitate mitral chord capture and also reduces the risk of myocardial perforation. Close the tip of the biopsy catheter before feeling a strong resistance. (This means that the catheter is attached to the myocardium. This can be also visually seen with fluoroscopy.) Confirm the location of the tip of the biopsy catheter under fluoroscopy (Fig. 1D) and echocardiography (Fig. 2A) (*see Note 8*). The optimal tip location is around the middle of the mitral valve plane and the papillary muscle plane, facing 4–5 o'clock (posterolateral wall) in the short axis view under echocardiography.
19. After a good location of the biopsy catheter tip is confirmed by echocardiography, pull back the biopsy catheter into the

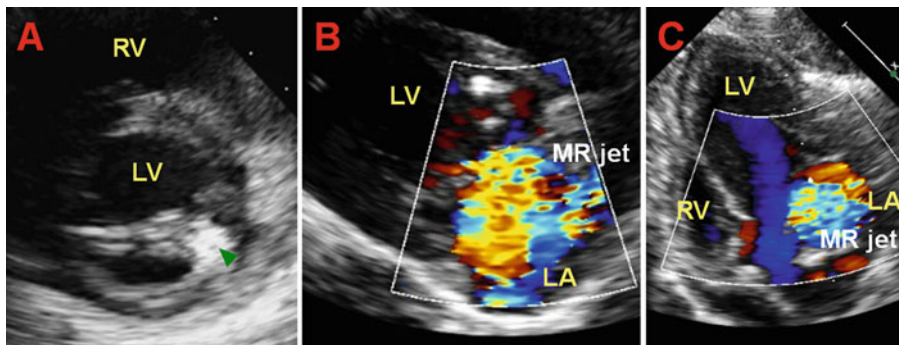


Fig. 2 Echocardiographic images during the procedure. **(A)** Short axis echocardiographic view at basal LV level during the antegrade procedure. Green arrowhead indicates the tip of the biopsy catheter. **(B, C)** Representative echocardiographic long axis and four chamber views showing the regurgitant flow after MR induction. (*LV* Left ventricular, *LA* Left atrium, *RV* Right ventricular, *MR* Mitral regurgitation)

steerable sheath. A loss of resistance can be felt when the chord is successfully severed (*see Note 9*).

20. Remove the biopsy catheter and flush the sheath. Evaluate the degree of MR with pressure, left ventriculography and echocardiography (*see Note 10*). Repeat steps 16–20 in Subheading 3.1 until desired degree of MR is established. (Figs. 1E, F and 2B, C)
21. Withdraw the steerable sheath and the pig-tail catheter.
22. Withdraw the sheaths from the vein and artery and achieve hemostasis by applying direct pressure to the site for several minutes.
23. Animals are treated daily with furosemide (50 mg) and nitroglycerin (5 mg) for three consecutive days, to prevent respiratory failure from acute congestive HF. Additionally, treat daily with intramuscular injection of gentamycin (80 mg) and cefazolin (25 mg/kg) for 3 days.

3.2 Retrograde Approach (*see Note 12*)

1. Repeat steps 1–4 in Subheading 3.1
2. Puncture the left carotid artery by using the Seldinger technique under echocardiographic guidance.
3. Insert 8 Fr long sheath into the carotid artery.
4. Administer heparin sodium at the dose of 200–300 U/kg IV to achieve an activated coagulation time of >250 s.
5. Advance the long sheath into the LV under fluoroscopic guidance.
6. Curve the tip of the biopsy catheter to J-shape (*see Note 13*).
7. Insert the biopsy catheter into the LV and slightly pull back the long sheath.

8. Rotate the sheath and the biopsy catheter and place it at the chordae tendinae of the lateral or medial part of the anterior leaflet using fluoroscopic and echocardiographic guidance.
9. After a good location of the biopsy catheter tip is confirmed by echocardiography, grasp the chord and pull back the biopsy catheter into the steerable sheath. A loss of resistance can be felt when the cord is successfully severed (*see Note 9*).
10. Repeat steps 20–23 in Subheading 3.1

4 Notes

1. For antegrade approach, length of the steerable sheath needs to be long enough to reach the LV through the atrial septum. For large pigs, check the necessary length before inserting the sheath.
2. All the protocols including analgesia, anesthesia, and antibacterial drugs are approved by the animal committee at the facility. Inhalational anesthetics can be used instead of propofol, however we experience vasodilatory effect with inhalational anesthetics, which may lower blood pressure and also cause under-estimation of the degree of MR after its induction.
3. Stretching the leg tightly will facilitate the vessel puncture. In young healthy animals, vessels can flexibly move and escape the needle when the legs are loosely stretched. Once the vascular accesses are established, loosen the tightened ropes.
4. Stiff end of the 0.025 inch wire can be used for puncturing the atrial septum instead of the Brockenbrough needle. Preshape the end as shown in Fig. 3. The size of the curve should be adjusted depending on the size of the animal (right atrium).
5. Pig tail catheter in the aorta will be the landmark for the aorta. Until the operator is well familiar with the anatomy, right atriogram may help understand the anatomy. When conducting the right atriogram, keep the fluoro-imaging long enough to capture the contrast flow into the LA, LV and the aorta. Intracardiac echo is also a useful tool to confirm the appropriate puncture site if it is available. However, once the operator has understood the anatomy and the catheter handling, fluoro-guidance is sufficient and we rarely experience complications associated with transseptal puncture.
6. Healthy pigs before MR induction have small LA. Advancing the needle too far can easily result in LA free wall puncture.
7. Use RAO 90° to determine the direction of the catheter. Rotating clockwise will rotate the catheter toward atrial side and counterclockwise will rotate the catheter toward the LV

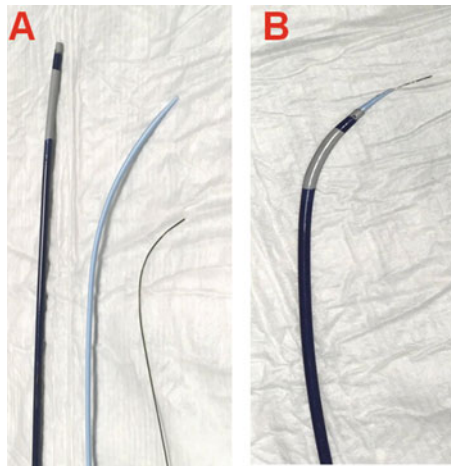


Fig. 3 The instrument description for the transseptal puncture. **(A)** Three components of the assembly: the steerable introducer, dilator, and a stiff wire. **(B)** The assembly with all three components put together. When manipulating the assembly to find the fossa ovalis, the stiff end of the wire should be concealed within the tip of the dilator. For puncturing the septum, the stiff end of the wire should be advanced for about 5 mm

side. AP view is useful in determining the depth of the sheath and the biopsy catheter from the septum toward LA free wall side.

8. Operator should be holding the catheter firmly, so that the grabbed chordae is not released. Repeat this step if the location in echocardiography is not ideal. Make sure that the catheter tip is not in the atrium. Severing the atrial wall leads to cardiac tamponade (*see Note 11*). When the tip is at the LV base, it can result in tear of the mitral valve itself. Meanwhile, when the chords are grasped too close to the papillary muscle, multiple chords can be cut after one attempt, which can result in massive MR.
9. Biopsy catheter needs to be tightly held so that the cord does not slip off.
10. We defined a successful acute severe MR as fulfilling at least one of the following criteria: angiographic (contrast dye reflux into the pulmonary veins) (Fig. 1e, f), echocardiographic (mitral regurgitation jet reaches the LA roof) (Fig. 2b, c), and hemodynamic (increase in LV end-diastolic pressure by 150%). This results in reproducible chronic HF. However, the mortality is high and depending on the goal of the projects, the criteria may be adjusted.
11. In case the pig developed cardiac tamponade, reverse heparin by injecting protamine sulfate as soon as possible. Puncture the pericardium from sub-sternum and insert a pigtail catheter.

Remove the blood until the bleeding stops. Echocardiography is useful to evaluate the amount of pericardial blood. Monitor the blood pressure and evaluate the hemodynamics continuously. Pericardial bleeding usually results in adhesions of the pericardium at the chronic stage. Animals should be excluded from the study if this can influence the study endpoints.

12. Femoral approach is possible using long guide sheath (7–8 Fr) with 5 Fr biopsy catheter. However, there is less controllability of the catheters and the procedure may take long. Because the steerable sheath is thick, placing this sheath in the artery may result in arterial dissection or post-procedure bleeding with high probability. If surgical access to the artery is available, this option may be considered.
13. Size of the curve should be adjusted based on the catheter positioning for grasping the mitral valve cord.

Acknowledgments

This work is supported by NIH R01 HL139963 (K.I.), HL117505, HL 119046, HL129814, 128072, HL131404, HL135093, a P50 HL112324 (R.J.H.), AHA-SDG 17SDG33410873 (K.I.), and two Transatlantic Fondation Leducq grants. We would like to acknowledge the Gene Therapy Resource Program (GTRP) of the National Heart, Lung, and Blood Institute, National Institutes of Health. O.B. was supported by the Deutsche Herzstiftung.

References

1. Nkomo VT, Gardin JM, Skelton TN et al (2006) Burden of valvular heart diseases: a population-based study. *Lancet* 368:1005–1011
2. Brillantes AM, Allen P, Takahashi T et al (1992) Differences in cardiac calcium release channel (ryanodine receptor) expression in myocardium from patients with end-stage heart failure caused by ischemic versus dilated cardiomyopathy. *Circ Res* 71:18–26
3. Sen L, Cui G, Fonarow GC et al (2000) Differences in mechanisms of SR dysfunction in ischemic vs. idiopathic dilated cardiomyopathy. *Am J Physiol Heart Circ Physiol* 279: H709–H718
4. Mosterd A, Hoes AW (2007) Clinical epidemiology of heart failure. *Heart* 93:1137–1146
5. Watanabe S, Fish K, Bonnet G et al (2017) Echocardiographic and hemodynamic assessment for predicting early clinical events in severe acute mitral regurgitation. *Int J Cardiovasc Imaging* 34(2):171–175



Chapter 26

Pig Model of Increased Cardiac Afterload Induced by Ascending Aortic Banding

Olympia Bikou, Satoshi Miyashita, and Kiyotake Ishikawa

Abstract

Increase in cardiac afterload as represented by hypertension is an established risk factor for cardiovascular diseases. Animal models of increased cardiac afterload offer studies aiming at identifying key molecular mechanisms and developing new therapeutic approaches. We have reported that banding of the ascending aorta in pigs results in significant cardiac hypertrophy and increased myocardial fibrosis at the chronic stages. These changes were accompanied by increased stiffness of the heart, but not by systolic dysfunction. In this chapter, we describe methods to surgically band the ascending aorta in pigs. After 3 months, animals develop systolic left ventricular pressure of >200 mmHg with above described changes in the heart.

Key words Heart failure, HFpEF, Diastolic dysfunction, Large animal, Chronic, Hypertrophic

1 Introduction

Patients with hypertension are at increased risk of suffering from myocardial infarction, stroke, and cardiovascular deaths [1]. Hypertension is also commonly found in patients suffering from heart failure with preserved ejection fraction, which currently has limited therapeutic approaches. Experimental studies also documented pathological changes attributed to increased afterload both in acute [2, 3] and chronic settings [4–6]. We have reported that banding of the ascending aorta in pigs results in significant cardiac hypertrophy and increased myocardial fibrosis at the chronic stages. These changes were accompanied by increased stiffness of the heart, but not by systolic dysfunction, thereby exhibiting similarities in the disease phenotype to heart failure with preserved ejection fraction. This pig model of increased cardiac afterload may thus lead to discovery of key molecular mechanisms and new therapeutic approaches for heart failure with preserved ejection fraction.

This chapter describes a protocol for creating a large animal model of pressure-overload induced heart failure by ascending aortic banding. Surgical aortic banding takes approximately 1 h

and the left ventricular pressure gradually increases as the animals grow. After 3 months, animals develop systolic left ventricular pressure of >200 mmHg with significant cardiac hypertrophy and increased fibrosis [4]. Systolic function remains preserved in this model in contrast to the rodent models of aortic constriction [7]. We have also reported that combination of aortic banding and myocardial infarction can exaggerate ischemic heart failure phenotype in pigs compared to myocardial infarction alone [5]. Degree of stenosis is adjusted by echocardiography during surgery and echocardiography can be used to serially monitor the development of cardiac hypertrophy and heart failure.

2 Materials

1. Standard surgical tools.
2. Electric cautery and grounding pad.
3. Anesthetics.
4. Sterile drape.
5. Silicon tube (Fig. 1).
6. Silicone Thoracic Drain.
7. Short ring to hold the silicon tube (we use a piece of ring cut from thoracic drain as shown in Fig. 1).
8. Clip (Fig. 1).
9. Umbilical tape.
10. Echocardiography.
11. Isoflurane.
12. Fentanyl transdermal patch, 25–50 µg/h.
13. Antibiotics.

3 Methods

1. After an appropriate acclimation period at the facility, schedule an animal for the surgery. Fast the animal overnight before surgery.
2. Sedate the animal and intubate for artificial ventilation. Start anesthesia and administer analgesics as well as preventive antibiotics.
3. Shave the surgical site as well as the hip area for placing the grounding pad.
4. Attach vital monitors including ECG electrodes and blood pressure monitoring cuff.

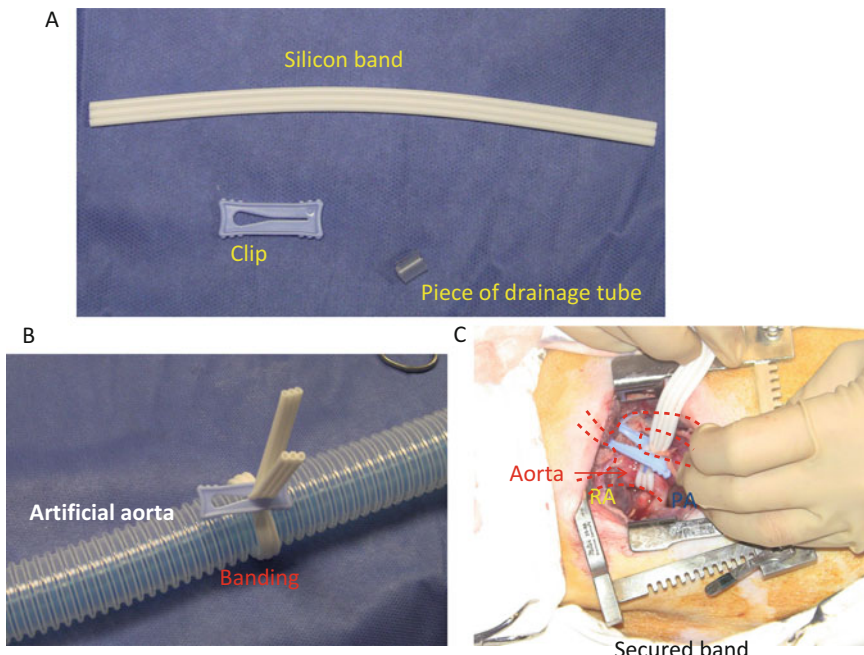


Fig. 1 Materials and scheme of aortic banding. **(A)** Materials used for banding the aorta. **(B)** Aortic banding on a mock aorta. Note that the ring (piece of drainage tube) is under the clip to keep both ends of band together. **(C)** Actual surgical banding of the aorta. Position of the Aorta is shown in dot lines. or (better)Dot lines indicate the position of the aorta.

5. Place the animal on a surgical table. Lightly pull and fix the upper limbs toward cranial direction (*see Note 1*).
6. Disinfect the surgical site and cover with a sterile drape.
7. Apply local anesthesia on the skin above the third intercostal space. The ribs can be felt over the skin (*see Note 2*). Wait for a while until the local anesthesia is in effect.
8. Make a 5 cm skin incision above the third intercostal space (*see Note 3*). Coagulate the bleeding spots using electrocautery.
9. Cut the lattisimus dorsi using electrocautery.
10. Cut the pleural membrane at the third intercostal space and widen the rib space using retractors (*see Note 4*). Obtain a good view of the pericardial sac inside the chest.
11. Use a wet gauze to push the lung out of the surgical window toward dorsal direction. Remember the number of gauzes placed inside the chest.
12. Pulsating pulmonary artery inside the pericardial space can be seen and felt. Make a small incision (3–4 cm) on the pericardium above the pulmonary artery (*see Note 5*).

13. Identify the aorta location by inserting a finger. Dissect the right side (bottom in surgical view) of the aorta using the finger.
14. Carefully and gently grasp the tunica adventitia of the pulmonary artery using forceps and pull it up. Make a small incision on the connective tissue between the pulmonary artery and the aorta.
15. Using a dull forceps, carefully dissect the connective tissues between the pulmonary artery and the aorta in the dorsal caudal direction (*see Note 6*). Gradually change the direction to the right (bottom in the surgical view) to dissect around the aorta. Insert a finger frequently to the right side of the aorta in order to understand the size of the aorta and to determine the exit site of the dissection (*see Note 7*).
16. Once the forceps are around the aorta, grasp the end of the silicon band and pull it through the dissected space for placing it around the aorta.
17. Place a ring and a clip on the silicon band and gradually tighten the banding (*see Note 8*).
18. Verify the degree of stenosis using echocardiography (Fig. 2). Pressure gradient can be estimated using continuous flow

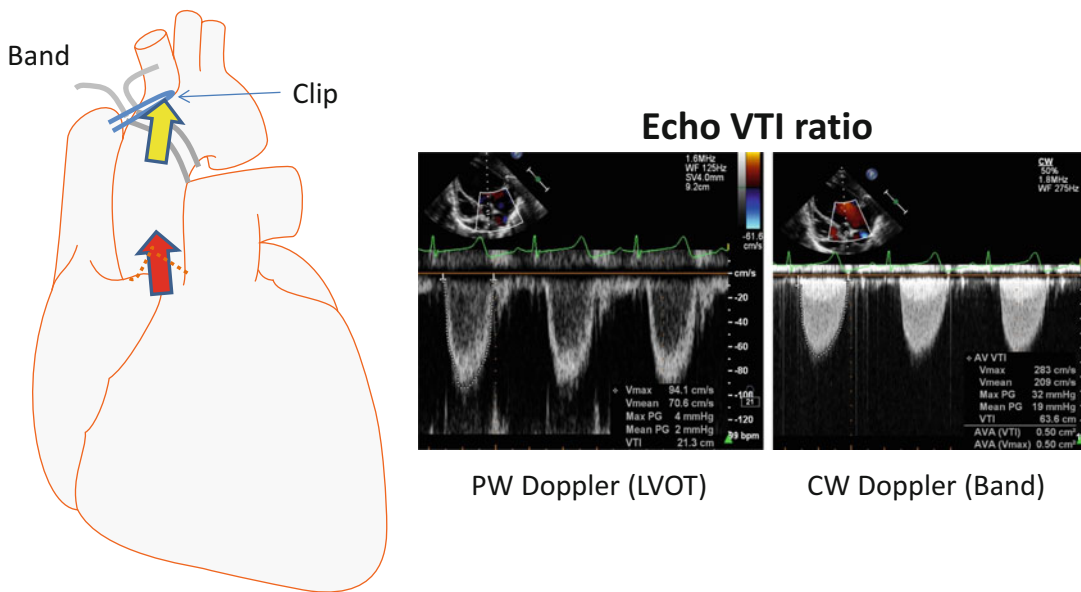


Fig. 2 Echocardiographic assessment of banding by calculating VTI ratio. Ratio of VTI at the banding site (continuous wave Doppler, placed at the point of the yellow arrow) and LV outflow tract (pulse wave Doppler, placed at the point of the red arrow) represents the relative stenosis against the LV outflow tract. The animal shown below underwent myocardial infarction first, and ascending aortic banding was added later. VTI ratio of 0.33 can be calculated by dividing LV out flow tract-VTI 21.3 (pulse wave Doppler, left) with stenosis-VTI 63.6 (continuous wave Doppler, right). LVOT: left ventricular outflow tract, PW: pulsed wave, CV: continuous wave

Doppler at the stenosis. Relative stenosis to LV outflow tract can be measured using the ratio of velocity time integrals (VTIs) at the LV outflow tract (using pulse wave Doppler) and the stenosis (using continuous wave Doppler) (*see Note 9*).

19. If the stenosis is too loose, tighten the band. If the stenosis is too tight, loosen (*see Notes 10 and 11*).
20. Fix the clip using an umbilical tape. Verify the degree of stenosis again using echocardiography before closing the chest.
21. Insert a drain in the chest through the fourth intercostal space. Remove the gauze that was placed to dislocate the lung. Connect an ambu bag and manually inflate the lung. Close the chest by approximating the ribs and suturing the muscles. Then, close the skin layer.
22. Remove air from the chest by applying negative pressure on the drain. Remove the drain and close the hole.
23. End anesthesia, apply a Fentanyl transdermal patch. Recover the animal and place the animal under continuous monitoring until its full recovery.
24. Echocardiography can be used to serially evaluate the degree of stenosis and development of hypertrophy.

4 Notes

1. Left forelimb should be pulled more cranially than the right forelimb so that the triceps do not overlap the third intercostal space.
2. Location of the incision should be marked after fixing the forelimbs as the skin layer can move by pulling the arms.
3. Avoid cutting the skin too close to the limb. Surgical wound can open easier than other locations due to the arm motion during the healing phase.
4. Securing good surgical view is key to the successful surgery. If the access or the views of surgical window is limited, consider widening the surgical window.
5. Left phrenic nerve runs on the dorsal side of the pericardium. Pay attention not to cut this nerve.
6. Narrow surgical space and side by side attachment of the pulmonary artery and the aorta preclude direct visualization inside the dissected space. Therefore, this step needs to be done blindly. L type forceps that have a diameter similar to the aorta facilitate dissection around the aorta.
7. Dissect gently and slowly. Do not apply strong force as the back side of the aorta is the atria that have very thin walls.

8. When the stenosis becomes significant, thrill can be felt by placing a finger on the aorta. At this point, the stenosis is still insufficient to induce heart failure in a reasonable time in normal pigs and the band should be tightened more after the thrill is sensed.
9. Pull and wiggle the band to release any constraint caused by surrounding tissues before evaluating the degree of the banding.
10. Align the echo Doppler beam direction and the flow direction to obtain accurate values. Failure to align the echo beam to flow results in underestimation of flow and pressure.
11. When the stenosis is too severe, heart rate usually increases and peripheral pressure decreases. Obtaining invasive peripheral arterial access for blood pressure monitoring is thus useful for evaluating the degree of stenosis. However, noninvasive blood pressure monitoring can also be used. In our experience, VTI ratio of around 0.2 against the LV outflow tract resulted in significant pressure overload (systolic LV pressure >200 mmHg) at the chronic stage (3–4 months) without causing acute death.

Acknowledgments

This work is supported by NIH R01 HL139963 (K.I.) and AHA-SDG 17SDG33410873 (K.I.). O.B. was supported by the Deutsche Herzstiftung.

References

1. Thune JJ, Signorovitch J, Kober L, Velazquez EJ, McMurray JJ, Califf RM et al (2008) Effect of antecedent hypertension and follow-up blood pressure on outcomes after high-risk myocardial infarction. *Hypertension* 51(1):48–54. <https://doi.org/10.1161/HYPERTENSIONAHA.107.093682>
2. Toischer K, Rokita AG, Unsold B, Zhu W, Kararigas G, Sossalla S et al (2010) Differential cardiac remodeling in preload versus afterload. *Circulation* 122(10):993–1003. <https://doi.org/10.1161/CIRCULATIONAHA.110.943431>
3. Nolan SE, Mannisi JA, Bush DE, Healy B, Weisman HF (1988) Increased afterload aggravates infarct expansion after acute myocardial infarction. *J Am Coll Cardiol* 12(5):1318–1325
4. Ishikawa K, Aguero J, Oh JG, Hammoudi N, Fish LA, Leonardson L et al (2015) Increased stiffness is the major early abnormality in a pig model of severe aortic stenosis and predisposes to congestive heart failure in the absence of systolic dysfunction. *J Am Heart Assoc* 4(5):e001925. <https://doi.org/10.1161/JAHA.115.001925>
5. Motloch LJ, Ishikawa K, Xie C, Hu J, Aguero J, Fish KM et al (2017) Increased afterload following myocardial infarction promotes conduction-dependent arrhythmias that are unmasked by hypokalemia. *JACC Basic Transl Sci* 2(3):258–269. <https://doi.org/10.1016/j.jacbs.2017.02.002>
6. Pfeffer MA, Braunwald E (1990) Ventricular remodeling after myocardial infarction. Experimental observations and clinical implications. *Circulation* 81(4):1161–1172
7. Furihata T, Kinugawa S, Takada S, Fukushima A, Takahashi M, Homma T et al (2016) The experimental model of transition from compensated cardiac hypertrophy to failure created by transverse aortic constriction in mice. *Int J Cardiol Heart Vasc* 11:24–28. <https://doi.org/10.1016/j.ijcha.2016.03.007>



Chapter 27

Large Porcine Model of Profound Acute Ischemic Cardiogenic Shock

Ole K. Møller-Helgestad, Hanne B. Ravn, and Jacob E. Møller

Abstract

Cardiogenic shock is one of the leading causes of death following acute myocardial infarction affecting 10% of patients with large myocardial infarcts with a subsequent mortality rate of 50%. Here we describe a large porcine model of acute ischemic cardiogenic shock. Acute left or right ventricular failure can be achieved with close to a 100% success rate by stepwise injection of microspheres into the left or right coronary artery, respectively, and the method allows for titration of heart failure to a prespecified level.

Key words Cardiogenic shock, Acute heart failure, Coronary ischemia, Microspheres, Pathophysiology, Hemodynamics, End-organ perfusion

1 Introduction

Cardiogenic shock is a serious complication to acute myocardial infarction with an in hospital mortality of 50% affecting as much as 10% of patients with large ST segment elevation myocardial infarction [1, 2]. It is a heterogeneous condition, ranging from severe distress on arrival to the hospital to more subtle symptoms gradually progressing into a circulatory collapse and end-organ hypoperfusion. For this reason clinical studies are difficult to perform, especially with respect to the effect of a therapeutic intervention. This warrants a large animal model, where cardiogenic shock is induced in a standardized manner, allowing the intervention to be performed at a prespecified hemodynamic state.

Fulminant cardiogenic shock is a state of end-organ hypoperfusion due to cardiac failure, where the pathophysiology is a downward spiral of ischemic myocardial injury causing systolic and diastolic dysfunction that result in decreased cardiac output and systemic blood pressure leading to decreased perfusion of the heart, which further exaggerates systolic and diastolic dysfunction [3]. It is most often caused by left ventricular failure but can also be caused by right ventricular failure [3]. The degree of systemic hypotension

and end-organ hypoperfusion with lactic acidosis is strongly associated with mortality [4–6]. An ideal animal model of cardiogenic shock should produce ischemic myocardial injury causing a reproducible degree of cardiac dysfunction leading to severe end-organ hypoperfusion with an increased arterial lactate. At the same time the model should be controllable to avoid extensive loss of animals while minimizing the risk of selection bias. Coronary artery occlusion–reperfusion mimics an acute myocardial infarct, but since swine are prone to ventricular fibrillation following a proximal complete coronary occlusion, the degree of cardiac dysfunction and circulatory impairment is unpredictable, consequently severe end-organ hypoperfusion and increased arterial lactate is mainly present if the animal has suffered a cardiac arrest [7, 8]. Acute coronary microembolization is a well-known method for producing ischemic myocardial dysfunction [9–12], and we present a protocol for inducing profound cardiogenic shock due to either failure of the left or right ventricle. The model can be used for end-organ pathophysiology studies during cardiogenic shock and specifically to evaluate pharmacologic and/or mechanical circulatory support used in management of cardiogenic shock. In summary, cardiogenic shock can be induced in approximately 45 min without the animals suddenly developing ventricular fibrillation. Microspheres are injected in a stepwise fashion every 3–10 min and entrapment of microspheres in the myocardium causes acute heart failure of either the left or right ventricle depending on which coronary artery the microspheres are injected into. The model allows for titration of ventricular failure to a predetermined hemodynamic state and asystole can develop within minutes in severe heart failure if no intervention is initiated.

2 Materials

We use animals weighing 70–80 kg. The procedure requires a suitable operating room including an operating table, ventilator, equipment for invasive hemodynamic monitoring, and a fluoroscopic imaging system.

2.1 Monitoring

1. Invasive blood pressure monitoring lines for measurement of systemic pressure, pulmonary artery pressure, and central venous pressure.
2. Electrocardiography (ECG) cables for three lead ECG monitoring.
3. Monitor screen for blood pressures and ECG.
4. A Swan-Ganz catheter with continuous monitoring of cardiac output and mixed venous oxygen saturation (CCOMbo

pulmonary artery catheter, Edwards Lifesciences LLC, Irvine, CA, USA).

5. A monitor screen for cardiac output (L/min), cardiac index (L/min/m²), and venous oxygen saturation (%) and core temperature (°C) surveillance.
6. Blood gas analyzer.
7. Syringes for drawing blood gas samples.

2.2 Anesthesia and Drugs

1. Intramuscular injection syringe containing premedication to relax the animal before inducing anesthesia.
2. Premedication: 0.2 mg/kg midazolam, 0.04 kg/kg medetomidine.
3. Peripheral venous catheter.
4. Anesthesia induction: propofol 5 mg/kg.
5. Cuffed endotracheal tube of appropriate size for intubation.
6. Ventilator.
7. Sevoflurane.
8. Fentanyl.
9. Isotonic saline, 1000 mL over 1 h followed by approximately 500 mL/h.
10. Anticoagulation: heparin i.v.
11. Antiarrhythmic: amiodarone.
12. Cardiac arrest kit (*see Note 1*).

2.3 Vascular Access (See Note 2)

1. Puncture needle (optionally connected to a syringe with saline mixed with heparin).
2. Ultrasound with a vascular access probe.
3. A 6 Fr (or other appropriate size) sheath introducer kit for the left carotid artery for catheterization of coronary arteries (*see Note 3*).
4. A 6 Fr (or other appropriate size) sheath introducer kit for arterial access (femoral) for systemic blood pressure monitoring.
5. A multilumen central venous access catheter kit (MACTM Arrow International Inc.) for the right external jugular vein for fluid administration and Swan-Ganz catheter (*see Note 4*).

2.4 Coronary Catheterization and Microembolization

1. A JL3.5 guide catheter.
2. Y-connector.
3. A stiff guidewire.
4. Introducer.

5. Soft tip, flexible body guidewire.
6. Contrast material for coronary angiography.
7. Appropriately sized syringe for injecting contrast.
8. 0.125 g Contour™ PVA-microspheres (Boston Scientific) ($\varnothing = 45\text{--}150 \mu\text{m}$) mixed in a container with 10 mL saline and 10 mL contrast (see Note 5). Stir constantly to avoid sedimentation.

3 Methods

Animals should be acclimatized in an appropriate facility close to the operating room, and fasted overnight with free access to water. Connect and prepare all monitoring systems prior to inducing anesthesia.

3.1 Inducing and Maintaining Anesthesia

1. Insert the needle connected to the syringe containing premedication into the neck musculature and gently infuse premedication. Wait until the animal has dozed off.
2. Insert a peripheral venous catheter into one of the ear veins and infuse drugs for inducing anesthesia (propofol). Use the peripheral vein for infusion of fentanyl and saline until gaining access to the right external jugular vein.
3. Intubate the animal following visualization of vocal cords by using a customized swine laryngoscope. Ensure proper position of endotracheal tube (ETT) by hand bagging and stethoscopy. Connect the ETT to the ventilator.
4. Ventilate the animal with a tidal volume of 6–8 mL/kg at a rate of 10–14/min with 20–50% oxygen and a positive end-expiratory pressure of 5 cm H₂O. Ventilator settings should be adjusted according to serial arterial blood gas analyses keeping pO₂ ≥ 12 kPa, pCO₂ between 4.5 and 6.5 kPa, and pH between 7.35 and 7.45.
5. Maintain anesthesia with Sevoflurane keeping mean alveolar concentration (MAC) 1.5–2% and fentanyl infusion 25–50 µg/kg/h.
6. Fixate the animal to the operating table in dorsal recumbency, and make sure the endotracheal tube is fixed properly to the animal.

3.2 Monitoring and Vascular Access

1. Place ECG electrodes and connect ECG cables.
2. Pull and fixate the legs of the animal caudally. In the femoral region, pulling the hind leg caudally will reveal a groove wherein the femoral vasculature is located.

3. Ultrasound guided, the vessel of interest is perforated by a needle (*see Note 6*). By using the Seldinger technique a guidewire is advanced through the needle. Make a skin incision close to the guidewire and exchange the needle with the sheath, which subsequently is advanced over the wire into the vessel, before removing the guidewire. Ensure correct intravascular sheath placement by the ability to draw blood before suturing the sheath to the skin. Repeat for all vascular accesses needed.
4. As soon as you have an arterial access, perform an arterial blood gas analysis and adjust ventilator settings accordingly and connect the arterial access to a pressure monitor.
5. When you have placed the multilumen central venous access catheter in the right external jugular vein, connect all fluids to the catheter and advance the Swan-Ganz catheter to the pulmonary artery. Connect the catheter to two separate pressure monitors (one for pulmonary arterial pressure and one for central venous pressure) and connect relevant cables to the Swan-Ganz monitor.
6. Perform *in vivo* calibration of the Swan-Ganz venous oxygen saturation. Initiate data collection for cardiac output measurement on the monitor.
7. Start infusing amiodarone when access to the right external jugular vein has been established with a rate of 4 mg/kg over 30 min followed by a continuous infusion rate of 0.8–1 mg/kg/h (*see Note 7*).
8. Inject 20,000 IU unfractionated heparin, when all vascular accesses have been established and repeat every 2 h.

3.3 Catheterizing the Coronary Arteries

Fluoroscopy is mandatory for catheterization of the coronary arteries.

1. Connect the y-connector to your JL 3.5 guide catheter and insert a stiff guidewire through the y-connector straightening the guide catheter leaving the wire tip just visible at the end of the catheter.
2. Advance the guide catheter through the sheath in the left carotid artery to the aortic root and remove the guidewire.
3. Alternate between gently rotate, advance and retreat the guide catheter until you gain access to the coronary artery of interest. Use contrast to confirm correct placement.
4. Insert the soft tip, flexible body guidewire through the y-connector using the introducer and place the guidewire distally in the coronary artery of interest securing catheter placement.

5. Take a time-out where you ensure all monitoring systems are up and running, all drugs has been infused and go over the experimental protocol.

3.4 Inducing Cardiogenic Shock by Microembilization

The described approach and results are based on injecting microspheres into the left coronary artery causing predominant left ventricular failure (Fig. 1). However, depending on the coronary artery anatomy, the right ventricle may be partly affected too. The model does also provide the possibility to generate cardiogenic shock due to predominant right ventricular failure (Fig. 2) by injecting microspheres into the right coronary artery. The approach described below causes a stable and reproducible decay in ventricular function that can be titrated to a desired level.

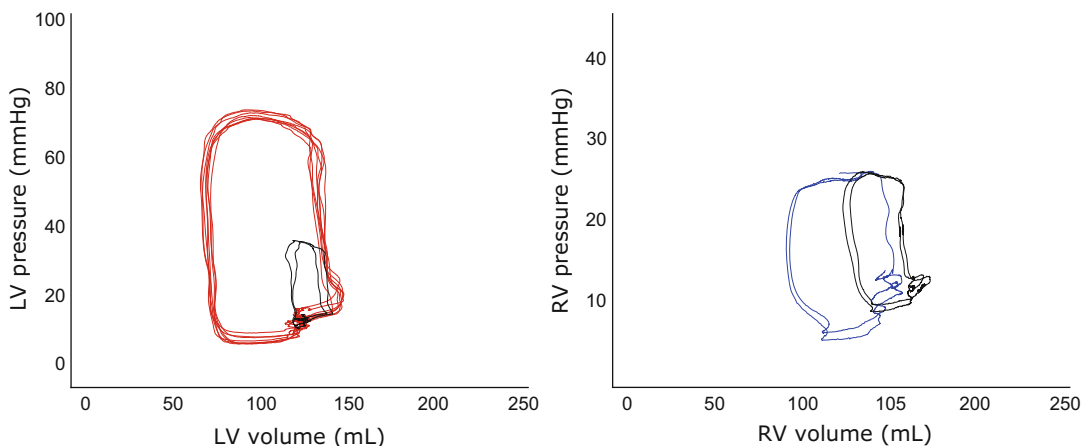


Fig. 1 Cardiogenic shock due to predominant left ventricular failure. Pressure–volume loop of the left (left panel) and right (right panel) ventricle at baseline (red and blue, respectively) and at cardiogenic shock (black)

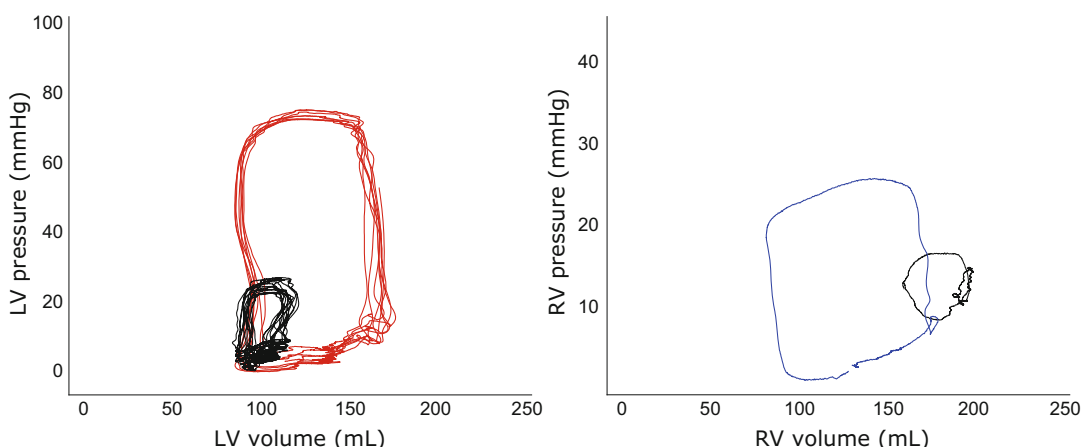


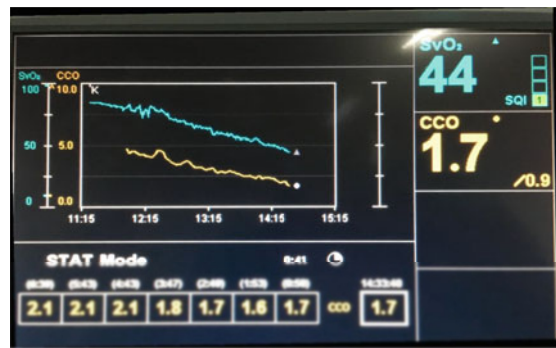
Fig. 2 Cardiogenic shock due to predominant right ventricular failure. Pressure–volume loop of the left (left panel) and right (right panel) ventricle at baseline (red and blue, respectively) and at cardiogenic shock (black)

1. Confirm that the guide catheter is located proximally in the target coronary artery (*see Note 8*).
2. Inject 1 mL microsphere solution and flush the guide catheter rapidly with a few milliliters of isotonic saline to completely flush the catheter (*see Note 9*).
3. Monitor impact of each bolus on systemic blood pressure, cardiac output and mixed venous oxygen saturation (*see Note 10*).
4. Repeat injections every 3–10 min, allowing the animals to completely stabilize between injections, until the desired and prespecified level of cardiac dysfunction has been reached based on arterial blood pressure, cardiac output and/or mixed venous oxygen saturation (*see Note 11*).
5. The number of boluses needed to cause profound cardiogenic shock associated with an increase in arterial lactate concentration indicating severe end-organ hypoperfusion varies from animal to animal but generally it can be achieved within 45 min (*see Note 12*). Figure 3 shows changes in hemodynamic parameters with incremental microsphere injections in a study series of 12 animals where the number of boluses ranged from 8 to 42.

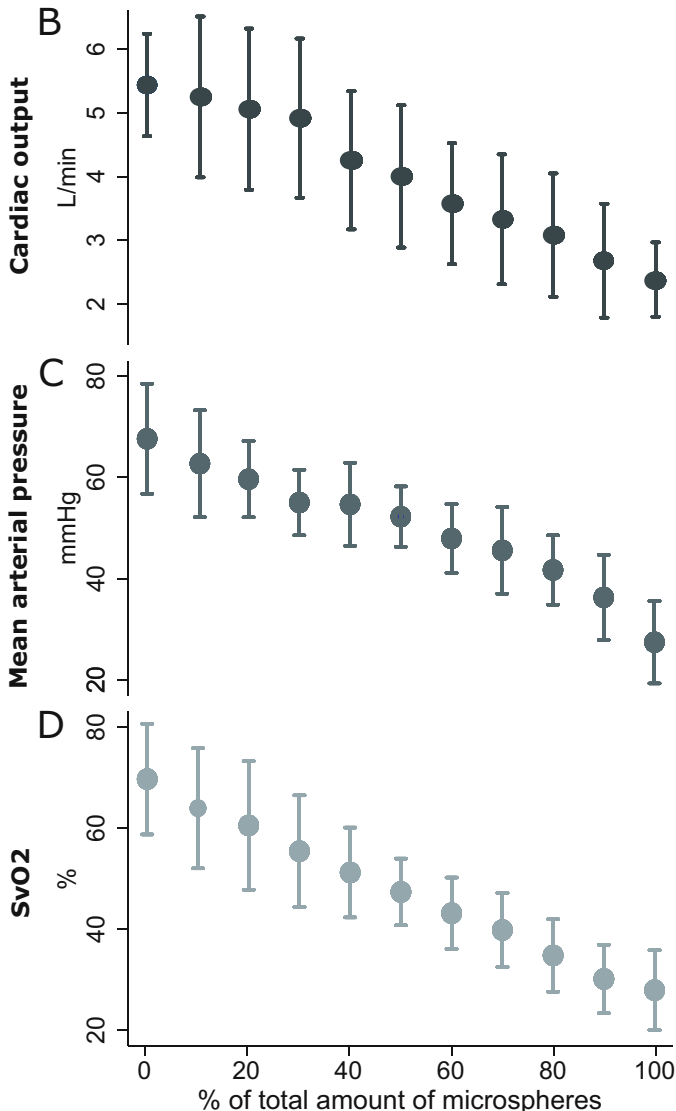
4 Notes

1. A cardiac arrest kit consisting of a defibrillator with handheld pads, as self-adhesive pads interfere with fluoroscopy, as well as epinephrine and amiodarone should be available and ready for immediate use. Although it is the purpose of the model to create hypotension, make sure to have a vasoconstrictive agent, e.g., a norepinephrine infusion, prepared and at place in a dedicated infusion pump for fast initiation as the pig may deteriorate quickly.
2. Vascular access can be achieved by either cut down or percutaneously guided by ultrasound. We recommend the percutaneous technique as it is less invasive for animals, reduces fluid loss from wound sites offering a more hemodynamic stable animal and saves time when the operator is skilled. The three specified access sites are a minimum to induce and monitor shock development. There are virtually no limits regarding how many catheters you can insert, and the pig has a well-developed vertebral arterial system and circle of Willis so it is possible to catheterize both carotid arteries without jeopardizing cerebral blood supply.
3. In pigs, the coronary arteries are easily catheterized through the left carotid artery.

A

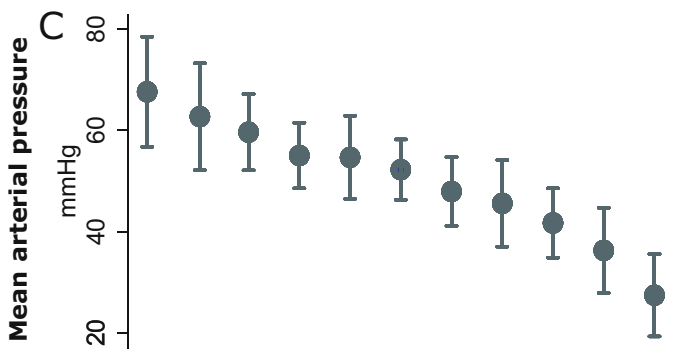


B



Mean arterial pressure

C

SvO₂

D

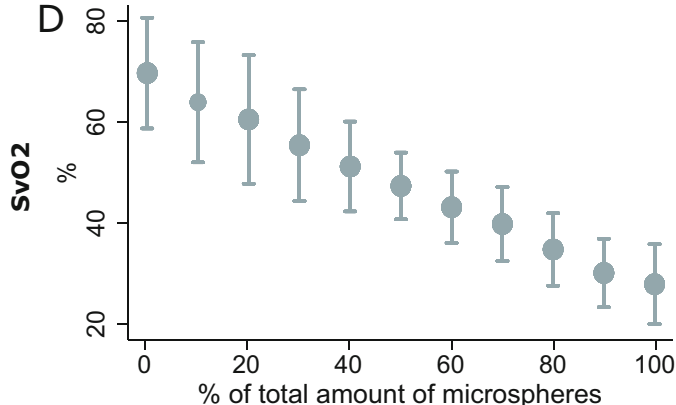


Fig. 3 Hemodynamic consequences to incremental microembolization in 12 female swine. (a) A photograph of the cardiac output monitor in one of the animals, light blue shows mixed venous oxygen saturation (SvO₂, %) and orange shows cardiac output (L/min). (b) Gradual reduction in cardiac output (L/min). (c) Gradual reduction in mean arterial pressure (mmHg). (d) Gradual reduction in SvO₂ (%). The dots indicate mean value and error bars indicate ± one standard deviation

4. Advancing the Swan-Ganz to the pulmonary artery can be easily done through the right jugular veins either pressure guided or by means of fluoroscopy.
5. In our experience, mixing the microspheres with saline and contrast results in fever arrhythmias and causes a more stable decrease of cardiac function compared to mixing it with saline alone.
6. Make sure to study porcine vasculature anatomy and where to locate vessels of interest.
7. Infusing the amiodarone bolus will cause some transient hemodynamic changes, e.g., reduction in systemic blood pressure [13] that normally resolves within 30 min.
8. Proximal placement of the catheter is a key issue, especially for the left coronary artery as both the LAD and LCx supplied myocardium has to be affected by microspheres to create profound cardiogenic shock. It is our experience that the LAD bed is filled and blocked before LCx when injecting the microspheres from the left main stem. If selective LAD/LCx bead microembolization is warranted it is possible to place a microcatheter in the preferred vessel.
9. It is our experience that injecting boluses larger than 1 mL increases the risk of circulatory collapse and cardiac arrest. Make sure that there is absolutely no air bubbles trapped in the guide catheter by gently pulling on the syringe before every injection of microspheres or saline, as an air bubble into the coronary circulation could cause immediate circulatory collapse.
10. With our stepwise injection protocol, arrhythmic events that require direct current shocks are very rare, and we have not experienced any in our studied animals.
11. It is our experience that you can inject boluses with a short time interval until mean systemic arterial blood pressure <45 mmHg and/or mixed venous oxygen saturation <45% and/or cardiac output <3 L/min. From this time point, animals seem to be more vulnerable and further injections of microspheres should be done cautiously and with sufficient time to stabilize between injections.
12. It is our experience that animals weighing 70–80 kg should be severely compromised hemodynamically (cardiac output <2.5 L/min and/or mean arterial blood pressure <35 mmHg and/or mixed venous oxygen saturation <35%) before an increase in arterial lactate becomes evident.

Acknowledgments

We thank Dr. Janus A Hyldebrandt, Dr. Ann Banke, Dr. Charlotte Svejstrup Rud, Dr. Nanna Louise Junker Udesen, Dr. Henrik Schmidt, and Professor Lisette Okkels Jensen for their significant contributions to the experimental studies, enabling us to prepare this chapter.

Reference

1. Goldberg RJ, Makam RC, Yarzebski J, McManus DD, Lessard D, Gore JM (2016) Decade-long trends (2001–2011) in the incidence and hospital death rates associated with the in-hospital development of cardiogenic shock after acute myocardial infarction. *Circ Cardiovasc Qual Outcomes* 9(2):117–125. <https://doi.org/10.1161/CIRCOUTCOMES.115.002359>
2. Obling L, Frydland M, Hansen R, Møller-Helgestad OK, Lindholm MG, Holmvang L, Ravn HB, Wiberg S, Thomsen JH, Jensen LO, Kjaergaard J, Møller JE, Hassager C (2017) Risk factors of late cardiogenic shock and mortality in ST-segment elevation myocardial infarction patients. *Eur Heart J Acute Cardiovasc Care* 7:7–15. <https://doi.org/10.1177/2048872617706503>
3. Reynolds HR, Hochman JS (2008) Cardiogenic shock: current concepts and improving outcomes. *Circulation* 117(5):686–697. <https://doi.org/10.1161/CIRCULATIONAHA.106.613596>
4. Sleeper LA, Reynolds HR, White HD, Webb JG, Dzavik V, Hochman JS (2010) A severity scoring system for risk assessment of patients with cardiogenic shock: a report from the SHOCK trial and registry. *Am Heart J* 160(3):443–450. <https://doi.org/10.1016/j.ahj.2010.06.024>
5. Haas SA, Lange T, Saugel B, Petzoldt M, Fuhrmann V, Metschke M, Kluge S (2016) Severe hyperlactatemia, lactate clearance and mortality in unselected critically ill patients. *Intensive Care Med* 42(2):202–210. <https://doi.org/10.1007/s00134-015-4127-0>
6. Vermeulen RP, Hoekstra M, Nijsten MW, van der Horst IC, van Pelt LJ, Jessurun GA, Jaarsma T, Zijlstra F, van den Heuvel AF (2010) Clinical correlates of arterial lactate levels in patients with ST-segment elevation myocardial infarction at admission: a descriptive study. *Crit Care* 14(5):R164. <https://doi.org/10.1186/cc9253>
7. Møller-Helgestad OK, Poulsen CB, Christiansen EH, Lassen JF, Ravn HB (2015) Support with intra-aortic balloon pump vs. Impella2.5 (R) and blood flow to the heart, brain and kidneys—an experimental porcine model of ischaemic heart failure. *Int J Cardiol* 178:153–158. <https://doi.org/10.1016/j.ijcard.2014.10.153>
8. Beurton A, Ducrocq N, Auchet T, Joineau-Groubatch F, Falanga A, Kimmoun A, Girerd N, Fay R, Vanhuyse F, Tran N, Levy B (2016) Beneficial effects of norepinephrine alone on cardiovascular function and tissue oxygenation in a pig model of cardiogenic shock. *Shock* 46(2):214–218. <https://doi.org/10.1097/SHK.0000000000000579>
9. Agress CM, Rosenberg MJ, Jacobs HI, Binder MJ, Schneiderman A, Clark WG (1952) Protracted shock in the closed-chest dog following coronary embolization with graded microspheres. *Am J Phys* 170(3):536–549
10. Hamburger WW, Priest WS, Bettman RB (1926) Experimental coronary embolism. *Am J Med Sci* 171:168–185. <https://doi.org/10.1097/00000441-192602010-00002>
11. Nordhaug D, Steensrud T, Korvald C, Aghajani E, Myrmel T (2002) Preserved myocardial energetics in acute ischemic left ventricular failure—studies in an experimental pig model. *Eur J Cardiothorac Surg* 22(1):135–142
12. Nordhaug D, Steensrud T, Muller S, Husnes KV, Myrmel T (2004) Intraaortic balloon pumping improves hemodynamics and right ventricular efficiency in acute ischemic right ventricular failure. *Ann Thorac Surg* 78(4):1426–1432. <https://doi.org/10.1016/j.athoracsur.2003.12.077>
13. Karlis G, Iacovidou N, Lelovas P, Niforopoulou P, Zacharioudaki A, Papalois A, Sunde K, Steen PA, Xanthos T (2014) Effects of early amiodarone administration during and immediately after cardiopulmonary resuscitation in a swine model. *Acta Anaesthesiol Scand* 58(1):114–122. <https://doi.org/10.1111/aas.12226>



Chapter 28

Chronic Pulmonary Artery Embolization Models in Large Animals

Jaume Aguero, Nadjib Hammoudi, Olympia Bikou, Kenneth M. Fish, Iratxe Zarragoikoetxea, Roger J. Hajjar, and Kiyotake Ishikawa

Abstract

A wide range of approaches have been described to develop animal models of pulmonary vascular disease (PWD). Clinical heterogeneity in patients with pulmonary hypertension (PH) has prompted development of different techniques to create PH models in several animal species with the objective to recapitulate specific PH/PWD phenotypes. Chronic thromboembolic PH (CTEPH) is a clinically important phenotype of PH with a documented prevalence of 0.4–9.1% in patients with history of pulmonary embolism. A well-established large animal model of CTEPH is thus necessary for studying this disease in preclinical research. Different experimental protocols with inconsistent outcomes have been reported in the literature.

We have focused on characterizing PH large animal models in a common framework; pulmonary hemodynamics, right ventricular (RV) function, and histological characterization of PWD. This research framework allows optimal evaluation of novel diagnostic tools, as well as new therapeutic strategies. The purpose of this protocol is to describe approaches to create experimental CTEPH models using recurrent pulmonary embolizations of dextran microspheres in swine. The key features of this experimental modeling approach are (1) nonsurgical, fully percutaneous techniques, (2) a minimum of four embolization procedures, with 1–2 month time period, (3) mild to moderate PH hemodynamics (mean PA pressure increase ~20–60%), (4) severe pulmonary vascular remodeling, (5) mild RV remodeling, and (6) a high reproducibility and low mortality (<10%).

Key words Pulmonary hypertension, Pulmonary embolization, Large animal disease models, Vascular remodeling, Pulmonary vascular disease

1 Introduction

A wide range of approaches have been described to develop animal models of pulmonary vascular disease (PWD). Clinical heterogeneity in patients with pulmonary hypertension (PH) has prompted development of different techniques to create PH models in several animal species with the objective to recapitulate specific PH/PWD phenotypes [1]. The appropriate technique for respective research purpose will depend on the target clinical disease phenotype, based on the current PH classification [1].

Chronic thromboembolic PH (CTEPH), also known as group 4 PH, typically occurs after an acute pulmonary embolism with an estimated clinical prevalence of 0.4–9.1% depending on different clinical series [2]. However, only ~75% of patients presenting CTEPH suffered prior acute thromboembolic events [3], suggesting a subclinical course in the natural history of CTEPH for reasons still poorly understood.

In general, acute pulmonary embolism progresses to CTEPH through incomplete pulmonary clot resolution resulting in clot organization, fibrotic changes, and chronic attachment to the pulmonary artery (PA) walls [4]. Therefore major vessel chronic obstruction is the main hallmark of CTEPH. However, involvement of small vessels or microvascular components has also been described, and is associated with persistent PH following surgical removal of the large PA obstructive thrombus (thromboendarterectomy procedure) [2, 4]. Microvascular disease in CTEPH has been identified as a consequence of small vessel thrombus obstruction or intrinsic arteriole wall disease occurring distal to both obstructed and nonobstructed vasculatures [2, 5].

Preclinical research in CTEPH requires well-established animal models that closely recapitulate the causes and phenotype of the clinical disease. A wide range of experimental protocols have been reported in the literature, many of them summarized in a recent report by our group (Table 3 in [6]). Because thrombus embolization model results in unsustained or inconsistent PH due to spontaneous thrombus dissolution, a number of variables have been modified in CTEPH models, including the embolic material (e.g., dextran microspheres, ceramic microspheres, air), number of procedures (e.g., continuous/daily, weekly, biweekly), and the experimental conditions (ventilation and oxygenation levels) during the assessment of the main functional endpoints [6–12]. Therefore, reported animal models of CTEPH are characterized by wide protocol heterogeneity. A common framework to characterize PH animal models typically includes three main endpoints: (1) functional evaluation of pulmonary hemodynamics, (2) functional assessment of right ventricular (RV) function, and (3) histological and molecular characterization of PVD and RV remodeling. In this regard, large animal models allow comprehensive PH studies using clinically relevant diagnostic tools, such as right heart catheterization and advanced imaging techniques, as well as histology and molecular level characterization. This research framework allows for optimal evaluation of novel diagnostic tools, as well as new therapeutic strategies.

The purpose of this chapter is to describe different approaches to experimentally model CTEPH using recurrent pulmonary embolizations of dextran microspheres in swine.

The key features of this experimental modeling approach are (1) a fully percutaneous technique that avoids surgical injury,

pulmonary adhesions, and potential infections and mortality related to thoracotomy procedures, (2) a minimum of four embolization procedures with 1–2 month study time period, depending on the target disease severity and the observation period or type of intervention, (3) mild to moderate PH hemodynamics (mean PA pressure increase ~20–60%), (4) severe pulmonary vascular remodeling, (5) mild RV remodeling as a marker of PH, and (6) a high reproducibility and low mortality (<10%).

2 Materials

2.1 Animal Preparation

For anesthesia induction and maintenance:

1. Telazol (tiletamine/zolazepam).
2. Propofol.
3. Respirator suitable for swine with adjustable inspiratory oxygen concentration.
4. ECG and pulse oximetry monitor.

2.2 Functional Evaluation: Hemodynamics and Echocardiography

1. Procedure room equipped with a fluoroscopy system (C-arm).
2. Standard cath pack for sterile percutaneous angiographies (syringes, towels, bowls, gauze).
3. Sheath introducer 8 French.
4. Swan-Ganz Catheter 7 French.
5. Capnograph.
6. Blood gas analyzer.
7. Pressure transducers.
8. Bupivacaine–HCl 0.5%.
9. Echocardiography machine equipped with broadband sector array transducer (5–1 MHz frequency range). For volumetric acquisition, a matrix array probe is necessary.
10. Ultrasound transmission gel.
11. Software for echocardiography images postprocessing. Several options are available depending on the echo machine manufacturer. These software allow 3D and strain analyses.

2.3 Embolization Model Creation

1. A 4 French coronary catheter with soft tip.
2. 0.035 inch vascular wire.
3. Intravenous iodinated contrast.
4. Dextran microspheres (100–300 µm diameter, coarse Sephadex G-50, Sigma-Aldrich).
5. Sterile silk sutures.

2.4 Histology Analysis

1. Embedding medium for frozen tissue specimens (optimal cutting temperature [O.C.T.]).
2. Wheat germ agglutinin (WGA) (conjugated to Oregon Green 488, 10 µg/mL) and phalloidin (conjugated to Alexa fluor 546, 165 nM).
3. Masson's Trichrome, Elastica Van-Gieson and Picosirius staining kits.

3 Methods

3.1 Animal Preparation

1. Fast the animals overnight.
2. Anesthesia is induced with intramuscular administration of 6.0 mg/kg Telazol. Orotracheal intubation is performed by trained personnel immediately after the animal is sedated, and peripheral oxygen saturation and heart rate are continuously monitored (*see Note 1*). A peripheral ear vein access is subsequently obtained.
3. Use intravenous propofol 8–10 mg/kg/h for hemodynamic evaluation (*see Note 2*).
4. Under sterile conditions, obtain a femoral vascular access using the Seldinger technique. For right heart catheterization with a 7 French Swan-Ganz catheter, place an 8-French sheath in the femoral vein. As an alternative, the jugular veins can also be accessed in swine but care must be taken to avoid undesired carotid artery punctures as a large hematoma around the trachea can result in respiratory failure post-extubation. Guidance of the percutaneous puncture using vascular echography is strongly recommended in available laboratories. Since repeated pulmonary embolization procedures as well as follow up hemodynamic studies are required in all protocols, vascular integrity should be maintained as much as possible for each procedure. Echo guidance of the percutaneous vascular punctures will minimize the number of attempts and prevent vascular injury problems. Heparin administration at each procedure (1000 units) will reduce the risk of total occlusion post-femoral vein punctures.
5. Place a Swan-Ganz catheter in the pulmonary artery to monitor right side hemodynamics during the procedure using fluoroscopic guidance (C-arm). Calibrate pressure sensor carefully. This is particularly important when measuring right side pressures as they are often much lower than left side pressures. Before measurements are obtained, hemodynamic stability must be established and the catheter locations should be confirmed with X-ray and pressure waves for every measurement.

3.2 Pulmonary Embolization Procedures. Protocol 1: Distal Embolization Model (See Note 3)

1. Dilute the dextran microspheres in 20 mL saline solution. In our experience, a key step is to prepare the dilution at least 2 h prior to injection for allowing the microspheres to swell before injection (*see Note 4*).
2. Inject the microspheres in the main PA through the tip lumen of the Swan-Ganz catheter to achieve even distribution of the microspheres to both lungs. Inject the diluted microspheres slowly, and wait a few minutes after half of the dose has been injected to check hemodynamic changes. If systemic arterial pressures are stable (systolic arterial pressure >80 mmHg), resume the injection procedure. The Swan-Ganz catheter should be placed in the main PA using fluoroscopy guidance (*see Note 5*).
3. During injection, continuous pulmonary and systemic hemodynamic monitoring is recommended. Excessive PA pressure increase and/or drop in systemic pressure suggest a low output status and further microspheres injection should be avoided.
4. After all microspheres are injected, collect necessary functional data relevant to the study, and proceed with animal recovery by first removing the vascular sheath.
5. Repeat embolization procedures are performed weekly. Following the first procedure, bring the animal back for preparation, anesthesia, vascular access and basal hemodynamics (**steps** in Subheading 3.1), and repeat **steps 1–4** in Subheading 3.2 (*see Note 6*).

3.3 Pulmonary Embolization Procedures. Protocol 2: Distal Embolization + Proximal Coiling (See Note 7)

1. Prepare the embolization and coiling materials: (a) dilute the dextran microspheres in 20 mL saline solution, as in Protocol 1; (b) cut sterile silk sutures into 3 cm length, and keep them dry for easier handling in subsequent steps.
2. Using fluoroscopy guidance, advance the Swan-Ganz catheter into the left PA, and inflate the balloon at the tip to completely occlude the blood flow into the left PA (Fig. 1). This is to prevent microsphere spilling to right PA as embolization causes retrograde flow during the RV diastole. Slowly inject diluted microspheres during 1 min. Deflate the balloon, and remove Swan-Ganz catheter (*see Note 8*).
3. Following microsphere delivery into the left PA, advance a 5 Fr coronary catheter with flexible tip to the left PA branch using a 0.035 inch wire. Inject contrast and confirm the catheter tip location. Carefully advance the catheter into smaller PA branches for coiling, as shown in Fig. 2.
4. To deliver 3 cm silk sutures, remove the wire and fill the catheter with contrast. This slows the backflow inside the catheter due to high viscosity of the contrast and makes it easier to

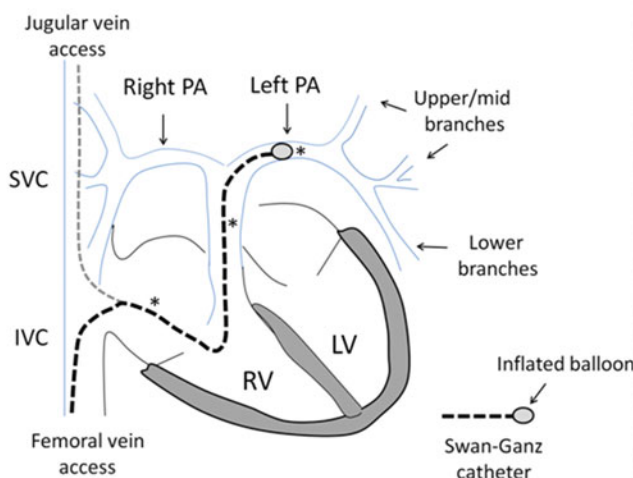
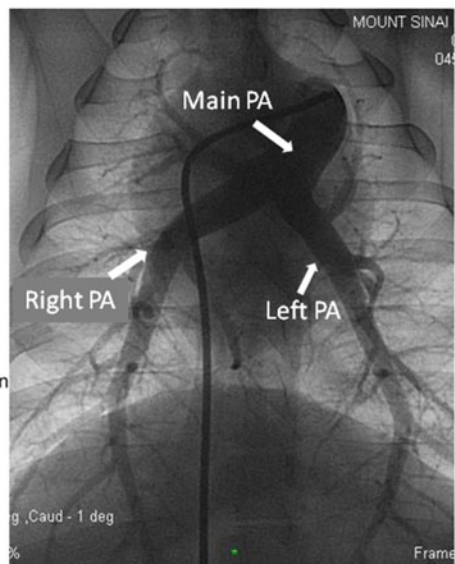
A**B**

Fig. 1 Scheme showing the balloon tipped catheter (Swan-Ganz) position for Protocol 2 Embolization procedure (A). Using femoral or jugular vein access, the catheter is advanced through the right heart cavities into the main PA and positioned in the left PA, before the takeoff of the first (upper) branches. The balloon is inflated to stop the antegrade flow. Right upper branch may take off closer to the main bifurcation and separate injection may be necessary for animals with difficulty in occluding the right PA. In panel B, PA angiography shows the right and left PA branching distribution in a pig from an anteroposterior fluoroscopy projection. Abbreviations: SVC Superior vena cava, IVC Inferior vena cava, PA Pulmonary artery, RV Right ventricle, LV Left ventricle

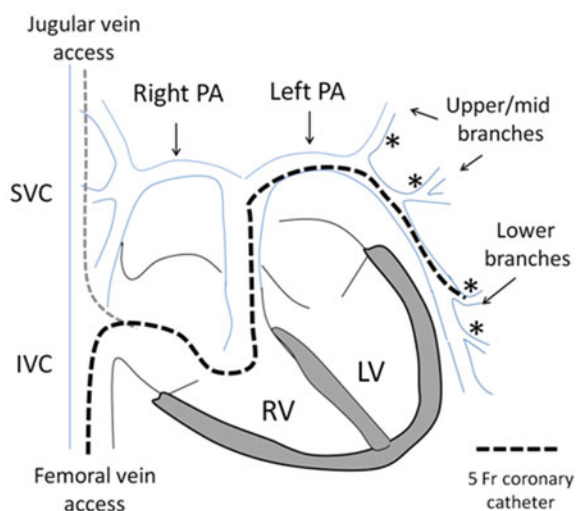
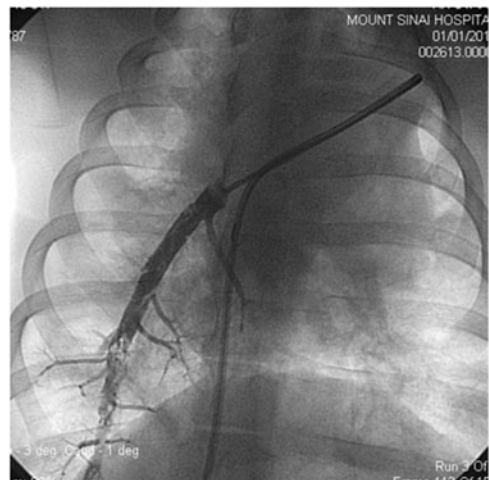
A**B**

Fig. 2 Scheme showing the coronary catheter position for Protocol 2 coil embolization procedure (A). After distal embolization, the catheter is advanced into the left PA, and secondary branches are identified using contrast injection. Once the catheter tip is stable at the proximal of the target branch, the silk suture "coils" are delivered. In panel B, lower right PA angiography shows flow obstructions in several branches following silk suture delivery. Abbreviations: see Fig. 1

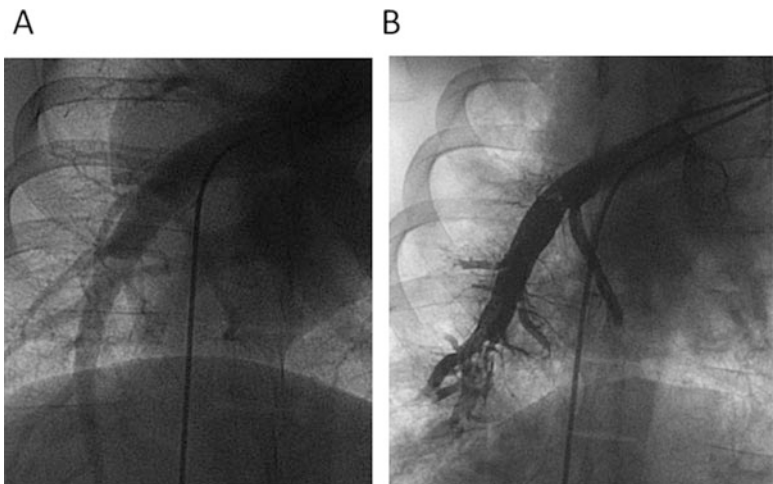


Fig. 3 Angiograms of the right lower pulmonary artery, before (**A**) and after (**B**) branch occlusions using silk sutures

insert sutures into the catheter (*see Note 9*). Insert a silk suture to the proximal end of the catheter, and flush the catheter with normal saline. This maneuver needs to be performed quickly so that the silk suture does not get stuck in the catheter due to its swelling (*see Note 10*). Following delivery, contrast can be injected to check the site of the vascular occlusion, and its effects on the regional pulmonary flow (Fig. 3).

5. Repeat steps **3** and **4** in Subheading **3.3** at several branches of the left PA: PA branches for the upper, mid and lower lobes. In the pig lung, upper lobes are small and the lower lobes are typically dominant. At least 2/3 of all prepared silk sutures will be delivered in lower lobe branches of the PA. Typically 20 of 3 cm silk sutures can be injected in each procedure.
6. One week later, bring the animal back and repeat animal preparation, vascular access and basal hemodynamic steps. Repeat steps **2–5** in Subheading **3.3** in the right PA (*see Note 11*).

3.4 Functional Evaluation of RV Performance (See Note 12)

Transthoracic echocardiography can be used for noninvasively imaging RV function. It is easy to perform at the animal facility whenever the equipment is available. The following protocol for image acquisition is recommended:

1. Under general anesthesia, as described in Subheading **3.1**. “Animal preparation” section, place the animal on right lateral recumbency.
2. Place ECG electrodes in upper and lower limbs. Carefully check that the ECG signal is optimal as most images will be acquired using ECG gating.

3. Stop the ventilator to induce brief apnea for acquiring echo videos. This is particularly important in gated acquisitions that require several beats (as for full-volume 3D clips).
4. For apical views, place the echocardiography probe in the sub-xiphoid position while the animal lays in right lateral recumbency. Modified apical views focusing on the RV are optimal for 2D and 3D acquisitions.
5. For parasternal long and short axis views, place the echocardiography probe below the upper right limb, while the animal is in left lateral recumbency.
6. The main acquisition modes and derived echocardiography parameters are summarized in Table 1.
7. Export DICOM files to a workstation (if available) for off-line analyses to obtain advanced quantitative parameters of RV dimensions and performance. For both 3D volumetric quantification and 2D strain analyses, image quality and endocardial border detection are key to obtain reproducible results.

3.5 Longitudinal In Vivo Model Evaluation of PH

We consider that there are two key factors that determine the phenotype of PVD/PH animal models by acute/recurrent embolizations: (1) time elapsed since the last embolization procedure, and (2) experimental conditions for right heart catheterization in anesthetized animals (anesthesia protocol and ventilation parameters) (*see Note 12*).

1. For final functional measurements and PVD assessment, allow at least 2 weeks since the last embolization procedure, to prevent overestimation of PH severity (this may be adjusted according to the purposes of each study).
2. Obtain serial pulmonary hemodynamic data (at least at the baseline and at the final follow up time point) under identical experimental conditions.
3. Conduct serial RV performance studies using several parameters to monitor chronic changes in cardiac chamber remodeling and functional impairment in response to sustained increased afterload.
4. For embolization Protocols 1 and 2, we have described serial functional data [6] according to the study timelines shown in Fig. 4.

3.6 Macroscopic Findings and Histology Analysis

1. At the final follow up time point, after all in vivo measurements have been performed, proceed to animal necropsy according to the animal procedure protocol. At lung explantation, obvious vessel occlusion with microspheres and silk sutures can be macroscopically found depending on the protocols of embolization (Fig. 5).

Table 1
Echocardiography imaging protocol for pulmonary hypertension models in swine

Acquisition mode	Parameters
<i>Left subcostal acoustic window</i>	
2D clip	LV volumes and ejection fraction (usually from LV four chamber view)
PW Doppler on LVOT	LVOT VTI (stroke volume estimation)
PW Doppler on mitral valve tips	LV diastolic function
DTI PW Doppler on mitral annulus (septal and lateral)	LV diastolic function
Color Doppler of aortic and mitral valve	Presence of valve regurgitation
3D LV	LV volumes
RV focused:	RV function parameters:
<ul style="list-style-type: none"> - 2D clip - M-mode of tricuspid annulus motion. - DTI PW Doppler of lateral tricuspid annulus - PW Doppler at the RV inflow - Color Doppler on tricuspid valve - CW Doppler on TR jet - 3D from RV 	<ul style="list-style-type: none"> - Fractional area change (%). - RV longitudinal strain curves (<i>see</i> Fig. 4) - TAPSE (mm). - Systolic wave velocity (s', cm/s) - RV Tei index. - Presence/severity of tricuspid regurgitation (TR). - Peak TR velocity (systolic RV pressure estimation). - 3D RV volumes.
<i>Right parasternal acoustic window</i>	
2D clip	LV function (short axis views), septal shift in pressure overload.
M Mode	RV wall thickness, RV diameter
Color Doppler on tricuspid valve	Presence/severity of tricuspid regurgitation.
CW Doppler on TR jet	Peak TR velocity (systolic RV pressure estimation)
PW Doppler on RVOT	RVOT flow VTI, PA flow acceleration time

CW Continuous wave (Doppler), LV Left ventricle, LVOT LV outflow tract, PA Pulmonary artery, PW Pulsed wave (Doppler), RV Right ventricle, RVOT RV outflow tract, TAPSE Tricuspid annular plane systolic excursion, TR Tricuspid regurgitation, VTI Velocity-time integral from the spectral Doppler signal

2. Following tissue fixation and sectioning, perform lung tissue staining with different kits (Masson's trichrome, elastic Van Gieson) to detect vascular remodeling and fibrosis (Fig. 6, *see Note 13*).
3. Right ventricular myocardial tissue specific staining allows evaluation of cardiomyocyte hypertrophy by cross-sectional area (wheat germ agglutinin costained with phalloidin). Stain with Masson's trichrome or Picosirius to quantify myocardial fibrosis.

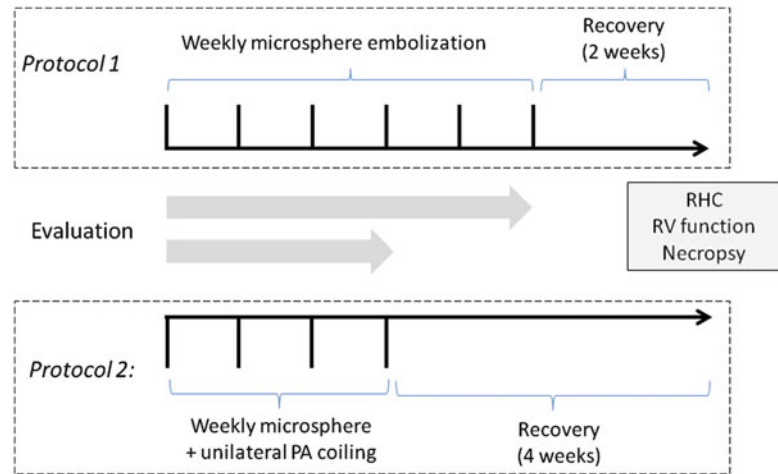


Fig. 4 Study timelines for embolization Protocols 1 and 2. Repeated acute embolization procedures are performed weekly to induce chronic PH. Recovery time period of 2–4 weeks after last injection is recommended before final functional measurements for chronic studies. Abbreviations: *RHC* Right heart catheterization

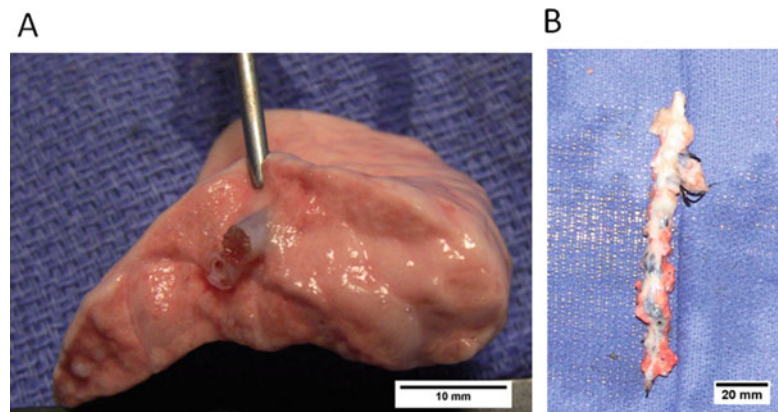


Fig. 5 Macroscopic necropsy examination shows vessel occlusion by microspheres (**A**) and silk sutures (**B**)

4 Notes

1. In animals with moderate to severe PH, hypoxia can significantly worsen the hemodynamics and animals can easily die from brief hypoxia periods. Oxygen should be supplied continuously during the preparation, and rapid intubation and immediate ventilation is necessary to prevent prolonged hypoxemia that may influence the stability of the hemodynamic evaluation.

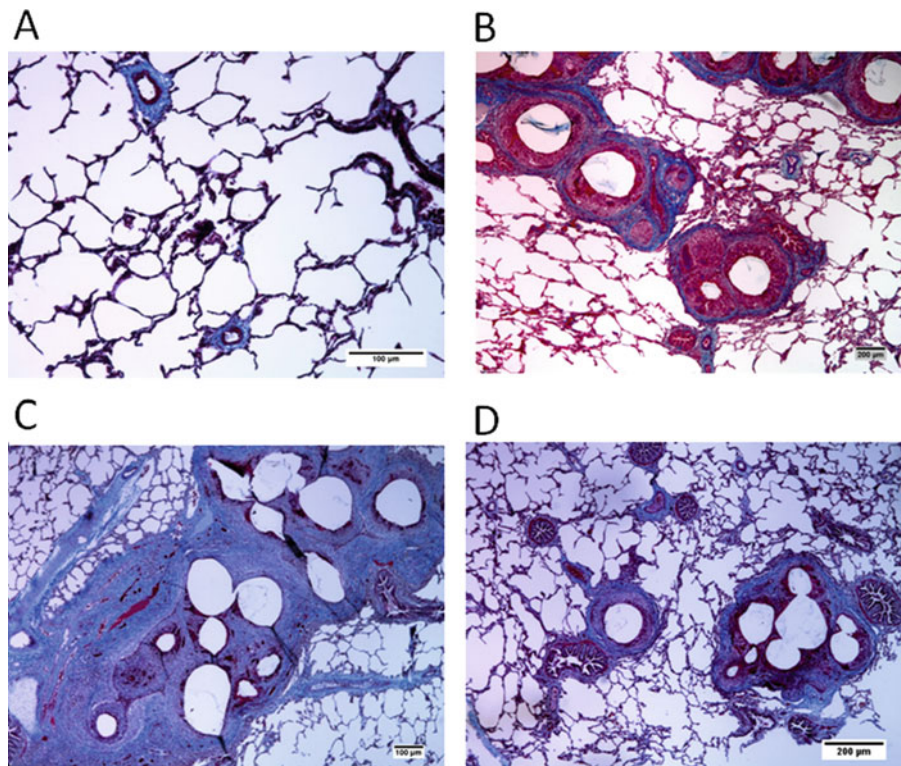


Fig. 6 Histology analysis in pulmonary embolization models. Masson's trichrome staining allows assessment of vascular remodeling including microsphere vessel occlusion and fibrosis in diseased animals (**B, C and D**) as compared to controls (**A**)

2. Certain anesthetic agents, including inhalational agents such as isoflurane (frequently used in experimental animal procedures) may exert vasodilatory effects that may result in underestimation of the pulmonary hemodynamics of the PH model.
3. In this protocol, only the distal vasculatures are targeted by PA injection of dextran microspheres. The dose is adjusted to the animal weight; however, the optimal dose depends on the animal species and strain. In our experience, a dose of 20 mg/kg of dextran microspheres in each procedure was well tolerated but induced severe acute PH in juvenile Yorkshire swine.
4. In some cases, we observed that direct dextran microspheres injection without prior swelling induced late-onset (2–4 h) severe respiratory distress resulting in high acute mortality. Other reports in sheep suggested use of nonsteroidal anti-inflammatory drugs to prevent or diminish the respiratory distress response [9].
5. In other protocols, microsphere injection is performed in the right atrium or from more periphery. Injection in the right

atrium may lead to a less accurate dosing associated with an entrapment in the RV, or uneven bilateral distribution.

6. The number and interval of the repeat embolization procedures will depend on the animal species and strain, as well as the target spectrum of the disease. In our scheme, we performed up to six embolization procedures allowing 1 week for animal recovery between each injection.
7. This protocol induces smaller increases in PA pressure during the acute embolization procedures, and in most cases without acute RV failure. Despite milder hemodynamic changes in the acute phase compared to the protocol 1 (distal embolization protocol), in the longer term, PA pressure is significantly elevated although partial recovery is observed after 1 week recovery period. Functional analysis of RV shows moderate, but significant signs of remodeling. In this protocol, distal and proximal PA vessels are sequentially targeted by local injection of dextran microspheres and local coiling (Embo+coiling). As in protocol 1, microsphere dose needs to be adjusted to the animal weight depending the animal species and breed. We used a dose of 20 mg/kg of dextran microspheres that were well tolerated and induced severe acute PH in the juvenile Yorkshire swine. In protocol 2, each Embo+coiling procedure is performed in only one lung for each procedure, alternating left and right with a weekly interval. The purpose of this is to improve hemodynamic tolerance and to minimize risk of acute decompensated RV failure.
8. After the first procedure, occlusion of the PA branch sometimes increases the PA pressure significantly and reduces cardiac output. As a result, heart rate will increase. Careful monitoring of the hemodynamics is necessary to avoid sustained low cardiac output status.
9. For the delivery of silk suture pieces, 5Fr coronary catheters are the best option, as larger catheters have greater backflow and make silk insertion more difficult, whereas silk pieces get stuck in the lumen of smaller catheters (4 Fr or smaller).
10. If the sutures get stuck inside the catheter, push the suture out by using 0.035 inch wire. If it cannot be pushed out, pull out the catheter and flush it outside, then place the catheter back into the PA branches.
11. In this procedure, at least four procedures are recommended (2 Embo+coiling procedures in right and left PA, respectively) with a recovery interval of 1 week, although this will depend on the animal species and breed as well as the target spectrum of disease. In our scheme, we performed up to six embolization procedures allowing 1 week for animal recovery between each of them.

12. Appropriate ventilation parameters are set depending on the investigators' needs. The following parameters provide stable and reproducible conditions under general anesthesia in our experience: oxygen inspiratory fraction 40%, 10 mL/kg tidal volume at 15 respirations per minute to maintain an end-tidal CO₂ between 35 and 45 mmHg as determined by capnography. A blood gas analyzer provides a detailed blood gas profile that can be particularly informative in diseased animals. Cardiac output is determined by thermodilution.

As mentioned above, some anesthesia drugs such as isoflurane have vasodilatory effects and can mask mild PH. Regarding the degree of PH, note that given the low PA pressure values in healthy animals under laboratory conditions (mean PA pressure ~15 mmHg), a mild increase of 5 mmHg results in a relative pressure rise of 33%. For this reason, all hemodynamic measurements require a very careful control of experimental conditions in order to consistently evaluate the "effect size" of the model creation, as well as the potential effects of novel therapies under investigation.

13. Occluded vessels with embolization material can be readily identified upon lung explant. Extensive vascular remodeling, including inflammatory infiltrates and occlusive vascular lesions are frequently found in the histology analyses.

Acknowledgments

This work is supported by NIH R01 HL139963 (K.I.), HL117505, HL 119046, HL129814, 128072, HL131404, HL135093, a P50 HL112324 (R.J.H.), AHA-SDG 17SDG33410873 (K.I.), and two Transatlantic Fondation Leducq grants. We would like to acknowledge the Gene Therapy Resource Program (GTRP) of the National Heart, Lung, and Blood Institute, National Institutes of Health. J.A. was supported by the Fundacion Alfonso Martin-Escudero. N.H. was supported by the French Federation of Cardiology.

References

1. Galie N, Humbert M, Vachiery J-L, Gibbs S, Lang I, Torbicki A, Simonneau G, Peacock A, Vonk Noordegraaf A, Beghetti M, Ghofrani A, Gomez Sanchez MA, Hansmann G, Klepetko W, Lancellotti P, Matucci M, McDonagh T, Pierard LA, Trindade PT, Zompatori M, Hoeper M (2016) 2015 ESC/ERS guidelines for the diagnosis and treatment of pulmonary hypertensionThe joint task force for the diagnosis and treatment of pulmonary hypertension of the European Society of Cardiology (ESC) and the European Respiratory Society (ERS): endorsed by: Association for European Paediatric and Congenital Cardiology (AEPC), International Society for Heart and Lung Transplantation (ISHLT). Eur Heart J 37(1):67–119
2. Lang IM, Madani M (2014) Update on chronic thromboembolic pulmonary hypertension. Circulation 130(6):508–518. <https:////>

- doi.org/10.1161/CIRCULATIONAHA.114.009309
3. Pepke-Zaba J, Delcroix M, Lang I, Mayer E, Jansa P, Ambroz D, Treacy C, D'Armini AM, Morsolini M, Snijder R, Bresser P, Torbicki A, Kristensen B, Lewczuk J, Simkova I, Barbera JA, de Perrot M, Hoeper MM, Gaine S, Speich R, Gomez-Sanchez MA, Kovacs G, Hamid AM, Jais X, Simonneau G (2011) Chronic thromboembolic pulmonary hypertension (CTEPH): results from an international prospective registry. *Circulation* 124(18):1973–1981. <https://doi.org/10.1161/CIRCULATIONAHA.110.015008>
 4. Simonneau G, Torbicki A, Dorfmuller P, Kim N (2017) The pathophysiology of chronic thromboembolic pulmonary hypertension. *Eur Respir Rev* 26(143). <https://doi.org/10.1183/16000617.0112-2016>
 5. Lang I (2015) Chronic thromboembolic pulmonary hypertension: a distinct disease entity. *Eur Respir Rev* 24(136):246–252. <https://doi.org/10.1183/16000617.00001115>
 6. Aguero J, Ishikawa K, Fish KM, Hammoudi N, Hadri L, Garcia-Alvarez A, Ibanez B, Fuster V, Hajjar RJ, Leopold JA (2015) Combination proximal pulmonary artery coiling and distal embolization induces chronic elevations in pulmonary artery pressure in swine. *PLoS One* 10(4):e0124526. <https://doi.org/10.1371/journal.pone.0124526>
 7. Garcia-Alvarez A, Fernandez-Friera L, Garcia-Ruiz JM, Nuno-Ayala M, Pereda D, Fernandez-Jimenez R, Guzman G, Sanchez-Quintana D, Alberich-Bayarri A, Pastor-Escuredo D, Sanz-Rosa D, Garcia-Prieto J, Gonzalez-Mirelis JG, Pizarro G, Jimenez-Borreguero LJ, Fuster V, Sanz J, Ibanez B (2013) Noninvasive monitoring of serial changes in pulmonary vascular resistance and acute vasodilator testing using cardiac magnetic resonance. *J Am Coll Cardiol* 62(17):1621–1631. <https://doi.org/10.1016/j.jacc.2013.07.037>
 8. Mercier O, Fadel E (2013) Chronic thromboembolic pulmonary hypertension: animal models. *Eur Respir J* 41(5):1200–1206. <https://doi.org/10.1183/09031936.00101612>
 9. Pohlmann JR, Akay B, Camboni D, Koch KL, Mervak BM, Cook KE (2012) A low mortality model of chronic pulmonary hypertension in sheep. *J Surg Res* 175(1):44–48. <https://doi.org/10.1016/j.jss.2011.02.049>
 10. Shelub I, van Grondelle A, McCullough R, Hofmeister S, Reeves JT (1984) A model of embolic chronic pulmonary hypertension in the dog. *J Appl Physiol Respir Environ Exerc Physiol* 56(3):810–815
 11. Weimann J, Zink W, Gebhard MM, Gries A, Martin E, Motsch J (2000) Effects of oxygen and nitric oxide inhalation in a porcine model of recurrent microembolism. *Acta Anaesthesiol Scand* 44(9):1109–1115. <https://doi.org/10.1034/j.1399-6576.2000.440913.x>
 12. Zhou X, Wang D, Castro CY, Hawkins H, Lynch JE, Liu X, Zwischenberger JB (2011) A pulmonary hypertension model induced by continuous pulmonary air embolization. *J Surg Res* 170(1):e11–e16. <https://doi.org/10.1016/j.jss.2011.04.030>



Chapter 29

Modeling Pulmonary Hypertension: A Pig Model of Postcapillary Pulmonary Hypertension

Olympia Bikou, Kiyotake Ishikawa, Kenneth M. Fish, Iratxe Zarragoikoetxea, Roger J. Hajjar, and Jaume Aguero

Abstract

Pulmonary hypertension (PH) is a pathophysiological condition defined as an increase in mean pulmonary arterial pressure ≥ 25 mmHg at rest assessed by right heart catheterization.

Based on hemodynamic criteria, precapillary PH is characterized by a mean pulmonary capillary wedge pressure ≤ 15 mmHg as opposed to the postcapillary PH by > 15 mmHg. Postcapillary PH is one of the most common forms of PH, often caused by left ventricular dysfunction and heart failure.

In this chapter, we describe protocols for creating a large animal model of postcapillary PH. It is induced by open chest surgery (lateral thoracotomy) to band the pulmonary veins. The model is characterized by low mortality, relatively easy surgical procedure with well reproducible results, and pulmonary and cardiac remodeling at the structural, functional, and molecular levels. The presence of right ventricular (RV) remodeling is of significant importance since right heart failure is the main cause of death in patients suffering from PH. One of the advantages of the model described in this chapter is that both adaptive and maladaptive forms of RV remodeling can be observed during the progression of the disease. This can help understand the progressive pathophysiology of RV failure in humans. Besides the description of the model, a detailed guidance of the RV functional assessment in pigs for both invasive (heart catheterization) and noninvasive (echocardiography) approaches is provided.

Key words Pulmonary hypertension, Animal model, Large animal, Postcapillary pulmonary hypertension, Right heart failure, Right heart echocardiography

1 Introduction

The current Guidelines of the European Society of Cardiology and the European Respiratory Society characterize pulmonary hypertension (PH) as a hemodynamic and pathophysiological condition defined as an increase in mean pulmonary arterial pressure (mPAP) ≥ 25 mmHg at rest assessed by right heart catheterization [1].

1.1 Classification

There is a broad spectrum of clinical conditions leading to PH. In order to organize different phenotypes of PH and to improve diagnosis, understanding and therapies, several classification

systems have been introduced. In the current *clinical classification* of PH by World Health Organization, five different groups are proposed. PH phenotypes are grouped together based on similarities in clinical presentation, pathological findings, hemodynamic characteristics and treatment strategies [1, 2]. The histopathological differences reflect various different pathogenesis, which provide clues for understanding PH and consequently developing new therapies [3].

Importantly, changes in the vascular pressure, vascular resistance, and vascular blood flow pattern lead to microscopical and macroscopical changes that can trigger and perpetuate PH [4]. From this standpoint, the need for a *hemodynamic classification* of PH has emerged. Various combinations of hemodynamic parameters including pulmonary capillary wedge pressure (PCWP), pulmonary vascular resistance (PVR) and cardiac output (CO) are taken into consideration for this categorization (Table 1) [1, 5]. Of extraordinary importance is the measurement of the PCWP. This parameter allows distinction between precapillary (PCWP \leq 15 mmHg) and postcapillary PH (PCWP $>$ 15 mmHg) [1, 5] in clinics. This distinction is important, since they differ in etiology, prognosis, and response to treatments [3] (Table 1).

Precapillary PH describes the hemodynamic condition of several PH phenotypes, such as idiopathic PH, PH due to lung diseases or chronic thromboembolic PH. Postcapillary PH is

Table 1
Hemodynamic classifications of pulmonary hypertension [1]

Definition	Hemodynamic characteristics	Clinical group
PH	mPAP \geq 25 mmHg	All
Precapillary PH	mPAP \geq 25 mmHg PCWP \leq 15 mmHg	1. Pulmonary arterial hypertension 3. PH due to lung diseases 4. Chronic thromboembolic PH 5. PH with unclear and/or multifactorial mechanisms
Postcapillary PH	mPAP \geq 25 mmHg PCWP $>$ 15 mmHg	2. PH due to left heart disease 5. PH with unclear and/or multifactorial mechanisms
Isolated postcapillary PH (Ipc-PH)	DPG $<$ 7 mmHg and/or PVR \leq 3 WU	
Combined postcapillary and precapillary PH (Cpc-PH)	DPG \geq 7 mmHg and/or PVR $>$ 3 WU	

PH Pulmonary hypertension, DPG Diastolic pressure gradient (diastolic PAP – mean PCWP), mPAP Mean pulmonary arterial pressure, PCWP Pulmonary capillary wedge pressure, PVR Pulmonary vascular resistance, WU Wood units

predominantly caused by systolic or diastolic left heart dysfunction. Other causes include congenital heart disease, veno-occlusive PH, and PH due to iatrogenic pulmonary vein stenosis (atrial fibrillation ablation procedures or lung transplantation). Elevated pressures in the left heart chambers result in elevated pressures in the pulmonary vascular system. Continuously elevated pulmonary pressure induces remodeling of the pulmonary vessels, leading to PH [6]. Postcapillary PH is undoubtedly one of the most common forms of PH, associated with high morbidity and mortality [5].

1.2 PH and the Right Ventricle (RV)

Regardless of the pathogenesis of PH and the vascular remodeling, right heart failure is the main cause of death in PH patients [7, 8]. Increased afterload forces the RV to adapt to it using a cascade of autocrine, paracrine, and neuroendocrine signaling as well as metabolic, molecular, inflammatory, and cellular remodeling. This initial adaptive response converts to a maladaptive RV dysfunction when PH persists. The mechanisms underlying this conversion are poorly understood, despite its importance in determining prognosis of PH patients [9]. To date, right heart failure specific pharmacotherapy has not been successfully developed in PH, in contrast to those for the left ventricle (LV) [8–10]. Evidently the elucidation of the molecular mechanisms that lead to RV-maladaptation is essential for development of new therapies.

1.3 The Need for Clinically Relevant PH Model

Despite the major advances in the therapeutic strategies for PH, the mortality rate remains high and the functional and hemodynamic parameters are essentially unchanged in many patients [8, 11]. This points out that essential molecular pathways have either not been identified or not therapeutically targeted yet. Animal models can help discover the central pathophysiology of PH. Considering the diversity and complexity of clinical PH presentation, it is apparent that we need more than one model to mimic PH associated diseases. Several animal models have served over the last decades to reveal the pathogenetic mechanisms of PH. The interested reader is referred to existing reviews on this topic [3, 12, 13].

1.4 What Do We Want to Model? What Is the Clinical Correlate?

In this chapter, we describe a large animal (pig) model of postcapillary PH.

Why postcapillary PH?

As pointed out above, postcapillary PH is one of the most common causes of PH [5, 14]. It is often associated with left heart failure, both with preserved and reduced ejection fraction [7]. The current guidelines do not support the use of therapies targeting pulmonary arterial hypertension in patients with heart failure with preserved ejection fraction accompanying PH [7]. Moreover, treatment of RV failure using pharmacotherapy for LV failure related PH has been largely unsuccessful. Not least the reason for the latter is that the mechanisms underlying in postcapillary PH are poorly

elucidated. Reproducible models of post capillary PH is needed to improve our understandings in disease mechanisms and to develop new therapies for this type of PH.

What do we need to model?

An animal model should recapitulate the clinical postcapillary PH condition. Ideally, the hemodynamic parameters and the macroscopical as well as microscopical vascular remodeling should imitate the postcapillary PH observed in humans. Moreover, a right heart pathophysiological adaption should be involved. The pig model described in this chapter meets these requirements. It is induced by open chest surgery (lateral thoracotomy) to band the pulmonary veins, which drain majority of the pulmonary blood flow into the left atrium (Fig. 1).

What are the advantages of this model?

Up to date, this is the only large animal model resembling the typical features of chronic postcapillary PH for both pulmonary vascular remodeling as well as right heart failure. Further, in this model, both adaptive and maladaptive RV responses to postcapillary PH can be observed [15], during the progression of the disease. This suggests that the model could pave the way for understanding the variable conditions of RV failure in humans [16]. Additionally, the model is characterized by low mortality and relatively easy surgical procedure with well reproducible results.

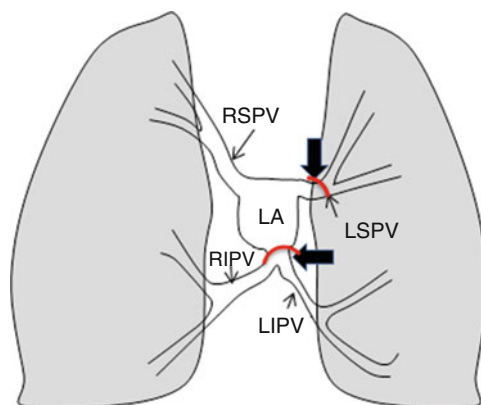


Fig. 1 Schematic representation of the anatomy of the pulmonary veins in swine. Superior pulmonary veins drain into the left atrium (LA) in separate ostia, whereas the inferior veins drain through a common ostium. To create the postcapillary PH model, both the left superior vein (LSPV) and the common inferior vein are banded (thick arrows). *RSPV* Right superior pulmonary vein, *RIPV* Right inferior pulmonary vein, *LSPV* Left superior pulmonary vein, *LIPV* Left inferior pulmonary vein, *LA* Left atrium. Arrows indicate the topography of the pulmonary veins. Red indicates the banding position

2 Materials

2.1 Reagents and Equipment

1. Syringes and needles.
2. Peripheral i.v. catheter, 22 G.
3. Laryngoscope and endotracheal tube.
4. Veterinary anesthesia ventilator, suitable for large animals.
5. Anesthesia syringe pump.
6. Vital and hemodynamic monitors.
7. Capnograph.
8. Ultrasound system for cardiology equipped with ultrasound transducer for adult cardiac exam (5–2 MHz).
9. 70% isopropyl alcohol and povidone-iodine.
10. Heating pad.
11. Sterile drapes.
12. Gauzes.
13. Standard surgical tools: Scissors, forceps, scalpel, needle holder, retractor, electric cautery.
14. Sutures: bioabsorbable and nylon sutures.
15. Cotton umbilical tape 1/8" × 18".
16. Silicone thoracic drain 22 Fr.
17. Transparent medical dressing.
18. Procedure room equipped with a fluoroscopy system (C-arm).
19. Standard cath pack for sterile percutaneous angiographies: syringes, towels, bowls, gauze.
20. Sheath introducer 7–8 French.
21. Swan-Ganz Catheter 7 French.
22. Blood gas analyzer.
23. Conductance micromanometer catheter for large animals (7 French).
24. Software Interface for pressure–volume signal data acquisition, calibration, and analysis.
25. Fogarty balloon catheter for inferior vena cava occlusions.

2.2 Drugs (Recommended Dose)

1. Telazol (tiletamine/zolazepam), (6.0–8.0 mg/kg).
2. Buprenorphine (0.6 mg).
3. Propofol (8–10 mg/kg/h).
4. Isoflurane (2–3%).
5. Local anesthetics.
6. Fentanyl transdermal patch, 25–50 µg/h.

7. Cefazolin (25 mg/kg).
8. Antibiotic ointment.
9. Furosemide.
10. Sodium chloride 0.9%.

3 Methods

The procedures described below have been set up in a swine model (10–20 kg) (*see Note 1*).

3.1 Animal Preparation

1. Fast the animal overnight. Provide free access to water.
2. Induce anesthesia by intramuscular administration of Telazol.
3. Transfer the animal to the preparation table and apply oxygen.
4. Monitor peripheral oxygen saturation and heart rate continuously.
5. Intubate the pig [17] (*see Note 2*)
6. Connect the animal to a ventilator. End-respiratory CO₂ measurement is recommended to adjust the tidal volume and ventilation rate (*see Note 3*)
7. Clean the ear as needed, and place an i.v. angiocatheter in the posterior auricular vein.
8. Clean and shave the left part of the thorax.
9. Administer intramuscular prophylactic antibiotics (Cefazolin, 25 mg/kg).
10. Apply preprocedural analgesics (e.g., buprenorphine, 0.03 mg/kg). Buprenorphine at higher dose is effective for 8–12 h and is therefore the preferred preprocedural pain medication.
11. Transfer the animal to the surgical suite.
12. Maintain anesthesia using propofol i.v.: if the animals are recovering from the sedation, initially administer a bolus of 3 mg/kg, then continue with 8–10 mg/kg/h (*see Note 4*).
13. Pulse oxymetry, ECG, heart rate and blood pressure should be continuously monitored throughout the procedure, including during anesthesia induction, maintenance and recovery.
14. Start intravenous saline infusion (BW (kg) × 5–10 mL) to correct dehydration from overnight fasting (*see Note 5*).
15. Position the pig on the right lateral decubitus, left side up. Place an electric cautery patch on the right side of the pig. Then tie and pull the forelegs toward head direction.
16. Clean the surgical area with alcohol and disinfect with povidone-iodine

3.2 Surgical Technique

Before starting the surgical procedure it is essential to be familiar with the anatomy of the pig heart as well as variations of the pulmonary veins. In pigs, there are commonly three vein ostia in the left atrium. Right superior pulmonary vein is draining blood from the right superior and middle lobes of the lung. Left superior pulmonary vein drains blood from the left superior lobe, and the common inferior pulmonary vein drains the blood from both sides of the inferior lobes [18]. The pulmonary veins that are banded in this model are the left superior and the common inferior pulmonary veins. Figure 1 displays the topography of the pig pulmonary veins as well as the banding sites.

1. Cover the pig with a large sterile drape and prepare surgical instruments. Use sterile techniques for all the surgical procedures. Ensure that the animal has an appropriate level of anesthesia before surgical incision (*see Note 4*).
2. Apply local anesthesia before performing the incision. Allow a few minutes for the drug to act.
3. The incision is carried out on the fifth intercostal space (*see Note 6*). The length of the incision depends on the size of the pig. Six centimeter is the length usually made in our procedures for a pig weighing 10–15 Kg.
4. Using electric cautery, dissect the muscle layers carefully.
5. Puncture the pleura using dull forceps during expiration to allow entry to the chest cavity. Widen the hole by manually dissecting the intercostal space along the ribs to open the chest (*see Note 7*). Displace the lung dorsally, and squeeze the lung with wet gauze as needed to obtain a good surgical window.
6. Identify left superior pulmonary vein. Make a small incision on the membrane surrounding the pulmonary vein and dissect it carefully using an angled forceps. Place an umbilical tape around the vein. The anatomic correlation to this is shown in Fig. 1 (*see Note 8*)
7. Adjust the surgical window to obtain a good view of the left atrium—common inferior pulmonary vein connection area. Carefully dissect the membrane using fine scissors and isolate common inferior pulmonary vein using blunt forceps. Place an umbilical tape around the vein (*see Notes 9 and 10*)
8. Place a fixed diameter plastic tube on top of the isolated common inferior vein and band the vein and the tube together with the umbilical tape. Remove the tube and check the size of the banded vein (Fig. 2a shows schematically how the band is placed around the reference tube to narrow the vein lumen). Do the same procedure on the left superior vein and shorten the umbilical tape (*see Note 11*).

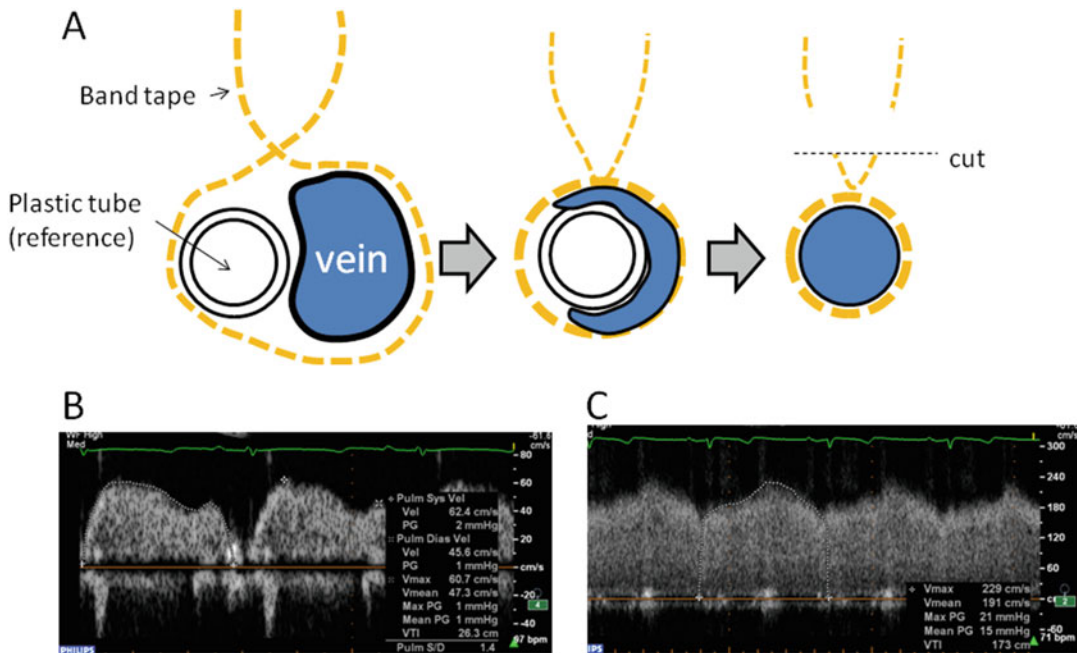


Fig. 2 Schematic illustration of the surgical procedure of pulmonary vein banding and echocardiographic evaluation. In **A**, the image depicts schematically how the band is placed around the reference tube to narrow the vein lumen, and the final effect after the plastic tube removal. In **B** and **C**, the effect of vein banding is confirmed by an increase in pulmonary vein velocities and mean gradient during systole and diastole (peak velocities increase from 40 to 60 cm/s to >150 cm/s, and mean gradient raises from 1 to 15 mmHg, on average)

9. Monitor the ECG and the heart rate. If the animal remains stable, chest can be closed (*see Note 12*). Create a small incision in the caudal side of the surgical site and make a small tunnel through sixth intercostal space. Place a drain tube through the tunnel for air removal after closing the surgical area.
10. Remove gauze on the lung and inflate the lung by giving an appropriate inhalation pressure.
11. Chest closure should be done in layers. Use bioabsorbable sutures for inside the body and nonabsorbable sutures for skin. Remove air by giving negative pressure to the drain tube. Close the wound. Clean the surgical site, place antibiotic ointment and cover with gauze.
12. Turn off isoflurane and recover the animal. Care must be taken to assess the recovery of spontaneous breathing for mechanical ventilation weaning and timely extubation. Keep the animal warm on heating pad.
13. Inject furosemide 4 mg/kg mg i.v. during recovery to prevent acute pulmonary congestion (*see Note 13*).

14. Administer antibiotics twice daily for 5 days after thoracotomy. Attach a fentanyl patch to the skin behind the ear for analgesia. Fixate if necessary. Check daily for signs of pain and symptoms of the animal. These may include but not limited to abnormal gait or posture, changes in appearance, reluctance to move, decreased appetite, escape, avoidance, and abnormal vocalization [19, 20]. Adapt the pain medication as needed.

3.3

Echocardiographic Functional Assessment of the PH Model

Assessment of RV remodeling and performance parameters, as well as invasive pulmonary hemodynamics, is the key to characterize chronic RV changes in response to sustained increased afterload.

Always perform baseline (before model creation) and follow up measurements to evaluate serial changes in individual animals.

1. Before starting the echocardiographic study, stabilize vital parameters (heart rate, oxygen saturation and anesthesia depth). Image acquisition is optimized using brief period of breath holds (<5 s) in particular for avoiding stitching artifacts in the 3D volume datasets that are obtained from consecutive beats (*see Note 14*).
2. Echocardiographic images will be obtained in the apical and in the parasternal views. For apical and left parasternal views, place the animal on right lateral recumbency. For right parasternal views, place the animal on left lateral recumbency. Table 2 summarizes the main echocardiographic views in the swine model, with focus on the relevant structures in PH models in each view.
3. Obtain pulmonary venous flow measurements in the left parasternal view (third or fourth intercostal space) during short breath holds. Display the pulmonary veins and apply color Doppler. Accelerated flow can be recognized as a scattered color after the pulmonary vein banding. Apply pulse-wave (PW) Doppler and adjust the scale for measuring the pulmonary venous flow. In Fig. 2B, C, the effect of vein banding is confirmed by an increase in pulmonary vein velocities and mean gradient during both systole and diastole.
4. Use apical approach to obtain RV longitudinal view and tricuspid annular plane systolic excursion (TAPSE). In pigs, apical approach provides five-chamber view with RV free wall delineation. Careful attention should be paid to image RV free-wall throughout the cycle, as it moves significantly in longitudinal direction. Frame rate should be adjusted to increase the image quality as much as possible while including all the RV myocardium and the tricuspid valve. Figure 3A, B shows apical RV focused imaging of normal (A) and dilated RV in the PH model (B). Postprocessing of these 2D images provides additional

Table 2**Image acquisition and parameter analysis in right heart echocardiography in pigs**

Probe position	Imaging mode	Parameters
Left parasternal	PW Doppler (pulmonary vein)	Pulmonary vein flow
Left subcostal	2D (RV inflow focused)	<ul style="list-style-type: none"> - Fractional area change (%). - RV longitudinal strain (postprocessing required) - 3D volumes and ejection fraction (postprocessing required)
	M-Mode (lateral tricuspid annulus)	TAPSE
	Tissue Doppler (lateral tricuspid annulus)	<ul style="list-style-type: none"> - Systolic wave velocity (s', cm/s) - RV Tei index.
	Color and CW Doppler (tricuspid valve)	Grade of tricuspid regurgitation and peak systolic gradient (pulmonary artery pressure estimation)
Right parasternal	2D (LV short axis, focus on septum)	LV function, septal shift in pressure overload RV wall thickness, RV diameter, RV/LV ratio
	Color and PW Doppler on RVOT	RVOT flow VTI, PA flow acceleration time, pulmonary regurgitation

PW Pulsed wave, 2D Two-dimensional, RV Right ventricle, 3D three-dimensional, TAPSE Tricuspid annular plane systolic excursion, LV Left ventricle, RVOT Right ventricular outflow tract, VTI Velocity time integral

quantitative parameters of RV performance (i.e., 2D longitudinal strain, Fig. 3C, D).

5. Quantitative assessment of tricuspid regurgitation, and trans-tricuspid flow velocities can be obtained with PW, color, and continuous-wave (CW) Doppler configurations (see Note 14).
6. Apply tissue Doppler on RV free-wall. Use fast sweep speed to obtain higher temporal resolution. Color Doppler should be applied to evaluate the presence of tricuspid regurgitation, followed by CW Doppler to measure the velocity if there is any. PW Doppler is applied on the RV inflow just proximal to the tricuspid valve to evaluate the inflow velocities.
7. Obtain 3DE images from the apex using 3D probe. Increase frame rate to obtain best available images with a focus placed on the RV. Use multiple loops to construct 3DE images depending on the availability of echocardiography machine function. Figure 3E, F show examples of normal and dilated RV in healthy and diseased PH animals.
8. In left lateral recumbency (right parasternal view, from third intercostal space), RV can be monitored just below the ribs. Apply M-mode and obtain clear images of RV free wall thickness throughout the cycle. Rotate the probe and obtain short axis views of the heart. Dilated RV and septal flattening can be

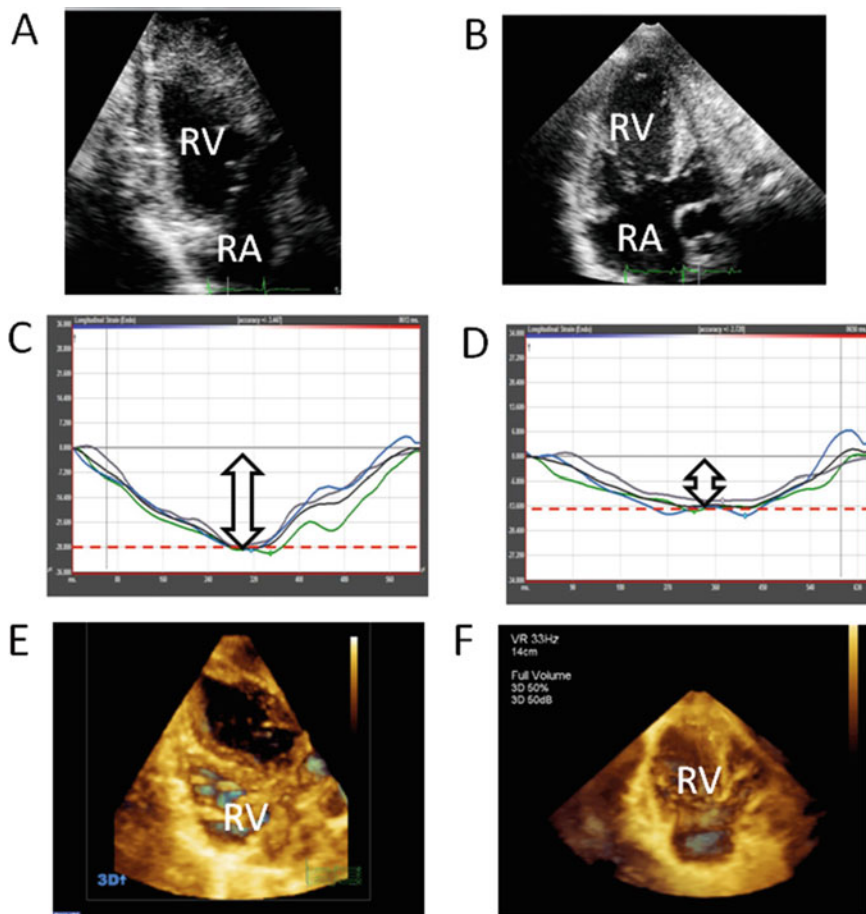


Fig. 3 Echocardiographic imaging of the RV in swine PH models. RV dimensions are assessed in apical RV focused 2D views (**A**, healthy, **B** diseased), that can be further postprocessed with specific software to derive quantitative strain parameters (arrows show peak longitudinal strain values in healthy (**C**), and PH model (**D**)). In the same apical view, 3D echocardiography of RV chamber provides volumetric information from control (**E**) and PH animals (**F**). Abbreviations: *RV* Right ventricle, *RA* Right atrium

observed in the advanced PH pigs. Figure 4 shows flattening and leftward septal shift in progressive PH.

9. Rotate the probe (clockwise from short axis view) and delineate tricuspid valve. Apply color Doppler and evaluate the presence of tricuspid regurgitation. When the regurgitation flow is eccentric, this view provides more accurate TR flow velocity by enabling more linear alignment of the flow and the Doppler axis.
10. Rotate the probe (clockwise from tricuspid view) and delineate the pulmonic valve. Apply color Doppler and evaluate the presence of pulmonic valve regurgitation. Apply pulse-wave Doppler on the proximal pulmonary artery and obtain pulmonary arterial flow. Increase the sweep speed for measuring the pulmonary arterial acceleration time.

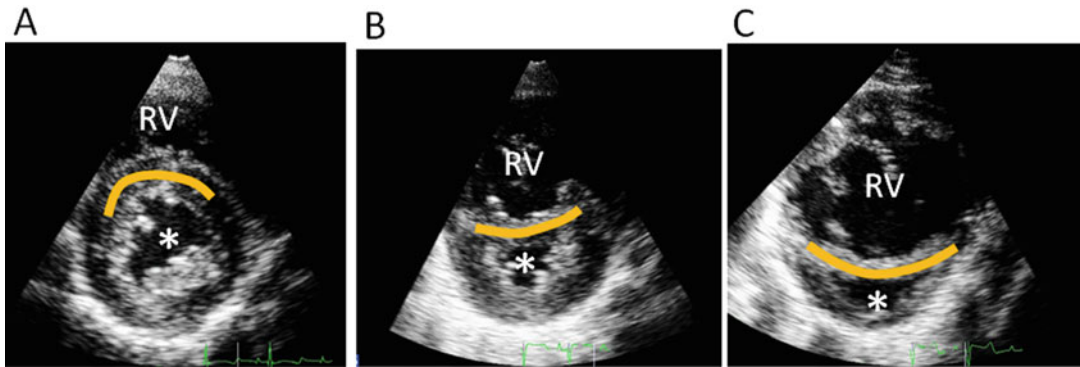


Fig. 4 In short axis views, septal shape (orange line overlay) can be assessed as a qualitative signs of PH. Images depict normal septal position at the end-systolic frame in a control animal (**A**), and progressive leftward-shift in the PH model (**B** and **C**). Abbreviations: *RV* Right ventricle, * identifies the left ventricular lumen

3.4 Hemodynamic Assessment of the RV, Right Heart Catheterization

1. Obtain serial pulmonary hemodynamic data (at least at the baseline and at the final follow up time point) under identical experimental conditions.
2. For right heart catheterization, a femoral vascular access is obtained under sterile conditions using the Seldinger technique. For right heart catheterization with a 7 French Swan-Ganz catheter, a 7–8-Fr sheath is placed in the femoral vein. As an alternative, the jugular veins can also be accessed in swine but care must be taken to avoid undesired carotid artery punctures.
3. Position the Swan-Ganz catheter in the pulmonary artery to obtain right side hemodynamics using fluoroscopic guidance. Calibrate pressure sensor carefully. Hemodynamic stability must be obtained and the catheter locations should be confirmed for every measurement.
4. Obtain the main hemodynamic parameters for PH assessment: right atrial (RA) pressure, systolic, diastolic, and mean pressures of the PA, PCWP from right and left lungs (see Note 15).
5. Measure cardiac output (CO) using the thermodilution method. Pulmonary vascular resistance (PVR) is calculated as (mean PA - PCWP)/CO.

3.5 Histological Analysis of the Lung and RV Tissue

1. At the final follow up time point, after all in vivo measurements have been performed, euthanize the animal under deep anesthesia and proceed with animal necropsy according to the animal procedure protocol.
2. Following tissue fixation and sectioning, perform lung tissue staining with different kits (Masson's trichrome, elastic Van Gieson) to detect vascular remodeling and fibrosis (see Note 16).

3. Right ventricular myocardial tissue specific staining allow for cardiomyocyte hypertrophy by cross-sectional area (wheat germ agglutinin costained with phalloidin). Stain with Masson's trichrome or Picosirius to quantify myocardial fibrosis.

4 Notes

1. In our experience, same degree of pulmonary vein stenosis in Yorkshire pigs and Yucatan mini pigs resulted in different outcomes. In specific, Yucatan mini pigs were much less tolerant to pulmonary hypertension compared to Yorkshire pigs and developed symptoms earlier. Therefore, strain difference should be taken into account when designing a study.
2. Pigs are difficult to intubate. Improper intubation can lead to trauma (laryngeal rupture, tube in the subcutaneous space). Before intubation the animal should be sedated, but careful attention should be paid to SpO₂ and heart rate (pulse) especially when the animals are sick from PH.
3. Pigs have fragile pulmonary tissue. In order to avoid damage by hyperinflation maintain ventilator pressure below 22 cm H₂O [17].
4. The anesthetic agent should be carefully chosen, as it can affect the endpoint measurements [21]. The preferred anesthesia in surgical procedures is volatile anesthetics (such as isoflurane 1–3%) as it has analgesic effect and can be adjusted according to the animal sedation status. However volatile anesthetics also have strong vasodilatory effects and can mask mild PH. Therefore we perform all echocardiographic and hemodynamic measurements under propofol anesthesia. Once the measurements are completed, anesthesia is switched to isoflurane before the surgical procedure. In the follow up time points (if no surgical intervention is planned), we only use intravenous anesthesia (propofol) for functional measurements.
5. Although animals have access to fluid overnight, they tend to be dehydrated in the morning without food. Evaluate the animal condition before infusion, because severely sick pigs could be volume-overloaded even after overnight fasting.
6. Obtaining good surgical view facilitates the banding procedure. Note that the lung lobes that cover pulmonary veins will be moved dorsally. Incision should be made on the site above the posterior end of the heart. If the fluoroscopy is available, the location of the heart can be determined before surgery.
7. Pay attention not to injure the lung while cutting the pleura. Bleeding is rarely caused by manual dissection. However, there

are relatively large vasculatures on the ventral part of the intercostals space, and widening the space too ventrally can injure these vessels and cause bleeding. For this surgery, there is no need to open the chest to this extent.

8. On the cranial side of the left superior pulmonary vein, azygos vein runs in parallel. Distinction is easy as oxygenated red blood runs in pulmonary veins. Azygos vein needs to be isolated from the pulmonary vein for banding.
9. The right half (bottom direction in surgical view) of the inferior common vein is usually very deep in the chest and cannot be easily accessed or visualized. The dissection of the vein needs to be done with extra care and gentle manipulation. Slowly dissect both visible sides of the vein (cranial and caudal sides) and scoop the vein with angled forceps. Never try to scoop by applying strong force. If it cannot be scooped, continue the dissection deeper in the surgical view until it can be scooped without applying strong force.
10. If the dissection is too distal from the left atrium, the right inferior pulmonary vein before merging into the common inferior pulmonary vein could be missed. Make sure that no pulmonary vein branches are missed before placing a band. Note that the inferior vena cava runs beneath the common inferior pulmonary vein. Do not band the inferior vena cava together.
11. The degree of stenosis that is created during the surgical procedure is a key aspect of this model. For a 10–15 kg Yorkshire swine, we used the cylinder part of a sterile 1 mL syringe (diameter of 4 mm) as a reference size to create reproducible degree of vein stenosis. We found that severe stenosis (using smaller cylinder size) induced severe postoperative pulmonary edema, whereas mild stenosis did not induce chronic PH during the follow up. Hence, the optimization of the surgical technique for creating the desired degree of stenosis is critical for achieving successful results. This optimization needs to take into account the size of the animal at the time of surgery, the growth rate, the anatomy of the pulmonary veins, and species as well as strains.
12. The heart rate will increase after banding by 5–10%. If the heart rate increases more than 15%, consider looser banding.
13. Excessive dehydration leads to low cardiac output due to low preload. Signs of low cardiac output are lethargy, effort breathing, and tachycardia. Meanwhile, signs of acute pulmonary congestion are lethargy, effort breathing, low oxygen saturation, tachycardia, and pink sputum. If the pig shows such symptoms postsurgery, careful evaluation using physiological signs, ECG, and echocardiography is necessary. Identifying the

condition of these two is usually very challenging, but the presence of pink sputum strongly suggests acute pulmonary congestion. If furosemide did not alleviate symptoms, volume loading should be considered.

14. Long breath holds should be avoided to prevent hypoxia as it dramatically increases the PA pressure (RV afterload) in sick pigs.
15. In this model the pulmonary vein banding can affect both lungs in different degrees due to anatomic variations and preferential banding of the left side veins. Therefore PCWP should be reported separately or as an average of measurements obtained from both sides.
16. For morphological evaluation, formaline fixed paraffin embedded tissues provide superior quality. However, when the immunohistochemistry is needed, frozen sections in OCT may be considered. The lung tissue is filled with air and is extremely difficult to cut with the cryotome unless the air is removed. For removing air, injection of saline–OCT (1:1) into the trachea or 24 h. fixation in 20% sucrose can be used. However, antibody reactivity should be evaluated for planned staining.

Acknowledgments

This work is supported by NIH R01 HL139963 (K.I.), HL117505, HL 119046, HL129814, 128072, HL131404, HL135093, a P50 HL112324 (R.J.H.), AHA-SDG 17SDG33410873 (K.I.), and two Transatlantic Fondation Leducq grants. We would like to acknowledge the Gene Therapy Resource Program (GTRP) of the National Heart, Lung, and Blood Institute, National Institutes of Health. J.A. was supported by the Fundacion Alfonso Martin-Escudero. O.B. was supported by the Deutsche Herzstiftung.

References

1. Galie N, Humbert M, Vachiery JL, Gibbs S, Lang I, Torbicki A, Simonneau G, Peacock A, Vonk Noordegraaf A, Beghetti M, Ghofrani A, Gomez Sanchez MA, Hansmann G, Klepetko W, Lancellotti P, Matucci M, McDonagh T, Pierard LA, Trindade PT, Zompatori M, Hoeper M, Aboyans V, Vaz Carneiro A, Achenbach S, Agewall S, Allanore Y, Asteggiano R, Paolo Badano L, Albert Barbera J, Bouvait H, Bueno H, Byrne RA, Carerj S, Castro G, Erol C, Falk V, Funck-Brentano C, Gorenflo M, Granton J, Iung B, Kiely DG, Kirchhof P, Kjellstrom B, Landmesser U, Lekakis J, Lionis C, Lip GY, Orfanos SE, Park MH, Piepoli MF, Ponikowski P, Revel MP, Rigau D, Rosenkranz S, Voller H, Luis Zamorano J (2016) 2015 ESC/ERS guidelines for the diagnosis and treatment of pulmonary hypertension: the joint task force for the diagnosis and treatment of pulmonary hypertension of the European Society of Cardiology (ESC) and the European Respiratory Society (ERS): endorsed by: Association for European Paediatric and Congenital Cardiology (AEPC), International Society for Heart and Lung

- Transplantation (ISHLT). Eur Heart J 37 (1):67–119. <https://doi.org/10.1093/eurheartj/ehv317>
2. Simonneau G, Galie N, Rubin LJ, Langleben D, Seeger W, Domenighetti G, Gibbs S, Lebrec D, Speich R, Beghetti M, Rich S, Fishman A (2004) Clinical classification of pulmonary hypertension. J Am Coll Cardiol 43(12 Suppl S):S5–S12S. <https://doi.org/10.1016/j.jacc.2004.02.037>
 3. Stenmark KR, Meyrick B, Galie N, Mooi WJ, McMurtry IF (2009) Animal models of pulmonary arterial hypertension: the hope for etiological discovery and pharmacological cure. Am J Physiol Lung Cell Mol Physiol 297(6):L1013–L1032. <https://doi.org/10.1152/ajplung.00217.2009>
 4. Dickinson MG, Bartelds B, Borgdorff MA, Berger RM (2013) The role of disturbed blood flow in the development of pulmonary arterial hypertension: lessons from preclinical animal models. Am J Physiol Lung Cell Mol Physiol 305(1):L1–L14. <https://doi.org/10.1152/ajplung.00031.2013>
 5. Humbert M, Montani D, Evgenov OV, Simonneau G (2013) Definition and classification of pulmonary hypertension. Handb Exp Pharmacol 218:3–29. https://doi.org/10.1007/978-3-642-38664-0_1
 6. Rich S, Rabinovitch M (2008) Diagnosis and treatment of secondary (non-category 1) pulmonary hypertension. Circulation 118 (21):2190–2199. <https://doi.org/10.1161/CIRCULATIONAHA.107.723007>
 7. Opitz CF, Hooper MM, Gibbs JS, Kaemmerer H, Pepke-Zaba J, Coghlann JG, Scelsi L, D'Alto M, Olsson KM, Ulrich S, Scholtz W, Schulz U, Grunig E, Vizza CD, Staehler G, Bruch L, Huscher D, Pittrow D, Rosenkranz S (2016) Pre-capillary, combined, and post-capillary pulmonary hypertension: a pathophysiological continuum. J Am Coll Cardiol 68(4):368–378. <https://doi.org/10.1016/j.jacc.2016.05.047>
 8. Lau EMT, Giannoulatou E, Celermajer DS, Humbert M (2017) Epidemiology and treatment of pulmonary arterial hypertension. Nat Rev Cardiol 14(10):603–614. <https://doi.org/10.1038/nrcardio.2017.84>
 9. Gomez-Arroyo J, Sandoval J, Simon MA, Dominguez-Cano E, Voelkel NF, Bogaard HJ (2014) Treatment for pulmonary arterial hypertension-associated right ventricular dysfunction. Ann Am Thorac Soc 11 (7):1101–1115. <https://doi.org/10.1513/AnnalsATS.201312-425FR>
 10. van Campen JS, de Boer K, van de Veerdonk MC, van der Bruggen CE, Allaart CP, Raijmakers PG, Heymans MW, Marcus JT, Harms HJ, Handoko ML, de Man FS, Vonk Noordegraaf A, Bogaard HJ (2016) Bisoprolol in idiopathic pulmonary arterial hypertension: an explorative study. Eur Respir J 48 (3):787–796. <https://doi.org/10.1183/13993003.00090-2016>
 11. Rosenkranz S, Gibbs JS, Wachter R, De Marco T, Vonk-Noordegraaf A, Vachiery JL (2016) Left ventricular heart failure and pulmonary hypertension. Eur Heart J 37 (12):942–954. <https://doi.org/10.1093/eurheartj/ehv512>
 12. Colvin KL, Yeager ME (2014) Animal models of pulmonary hypertension: matching disease mechanisms to etiology of the human disease. J Pulm Respir Med 4(4):198. <https://doi.org/10.4172/2161-105X.1000198>
 13. Maarmann G, Lecour S, Butrous G, Thienemann F, Sliwa K (2013) A comprehensive review: the evolution of animal models in pulmonary hypertension research; are we there yet? Pulm Circ 3(4):739–756. <https://doi.org/10.1086/674770>
 14. Pereda D, Garcia-Alvarez A, Sanchez-Quintana D, Nuno M, Fernandez-Friera L, Fernandez-Jimenez R, Garcia-Ruiz JM, Sandoval E, Aguero J, Castella M, Hajjar RJ, Fuster V, Ibanez B (2014) Swine model of chronic postcapillary pulmonary hypertension with right ventricular remodeling: long-term characterization by cardiac catheterization, magnetic resonance, and pathology. J Cardiovasc Transl Res 7(5):494–506. <https://doi.org/10.1007/s12265-014-9564-6>
 15. Aguero J, Ishikawa K, Hadri L, Santos-Gallego C, Fish K, Hammoudi N, Chaanine A, Torquato S, Naim C, Ibanez B, Pereda D, Garcia-Alvarez A, Fuster V, Sen-gupta PP, Leopold JA, Hajjar RJ (2014) Characterization of right ventricular remodeling and failure in a chronic pulmonary hypertension model. Am J Phys Heart Circ Phys 307(8):H1204–H1215. <https://doi.org/10.1152/ajpheart.00246.2014>
 16. Gomez-Arroyo JN, Yu PB (2016) Animal models of pulmonary hypertension. In: Maron BA, Zamanian RT, Waxman AB (eds) Pulmonary hypertension. Springer, Cham
 17. Swindle MM (2007) Swine in the laboratory surgery, anesthesia, imaging, and experimental techniques. CRC Press, Boca Raton
 18. Vandecasteele T, Vandeveld K, Doom M, Van Mulken E, Simoens P, Cornillie P (2015) The

- pulmonary veins of the pig as an anatomical model for the development of a new treatment for atrial fibrillation. *Anat Histol Embryol* 44(1):1–12. <https://doi.org/10.1111/ahe.12099>
19. Bradbury AG, Eddleston M, Clutton RE (2016) Pain management in pigs undergoing experimental surgery; a literature review (2012–4). *Br J Anaesth* 116(1):37–45. <https://doi.org/10.1093/bja/aev301>
20. Ison SH, Clutton RE, Di Giminiani P, Rutherford KM (2016) A review of pain assessment in pigs. *Front Vet Sci* 3:108. <https://doi.org/10.3389/fvets.2016.00108>
21. Lecour S, Botker HE, Condorelli G, Davidson SM, Garcia-Dorado D, Engel FB, Ferdinand P, Heusch G, Madonna R, Ovize M, Ruiz-Meana M, Schulz R, Sluijter JP, Van Laake LW, Yellon DM, Hausenloy DJ (2014) ESC working group cellular biology of the heart: position paper: improving the pre-clinical assessment of novel cardioprotective therapies. *Cardiovasc Res* 104(3):399–411. <https://doi.org/10.1093/cvr/cvu225>



Chapter 30

Development and Multiparametric Evaluation of Experimental Atherosclerosis in Rabbits

Max L. Senders, Mark E. Lobatto, Raphael Soler, Olivier Lairez, Carlos Pérez-Medina, Claudia Calcagno, Zahi A. Fayad, Willem J. M. Mulder, and Francois Fay

Abstract

Several animal models have been developed to study atherosclerosis. Here we present a rabbit atherosclerosis model generated by surgical denudation of the aortic endothelium in combination with a high-fat and cholesterol-enriched diet. This model is characterized by the formation of vascular lesions that exhibit several hallmarks of human atherosclerosis. Due to the rabbit's relative large size, as compared to rodents, this model is suited for the imaging-guided evaluation of novel therapeutic strategies using clinical scanners. In this chapter, we present an extensive outline of the procedures to induce aortic atherosclerotic lesions in rabbits as well as methods to evaluate the disease, including noninvasive *in vivo* multiparametric imaging and histopathology.

Key words New Zealand White rabbit, Rabbit atherosclerosis model, Translational, Imaging model, PET/MRI

1 Introduction

Atherosclerosis is the major pathophysiological mechanism responsible for cardiovascular events such as myocardial infarction and stroke [1]. Several animal models have been developed to unravel these underlying pathological pathways, ranging from recruitment and proliferation of immune cells and subsequent inflammation to lipid accumulation resulting in foam cell formation. While most rodent models lack important human plaque characteristics [2], such as small lesion size and the absence of neovascularization, the use of pig, sheep or nonhuman primate atherosclerosis models is economically and logically challenging. In this context, the rabbit model may represent the perfect trade-off. New Zealand White (NZW) rabbits are excellently suited as they establish a favorable body size relatively fast. The induction of atherosclerosis

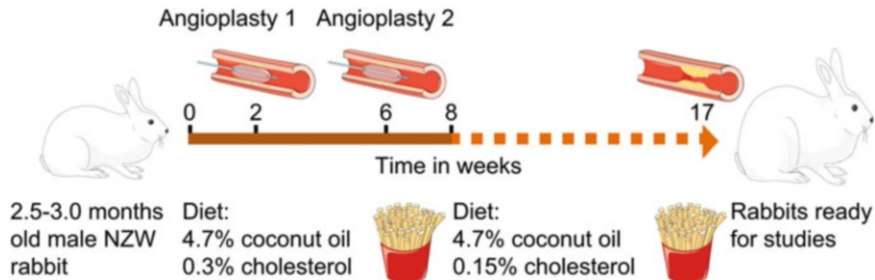


Fig. 1 Outline of the experimental procedures

is achieved by a combination of a double balloon injury—to denude the endothelial layer—and a high-fat and cholesterol-enriched diet (Fig. 1). This protocol induces inflammation and facilitates lipid accumulation in the aortic vessel wall [3, 4]. The thus induced plaques show several aspects of the so-called human vulnerable plaques [3], including extensive macrophage-rich areas, hypoxia induced neovascularization and substantial plaque size [5, 6]. The size of this model's abdominal aorta, which is comparable to human coronary arteries, facilitates noninvasive imaging using clinical systems. This allows the noninvasive study of aortic plaques' anatomical as well as compositional features. For example, computed tomography (CT) can be applied to study calcifications [7], magnetic resonance imaging (MRI) to study plaque area (T2-weighted MRI) [8, 9], dynamic contrast enhanced-MRI for neovascularization [10, 11] and macrophage burden using iron oxide-T2*-MRI [12–14]. Molecular imaging of atherosclerosis can be achieved by positron emission tomography (PET), including ¹⁸F-fluorodeoxyglucose-PET to assess plaque inflammation/hypoxia [15, 16], ¹⁸F-fluorothymidine-PET to assess macrophage proliferation [17], and ¹⁸F-sodiumfluoride-PET to evaluate microcalcifications [18–20]. Finally, immunohistochemistry may be used to assess and validate plaque severity at the microscopic level.

In summary, the New Zealand White rabbit subjected to double balloon injury and a high-fat and cholesterol-enriched diet is an excellent model to investigate atherosclerosis biology, to develop and evaluate novel diagnostics and to study cardiovascular therapies. Moreover, with this model formation of significant plaques can be achieved in 17 weeks with a survival rate of 95%. This chapter provides an overview of the requisites to induce atherosclerotic lesions in rabbits, including specifics on the diet and a step-by-step approach to denude the endothelial layer by angioplasty. Finally, several methods to evaluate and validate the atherosclerotic lesions are presented, including noninvasive *in vivo* multimodal imaging and histopathology of rabbit plaques.

2 Materials

2.1 Diet

1. Rabbit high-fat, cholesterol-enriched diet (**i**) containing 4.7% coconut oil with 0.3% cholesterol.
2. Rabbit high-fat, cholesterol-enriched diet (**ii**) containing 4.7% coconut oil with 0.15% cholesterol.

2.2 Surgical Procedure

2.2.1 Surgical Instruments and Equipment (See Table 1 and Fig. 2)

All instruments and solutions need to be sterile.

1. Sodium chloride 0.9% w/v solution.
 2. Iopamidol (Bracco Diagnostics, Monroe Township, NJ, USA).
 3. 4-French Fogarty embolectomy catheter.
 4. 20/30 Indeflator.
 5. Vein pick catheter introducer.
 6. Silk 2-0 suture Au3.
 7. Absorbable 3-0 sutures.
 8. Prolene sutures 2.0.
 9. Syringes, 5 and 10 mL.
 10. Sterile gauze (4 × 4 inches).
 11. Sterile cotton tipped applicators.
 12. Basic surgical instruments including: scalpel, retractor, and small curved Metzenbaum scissors (Fig. 2).
 13. Fluoroscopic system, such as Allura Xper FD20/10.
 14. X-ray protective lead apron.
- 2.2.2 Anesthesia
1. Lidocaine hydrochloride 1% w/v solution.
 2. Ketamine (100 mg/mL) and xylazine (20 mg/mL) solution.
 3. Veterinarian *anesthesia* and breathing system.
 4. Anesthesia monitoring: pulse oximeter.
- 2.3 Noninvasive Multiparametric Imaging Evaluation of Atherosclerosis
1. Clinical 3 Tesla Biograph mMR (Siemens, Erlangen, Germany).
 2. Ketamine (100 mg/mL) and xylazine (20 mg/mL) solutions.
 3. Pediatric Foley catheter 8 Fr.
 4. Urine leg bag.
 5. Isoflurane.
 6. Veterinarian *anesthesia* and breathing system.
 7. Contrast agent for MRI such as gadopentetate dimeglumine (Magnevist®).
 8. Computer for imaging reconstruction and analysis, including software such as Matlab and Osirix.

2.4 Euthanasia and Harvesting of Aorta and Organs

1. Pentobarbital sodium.
2. Intravenous catheter with a 500 mL bag of (heparinized) saline attached.
3. Second rabbit instrument set as shown in Table 1 and Fig. 2 for ex vivo applications.

Table 1
List of surgical instruments used during the balloon denudation procedure

Instrument	Function
Sterile tray	Sterilization of the instruments
Scalpel	Skin incision
Surgical forceps	Skin incision
Anatomical forceps	Opening of the surgical site
Beckman retractor	Visualization of the surgical site
Metzenbaum scissors	Dissection of the musculature and opening of the artery
Needle holder	Suturing
Introducer	Introduce catheter in artery
Disposable inflation device	Inflation of the balloon during angioplasty
Sterile bowl	Mixing of the iopamidol
Towel clamps	Hold the surgical drapes in place

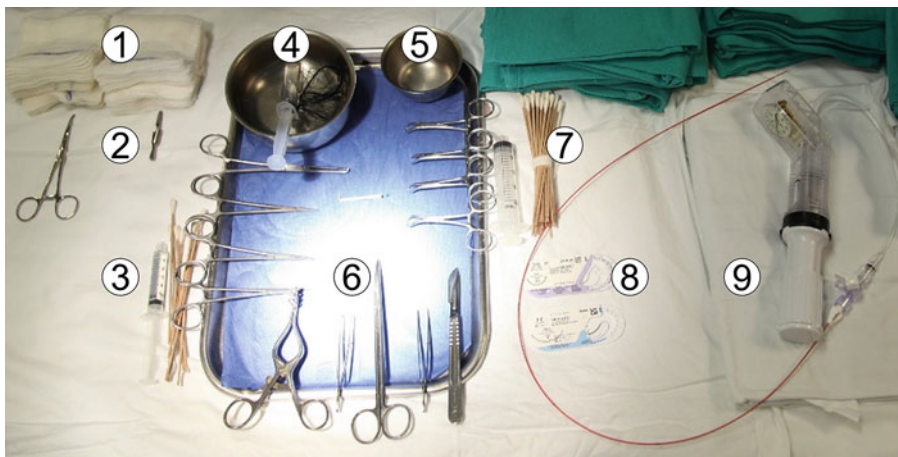


Fig. 2 Surgical instruments and equipment. (1) Sterile gauze. (2) arterial clip. (3) syringe filled with lidocaine. (4) sodium chloride solution with wet silk sutures. (5) iopamidol:saline solution (1:1). (6) surgical instruments. (7) sterile cotton tipped applicators. (8) 4-F Fogarty embolectomy catheter mounted on, (9) 20/30 indeflator

2.5 Histological Validation of Atherosclerotic Lesions

1. Formalin.
2. Paraffin.
3. Standard hematoxylin and eosin staining solutions.
4. Monoclonal Mouse Anti-Rabbit Macrophage, Clone RAM11.
5. Peroxidase-based immunohistochemical visualization kit to enhance visualization of the antibodies.

3 Methods

3.1 Regulatory

All experiments involving the use of animals should be performed in accordance with protocols approved by the Institutional Animal Care and Use Committee (IACUC) of your institution and follow national/international guidelines for animal welfare. Imaging experiments involving radiation should be performed in accordance with protocols approved by the radiation safety committee of your institution.

3.2 Diet

1. Obtain male New Zealand White (NZW) rabbit 2.5–3.0 months old.
2. Rabbits may be housed in single or paired cages and receive a regular chow and water ad libitum.
3. When rabbits reach a target weight from 2.5 to 3.0 kg, change the diet to the high-fat, cholesterol-enriched diet (**i**) containing 4.7% coconut oil and 0.3% cholesterol.
4. Two weeks after diet initiation, perform an angioplasty of the aorta using either femoral artery for entrance (*see Subheading 3.3*).
5. Four weeks after the first procedure, the contralateral femoral artery is used for entry, to repeat the angioplasty of the aorta.
6. Eight weeks after cholesterol-enriched diet initiation (2 weeks after the last angioplasty) the diet is changed to diet (**ii**) containing 4.7% coconut oil and 0.15% cholesterol (*see Note 1*).
7. After approximately 17 weeks, the animals have developed atherosclerotic lesions detectable with clinical imaging systems. When rabbits are kept on diet (**ii**) for prolonged periods they will develop advanced atherosclerotic lesions.

3.3 Surgical Procedure

3.3.1 Animal Preparation

1. Use a preparation room to sedate the rabbit with an intramuscular injection of ketamine (35 mg/kg) and xylazine (5 mg/kg) (*see Note 2*).
2. Shave the inguinal area, collect the fur and disinfect the surgical area with Iodopovidone and alcohol.

3. The rabbit can then be moved to the surgical suite. Place the rabbit in supine position in a holder on the operating table with the hind limb in a relaxed position (*see Note 3*). The position of the surgeon should be in line with the hind limbs of the rabbit.
4. Make sure the neck is in an extended position and place a facemask over the head to provide oxygen for the full length of the procedure using a veterinarian *anesthesia* and breathing system.
5. The rabbit heart rate and oxygen saturation should be monitored with a pulse oximeter attached to a front paw.
6. Organize the surgical instruments and prepare the embolectomy catheter. Use 1:1 ratio to dilute the Iopamidol with sterilized saline.
7. Place surgical drapes covering the rabbit up to the oxygen mask, only exposing the disinfected surgical area (Fig. 3a: 1) (*see Note 4*).

3.3.2 Angioplasty of the Aorta

1. Palpate the inguinal area to locate the femoral artery just below the inguinal ligament. Subsequently draw a line from the femoral artery toward the knee joint over a length of approximately 3–5 cm.
2. Apply local anesthesia using lidocaine and make a skin incision, proximal to distal, over the full length of trajectory identified in **step 1** (Fig. 3a: 2).
3. After opening the skin, bluntly separate the adductor muscles from the quadriceps muscle to allow visualization of the femoral neurovascular bundle. This can be achieved using the curved Metzenbaum scissors (*see Note 5*).
4. After separating the musculature, locate the femoral neurovascular bundle and use the self-retaining retractor to retain easy access to the surgical area. In addition, the incision may be enlarged to improve visualization.
5. Isolate the femoral neurovascular bundle by using cotton tipped applicators to separate it from the surrounding tissue (Fig. 3a: 3).
6. Identify and isolate the femoral artery from the neurovascular bundle using the curved-tip forceps or a smaller curved Metzenbaum scissors and cotton tipped applicators (*see Note 6*).
7. Isolate the femoral artery at the distal end and use a silk 2-0 filament to ligate the artery (Fig. 3a: 4, enlargement in 3b) (*see Note 7*).
8. Circumferentially remove the adventitial layer and remaining associated fat surrounding the femoral artery (*see Note 8*).

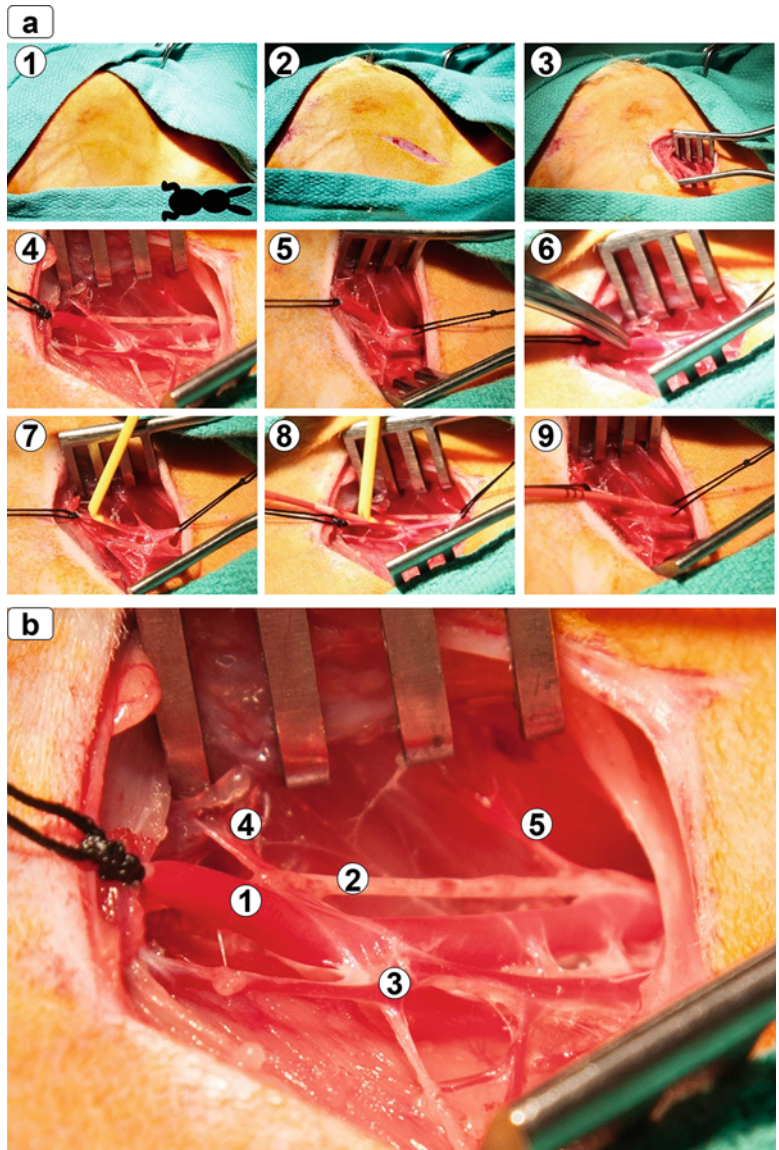


Fig. 3 Isolation of the artery and introduction of the catheter. (a) Surgical procedures. (1) The rabbit in supine position with the hind limb relaxed (the orientation of the animal is indicated by the rabbit shape). (2) A 3–5 cm incision is made from below the inguinal ligament to the knee joint. (3) The adductor muscles are separated from the quadriceps muscle to allow visualization of the femoral neurovascular bundle. (4) The femoral artery is isolated from the neurovascular bundle and a ligation is made at the most distal part of the artery. (5) A vascular loop is positioned around the proximal part of the femoral artery and put under tension. (6) A small longitudinal incision in the artery is made as distally as possible. (7) The introducer is placed in the lumen of the artery. (8) With the help of the introducer, the catheter is inserted in the artery. (9) The catheter is advanced up to the left subclavian artery (~30 cm, mark with three stripes). (b) Magnification of the neurovascular bundle. (1) Femoral artery. (2) Femoral nerve. (3) Femoral vein. (4 and 5) Branches from the femoral artery

9. Place a vascular loop (silk 2.0) around the proximal part of the femoral artery and put it under tension (Fig. 3a: 5) (*see Note 9*).
10. Soak a cotton tip applicator with lidocaine and gently stroke over the artery to enhance vasodilatation and allow easier access when introducing the catheter (*see Note 10*).
11. Use the Metzenbaum scissors or scalpel to make a small longitudinal incision in the artery as distally as possible, while keeping pressure on the proximal loop to prevent unnecessary blood loss (Fig. 3a: 6).
12. Use the introducer to facilitate insertion of the catheter into the artery while easing the pressure on the proximal loop (Fig. 3a: 7, 8) (*see Note 11*).
13. Advance the catheter up to the left subclavian artery, this is approximately 30 cm (marked with three stripes) (Fig. 3a: 9) (*see Note 12*).
14. Use the X-ray beam to ensure the whole aorta, i.e., from the aortic arch to the iliac bifurcation, is in the field of view (*see Note 13*).
15. Gently inflate the balloon with the diluted contrast until you reach a pressure of around 1.5–2.0 atmospheres (atm), the balloon will now be visualized. Based on the resistance of the vessel you may alter the pressure (Fig. 4: 1).
16. Retract the catheter over the entire length of the aorta until the iliac bifurcation is reached. Fully deflate the balloon when the catheter is in the iliac artery and stop the X-ray (Fig. 4: 2, 3) (*see Note 14*).
17. Repeat steps 13–16 two more times.
18. After retracting the balloon the final time, keep pressure on the proximal vascular loop while removing the catheter from the artery. After the catheter is completely removed, ligate the

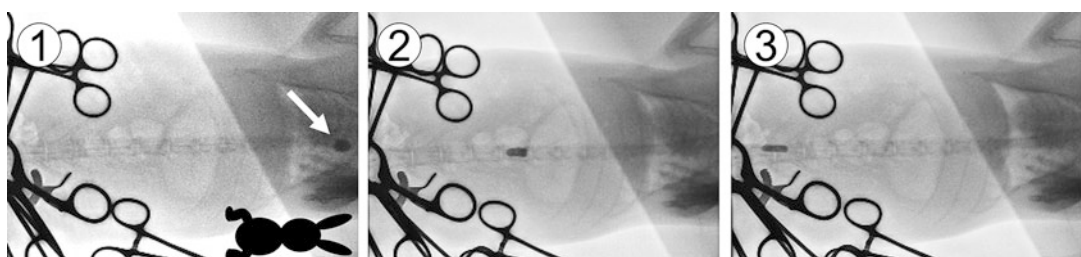


Fig. 4 Visualization of the angioplasty by fluoroscopy. (1) The X-ray beam is placed with the aortic arch and the iliac bifurcation in the field of view (the orientation of the animal is indicated by the rabbit shape). The balloon is gently inflated and visualized (white arrow). (2) The catheter is slowly retracted over the entire length of the aorta. Passing the diaphragm, resistance may be felt, for which the balloon should be marginally deflated. (3) Once the iliac bifurcation is reached the balloon is fully deflated and the X-rays should be stopped



Fig. 5 Closure of the incision. (1) As the catheter is removed, the femoral artery is ligated using the proximal loop (silk 2-0). The surgical site is cleaned and inspected for active bleedings. (2) The musculature is approximated using interrupted absorbable 3-0 sutures. (3) The skin is closed with a continuous 2.0 Prolene suture

femoral artery using the proximal vascular loop (Fig. 5: 1) (*see Note 15*).

19. Check for any active bleedings and rinse the surgical site with saline. Clean the area and remove any remaining blood clots (*see Note 16*).
20. Approximate the musculature using 2–4 interrupted sutures (Vicryl 3-0). Apply lidocaine to prolong local analgesia after surgery (Fig. 5: 2).
21. Close the skin with a continuous suture using Prolene 2.0 (Fig. 5: 3) (*see Note 17*).

3.3.3 Postoperative Care and Monitoring

1. Place an e-collar or protective materials on the wound to avoid self-mutilation or contamination of the surgical site until the wound is fully healed.
2. After surgery, check the rabbit daily for any symptoms of distress, blood loss, infections, dehiscence or nerve damage until 7–10 days postsurgery.
3. Treat mild complications such as an infection, with local antibiotic cream, or systemically if needed. Dehiscence can be treated by surgically reopening the wound for inspection and debridement.
4. In case of an active postoperative bleeding, severe dehydration, or signs of significant distress, euthanasia is strongly recommended to prevent any inhumane suffering. In addition, IACUC protocols should describe clear humane endpoints.

3.3.4 Survival

After initial recovery, rabbits may experience (reversible) nerve damage (*see Note 18*), which may induce self-mutilation. Euthanasia is required if walking is impaired or paralysis is observed. Wound infections are rare (<1%) and can be treated with local antibiotic therapy in most cases. When infections persist, systemic treatment should be started before surgical debridement of the wound is

considered. When rabbits experience a slower recovery, loss of weight is common and often reversible. However, when more than 20% loss of body weight is observed, further analysis, support and euthanasia should be considered.

Because of the added oil and cholesterol to the diet, rabbits will develop a fatty liver that may eventually result in liver failure and death. Therefore, it is a necessity to monitor the rabbits and check for signs of jaundice regularly (*see Note 19*). When signs of liver failure are suspected, blood can be drawn for analysis of liver function and animals should receive extra dietary support. In addition, the rabbit should be used for terminal experiments within a short time frame.

3.4 Noninvasive Multiparametric Imaging Evaluation of Atherosclerosis

3.4.1 Preparation of the Animal for Imaging

1. When imaging with ^{18}F -fluorodeoxyglucose (^{18}F -FDG), fast the rabbit 4 hours prior to injection.
2. Place intravenous catheters using the marginal ear veins in both ears; attach a stopcock with a short i.v. line.
3. Use either of the i.v. entries to inject the ^{18}F -FDG dose (1 mCi/kg).
4. Anesthetize the rabbits 2.5 h after injection using an intramuscular injection of ketamine (35 mg/kg) and xylazine (5 mg/kg) and empty the bladder using a pediatric Foley catheter and attach a urine bag.
5. Transport the rabbit to the PET/MRI system (make sure all metals are removed).
6. Place the rabbit in the middle of the bed, feet first, supine position, and place a facemask over the head to provide an oxygen/isoflurane mixture for the full length of the procedure using a veterinarian *anesthesia* and breathing system (Penlon Ltd., Abingdon, UK).
7. Place a body matrix coil or knee coil around the rabbit covering at least the abdominal region (*see Note 20*).
8. Prepare the automatic injector to administer the MR contrast agent and connect together with saline (for flushing) to the unused i.v. catheter for the dynamic contrast enhanced magnetic resonance imaging (DCE-MRI) scan.

3.4.2 PET/MR Imaging

1. Start the PET scan to quantify the ^{18}F -FDG signal in the abdominal aorta, and a time-of-flight (TOF) MR scan for anatomical localization (Fig. 6a).
2. After the TOF is finished, start a 3D T2-weighted MR sequence to assess the vessel wall area (Fig. 6b).
3. Start the dynamic contrast-enhanced (DCE)-MRI sequence to evaluate vessel wall permeability [21], and inject Magnevist after several frames have been acquired during the dynamic MR sequence (Fig. 6c).

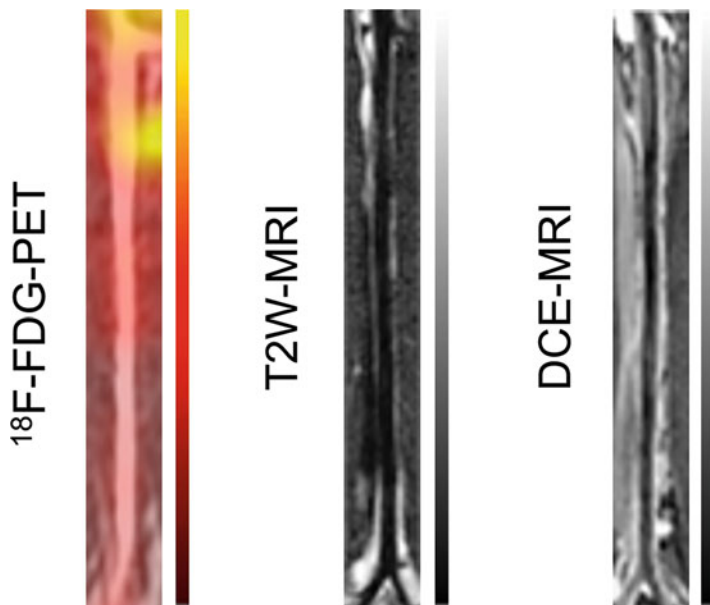


Fig. 6 Noninvasive PET/MR imaging evaluation of atherosclerosis. Representative coronal aortic fused PET/MR images of ^{18}F -FDG-PET (3 h after injection, *left*), T2-weighted MRI (*middle*) and dynamic contrast enhanced-MRI (*right*). Lesions can be found along the full length of the aorta

3.4.3 Reconstruction and Imaging Analysis

1. When necessary, offline PET reconstruction may be performed using vendor-specific tools, either alone or in combination with custom-made software to interface with them.
2. DCE-MRI data are typically analyzed using custom-made software. Custom-made software may be written in Matlab, javascript or other programming language with libraries readily available to handle imaging data as extensively discussed elsewhere [11].
3. Processed (DCE-MRI) or raw (plaque size, PET) images can be processed using readily available image analysis software, such as Osirix or similar DICOM analysis software by manually drawing regions of interest (ROIs) on the infrarenal abdominal aorta and other tissues of interest [11].

3.5 Euthanasia and Harvesting of Aorta and Organs

3.5.1 Euthanasia and Perfusion

1. Use an intravenous injection of 100 mg/kg pentobarbital sodium to euthanize the rabbit.
2. Make an incision from the jugular notch to the pubic bone.
3. Use scissors or a bone cutter to perform a sternotomy to facilitate better vision of the heart and thoracic aorta, while a self-retaining retractor is used to keep the thorax opened.
4. Place an intravenous catheter in the left ventricle to perfuse the rabbit with a minimum of 500 mL (heparinized) saline and make an incision in the portal vein to drain the blood and saline.



Fig. 7 Histological validation of atherosclerotic lesions. Conventional hematoxylin and eosin (*top*) and RAM-11 (*bottom*) for macrophage staining of aortas from healthy controls fed a regular chow diet (*left*), atherosclerotic rabbits that underwent the double balloon injury in combination with a high-fat and cholesterol-enriched diet for 17 weeks (*middle*) and 34 weeks (*right*)

3.5.2 Harvesting of the Aorta and Organs

1. Dissect the aorta from the heart to the iliac bifurcation.
2. Rinse the aorta again using saline.
3. Finally, cut the aorta in 5 mm thick pieces and preserve in formalin for histological analysis.

3.6 Histological Validation of Atherosclerotic Lesions

1. Remove the blocks from the formalin solution and embed them in paraffin.
2. Cut 7 µm thick sections, preferably two sections per slide.
3. Let the slides dry for at least 24 h in a 37 °C preheated oven.
4. Conventional hematoxylin and eosin (H&E) staining and RAM-11 staining for macrophages (Fig. 7) can be performed according to manufacturer's protocol.

4 Notes

1. Diet with 0.3% cholesterol (**i**) is changed to diet (**ii**) with a lower amount of added cholesterol (0.15%), to prevent liver failure before plaques have been induced.
2. In our experience, one intramuscular injection will be sufficient to keep the rabbit anesthetized for the whole procedure (30–45 min). If needed, an additional injection can be given.
3. Having the leg relaxed prevents an artificial bend in the iliac artery easing access when introducing the catheter.

4. It is important to cover the rabbit's body to prevent hypothermia. In addition, cover the nonsurgical area to prevent infection that can be caused by loose fur.
5. This is a crucial step: you need to be careful when bluntly dissecting not to hit the femoral nerve, artery, or vein. Before separation, removing the fascia may help to identify muscle fiber direction and facilitate proper separation.
6. The artery has a bright red color compared to the purple hue of the vein, due to the difference in oxygenation. The femoral nerve can be identified as the white structure. Be careful not to manipulate the nerve with anything else than the cotton tipped applicators, and do not stretch it. This may result in severe nerve damage, for which the animals may need to be euthanized.
7. Placing a ligation on the distal side of the artery first facilitates vasodilatation, easing further separation if needed. The silk filament should be wetted in saline solution to ease the surgical knot.
8. Removing the adventitial layer will allow vasodilatation of the artery. However, without this layer, the artery is more fragile and thus prone to rupture. Small peripheral arteries may be located near the incision site. It is recommended to save these small branches, to facilitate collateral artery formation. Nevertheless, ligation might be considered when the branches are put under tension to prevent any blood spill as they are prone to rupture.
9. Make sure the distance between the first knot and this loop is long enough to allow access for the catheter. After the denudation is completed, this loop will be used to ligate the proximal part of the femoral artery.
10. In order to ease introduction of the catheter, apply lidocaine on the artery until the diameter of the artery has approximately doubled in size.
11. Work as parallel to the vessel as possible to prevent a puncture in the artery while introducing the catheter. Make sure the catheter has not been introduced between the adventitia and media layers of the vessel wall.
12. Do not apply too much force while inserting the catheter into the artery; if the catheter gets stuck, retract it a little and try again. Ensure the adventitial layer is removed from the part of artery that will be used for catheter introduction. Forcing the catheter into the artery may cause rupture of the femoral artery.
13. To reduce radiation exposure, while wearing a radiation protection apron, try to stay as far away from the X-ray beam as possible.

14. While retracting the catheter, you should deflate the balloon slowly if you encounter any resistance, especially when passing the diaphragm. As a result of the first surgery, stenotic regions will develop along the aorta, which may increase the chance of aneurysms if the balloon is not deflated well enough during the second surgery.
15. After ligation of the femoral artery, formation of new collateral arteries will develop over time and prevent progression of limb ischemia.
16. Any hematomas left in the wound will increase the chance of infection and can induce hitching and possibly self-mutilation.
17. Keep the ends long to enable easy removal after the fur has regrown. The sutures can be removed 10–14 days after surgery.
18. Most nerve damage observed after the procedure is reversible and recovers between several hours up to 3 days after the surgery. If the nerve damage persists after day 3, it is very likely to be permanent and requires animal humane termination; however, this complication only occurs in less than 2% of the surgeries.
19. Rabbit behavior may be altered resulting in decreased activity and responsiveness. Signs of liver failure are first presented as a yellow glaze in the ears, around the eyes and the nose. We found that approximately 10% of the rabbits developed liver failure, but only after 6–12 months were spent on the cholesterol-enriched, high-fat diet.
20. Make sure to place the rabbit in a stable position to prevent it from rolling over and induce movement artifacts without causing attenuation. Linen may be used to stabilize the sides.

Acknowledgments

We would like to thank all the members of the large animal unit of the Center for Comparative Medicine and Surgery at the Icahn School of Medicine at Mount Sinai for their continual excellent technical support with this model. We also would like to thank René-Paul Lafarie for the great pictures of the angioplasty procedure. Histology images presented here were performed at the Microscopy Core at Icahn School of Medicine at Mount Sinai. PET/MR imaging was performed at the TMII Imaging Core at Icahn School of Medicine at Mount Sinai.

All experiments presented in this chapter were performed in accordance with protocols approved by the Radiation Safety Committee and the Institutional Animal Care and Use Committee of the Icahn School of Medicine at Mount Sinai and followed

National Institutes of Health guidelines for animal welfare. Some of the artworks present in Fig. 1 are adapted from Servier Medical Art and used under a Creative Commons Attribution 3.0 Unported License.

Funding

This research was supported by “De Drie Lichten” Foundation in The Netherlands (M.L.S.), the American Heart Association 17PRE33660729 (M.L.S.), the National Heart, Lung, and Blood Institute (NHLBI), and the National Institutes of Health (NIH), as a Program of Excellence in Nanotechnology (PEN) Award, Contract #HHSN268201000045C, NIH/NIBIB R01 EB009638 (Z.A.F.), Harold S. Geneen Charitable Trust Award (Z.A.F.), R01 HL125703 (W.J.M.M.), NWO Vidi 91713324 (W.J.M.M.), and PSC-CUNY (F.F.).

References

- Hansson GK (2005) Inflammation, atherosclerosis, and coronary artery disease. *N Engl J Med* 352(16):1685–1695. <https://doi.org/10.1056/NEJMra043430>
- Bentzon JF, Falk E (2010) Atherosclerotic lesions in mouse and man: is it the same disease? *Curr Opin Lipidol* 21:434–440. <https://doi.org/10.1097/MOL.0b013e32833ded6a>
- Virmani R, Burke AP, Farb A, Kolodgie FD (2006) Pathology of the vulnerable plaque. *J Am Coll Cardiol* 47((8):C13–C18. <https://doi.org/10.1016/j.jacc.2005.10.065>
- Falk E, Nakano M, Bentzon JF, Finn AV, Virmani R (2013) Update on acute coronary syndromes: the pathologists’ view. *Eur Heart J* 34 (10):719–728. <https://doi.org/10.1093/euroheartj/ehs411>
- Bocan TMA, Mueller SB, Mazur MJ, Uhendorf PD, Brown EQ, Kieft KA (1993) The relationship between the degree of dietary-induced hypercholesterolemia in the rabbit and atherosclerotic lesion formation. *Atherosclerosis* 102:9–22
- Falk E (2006) Pathogenesis of atherosclerosis. *J Am Coll Cardiol* 47(8 Suppl):C7–C12. <https://doi.org/10.1016/j.jacc.2005.09.068>
- Motoyama S, Kondo T, Sarai M, Sugiura A, Harigaya H, Sato T, Inoue K, Okumura M, Ishii J, Anno H, Virmani R, Ozaki Y, Hishida H, Narula J (2007) Multislice computed tomographic characteristics of coronary lesions in acute coronary syndromes. *J Am Coll Cardiol* 50(4):319–326. <https://doi.org/10.1016/j.jacc.2007.03.044>
- Mateo J, Izquierdo-Garcia D, Badimon JJ, Fayad ZA, Fuster V (2014) Noninvasive assessment of hypoxia in rabbit advanced atherosclerosis using 18F-fluoromisonidazole positron emission tomographic imaging. *Circ Cardiovasc Imaging* 7(2):312–320. <https://doi.org/10.1161/CIRCIMAGING.113.001084>
- Tarkin JM, Dweck MR, Evans NR, Takx RAP, Brown AJ, Tawakol A, Fayad ZA, Rudd JHF (2016) Imaging atherosclerosis. *Circ Res* 118 (4):750–769. <https://doi.org/10.1161/CIRCRESAHA.115.306247>
- Lobatto ME, Z a F, Silvera S, Vucic E, Calcagno C, Mani V, Dickson SD, Nicolay K, Banciu M, Schiffelers RM, Metselaar JM, Van Bloois L, Wu H-S, Fallon JT, Rudd JH, Fuster V, E a F, Storm G, Mulder WJM (2010) Multimodal clinical imaging to longitudinally assess a nanomedical anti-inflammatory treatment in experimental atherosclerosis. *Mol Pharm* 7(6):2020–2029. <https://doi.org/10.1021/mp100309y>
- Calcagno C, Lobatto ME, Dyvorne H, Robson PM, Millon A, Senders ML, Lairez O, Ramachandran S, Coolen BF, Black A, Mulder WJM, Fayad ZA (2015) Three-dimensional dynamic contrast-enhanced MRI for the accurate, extensive quantification of microvascular permeability in atherosclerotic plaques. *NMR Biomed* 28(10):1304–1314. <https://doi.org/10.1002/nbm.3369>
- Kelher EJ, Ye Y, Wojtkiewicz GR, Aguirre AD, Tricot B, Senders ML, Groenen H, Fay F, Perez-Medina C, Calcagno C, Carlucci G,

- Reiner T, Sun Y, Courties G, Iwamoto Y, Kim H, Wang C, Chen JW, Swirski FK, Wey H, Hooker J, Fayad ZA, Mulder WJM, Weissleder R, Nahrendorf M (2017) Polyglucose nanoparticles with renal elimination and macrophage avidity facilitate PET imaging in ischaemic heart disease. *Nat Commun* 8:14064. <https://doi.org/10.1038/ncomms14064>
13. Ruehm SG, Corot C, Vogt P, Kolb S, Debatin JF (2001) Magnetic resonance imaging of atherosclerotic plaque with ultrasmall superparamagnetic particles of iron oxide in hyperlipidemic rabbits. *Circulation* 103 (3):415–422. <https://doi.org/10.1161/01.CIR.103.3.415>
14. Tang TY, Howarth SPS, Miller SR, Graves MJ, Patterson AJ, U-King-Im JM, Li ZY, Walsh SR, Brown AP, Kirkpatrick PJ, Warburton EA, Hayes PD, Varty K, Boyle JR, Gaunt ME, Zalewski A, Gillard JH (2009) The ATHER-OMA (Atorvastatin Therapy: Effects on Reduction of Macrophage Activity) study. Evaluation using ultrasmall superparamagnetic iron oxide-enhanced magnetic resonance imaging in carotid disease. *J Am Coll Cardiol* 53(22):2039–2050. <https://doi.org/10.1016/j.jacc.2009.03.018>
15. Tawakol A, Migrino RQ, Hoffmann U, Abbara S, Houser S, Gewirtz H, Muller JE, Brady TJFA (2005) Noninvasive in vivo measurement of vascular inflammation with F-18 fluorodeoxyglucose positron emission tomography. *J Nucl Cardiol* 12(3):294–301. <https://doi.org/10.1016/j.nuclcard.2005.03.002>
16. Vucic E, Dickson SD, Calcagno C, Rudd JHF, Moshier E, Hayashi K, Mounessa JS, Roitman M, Moon MJ, Lin J, Tsimikas S, Fisher EA, Nicolay K, Fuster V, Fayad ZA (2009) Pioglitazone modulates vascular inflammation in atherosclerotic rabbits noninvasive assessment with FDG-PET-CT and dynamic contrast-enhanced MR imaging. *JACC Cardiovasc Imaging* 4(10):1100–1109. <https://doi.org/10.1016/j.jcmg.2011.04.020>
17. Ye Y, Calcagno C, Binderup T, Courties G, Keliher E, Wojtkiewicz GR, Iwamoto Y, Tang J, Perez-Medina C, Mani V, Ishino S, Johnbeck CB, Knigge U, Fayad ZA, Libby P, Weissleder R, Tawakol A, Dubey S, Belanger AP, Di Carli MF, Swirski FK, Kjær A, Mulder W, Nahrendorf M (2015) Imaging macrophage and hematopoietic progenitor proliferation in atherosclerosis. *Circ Res* 117 (10):835–845. <https://doi.org/10.1161/CIRCRESAHA.115.307024>
18. Joshi NV, Vesey AT, Williams MC, Shah ASV, Calvert PA, Craighead FHM, Yeoh SE, Wallace W, Salter D, Fletcher AM, Van Beek EJR, Flapan AD, Uren NG, Behan MWH, Cruden NLM, Mills NL, Fox KAA, Rudd JHF, Dweck MR, Newby DE (2014) 18F-fluoride positron emission tomography for identification of ruptured and high-risk coronary atherosclerotic plaques: a prospective clinical trial. *Lancet* 383(9918):705–713. [https://doi.org/10.1016/S0140-6736\(13\)61754-7](https://doi.org/10.1016/S0140-6736(13)61754-7)
19. Irkle A, Vesey AT, Lewis DY, Skepper JN, Bird JLE, Dweck MR, Joshi FR, Gallagher FA, Warburton EA, Bennett MR, Brindle KM, Newby DE, Rudd JH, Davenport AP (2015) Identifying active vascular microcalcification by 18F-sodium fluoride positron emission tomography. *Nat Commun* 6:7495. <https://doi.org/10.1038/ncomms8495>
20. Dweck MR, Chow MWL, Joshi NV, Williams MC, Jones C, Fletcher AM, Richardson H, White A, McKillop G, van Beek EJR, Boon NA, Rudd JHF, Newby DE (2012) Coronary arterial 18F-sodium fluoride uptake: a novel marker of plaque biology. *J Am Coll Cardiol* 59(17):1539–1548. <https://doi.org/10.1016/j.jacc.2011.12.037>
21. Calcagno C, Mani V, Ramachandran S, Fayad ZA (2010) Dynamic contrast enhanced (DCE) magnetic resonance imaging (MRI) of atherosclerotic plaque angiogenesis. *Angiogenesis* 13 (2):87–99. <https://doi.org/10.1007/s10456-010-9172-2>

INDEX

A

- Acquired cardiomyopathy 145–158
Acute heart failure 276, 344
Acute myocardial infarction 281, 343
Adeno-associated virus 134
Adventitial lineage cells 254, 258, 262, 265–267
Anesthesia 137, 139, 140, 180,
 185, 186, 189–192, 202, 203, 209, 210, 213,
 222, 223, 227, 245, 247, 254, 256, 270, 275,
 282–284, 297, 299, 303, 310–312, 317, 318,
 329, 333, 338, 341, 345, 346, 355–357, 359,
 360, 365, 371–374, 376, 379, 387, 390, 394
Angioplasty 253, 386, 389, 390, 392
Animal model 7–9, 28, 146,
 175, 221, 227, 233, 253, 282, 296, 327, 337,
 343, 344, 353, 354, 360, 368, 370, 385
Aortocaval fistula 269–276
Arrhythmia 19, 31, 125,
 126, 134, 135, 138, 142, 205, 284, 286–289,
 292, 293, 300–302, 320, 351
Arterial thrombosis 162, 243, 269, 291
Arterial-venous fistulae (AVF) 269–273, 275, 276
AVF, *see* Arterial-venous fistulae (AVF)
Ascending aortic banding (AAB) 196–198,
 202, 205, 337–339, 341, 342
Atherosclerosis model 385
Atrial
 cardiomyocyte 39–48

B

- Badimon chamber 169
Balloon occlusion 284, 287, 290, 293
Biopsy catheter 329–335
Blood
 flow 124, 128, 133,
 162, 163, 165, 166, 168, 169, 192, 260, 262,
 272, 273, 275, 286, 312, 313, 319, 357, 368, 370
Blood-vessel wall interaction 161

C

- Calcium
 handling 93–103, 195
Canine
 heart failure model 309–314, 316–323

Cardiac

- angiography 282
differentiation 61, 62, 67, 75,
 77, 79, 85–87, 90, 91
electrophysiology 7, 17–33
function 4, 7, 192, 223, 292, 318, 322, 351
ischemia 8, 282
remodeling 51, 53, 211, 213
Cardiogenic shock 343–349, 351
Cardiomyocyte
 differentiation 55–65, 67–77, 81, 82, 148
 isolation 5, 40, 49, 50, 103
Cardiotoxicity 6, 8, 28, 221, 222, 225, 227
Cardiovascular diseases 3–10, 68,
 134, 156, 175, 215
Catheter based 9, 281–293
Cell
 culture 7, 32, 50, 56–58, 60–62, 68,
 69, 71–73, 76, 80, 83, 102
 isolation 5, 40,
 42, 48–50, 52, 62, 103
Chronic 7–9, 134, 184,
 207, 208, 215, 222, 244, 248, 250, 281, 292,
 293, 296, 311, 327, 328, 334, 335, 337, 342,
 353–361, 363–365, 368, 370, 374, 380
Clinical application 9, 328
Collagenase digestion 49, 51
Congestive heart failure 289, 310, 332
Contractility 4, 5, 93–103, 118,
 129, 131, 145, 184, 191, 200, 310
Coronary
 artery disease 133, 145
 artery ligation 181
 ischemia 7–9, 51, 107, 115, 133, 282
 perfusion pressure 109, 111,
 122, 125, 128, 130
Cross-circulation 6, 118, 120,
 121, 123–125, 128, 129
Cryo-injury 154, 155
- D
Diastolic dysfunction 197, 343
Dilated cardiomyopathy 145, 146, 153, 309, 310
Doxorubicin (Dox) 8, 146,
 154, 155, 158, 221, 223

E

- Echocardiography 118, 186,
 189–192, 197, 199, 201–203, 209–211, 213,
 222–225, 227, 282–285, 297, 300–302, 316,
 322, 331–335, 338, 340, 341, 355, 359, 360,
 376, 377
- Electrophysiology 4, 7, 17–33
- Embolic coil 283, 288, 293
- Embryoid body (EB) 55, 56,
 59–62, 64, 65, 79, 80, 85, 87–91
- Embryonic stem cells (ESCs) 4, 6,
 55–65, 67–77, 79
- End-organ perfusion 343
- Endothelial cell denudation 161, 264
- Energetics 117, 126
- Equivalent Emax (eEmax) 118, 129, 130
- ESCs, *see* Embryonic stem cells (ESCs)
- Experimental modeling 354
- Ex vivo 6, 7, 55, 108,
 117, 118, 134, 135, 138–141, 161–169, 178,
 181, 209, 310, 388
- Excitation-contraction coupling 126, 127
- Extracellular matrix remodeling 195, 197, 200

F

- Femoral artery (FA) 253, 257–262,
 264, 265, 267, 290, 311, 317, 319, 329, 389,
 390, 393, 397, 398
- Fibrosis 30, 32, 51, 53,
 198, 200, 201, 204, 209, 215, 219, 228, 337,
 338, 361, 363, 376, 379
- Fistula maturation 274

G

- Gene therapy 134

H

- Heart 9
 development 7, 9, 51, 56,
 68, 139, 338, 368
 disease 3, 6, 8, 9, 56, 68, 93,
 118, 134, 145, 146, 175, 183, 195, 215, 281,
 295, 327, 337, 368–370
 failure 8, 9, 31, 118, 128,
 134, 145, 175–181, 183, 184, 190, 191,
 195–205, 207–216, 243, 276, 281, 289, 295,
 296, 309–314, 316–323, 327–335, 337, 338,
 342–344, 368, 370
 failure with preserved ejection fraction (*see* HFpEF)
 rate 43–45, 96,
 107, 111, 113, 118, 125, 127, 128, 140, 184,
 189, 192, 203, 205, 210, 227, 281–284, 296,

- 301, 303, 309, 312, 322, 342, 356, 364, 372,
 374, 379, 380, 390
- Hemodialysis access 269
- Hemodynamics 4, 7, 125, 203,
 205, 240, 243, 244, 251, 288, 296, 302, 316,
 318–320, 322, 334, 335, 343, 344, 349–351,
 354–357, 359, 360, 362–365, 367, 368, 370,
 371, 374, 376, 379
- HFpEF 9, 337, 368
- Human
 embryonic stem cells 4, 55,
 62, 67, 69–72, 74, 76
 induced pluripotent stem cells 4, 6, 7,
 21, 79–92, 146, 148–151, 153, 156, 158
 pluripotent stem cells 4, 6, 40, 55,
 56, 67, 68, 79–92, 146
- Human engineered cardiac tissues (hECTs) 145, 146,
 149–158
- Hypertrophy 5, 51, 102,
 118, 183, 184, 190, 195, 197, 198, 203, 209,
 228, 233, 234, 237, 248, 337, 338, 341, 361, 379
- Hypoxia 5, 8, 51, 110,
 112, 114, 115, 243–251, 293, 362, 381, 386
- I**
- Imaging 5, 7, 9, 20,
 134, 137, 140, 152, 179, 181, 190, 191, 210,
 224, 225, 227, 282, 284, 286, 302, 330, 333,
 344, 354, 359, 374, 376, 377, 386, 387, 389,
 394–395
- Induced pluripotent stem cells (iPS) cells 4, 6, 7,
 40, 68, 75, 79–92, 146
- In silico 3, 4, 19, 20, 25, 31, 32
- Intracellular calcium (Ca^{2+}) 26, 28, 93
- Intracoronary 126, 127, 129
- Intraluminal drug delivery 269–276
- In vitro
 differentiation 56, 62, 67, 70, 75
- In vivo 3–10, 32, 56,
 68, 79, 111, 113, 118, 134, 135, 146, 162, 175,
 178, 209, 210, 310, 347, 360, 376, 386
- Ion Channels 4, 5, 19, 21–28, 32, 39, 93, 135
- iPS cells, *see* Induced pluripotent stem cells (iPS) cells
- Irreversible cardiac damage 133
- Ischemia 5, 7–9, 51, 107,
 114, 115, 133–142, 179, 181, 215, 276, 282,
 289, 293, 398
- Ischemia–reperfusion (I/R) 5, 107,
 114, 115, 133–142, 179, 181, 215, 282, 289, 293
- Ischemic 295
 heart disease 281, 282, 295
 heart failure 310, 327, 338, 343, 344
 mitral regurgitation 9, 299, 295–ENF
- Isoproterenol 207–219

L

- Langendorff
retrograde heart perfusion 6, 40, 107–115, 117
- Large animal
disease models 9, 370
- Left atrial
enlargement 285
- Left ventricle (LV) 52, 96,
102, 109, 112–115, 117–121, 124–127,
129–131, 178–181, 183, 184, 191, 195–200,
202–205, 210, 211, 225, 237, 248, 284, 285,
293, 295–298, 302, 305, 310–313, 318, 319,
321, 327, 328, 330–334, 340–342, 358, 361,
368, 376, 395
- Left ventricular
ejection fraction 198, 199,
202, 221, 225, 227, 311, 361, 368
- pressure 107, 109,
112–114, 117, 119–122, 124–126, 131, 185,
195, 197, 198, 200, 205, 302, 310–312, 314,
319–322, 331, 334, 338, 342, 343

M

- Magnetic resonance imaging (MRI) 387, 394, 395
- Mathematical modeling 18
- Mechanical work 126
- Mechanoenergetics 118, 129
- Microspheres 344, 346,
348, 349, 351, 354, 355, 357, 360, 362–364
- Microsurgery 185, 272
- Mitochondria 228
- Mitral
insufficiency 328
- regurgitation 9, 284, 299, 327–335, 295–ENF
- Modeling 3–6, 17–33,
354, 367, 368, 370–374, 376, 377, 379–381
- Models of disease v, 9, 51, 146
- Monocrotaline (MCT) 8, 233–241, 244
- Mouse
embryonic stem cell 55–65, 67
model 8, 92, 207–216,
243–251, 253–267, 269
strains 208, 210, 211, 213, 214, 216
- MRI, *see* Magnetic resonance imaging (MRI)
- Myocardial
infarction 8, 9, 32, 68,
92, 175, 176, 178–181, 183, 281–293, 295, 298,
299, 301, 302, 327, 337, 338, 343, 385
remodeling 195, 197

N

- Neointima hyperplasia 244, 253,
254, 262, 265–267

- New Zealand White rabbit 386
- Non-ischemic 9, 145, 146, 154, 179, 310, 327

O

- Optical mapping 7, 20, 136, 137, 139–141
- Osmotic pump 8, 207–216
- Ovine 299, 295–ENF
- Oxygen consumption 7, 124

P

- Pacing-induced heart failure 309–323
- Papillary muscle (PM) 191, 198,
199, 202, 205, 285, 296, 298, 301, 327, 330,
331, 334
- Pathophysiology 3, 7, 20, 161,
162, 233, 301, 328, 343, 344, 368
- Perfusion 6, 7, 40,
43–45, 50, 51, 94–97, 101, 102, 107–115, 117,
119, 120, 122–125, 128, 130, 137, 139–142,
161–169, 180, 241, 292, 343, 395
- Peripheral artery 253, 256–258, 263–265, 267
- Permanent coronary occlusion 289, 293
- Pharmacology 31
- Phenotypes 9, 146,
153, 158, 184, 190, 191, 195–199, 201, 213,
234, 337, 338, 353, 354, 360, 367, 368
- Pig 164, 281–293,
328, 329, 332–334, 337–339, 341, 342, 359,
367, 368, 370–374, 376, 377, 379–381, 385
- Platelet
function 161, 168
- Pluripotent stem cells 4, 6, 40,
56, 67, 68, 79–92, 146
- Porcine 57, 69, 80, 162, 164, 165, 343–349, 351
- Positron emission tomography (PET) 386,
394, 395
- Post-capillary pulmonary hypertension 9, 367,
368, 370–374, 376, 377, 379–381
- Pre-clinical
heart failure model 309
- Pressure-overload (PO) 8, 9,
183–185, 190, 191, 195–205, 337, 342, 361, 376
- Pressure-volume area (PVA) 117, 126, 129
- Pulmonary
embolization 354, 356, 357, 359, 363
hypertension 8, 9, 234, 244,
353, 367, 368, 370–374, 376, 377, 379–381
vascular disease 353
vein 124, 330, 334, 369,
370, 373, 374, 376, 379, 380
vein banding 370, 373, 381
- Pulmonary artery hypertension
model 233–241

Pulmonary vascular remodeling 234, 244, 355, 370

Q

Quantitative systems 31

R

Rabbit

 atherosclerosis model 385, 386

Rat 5, 8, 40, 41, 43, 49–51, 53, 107–115, 117–131, 135–137, 139, 178, 179, 195–205, 221–228, 233, 235, 237, 256, 266

Reaggregation 87, 91

Right heart

 echocardiography 376
 failure 9, 368, 370

Right ventricle

 failure 343, 348
 hypertrophy 248

Right ventricular failure 343, 348

Rodent 8, 9, 139, 175, 176, 178, 195, 234, 244, 245, 338, 385

S

Sheep 9, 175, 287, 296–299, 301, 310, 363, 385

shRNA 135, 137

Small animals 8, 118, 176, 185, 201, 209, 212

Stem cells 4, 6, 21, 31–33, 40, 55–65, 67–77, 79–92, 145, 147, 150, 254

Sugen 5416 243–251

Surgical 8, 9, 41, 43, 44, 94, 96, 101, 118, 120, 121, 124, 125, 127, 162–165, 175, 176, 178, 180, 183–186, 188, 201–203, 209, 210, 212–214, 235–237, 239, 245, 247, 251, 254–258, 262, 270, 284, 296, 299–301, 303, 310–314, 316, 317, 320, 321, 335, 337–341, 354, 370–375, 379, 380, 387, 389–394, 397

Systems biology 18

T

Tachycardia-induced heart failure 309

Tethering 295

Thoracotomy 188, 202, 296, 297, 302, 314, 321, 355, 370, 375

Thrombosis 7, 161–169, 243, 269, 276

Thrombus 161, 162, 166–169, 286, 288, 291, 293, 354

Tissue
 collection 152, 213
 engineering 7, 145–158

Torsades de Pointes (TdP) 28, 31

Translational 17, 18, 146

Translocator protein (TSPO) 133–142

Trans-septal 328, 333

Transverse aortic constriction (TAC) 183–192

TAC, *see* Transverse aortic constriction (TAC)

Traszmab (Trz) 221–223, 227

Troponin 84, 88–91, 225–227

U

Ultrasound 186, 189, 190, 210, 211, 274, 275, 284, 286, 290, 297, 301, 345, 347, 349, 355, 371

V

Vascular remodeling 8, 233, 234, 243, 253–267, 355, 361, 363, 365, 368, 370, 376

Venous thrombosis 161

Ventricular
 cardiomyocyte 19, 21, 25, 39–48, 209, 361, 379

 tachycardia 28, 142, 289, 290

Ventricular fibrillation 205, 320, 344

Virchow's triad 162

Volume-overload 9, 327, 379

W

Wire injury 8, 253–267

Wnt signaling 70, 74, 75